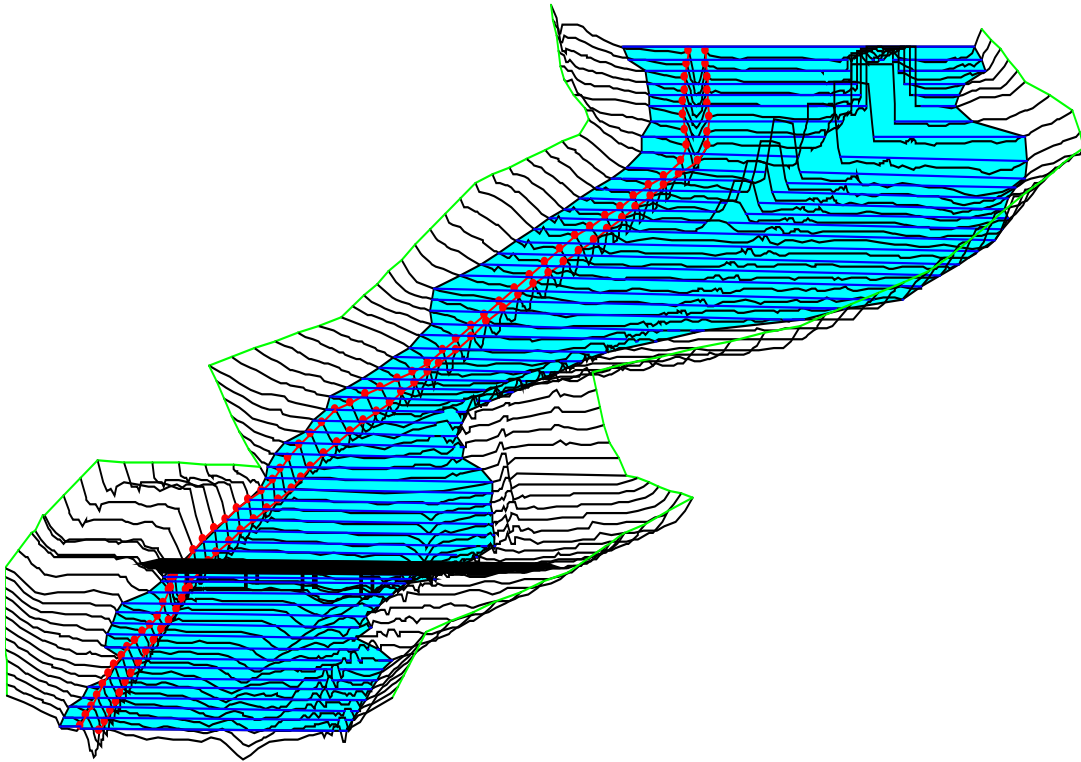**US Army Corps
of Engineers**
Hydrologic Engineering Center

HEC-RAS
River Analysis System

Hydraulic Reference Manual
Version 5.0
February 2016

CPD-69

1. AGENCY USE ONLY *(Leave blank)*	**2. REPORT DATE** February, 2016	**3. REPORT TYPE AND DATES COVERED** Computer Program Documentation	
4. TITLE AND SUBTITLE HEC-RAS, River Analysis System Hydraulic Reference Manual			**5. FUNDING NUMBERS**
6. AUTHOR(S) Gary W. Brunner			
7. PERFORMING ORGANIZATION NAME(S) AND ADDRESS(ES) US ARMY CORPS OF ENGINEERS HYDROLOGIC ENGINEERING CENTER (HEC) 609 Second Street Davis, CA 95616-4687			**8. PERFORMING ORGANIZATION REPORT NUMBER** CPD-69
9. SPONSORING / MONITORING AGENCY NAME(S) AND ADDRESS(ES)			**10. SPONSORING / MONITORING AGENCY REPORT NUMBER**
11. SUPPLEMENTARY NOTES			
12a. DISTRIBUTION / AVAILABILITY STATEMENT Approved for Public Release. Distribution is unlimited.			**12b. DISTRIBUTION CODE**

13. ABSTRACT *(Maximum 200 words)*

The U.S. Army Corps of Engineers' River Analysis System (HEC-RAS) is software that allows you to perform one-dimensional steady and unsteady flow river hydraulics calculations.

HEC-RAS is an integrated system of software, designed for interactive use in a multi-tasking, multi-user network environment. The system is comprised of a graphical user interface (GUI), separate hydraulic analysis components, data storage and management capabilities, graphics and reporting facilities.

The HEC-RAS system contains four one-dimensional hydraulic analysis components for: (1) steady flow water surface profile computations; (2) unsteady flow simulation; (3) movable boundary sediment transport computations; and (4) temperature and water quality constituent transport modeling.. A key element is that all four components use a common geometric data representation and common geometric and hydraulic computation routines. In addition to the four hydraulic analysis components, the system contains several hydraulic design features that can be invoked once the basic water surface profiles are computed.

14. SUBJECT TERMS water surface profiles, river hydraulics, steady and unsteady flow, One-dimensional and two-dimensional hydrodynamics, computer program			**15. NUMBER OF PAGES** 547
			16. PRICE CODE
17. SECURITY CLASSIFICATION OF REPORT UNCLASSIFIED	**18. SECURITY CLASSIFICATION OF THIS PAGE** UNCLASSIFIED	**19. SECURITY CLASSIFICATION OF ABSTRACT** UNCLASSIFIED	**20. LIMITATION OF ABSTRACT** UNLIMITED

HEC-RAS

River Analysis System

Hydraulic Reference Manual

Version 5.0

February 2016

River Analysis System, HEC-RAS

The HEC-RAS executable code and documentation was developed with U.S. Federal Government resources and is therefore in the public domain. It may be used, copied, distributed, or redistributed freely. However, it is requested that HEC be given appropriate acknowledgment in any subsequent use of this work.

HEC cannot provide technical support for this software to non-Corps users. See our software vendors list (on our web page) to locate organizations that provide the program, documentation, and support services for a fee. However, we will respond to all documented instances of program errors. Documented errors are bugs in the software due to programming mistakes not model problems due to user-entered data.

This document contains references to product names that are trademarks or registered trademarks of their respective owners. Use of specific product names does not imply official or unofficial endorsement. Product names are used solely for the purpose of identifying products available in the public market place.

Microsoft, Windows, and Excel are registered trademarks of Microsoft Corp. ArcView is a trademark of ESRI, Inc.

Terms and Conditions of Use:

Use of the software described by this document is controlled by certain terms and conditions. The user must acknowledge and agree to be bound by the terms and conditions of usage before the software can be installed or used. The software described by this document can be downloaded for free from our internet site (www.hec.usace.army.mil).

The United States Government, US Army Corps of Engineers, Hydrologic Engineering Center ("HEC") grants to the user the rights to install Watershed Analysis Tool (HEC-RAS) "the Software" (either from a disk copy obtained from HEC, a distributor or another user or by downloading it from a network) and to use, copy and/or distribute copies of the Software to other users, subject to the following Terms and Conditions for Use:

All copies of the Software received or reproduced by or for user pursuant to the authority of this Terms and Conditions for Use will be and remain the property of HEC.

User may reproduce and distribute the Software provided that the recipient agrees to the Terms and Conditions for Use noted herein.

HEC is solely responsible for the content of the Software. The Software may not be modified, abridged, decompiled, disassembled, unobfuscated or reverse engineered. The user is solely responsible for the content, interactions, and effects of any and all amendments, if present, whether they be extension modules, language resource bundles, scripts or any other amendment.

The name "HEC-RAS" must not be used to endorse or promote products derived from the Software. Products derived from the Software may not be called "HEC- RAS " nor may any part of the "HEC- RAS " name appear within the name of derived products.

No part of this Terms and Conditions for Use may be modified, deleted or obliterated from the Software.

No part of the Software may be exported or re-exported in contravention of U.S. export laws or regulations.

Waiver of Warranty:

THE UNITED STATES GOVERNMENT AND ITS AGENCIES, OFFICIALS, REPRESENTATIVES, AND EMPLOYEES, INCLUDING ITS CONTRACTORS AND SUPPLIERS PROVIDE HEC-WAT \"AS IS,\" WITHOUT ANY WARRANTY OR CONDITION, EXPRESS, IMPLIED OR STATUTORY, AND SPECIFICALLY DISCLAIM ANY IMPLIED WARRANTIES OF TITLE, MERCHANTABILITY, FITNESS FOR A PARTICULAR PURPOSE AND NON-INFRINGEMENT.

Depending on state law, the foregoing disclaimer may not apply to you, and you may also have other legal rights that vary from state to state.

Limitation of Liability:

IN NO EVENT SHALL THE UNITED STATES GOVERNMENT AND ITS
AGENCIES, OFFICIALS, REPRESENTATIVES, AND EMPLOYEES, INCLUDING
ITS CONTRACTORS AND SUPPLIERS, BE LIABLE FOR LOST PROFITS OR ANY
SPECIAL, INCIDENTAL OR CONSEQUENTIAL DAMAGES ARISING OUT OF OR
IN CONNECTION WITH USE OF HEC-WAT REGARDLESS OF CAUSE,
INCLUDING NEGLIGENCE.

THE UNITED STATES GOVERNMENT'S LIABILITY, AND THE LIABILITY OF
ITS AGENCIES, OFFICIALS, REPRESENTATIVES, AND EMPLOYEES,
INCLUDING ITS CONTRACTORS AND SUPPLIERS, TO YOU OR ANY THIRD
PARTIES IN ANY CIRCUMSTANCE IS LIMITED TO THE REPLACEMENT OF
CERTIFIED COPIES OF HEC-WAT WITH IDENTIFIED ERRORS CORRECTED.
Depending on state law, the above limitation or exclusion may not apply to you.

Indemnity:

As a voluntary user of HEC- RAS you agree to indemnify and hold the United States
Government, and its agencies, officials, representatives, and employees, including its
contractors and suppliers, harmless from any claim or demand, including reasonable
attorneys' fees, made by any third party due to or arising out of your use of HEC- RAS or
breach of this Agreement or your violation of any law or the rights of a third party.

Assent:

By using this program you voluntarily accept these terms and conditions. If you do not
agree to these terms and conditions, uninstall the program and return any program
materials to HEC (if you downloaded the program and do not have disk media, please
delete all copies, and cease using the program.)

Table of Contents

Foreword

The U.S. Army Corps of Engineers' River Analysis System (HEC-RAS) is software that allows you to perform one-dimensional steady flow hydraulics; one and two-dimensional unsteady flow river hydraulics calculations; quasi Unsteady and full unsteady flow sediment transport-mobile bed modeling; water temperature analysis; and generalized water quality modeling (nutrient fate and transport).

The first version of HEC-RAS (version 1.0) was released in July of 1995. Since that time there have been several major releases of this software package, including versions: 1.1; 1.2; 2.0; 2.1; 2.2; 3.0, 3.1, 3.1.1, 3.1.2, 3.1.3, 4.0, 4.1 and now version 5.0 in 2015.

The HEC-RAS software was developed at the Hydrologic Engineering Center (HEC), which is a division of the Institute for Water Resources (IWR), U.S. Army Corps of Engineers.

The software was designed by Mr. Gary W. Brunner, leader of the HEC-RAS development team. The user interface and graphics were programmed by Mr. Mark R. Jensen. The steady flow water surface profiles computational module and the majority of the one-dimensional unsteady flow computations modules was programmed by Mr. Steven S. Piper. The One-dimensional unsteady flow matrix solution algorithm was developed by Dr. Robert L. Barkau (Author of UNET and HEC-UNET).

The two-dimensional unsteady flow modeling capabilities were developed by Gary W. Brunner, Mark R. Jensen, Steve S. Piper, Ben Chacon (Resource Management Consultants, RMA), and Alex J. Kennedy.

The sediment transport interface module was programmed by Mr. Stanford A. Gibson. The quasi unsteady flow computational sediment transport capabilities were developed by Stanford A. Gibson and Steven S. Piper. The Unsteady flow sediment transport modules were developed by Stanford A. Gibson, Steven S. Piper, and Ben Chacon (RMA). Special thanks to Mr. Tony Thomas (Author of HEC-6 and HEC-6T) for his assistance in developing the quasi-unsteady flow sediment transport routines used in HEC-RAS.

The water quality computational modules were designed and developed by Mr. Mark R. Jensen, Dr. Cindy Lowney and Zhonglong Zhang (ERDC-RDE-EL-MS).

The spatial data and mapping tools (RAS-Mapper) were developed by Mark R. Jensen, Cameron T. Ackerman, and Alex J. Kennedy.

The interface for channel design/modifications was designed and developed by Mr. Cameron T. Ackerman and Mr. Mark R. Jensen. The stable channel design functions were programmed by Mr. Chris R. Goodell.

The routines that import HEC-2 and UNET data were developed by Ms. Joan Klipsch. The routines for modeling ice cover and wide river ice jams were developed by Mr. Steven F. Daly of the Cold Regions Research and Engineering Laboratory (CRREL).

Many other HEC staff members have made contributions in the development of this software, including: Mr. Vern R. Bonner, Mr. Richard Hayes, Mr. John Peters, Mr. Al Montalvo, and Dr. Michael Gee. Mr. Matt Fleming was the Chief of the H&H Division, and Mr. Chris Dunn was the director during the development of this version of the software.

This manual was written by Mr. Gary W. Brunner. Chapter 12 was written by Mr. Chris R. Goodell, and Chapter 13 was written by Mr. Stanford Gibson.

Part of Chapter 2 (2D Computational Theory) was written by Mr. Ben Chacon (Resource Management Consultants, RMA).

HEC-RAS uses the following third party libraries:

1. Hierarchical Data Format (HDF) – HEC-RAS uses the HDF5 libraries in both the User Interface and the Computational engines for writing and reading data to binary files that follow the HDF5 standards. The HDF Group: http://www.hdfgroup.org/HDF5/

2. Geospatial Data Abstraction Library (GDAL) – HEC-RAS uses the GDAL libraries in the HEC-RAS Mapper tool. These libraries are use for all Geospatial data rendering, coordinate transformations, etc…   GDAL: http://www.gdal.org/

3. Bitmiracle LibTiff .Net. LibTiff.Net provides support for the Tag Image File Format (TIFF), a widely used format for storing image data. Bitmiricle: http://bitmiracle.com/libtiff/

4. Oxyplot – 2 dimensional X-Y plots in HEC-RAS Mapper. Oxyplot: http://oxyplot.org/

5. SQLite – Reading and writing database files. SQLite: https://www.sqlite.org/

6. cURL - HTTP support for GDAL http://curl.haxx.se/

CHAPTER 1

Introduction

Welcome to the Hydrologic Engineering Center's River Analysis System (HEC-RAS). This software allows you to perform one-dimensional steady, one and two dimensional unsteady flow hydraulics, sediment transport/mobile bed computations, water temperature modeling, and generalized water quality modeling (nutrient fate and transport).

This manual documents the hydraulic capabilities of the Steady and unsteady flow portion of HEC-RAS, as well as sediment transport computations.

This chapter discusses the general philosophy of HEC-RAS and gives you a brief overview of the hydraulic capabilities of the modeling system. Documentation for HEC-RAS is discussed, as well as an overview of this manual.

Contents

■ General Philosophy of the Modeling System

■ Overview of Hydraulic Capabilities

■ HEC-RAS Documentation

■ Overview of This Manual

General Philosophy of the Modeling System

HEC-RAS is an integrated system of software, designed for interactive use in a multi-tasking, multi-user network environment. The system is comprised of a graphical user interface (GUI), separate hydraulic analysis components, data storage and management capabilities, graphics and reporting facilities.

The HEC-RAS system contains four one-dimensional river analysis components for: (1) steady flow water surface profile computations; (2) unsteady flow simulation (one-dimensional and two-dimensional hydrodynamics); (3) movable boundary sediment transport computations; and (4) water quality analysis. A key element is that all four components use a common geometric data representation and common geometric and hydraulic computation routines. In addition to the four river analysis components, the system contains several hydraulic design features that can be invoked once the basic water surface profiles are computed.

The current version of HEC-RAS supports Steady and Unsteady flow water surface profile calculations; combined 1D and 2D hydrodynamics; sediment transport/mobile bed computations; water temperature analysis; water quality analyses (Nutrient transport and fate); and spatial mapping of many computed parameters (Depth, water surface elevation, velocity, etc…). New features and additional capabilities will be added in future releases.

Overview of Hydraulic Capabilities

HEC-RAS is designed to perform one-dimensional (1D), two-dimensional (2D), or combined 1D and 2D hydraulic calculations for a full network of natural and constructed channels. The following is a description of the major hydraulic capabilities of HEC-RAS.

Steady Flow Water Surface Profiles. This component of the modeling system is intended for calculating water surface profiles for steady gradually varied flow. The system can handle a single river reach, a dendritic system, or a full network of channels. The steady flow component is capable of modeling subcritical, supercritical, and mixed flow regime water surface profiles.

The basic computational procedure is based on the solution of the one-dimensional energy equation. Energy losses are evaluated by friction (Manning's equation) and contraction/expansion (coefficient multiplied by the change in velocity head). The momentum equation is utilized in situations where the water surface profile is rapidly varied. These situations include mixed flow regime calculations (i.e., hydraulic jumps), hydraulics of bridges, and evaluating profiles at river confluences (stream junctions).

The effects of various obstructions such as bridges, culverts, weirs, spillways and other structures in the flood plain may be considered in the computations. The steady flow system is designed for application in flood plain management and flood insurance studies to evaluate floodway encroachments. Also, capabilities are available for assessing the change in water surface profiles due to channel improvements, and levees.

Special features of the steady flow component include: multiple plan analyses; multiple profile computations; multiple bridge and/or culvert opening analysis, and split flow optimization at stream junctions and lateral weirs and spillways.

Unsteady Flow Simulation. This component of the HEC-RAS modeling system is capable of simulating one-dimensional unsteady flow; two-dimensional unsteady flow; or combined 1D and 2D unsteady flow modeling through a full network of open channels. The 1D unsteady flow equation solver was adapted from Dr. Robert L. Barkau's UNET model (Barkau, 1992 and HEC, 1997). This 1D unsteady flow component was developed primarily for subcritical flow regime calculations. The 2D unsteady flow equation solver was developed at HEC, and was directly integrated into the HEC-RAS Unsteady flow engine in order to facilitate combined 1D and 2D hydrodynamic modeling.

The hydraulic calculations for cross-sections, bridges, culverts, and other hydraulic structures that were developed for the steady flow component were incorporated into the unsteady flow module. Additionally, the unsteady flow component has the ability to model storage areas and hydraulic connections between storage areas; 2D Flow Areas; and between stream reaches.

Sediment Transport/Movable Boundary Computations. This component of the modeling system is intended for the simulation of one-dimensional sediment transport/movable boundary calculations resulting from scour and deposition over moderate time periods (typically years, although applications to single flood events will be possible).

The sediment transport potential is computed by grain size fraction, thereby allowing the simulation of hydraulic sorting and armoring. Major features include the ability to model a full network of streams, channel dredging, various levee and encroachment alternatives, and the use of several different equations for the computation of sediment transport.

The model is designed to simulate long-term trends of scour and deposition in a stream channel that might result from modifying the frequency and duration of the water discharge and stage, or modifying the channel geometry. This system can be used to evaluate deposition in reservoirs, design channel contractions required to maintain navigation depths, predict the influence of dredging on the rate of deposition, estimate maximum possible scour during large flood events, and evaluate sedimentation in fixed channels.

Water Quality Analysis. This component of the modeling system is intended to allow the user to perform riverine water quality analyses. The current version of HEC-RAS can perform detailed temperature analysis and transport of a limited number of water quality constituents (Algae, Dissolved Oxygen, Carbonaceuos Biological Oxygen Demand, Dissolved Orthophosphate, Dissolved Organic Phosphorus, Dissolved Ammonium Nitrate, Dissolved Nitrite Nitrogen, Dissolved Nitrate Nitrogen, and Dissolved Organic Nitrogen). Future versions of the software will include the ability to perform the transport of several additional water quality constituents.

HEC-RAS Documentation

The HEC-RAS package includes several documents, each are designed to help the modeler learn to use a particular aspect of the modeling system. The documentation has been divided into the following three categories:

Documentation	**Description**
User's Manual	This manual is a guide to using the HEC-RAS. The manual provides an introduction and overview of the modeling system, installation instructions, how to get started, simple examples, detailed descriptions of each of the major modeling components, and how to view graphical and tabular output.
Hydraulic Reference Manual	This manual describes the theory and data requirements for the hydraulic calculations performed by HEC-RAS. Equations are presented along with the assumptions used in their derivation. Discussions are provided on how to estimate model parameters, as well as guidelines on various modeling approaches.
Applications Guide	This document contains a series of examples that demonstrate various aspects of the HEC-RAS. Each example consists of a problem statement, data requirements, general outline of solution steps, displays of key input and output screens, and discussions of important modeling aspects.
2D Modeling with HEC-RAS	This manual describes how to utilize the 2D hydrodynamic modeling capabilities within HEC-RAS. Discussions include: developing terrain models for 2D modeling; developing combined 1D/2D integrated models; running the combined 1D/2D model; and viewing output for combined 1D/2D models.

Overview of This Manual

This manual presents the theory and data requirements for hydraulic calculations in the HEC-RAS system. The manual is organized as follows:

- ■ Chapter 2 provides an overview of the hydraulic calculations theory in HEC-RAS.

- ■ Chapter 3 describes the basic data requirements to perform the various hydraulic analyses available.

- ■ Chapter 4 is an overview of some of the optional hydraulic capabilities of the HEC-RAS software.

- ■ Chapters 5, 6, 7, and 8 provide detailed discussions on modeling bridges; culverts; multiple openings; inline structures (weirs and gated spillways), and lateral structures.

- ■ Chapter 9 describes how to perform floodway encroachment calculations.

- ■ Chapter 10 describes how to use HEC-RAS to compute scour at bridges.

- ■ Chapter 11 describes how to model ice-covered rivers.

- ■ Chapter 12 describes the equations and methodologies for stable channel design within HEC-RAS.

- ■ Chapter 13 describes the equations and methodologies for performing one-dimensional sediment transport, erosion, and deposition computations.

- ■ Chapter14 describes how to perform a Dambreak study with HEC-RAS.

- ■ Appendix A provides a list of all the references for the manual.

- ■ Appendix B is a summary of the research work on "Flow Transitions in Bridge Backwater Analysis."

- ■ Appendix C is a write up on the computational differences between HEC-RAS and HEC-2.

- ■ Appendix D is a write up on the "Computation of the WSPRO Discharge Coefficient and Effective Flow Length

CHAPTER 2

Theoretical Basis for One-Dimensional and Two-Dimensional Hydrodynamic Calculations

This chapter describes the methodologies used in performing the one-dimensional (1D) steady flow and unsteady flow calculations, as well as the two-dimensional (2D) unsteady flow calculations within HEC-RAS. The basic equations are presented along with discussions of the various terms. Solution schemes for the various equations are described. Discussions are provided as to how the equations should be applied, as well as applicable limitations.

Contents

■ General

■ 1D Steady Flow Water Surface Profiles

■ 1D Unsteady Flow Computations

■ 2D Unsteady Flow Computations

General

This chapter describes the theoretical basis for one-dimensional water surface profile calculations and the two-dimensional hydrodynamic calculations. Discussions contained in this chapter are limited to steady flow water surface profile calculations and unsteady flow routing (1D, 2D, and combined 1D/2D).

1D Steady Flow Water Surface Profiles

HEC-RAS is currently capable of performing 1D water surface profile calculations for steady gradually varied flow in natural or constructed channels. Subcritical, supercritical, and mixed flow regime water surface profiles can be calculated. Topics discussed in this section include: equations for basic profile calculations; cross section subdivision for conveyance calculations; composite Manning's n for the main channel; evaluation of the mean kinetic energy head (velocity weighting coefficient alpha); friction loss evaluation; contraction and expansion losses; computational procedure; critical depth determination; applications of the momentum equation; air entrainment in high velocity streams; and limitations of the steady flow model.

Equations for Basic Profile Calculations

Water surface profiles are computed from one cross section to the next by solving the Energy equation with an iterative procedure called the standard step method. The Energy equation is written as follows:

$$Z_2 + Y_2 + \frac{a_2 V_2^2}{2g} = Z_1 + Y_1 + \frac{a_1 V_1^2}{2g} + h_e \tag{2-1}$$

Where: Z_1, Z_2 = elevation of the main channel inverts

Y_1, Y_2 = depth of water at cross sections

V_1, V_2 = average velocities (total discharge/ total flow area)

a_1, a_2 = velocity weighting coefficients

g = gravitational acceleration

h_e = energy head loss

A diagram showing the terms of the energy equation is shown in Figure 2-1.
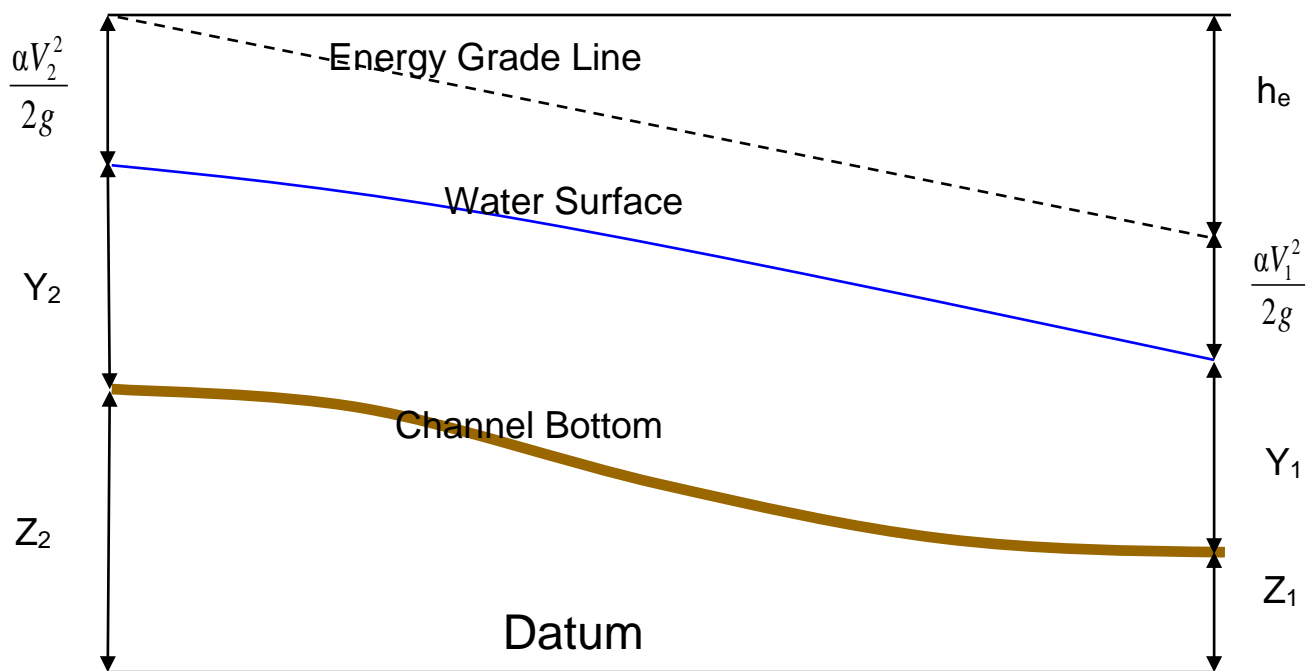
Figure 2-1 Representation of Terms in the Energy Equation

The energy head loss (h_e) between two cross sections is comprised of friction losses and contraction or expansion losses. The equation for the energy head loss is as follows:

$$h_e = L\overline{S}_f + C\left|\frac{a_2 V_2^2}{2g} - \frac{a_1 V_1^2}{2g}\right|$$

(2-2)

Where: L = discharge weighted reach length

$\overline{S}_f$ = representative friction slope between two sections

C = expansion or contraction loss coefficient

The distance weighted reach length, L, is calculated as:

$$L = \frac{L_{lob}\overline{Q}_{lob} + L_{ch}\overline{Q}_{ch} + L_{rob}\overline{Q}_{rob}}{\overline{Q}_{lob} + \overline{Q}_{ch} + \overline{Q}_{rob}}$$

(2-3)

where: L_{lob}, L_{ch}, L_{rob} = cross section reach lengths specified for flow in the left overbank, main channel, and right overbank, respectively

$\overline{Q}_{lob} + \overline{Q}_{ch} + \overline{Q}_{rob}$ = arithmetic average of the flows between sections for the left overbank, main channel, and right overbank, respectively

Cross Section Subdivision for Conveyance Calculations

The determination of total conveyance and the velocity coefficient for a cross section requires that flow be subdivided into units for which the velocity is uniformly distributed. The approach used in HEC-RAS is to subdivide flow in the **overbank** areas using the input cross section n-value break points (locations where n-values change) as the basis for subdivision (Figure 2-2). Conveyance is calculated within each subdivision from the following form of Manning's equation (based on English units):

$$Q = KS_f^{1/2} \tag{2-4}$$

$$K = \frac{1.486}{n} AR^{2/3} \tag{2-5}$$

where: K = conveyance for subdivision

n = Manning's roughness coefficient for subdivision

A = flow area for subdivision

R = hydraulic radius for subdivision (area / wetted perimeter)

S_f = slope of the energy gradeline

The program sums up all the incremental conveyances in the overbanks to obtain a conveyance for the left overbank and the right overbank. The main channel conveyance is normally computed as a single conveyance element. The total conveyance for the cross section is obtained by summing the three subdivision conveyances (left, channel, and right).
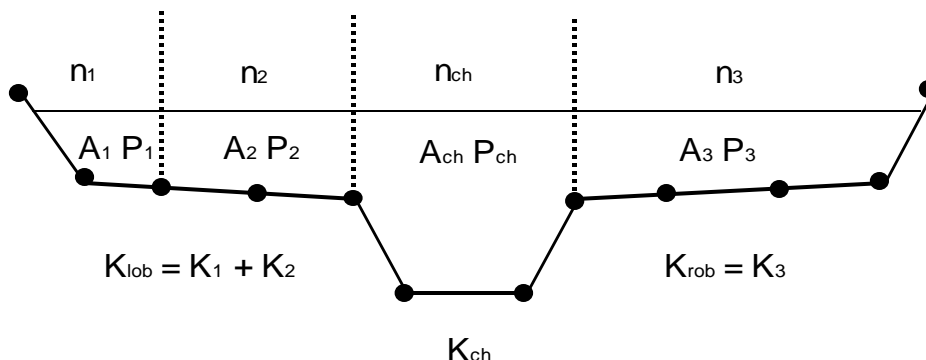
Figure 2-2 HEC-RAS Default Conveyance Subdivision Method

An alternative method available in HEC-RAS is to calculate conveyance between every coordinate point in the overbanks (Figure 2.3). The conveyance is then summed to get the total left overbank and right overbank values. This method is used in the Corps HEC-2 program. The method has been retained as an option within HEC-RAS in order to reproduce studies that were originally developed with HEC-2.
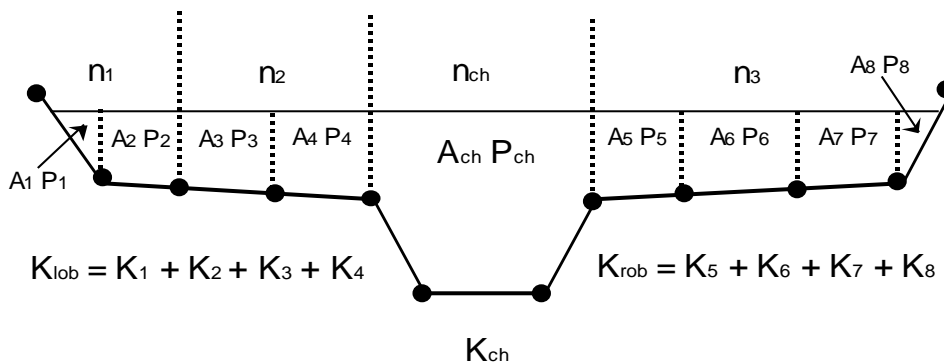
Figure 2-3 Alternative Conveyance Subdivision Method (HEC-2 style)

The two methods for computing conveyance will produce different answers whenever portions on the overbank have ground sections with significant vertical slopes. In general, the HEC-RAS default approach will provide a lower total conveyance for the same water surface elevation.

In order to test the significance of the two ways of computing conveyance, comparisons were performed using 97 data sets from the HEC profile accuracy study (HEC, 1986). Water surface profiles were computed for the 1% chance event using the two methods for computing conveyance in HEC-RAS. The results of the study showed that the HEC-RAS default approach will generally produce a higher computed water surface elevation. Out of the 2048 cross section locations, 47.5% had computed water surface elevations within 0.10 ft. (30.48 mm), 71% within 0.20 ft. (60.96 mm), 94.4% within 0.4 ft. (121.92 mm), 99.4% within 1.0 ft. (304.8 mm), and one cross section had a difference of 2.75 ft. (0.84 m). Because the differences tend to be in the same direction, some effects can be attributed to propagation of downstream differences.

The results from the conveyance comparisons do not show which method is more accurate, they only show differences. In general, it is felt that the HEC-RAS default method is more commensurate with the Manning equation and the concept of separate flow elements. Further research, with observed water surface profiles, will be needed to make any conclusions about the accuracy of the two methods.

Composite Manning's n for the Main Channel

Flow in the main channel is not subdivided, except when the roughness coefficient is changed within the channel area. HEC-RAS tests the applicability of subdivision of roughness within the main channel portion of a cross section, and if it is not applicable, the program will compute a single composite n value for the entire main channel. The program determines if the main channel portion of the cross section can be subdivided or if a composite main channel n value will be utilized based on the following criterion: if a main channel side slope is steeper than 5H:1V and the main channel has more than one n-value, a composite roughness n_c will be computed [Equation 6-17, Chow, 1959]. The channel side slope used by HEC-RAS is defined as the horizontal distance between adjacent n-value stations within the main channel over the difference in elevation of these two stations (See SL and SR of Figure 2.4).

ROCKY RIVER TEST 2
Cross-section 3.000
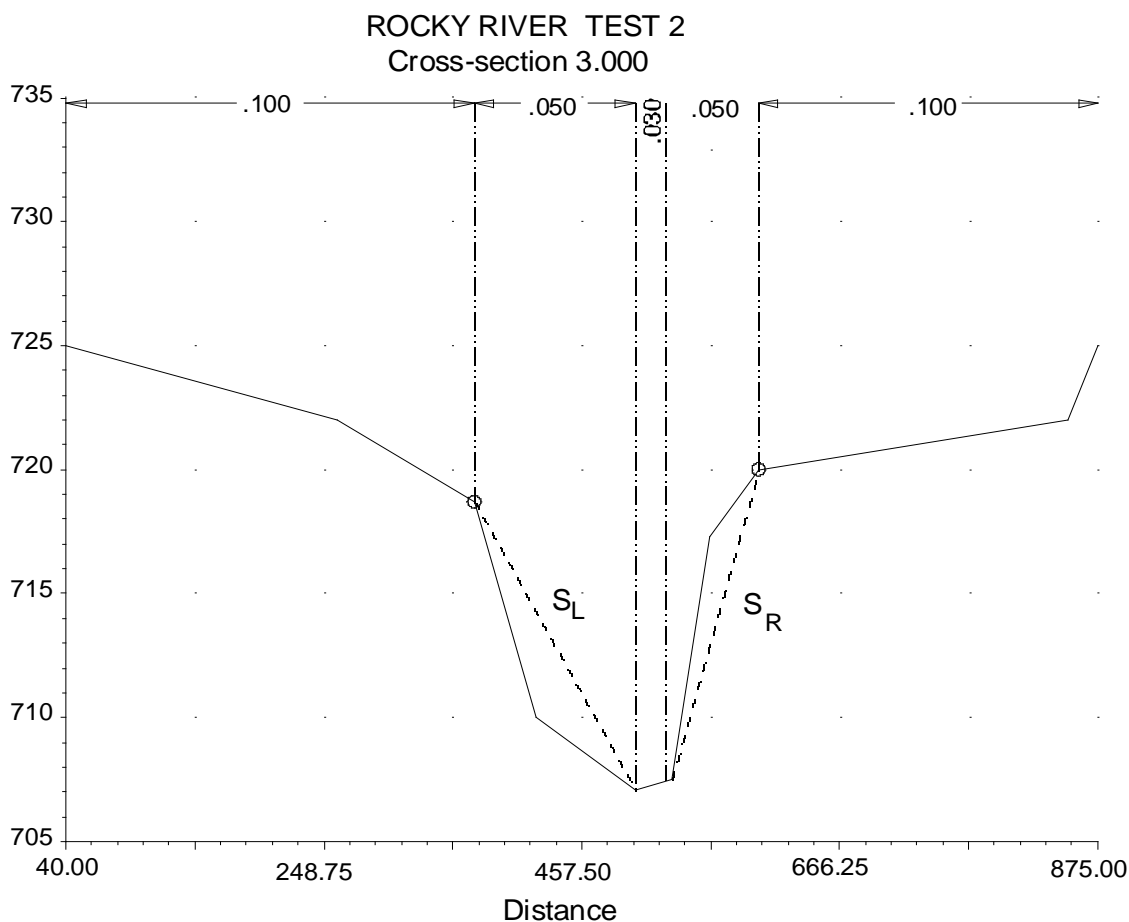
Figure 2-4 Definition of Bank Slope for Composite n_c Calculation

For the determination of n_c, the main channel is divided into N parts, each with a known wetted perimeter P_i and roughness coefficient n_i.

$$n_c = \left[\frac{\sum_{i=1}^{N} \left(P_i n_i^{1.5} \right)}{P} \right]^{2/3}$$

(2-6)

Where: n_c =   composite or equivalent coefficient of roughness

P =   wetted perimeter of entire main channel

P_i =   wetted perimeter of subdivision I

n_i =   coefficient of roughness for subdivision

The computed composite n_c should be checked for reasonableness. The computed value is the composite main channel n value in the output and summary tables.

Evaluation of the Mean Kinetic Energy Head

Within the 1D river reach segments, only a single water surface and therefore a single mean energy are computed at each cross section. For a given water surface elevation, the mean energy is obtained by computing a flow weighted energy from the three subsections of a cross section (left overbank, main channel, and right overbank). Figure 2-5 below shows how the mean energy would be obtained for a cross section with a main channel and a right overbank (no left overbank area).
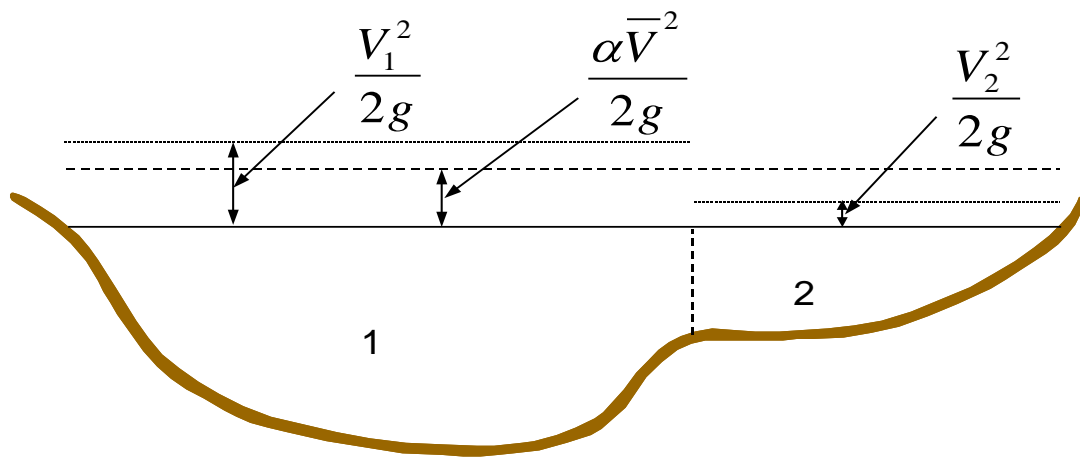
V_1 = mean velocity for subarea 1

V_2 = mean velocity for subarea 2

Figure 2-5 Example of How Mean Energy is Obtained

To compute the mean kinetic energy it is necessary to obtain the velocity head weighting coefficient alpha. Alpha is calculated as follows:

Mean Kinetic Energy Head = Discharge-Weighted Velocity Head

$$\alpha \frac{\overline{V}^2}{2g} = \frac{Q_1 \frac{V_1^2}{2g} + Q_2 \frac{V_2^2}{2g}}{Q_1 + Q_2} \tag{2-7}$$

$$\alpha = \frac{2g\left[Q_1\frac{V_1^2}{2g} + Q_2\frac{V_2^2}{2g}\right]}{(Q_1 + Q_2)\overline{V}^2} \tag{2-8}$$

$$\alpha = \frac{Q_1V_1^2 + Q_2V_2^2}{(Q_1 + Q_2)\overline{V}^2} \tag{2-9}$$

In General:

$$\alpha = \frac{\left[Q_1V_1^2 + Q_2V_2^2 + \cdots + Q_NV_N^2\right]}{Q\overline{V}^2} \tag{2-10}$$

The velocity coefficient, α, is computed based on the conveyance in the three flow elements: left overbank, right overbank, and channel. It can also be written in terms of conveyance and area as in the following equation:

$$\alpha = \frac{(A_t)^2\left[\dfrac{K_{lob}^3}{A_{lob}^2} + \dfrac{K_{ch}^3}{A_{ch}^2} + \dfrac{K_{rob}^3}{A_{rob}^2}\right]}{K_t^3} \tag{2-11}$$

Where: A_t =   total flow area of cross section

A_{lob}, A_{ch}, A_{rob} =   flow areas of left overbank, main channel
and right overbank, respectively

K_t =   total conveyance of cross section

K_{lob}, K_{ch}, K_{rob} =   conveyances of left overbank, main channel and right overbank

Friction Loss Evaluation

Friction loss is evaluated in HEC-RAS as the product of $\overline{S}_f$ and *L* (Equation 2-2), where $\overline{S}_f$ is the representative friction slope for a reach and *L* is defined by Equation 2-3. The friction slope (slope of the energy gradeline) at each cross section is computed from Manning's equation as follows:

$$S_f = \left(\frac{Q}{K}\right)^2 \tag{2-12}$$

Alternative expressions for the representative reach friction slope S_f in HEC-RAS are as follows:

Average Conveyance Equation

$$\overline{S}_f = \left(\frac{Q_1 + Q_2}{K_1 + K_2}\right)^2 \tag{2-13}$$

Average Friction Slope Equation

$$\overline{S}_f = \frac{S_{f1} + S_{f2}}{2} \tag{2-14}$$

Geometric Mean Friction Slope Equation

$$\overline{S}_f = \sqrt{S_{f1} \times S_{f2}} \tag{2-15}$$

Harmonic Mean Friction Slope Equation

$$\overline{S}_f = \frac{2\left(S_{f1} \times S_{f2}\right)}{S_{f1} + S_{f2}} \tag{2-16}$$

Equation 2-13 is the "default" equation used by the program; that is, it is used automatically unless a different equation is selected by the user. The program also contains an option to select equations, depending on flow regime and profile type (e.g., S1, M1, etc.). Further discussion of the alternative methods for evaluating friction loss is contained in Chapter 4, "Overview of Optional Capabilities."

Contraction and Expansion Loss Evaluation

Contraction and expansion losses in HEC-RAS are evaluated by the following equation:

$$h_{ce} = C\left|\frac{\alpha_1 V_1^2}{2g} - \frac{\alpha_2 V_2^2}{2g}\right| \tag{2-17}$$

Where: *C*   = the contraction or expansion coefficient

The program assumes that a contraction is occurring whenever the velocity head downstream is greater than the velocity head upstream. Likewise, when the velocity head upstream is greater than the velocity head downstream, the program assumes that a flow expansion is occurring. Typical *C* values can be found in Chapter 3, "Basic Data Requirements."

Computation Procedure

The unknown water surface elevation at a cross section is determined by an iterative solution of Equations 2-1 and 2-2. The computational procedure is as follows:

1. Assume a water surface elevation at the upstream cross section (or downstream cross section if a supercritical profile is being calculated).

2. Based on the assumed water surface elevation, determine the corresponding total conveyance and velocity head.

3. With values from step 2, compute $\bar{S}_f$ and solve Equation 2-2 for h_e.

4. With values from steps 2 and 3, solve Equation 2-1 for WS2.

5. Compare the computed value of WS2 with the value assumed in step 1; repeat steps 1 through 5 until the values agree to within .01 feet (.003 m), or the user-defined tolerance.

The criterion used to assume water surface elevations in the iterative procedure varies from trial to trial. The first trial water surface is based on projecting the previous cross section's water depth onto the current cross section. The second trial water surface elevation is set to the assumed water surface elevation plus 70% of the error from the first trial (computed W.S. - assumed W.S.). In other words, W.S. new = W.S. assumed + 0.70 * (W.S. computed - W.S. assumed). The third and subsequent trials are generally based on a "Secant" method of projecting the rate of change of the difference between computed and assumed elevations for the previous two trials. The equation for the secant method is as follows:

$$WS_I = WS_{I-2} - Err_{I-2} * Assum\_Diff / Err\_Diff \qquad (2-18)$$

Where: WS_I = the new assumed water surface

WS_{I-1} = the previous iteration's assumed water surface

WS_{I-2} = the assumed water surface from two trials previous

Err_{I-2} = the error from two trials previous (computed water surface minus assumed from the I-2 iteration)

$Assum\_Diff$ = the difference in assumed water surfaces from the previous two trials. Err Assum = WS_{I-2} - WS_{I-1}

Err_Diff = the difference in the previous error (Err_{I-2}) and the current error (Err_{I-1}). $Err\_Diff = Err_{I-2} - Err_{I-1}$

The change from one trial to the next is constrained to a maximum of 50 percent of the assumed depth from the previous trial. On occasion the secant method can fail if the value of Err_Diff becomes too small. If the Err_Diff is less than 1.0E-2, then the secant method is not

used. When this occurs, the program computes a new guess by taking the average of the assumed and computed water surfaces from the previous iteration.

The program is constrained by a maximum number of iterations (the default is 20) for balancing the water surface. While the program is iterating, it keeps track of the water surface that produces the minimum amount of error between the assumed and computed values. This water surface is called the minimum error water surface. If the maximum number of iterations is reached before a balanced water surface is achieved, the program will then calculate critical depth (if this has not already been done). The program then checks to see if the error associated with the minimum error water surface is within a predefined tolerance (the default is 0.3 ft or 0.1 m). If the minimum error water surface has an associated error less than the predefined tolerance, and this water surface is on the correct side of critical depth, then the program will use this water surface as the final answer and set a warning message that it has done so. If the minimum error water surface has an associated error that is greater than the predefined tolerance, or it is on the wrong side of critical depth, the program will use critical depth as the final answer for the cross section and set a warning message that it has done so. The rationale for using the minimum error water surface is that it is probably a better answer than critical depth, as long as the above criteria are met. Both the minimum error water surface and critical depth are only used in this situation to allow the program to continue the solution of the water surface profile. Neither of these two answers are considered to be valid solutions, and therefore warning messages are issued when either is used. In general, when the program cannot balance the energy equation at a cross section, it is usually caused by an inadequate number of cross sections (cross sections spaced too far apart) or bad cross section data. Occasionally, this can occur because the program is attempting to calculate a subcritical water surface when the flow regime is actually supercritical.

When a balanced water surface elevation has been obtained for a cross section, checks are made to ascertain that the elevation is on the right side of the critical water surface elevation (e.g., above the critical elevation if a subcritical profile has been requested by the user). If the balanced elevation is on the wrong side of the critical water surface elevation, critical depth is assumed for the cross section and a warning message to that effect is displayed by the program. The program user should be aware of critical depth assumptions and determine the reasons for their occurrence, because in many cases they result from reach lengths being too long or from misrepresentation of the effective flow areas of cross sections.

For a subcritical profile, a preliminary check for proper flow regime involves checking the Froude number. The program calculates the Froude number of the balanced water surface for both the main channel only and the entire cross section. If either of these two Froude numbers are greater than 0.94, then the program will check the flow regime by calculating a more accurate estimate of critical depth using the minimum specific energy method (this method is described in the next section). A Froude number of 0.94 is used instead of 1.0, because the calculation of Froude number in irregular channels is not accurate. Therefore, using a value of 0.94 is conservative, in that the program will calculate critical depth more often than it may need to.

For a supercritical profile, critical depth is automatically calculated for every cross section, which enables a direct comparison between balanced and critical elevations.

Critical Depth Determination

Critical depth for a cross section will be determined if any of the following conditions are satisfied:

(1)   The supercritical flow regime has been specified.

(2)   The calculation of critical depth has been requested by the user.

(3)   This is an external boundary cross section and critical depth must be determined to ensure the user entered boundary condition is in the correct flow regime.

(4)   The Froude number check for a subcritical profile indicates that critical depth needs to be determined to verify the flow regime associated with the balanced elevation.

(5)   The program could not balance the energy equation within the specified tolerance before reaching the maximum number of iterations.

The total energy head for a cross section is defined by:

$$H = WS + \frac{aV^2}{2g} \tag{2-19}$$

Where: H =   total energy head

WS =   water surface elevation

$\dfrac{aV^2}{2g}$ =   velocity head

The critical water surface elevation is the elevation for which the total energy head is a minimum (i.e., minimum specific energy for that cross section for the given flow). The critical elevation is determined with an iterative procedure whereby values of WS are assumed and corresponding values of H are determined with Equation 2-19 until a minimum value for H is reached.
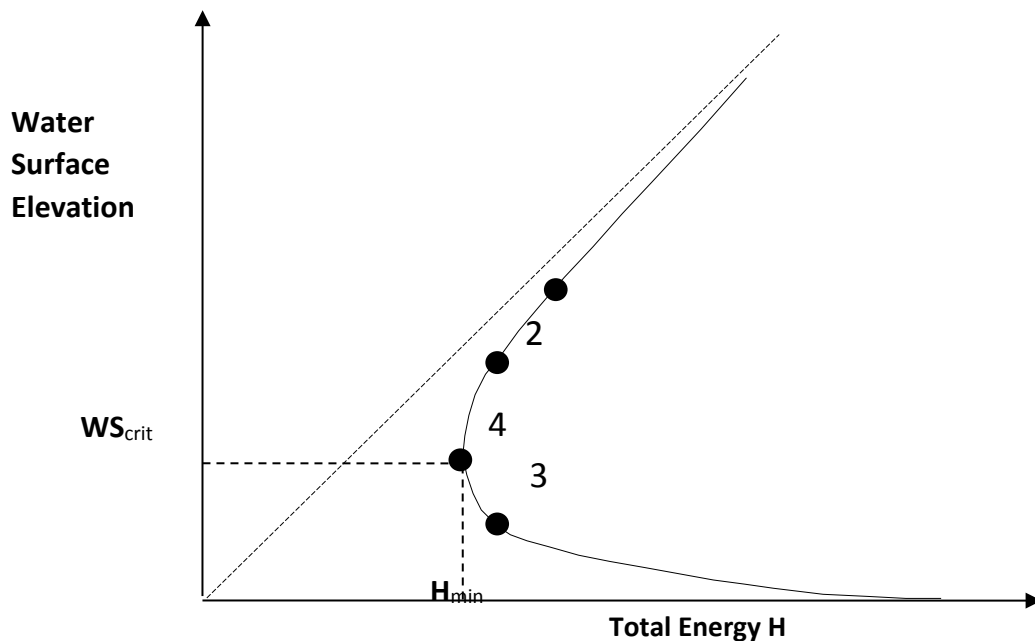
Figure 2-6 Energy vs. Water Surface Elevation Diagram

The HEC-RAS program has two methods for calculating critical depth: a "parabolic" method and a "secant" method. The parabolic method is computationally faster, but it is only able to locate a single minimum energy. For most cross sections there will only be one minimum on the total energy curve, therefore the parabolic method has been set as the default method (the default method can be changed from the user interface). If the parabolic method is tried and it does not converge, then the program will automatically try the secant method.

In certain situations it is possible to have more than one minimum on the total energy curve. Multiple minimums are often associated with cross sections that have breaks in the total energy curve. These breaks can occur due to very wide and flat overbanks, as well as cross sections with levees and ineffective flow areas. When the parabolic method is used on a cross section that has multiple minimums on the total energy curve, the method will converge on the first minimum that it locates. This approach can lead to incorrect estimates of critical depth. If the user thinks that the program has incorrectly located critical depth, then the secant method should be selected and the model should be re-simulated.

The "parabolic" method involves determining values of H for three values of WS that are spaced at equal ΔWS intervals. The WS corresponding to the minimum value for H, defined by a parabola passing through the three points on the H versus WS plane, is used as the basis for the next assumption of a value for WS. It is presumed that critical depth has been obtained when there is less than a 0.01 ft. (0.003 m) change in water depth from one iteration to the next and provided the energy head has not either decreased or increased by more than .01 feet (0.003 m).

The "secant" method first creates a table of water surface versus energy by slicing the cross section into 30 intervals. If the maximum height of the cross section (highest point to lowest point) is less than 1.5 times the maximum height of the main channel (from the highest main channel bank station to the invert), then the program slices the entire cross section into 30 equal intervals. If this is not the case, the program uses 25 equal intervals from the invert to the highest main channel bank station, and then 5 equal intervals from the main channel to the top of the cross section. The program then searches this table for the location of local minimums. When a point in the table is encountered such that the energy for the water surface immediately above and immediately below are greater than the energy for the given water surface, then the general location of a local minimum has been found. The program will then search for the local minimum by using the secant slope projection method. The program will iterate for the local minimum either thirty times or until the critical depth has been bounded by the critical error tolerance. After the local minimum has been determined more precisely, the program will continue searching the table to see if there are any other local minimums. The program can locate up to three local minimums in the energy curve. If more than one local minimum is found, the program sets critical depth equal to the one with the minimum energy. If this local minimum is due to a break in the energy curve caused by overtopping a levee or an ineffective flow area, then the program will select the next lowest minimum on the energy curve. If all of the local minimums are occurring at breaks in the energy curve (caused by levees and ineffective flow areas), then the program will set critical depth to the one with the lowest energy. If no local minimums are found, then the program will use the water surface elevation with the least energy. If the critical depth that is found is at the top of the cross section, then this is probably not a real critical depth. Therefore, the program will double the height of the cross section and try again. Doubling the height of the cross section is accomplished by extending vertical walls at the first and last points of the section. The height of the cross section can be doubled five times before the program will quit searching.

Applications of the Momentum Equation

Whenever the water surface passes through critical depth, the energy equation is not considered to be applicable. The energy equation is only applicable to gradually varied flow situations, and the transition from subcritical to supercritical or supercritical to subcritical is a rapidly varying flow situation. There are several instances when the transition from subcritical to supercritical and supercritical to subcritical flow can occur. These include significant changes in channel slope, bridge constrictions, drop structures and weirs, and stream junctions. In some of these instances empirical equations can be used (such as at drop structures and weirs), while at others it is necessary to apply the momentum equation in order to obtain an answer.

Within HEC-RAS, the momentum equation can be applied for the following specific problems: the occurrence of a hydraulic jump; low flow hydraulics at bridges; and stream junctions. In order to understand how the momentum equation is being used to solve each of the three problems, a derivation of the momentum equation is shown here. The application of the momentum equation to hydraulic jumps and stream junctions is discussed in detail in Chapter 4. Detailed discussions on applying the momentum equation to bridges can be found in Chapter 5.

The momentum equation is derived from Newton's second law of motion:

Force = Mass x Acceleration (change in momentum)

$$\sum F_x = m\,a \qquad\qquad\text{(2-20)}$$

Applying Newton's second law of motion to a body of water enclosed by two cross sections at locations 1 and 2 (Figure 2-7), the following expression for the change in momentum over a unit time can be written:

$$P_2 - P_1 + W_x - F_f = Q\,\rho\,\Delta V_x \qquad\qquad\text{(2-21)}$$

Where: P = Hydrologic pressure force at locations 1 and 2.

W_x = Force due to the weight of water in the X direction.

F_f = Force due to external friction losses from 2 and 1.

Q = Discharge

ρ = Density of water

ΔV_x = Change on velocity from 2 to 1, in the X direction.
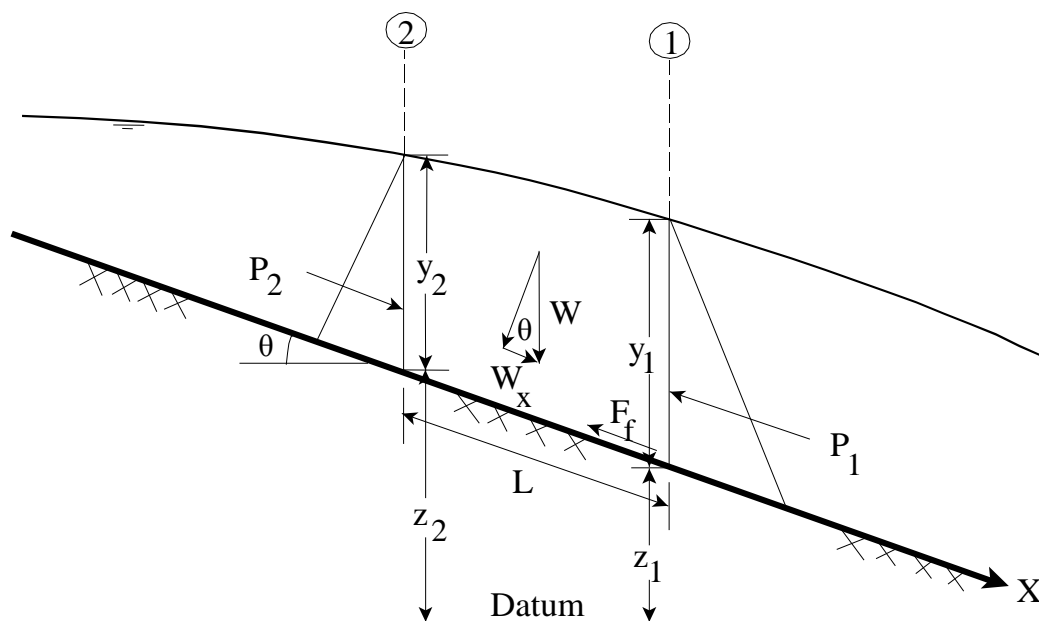
Figure 2-7 Application of the Momentum Principle

Hydrostatic Pressure Forces:

The force in the X direction due to hydrostatic pressure is:

$$P = \gamma\, A \overline{Y} \cos\theta \tag{2-22}$$

The assumption of a hydrostatic pressure distribution is only valid for slopes less than 1:10. The *cos* ϑ for a slope of 1:10 (approximately 6 degrees) is equal to 0.995. Because the slope of ordinary channels is far less than 1:10, the *cos* ϑ correction for depth can be set equal to 1.0 (Chow, 1959). Therefore, the equations for the hydrostatic pressure force at sections 1 and 2 are as follows:

$$P_1 = \gamma A_1 \overline{Y}_1 \tag{2-23}$$

$$P_2 = \gamma A_2 \overline{Y}_2 \tag{2-24}$$

Where: γ = Unit weight of water

A_i = Wetted area of the cross section at locations 1 and 2

$\overline{Y}_i$ = Depth measured from water surface to the centroid of the cross sectional area at locations 1 and 2.

Weight of Water Force:

Weight of water = (unit weight of water) x (volume of water)

$$W = \gamma \left(\frac{A_1 + A_2}{2} \right) L \tag{2-25}$$

$$W_x = W \times \sin \theta \tag{2-26}$$

$$\sin \theta = \frac{z_2 - z_1}{L} = S_0 \tag{2-27}$$

$$W_x = \gamma \left(\frac{A_1 + A_2}{2} \right) L S_0 \tag{2-28}$$

Where: L = Distance between sections 1 and 2 along the X axis

S_o = Slope of the channel, based on mean bed elevations

Z_i = Mean bed elevation at locations 1 and 2

Force of External Friction:

$$F_f = \tau \overline{P} L \tag{2-29}$$

Where: τ = Shear stress

$\overline{P}$ = Average wetted perimeter between sections 1 and 2

$$\tau = \gamma \overline{R} \overline{S}_f \tag{2-30}$$

Where: $\overline{R}$ = Average hydraulic radius (R = A/P)

$\overline{S}_f$ = Slope of the energy grade line (friction slope)

$$F_f = \gamma \frac{\overline{A}}{\overline{P}} \overline{S}_f \overline{P} L \tag{2-31}$$

$$F_f = \gamma \left(\frac{A_1 + A_2}{2} \right) \overline{S}_f \, L \tag{2-32}$$

Mass times Acceleration:

$$ma = Q \rho \Delta V_x \tag{2-33}$$

$$\rho = \frac{\gamma}{g} \quad and \quad \Delta V_x = \left(\beta_1 V_1 - \beta_2 V_2 \right)$$

$$ma = \frac{Q\gamma}{g} \left(\beta_1 V_1 - \beta_2 V_2 \right) \tag{2-34}$$

Where: β   = momentum coefficient that accounts for a varying velocity distribution in irregular channels

Substituting Back into Equation 2-21, and assuming Q can vary from 2 to 1:

$$\gamma A_2 \overline{Y}_2 - \gamma A_1 \overline{Y}_1 + \gamma \left(\frac{A_1 + A_2}{2} \right) L S_0 - \gamma \left(\frac{A_1 + A_2}{2} \right) L \overline{S}_f = \frac{Q_1 \gamma}{g} \beta_1 V_1 - \frac{Q_2 \gamma}{g} \beta_2 V_2 \tag{2-35}$$

$$\frac{Q_2 \beta_2 V_2}{g} + A_2 \overline{Y}_2 + \left(\frac{A_1 + A_2}{2} \right) L S_0 - \left(\frac{A_1 + A_2}{2} \right) L \overline{S}_f = \frac{Q_1 \beta_1 V_1}{g} + A_1 \overline{Y}_1 \tag{2-36}$$

$$\frac{Q_2^2 \beta_2}{g A_2} + A_2 \overline{Y}_2 + \left(\frac{A_1 + A_2}{2} \right) L S_0 - \left(\frac{A_1 + A_2}{2} \right) L \overline{S}_f = \frac{Q_1^2 \beta_1}{g A_1} + A_1 \overline{Y}_1 \tag{2-37}$$

Equation 2-37 is the functional form of the momentum equation that is used in HEC-RAS. All applications of the momentum equation within HEC-RAS are derived from equation 2-37.

Air Entrainment in High Velocity Streams

For channels that have high flow velocity, the water surface may be slightly higher than otherwise expected due to the entrainment of air. While air entrainment is not important for most rivers, it can be significant for highly supercritical flows (Froude numbers greater than 1.6). HEC-RAS now takes this into account with the following two equations (EM 1110-2-1601, plate B-50):

For Froude numbers less than or equal to 8.2,

$$D_a = 0.906 \, D \, (e)^{0.061F}$$

<div align="right">(2-38)</div>

For Froude numbers greater than 8.2,

$$D_a = 0.620 \, D \, (e)^{0.1051F}$$

<div align="right">(2-39)</div>

> Where: D_a = water depth with air entrainment
>
> D = water depth without air entrainment
>
> e = numerical constant, equal to 2.718282
>
> F = Froude number

A water surface with air entrainment is computed and displayed separately in the HEC-RAS tabular output. In order to display the water surface with air entrainment, the user must create their own profile table and include the variable "WS Air Entr." within that table. This variable is not automatically displayed in any of the standard HEC-RAS tables.

1D Steady Flow Program Limitations

The following assumptions are implicit in the analytical expressions used in the current version of the program:

> (1)   Flow is steady.
>
> (2)   Flow is gradually varied. (Except at hydraulic structures such as: bridges; culverts; and weirs. At these locations, where the flow can be rapidly varied, the momentum equation or other empirical equations are used.)
>
> (3)   Flow is one dimensional (i.e., velocity components in directions other than the direction of flow are not accounted for).
>
> (4)   River channels have "small" slopes, say less than 1:10.

Flow is assumed to be steady because time dependant terms are not included in the energy equation (Equation 2-1). Flow is assumed to be gradually varied because Equation 2-1 is based on the premise that a hydrostatic pressure distribution exists at each cross section. At locations where the flow is rapidly varied, the program switches to the momentum equation or other empirical equations. Flow is assumed to be one-dimensional because Equation 2-19 is based on the premise that the total energy head is the same for all points in a cross section.

The limit on slope as being less than 1:10 is based on the fact that the true derivation of the energy equation computes the vertical pressure head as:

$$H_p = d\ \cos\theta$$

Where: H_p = vertical pressure head

d = depth of the water measured perpendicular to the channel bottom.

θ = the channel bottom slope expressed in degrees.

For a channel bottom slope of 1:10 (5.71 degrees) or less, the cos(θ) is 0.995. So instead of using $d \cos(\theta)$, the vertical pressure head is approximated as d and is used as the vertical depth of water. As you can see for a slope of 1:10 or less, this is a very small error in estimating the vertical depth (.5 %).

If HEC-RAS is used on steeper slopes, you must be aware of the error in the depth computation introduced by the magnitude of the slope. Below is a table of slopes and the cos(θ):

Slope	Degrees	Cos (θ)
1:10	5.71	0.995
2:10	11.31	0.981
3:10	16.70	0.958
4:10	21.80	0.929
5:10	26.57	0.894

If you use HEC-RAS to perform the computations on slopes steeper than 1:10, you would need to divide the computed depth of water by the cos(θ) in order to get the correct depth of water. Also, be aware that very steep slopes can introduce air entrainment into the flow, as well as other possible factors that may not be taken into account within HEC-RAS.

1D Unsteady Flow Hydrodynamics

The physical laws which govern the flow of water in a stream are: (1) the principle of conservation of mass (continuity), and (2) the principle of conservation of momentum. These laws are expressed mathematically in the form of partial differential equations, which will hereafter be referred to as the continuity and momentum equations. The derivations of these equations are presented in this chapter based on a paper by James A. Liggett from the book *Unsteady Flow in Open Channels* (Mahmmod and Yevjevich, 1975).

Continuity Equation

Consider the elementary control volume shown in Figure 2-8. In this figure, distance x is measured along the channel, as shown. At the midpoint of the control volume the flow and total flow area are denoted Q(x,t) and A_T, respectively. The total flow area is the sum of active area A and off-channel storage area S.
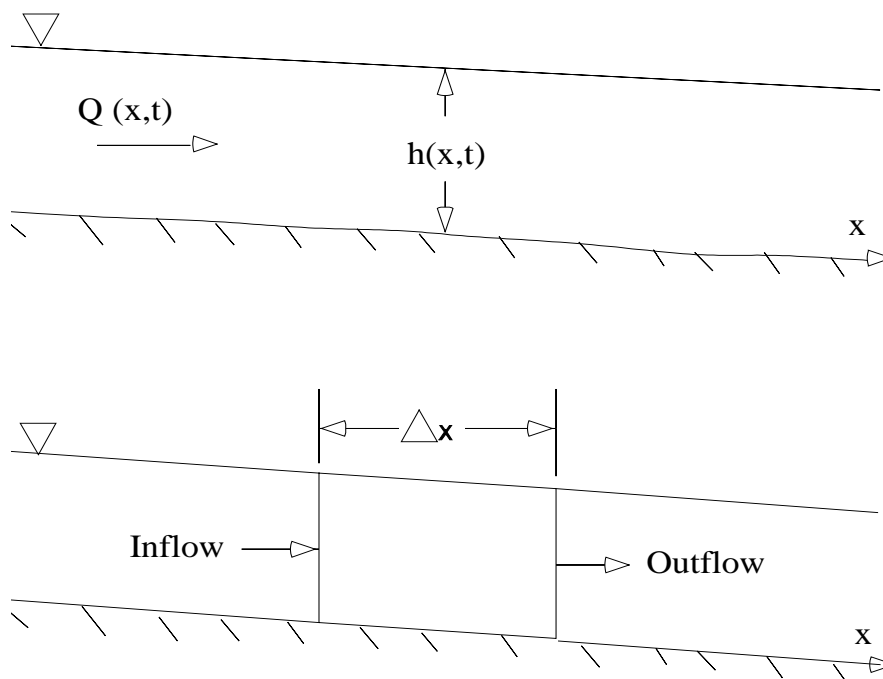
Figure 2-8 Elementary Control Volume for Derivation of Continuity and Momentum Equations.

Conservation of mass for a control volume states that the net rate of flow into the volume be equal to the rate of change of storage inside the volume. The rate of inflow to the control volume may be written as:

$$Q - \frac{\partial Q}{\partial x}\frac{\Delta x}{2} \qquad\qquad (2\text{-}40)$$

the rate of outflow as:

$$Q + \frac{\partial Q}{\partial x}\frac{\Delta x}{2}$$

(2-41)

and the rate of change in storage as:

$$\frac{\partial A_T}{\partial t}\Delta x$$

(2-42)

Assuming that Δx is small, the change in mass in the control volume is equal to:

$$\rho\frac{\partial A_T}{\partial t}\Delta x = \rho\left[\left(Q - \frac{\partial Q}{\partial x}\frac{\Delta x}{2}\right) - \left(Q + \frac{\partial Q}{\partial x}\frac{\Delta x}{2}\right) + Q_l\right]$$

(2-43)

Where Q_l is the lateral flow entering the control volume and ρ is the fluid density. Simplifying and dividing through by $p\Delta x$ yields the final form of the continuity equation:

$$\frac{\partial A_T}{\partial t} + \frac{\partial Q}{\partial x} - q_l = 0$$

(2-44)

in which q_l is the lateral inflow per unit length.

Momentum Equation

Conservation of momentum is expressed by Newton's second law as:

$$\sum F_x = \frac{d\vec{M}}{dt}$$

(2-45)

Conservation of momentum for a control volume states that *the net rate of momentum entering the volume (momentum flux) plus the sum of all external forces acting on the volume be equal to the rate of accumulation of momentum*. This is a vector equation applied in the x-direction. The momentum flux (MV) is the fluid mass times the velocity vector in the direction of flow. Three forces will be considered: (1) pressure, (2) gravity and (3) boundary drag, or friction force.

Pressure forces: Figure 2-9 illustrates the general case of an irregular cross section. The pressure distribution is assumed to be hydrostatic (pressure varies linearly with depth) and the total pressure force is the integral of the pressure-area product over the cross section. After Shames (1962), the pressure force at any point may be written as:

$$F_P = \int_0^h \rho\, g\, (h - y)\, T(y)\, dy \tag{2-46}$$

where h is the depth, y the distance above the channel invert, and $T(y)$ a width function which relates the cross section width to the distance above the channel invert.

If F_P is the pressure force in the x-direction at the midpoint of the control volume, the force at the upstream end of the control volume may be written as:

$$F_P - \frac{\partial F_P}{\partial x} \frac{\Delta x}{2} \tag{2-47}$$

and at the downstream end as:

$$F_P + \frac{\partial F_P}{\partial x} \frac{\Delta x}{2} \tag{2-48}$$
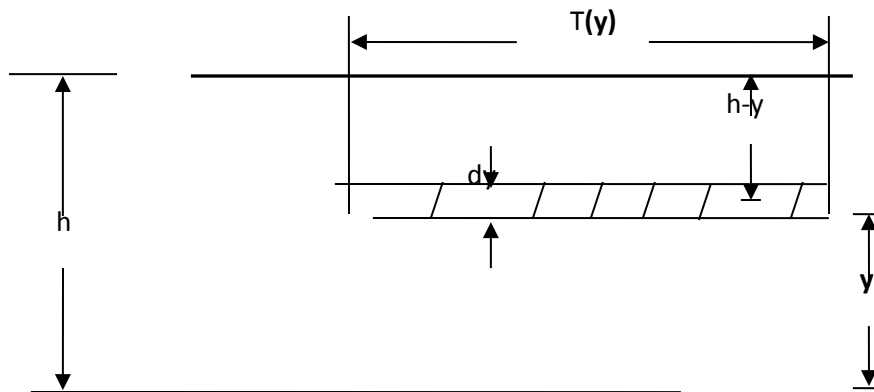
Figure 2-9 Illustration of Terms Associated with Definition of Pressure Force

The sum of the pressure forces for the control volume may therefore be written as:

$$F_{Pn} = \left| F_P - \frac{\partial F_P}{\partial x} \frac{\Delta x}{2} \right| - \left| F_P + \frac{\partial F_P}{\partial x} \frac{\Delta x}{2} \right| + F_B \tag{2-49}$$

Where F_{Pn} is the net pressure force for the control volume, and F_B is the force exerted by the banks in the x-direction on the fluid. This may be simplified to:

$$F_{Pn} = -\frac{\partial F_P}{\partial x} \Delta x + F_B \tag{2-50}$$

Differentiating equation 2-46 using Leibnitz's Rule and then substituting in equation 2-50 results in:

$$F_{Pn} = -\rho\, g\Delta x\left[\frac{\partial h}{\partial x}\int_0^h T(y)dy + \int_0^h (h-y)\frac{\partial T(y)}{\partial x}dy\right] + F_B \qquad (2\text{-}51)$$

The first integral in equation 2-51 is the cross-sectional area, A. The second integral (multiplied by $-\rho g\Delta x$) is the pressure force exerted by the fluid on the banks, which is exactly equal in magnitude, but opposite in direction to F_B. Hence the net pressure force may be written as:

$$F_{Pn} = -\rho\, g\, A\frac{\partial h}{\partial x}\Delta x \qquad (2\text{-}52)$$

Gravitational force: The force due to gravity on the fluid in the control volume in the x-direction is:

$$F_g = \rho\, gA\,\sin\theta\,\Delta x \qquad (2\text{-}53)$$

here θ is the angle that the channel invert makes with the horizontal. For natural rivers θ is small and $\sin\theta \approx \tan\theta = -\partial Z_0/\partial X$, where z_0 is the invert elevation. Therefore the gravitational force may be written as:

$$F_g = -\rho gA\frac{\partial z_0}{\partial x}\Delta x \qquad (2\text{-}54)$$

This force will be positive for negative bed slopes.

Boundary drag (friction force): Frictional forces between the channel and the fluid may be written as:

$$F_f = -\tau_o P\Delta x \qquad (2\text{-}55)$$

where τ_o is the average boundary shear stress (force/unit area) acting on the fluid boundaries, and P is the wetted perimeter. The negative sign indicates that, with flow in the positive x-direction, the force acts in the negative x-direction. From dimensional analysis, τ_o may be expressed in terms of a drag coefficient, C_D, as follows:

$$\tau_0 = \rho C_D V^2 \qquad (2\text{-}56)$$

The drag coefficient may be related to the Chezy coefficient, C, by the following:

$$C_D = \frac{g}{C^2} \tag{2-57}$$

Further, the Chezy equation may be written as:

$$V = C\sqrt{RS_f} \tag{2-58}$$

Substituting equations 2-56, 2-57, and 2-58 into 2-55, and simplifying, yields the following expression for the boundary drag force:

$$F_f = -\rho g A S_f \Delta x \tag{2-59}$$

where S_f is the friction slope, which is positive for flow in the positive x-direction. The friction slope must be related to flow and stage. Traditionally, the Manning and Chezy friction equations have been used. Since the Manning equation is predominantly used in the United States, it is also used in HEC-RAS. The Manning equation is written as:

$$S_f = \frac{Q|Q|n^2}{2.208 R^{4/3} A^2} \tag{2-60}$$

where R is the hydraulic radius and n is the Manning friction coefficient.

Momentum flux: With the three force terms defined, only the momentum flux remains. The flux entering the control volume may be written as:

$$\rho \left[QV - \frac{\partial QV}{\partial x} \frac{\Delta x}{2} \right] \tag{2-61}$$

and the flux leaving the volume may be written as:

$$\rho \left[QV + \frac{\partial QV}{\partial x} \frac{\Delta x}{2} \right] \tag{2-62}$$

Therefore the net rate of momentum (momentum flux) entering the control volume is:

$$- \rho \frac{\partial QV}{\partial x} \Delta x \tag{2-63}$$

Since the momentum of the fluid in the control volume is $\rho Q \Delta x$, the rate of accumulation of momentum may be written as:

$$\frac{\partial}{\partial t}\left(\rho Q \Delta x\right) = \rho \Delta x \frac{\partial Q}{\partial t} \tag{2-64}$$

Restating the principle of conservation of momentum:

The net rate of momentum (momentum flux) *entering the volume* (2-63) *plus the sum of all external forces acting on the volume* [(2-52) + (2-54) + (2-59)] *is equal to the rate of accumulation of momentum* (2-64). Hence:

$$\rho \Delta x \frac{\partial Q}{\partial t} = -\rho \frac{\partial QV}{\partial x}\Delta x - \rho g A \frac{\partial h}{\partial x}\Delta x - \rho g A \frac{\partial z_0}{\partial x}\Delta x - \rho g A S_f \Delta x \tag{2-65}$$

The elevation of the water surface, z, is equal to $z_0 + h$. Therefore:

$$\frac{\partial z}{\partial x} = \frac{\partial h}{\partial x} + \frac{\partial z_0}{\partial x} \tag{2-66}$$

where $\partial z / \partial x$ is the water surface slope. Substituting (2-66) into (2-65), dividing through by $\rho \Delta x$ and moving all terms to the left yields the final form of the momentum equation:

$$\frac{\partial Q}{\partial t} + \frac{\partial QV}{\partial x} + gA\left(\frac{\partial z}{\partial x} + S_f\right) = 0 \tag{2-67}$$

Application of the 1D Unsteady Flow Equations within HEC-RAS

Figure 2-10 illustrates the two-dimensional characteristics of the interaction between the channel and floodplain flows. When the river is rising water moves laterally away from the channel, inundating the floodplain and filling available storage areas. As the depth increases, the floodplain begins to convey water downstream generally along a shorter path than that of the main channel. When the river stage is falling, water moves toward the channel from the overbank supplementing the flow in the main channel.
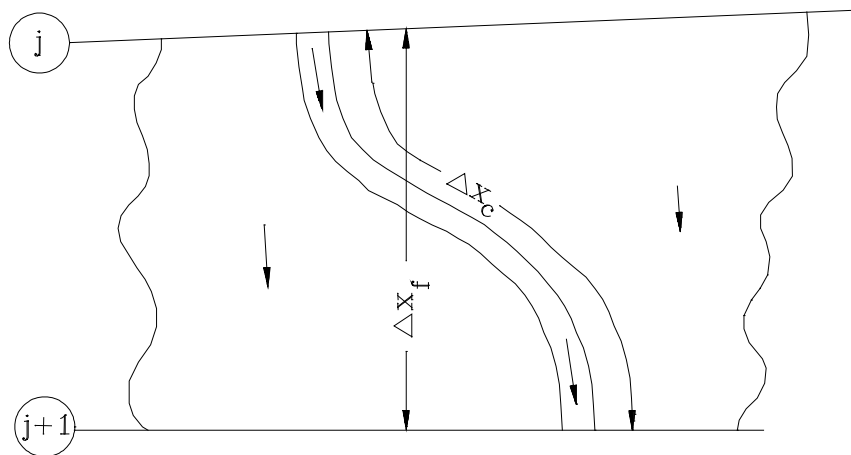
Figure 2-10 Channel and floodplain flows

Because the primary direction of flow is oriented along the channel, this two-dimensional flow field can often be accurately approximated by a one-dimensional representation. Off-channel ponding areas can be modeled with storage areas that exchange water with the channel. Flow in the overbank can be approximated as flow through a separate channel.

This channel/floodplain problem has been addressed in many different ways. A common approach is to ignore overbank conveyance entirely, assuming that the overbank is used only for storage. This assumption may be suitable for large streams such as the Mississippi River where the channel is confined by levees and the remaining floodplain is either heavily vegetated or an off-channel storage area. Fread (1976) and Smith (1978) approached this problem by dividing the system into two separate channels and writing continuity and momentum equations for each channel. To simplify the problem they assumed a horizontal water surface at each cross section normal to the direction of flow; such that the exchange of momentum between the channel and the floodplain was negligible and that the discharge was distributed according to conveyance, i.e.:

$$Q_c = \phi Q \qquad\qquad (2\text{-}68)$$

Where: Q_c =   flow in channel,

Q =   total flow,

ϕ = $K_c / (K_c + K_f),$

K_c =   conveyance in the channel, and,

K_f =   conveyance in the floodplain,

With these assumptions, the one-dimensional equations of motion can be combined into a single set:

$$\frac{\partial A}{\partial t} + \frac{\partial (\Phi Q)}{\partial x_c} + \frac{\partial [(1 - \Phi) Q]}{\partial x_f} = 0 \tag{2-69}$$

$$\frac{\partial Q}{\partial t} + \frac{\partial (\Phi^2 Q^2 / A_c)}{\partial x_c} + \frac{\partial ((1 - \Phi)^2 Q^2 / A_f)}{\partial x_f} + gA_c \left[\frac{\partial Z}{\partial x_c} + S_{fc} \right] + gA_f \left[\frac{\partial z}{\partial x_f} + S_{ff} \right] = 0 \tag{2-70}$$

in which the subscripts c and f refer to the channel and floodplain, respectively. These equations were approximated using implicit finite differences, and solved numerically using the Newton-Raphson iteration technique. The model was successful and produced the desired effects in test problems. Numerical oscillations, however, can occur when the flow at one node, bounding a finite difference cell, is within banks and the flow at the other node is not.

Expanding on the earlier work of Fread and Smith, Barkau (1982) manipulated the finite difference equations for the channel and floodplain and defined a new set of equations that were computationally more convenient. Using a velocity distribution factor, he combined the convective terms. Further, by defining an equivalent flow path, Barkau replaced the friction slope terms with an equivalent force.

The equations derived by Barkau are the basis for the unsteady flow solution within the HEC-RAS software. These equations were derived above. The numerical solution of these equations is described in the next sections.

Implicit Finite Difference Scheme

The most successful and accepted procedure for solving the one-dimensional unsteady flow equations is the four-point implicit scheme, also known as the box scheme (Figure 2-11). Under this scheme, space derivatives and function values are evaluated at an interior point, (n+θ) Δt. Thus values at (n+1) Δt enter into all terms in the equations. For a reach of river, a system of simultaneous equations results. The simultaneous solution is an important aspect of this scheme because it allows information from the entire reach to influence the solution at any one point. Consequently, the time step can be significantly larger than with explicit numerical

schemes. Von Neumann stability analyses performed by Fread (1974), and Liggett and Cunge (1975), show the implicit scheme to be unconditionally stable (theoretically) for $0.5 < \theta \le 1.0$, conditionally stable for $\theta = 0.5$, and unstable for $\theta < 0.5$. In a convergence analysis performed by the same authors, it was shown that numerical damping increased as the ratio $\lambda/\Delta x$ decreased, where λ is the length of a wave in the hydraulic system. For streamflow routing problems where the wavelengths are long with respect to spatial distances, convergence is not a serious problem.

In practice, other factors may also contribute to the non-stability of the solution scheme. These factors include dramatic changes in channel cross-sectional properties, abrupt changes in channel slope, characteristics of the flood wave itself, and complex hydraulic structures such as levees, bridges, culverts, weirs, and spillways.   In fact, these other factors often overwhelm any stability considerations associated with θ. **Because of these factors, any model application should be accompanied by a sensitivity study, where the accuracy and the stability of the solution are tested with various time and distance intervals.**
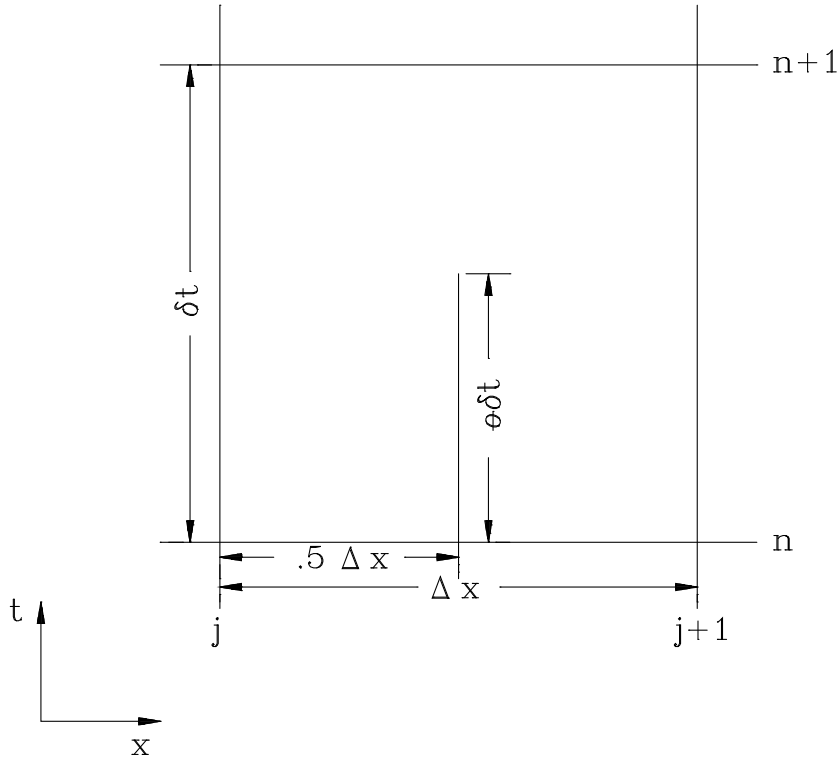
Figure 2-11 Typical finite difference cell.

The following notation is defined:

$$f_j = f_j^{\ n} \tag{2-71}$$

and:

$$\Delta f_j = f_j^{\ n+1} - f_j^{\ n} \tag{2-72}$$

then:

$$f_j^{\ n+1} = f_j + \Delta f_j \tag{2-73}$$

The general implicit finite difference forms are:

1. Time derivative

$$\frac{\partial f}{\partial t} \approx \frac{\Delta f}{\Delta t} = \frac{0.5\left(\Delta f_{j+1} + \Delta f_j\right)}{\Delta t} \tag{2-74}$$

2. Space derivative

$$\frac{\partial f}{\partial x} \approx \frac{\Delta f}{\Delta x} = \frac{\left(f_{j+1} - f_j\right) + \theta\left(\Delta f_{j+1} - \Delta f_j\right)}{\Delta x} \tag{2-75}$$

3.   Function value

$$f \approx \bar{f} = 0.5\left(f_j + f_{j+1}\right) + 0.5\theta\left(\Delta f_j + \Delta f_{j+1}\right)$$

(2-76)

Continuity Equation

The continuity equation describes conservation of mass for the one-dimensional system. From previous text, with the addition of a storage term, S, the continuity equation can be written as:

$$\frac{\partial A}{\partial t} + \frac{\partial S}{\partial t} + \frac{\partial Q}{\partial x} - q_1 = 0$$

(2-77)

Where: x =   distance along the channel,

t =   time,

Q =   flow,

A =   cross-sectional area,

S =   storage from non conveying portions of cross section,

q_l =   lateral inflow per unit distance.

The above equation can be written for the channel and the floodplain:

$$\frac{\partial Q_c}{\partial x_c} + \frac{\partial A_c}{\partial t} = q_f$$

(2-78)

and:

$$\frac{\partial Q_f}{\partial x_f} + \frac{\partial A_f}{\partial t} + \frac{\partial S}{\partial t} = q_c + q_l$$

(2-79)

where the subscripts c and f refer to the channel and floodplain, respectively, q_l is the lateral inflow per unit length of floodplain, and q_c and q_f are the exchanges of water between the channel and the floodplain.

NOTE: The HEC-RAS Unsteady flow engine combines the properties of the left and right overbank into a single flow compartment called the floodplain. Hydraulic properties for the

floodplain are computed by combining the left and right overbank elevation vs Area, conveyance, and storage into a single set of relationships for the floodplain portion of the cross section. The reach length used for the floodplain area is computed by taking the arithmetic average of the left and right overbank reach lengths (L$_L$ + L$_R$)/2 = L$_F$. The average floodplain reach length is used in both the continuity and momentum equations to compute their respective terms for a combined floodplain compartment (Left and right overbank combined together).

This is different than what is done in the Steady Flow computational engine (described above in the previous section), in which the left and right overbank are treated completely separately.

Equations 2-78 and 2-79 are now approximated using implicit finite differences by applying Equations 2-74 through 2-76:

$$\frac{\Delta Q_c}{\Delta x_c} + \frac{\Delta A_c}{\Delta t} = \overline{q}_f \tag{2-80}$$

$$\frac{\Delta Q_f}{\Delta x_f} + \frac{\Delta A_f}{\Delta t} + \frac{\Delta S}{\Delta t} = \overline{q}_c + \overline{q}_l \tag{2-81}$$

The exchange of mass is equal but not opposite in sign such that $\Delta x_c q_c = -q_f \Delta x_f$. Adding the above equations together and rearranging yields:

$$\Delta Q + \frac{\Delta A_c}{\Delta t} \Delta x_c + \frac{\Delta A_f}{\Delta t} \Delta x_f + \frac{\Delta S}{\Delta t} \Delta x_f - \overline{Q}_l = 0 \tag{2-82}$$

Where: $\overline{Q}_l$ = the average lateral inflow.

Δx_c = the length of the main channel between two cross sections.

Δx_f = the length of the floodplain between two cross sections (computed as the arithmetic average of the left and right overbank reach lengths)

Momentum Equation

The momentum equation states that the rate of change in momentum is equal to the external forces acting on the system. From Appendix A, for a single channel:

$$\frac{\partial Q}{\partial t} + \frac{\partial (VQ)}{\partial x} + gA\left(\frac{\partial z}{\partial x} + S_f\right) = 0 \tag{2-83}$$

Where: g = acceleration of gravity

S_f = friction slope,

$$V \quad = \quad \text{velocity.}$$

The above equation can be written for the channel and for the floodplain:

$$\frac{\partial Q_c}{\partial t} + \frac{\partial (V_c Q_c)}{\partial x_c} + gA_c \left(\frac{\partial z}{\partial x_c} + S_{fc} \right) = M_f \qquad (2\text{-}84)$$

$$\frac{\partial Q_f}{\partial t} + \frac{\partial (V_f Q_f)}{\partial x_f} + gA_f \left(\frac{\partial z}{\partial x_f} + S_{ff} \right) = M_c \qquad (2\text{-}85)$$

where M_c and M_f are the momentum fluxes per unit distance exchanged between the channel and floodplain, respectively. Note that in Equations 2-84 and 2-85 the water surface elevation is not subscripted. An assumption in these equations is that the water surface is horizontal at any cross section perpendicular to the flow. Therefore, the water surface elevation is the same for the channel and the floodplain at a given cross section.

Using Equations 2-74 through 2-76, the above equations are approximated using finite differences:

$$\frac{\Delta Q_c}{\Delta t} + \frac{\Delta (V_c Q_c)}{\Delta x_c} + g\, \overline{A}_c \left(\frac{\Delta z}{\Delta x_c} + \overline{S}_{fc} \right) = M_f \qquad (2\text{-}86)$$

$$\frac{\Delta Q_f}{\Delta t} + \frac{\Delta (V_f Q_f)}{\Delta x_f} + g\, \overline{A}_f \left(\frac{\Delta z}{\Delta x_f} + \overline{S}_{ff} \right) = M_c \qquad (2\text{-}87)$$

Note that $\Delta x_c M_c = -\Delta x_f M_f$ (due to the horizontal water surface assumption).

Adding and rearranging the above equations yields:

$$\frac{\Delta(Q_c \Delta x_c + Q_f \Delta x_f)}{\Delta t} + \Delta(V_c Q_c) + \Delta(V_f Q_f) + g(A_c + A_f)\Delta z + g\overline{A}_c \overline{S}_{fc} \Delta x_c + g\overline{A}_f \overline{S}_{ff} \Delta x_f = 0 \quad (2\text{-}88)$$

The final two terms define the friction force from the banks acting on the fluid. An equivalent force can be defined as:

$$g\overline{A}\,\overline{S}_f \Delta x_e = g\overline{A}_c \overline{S}_{fc} \Delta x_c + g\overline{A}_f \overline{S}_{ff} \Delta x_f \qquad (2\text{-}89)$$

where: Δx_e =   equivalent flow path,

          S_f =   friction slope for the entire cross section,

$$A \quad = \quad \overline{A}_c + \overline{A}_f .$$

Now, the convective terms can be rewritten by defining a velocity distribution factor:

$$\beta = \frac{(V_c^{\,2} A_c + V_f^{\,2} A_f)}{V^2 A} = \frac{(V_c Q_c + V_f Q_f)}{QV} 0 \tag{2-90}$$

then:

$$\Delta(\beta VQ) = \Delta(V_c Q_c) + \Delta(V_f Q_f) \tag{2-91}$$

The final form of the momentum equation is:

$$\frac{\Delta(Q_c \Delta x_c + Q_f \Delta x_f)}{\Delta t} + \Delta(\beta VQ) + g\overline{A}\Delta z + g\overline{A}\,\overline{S}_f \Delta x_e = 0 \tag{2-92}$$

A more familiar form is obtained by dividing through by Δx_e :

$$\frac{\Delta(Q_c \Delta x_c + Q_f \Delta x_f)}{\Delta t \Delta x_e} + \frac{\Delta(\beta VQ)}{\Delta x_e} + g\overline{A}(\frac{\Delta z}{\Delta x_e} + \overline{S}_f) = 0 \tag{2-93}$$

Added Force Term

The friction and pressure forces from the banks do not always describe all the forces that act on the water. Structures such as bridge piers, navigation dams, and cofferdams constrict the flow and exert additional forces, which oppose the flow. In localized areas these forces can predominate and produce a significant increase in water surface elevation (called a "swell head") upstream of the structure.

For a differential distance, dx, the additional forces in the contraction produce a swell head of dh_l. This swell head is only related to the additional forces. The rate of energy loss can be expressed as a local slope:

$$S_h = \frac{dh_l}{dx} \tag{2-94}$$

The friction slope in Equation 2-93 can be augmented by this term:

$$\frac{\partial Q}{\partial t} + \frac{\partial (VQ)}{\partial x} + gA\left(\frac{\partial z}{\partial x} + S_f + S_h\right) = 0 \tag{2-95}$$

For steady flow, there are a number of relationships for computation of the swell head upstream of a contraction. For navigation dams, the formulas of Kindsvater and Carter, d'Aubuisson (Chow, 1959), and Nagler were reviewed by Denzel (1961). For bridges, the

formulas of Yarnell (WES, 1973) and the Federal Highway Administration (FHWA, 1978) can be used. These formulas were all determined by experimentation and can be expressed in the more general form:

$$h_l = C \frac{V^2}{2g}$$

(2-96)

where h_l is the head loss and C is a coefficient. The coefficient C is a function of velocity, depth, and the geometric properties of the opening, but for simplicity, it is assumed to be a constant. The location where the velocity head is evaluated varies from method to method. Generally, the velocity head is evaluated at the tailwater for tranquil flow and at the headwater for supercritical flow in the contraction.

If h_l occurs over a distance Δx_e, then $h_l = \overline{S}_h \Delta x_e$ and $\overline{S}_h = h_l / \Delta x_e$ where $\overline{S}_h$ is the average slope over the interval Δx_e. Within HEC-RAS, the steady flow bridge and culvert routines are used to compute a family of rating curves for the structure. During the simulation, for a given flow and tailwater, a resulting headwater elevation is interpolated from the curves. The difference between the headwater and tailwater is set to h_l and then $\overline{S}_h$ is computed. The result is inserted in the finite difference form of the momentum equation (Equation 2-93), yielding:

$$\frac{\Delta\left(Q_c \Delta x_c + Q_f \Delta x_f\right)}{\Delta t \Delta x_e} + \frac{\Delta(\beta VQ)}{\Delta x_e} + g\overline{A}\left(\frac{\Delta z}{\Delta x_e} + \overline{S}_f + \overline{S}_h\right) = 0$$

(2-97)

Lateral Influx of Momentum

At stream junctions, the momentum as well as the mass of the flow from a tributary enters the receiving stream. If this added momentum is not included in the momentum equation, the entering flow has no momentum and must be accelerated by the flow in the river. The lack of entering momentum causes the convective acceleration term, $\partial(VQ)/\partial x$, to become large. To balance the spatial change in momentum, the water surface slope must be large enough to provide the force to accelerate the fluid. Thus, the water surface has a drop across the reach where the flow enters creating backwater upstream of the junction on the main stem. When the tributary flow is large in relation to that of the receiving stream, the momentum exchange may be significant. The confluence of the Mississippi and Missouri Rivers is such a juncture. During a large flood, the computed decrease in water surface elevation over the Mississippi reach is over 0.5 feet if the influx of momentum is not properly considered.

The entering momentum is given by:

$$M_l = \xi \frac{Q_l V_l}{\Delta x}$$ (2-98)

Where: Q_l =   lateral inflow,

V_l =   average velocity of lateral inflow,

ξ =   fraction of the momentum entering the receiving stream.

The entering momentum is added to the right side of Equation 2-97, hence:

$$\frac{\Delta\left(Q_c \Delta x_c + Q_f \Delta x_f\right)}{\Delta t \Delta_{xe}} + \frac{\Delta(\beta V Q)}{\Delta x_e} + g\overline{A}\left(\frac{\Delta z}{\Delta x_e} + \overline{S}_f + \overline{S}_h\right) = \xi \frac{Q_l V_l}{\Delta x_e}$$ (2-99)

Equation 2-99 is only used at stream junctions in a dendritic model.

Finite Difference Form of the Unsteady Flow Equations

Equations 2-77 and 2-83 are nonlinear. If the implicit finite difference scheme is directly applied, a system of nonlinear algebraic equations results. Amain and Fang (1970), Fread (1974, 1976) and others have solved the nonlinear equations using the Newton-Raphson iteration technique. Apart from being relatively slow, that iterative scheme can experience troublesome convergence problems at discontinuities in the river geometry. To avoid the nonlinear solution, Preissmann (as reported by Liggett and Cunge, 1975) and Chen (1973) developed a technique for linearizing the equations. The following section describes how the finite difference equations are linearized in HEC-RAS.

Linearized, Implicit, Finite Difference Equations

The following assumptions are applied:

1.   If $f \bullet f >> \Delta f \bullet \Delta f$, then $\Delta f \bullet \Delta f = 0$ (Preissmann as reported by Liggett and Cunge, 1975).

2.   If $g = g(Q, z)$, then Δg can be approximated by the first term of the Taylor Series, i.e.:

$$\Delta g_j = \left(\frac{\partial g}{\partial Q}\right)_j \Delta Q_j + \left(\frac{\partial g}{\partial z}\right)_j \Delta z_j$$ (2-100)

3. If the time step, Δt, is small, then certain variables can be treated explicitly; hence $hj^{n+1} \approx hj^{n}$ and $\Delta hj \approx 0$.

Assumption 2 is applied to the friction slope, S_f and the area, A. Assumption 3 is applied to the velocity, V, in the convective term; the velocity distribution factor, β; the equivalent flow path, x; and the flow distribution factor, ϕ.

The finite difference approximations are listed term by term for the continuity equation in Table 2-1 and for the momentum equation in Table 2-2. If the unknown values are grouped on the left-hand side, the following linear equations result:

$$CQ1_{j}\Delta Q_{j} + CZ1_{j}\Delta z_{j} + CQ2_{j}\Delta Q_{j+1} + CZ2_{j}\Delta z_{j+1} = CB_{j} \qquad \text{(2-101)}$$

$$MQ1_{j}\Delta Q_{j} + MZ1_{j}\Delta z_{j} + MQ2_{j}\Delta Q_{j+1} + MZ2_{j}\Delta z_{j+1} = MB_{j} \text{ (2-102)}$$

Table 2-1

Finite Difference Approximation of the Terms in the Continuity Equation

Term	Finite Difference Approximation
ΔQ	$(Q_{j+1} - Q_{j}) + \theta(\Delta Q_{j+1} - \Delta Q_{j})$
$\dfrac{\partial A_c}{\partial t}\Delta x_c$	$0.5\Delta x_{cj}\dfrac{\left(\dfrac{dA_c}{dz}\right)_{j}\Delta z_{j} + \left(\dfrac{dA_c}{dz}\right)_{j+1}\Delta z_{j+1}}{\Delta t}$
$\dfrac{\partial A_f}{\partial t}\Delta x_f$	$0.5\Delta x_{fj}\dfrac{\left(\dfrac{dA_f}{dz}\right)_{j}\Delta z_{j} + \left(\dfrac{dA_f}{dz}\right)_{j+1}\Delta z_{j+1}}{\Delta t}$
$\dfrac{\partial S}{\partial t}\Delta x_f$	$0.5\Delta x_{fj}\dfrac{\left(\dfrac{dS}{dz}\right)_{j}\Delta z_{j} + \left(\dfrac{dS}{dz}\right)_{j+1}\Delta z_{j+1}}{\Delta t}$

Table 2-2
Finite Difference Approximation of the Terms in the Momentum Equation

Term	Finite Difference Approximation
$\dfrac{\partial(Q_c \Delta x_c + Q_f \Delta x_f)}{\partial t \Delta x_e}$	$\dfrac{0.5}{\Delta x_e \partial t}(\partial Q_{cj} \Delta x_{cj} + \partial Q_{fj} \Delta x_{fj} + \partial Q_{cj+1} \Delta x_{cj} + \partial Q_{fj+1} \Delta x_{fj})$
$\dfrac{\Delta \beta VQ}{\Delta x_{ej}}$	$\dfrac{1}{\Delta x_{ej}}\left[(\beta VQ)_{j+1} - (\beta VQ)_j\right] + \dfrac{\theta}{\Delta x_{ej}}\left[(\beta VQ)_{j+1} - (\beta VQ)_j\right]$
$g\overline{A}\dfrac{\Delta z}{\Delta x_e}$	$g\overline{A}\left[\dfrac{z_{j+1} - z_j}{\Delta x_{ej}} + \dfrac{\theta}{\Delta x_{ej}}(\Delta z_{j+1} - \Delta z_j)\right] + \theta g \Delta \overline{A}\dfrac{(z_{j+1} - z_j)}{\Delta x_{ej}}$
$g\overline{A}(\overline{S}_f + \overline{S}_h)$	$g\overline{A}(\overline{S}_f + \overline{S}_h) + 0.5\theta g\overline{A}\left[(\Delta S_{fj+1} + \Delta S_{fj}) + (\Delta S_{hj+1} + \Delta S_{hj})\right] + 0.5\theta g(\overline{S}_f + \overline{S}_h)(\Delta A_j + \Delta A_{j+1})$
$\overline{A}$	$0.5(A_{j+1} + A_j)$
$\overline{S}_f$	$0.5(S_{fj+1} + S_{fj})$
∂A_j	$\left(\dfrac{dA}{dZ}\right)_j \Delta z_j$
∂S_{fj}	$\left(\dfrac{-2S_f}{K}\dfrac{dK}{dz}\right)_j \Delta z_j + \left(\dfrac{2S_f}{Q}\right)_j \Delta Q_j$
$\partial \overline{A}$	$0.5(\Delta A_j + \Delta A_{j+1})$

The values of the coefficients are defined in Tables 2-3 and 2-4.

Table 2-3

Coefficients for the Continuity Equation

Coefficient	Value
$CQ1_j$	$\dfrac{-\theta}{\Delta x_{ej}}$
$CZ1_j$	$\dfrac{0.5}{\Delta t \Delta x_{ej}}\left[\left(\dfrac{dA_c}{dz}\right)_j \Delta x_{cj} + \left(\dfrac{dA_f}{dz} + \dfrac{dS}{dz}\right)_j \Delta x_{fj}\right]$
$CQ2_j$	$\dfrac{\theta}{\Delta x_{ej}}$
$CZ2_j$	$\dfrac{0.5}{\Delta t \Delta x_{ej}}\left[\left(\dfrac{dA_c}{dz}\right)_{j+1} \Delta x_{cj} + \left(\dfrac{dA_f}{dz} + \dfrac{dS}{dz}\right)_{j+1} \Delta x_{fj}\right]$
CB_j	$-\dfrac{Q_{j+1} - Q_j}{\Delta x_{ej}} + \dfrac{Q_j}{\Delta x_{ej}}$

Table 2-4

Coefficients of the Momentum Equation

Term	Value
$MQ1_j$	$0.5 \dfrac{\Delta x_{cj} \phi_j + \Delta x_{fj}(1-\phi_j)}{\Delta x_{ej} \Delta t} - \dfrac{\beta_j V_j \theta}{\Delta x_{ej}} + \theta g \overline{A} \dfrac{(S_{fj} + S_{hj})}{Q_j}$
$MZ1_j$	$\dfrac{-gA\theta}{\Delta x_{ej}} + 0.5g(z_{j+1} - z_j)\left(\dfrac{dA}{dz}\right)_j \left(\dfrac{\theta}{\Delta x_{ej}}\right) - g\theta\overline{A}\left[\left(\dfrac{dK}{dz}\right)_j\left(\dfrac{S_{fj}}{K_j}\right) + \left(\dfrac{dA}{dz}\right)_j\left(\dfrac{S_{hj}}{A_j}\right)\right] + 0.5\theta g\left(\dfrac{dA}{dz}\right)_j (\overline{S}_f + \overline{S}_h)$
$MQ2_j$	$0.5\left[\Delta x_{cj}\phi_{j+1} + \Delta x_{fj}(1-\phi_{j+1})\right]\left(\dfrac{1}{\Delta x_{ej}\Delta t}\right) + \beta_{j+1} V_{j+1}\left(\dfrac{\theta}{\Delta x_{ej}}\right) + \dfrac{\theta gA}{Q_{j+1}}(S_{fj+1} + S_{hj+1})$
$MZ2_j$	$\dfrac{g\overline{A}\theta}{\Delta x_{ej}} + 0.5g(z_{j+1} - z_j)\left(\dfrac{dA}{dz}\right)_{j+1}\left(\dfrac{\theta}{\Delta x_{ej}}\right) - \theta g\overline{A}\left[\left(\dfrac{dK}{dz}\right)_{j+1}\left(\dfrac{S_{fj+1}}{K_{j+1}}\right) + \left(\dfrac{dA}{dz}\right)_{j+1}\left(\dfrac{S_{hj+1}}{A_{j+1}}\right)\right] + 0.5\theta g\left(\dfrac{dA}{dz}\right)_{j+1}(\overline{S}_f + \overline{S}_h)$
MB_j	$-\left[\left(\beta_{j+1} V_{j+1} Q_{j+1} - \beta_j V_j Q_j\right)\left(\dfrac{1}{\Delta x_{ej}}\right) + \left(\dfrac{g\overline{A}}{\Delta x_{ej}}\right)(z_{j+1} - z_j) + g\overline{A}(\overline{S}_f + \overline{S}_h)\right]$

Flow Distribution Factor

The distribution of flow between the channel and floodplain must be determined. The portion of the flow in the channel is given by:

$$\phi_j = \frac{Q_{cj}}{Q_{cj} + Q_{fj}}$$

(2-103)

Fread (1976) assumed that the friction slope is the same for the channel and floodplain, thus the distribution is given by the ratio of conveyance:

$$\phi_j = \frac{K_{cj}}{K_{cj} + K_{fj}}$$

(2-104)

Equation 2-104 is used in the HEC-RAS model.

Equivalent Flow Path

The equivalent flow path is given by:

$$\Delta x_e = \frac{\overline{A}_c \overline{S}_{fc} \Delta x_c + \overline{A}_f \overline{S}_{ff} \Delta x_f}{\overline{A} \overline{S}_f}$$

(2-105)

If we assume:

$$\overline{\phi} = \frac{\overline{K}_c}{\overline{K}_c + \overline{K}_f}$$

(2-106)

where $\overline{\phi}$ is the average flow distribution for the reach, then:

$$\Delta x_e = \frac{\overline{A}_c \Delta x_c + \overline{A}_f \Delta x_f}{\overline{A}}$$

(2-107)

Since Δx_e is defined explicitly:

$$\Delta x_{ej} = \frac{(A_{cj} + A_{cj+1})\Delta x_{cj} + (A_{fj} + A_{fj+1})\Delta x_{fj}}{A_j + A_{j+1}}$$

(2-108)

Boundary Conditions

For a reach of river there are N computational nodes which bound N-1 finite difference cells. From these cells 2N-2 finite difference equations can be developed. Because there are 2N unknowns (ΔQ and Δz for each node), two additional equations are needed. These equations are provided by the boundary conditions for each reach, which for subcritical flow, are required at the upstream and downstream ends.

Interior Boundary Conditions (for Reach Connections)

A network is composed of a set of M individual reaches. Interior boundary equations are required to specify connections between reaches. Depending on the type of reach junction, one of two equations is used:

Continuity of flow:

$$\sum_{i=1}^{l} S_{gi} Q_i = 0 \qquad (2\text{-}109)$$

Where: l = the number of reaches connected at a junction,

S_{gi} = -1 if i is a connection to an upstream reach, +1 if i is a connection to a downstream reach,

Q_i = discharge in reach i.

The finite differences form of Equation 2-109 is:

$$\sum_{i=1}^{l-1} MU_{mi} \Delta Q_i + MUQ_m \Delta Q_K = MUB_m \qquad (2\text{-}110)$$

Where: MU_{mi} = θ S_{gi},

MUQ_m = θ S_{gK},

MUB_m = $- \displaystyle\sum_{i=1}^{l} S_{gi} Q_i$

Continuity of stage:

$$z_k = z_c \qquad\qquad (2\text{-}111)$$

where z_k, the stage at the boundary of reach k, is set equal to z_c, a stage common to all stage boundary conditions at the junction of interest. The finite difference form of Equation 2-111 is:

$$MUZ_m \Delta z_k - MU_m \Delta z_c = MUB_m \qquad\qquad (2\text{-}112)$$

where: MUZ_m = 0,

   MU_m = 0,

   MUB_m = $z_c - z_k$.

With reference to Figure 2-12, HEC-RAS uses the following strategy to apply the reach connection boundary condition equations:

- Apply flow continuity to reaches upstream of flow splits and downstream of flow combinations (reach 1 in Figure 2-12). Only one flow boundary equation is used per junction.

- Apply stage continuity for all other reaches (reaches 2 and 3 in Figure 2-12). Z_c is computed as the stage corresponding to the flow in reach 1. Therefore, stage in reaches 2 and 3 will be set equal to Z_c.

Upstream Boundary Conditions

Upstream boundary conditions are required at the upstream end of all reaches that are not connected to other reaches or storage areas. An upstream boundary condition is applied as a flow hydrograph of discharge versus time. The equation of a flow hydrograph for reach m is:

$$\Delta Q_k^{n+1} = Q_k^n - Q_k \qquad\qquad (2\text{-}113)$$

where k is the upstream node of reach m. The finite difference form of Equation 2-113 is:

$$MUQ_m \Delta dQ_K = MUB_m \qquad\qquad (2\text{-}114)$$

where: MUQ_m = 1,

   MUB_m = $Q_1^{n+1} - Q_1^n$.
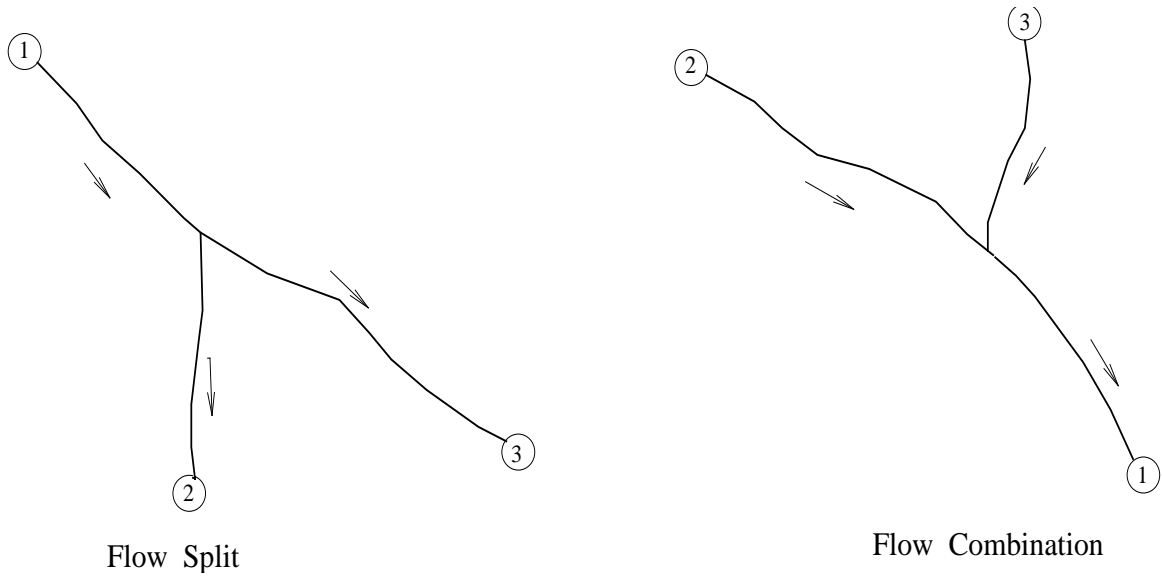
Figure 2-12 Typical flow split and combination.

Downstream Boundary Conditions

Downstream boundary conditions are required at the downstream end of all reaches which are not connected to other reaches or storage areas. Four types of downstream boundary conditions can be specified:

• a stage hydrograph,

• a flow hydrograph,

• a single-valued rating curve,

• Normal Depth from Manning's equation.

Stage Hydrograph. A stage hydrograph of water surface elevation versus time may be used as the downstream boundary condition if the stream flows into a backwater environment such as an estuary or bay where the water surface elevation is governed by tidal fluctuations, or where it flows into a lake or reservoir of known stage(s). At time step $(n+1)\Delta t$, the boundary condition from the stage hydrograph is given by:

$$\Delta Z_N = Z_N^{n+1} - Z_N^n \qquad (2\text{-}115)$$

The finite difference form of Equation 2-115 is:

$$CDZ_m \, \Delta Z_N = CDB_m$$

(2-116)

where: CDZ_m = 1,

CDB_m = $z_N^{n+1} - z_N^n$.

Flow Hydrograph. A flow hydrograph may be used as the downstream boundary condition if recorded gage data is available and the model is being calibrated to a specific flood event. At time step $(n+1)\Delta t$, the boundary condition from the flow hydrograph is given by the finite difference equation:

$$CDQ_m \Delta Q_N = CDB_m$$

(2-117)

where: CDQ_m = 1,

CDB_m = $Q_N^{n+1} - Q_N^n$.

Single Valued Rating Curve. The single valued rating curve is a monotonic function of stage and flow. An example of this type of curve is the steady, uniform flow rating curve. The single valued rating curve can be used to accurately describe the stage-flow relationship of free outfalls such as waterfalls, or hydraulic control structures such as spillways, weirs or lock and dam operations. When applying this type of boundary condition to a natural stream, caution should be used. If the stream location would normally have a looped rating curve, then placing a single valued rating curve as the boundary condition can introduce errors in the solution. Too reduce errors in stage, move the boundary condition downstream from your study area, such that it no longer affects the stages in the study area. Further advice is given in (USACE, 1993).

At time $(n+1)\Delta t$ the boundary condition is given by:

$$Q_N + \theta \Delta Q_N = D_{k-1} + \frac{D_k - D_{k-1}}{S_k - S_{k-1}} \left(z_N + \Delta z_N - S_{k-1} \right)$$

(2-118)

Where: D_k = K^{th} discharge ordinate,

S_k = K^{th} stage ordinate.

After collecting unknown terms on the left side of the equation, the finite difference form of Equation 2-118 is:

$$CDQ_m \Delta Q_N + CDZ_m \Delta z_N = CDB_m$$

(2-119)

where: $CDQ_m = \theta,$

$$CDZ_m = \frac{D_k - D_{k-1}}{S_k - S_{k-1}},$$

$$CDB_m = Q_N + D_{k-1} + \frac{D_k - D_{k-1}}{S_k - S_{k-1}}(z_N - S_{k-1}).$$

Normal Depth. Use of Manning's equation with a user entered friction slope produces a stage considered to be normal depth if uniform flow conditions existed. Because uniform flow conditions do not normally exist in natural streams, this boundary condition should be used far enough downstream from your study area that it does not affect the results in the study area. Manning's equation may be written as:

$$Q = K\left(S_f\right)^{0.5} \tag{2-120}$$

where: K represents the conveyance and S_f is the friction slope.

Skyline Solution of a Sparse System of Linear Equations

The finite difference equations along with external and internal boundary conditions and storage area equations result in a system of linear equations which must be solved for each time step:

$$Ax = b \tag{2-121}$$

in which: A = coefficient matrix,

x = column vector of unknowns,

b = column vector of constants.

For a single channel without a storage area, the coefficient matrix has a band width of five and can be solved by one of many banded matrix solvers.

For network problems, sparse terms destroy the banded structure. The sparse terms enter and leave at the boundary equations and at the storage areas. Figure 2-13 shows a simple system with four reaches and a storage area off of reach 2. The corresponding coefficient matrix is shown in Figure 2-14. The elements are banded for the reaches but sparse elements appear at the reach boundaries and at the storage area. This small system is a trivial problem to solve, but systems with hundreds of cross sections and tens of reaches pose a major numerical problem because of the sparse terms. Even the largest computers cannot store the coefficient matrix for a moderately sized problem, furthermore, the computer time required to solve such a large

matrix using Gaussian elimination would be very large. Because most of the elements are zero, a majority of computer time would be wasted.
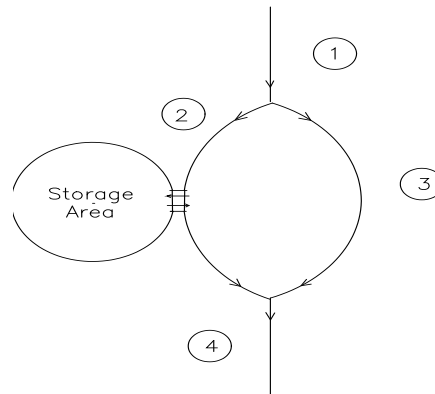
Figure 2-13 Simple network with four reaches and a storage area.
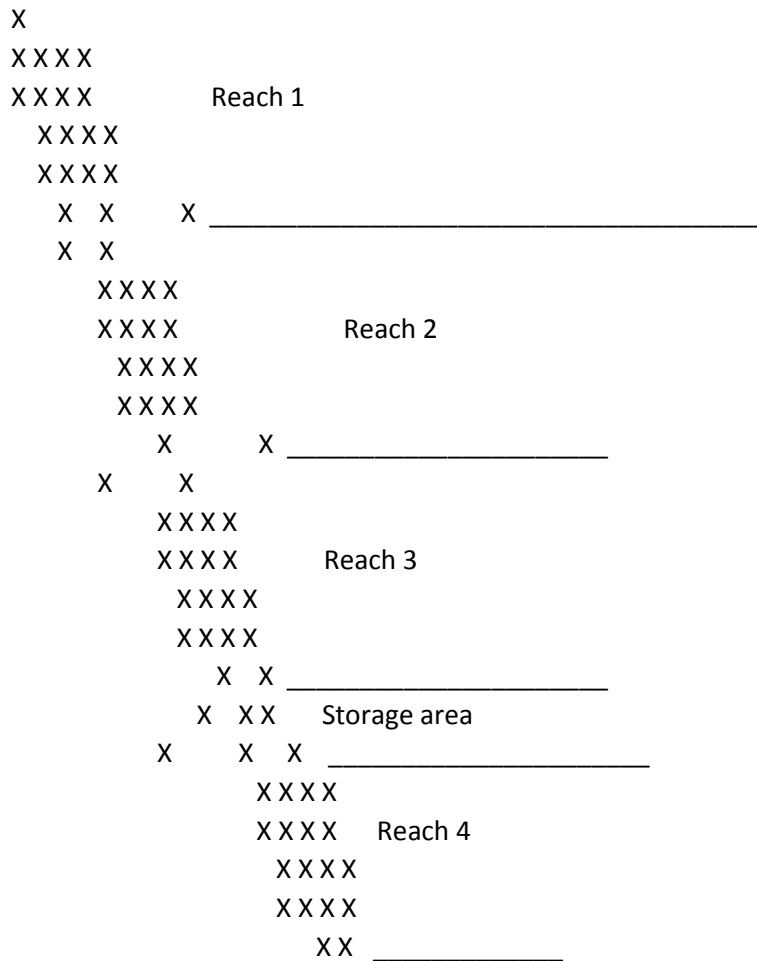
Figure 2-14 Example Sparse coefficient matrix resulting from simple linear system. Note, sparse terms enter and disappear at storage areas and boundary equations.

Three practical solution schemes have been used to solve the sparse system of linear equations: Barkau (1985) used a front solver scheme to eliminate terms to the left of the diagonal and pointers to identify sparse columns to the right of the diagonal. Cunge et al. (1980) and Shaffranekk (1981) used recursive schemes to significantly reduce the size of the sparse coefficient matrix. Tucci (1978) and Chen and Simons (1979) used the skyline storage scheme (Bathe and Wilson, 1976) to store the coefficient matrix. The goal of these schemes is to more effectively store the coefficient matrix. The front solver and skyline methods identify and store only the significant elements. The recursive schemes are more elegant, significantly reducing the number of linear equations. All use Gaussian elimination to solve the simultaneous equations.

A front solver performs the reduction pass of Gauss elimination before equations are entered into a coefficient matrix. Hence, the coefficient matrix is upper triangular. To further reduce storage, Barkau (1985) proposed indexing sparse columns to the right of the band, thus, only the band and the sparse terms were stored. Since row and column operations were minimized, the procedure should be as fast if not faster than any of the other procedures. But, the procedure could not be readily adapted to a wide variety of problems because of the way that the sparse terms were indexed. Hence, the program needed to be re-dimensioned and recompiled for each new problem.

The recursive schemes are ingenious. Cunge credits the initial application to Friazinov (1970). Cunge's scheme and Schaffranek's scheme are similar in approach but differ greatly in efficiency. Through recursive upward and downward passes, each single routing reach is transformed into two transfer equations which relate the stages and flows at the upstream and downstream boundaries. Cunge substitutes the transfer equations in which M is the number of junctions. Schraffranek combines the transfer equations with the boundary equations, resulting in a system of $4N$ equations in which N is the number of individual reaches. The coefficient matrix is sparse, but the degree is much less than the original system.

By using recursion, the algorithms minimize row and column operations. The key to the algorithm's speed is the solution of a reduced linear equation set. For smaller problems Gaussian elimination on the full matrix would suffice. For larger problems, some type of sparse matrix solver must be used, primarily to reduce the number of elementary operations. Consider, for example, a system of 50 reaches. Schaffranek's matrix would be 200 X 200 and Cunge's matrix would be 50 X 50, 2.7 million and 42,000 operations respectively (the number of operations is approximately $1/3 \, n^3$ where n is the number of rows).

Another disadvantage of the recursive scheme is adaptability. Lateral weirs which discharge into storage areas or which discharge into other reaches disrupt the recursion algorithm. These weirs may span a short distance or they may span an entire reach. The recursion algorithm, as presented in the above references, will not work for this problem. The algorithm can be adapted, but no documentation has yet been published.

Skyline is the name of a storage algorithm for a sparse matrix. In any sparse matrix, the non-zero elements from the linear system and from the Gaussian elimination procedure are to the left of the diagonal and in a column above the diagonal. This structure is shown in Figure 2-14. Skyline stores these inverted "L shaped" structures in a vector, keeping the total storage at a

minimum. Elements in skyline storage are accessed by row and column numbers. Elements outside the "L" are returned as zero, hence the skyline matrix functions exactly as the original matrix. Skyline storage can be adapted to any problem.

The efficiency of Gaussian elimination depends on the number of pointers into skyline storage. Tucci (1978) and Chen and Simons (1979) used the original algorithm as proposed by Bathe and Wilson (1976). This algorithm used only two pointers, the left limit and the upper limit of the "L", thus, a large number of unnecessary elementary operations are performed on zero elements and in searching for rows to reduce. Their solution was acceptable for small problems, but clearly deficient for large problems. Using additional pointers reduces the number of superfluous calculations. If the pointers identify all the sparse columns to the right of the diagonal, then the number of operations is minimized and the performance is similar to the front solver algorithm.

<u>Skyline Solution Algorithm</u>

The skyline storage algorithm was chosen to store the coefficient matrix. The Gauss elimination algorithm of Bathe and Wilson was abandoned because of its poor efficiency. Instead a modified algorithm with seven pointers was developed. The pointers are:

1)   IDIA(IROW) - index of the diagonal element in row IROW in skyline storage.

2)   ILEFT(IROW) - number of columns to the left of the diagonal.

3)   IHIGH(IROW) - number of rows above the diagonal.

4)   IRIGHT(IROW) - number of columns in the principal band to the right of the diagonal.

5)   ISPCOL(J,IROW) - pointer to sparse columns to the right of the principal band.

6)   IZSA(IS) - the row number of storage area IS.

7)   IROWZ(N) - the row number of the continuity equation for segment N.

The pointers eliminate the meaningless operations on zero elements. This code is specifically designed for flood routing through a full network.

Computational Procedure

The solution of the water surface elevation at all cross sections, storage areas, and 2D Flow Area cells follows this computational procedure:

1. The solver makes an initial trial at the water surface, flows, derivatives etc… The unsteady flow equations are solved in the implicit finite difference matrix solver (we use a solver called the Skyline Matrix solver) for the 1D nodes. A 2D implicit finite volume solution algorithm is used for the 2D flow areas (See the 2D Theory section below in this chapter).
2. All computational nodes (cross sections, storage areas, and now 2D cells) are checked to see if the computed water surface minus the previous values are less than the numerical solution tolerance.
3. If the error is less than the numerical solution tolerance, then it is finished for that time step; it uses those answers as the correct solution for the time step, and moves on to the next time step.
4. If the numerical error is greater than the tolerance at any node, it iterates, meaning it makes a new estimate of all the derivatives and solves the equations again.
5. During the iteration process, if it comes up with a solution in which the numerical error is less than the tolerance at all locations, it is done and it uses that iteration as the correct answers, and goes on to the next time step.
6. During the iteration (and even first trial) process, the program saves the trial with the least amount of numerical error as being the best solution so far. All water surfaces and flows are saved at all locations.
7. Any iteration that produces a better answer, but does not meet the tolerance, is saved as the current best solution.
8. If the solution goes to the maximum number of iterations (20 by default), then it prints out a warning. However it uses the trial/iteration that had the best answer. It also prints out the location that had the greatest amount of numerical error and the magnitude of that error.
9. This happens even if one of the trials/iterations causes the matrix to go completely unstable. It still does this process and often can find a trial that is not unstable, but does not produce an error less than the numerical tolerance, so it goes with that iteration and moves on.

2D Unsteady Flow Hydrodynamics

Introduction

The Navier-Stokes equations describe the motion of fluids in three dimensions. In the context of channel and flood modeling, further simplifications are imposed. One simplified set of equations is the Shallow Water (SW) equations. Incompressible flow, uniform density and hydrostatic pressure are assumed and the equations are Reynolds averaged so that turbulent motion is approximated using eddy viscosity. It is also assumed that the vertical length scale is much smaller than the horizontal length scales. As a consequence, the vertical velocity is small and pressure is hydrostatic, leading to the differential form of the SW equations derived in subsequent sections.

In some shallow flows the barotropic pressure gradient (gravity) term and the bottom friction terms are the dominant terms in the momentum equations and unsteady, advection, and viscous terms can be disregarded. The momentum equation then becomes the two dimensional form of the Diffusion Wave Approximation. Combining this equation with mass conservation yields a one equation model, known as the Diffusive Wave Approximation of the Shallow Water (DSW) equations.

Furthermore, in order to improve computation time, a sub-grid bathymetry approach can be used. The idea behind this approach is to use a relatively coarse computational grid and finer scale information about the underlying topography (Casulli, 2008). The mass conservation equation is discretized using a finite volume technique. The fine grid details are factored out as parameters representing multiple integrals over volumes and face areas. As a result, the transport of fluid mass accounts for the fine scale topography inside of each discrete cell. Since this idea relates only to the mass equation, it can be used independent of the version of the momentum equation. In the sections below, sub-grid bathymetry equations are derived in the context of both; full Shallow Water (SW) equations and Diffusion Wave (DSW) equations.
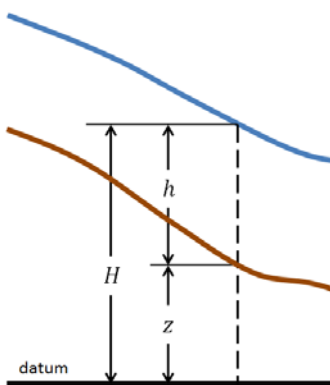
In a subsequent section, the grid requirements are laid out and further notation is defined in order to develop a numerical solution algorithm.

The section about numerical methods describes the details of the finite volume implementation. That section details the way in which the different terms of the equations are discretized and how the non-linear problem is transformed into a system of equations with variable coefficients. The global algorithm to solve the general unsteady problem is also explained in detail.

Through this document it will be assumed that the bottom surface elevation is given by z(x,y); the water depth is h(x,y,t); and the water surface elevation is:

$$H(x, y, t) = z(x, y) + h(x, y, t) \qquad \text{(2-122)}$$

Hydraulic Equations

Mass Conservation

Assuming that the flow is incompressible, the unsteady differential form of the mass conservation (continuity) equation is:

$$\frac{\partial H}{\partial t} + \frac{\partial (hu)}{\partial x} + \frac{\partial (hv)}{\partial y} + q = 0 \qquad \text{(2-123)}$$

where t is time, u and v are the velocity components in the x- and y- direction respectively and q is a source/sink flux term.

In vector form, the continuity equation takes the form:

$$\frac{\partial H}{\partial t} + \nabla \bullet hV + q = 0 \qquad \text{(2-124)}$$

where V=(u,v) is the velocity vector and the differential operator del (∇) is the vector of the partial derivative operators given by $\nabla = (\partial / \partial x, \partial / \partial y)$.

Integrating over a horizontal region with boundary normal vector *n* and using Gauss' Divergence theorem, the integral form of the equation is obtained:

$$\frac{\partial}{\partial t} \iiint\limits_{\Omega} d\Omega + \iint\limits_{S} V \bullet n dS + Q = 0 \qquad \text{(2-125)}$$

The volumetric region Ω represents the three-dimensional space occupied by the fluid. The side boundaries are given by S. It is assumed that Q represents any flow that crosses the bottom surface (infiltration) or the top water surface of Ω (evaporation or rain). The source/sink flow term Q is also convenient to represent other conditions that transfer mass into, within or out of the system, such as pumps. Following the standard sign conventions, sinks are positive and sources are negative

This integral form of the continuity equation will be appropriate in order to follow a sub-grid bathymetry approach in subsequent sections. In this context, the volume Ω will represent a finite volume cell and the integrals will be computed using information about the fine underlying topography.

Sub-grid Bathymetry. Modern advances in the field of airborne remote sensing can provide very high resolution topographic data. In many cases the data is too dense to be feasibly used directly as a grid for the numerical model. This presents a dilemma in which a relatively coarse computational grid must be used to produce a fluid simulation, but the fine topographic features should be incorporated in the computation.
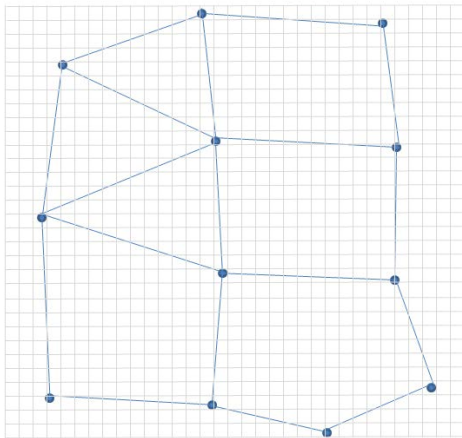
The solution to this problem that HEC-RAS uses is the sub-grid bathymetry approach (Casulli, 2008). The computational grid cells contain some extra information such as hydraulic radius, volume and cross sectional area that can be pre-computed from the fine bathymetry. The high resolution details are lost, but enough information is available so that the coarser numerical method can account for the fine bathymetry through mass conservation. For many applications this method is appropriate because the free water surface is smoother than the bathymetry so a coarser grid can effectively be used to compute the spatial variability in free surface elevation.

In the figure above, the fine grid is represented by the Cartesian grid in gray and the computational grid is displayed in blue.

The volume triple integral of equation 2-125 represents the volume Ω of a horizontally bounded region. Assuming that it is a function of the water surface elevation H, the first term of the equation is discretized as:

$$\frac{\partial}{\partial t}\iiint_{\Omega} d\Omega = \frac{\Omega\left(H^{n+1}\right) - \Omega\left(H^{n}\right)}{\Delta t} \tag{2-126}$$

where the superscripts are used to index time-steps and the difference between two consecutive time-steps is Δt.

If the cells are assumed to have a polygonal shape, the boundary double integral of equation 2-125**Error! Reference source not found.** can be written as a sum over the vertical faces of the volumetric region

$$\iint_{S} V \bullet n dS = \sum_{k} V_{k} \bullet n_{k} A_{k}\left(H\right) \tag{2-127}$$

where V_{k} and n_{k} are the average velocity and unit normal vector at face k and A_{k} (H) is the area of face k as a function of water elevation, in the spirit of the sub-grid bathymetry technique. In Figure 2-15, the left figure represents the shape of a face as seen in the fine grid and the corresponding function for face area A_{k} in terms of the water surface elevation H.
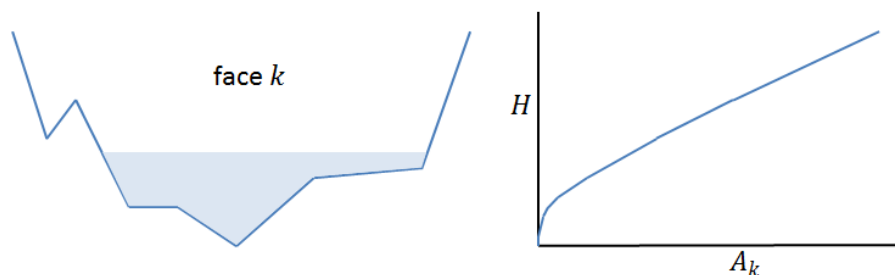
Figure 2-15. Cell Face Terrain Data and Property Table.

Equations 2-126 and 2-127 can be substituted back into equation 2-125 to obtain the sub-grid bathymetry mass conservation equation:

$$\frac{\Omega\left(H^{n+1}\right)-\Omega\left(H^{n}\right)}{\Delta t}+\sum_{k}V_{k}\bullet n_{k}A_{k}\left(H\right)+Q=0 \qquad (2\text{-}128)$$

Notice that this equation requires some knowledge of sub-grid bathymetry, mainly the cell volume $\Omega(H)$ and the face areas A_k (H) as functions of the water elevation H. However, if this information is not available, the classical "box scheme" can be very easily recovered by making $\Omega(H)$=P*h and $A_{k}\left(H\right)=\ell_{k}*h$, where P is the cell area, ℓ_{k} is the length of the edge k (both independently of H) and h=H-z is the water depth.

Some special considerations will be necessary for dry cells. Notice that in the case where the cell volume Ω is zero, dry cells remain dry until they have a volume gain from balancing an inflow from one of their faces or from the source term. If the face k of a cell is dry, the area A_k is zero and the system of equations will be missing the term V_k, so it is undefined. However, it will be shown in subsequent sections that the momentum equation for dry cells will yield zero velocity in the limit. Consequently, the process of wetting and drying is continuous and consistent with the equations, even though computationally, dry cells must be handled as a special case.

Momentum Conservation

When the horizontal length scales are much larger than the vertical length scale, volume conservation implies that the vertical velocity is small. The Navier-Stokes vertical momentum equation can be used to justify that pressure is nearly hydrostatic. In the absence of baroclinic pressure gradients (variable density), strong wind forcing and non-hydrostatic pressure, a vertically-averaged version of the momentum equation is adequate. Vertical velocity and vertical derivative terms can be safely neglected (in both mass and momentum equations). The shallow water equations are obtained.

$$\frac{\partial u}{\partial t}+u\frac{\partial u}{\partial x}+v\frac{\partial u}{\partial y}=-g\frac{\partial H}{\partial x}+v_{t}\left(\frac{\partial^{2}u}{\partial x^{2}}+\frac{\partial^{2}u}{\partial y^{2}}\right)-c_{f}u+fv \qquad (2\text{-}129)$$

$$\frac{\partial v}{\partial t} + u \frac{\partial v}{\partial x} + v \frac{\partial v}{\partial y} = -g \frac{\partial H}{\partial y} + v_t \left(\frac{\partial^2 v}{\partial x^2} + \frac{\partial^2 v}{\partial y^2} \right) - c_f v + fu \qquad \text{(2-130)}$$

Where u and v are the velocities in the Cartesian directions, g is the gravitational acceleration, v_t is the horizontal eddy viscosity coefficient, c_f is the bottom friction coefficient, R is the hydraulic radius and f is the Coriolis parameter.

The left hand side of the equation contains the acceleration terms. The right hand side represents the internal or external forces acting on the fluid. The left and right hand side term are typically organized in such a way in accordance with Newton's second law, from which the momentum equations are ultimately derived.

The momentum equations can also be rendered as a single differential vector form. The advantage of this presentation of the equation is that it becomes more compact and easily readable. The vector form of the momentum equation is:

$$\frac{\partial V}{\partial t} + V \bullet \nabla V = -g \nabla H + v_t \nabla^2 V - c_f V + fk \times V \qquad \text{(2-131)}$$

where the differential operator del (∇) is the vector of the partial derivative operators given by $\nabla = (\partial / \partial x, \partial / \partial y)$ and k is the unit vector in the vertical direction.

Every term of the vector equation has a clear physical counterpart. From left to right there is the unsteady acceleration, convective acceleration, barotropic pressure term, eddy diffusion, bottom friction and Coriolis term.

A dimensional analysis shows that when the water depth is very small the bottom friction term dominates the equation. As a consequence, equation 2-131 for dry cells takes the limit form $V = 0$. As before, dry cells are computationally treated as a special case, but the result is continuous and physically consistent during the process of wetting or drying.

Acceleration. The Eulerian acceleration terms on the left, can be condensed into a Lagrangian derivative acceleration term taken along the path moving with the velocity term:

$$\frac{DV}{Dt} = \frac{\partial V}{\partial t} + V \bullet \nabla V \qquad \text{(2-132)}$$

Other names usually given to this term are substantial, material and total derivative. The use of the Lagrangian derivative will become evident in subsequent sections when it will be seen that its discretization reduces Courant number constraints and yields a more robust solution method.

Gravity. If the flow surface is not horizontal, the weight of contiguous water columns with different heights will produce a pressure gradient referred to in the uniform density case as a barotropic pressure gradient. This is expressed by the first term on the right hand side of equation 2-131.

Latitude affects the value of g by as much as ±0.3%, due to the rotation of Earth and the equatorial bulge. According to the Somigliana formula:

$$g = g_o \left(\frac{1 + k \sin^2 \varphi}{\sqrt{1 - e^2 \sin^2 \varphi}} \right) \tag{2-133}$$

where φ is latitude, g_0 = 9.7803267715 m/s² (32.0876862582 ft/s²) is the gravitational acceleration at the equator, k = 0.0019318514 is the normal gravity constant and e = 0.0066943800 is the square of the eccentricity of the Earth.

Eddy Viscosity. Turbulence is a complex phenomenon of chaotic (turbulent) fluid motion and eddies spanning a wide range of length scales. Many of the length scales are too small to be feasibly resolved by a discrete numerical model, so turbulent flow mixing is modeled as a gradient diffusion process. In this approach, the diffusion rate is cast as the eddy viscosity coefficient v_t.

The Eddy viscosity coefficient can be parameterized as follows,

$$v_t = Dhu_* \tag{2-134}$$

where D is a non-dimensional empirical constant and u_* is the shear velocity, which can be computed as:

$$u_* = \sqrt{gRS} = \frac{\sqrt{g}}{C}|V| = \frac{n\sqrt{g}}{R^{1/6}}|V| \tag{2-135}$$

R is the hydraulic radius and S denotes the energy slope, which can be computed using Chézy formula from the next section, and further simplified using Manning formula, also explained later.

The diffusion is assumed to be isotropic. The empirical values D_L and D_T are assumed to be identical. The mixing coefficient D is an empirical value that varies with the geometry and bottom/wall surface. Some values for D are provided in table 5 below:

Table 5. Eddie Viscosity Transverse Mixing Coefficients

D	Mixing Intensity	Geometry and surface
0.11 to 0.26	Little mixing	Straight channel, smooth surface
0.30 to 0.77	Moderate mixing	Gentle meanders, moderate surface irregularities
2.0 to 5.0	Strong mixing	Strong meanders, rough surface

Bottom Friction. Using the Chézy formula, the bottom friction coefficient is given by

$c_f = \dfrac{g|V|}{C^2 R}$, where g is the gravitational acceleration, $|V|$ is the magnitude of the velocity vector, C is the Chézy coefficient and R is the hydraulic radius. Notice that the Chézy coefficient is not dimensionless. It is measured in $m^{1/2}/s$ in the SI system and $ft^{1/2}/s$ in the U.S. customary system.

Empirical results show that the Chézy coefficient can be approximated using the Gauckler-Manning-Strickler formula, or Manning's formula for short. This relation states that the Chézy coefficient C is related to the hydraulic radius R by the formula $C=R^{1/6}/n$, where n is an empirically derived roughness coefficient known as Manning's n. As expected, the coefficient n is not independent of units and is usually measured in $s/m^{1/3}$ in the SI system. To transform to the U.S. customary system the conversion constant is 1.48592 $(ft/m)^{1/3}$.

Using Manning's formula, the bottom friction coefficient is now given by:

$$c_f = \frac{n^2 g|V|}{R^{4/3}}$$

(2-136)

Coriolis Effect. The last term of the momentum equation relates to the Coriolis Effect. It accounts for the fact that the frame of reference of the equation is attached to the Earth, which is rotating around its axis. The vertical component of the Coriolis term is disregarded in agreement with the shallow water assumptions. The apparent horizontal force felt by any object in the rotating frame is proportional to the Coriolis parameter given by:

$$f = 2\omega \sin \varphi$$

(2-137)

where ω = 0.00007292115855306587/s is the sidereal angular velocity of the Earth and φ is the latitude.

Diffusion Wave Approximation of the Shallow Water Equations

In the previous section, the Manning formula was used to estimate the Chézy coefficient. If further constraints are assumed on the physics of the flow, a relation between barotropic pressure gradient and bottom friction is obtained from the diffusion wave form of the momentum equation. This relation is extremely useful due to its simplicity. However it must be noted that it can be applied only in a narrower scope than the more general momentum

equation studied before. Under the conditions described in this section, the Diffusion Wave equation can be used in place of the momentum equation. It will be seen in subsequent sections that the corresponding model becomes a one equation model known as the Diffusion Wave Approximation of the Shallow Water equations (DSW).

Up to this point, we have described the hydraulics for momentum. From now on the discussion will gear towards the formulation and numerics of the solution. It will be convenient to denote the hydraulic radius and the face cross section areas as a function of the water surface elevation H, so R= R(H), A=A(H).

Diffusion-Wave Form of the Momentum Equation. In shallow frictional and gravity controlled flow; unsteady, advection, turbulence and Coriolis terms of the momentum equation can be disregarded to arrive at a simplified version. Flow movement is driven by barotropic pressure gradient balanced by bottom friction. Simplifying the momentum equation results in:

$$\frac{n^2 |V| V}{(R(H))^{4/3}} = -\nabla H \tag{2-138}$$

Dividing both sides of the equation by the square root of their norm, the equation can be rearranged into the more classical form,

$$V = \frac{-(R(H))^{2/3}}{n} \frac{\nabla H}{|\nabla H|^{1/2}} \tag{2-139}$$

where V is the velocity vector, R is the hydraulic radius, ∇H is the surface elevation gradient and *n* is the empirically derived Manning's *n*.

Diffusion-wave approximation of the Shallow Water Equations. When the velocity is determined by a balance between barotropic pressure gradient and bottom friction, the Diffusion Wave form of the Momentum equation 2-139 can be used in place of the full momentum equation and the corresponding system of equations can in fact be simplified to a one equation model. Direct substitution of Diffusion Wave equation 2-139 in the mass conservation equation **Error! Reference source not found.** yields the classical differential form of the Diffusion Wave Approximation of the Shallow Water (DSW) equations:

$$\frac{\partial H}{\partial t} - \nabla \bullet \beta \nabla H + q = 0 \tag{2-140}$$

Where: $\beta = \dfrac{(R(H))^{5/3}}{n |\nabla H|^{1/2}}$

If bathymetry information is of interest, the Diffusion Wave equation 2-139 can also be substituted into the sub-grid bathymetry form of the continuity equation 2-128 to obtain the equation:

$$\frac{\Omega(H^{n+1}) - \Omega(H^n)}{\Delta t} - \sum_k \alpha \nabla H \bullet n + Q = 0 \qquad (2\text{-}141)$$

Where $\alpha = \alpha(H) = \dfrac{(R(H))^{2/3} A_k(H)}{n|\nabla H|^{1/2}}$ and as seen in equation 2-128, $\Omega(H^n)$ is the cell volume

at time *n* and $A_k(h)$ is the area of face *k*, as functions of water elevation.

Once the DSW equation has been solved, the velocities can be recovered by substituting the water elevation back into the Diffusion Wave equation 2-140.

Boundary Conditions

At any given time step, boundary conditions must be given at all the edges of the domain. Within HEC-RAS they can be of three different kinds;

- **Water surface elevation**: The value of the water surface elevation $H=H_b$ is given at one of the boundary edges.
- **Water surface gradient**: The slope of the water surface S_b in the direction normal to the boundary is imposed. This condition is expressed as:

$$\nabla H \bullet n = S_b \qquad (2\text{-}142)$$

- **Flow**: The flow Q_b that crosses the boundary is provided. In the continuity equation 2-125, this condition is implemented by direct substitution into the flow formula of the corresponding boundary faces. More formally, the surface integral in equation 2-125 is constrained by the condition:

$$\iint_b V \bullet n \, dS = Q_b \qquad (2\text{-}143)$$

Where the integral is taken over the boundary surface on which the boundary condition applies.

If a sub-grid bathymetry approach is preferred, a constraint on the form of equation 2-128 must be used and the boundary condition takes the form:

$$V_b \bullet n_b A_b(H) = Q_b \qquad (2\text{-}144)$$

Where again the index refers to the face on which the boundary condition applies.

Grid and Dual Grid

In order to efficiently take advantage of the numerical methods described later, the domain must be subdivided into non-overlapping polygons to form a grid. To provide the maximum flexibility, the solver does not require the grid to be structured or even orthogonal. However if orthogonality exists in all or part of the grid, the numerical solver will take advantage of it to improve computational speed. This will be covered in detail in the following section.

The solver does not have any inherent restrictions with respect to the number of sides of the polygonal cells (however, we have set a limit of 8 sides for efficiency and saving memory space). However, it is required that grid cells are convex. It must be emphasized that the choice of a grid is extremely important because the stability and accuracy of the solution depend greatly on the size, orientation and geometrical characteristics of the grid elements.

Because of second order derivative terms and the differential nature of the relationship between variables, a dual grid will be necessary in addition to the regular grid in order to numerically model the differential equations. The dual grid also spans the domain and is characterized by defining a correspondence between dual nodes and regular grid cells and similarly between dual cells and regular grid nodes.
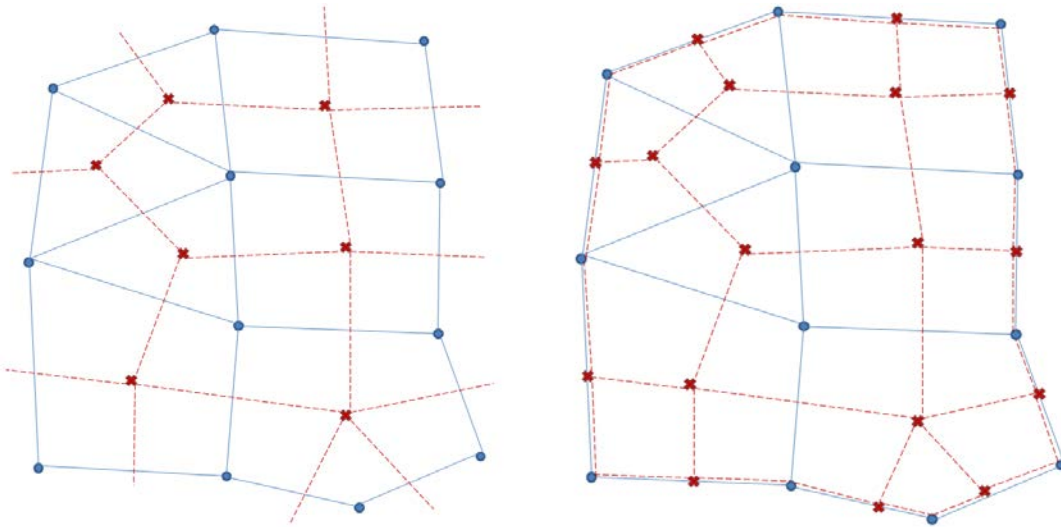
In the figure above, the grid nodes and edges are represented by dots and solid lines; the dual grid nodes and edges are represented by crosses and dashed lines.

From the mathematical point of view sometimes the grid is augmented with a cell "at infinity" and analogously, the dual grid is augmented with a node "at infinity". With these extra additions, the grid and its dual have some interesting properties. For instance, the dual edges intersect the regular edges and the two groups are in a one-to-one correspondence. Similarly, the dual cells are in a one-to-one correspondence with the grid nodes and the dual nodes are in a one-to-one correspondence with the grid cells. Moreover, the dual of the dual grid is the original grid.

However, in the context of a numerical simulation, extending the grid to infinity is impractical. The dual grid is therefore truncated by adding dual nodes on the center of the boundary edges and dual edges along the boundary joining the boundary dual nodes. The one-to-one correspondences of the infinite model do not carry over to the truncated model, but some slightly more complex relations can be obtained. For instance, the dual nodes are now in one-to-one correspondence with the set of grid cells and grid boundary edges. For this reason, the

boundary edges are considered as a sort of topological artificial cells with no area which are extremely useful when setting up boundary conditions.

In the context of the equations described in this document, it is convenient to numerically compute the water surface elevation *H* at the grid cell centers (including artificial cells), the velocity perpendicular to the faces (determining the flow transfer across the faces), and the velocity vector *V* at the face points.

Numerical Methods

A hybrid discretization scheme combining finite differences and finite volumes is used to take advantage of orthogonality in grids. The discrete solution for the hydraulic equations is computed using a Newton-like solution technique explained later.

Finite Difference Approximations

A finite difference scheme expresses a derivative as the difference of two quantities. This technique has already been tacitly used in equation 2-128, to discretize the volume derivative in time as the difference of the volumes at times *n* and *n+1* and divided by the time-step Δt,

$$\frac{\partial \Omega}{\partial t} \approx \frac{\Omega\left(H^{n+1}\right) - \Omega\left(H^{n}\right)}{\Delta t} \tag{2-145}$$

Finite differences in space work identically. Given two adjacent cells j_1 and j_2 with water surface elevation H_1 and H_2 respectively, the directional derivative in the direction n' determined by the cell centers is approximated by

$$\nabla H \bullet n' = \frac{\partial H}{\partial n'} \approx \frac{H_2 - H_1}{\Delta n'} \tag{2-146}$$

where $\Delta n'$ is the distance between the cell centers.

The orientation of the derivative is important. In the example below (Figure 2-16), the derivative is oriented from cell i_1 to cell i_2, towards the right of the picture. To reverse orientation, just reverse the position of the sub-indices.
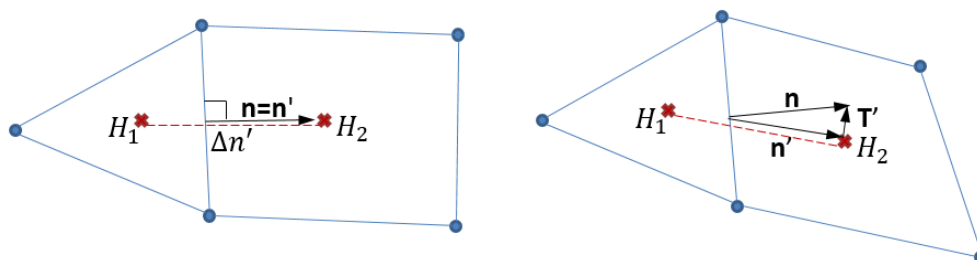
Figure 2-16. Cell Directional Derivatives

If the direction n' happens to be orthogonal to the face between the cells, the grid is said to be locally orthogonal at this face. This is the situation depicted on the left image in Figure 2-16. In

this case, the formula above is sufficient to compute the normal water surface derivative of equation 2-141. In general, this condition is not satisfied and the finite difference technique is supplemented by a finite volume technique, as will be seen soon.

Finite Volume Approximations

A finite volume approach is used to discretize equation 2-141 when the grid is not locally orthogonal. Moreover, the finite volume technique will also be used to approximate other differential terms such as eddy viscosity.

In the spirit of the finite volume technique, the value of the gradient term ∇H at a grid face is approximated as an average over dual cells and Gauss' divergence theorem is applied to obtain the formula

$$\nabla H \approx \frac{\oint_L H \, n \, dL}{A'} \tag{2-147}$$

Where L is the dual cells boundary and A' is the area of the dual cells, shaded in the Figure 2-17. As the dual cells form a polygon, the line integral can be written as a sum over the dual cell faces. The dual face k' joining dual nodes j_1 and j_2 contributes a term $n_{k'} l_{k'}(H_1+H_2)/2$ to the line integral, where $l_{k'}$ is the length of dual face k', $n_{k'}$ is the unit outward normal vector at dual face k' and H_1, H_2 are the water elevation values at the cell centers j_1 and j_2 as shown on the figure on the left.
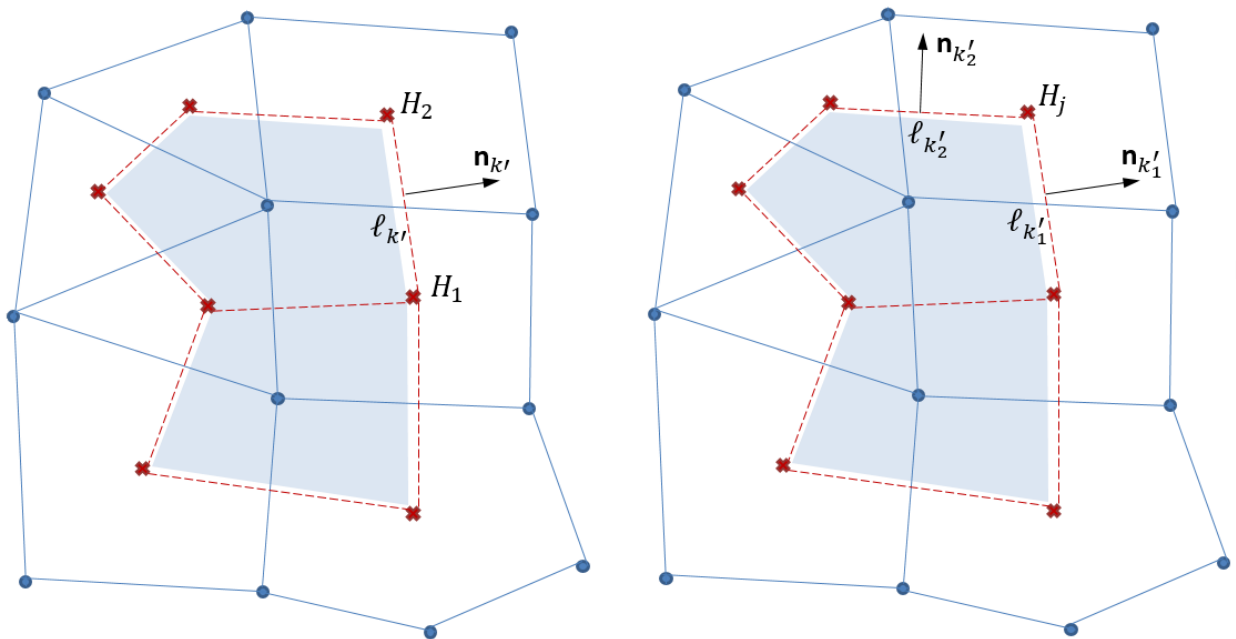
Figure 2-17. Cell and Dual Cell Finite Volume Formulation

Grouping terms by cell index j, the finite volume approximation of the gradient becomes the multi-linear formula

$$\nabla H \approx \sum_j c_j H_j \tag{2-148}$$

where the sum is over all cells (dual nodes) around the calculation face, H_j is the value of the water elevation at the cell j and the vector constants $c_j = \left(n_{k_1'}l_{k_1'} + n_{k_2'}l_{k_2'}\right)/2A'$ depend on the local grid geometry at the dual faces k'_1 and k'_2 neighboring dual node (cell) j and the dual area A', as seen on the figure. The values $l_{k_1'}$, $l_{k_2'}$ and the unit vectors $n_{k_1'}$, $n_{k_2'}$ represent respectively the length and the outward normal to the dual faces k'_1 and k'_2.

Directional derivatives in an arbitrary direction T' are readily computed using the formula

$$\frac{\partial H}{\partial T'} = \nabla H \bullet T' \approx \sum_j c_j' H_j \tag{2-149}$$

where the scalar constants $c_j' = \left(n_{k_1'}l_{k_1'} + n_{k_2'}l_{k_2'}\right)\bullet T'/(2A')$ absorbed the dot product with T'.

Applying a similar argument on the grid instead of the dual grid, the gradient of the velocity ∇V can be computed at a grid cell. The argument can be repeated sequentially in order to compute higher order derivatives. For instance, once ∇V is known at all grid cells, the Laplacian terms $\nabla^2 V$ can be computed at the grid nodes by the process described before.

Hybrid Discretization

As seen in previous sections, normal derivatives on the faces of an orthogonal grid can be approximated using finite differences. If the grid is not locally orthogonal, the normal derivative must be split as the sum of a finite difference and a finite volume approximation.

Let *n* be the direction normal to a face and *T = k x n* be the direction orthogonal to n, where k is the unit vector in the vertical direction. Similarly, let *n'* be the direction determined by the cell centers on both sides of the face and *T' = k x n'* be the direction orthogonal to *n'*.

An algebraic manipulation yields the relation

$$\frac{\partial H}{\partial n} = \left(n \bullet n'\right)\frac{\partial H}{\partial n'} + \left(n \bullet T'\right)\frac{\partial H}{\partial T'} \tag{2-150}$$

The first derivative on the right hand side is computed using the finite difference approximation, while the other derivative is computed using the finite volume approximation.

Note that the formula is linear on *H*. It can be written as

$$\nabla H \bullet n = \frac{\partial H}{\partial n} \approx \sum_j c_{j'} H_j \tag{2-151}$$

where the coefficients $c_{j'}$ are a combination of the finite difference terms $\pm 1/\Delta n'$ and the finite volume terms c_j'.

It is immediately evident that locally orthogonal grids produce two-point discretization stencils, while non-orthogonal grids require a larger stencil. Consequentially, locally orthogonal grids yield systems with smaller band-widths that can be solved more efficiently. A pre-process routine is used to identify regions of local grid orthogonality and advising the discretization techniques to implement purely finite difference approximations in those regions.

Numerical DSW Solver

Discrete Scheme for DSW Equations. Finite differences are used to discretize time derivatives and hybrid approximations are used to discretize spatial derivatives. The generalized Crank-Nicolson method is used to weight the contribution of variables at time steps *n* and *n+1*. Equation 2-141 is rewritten grouping similar terms and taking advantage of the linearity of equation 2-151,

$$\Omega\left(H^{n+1}\right) + \sum_j a_j \left((1-\theta)H_j^n + \theta H_j^{n+1}\right) = d \tag{2-152}$$

where the sum is over all cells around the computational cell where the equation is being solved. The coefficients a_j are a function of terms Δt and α from equation 2-141 and $c'_{j'}$ of equation 2-151. The right hand side term is given by $d = \Omega\left(H^n\right) - \Delta t Q$.

Collecting together terms that refer to the same cell and moving all terms involving time step *n* to the right hand side of the equation, the equation takes the form.

$$\Omega\left(H^{n+1}\right) + \theta\sum_j a_j H_j^{n+1} = d - (1-\theta)\sum_j a_j H_j^n \tag{2-153}$$

There is an equation of this form for every cell in the domain. Before proceeding, the system of equation for all cells is written in a more compact vector notation.

$$\Omega(H) + \Psi H = b \tag{2-154}$$

Where Ω is the vector of all cell volumes, *H* is the vector of all cell water elevations at time *n+1*, Ψ is the coefficient matrix of the system and *b* is the right-hand-side vector.

If the coefficients are lagged, the system of equations is mildly non-linear due to the bathymetric relationship for Ω as a function of *H*. The Jacobian (derivative) of Ω with respect to *H* is given by another bathymetric relationship *P(H)*: the diagonal matrix of cell wet surface areas. If this information is known, a Newton-like technique can be applied to solve the system of equations, producing the iterative formula,

$$H^{m+1} = H^m - \left(P\left(H^m\right) + \Psi\right)^{-1}\left(\Omega\left(H^m\right) + \Psi H^m - b\right) \tag{2-155}$$

where *m denotes* the iteration index (not to be confused with the time-step).

Robustness and Stability. When there are no fluxes the coefficients are $a_j=0$ and Q=0 so the water surface is identical to the previous step. In particular, dry cells remain dry until water flows into them.

Equation 2-141 implies that the coefficients a_j of equation 2-153 will depend on the value of the water surface. In order to maintain consistency with the generalized Crank Nicolson method, the terms a_j must be evaluated at time *n+ϑ*, $H = (1-\theta)H_j^n + \theta H_j^{n+1}$, creating a circular dependence on the solution of the system of equations. This situation is typical of nonlinear systems and is corrected through iteration. This is presented in steps 5–8 below.

The linearized scheme is unconditionally stable for $1/2 \le \theta \le 1$. When $\theta < 1/2$ the scheme is stable if

$$\frac{\Delta t}{(\Delta x)^2} < \frac{1}{2-4\theta} \tag{2-156}$$

When ϑ=1, the scheme obtained is implicit. It corresponds to using backward differences in time and positioning the spatial derivatives at step *n+1*. When ϑ=1/2, this is the Crank-Nicolson scheme obtained from central differences in time and positioning the spatial derivatives at n+1/2.

The linearized scheme is second order accurate in space. The time accuracy depends of the choice of ϑ; for instance, for ϑ=1 it is first order accurate and for ϑ=1/2 it is second order accurate.

Discrete Boundary Conditions. Flow boundary conditions are also discretized;

- The water surface elevation boundary condition is directly implemented as $H^{n+1}=H_b$.
- The water energy gradient condition is carried out simply as the finite volume approximation of equation 2-142.
- The flow boundary condition is similarly implemented as a condition on the water surface gradient using equation 2-154**Error! Reference source not found.**, a finite volume approximation of Manning equation 2-139. A rotation of the local coordinate system is necessary since in general the direction normal to the boundary does not coincide with the Cartesian directions.

Solution Algorithm. The complete solution algorithm is given here:

1. The geometry, local orthogonality and sub-grid bathymetry data is obtained or pre-computed.
2. Solution starts with H^0 as the provided initial condition at time-step $n = 0$.
3. Boundary conditions are provided for the next time step $n+1$.
4. Initial guess $H^{n+1}=H^n$.

5. Compute the θ-averaged water elevation $H = (1-\theta)H_j^n + \theta H_j^{n+1}$ and sub-grid bathymetry quantities that depend on it (face areas, fluid surface areas, hydraulic radii, Manning's n, etc.).
6. The coefficients a_j are computed and the system of equations 2-154 is assembled.
7. The system of equations 2-154 is solved iteratively using the Newton-like algorithm with the given boundary conditions to obtain a candidate solution H^{n+1}.
8. If the residual (or alternatively, the correction) is larger than a given tolerance (and the maximum number of iterations has not been reached), go back to step 5; otherwise continue with the next step.
9. The computed H^{n+1} is accepted and the velocities V^{n+1} can be calculated using the discrete version of equation 2-139, using equations 2- 146 and 2-148.
10. Increment n. If there are more time steps go back to step 3, otherwise end.

The loop provided by steps 5–8 has the purpose of updating the coefficients a_j so that the solution of the nonlinear system (rather than its linearization) is obtained at every time step. As expected, a fully nonlinear solution has very desirable properties such as wetting several cells or updating coefficients that are evaluated at time $n+\vartheta$.

The implementation of this algorithm takes full advantage of computational vectorization and parallelization. For instance, in step 5 the equation $H = (1-\theta)H_j^n + \theta H_j^{n+1}$ is computed using vectorized operations and then in step 6 the coefficients a_j are computed in parallel using either all available cores or a number of cores determined by the user. Similarly, operations in steps 8 and 9 were also vectorized whenever possible. Additionally, the sparse linear system in step 7 is solved using the Intel MKL PARDISO library. For large sparse linear systems, this solver uses a combination of parallel left- and right- looking supernode pivoting techniques to improve its LDU factorization process (Schenk, et al., 2004), (Schenk, et al., 2006). The solution of step 7 takes full advantage of the solver's memory efficiency and multi-thread features. Moreover, in order to reduce overhead, all matrices are stored using the Compressed Sparse Row (CSR) format consistent with the requirements of Intel PARDISO solver (Schenk, et al., 2011).

Numerical SW Solver

Discrete Scheme for SW Equations. The SW equations express volume and momentum conservation. The continuity equation is discretized using finite volume approximations. For the momentum equation, the type of discretization will vary depending on the term. The Crank-Nicolson method is also used to weight the contribution of variables at time steps *n* and *n+1*. However, the different nature of the equations will call for the use of a more elaborate solver scheme.

Mass Conservation. The continuity equation can be assembled following a process that mimics the construction of the DSW scheme, Equation 2-128 is rewritten grouping terms according to face index *k* around a given computational cell,

$$\frac{\Omega(H^{n+1}) - \Omega(H^n)}{\Delta t} + \sum_k \pm A_k(H)\left((1-\theta)(u_N)_k^n + \theta(u_N)_k^{n+1}\right) + Q = 0 \quad \text{(2-157)}$$

where Δt is the time step, and the velocities have been interpolated in time using the generalized Crank-Nicolson method (which is used to weight the contribution of velocities at time steps *n* and *n+1*). Since the momentum equation is rotation invariant, it will be assumed that $\pm(u_N)$ is in the outward direction orthogonal to the face *k*. The sign in the summation term is chosen according to this orientation principle.

Following the same approach used for the DSW equations, the velocities will be expressed as a linear combination of water surface elevation at neighboring cells and terms will be grouped according to their spatial and time indices. All terms related to the time step *n* will be moved to the right hand side yielding an equation of the form 2-154.

Momentum Equation. Since velocities are computed on the grid faces, the momentum equations are not located on a computational cell, but rather on a computational face. The discrete equations are built based on a semi-implicit scheme in which only the acceleration, barotropic pressure gradient and bottom friction terms contain variables for which the equation is solved. Other terms of the momentum equation are still computed based on the ϑ-method, but their contribution is smaller and so they are considered explicit forcing function terms and moved to the right hand side of the linearized system.

Acceleration

Acceleration terms are discretized using a semi-Lagrangian approach. The Lagrangian form of the advection shown in equation 2-132 is discretized as a derivative taken along the path moving with the velocity term:

$$\frac{DV}{Dt} \approx \frac{V^{n+1} - V_x^n}{\Delta t} \quad \text{(2-158)}$$

Where V^{n+1} is located at the computational face and V_x^n is evaluated at a location *X*. This location is found by integrating the velocity field back in time starting from the location of the computational face. Location *X* does not in general correspond to a face, so an interpolation technique must be applied. Interpolation in general will not be linear, since the cells are not required to satisfy any constraint in terms of the number of edges. However it is required that the interpolation algorithm gives consistent values at the boundaries between cells, independent of which cell is used to compute the interpolation. Due to those conditions an interpolation technique based on generalized barycentric coordinates is implemented.

Integration of the velocity is done in steps using the interpolated velocity field in each cell. In practice, this is equivalent to subdividing the integration time step into smaller sub-steps with a Courant number of one or less and increases the robustness of the computation. In contrast to

the explicit Eulerian framework, the semi-Lagrangian scheme allows for the use of large time steps without limiting the stability and with a much reduced artificial diffusion (regarded as the interpolation error).

Barotropic Pressure Gradient

Recall that the momentum equation is computed at the nodes, but the water elevation term is computed at the center of the cells. This makes equation 2-148 an ideal candidate to discretize the barotropic pressure gradient:

$$-g\nabla H \approx -g\sum_{j} c_j \left((1-\theta)H_j^n + \theta H_j^{n+1}\right)$$
(2-159)

The sum is over all cells (dual nodes) around the node and the coefficients c_j are computed as in equation 2-148 . The gravitational acceleration g accounts for latitudinal variation as specified in equation 2-133. The sum of ϑ–weighted terms accounts for the fact that the ϑ-scheme is used to compute H_j at the cell j. As a consequence, the barotropic pressure gradient term will consist of two parts; an implicit term with weight ϑ and an explicit term with weight *1-ϑ*.

Eddy Viscosity

The eddy diffusivity coefficient is implicitly defined in terms of water surface elevations and velocities. The coefficient must be updated for every iteration of the solution steps 6-10 of the algorithm presented later.

The computation of the eddy diffusivity starts by calculating the shear velocity u_* using equation 2-135. The shear velocity formula itself relies on other quantities that must be previously computed;

- The constant of gravitational acceleration g, pre-computed once using equation 2-133;
- For every time-step and for every face, the hydraulic radius R which is obtained from the sub-grid bathymetry data. The solver must maintain a table relating the hydraulic radius to the water elevation. This table will be pre-computed once from the fine grid data.
- The Manning's n, also depends on the sub-grid bathymetry. For every time-step and for every face this quantity is interpolated from a pre-computed table.
- The velocity vector is from the previous time-step $V=V^n$.

Once the shear velocity is computed at each face, equations 2-134 and 2-135 are used to calculate the eddy diffusivity tensor.

The Laplacian terms will be computed as a field, at all nodes of the grid and then spatially interpolated at the location X obtained from the acceleration advection. The Laplacian field is

explicit in the numerical solution so it will depend only on values computed for the previous time step. As a consequence, the Laplacian field is computed only once per time step even if the solution process requires several iterations as in steps 6-10 of the solution algorithm below.

The Laplacian terms are calculated using a standard finite volume approach. Since the velocity is known at the nodes, the gradients can be computed for the cells by a simple application of the Gauss' Divergence Theorem on a grid cell. Following a recipe completely analogous to the dual of equation 2-148, the velocity gradient is given by:

$$\nabla V \approx \sum_i c_i' V_i^n \qquad (2\text{-}160)$$

where the sum is over all nodes around a cell and the vector coefficients c_j' are computed from geometrical characteristics of the grid such as cell areas, face normals and face lengths. Notice that the velocities are taken from the previous time step.

Once the gradients are known for the cells, the Gauss' Divergence theorem can now be applied on a dual cell. Again, an equation analogous to equation 2-148 is:

$$\nabla^2 V \approx \sum_j d_j' \nabla V_j \approx \sum_j d_j' \sum_i c_i' V_i^n \qquad (2\text{-}161)$$

where, as a dual analogous to the previous equation, the first sum is over all cells around a node and the vector coefficients d_j' are computed from the geometry of the dual grid. The last sum on the right hand side of the equation is now indexed over all nodes around cell j. A linear equation is obtained expressing the Laplacian of the velocity at a node as a linear combination of the velocities at and around the node, and then interpolating to any location on the grid.

Once the Laplacian field is known, the Laplacian term is spatially interpolated using generalized barycentric coordinates to obtain $(\nabla^2 V)_X^n$. The location X where this quantity is interpolated is obtained from the acceleration advection.

The eddy diffusion term is finally assembled by multiplying the diffusion coefficient times the Laplacian term.

Bottom Friction

The bottom friction coefficient c_f is computed using equation 2-136. As in the previous section, this term will also depend on other quantities such as the gravitational acceleration, hydraulic radius, Manning's n and the velocity.

However, extra care must be taken with the bottom friction due to the fact that the term is used implicitly in the equations. Since a Crank-Nicolson type of scheme is being used, the coefficient c_f is computed from ϑ-averaged variables located at time $n+\vartheta$ and is therefore a ϑ-weighted average of the corresponding values at times n and $n+1$. The bottom friction coefficient c_f is therefore not computed once per time step, but as many times as iterations are required for convergence, through the iteration process of steps 6-10, as it will be seen in the algorithm

description below. At each of those iterations, a new bottom friction term $-c_f V^{n+1}$ is computed similarly to other implicit terms. The velocity V used in the bottom friction formula is completely implicit for stability purposes.

Coriolis Effect

The Coriolis term is typically the smallest magnitude term in the momentum equations, but it is also the easiest to compute. The Coriolis parameter f is a pre-computed constant that does not change between time-steps and does not depend on sub-grid bathymetry. According to the generalized Crank-Nicolson formula along a streamline, the Coriolis term reduces to:

$$fk \times V \approx \begin{pmatrix} f\left((1-\theta)v_X^n + \theta v^{n+1}\right) \\ -f\left((1-\theta)u_X^n + \theta u^{n+1}\right) \end{pmatrix} \qquad (2\text{-}162)$$

in the Cartesian oriented system used for the velocities. The location X where this quantity is interpolated is obtained from the acceleration advection.

As with other implicit terms in the momentum equation, this vector is computed once per iteration.

Normal Velocity. The solution of the momentum equation uses a fractional-step technique. The first fractional step contains only acceleration and Coriolis terms. The discretization formulas described above yields a vector equation for the velocity. If the coefficients are lagged, this equation is linear on the velocity terms V^n and V^{n+1} and the water surface elevation terms H^n and H^{n+1}. The momentum equation contains some velocity cross-terms arising from the Coriolis force. Grouping velocity terms yields the formula:

$$\begin{pmatrix} 1 & -\theta\Delta tf \\ \theta\Delta tf & 1 \end{pmatrix}\begin{pmatrix} u_*^{n+1} \\ v_*^{n+1} \end{pmatrix} = \begin{pmatrix} u_X^n + (1-\theta)\Delta tfv_X^n \\ v_X^n + (1-\theta)\Delta tfu_X^n \end{pmatrix} \qquad (2\text{-}163)$$

where the right hand side is a linear formula in terms of the velocities and water surface elevations. An explicit formula for V_*^{n+1} without any cross-terms is obtained by

$$V_*^{n+1} = \begin{pmatrix} u_*^{n+1} \\ v_*^{n+1} \end{pmatrix} = \begin{pmatrix} 1 & -\theta\Delta tf \\ \theta\Delta tf & 1 \end{pmatrix}^{-1}\begin{pmatrix} u_X^n + (1-\theta)\Delta tfv_X^n \\ v_X^n + (1-\theta)\Delta tfu_X^n \end{pmatrix} \qquad (2\text{-}164)$$

The second fractional step adds the pressure gradient, eddy viscosity and bottom friction terms according to the discretization formulas developed earlier.

Finally, the normal component $(u_N)^{n+1}$ of the velocity is obtained by a dot product with the face normal vector and substituting back in the continuity equation 2-157 an equation of the form 2-154 is obtained.

Robustness and Stability

When there are no fluxes into a cell the mass conservation equation becomes $H_t=0$, so the water surface is identical to the previous step. In particular, dry cells remain dry until water flows into them.

In the momentum equation, as water depth decreases to zero, all forces tend to zero. However, the bottom friction is the dominant force, so velocities also go to zero in the limit. As a consequence, it is consistent to assume that dry cells have a flow velocity of zero. The momentum equation for dry faces becomes $\partial V/\partial t=0$ and dry faces continue to have zero velocity until water flows into them.

As seen in previous sections, both mass and momentum equations are non-linear. Similarly to the DSW solver, an iterative process must be applied. This idea is presented in steps 6–9 below.

In contrast with an explicit Eulerian scheme, the semi-Lagrangian scheme for the computation of acceleration has the advantage of avoiding a CFL condition based on velocity. For the case $\frac{1}{2} \leq \vartheta \leq 1$, the main condition for stability results from the explicit diffusion term,

$$\Delta t < \frac{(\Delta x)^2}{2v}$$

(2-165)

This condition allows a larger time step than typical stability conditions originating from Eulerian advection schemes.

The linearized scheme is second order accurate in space. The time accuracy depends of the choice of ϑ; for instance, for $\vartheta=1$ it is first order accurate and for $\vartheta=1/2$ it is second order accurate.

Discrete Boundary Conditions

Flow boundary conditions are also discretized;

- The water surface elevation boundary condition is directly implemented as $H^{n+1}=H_b$.
- The water surface gradient condition is carried out simply as the finite volume approximation of equation 2-142.
- The flow boundary condition can be implemented by directly using equation 2-144. A rotation of the local coordinate system is necessary since in general the direction normal to the boundary does not coincide with the Cartesian directions.

Solution Algorithm

The complete solution algorithm is given here:

1. The geometry, local orthogonality and sub-grid bathymetry data is obtained or pre-computed.

2. Solution starts with H^0 and u_N^0 as the provided initial condition at time-step *n=0*.

3. Boundary conditions are provided for the next time step *n+1*.

4. Initial guess $H^{n+1} = H^n$ and $u_N^{n+1} = u_N^n$.

5. Compute explicit terms that remain constant through the time step compute, such as the diffusion Laplacian field.

6. Compute θ–averaged water elevation $H = (1-\theta)H_j^n + \theta H_j^{n+1}$ and sub-grid bathymetry quantities that depend on it (face areas, fluid surface areas, hydraulic radii, Manning's *n*, etc.).

7. A system of equations is assembled for the continuity at the cells as described in the previous sections.

8. The system of equations is solved iteratively using the Newton-like algorithm with the given boundary conditions to obtain a candidate solution H^{n+1}.

9. Velocities u_N^{n+1} are computed according to equation 2-164.

10. If the residual (or alternatively, the correction) is larger than a given tolerance (and the maximum number of iterations has not been reached), go back to step 6; otherwise, continue with the next step.

11. The computed solution is accepted.

12. Increment *n*. If there are more time steps go back to step 3, otherwise end.

The loop provided by steps 6–10 has the purpose of updating the coefficients of the system of equations, so that the solution of the nonlinear system (rather than its linearization) is obtained at every time step. As expected, a fully nonlinear solution has very desirable properties such as wetting several cells and propagating waves though several cells in a single time step.

Similar to the DSW solver, the implementation of this algorithm takes full advantage of computational vectorization and parallelization. Vectorization is used extensively in terms with an explicit discretization in terms of algebraic operations, such as the coefficients for diffusion, Coriolis and bottom friction terms. Simple algebraic steps of the algorithm like steps 4, 6 and 9 are completely vectorized. Parallelization is implemented in terms with a more constructive description such as algorithms, and conditional statements. Examples of such are the sub-grid bathymetry table searches, continuity equation coefficients, semi-Lagrangian advection, barotropic pressure gradient terms and the computation of the Laplacian in the eddy diffusion term. Similarly, algorithmic operations in steps 7 and 8 were also parallelized.

As in previous sections, the sparse linear system in step 7 is solved using the Intel PARDISO library, taking full advantage of its memory efficiency and multi-thread features. To reduce overhead, all matrices are stored using the Compressed Storage Row (CSR) format consistent with the requirements of PARDISO's solver (Schenk, et al., 2011).

CHAPTER 3

Basic Data Requirements

This chapter describes the basic data requirements for performing the one-dimensional flow calculations within HEC-RAS. The basic data are defined and discussions of applicable ranges for parameters are provided.

Contents

■ General

■ Geometric Data

■ Steady Flow Data

■ Unsteady Flow Data

General

The main objective of the HEC-RAS program is quite simple - to compute water surface elevations at all locations of interest for either a given set of flow data (steady flow simulation), or by routing hydrographs through the system (unsteady flow simulation). The data needed to perform these computations are divided into the following categories: geometric data; steady flow data; unsteady flow data; sediment data; and water quality data. Geometric data are required for any of the analyses performed within HEC-RAS. The other data types are only required if you are going to do that specific type of analysis (i.e., steady flow data are required to perform a steady flow water surface profile computation). The current version of HEC-RAS can perform either steady or unsteady flow computations.

Geometric Data

The basic geometric data consist of establishing the connectivity of the river system (River System Schematic); cross section data; reach lengths; energy loss coefficients (friction losses, contraction and expansion losses); stream junction information; storage areas; and 2D Flow Areas. Hydraulic structure data (bridges, culverts, spillways, weirs, etc...), which are also considered geometric data, will be described in later chapters.

Study Limit Determination

When performing a hydraulic study, it is normally necessary to gather data both upstream of and downstream of the study reach. Gathering additional data upstream is necessary in order to evaluate any upstream impacts due to construction alternatives that are being evaluated within the study reach (Figure 3-1). The limits for data collection upstream should be at a distance such that the increase in water surface profile resulting from a channel modification converges with the existing conditions profile. Additional data collection downstream of the study reach is necessary in order to prevent any user-defined boundary condition from affecting the results within the study reach. In general, the water surface at the downstream boundary of a model is not normally known. The user must estimate this water surface for each profile to be computed. A common practice is to use Manning's equation and compute normal depth as the starting water surface. The actual water surface may be higher or lower than normal depth. The use of normal depth will introduce an error in the water surface profile at the boundary. In general, for subcritical flow, the error at the boundary will diminish as the computations proceed upstream. In order to prevent any computed errors within the study reach, the unknown boundary condition should be placed far enough downstream such that the computed profile will converge to a consistent answer by the time the computations reach the downstream limit of the study.
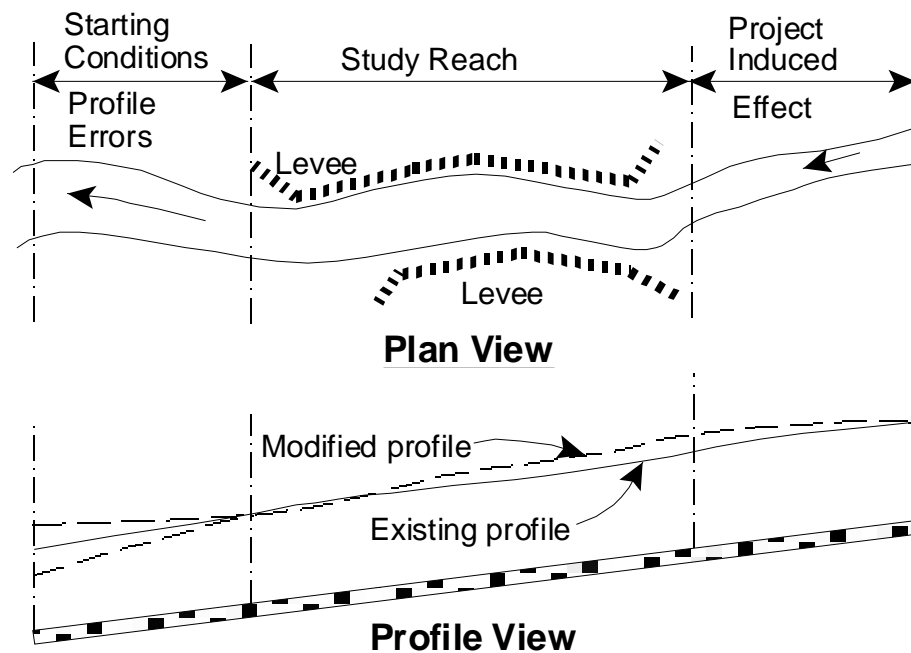
Figure 3-1 Example Study Limit Determination

The River System Schematic

The river system schematic is required for any geometric data set within the HEC-RAS system. The schematic defines how the various river reaches, storage areas, and 2D flow areas are connected, as well as establishing a naming convention for referencing all the other data. The river system schematic is developed by drawing and connecting the various hydraulic elements of the system within the geometric data editor (see Chapter 6 of the HEC-RAS User's Manual for details on how to develop the schematic from within the user interface). The user is required to develop the river system schematic before any other data can be entered.

Each river reach on the schematic is given a unique identifier. As other river reach data are entered, the data are referenced to a specific reach of the schematic. For example, each cross section must have a "River", "Reach" and "River Station" identifier. The river and reach identifiers defines which reach the cross section lives in, while the river station identifier defines where that cross section is located within the reach, with respect to the other cross sections for that reach. The connectivity of reaches is very important in order for the model to understand how the computations should proceed from one reach to the next. The user is required to draw each reach from upstream to downstream, in what is considered to be the positive flow direction. The connecting of reaches is considered a junction. Junctions should only be established at locations where two or more streams come together or split apart. Junctions cannot be established with a single reach flowing into another single reach. These two reaches must be combined and defined as one reach. An example river system schematic is shown in Figure 3-2.
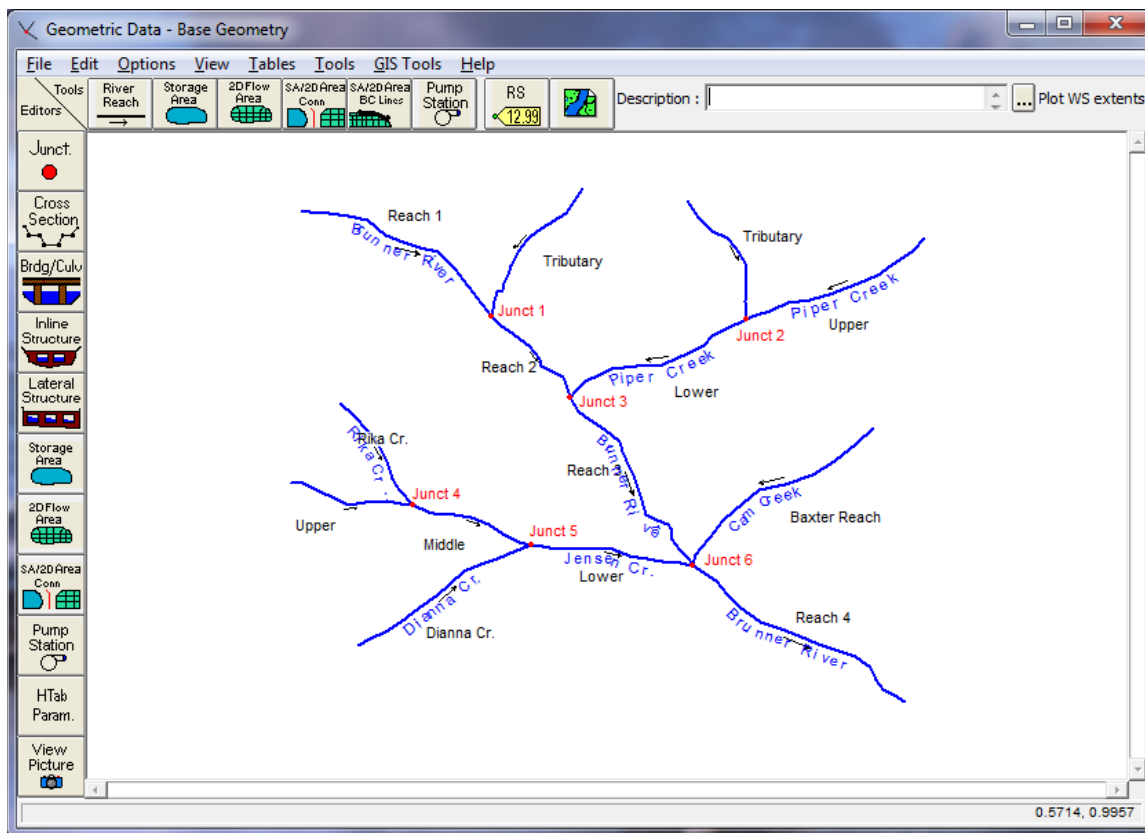
Figure 3-2 Example River System Schematic.

The example schematic shown in Figure 3-2 is for a dendritic river system. Arrows are automatically drawn on the schematic in the assumed positive flow direction. Junctions (red circles) are automatically formed as reaches are connected. As shown, the user is require to provide a river and reach identifier for each reach, as well as an identifier for each junction.

HEC-RAS has the ability to model river systems that range from a single reach model to complicated networks. A "network" model is where river reaches split apart and then come back together, forming looped systems. An example schematic of a looped stream network is shown in Figure 3-3.
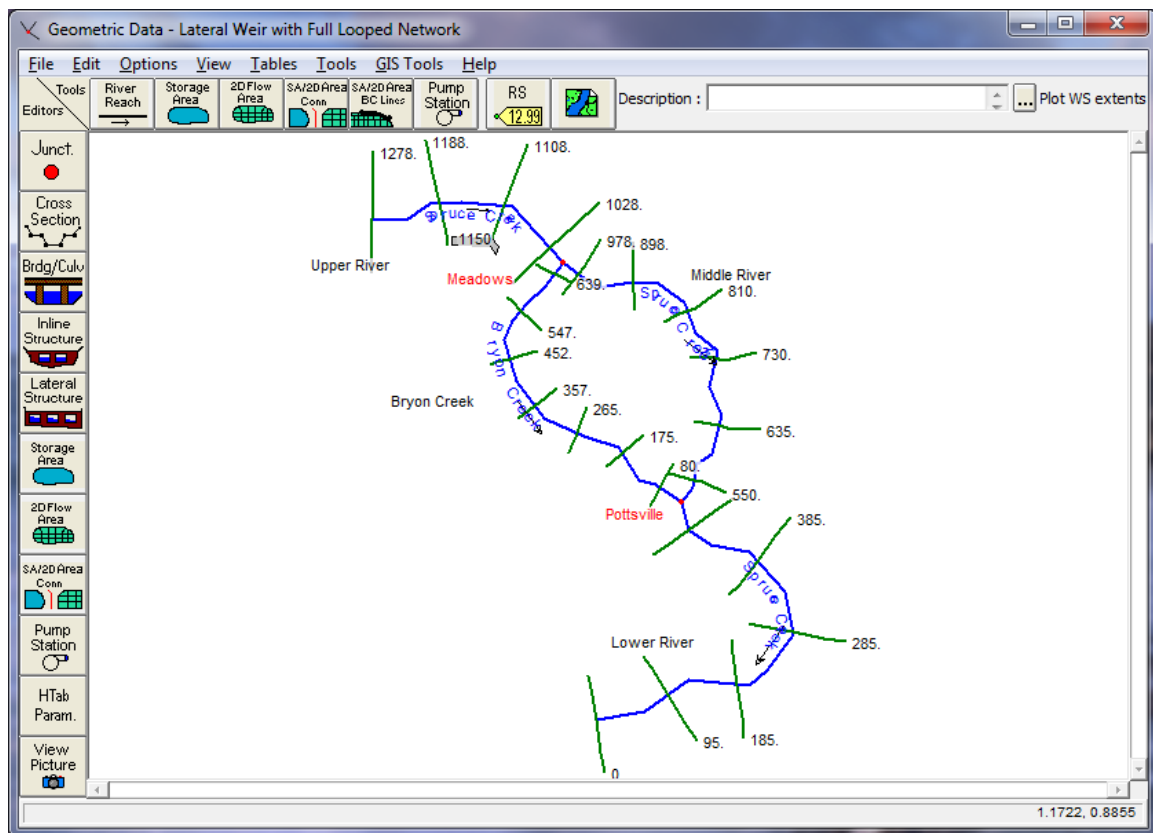
Figure 3-3 Example Schematic for a Looped Network of Reaches

The river system schematic shown in Figure 3-3 demonstrates the ability of HEC-RAS to model flow splits as well as flow combinations. The current version of the steady flow model within HEC-RAS does not determine the amount of flow going to each reach at a flow split, unless the user turns on the split flow optimization option.

Cross Section Geometry

Boundary geometry for the analysis of flow in natural streams is specified in terms of ground surface profiles (cross sections) and the measured distances between them (reach lengths). Cross sections are located at intervals along a stream to characterize the flow carrying capability of the stream and its adjacent floodplain. They should extend across the entire floodplain and should be perpendicular to the anticipated flow lines. Occasionally it is necessary to layout cross-sections in a curved or dog-leg alignment to meet this requirement. Every effort should be made to obtain cross sections that accurately represent the stream and floodplain geometry.

An example of laying out cross sections is shown below in Figure 3-4. The general approach to laying out cross sections is to ensure that the cross sections are perpendicular to the flow lines. This requires an estimation of what the flow lines will look like in the overbank areas away from the main channel. One option is to draw a stream center line down the main channel along what is perceived to be the center of mass of flow. The same thing should be done for the left overbank and the right overbank. The assumed flow paths for the channel and overbank areas are shown as dashed lines in Figure 3-4. These lines will not only help in drawing the cross

sections perpendicular to the flow lines, but they also represent the path for measuring the reach lengths between the cross sections.
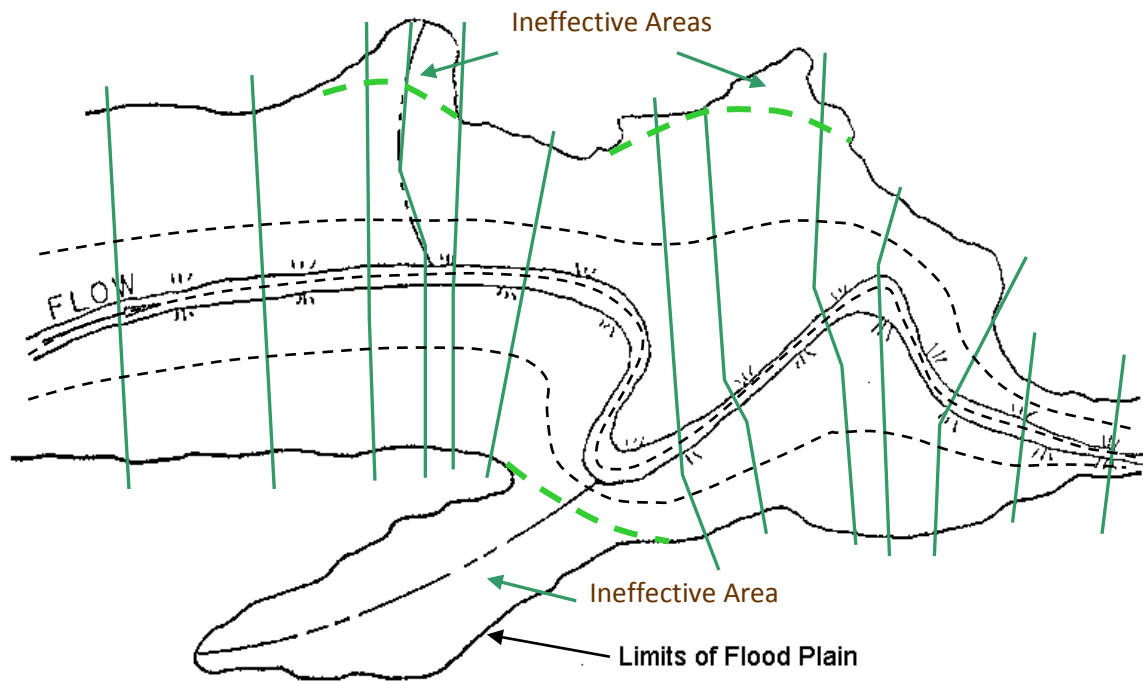
Figure 3-4 Example Cross Section Layout

Cross sections are required at representative locations throughout a stream reach and at locations where changes occur in discharge, slope, shape, or roughness, at locations where levees begin or end and at bridges or control structures such as weirs. Where abrupt changes occur, several cross sections should be used to describe the change regardless of the distance. Cross section spacing is also a function of stream size, slope, and the uniformity of cross section shape. In general, large uniform rivers of flat slope normally require the fewest number of cross sections per mile. The purpose of the study also affects spacing of cross sections. For instance, navigation studies on large relatively flat streams may require closely spaced (e.g., 200 feet) cross sections to analyze the effect of local conditions on low flow depths, whereas cross sections for sedimentation studies, to determine deposition in reservoirs, may be spaced at intervals on the order of thousands of feet.

The choice of friction loss equation may also influence the spacing of cross sections. For instance, cross section spacing may be maximized when calculating an M1 profile (backwater profile) with the average friction slope equation or when the harmonic mean friction slope equation is used to compute M2 profiles (draw down profile). The HEC-RAS software provides the option to let the program select the averaging equation.

Each cross section in an HEC-RAS data set is identified by a River, Reach, and River Station label. The cross section is described by entering the station and elevation (X-Y data) from left to right,

with respect to looking in the downstream direction. The River Station identifier may correspond to stationing along the channel, mile points, or any fictitious numbering system. The numbering system must be consistent, in that the program assumes that higher numbers are upstream and lower numbers are downstream.

Each data point in the cross section is given a station number corresponding to the horizontal distance from a starting point on the left. Up to 500 data points may be used to describe each cross section. Cross section data are traditionally defined looking in the downstream direction. The program considers the left side of the stream to have the lowest station numbers and the right side to have the highest. Cross section data are allowed to have negative stationing values. Stationing must be entered from left to right in increasing order. However, more than one point can have the same stationing value. The left and right stations separating the main channel from the overbank areas must be specified on the cross section data editor. End points of a cross section that are too low (below the computed water surface elevation) will automatically be extended vertically and a note indicating that the cross section had to be extended will show up in the output for that section. The program adds additional wetted perimeter for any water that comes into contact with the extended walls.

Other data that are required for each cross section consist of: downstream reach lengths; roughness coefficients; and contraction and expansion coefficients. These data will be discussed in detail later in this chapter.

Numerous program options are available to allow the user to easily add or modify cross section data. For example, when the user wishes to repeat a surveyed cross section, an option is available from the interface to make a copy of any cross section. Once a cross section is copied, other options are available to allow the user to modify the horizontal and vertical dimensions of the repeated cross section data. For a detailed explanation on how to use these cross section options, see chapter 6 of the HEC-RAS user's manual.

Optional Cross Section Properties

A series of program options are available to restrict flow to the effective flow areas of cross sections. Among these capabilities are options for: ineffective flow areas; levees; and blocked obstructions. All of these capabilities are available from the "Options" menu of the Cross Section Data editor.

Ineffective Flow Areas. This option allows the user to define areas of the cross section that will contain water that is not actively being conveyed (ineffective flow). Ineffective flow areas are often used to describe portions of a cross section in which water will pond, but the velocity of that water, in the downstream direction, is close to zero. This water is included in the storage calculations and other wetted cross section parameters, but it is not included as part of the active flow area. When using ineffective flow areas, no additional wetted perimeter is added to the active flow area. An example of an ineffective flow area is shown in Figure 3-5. The cross-hatched area on the left of the plot represents what is considered to be the ineffective flow.

Two alternatives are available for setting ineffective flow areas. The first option allows the user to define a left station and elevation and a right station and elevation (normal ineffective areas).

When this option is used, and if the water surface is below the established ineffective elevations, the areas to the left of the left station and to the right of the right station are considered ineffective. Once the water surface goes above either of the established elevations, then that specific area is no longer considered ineffective.

The second option allows for the establishment of blocked ineffective flow areas. Blocked ineffective flow areas require the user to enter an elevation, a left station, and a right station for each ineffective block. Up to ten blocked ineffective flow areas can be entered at each cross section. Once the water surface goes above the elevation of the blocked ineffective flow area, the blocked area is no longer considered ineffective.
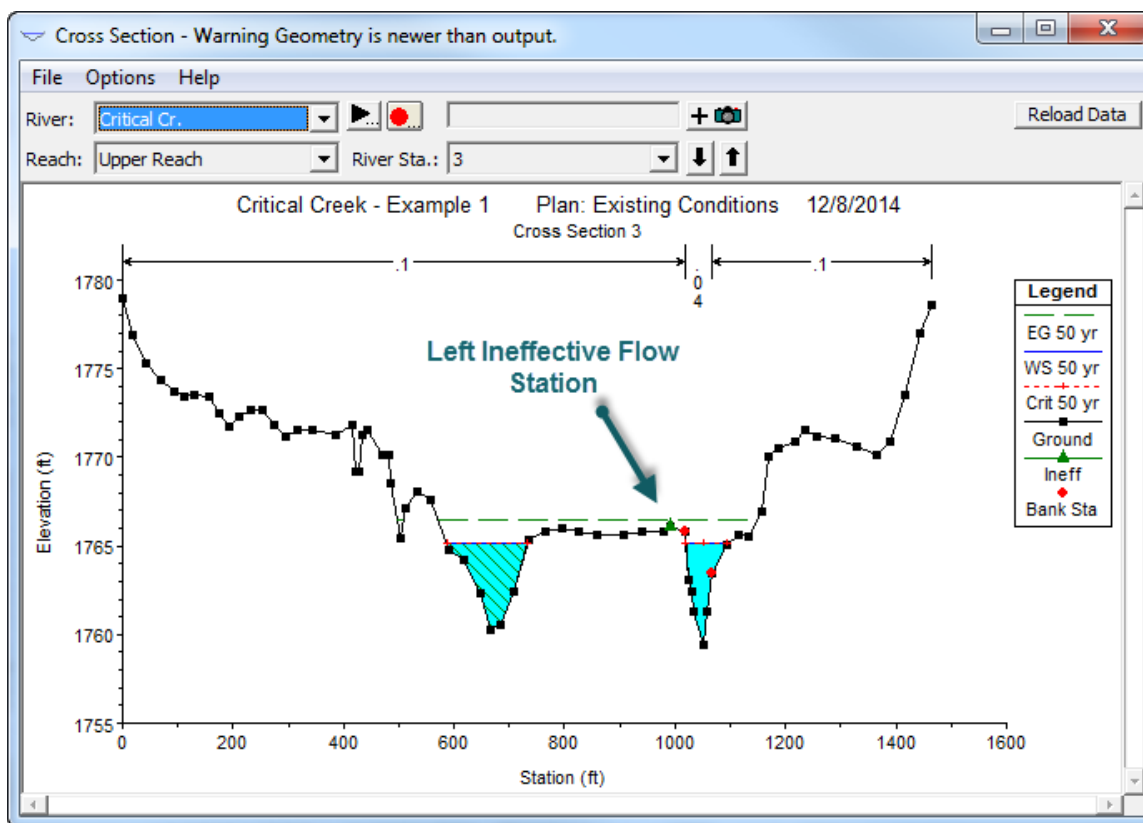
Figure 3-5 Cross section with normal ineffective flow areas

Levees. This option allows the user to establish a left and/or right levee station and elevation on any cross section. When levees are established, no water can go to the left of the left levee station or to the right of the right levee station until either of the levee elevations are exceeded. Levee stations must be defined explicitly, or the program assumes that water can go anywhere within the cross section. An example of a cross section with a levee on the left side is shown in Figure 3-6. In this example the levee station and elevation is associated with an existing point on the cross section

The user may want to add levees into a data set in order to see what effect a levee will have on the water surface. A simple way to do this is to set a levee station and elevation that is above the existing ground. If a levee elevation is placed above the existing geometry of the cross section, then a vertical wall is placed at that station up to the established levee height. Additional wetted perimeter is included when water comes into contact with the levee wall. An example of this is shown in Figure 3-7.
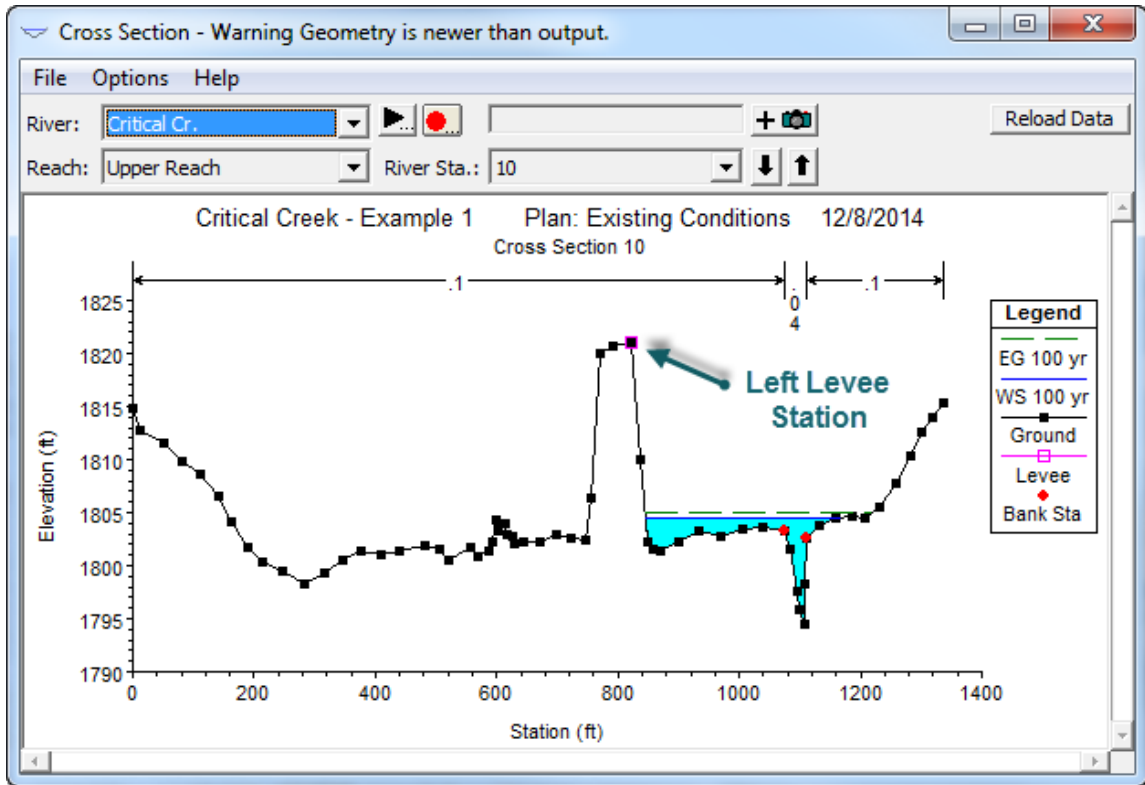
Figure 3-6 Example of the Levee Option
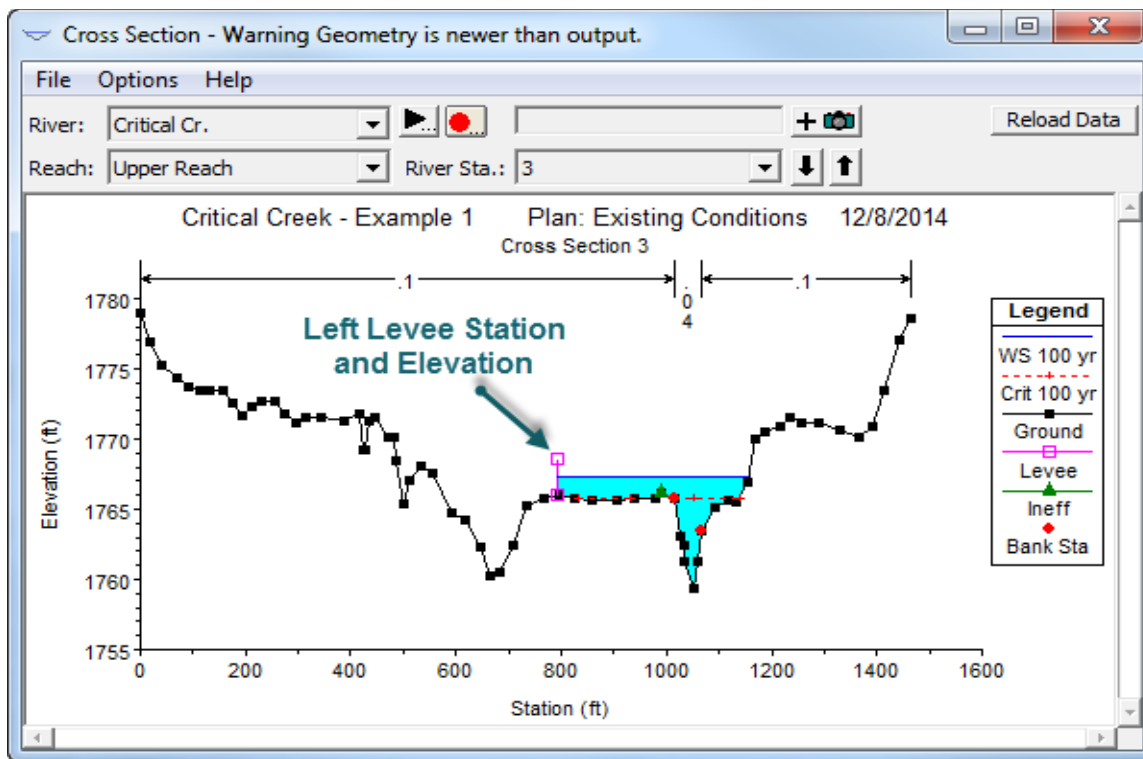
Figure 3-7 Example Levee Added to a Cross Section

Obstructions. This option allows the user to define areas of the cross section that will be permanently blocked out. Obstructions decrease flow area and add wetted perimeter when the water comes in contact with the obstruction. A obstruction does not prevent water from going outside of the obstruction.

Two alternatives are available for entering obstructions. The first option allows the user to define a left station and elevation and a right station and elevation (normal obstructions). When this option is used, the area to the left of the left station and to the right of the right station will be completely blocked out. An example of this type of obstruction is shown in Figure 3-8.
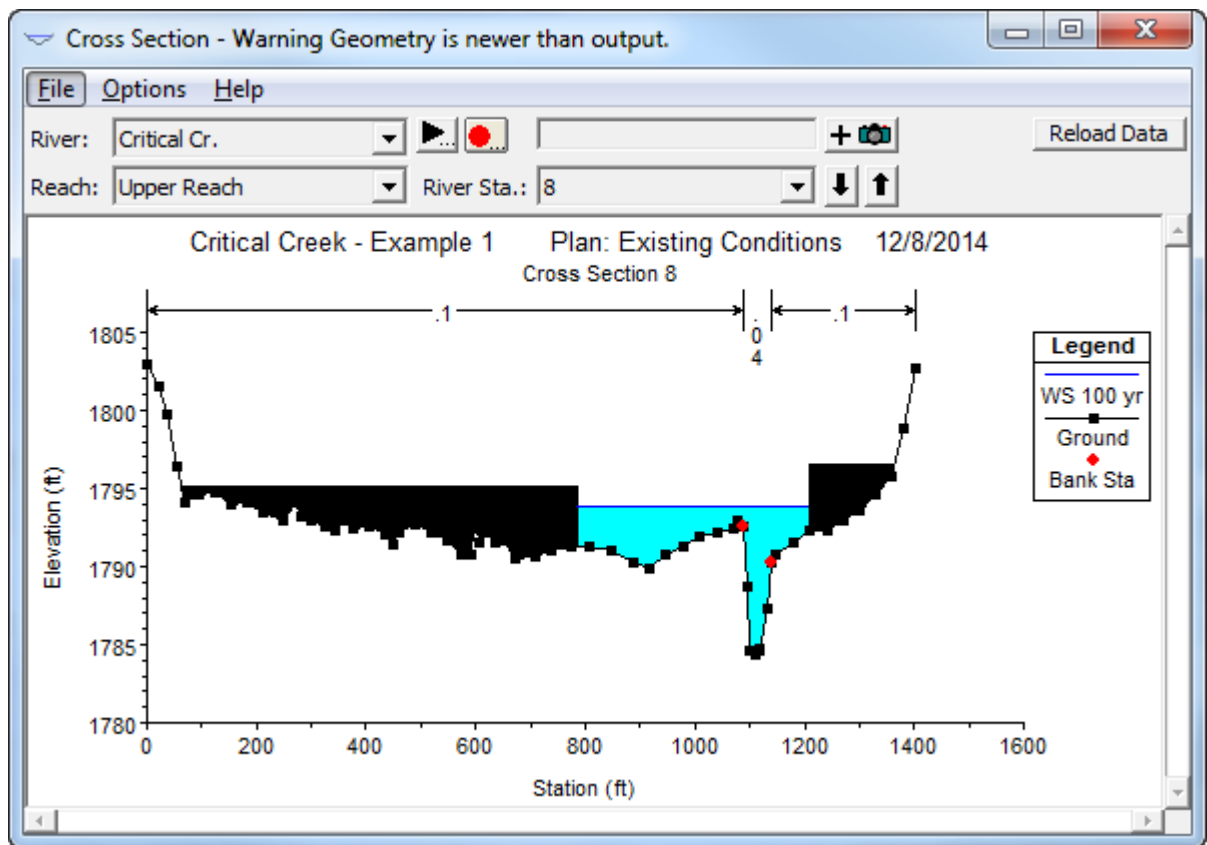
Figure 3-8 Example of Normal Obstructions

The second option, for obstructions, allows the user to enter up to 20 individual blocks (Multiple Blocks). With this option the user enters a left station, a right station, and an elevation for each of the blocks. An example of a cross section with multiple blocked obstructions is shown in Figure 3-9.
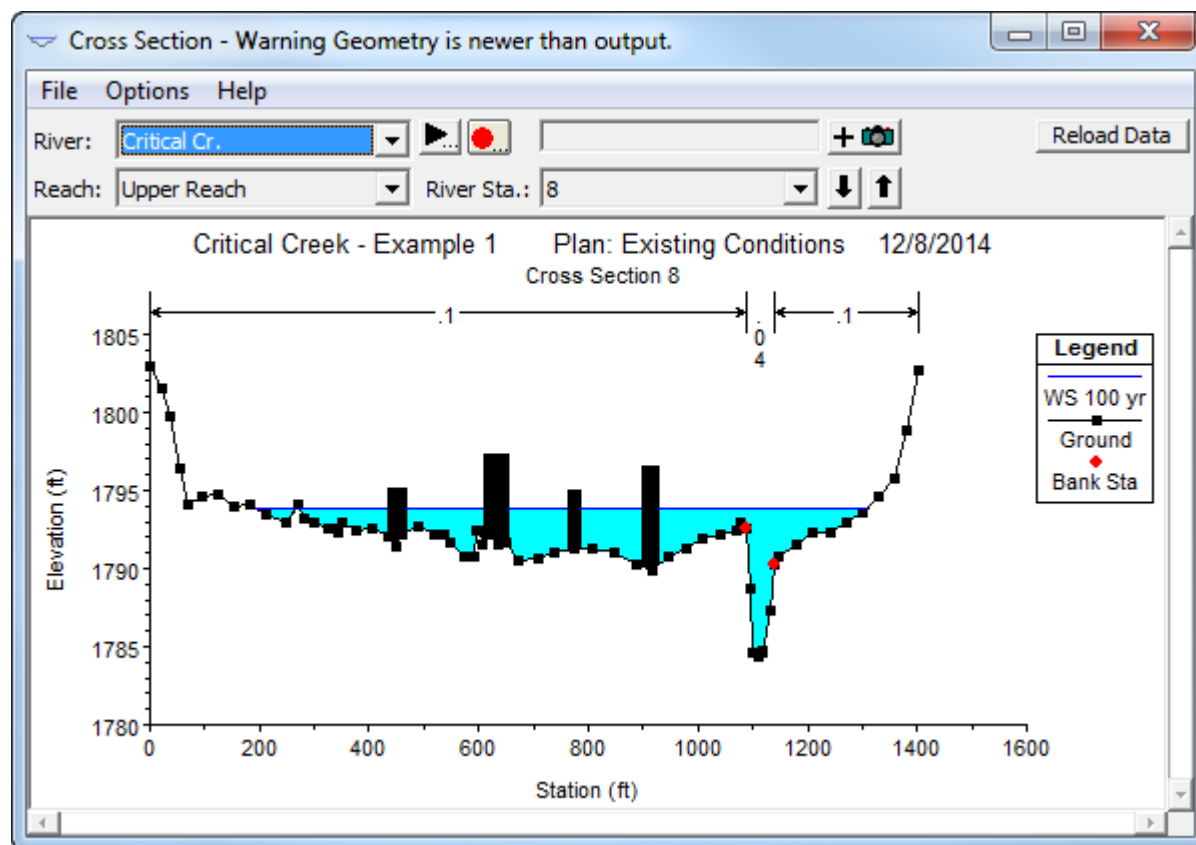
Figure 3-9 Example Cross Section WIth Multiple Blocked Obstructions

Reach Lengths

The measured distances between cross sections are referred to as reach lengths. The reach lengths for the left overbank, right overbank and channel are specified on the cross section data editor. Channel reach lengths are typically measured along the thalweg. Overbank reach lengths should be measured along the anticipated path of the center of mass of the overbank flow. Often, these three lengths will be of similar value. There are, however, conditions where they will differ significantly, such as at river bends, or where the channel meanders and the overbanks are straight. Where the distances between cross sections for channel and overbanks are different, a discharge-weighted reach length is determined based on the discharges in the main channel and left and right overbank segments of the reach (see Equation 2-3, of chapter 2).

Energy Loss Coefficients

Several types of loss coefficients are utilized by the program to evaluate energy losses: (1) Manning's n values or equivalent roughness "k" values for friction loss, (2) contraction and expansion coefficients to evaluate transition (shock) losses, and (3) bridge and culvert loss coefficients to evaluate losses related to weir shape, pier configuration, pressure flow, and

entrance and exit conditions. Energy loss coefficients associated with bridges and culverts will be discussed in chapters 5 and 6 of this manual.

Manning's n. Selection of an appropriate value for Manning's n is very significant to the accuracy of the computed water surface elevations. The value of Manning's n is highly variable and depends on a number of factors including: surface roughness; vegetation; channel irregularities; channel alignment; scour and deposition; obstructions; size and shape of the channel; stage and discharge; seasonal changes; temperature; and suspended material and bedload.

In general, Manning's n values should be calibrated whenever observed water surface elevation information (gaged data, as well as high water marks) is available. When gaged data are not available, values of n computed for similar stream conditions or values obtained from experimental data should be used as guides in selecting n values.

There are several references a user can access that show Manning's n values for typical channels. An extensive compilation of n values for streams and floodplains can be found in Chow's book "Open-Channel Hydraulics" [Chow, 1959]. Excerpts from Chow's book, for the most common types of channels, are shown in Table 3-1 below. Chow's book presents additional types of channels, as well as pictures of streams for which n values have been calibrated.

Table 3-1 Manning's 'n' Values

Type of Channel and Description	Minimum	Normal	Maximum
A. *Natural Streams*			
1. **Main Channels**			
a. Clean, straight, full, no rifts or deep pools	0.025	0.030	0.033
b. Same as above, but more stones and weeds	0.030	0.035	0.040
c. Clean, winding, some pools and shoals	0.033	0.040	0.045
d. Same as above, but some weeds and stones	0.035	0.045	0.050
e. Same as above, lower stages, more ineffective slopes and sections	0.040	0.048	0.055
f. Same as "d" but more stones	0.045	0.050	0.060
g. Sluggish reaches, weedy. deep pools	0.050	0.070	0.080
h. Very weedy reaches, deep pools, or floodways with heavy stands of timber and brush	0.070	0.100	0.150
2. **Flood Plains**			
a. Pasture no brush			
1. Short grass	0.025	0.030	0.035
2. High grass	0.030	0.035	0.050
b. Cultivated areas			
1. No crop	0.020	0.030	0.040
2. Mature row crops	0.025	0.035	0.045
3. Mature field crops	0.030	0.040	0.050
c. Brush			
1. Scattered brush, heavy weeds	0.035	0.050	0.070
2. Light brush and trees, in winter	0.035	0.050	0.060
3. Light brush and trees, in summer	0.040	0.060	0.080
4. Medium to dense brush, in winter	0.045	0.070	0.110
5. Medium to dense brush, in summer	0.070	0.100	0.160
d. Trees			
1. Cleared land with tree stumps, no sprouts	0.030	0.040	0.050
2. Same as above, but heavy sprouts	0.050	0.060	0.080
3. Heavy stand of timber, few down trees, little undergrowth, flow below branches	0.080	0.100	0.120
4. Same as above, but with flow into branches	0.100	0.120	0.160
5. Dense willows, summer, straight	0.110	0.150	0.200
3. **Mountain Streams, no vegetation in channel, banks usually steep, with trees and brush on banks submerged**			
a. Bottom: gravels, cobbles, and few boulders	0.030	0.040	0.050
b. Bottom: cobbles with large boulders	0.040	0.050	0.070

Table 3-1 (Continued) Manning's 'n' Values

Type of Channel and Description	Minimum	Normal	Maximum
B. *Lined or Built-Up Channels*			
1. **Concrete**			
a. Trowel finish	0.011	0.013	0.015
b. Float Finish	0.013	0.015	0.016
c. Finished, with gravel bottom	0.015	0.017	0.020
d. Unfinished	0.014	0.017	0.020
e. Gunite, good section	0.016	0.019	0.023
f. Gunite, wavy section	0.018	0.022	0.025
g. On good excavated rock	0.017	0.020	
h. On irregular excavated rock	0.022	0.027	
2. **Concrete bottom float finished with sides of:**			
a. Dressed stone in mortar	0.015	0.017	0.020
b. Random stone in mortar	0.017	0.020	0.024
c. Cement rubble masonry, plastered	0.016	0.020	0.024
d. Cement rubble masonry	0.020	0.025	0.030
e. Dry rubble on riprap	0.020	0.030	0.035
3. **Gravel bottom with sides of:**			
a. Formed concrete	0.017	0.020	0.025
b. Random stone in mortar	0.020	0.023	0.026
c. Dry rubble or riprap	0.023	0.033	0.036
4. **Brick**			
a. Glazed	0.011	0.013	0.015
b. In cement mortar	0.012	0.015	0.018
5. **Metal**			
a. Smooth steel surfaces	0.011	0.012	0.014
b. Corrugated metal	0.021	0.025	0.030
6. **Asphalt**			
a. Smooth	0.013	0.013	
b. Rough	0.016	0.016	
7. **Vegetal lining**	0.030		0.500

Table 3-1 (Continued) Manning's 'n' Values

Type of Channel and Description	Minimum	Normal	Maximum
C. *Excavated or Dredged Channels*			
1. **Earth, straight and uniform**			
a. Clean, recently completed	0.016	0.018	0.020
b. Clean, after weathering	0.018	0.022	0.025
c. Gravel, uniform section, clean	0.022	0.025	0.030
d. With short grass, few weeds	0.022	0.027	0.033
2. **Earth, winding and sluggish**			
a. No vegetation	0.023	0.025	0.030
b. Grass, some weeds	0.025	0.030	0.033
c. Dense weeds or aquatic plants in deep channels	0.030	0.035	0.040
d. Earth bottom and rubble side	0.028	0.030	0.035
e. Stony bottom and weedy banks	0.025	0.035	0.040
f. Cobble bottom and clean sides	0.030	0.040	0.050
3. **Dragline-excavated or dredged**			
a. No vegetation	0.025	0.028	0.033
b. Light brush on banks	0.035	0.050	0.060
4. **Rock cuts**			
a. Smooth and uniform	0.025	0.035	0.040
b. Jagged and irregular	0.035	0.040	0.050
5. **Channels not maintained, weeds and brush**			
a. Clean bottom, brush on sides	0.040	0.050	0.080
b. Same as above, highest stage of flow	0.045	0.070	0.110
c. Dense weeds, high as flow depth	0.050	0.080	0.120
d. Dense brush, high stage	0.080	0.100	0.140

Other sources that include pictures of selected streams as a guide to n value determination are available (Fasken, 1963; Barnes, 1967; and Hicks and Mason, 1991). In general, these references provide color photos with tables of calibrated n values for a range of flows.

Although there are many factors that affect the selection of the n value for the channel, some of the most important factors are the type and size of materials that compose the bed and banks of a channel, and the shape of the channel. Cowan (1956) developed a procedure for estimating the effects of these factors to determine the value of Manning's n of a channel. In **Cowan's procedure**, the value of n is computed by the following equation:

$$n = (n_b + n_1 + n_2 + n_3 + n_4)m \tag{3-1}$$

Where: n_b =   Base value for n for a straight uniform, smooth channel in natural
materials

n_1 =   Value added to correct for surface irregularities

n_2 =   Value for variations in shape and size of the   channel

n_3 =   Value for obstructions

n_4 =   Value for vegetation and flow conditions

m =   Correction factor to account for meandering of the channel

A detailed description of Cowan's method can be found in "Guide for Selecting Manning's
Roughness Coefficients for Natural Channels and Flood Plains" (FHWA, 1984). This report was
developed by the U.S. Geological Survey (Arcement, 1989) for the Federal Highway
Administration. The report also presents a method similar to Cowan's for developing Manning's
n values for flood plains, as well as some additional methods for densely vegetated flood plains.

Limerinos (1970) related n values to hydraulic radius and bed particle size based on samples
from 11 stream channels having bed materials ranging from small gravel to medium size
boulders. The Limerinos equation is as follows:

$$n = \frac{(0.0926)R^{1/6}}{1.16 + 2.0\log\left(\dfrac{R}{d_{84}}\right)} \tag{3-2}$$

Where: R = Hydraulic radius, in feet (data range was 1.0 to 6.0 feet)

d_{84} = Particle diameter, in feet, that equals or exceeds that of 84 percent of
the particles (data range was 1.5 mm to 250 mm)

The Limerinos equation (3-2) fit the data that he used very well, in that the coefficient of
correlation $\overline{R}^2$ = 0.88 and the standard error of estimates for values of $n/R^{1/6}$ = 0.0087.
Limerinos selected reaches that had a minimum amount of roughness, other than that caused
by the bed material. The Limerinos equation provides a good estimate of the base n value. The
base n value should then be increased to account for other factors, as shown above in Cowen's
method.

Jarrett (1984) developed an equation for high gradient streams (slopes greater than 0.002).
Jarrett performed a regression analysis on 75 data sets that were surveyed from 21 different
streams. Jarrett's equation for Manning's n is as follows:

$$n = 0.39 S^{0.38} R^{-0.16}$$ (3-3)

Where: S =   The friction slope. The slope of the water surface can be used when the friction slope is unknown.

R =   The Hydraulic Radius of the main channel at bank full flow.

Jarrett (1984) states the following limitations for the use of his equation:

1.   The equations are applicable to natural main channels having stable bed and bank materials (gravels, cobbles, and boulders) without backwater.

2.   The equations can be used for slopes from 0.002 to 0.04 and for hydraulic radii from 0.5 to 7.0 feet (0.15 to 2.1 m). The upper limit on slope is due to a lack of verification data available for the slopes of high-gradient streams. Results of the regression analysis indicate that for hydraulic radius greater than 7.0 feet (2.1 m), n did not vary significantly with depth; thus extrapolating to larger flows should not be too much in error as long as the bed and bank material remain fairly stable.

3.   During the analysis of the data, the energy loss coefficients for contraction and expansion were set to 0.0 and 0.5, respectively.

4.   Hydraulic radius does not include the wetted perimeter of bed particles.

5.   These equations are applicable to streams having relatively small amounts of suspended sediment.

Because Manning's n depends on many factors such as the type and amount of vegetation, channel configuration, stage, etc., several options are available in HEC-RAS to vary n. When three n values are sufficient to describe the channel and overbanks, the user can enter the three n values directly onto the cross section editor for each cross section. Any of the n values may be changed at any cross section. Often three values are not enough to adequately describe the lateral roughness variation in the cross section; in this case the "Horizontal Variation of n Value" should be selected from the "Options" menu of the cross section editor. If n values change within the channel, the criterion described in Chapter 2, under composite n values, is used to determine whether the n values should be converted to a composite value using Equation 2-5.

Equivalent Roughness "k". An equivalent roughness parameter "k", commonly used in the hydraulic design of channels, is provided as an option for describing boundary roughness in HEC-RAS. Equivalent roughness, sometimes called "roughness height," is a measure of the linear dimension of roughness elements, but is not necessarily equal to the actual, or even the average, height of these elements. In fact, two roughness elements with different linear dimensions may have the same "k" value because of differences in shape and orientation [Chow, 1959].

The advantage of using equivalent roughness "k" instead of Manning's "n" is that "k" reflects changes in the friction factor due to stage, whereas Manning's "n" alone does not. This influence can be seen in the definition of Chezy's "C" (English units) for a rough channel (Equation 2-6, USACE, 1991):

$$C = 32.6 \log_{10} \left[\frac{12.2R}{k} \right] \qquad (3\text{-}4)$$

Where: C = Chezy roughness coefficient

R = hydraulic radius (feet)

k = equivalent roughness (feet)

Note that as the hydraulic radius increases (which is equivalent to an increase in stage), the friction factor "C" increases. In HEC-RAS, "k" is converted to a Manning's "n" by using the above equation and equating the Chezy and Manning's equations (Equation 2-4, USACE, 1991) to obtain the following:

English Units:

$$n = \frac{1.486 R^{1/6}}{32.6 \, \log_{10} \left[12.2 \dfrac{R}{k} \right]} \qquad (3\text{-}5)$$

Metric Unit:

$$n = \frac{R^{1/6}}{18 \, \log_{10} \left[12.2 \dfrac{R}{k} \right]} \qquad (3\text{-}6)$$

where: n =   Manning's roughness coefficient

Again, this equation is based on the assumption that all channels (even concrete-lined channels) are "hydraulically rough." A graphical illustration of this conversion is available [USACE, 1991].

Horizontal variation of "k" values is described in the same manner as horizontal variation of Manning's "n" values. See chapter 6 of the HEC-RAS user's manual, to learn how to enter k values into the program. Up to twenty values of "k" can be specified for each cross section.

Tables and charts for determining "k" values for concrete-lined channels are provided in EM 1110-2-1601 [USACE, 1991]. Values for riprap-lined channels may be taken as the theoretical spherical diameter of the median stone size. Approximate "k" values [Chow, 1959] for a variety of bed materials, including those for natural rivers are shown in Table 3-2.

Table 3-2

Equivalent Roughness Values of Various Bed Materials

	k
	(Feet)
Brass, Cooper, Lead, Glass	0.0001 - 0.0030
Wrought Iron, Steel	0.0002 - 0.0080
Asphalted Cast Iron	0.0004 - 0.0070
Galvanized Iron	0.0005 - 0.0150
Cast Iron	0.0008 - 0.0180
Wood Stave	0.0006 - 0.0030
Cement	0.0013 - 0.0040
Concrete	0.0015 - 0.0100
Drain Tile	0.0020 - 0.0100
Riveted Steel	0.0030 - 0.0300
Natural River Bed	0.1000 - 3.0000

The values of "k" (0.1 to 3.0 ft.) for natural river channels are normally much larger than the actual diameters of the bed materials to account for boundary irregularities and bed forms.

Contraction and Expansion Coefficients. Contraction or expansion of flow due to changes in the cross section is a common cause of energy losses within a reach (between two cross sections). Whenever this occurs, the loss is computed from the contraction and expansion coefficients specified on the cross section data editor. The coefficients, which are applied between cross sections, are specified as part of the data for the upstream cross section. The coefficients are multiplied by the absolute difference in velocity heads between the current cross section and the next cross section downstream, which gives the energy loss caused by the transition (Equation 2-2 of Chapter 2). Where the change in river cross section is small, and the flow is subcritical, coefficients of contraction and expansion are typically on the order of 0.1 and 0.3, respectively. When the change in effective cross section area is abrupt such as at bridges, contraction and expansion coefficients of 0.3 and 0.5 are often used. On occasion, the coefficients of contraction and expansion around bridges and culverts may be as high as 0.6 and 0.8, respectively. These values may be changed at any cross section. For additional information concerning transition losses and for information on bridge loss coefficients, see chapter 5, Modeling Bridges. Typical values for contraction and expansion coefficients, for subcritical flow, are shown in Table 3-3 below.

Table 3-3

Subcritical Flow Contraction and Expansion Coefficients

	Contraction	Expansion
No transition loss computed	0.0	0.0
Gradual transitions	0.1	0.3
Typical Bridge sections	0.3	0.5
Abrupt transitions	0.6	0.8

The maximum value for the contraction and expansion coefficient is one (1.0). **Note: In general, the empirical contraction and expansion coefficients should be lower for supercritical flow**. In supercritical flow the velocity heads are much greater, and small changes in depth can cause large changes in velocity head. Using contraction and expansion coefficients that would be typical for subcritical flow can result in over estimation of the energy losses and oscillations in the computed water surface profile. In constructed trapezoidal and rectangular channels, designed for supercritical flow, the user should set the contraction and expansion coefficients to zero in the reaches where the cross sectional geometry is not changing shape. In reaches where the flow is contracting and expanding, the user should select contraction and expansion coefficients carefully. Typical values for gradual transitions in supercritical flow would be around 0.01 for the contraction coefficient and 0.03 for the expansion coefficient. As the natural transitions begin to become more abrupt, it may be necessary to use higher values, such as 0.05 for the contraction coefficient and 0.2 for the expansion coefficient. If there is no contraction or expansion, the user may want to set the coefficients to zero for supercritical flow.

Stream Junction Data

Stream junctions are defined as locations where two or more streams come together or split apart. Junction data consists of reach lengths across the junction and tributary angles (only if the momentum equation is selected). Reach lengths across the junction are entered in the Junction Data editor. This allows for the lengths across very complicated confluences (e.g., flow splits) to be accommodated. An example of this is shown in Figure 3-10.

Figure 3-10 Example of a Stream Junction
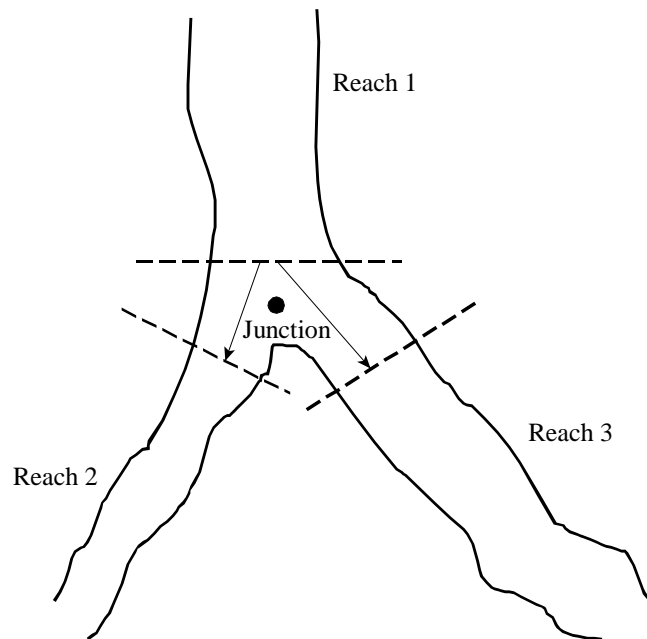
As shown in Figure 3-10, using downstream reach lengths, for the last cross section in Reach 1, would not adequately describe the lengths across the junction. It is therefore necessary to describe lengths across junctions in the Junction Data editor. For the example shown in Figure 3-10, two lengths would be entered. These lengths should represent the average distance that the water will travel from the last cross section in Reach 1 to the first cross section of the respective reaches.

In general, the cross sections that bound a junction should be placed as close together as possible. This will minimize the error in the calculation of energy losses across the junction.

In HEC-RAS, for steady flow hydraulic computations, a junction can be modeled by either the energy equation (Equation 2-1 of chapter 2) or the momentum equation. The energy equation does not take into account the angle of any tributary coming in or leaving the main stream, while the momentum equation does. In most cases, the amount of energy loss due to the angle of the tributary flow is not significant, and using the energy equation to model the junction is more than adequate. However, there are situations where the angle of the tributary can cause significant energy losses. In these situations it would be more appropriate to use the momentum approach. When the momentum approach is selected, an angle for all tributaries of the main stem must be entered. A detailed description of how junction calculations are made can be found in Chapter 4 of this manual.

For Unsteady flow computations, HEC-RAS has two options for the hydraulic computations at a junction. The default option is a very simple assumption that the water surface computed at the downstream side of a flow combining junction, is used for the cross sections just upstream of the junction. If this is not a good assumption (such as for steeper river systems), there is an option to perform an energy balance across the junction in order to compute the upstream water surface elevations.

Steady Flow Data

Steady flow data are required in order to perform a steady water surface profile calculation. Steady flow data consist of: flow regime; boundary conditions; and discharge information (peak flows or flow data from a specific instance in time).

Flow Regime

Profile computations begin at a cross section with known or assumed starting conditions and proceed upstream for subcritical flow or downstream for supercritical flow. The flow regime (subcritical, supercritical, or mixed flow regime) is specified on the Steady Flow Analysis window of the user interface. Subcritical profiles computed by the program are constrained to critical depth or above, and supercritical profiles are constrained to critical depth or below. In cases where the flow regime will pass from subcritical to supercritical, or supercritical to subcritical, the program should be run in a mixed flow regime mode. For a detailed discussion of mixed flow regime calculations, see Chapter 4 of this manual.

Boundary Conditions

Boundary conditions are necessary to establish the starting water surface at the ends of the river system (upstream and downstream). A starting water surface is necessary in order for the program to begin the calculations. In a subcritical flow regime, boundary conditions are only necessary at the downstream ends of the river system. If a supercritical flow regime is going to be calculated, boundary conditions are only necessary at the upstream ends of the river system. If a mixed flow regime calculation is going to be made, then boundary conditions must be entered at all ends of the river system.

The boundary conditions editor contains a table listing every reach. Each reach has an upstream and a downstream boundary condition. Connections to junctions are considered internal boundary conditions. Internal boundary conditions are automatically listed in the table, based on how the river system was defined in the geometric data editor. The user is only required to enter the necessary external boundary conditions. There are four types of boundary conditions available to the user:

Known Water Surface Elevations - For this boundary condition the user must enter a known water surface elevation for each of the profiles to be computed.

Critical Depth - When this type of boundary condition is selected, the user is not required to enter any further information. The program will calculate critical depth for each of the profiles and use that as the boundary condition.

Normal Depth - For this type of boundary condition, the user is required to enter an energy slope that will be used in calculating normal depth (using Manning's equation) at that location. A normal depth will be calculated for each profile based on the user-entered slope. In general, the energy slope can be approximated by using the average slope of the channel, or the average slope of the water surface in the vicinity of the cross section.

Rating Curve - When this type of boundary condition is selected, a pop up window appears allowing the user to enter an elevation versus flow rating curve. For each profile, the elevation is interpolated from the rating curve given the flow, using linear interpolation between the user-entered points.

Whenever the water surface elevations at the boundaries of the study are unknown; and a user defined water surface is required at the boundary to start the calculations; the user must either estimate the water surface, or select normal depth or critical depth. Using an estimated water surface will incorporate an error in the water surface profile in the vicinity of the boundary condition. If it is important to have accurate answers at cross sections near the boundary condition, additional cross sections should be added. If a subcritical profile is being computed, then additional cross sections need only be added below the downstream boundaries. If a supercritical profile is being computed, then additional cross sections should be added upstream of the relevant upstream boundaries. If a mixed flow regime profile is being computed, then cross sections should be added upstream and downstream of all the relevant boundaries. In order to test whether the added cross sections are sufficient for a particular boundary condition, the user should try several different starting elevations at the boundary condition, for the same discharge. If the water surface profile converges to the same answer, by the time the computations get to the cross sections that are in the study area, then enough sections have been added, and the boundary condition is not affecting the answers in the study area.

Discharge Information

Discharge information is required at each cross section in order to compute the water surface profile. Discharge data are entered from upstream to downstream for each reach. At least one flow value must be entered for each reach in the river system. Once a flow value is entered at the upstream end of a reach, it is assumed that the flow remains constant until another flow value is encountered with the same reach. The flow rate can be changed at any cross section within a reach. However, the flow rate cannot be changed in the middle of a bridge, culvert, or stream junction. Flow data must be entered for the total number of profiles that are to be computed.

Unsteady Flow Data

Unsteady flow data are required in order to perform an unsteady flow analysis. Unsteady flow data consists of boundary conditions (external and internal), as well as initial conditions.

Boundary Conditions

Boundary conditions must be established at all of the open ends of the river system being modeled. Upstream ends of a river system can be modeled with the following types of boundary conditions: flow hydrograph (most common upstream boundary condition); stage hydrograph; flow and stage hydrograph. Downstream ends of the river system can be modeled with the following types of boundary conditions: rating curve, normal depth (Manning's equation); stage hydrograph; flow hydrograph; stage and flow hydrograph.

Boundary conditions can also be established at internal locations within the river system. The user can specify the following types of boundary conditions at internal cross sections: lateral inflow hydrograph; uniform lateral inflow hydrograph; groundwater interflow; and Internal Stage and flow hydrograph. Additionally, any gated structures that are defined within the system (inline, lateral, or between storage areas and/or 2D flow areas) could have the following types of boundary conditions in order to control the gates: time series of gate openings; elevation controlled gate; navigation dam; Rules; or internal observed stage and flow.

Initial Conditions

In addition to boundary conditions, the user is required to establish the initial conditions (flow and stage) at all nodes in the system at the beginning of the simulation. Initial conditions can be established in two different ways. The most common way is for the user to enter flow data for each reach, and then have the program compute water surface elevations by performing a steady flow backwater analysis. A second method can only be done if a previous run was made. This method allows the user to write a file of flow and stage from a previous run, which can then be used as the initial conditions for a subsequent run.

In addition to establishing the initial conditions within the river system, the user must define the starting water surface elevation in any storage areas and 2D flow area that are defined. This is accomplished from the initial conditions editor. The user can enter a stage for each storage area within the system. 2D Flow areas have several ways of establishing initial conditions within the 2D flow area.

For more information on unsteady flow data, please review chapter 8 of the HEC-RAS User's manual.

CHAPTER 4

Overview of Optional Capabilities

HEC-RAS has numerous optional capabilities that allow the user to model unique situations. This chapter describes some of the optional capabilities available for performing a hydraulic analysis. For additional steady flow computational options, see Chapter 7. For information on Unsteady Flow computational options, see Chapter 8. Some of the more commonly used option capabilities include (but not limited to): multiple profile analysis; multiple plan analysis; optional friction loss equations; cross section interpolation; mixed flow regime calculations; modeling stream junctions; flow distribution calculations; split flow optimization; pressurized pipe flow; estimating ungaged area inflows.

Contents

■ Multiple Profile Analysis

■ Multiple Plan Analysis

■ Optional Friction Loss Equations

■ Cross Section Interpolation

■ Mixed Flow Regime Calculations

■ Modeling Stream Junctions

■ Flow Distribution Calculations

■ Split Flow Optimization

■ Pressurized Pipe Flow

■ Estimating Ungaged Area Inflows

Multiple Profile Analysis

HEC-RAS can compute up to 25000 profiles, for the same geometric data, within a single execution of the steady flow computations. The number of profiles to be computed is defined as part of the steady flow data. When more than one profile is requested, the user must ensure that flow data and boundary conditions are established for each profile. Once a multiple profile computation is made, the user can view output, in a graphical and tabular mode, for any single profile or combination of profiles.

For an unsteady flow analysis, the user can have detailed output computed for the maximum water surface profile, as well as profiles that represent specific instances in time during the unsteady flow simulation. The user can request detailed output for up to 25000 specific time slices.

Warning, as the number of profiles (steady flow) or time slices (unsteady flow) is increased, the size of the output files will also increase.

Multiple Plan Analysis

The HEC-RAS system has the ability to compute water surface profiles for a number of different characterizations (plans) of the river system. Modifications can be made to the geometry and/or flow data, and then saved in separate files. Plans are then formulated by selecting a particular geometry file and a particular flow file. The multiple plan option is useful when, for example, a comparison of existing conditions and future channel modifications are to be analyzed. Channel modifications can consist of any change in the geometric data, such as: the addition of a bridge or culvert; channel improvements; the addition of levees; changes in n values due to development or changes in vegetation; etc. The multiple plan option can also be used to perform a design of a specific geometric feature. For example, if you were sizing a bridge opening, a separate geometry file could be developed for a base condition (no bridge), and then separate geometry files could be developed for each possible bridge configuration. A plan would then consist of selecting a flow file and one of the geometry files. Computations are performed for each plan individually. Once the computations are performed for all the plans, the user can then view output in a graphical and tabular mode for any single plan or combination of plans.

Optional Friction Loss Equations

This option can be used in both steady flow and unsteady flow water surface profile calculations. The friction loss between adjacent cross sections is computed as the product of the representative rate of friction loss (friction slope) and the weighted-average reach length. The program allows the user to select from the following previously defined friction loss equations:

●   Average Conveyance (Equation 2-13)

●   Average Friction Slope (Equation 2-14)

●   Geometric Mean Friction Slope (Equation 2-15)

●   Harmonic Mean Friction Slope (Equation 2-16)

●   HEC-6 Slope Averaging Method

Any of the above friction loss equations will produce satisfactory estimates provided that reach lengths are not too long. The advantage sought in alternative friction loss formulations is to be able to maximize reach lengths without sacrificing profile accuracy.

Equation 2-13, the average conveyance equation, is the friction loss formulation that has been set as the default method within HEC-RAS. This equation is viewed as giving the best overall results for a range of profile types (M1, M2, etc). Research (Reed and Wolfkill, 1976) indicates that Equation 2-14 is the most suitable for M1 profiles. (Suitability as indicated by Reed and Wolfkill is the most accurate determination of a known profile with the least number of cross sections.) Equation 2-15 is the standard friction loss formulation used in the FHWA/USGS step-backwater program WSPRO (Sherman, 1990). Equation 2-16 has been shown by Reed and Wolfkill to be the most suitable for M2 profiles.

Another feature of this capability is to select the most appropriate of the preceding four equations on a cross section by cross section basis depending on flow conditions (e.g., M1, S1, etc.) within the reach. At present, however, the criteria for this automated method (shown in Table 4-1), does not select the best equation for friction loss analysis in reaches with significant lateral expansion, such as the reach below a contracted bridge opening.

The selection of friction loss equations is accomplished from the Options menu on the Steady Flow Analysis window.

Table 4-1 Criteria Utilized to Select Friction Equation

Profile Type	Is friction slope at current cross section greater than friction slope at preceding cross section?	Equation Used
Subcritical (M1, S1)	Yes	Average Friction Slope (2-14)
Subcritical (M2)	No	Harmonic Mean (2-16)
Supercritical (S2)	Yes	Average Friction Slope (2-14)
Supercritical (M3, S3)	No	Geometric Mean (2-15)

Cross Section Interpolation

Occasionally it is necessary to supplement surveyed cross section data by interpolating cross sections between two surveyed sections. Interpolated cross sections are often required when the change in velocity head is too large to accurately determine the change in the energy gradient. An adequate depiction of the change in energy gradient is necessary to accurately model friction losses as well as contraction and expansion losses. When cross sections are spaced too far apart, the program may end up defaulting to critical depth.

The HEC-RAS program has the ability to generate cross sections by interpolating the geometry between two user entered cross sections. The geometric interpolation routines in HEC-RAS are based on a string model, as shown in Figure 4-1
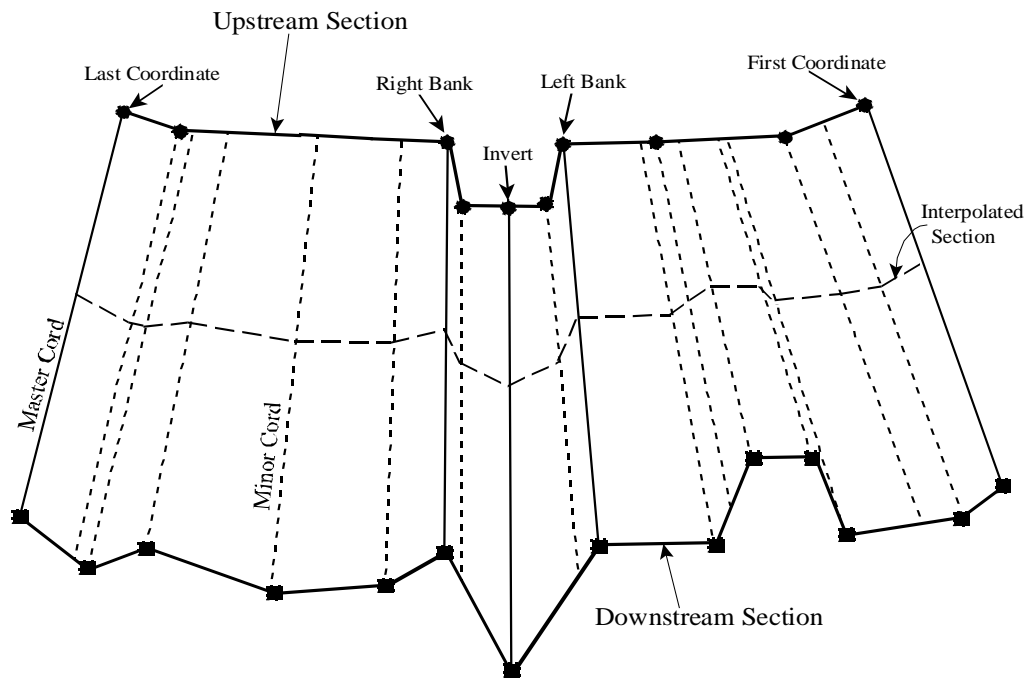
Figure 4-1 String Model for Geometric Cross Section Interpolation

The string model in HEC-RAS consists of cords that connect the coordinates of the upstream and downstream cross sections. The cords are classified as "Master Cords" and "Minor Cords." The master cords are defined explicitly as to the number and starting and ending location of each cord. The default number of master cords is five. The five default master cords are based on the following location criteria:

        1. First coordinate of the cross section (May be equal to left bank).

        2. Left bank of main channel (Required to be a master cord).

        3. Minimum elevation point in the main channel.

        4. Right bank of main channel (Required to be a master cord).

        5. Last coordinate of the cross section (May be equal to right bank).

The interpolation routines are not restricted to a set number of master cords. At a minimum, there must be two master cords, but there is no maximum. Additional master cords can be added by the user. This is explained in Chapter 6 of the HEC-RAS user's manual, under cross section interpolation.

The minor cords are generated automatically by the interpolation routines. A minor cord is generated by taking an existing coordinate in either the upstream or downstream section and establishing a corresponding coordinate at the opposite cross section by either matching an existing coordinate or interpolating one. The station value at the opposite cross section is determined by computing the proportional distance that the known coordinate represents between master chords, and then applying the proportion to the distance between master cords of the opposite section. The number of minor cords will be equal to the sum of all the coordinates in the upstream and downstream sections minus the number of master cords.

Once all the minor cords are computed, the routines can then interpolate any number of sections between the two known cross sections. Interpolation is accomplished by linearly interpolating between the elevations at the ends of a cord. Interpolated points are generated at all of the minor and master cords. The elevation of a particular point is computed by distance weighting, which is based on how far the interpolated cross section is from the user known cross sections.

The interpolation routines will also interpolate roughness coefficients (Manning's n). Interpolated cross section roughness is based on a string model similar to the one used for geometry. Cords are used to connect the breaks in roughness coefficients of the upstream and downstream sections. The cords are also classified as master and minor cords. The default number of master cords is set to four, and are located based on the following criteria:

     1. First coordinate of the cross section (may be equal to left bank).

     2. Left bank of main channel.

     3. Right bank of main channel.

     4. Last coordinate of the cross section (may be equal to right bank).

When either of the two cross sections has more than three n values, additional minor cords are added at all other n value break points. Interpolation of roughness coefficients is then accomplished in the same manner as the geometry interpolation.

In addition to the Manning's n values, the following information is interpolated automatically for each generated cross section: downstream reach lengths; main channel bank stations; contraction and expansion coefficients; normal ineffective flow areas; levees; and normal blocked obstructions. Ineffective flow areas, levees, and blocked obstructions are only interpolated if both of the user-entered cross sections have these features turned on.

Cross section interpolation is accomplished from the user interface. To learn how to perform the interpolation, review the section on interpolating in Chapter 6 of the HEC-RAS user's manual.

Mixed Flow Regime Calculations

The HEC-RAS software has the ability to perform subcritical, supercritical, or mixed flow regime calculations. The Specific Force equation is used in HEC-RAS to determine which flow regime is controlling, as well as locating any hydraulic jumps. The equation for Specific Force is derived from the momentum equation (Equation 2-37). When applying the momentum equation to a very short reach of river, the external force of friction and the force due to the weight of water are very small, and can be ignored. The momentum equation then reduces to the following equation:

$$\frac{Q_1^2 \, \beta_1}{g \, A_1} + A_1 \, \overline{Y}_1 = \frac{Q_2^2 \, \beta_2}{g \, A_2} + A_2 \, \overline{Y}_2 \tag{4-1}$$

Where: Q = Discharge at each section

β = Momentum coefficient (similar to alpha)

A = Total flow area

$\overline{Y}$ = Depth from the water surface to centroid of the area

g = Gravitational acceleration

The two sides of the equation are analogous, and may be expressed for any channel section as a general function:

$$SF = \frac{Q^2 \, \beta}{g \, A} + A\overline{Y} \tag{4-2}$$

The generalized function (equation 4-2) consists of two terms. The first term is the momentum of the flow passing through the channel cross section per unit time. This portion of the equation is considered the dynamic component. The second term represents the momentum of the static component, which is the force exerted by the hydrostatic pressure of the water. Both terms are essentially a force per unit weight of water. The sum of the two terms is called the Specific Force (Chow, 1959).

When the specific force equation is applied to natural channels, it is written in the following manner:

$$SF = \frac{Q^2 \, \beta}{g \, A_m} + A_t \, \overline{Y} \tag{4-3}$$

Where: A_m = Flow area in which there is motion

A_t = Total flow area, including ineffective flow areas

The mixed flow regime calculations for steady flow analysis in HEC-RAS are performed as follows:

1.   First, a subcritical water surface profile is computed starting from a known downstream boundary condition. During the subcritical calculations, all locations where the program defaults to critical depth are flagged for further analysis.

2.   Next the program begins a supercritical profile calculation starting upstream. The program starts with a user specified upstream boundary condition. If the boundary condition is supercritical, the program checks to see if it has a greater specific force than the previously computed subcritical water surface at this location. If the supercritical boundary condition has a greater specific force, then it is assumed to control, and the program will begin calculating a supercritical profile from this section. If the subcritical answer has a greater specific force, then the program begins searching downstream to find a location where the program defaulted to critical depth in the subcritical run. When a critical depth is located, the program uses it as a boundary condition to begin a supercritical profile calculation.

3.   The program calculates a supercritical profile in the downstream direction until it reaches a cross section that has both a valid subcritical and a supercritical answer. When this occurs, the program calculates the specific force of both computed water surface elevations. Whichever answer has the greater specific force is considered to be the correct solution. If the supercritical answer has a greater specific force, the program continues making supercritical calculations in the downstream direction and comparing the specific force of the two solutions. When the program reaches a cross section whose subcritical answer has a greater specific force than the supercritical answer, the program assumes that a hydraulic jump occurred between that section and the previous cross section.

4.   The program then goes to the next downstream location that has a critical depth answer and continues the process.

An example mixed flow profile, from HEC-RAS, is shown in Figure 4-2. This example was adapted from problem 9-8, page 245, in Chow's "Open Channel Hydraulics" (Chow, 1959).
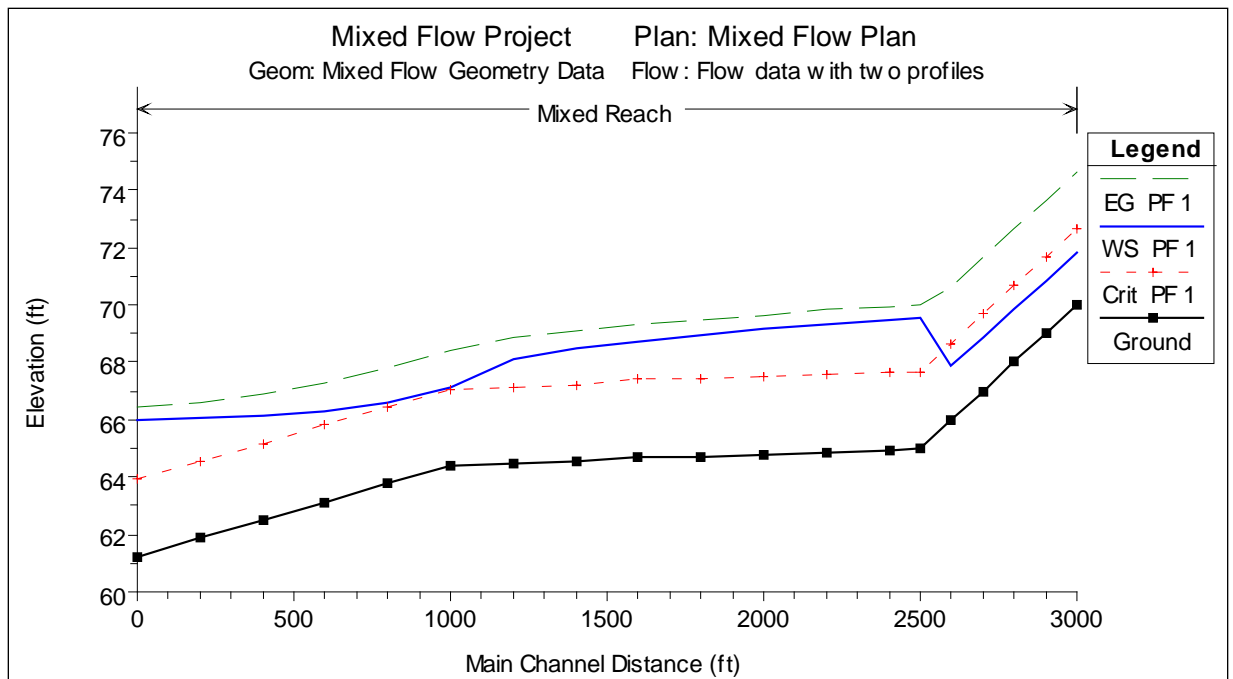
Figure 4-2 Example Mixed Flow Regime Profile from HEC-RAS

As shown in Figure 4-2, the flow regime transitions from supercritical to subcritical just before the first break in slope.

Modeling Stream Junctions

This option is only available for steady flow water surface profile calculations. Stream junctions can be modeled in two different ways within HEC-RAS. The default method is an energy based solution. This method solves for water surfaces across the junction by performing standard step backwater and forewater calculations through the junction. The method does not account for the angle of any of the tributary flows. Because most streams are highly subcritical flow, the influence of the tributary flow angle is often insignificant. If the angle of the tributary plays an important role in influencing the water surface around the junction, then the user should switch to the alternative method available in HEC-RAS, which is a momentum based method. The momentum based method is a one dimensional formulation of the momentum equation, but the angles of the tributaries are used to evaluate the forces associated with the tributary flows. There are six possible flow conditions that HEC-RAS can handle at a junction:

1. Subcritical flow - flow combining

2. Subcritical flow - flow split

3. Supercritical flow - flow combining

4. Supercritical flow- flow split

5. Mixed flow regime - flow combining

6. Mixed flow regime - flow split

The most common situations are the subcritical flow cases (1) and (2). The following is a discussion of how the energy method and the momentum based method are applied to these six flow cases.

Energy Based Junction Method

The energy-based method solves for water surfaces across the junction by performing standard step calculations with the one dimensional energy equation (Equation 2-1). Each of the six cases are discussed individually.

Case 1: Subcritical Flow - Flow Combining.

An example junction with flow combining is shown in Figure 4-3. In this case, subcritical flow calculations are performed up to the most upstream section of reach 3. From here, backwater calculations are performed separately across the junction for each of the two upstream reaches. The water surface at reach 1, station 4.0 is calculated by performing a balance of energy from station 3.0 to 4.0. Friction losses are based on the length from station 4.0 to 3.0 and the average friction slope between the two sections. Contraction or expansion losses are also evaluated across the junction. The water surface for the downstream end of reach 2 is calculated in the same manner. The energy equation from station 3.0 to 4.0 is written as follows:
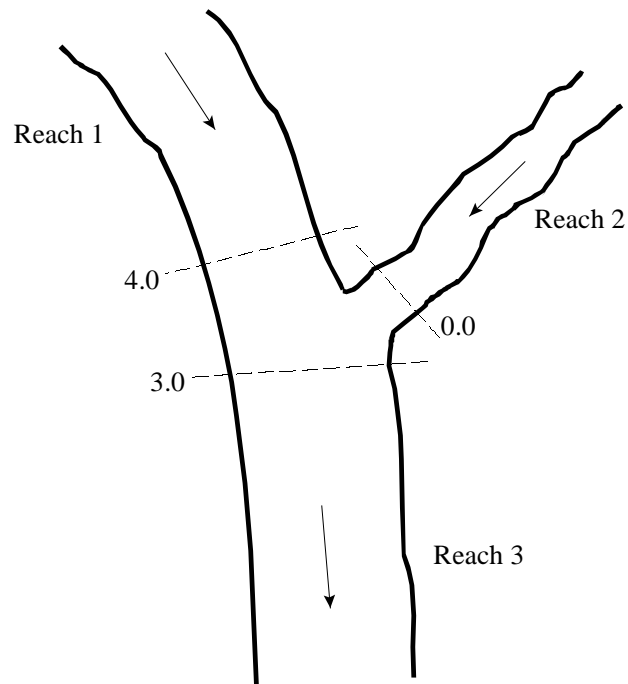
Figure 4-3 Example Junction with Flow Combining.

$$WS_4 + \frac{\alpha_4 V_4^2}{2g} = WS_3 + \frac{\alpha_3 V_3^2}{2g} + L_{4-3}\,\overline{S}_{f_{4-3}} + C\left|\frac{\alpha_4 V_4^2}{2g} - \frac{\alpha_3 V_3^2}{2g}\right| \qquad (4\text{-}4)$$

Case 2: Subcritical Flow - Flow Split

For this case, a subcritical water surface profile is calculated for both reaches 2 and 3, up to river stations 2.0 and 3.0 (see Figure 4-4). The program then calculates the specific force (momentum) at the two locations. The cross section with the greater specific force is used as the downstream boundary for calculating the water surface across the junction at river station 4.0. For example, if cross section 3.0 had a greater specific force than section 2.0, the program will compute a backwater profile from station 3.0 to station 4.0 in order to get the water surface at 4.0.
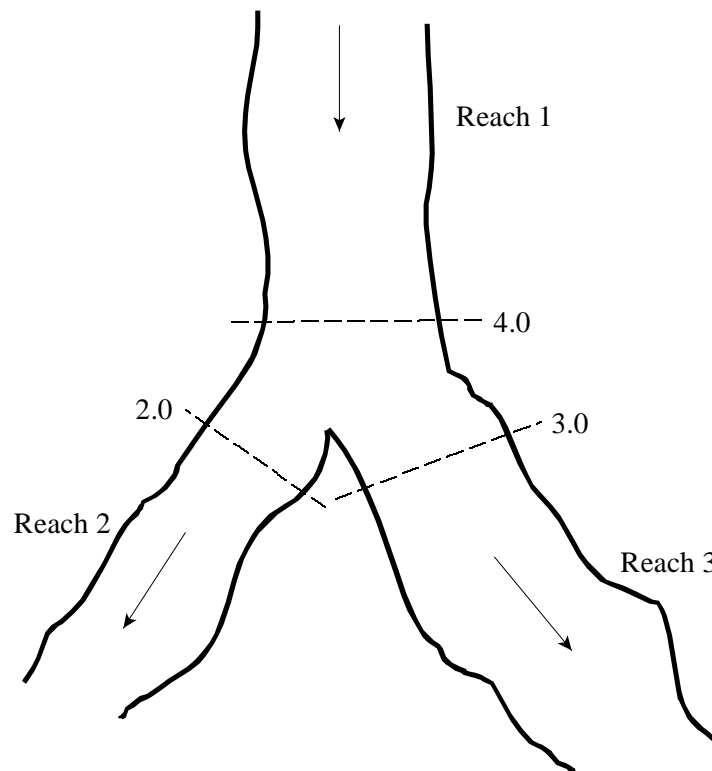
Figure 4-4 Example Flow Split at a Junction

Currently the HEC-RAS program assumes that the user has entered the correct flow for each of the three reaches. In general, the amount of flow going to reach 2 and reach 3 is unknown. In order to obtain the correct flow distribution at the flow split, the user must perform a trial and error process. This procedure involves the following:

1. Assume an initial flow split at the junction.

2. Run the program in order to get energies and water surfaces at all the locations around the junction.

3. Compare the energy at stations 2.0 and 3.0. If they differ by a significant magnitude, then the flow distribution is incorrect. Re-distribute the flow by putting more flow into the reach that had the lower energy.

4. Run the program again and compare the energies. If the energy at stations 2.0 and 3.0 still differ significantly, then re-distribute the flow again.

5. Keep doing this until the energies at stations 2.0 and 3.0 are within a reasonable tolerance.

Ideally it would be better to perform a backwater from station 2.0 to 4.0 and also from station 3.0 to 4.0, and then compare the two computed energies at the same location. Since the program only computes one energy at station 4.0, the user must compare the energies at the

downstream cross sections. This procedure assumes that the cross sections around the junction are spaced closely together.

Case 3: Supercritical Flow - Flow Combining

In this case, a supercritical water surface profile is calculated for all of reach 1 and 2, down to stations 4.0 and 0.0 (see Figure 4-5). The program calculates the specific force at stations 4.0 and 0.0, and then takes the stream with the larger specific force as the controlling stream. A supercritical forewater calculation is made from the controlling upstream section down to station 3.0.
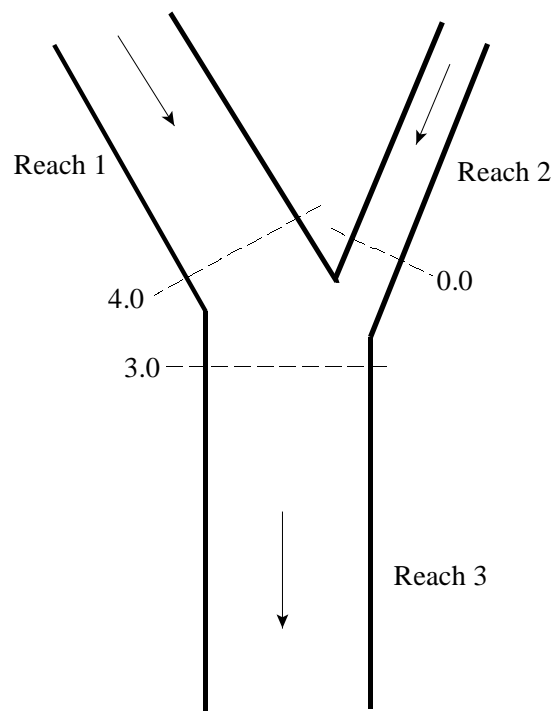
Figure 4-5 Example Supercritical Flow Combine

Case 4: Supercritical Flow - Flow Split

In this case a supercritical water surface profile is calculated down to station 4.0 of reach 1 (see Figure 4-6). The water surfaces at sections 3.0 and 2.0 are calculated by performing separate forewater calculations from station 4.0 to station 2.0, and then from station 4.0 to 3.0.
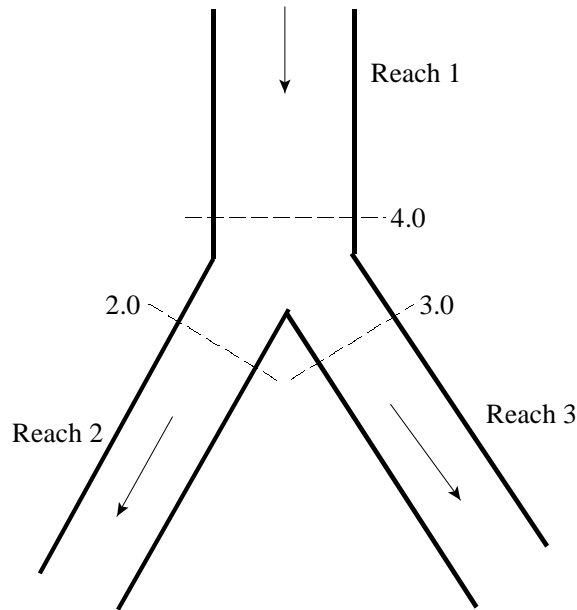
Figure 4-6 Example Supercritical Flow Split

Case 5: Mixed Flow Regime - Flow Combining

In the case of mixed flow, a subcritical profile calculation is made through the junction as described previously (see Figure 4-7). If the flow remains subcritical during the supercritical flow calculations, then the subcritical answers are assumed to be correct. If, however, the flow at either or both of the cross sections upstream of the junction is found to have supercritical flow controlling, then the junction must be re-calculated. When one or more of the upstream sections is supercritical, the program will calculate the specific force of all the upstream sections. If the supercritical sections have a greater specific force than the subcritical sections, then the program assumes that supercritical flow will control. The program then makes a forewater calculation from the upstream section with the greatest specific force (let's say section 4.0) to the downstream section (section 3.0).
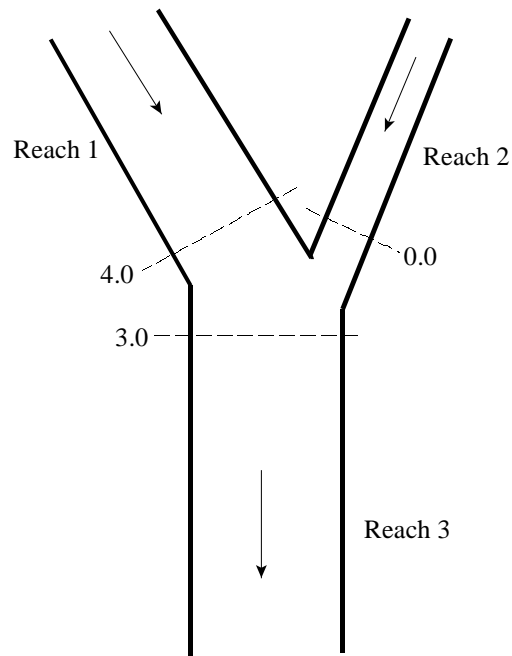
Figure 4-7 Example of Mixed Flow Regime at a Flow Combine

The program next computes the specific force of both the subcritical and supercritical answers at section 3.0. If the supercritical answer at section 3.0 has a lower specific force than the previously computed subcritical answer, then the program uses the subcritical answer and assumes that a hydraulic jump occurred at the junction. If the supercritical answer has a greater specific force, then the program continues downstream with forewater calculations until a hydraulic jump is encountered. Also, any upstream reach that is subcritical must be recomputed. For example, if reach two is subcritical, the water surface at section 0.0 was based on a backwater calculation from section 3.0 to 0.0. If section 3.0 is found to be supercritical, the water surface at section 0.0 is set to critical depth, and backwater calculations are performed again for reach 2. If there are any reaches above reach 2 that are affected by this change, then they are also recomputed.

<u>Case 6</u>: Mixed Flow Regime - Split Flow
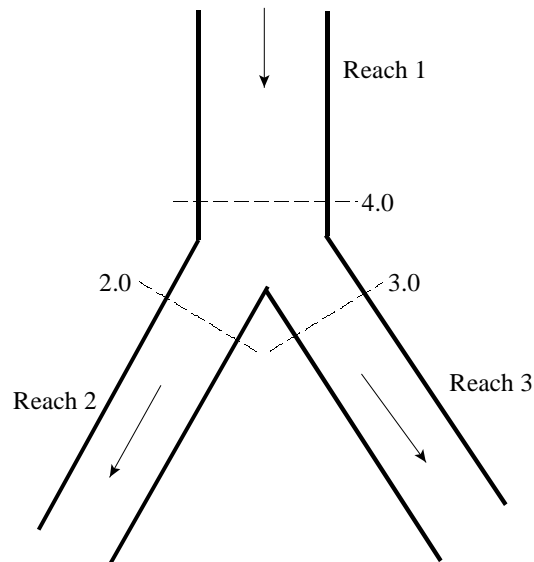
Figure 4-8 Example of Mixed Flow Regime at a Flow Split

In this case, a subcritical profile through the junction is computed as described previously. If during the supercritical flow pass it is found that section 4.0 (Figure 4-8) is actually supercritical, the program will perform forewater calculations across the junction. The program will make a forewater calculation from section 4.0 to 2.0 and then from 4.0 to 3.0. The program will then calculate the specific force of the subcritical and supercritical answers at sections 2.0 and 3.0. Which ever answer has the greater specific force is assumed to be correct for each location. Normal mixed flow regime calculations continue on downstream from the junction.

Momentum Based Junction Method

The user can choose a momentum-based method to solve the junction problem instead of the default energy based method. As described previously, there are six possible flow conditions at the junction. The momentum-based method uses the same logic as the energy based method for solving the junction problem. The only difference is that the momentum-based method solves for the water surfaces across the junction with the momentum equation.

Also, the momentum equation is formulated such that it can take into account the angles at which reaches are coming into or leaving the junction. To use the momentum based method, the user must supply the angle for any reach who's flow lines are not parallel to the main stem's flow lines. An example of a flow combining junction is shown below in Figure 4-9. In this example, angles for both reaches 1 and 2 could be entered. Each angle is taken from a line that is perpendicular to cross-section 3.0 of reach 3.
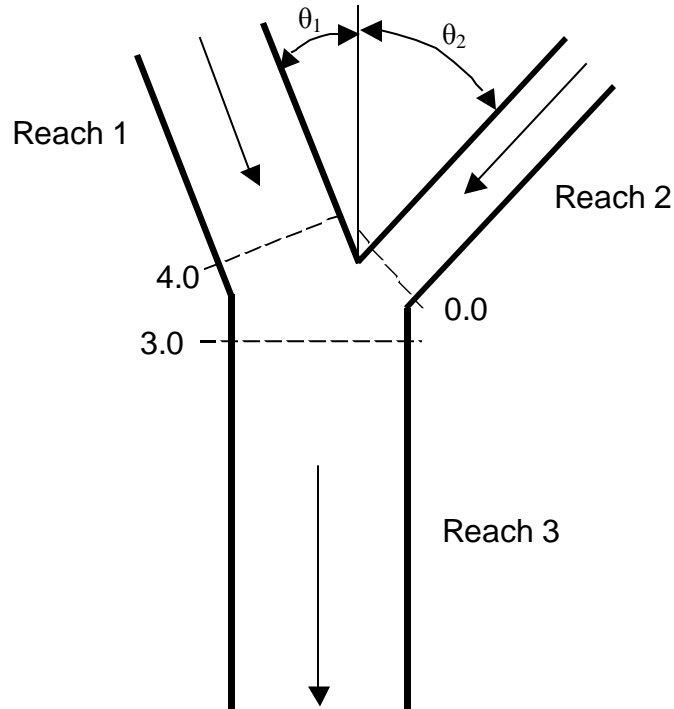
Figure 4-9 Example Geometry for Applying the Momentum Equation to a Flow Combining Junction

For subcritical flow, the water surface is computed up to section 3.0 of reach 3 by normal standard step backwater calculations. If the momentum equation is selected, the program solves for the water surfaces at sections 4.0 and 0.0 by performing a momentum balance across the junction. The momentum balance is written to only evaluate the forces in the X direction (the direction of flow based on cross section 3.0 of reach 3). For this example the equation is as follows:

$$SF_3 = SF_4 \cos\theta_1 - F_{f_{4-3}} + W_{x_{4-3}} + SF_0 \cos\theta_2 - F_{f_{0-3}} + W_{x_{0-3}} \qquad (4\text{-}5)$$

Where: SF = Specific Force (as define in Equation 4-3)

The frictional and the weight forces are computed in two segments. For example, the friction and weight forces between sections 4.0 and 3.0 are based on the assumption that the centroid of the junction is half the distance between the two sections. The first portion of the forces are computed from section 4.0 to the centroid of the junction, utilizing the area at cross section 4.0. The second portion of the forces are computed from the centroid of the junction to section 3.0, using a flow weighted area at section 3.0. The equations to compute the friction and weight forces for this example are as follows:

Forces due to friction:

$$F_{f_{4-3}} = \overline{S}_{f_{4-3}} \frac{L_{4-3}}{2} A_4 \cos \theta_1 + \overline{S}_{f_{4-3}} \frac{L_{4-3}}{2} A_3 \frac{Q_4}{Q_3} \qquad (4\text{-}6)$$

$$F_{f_{0-3}} = \overline{S}_{f_{0-3}} \frac{L_{0-3}}{2} A_0 \cos \theta_2 + \overline{S}_{f_{0-3}} \frac{L_{0-3}}{2} A_3 \frac{Q_0}{Q_3} \qquad (4\text{-}7)$$

Forces due to weight of water:

$$W_{x_{4-3}} = S_{0_{4-3}} \frac{L_{4-3}}{2} A_4 \cos \theta_1 + S_{0_{4-3}} \frac{L_{4-3}}{2} A_3 \frac{Q_4}{Q_3} \qquad (4\text{-}8)$$

$$W_{x_{0-3}} = S_{0_{0-3}} \frac{L_{0-3}}{2} A_0 \cos \theta_2 + S_{0_{0-3}} \frac{L_{0-3}}{2} A_3 \frac{Q_0}{Q_3} \qquad (4\text{-}9)$$

To solve the momentum balance equation (Equation 4-5) for this example, the following assumptions are made:

1. The water surface elevations at section 4.0 and 0.0 are solved simultaneously, and are assumed to be equal to each other. This is a rough approximation, but it is necessary in order to solve Equation 4-5. Because of this assumption, the cross sections around the junction should be closely spaced in order to minimize the error associated with this assumption.

2. The area used at section 3.0 for friction and weight forces is distributed between the upper two reaches by using a flow weighting. This is necessary in order not to double account for the flow volume and frictional area.

When evaluating supercritical flow at this type of junction (Figure 4-9), the water surface elevations at sections 4.0 and 0.0 are computed from forewater calculations, and therefore the water surface elevations at section 3.0 can be solved directly from equation 4-5.

For mixed flow regime computations, the solution approach is the same as the energy based method, except the momentum equation is used to solve for the water surfaces across the junction.

An example of applying the momentum equation to a flow split is shown in Figure 4-10 below:
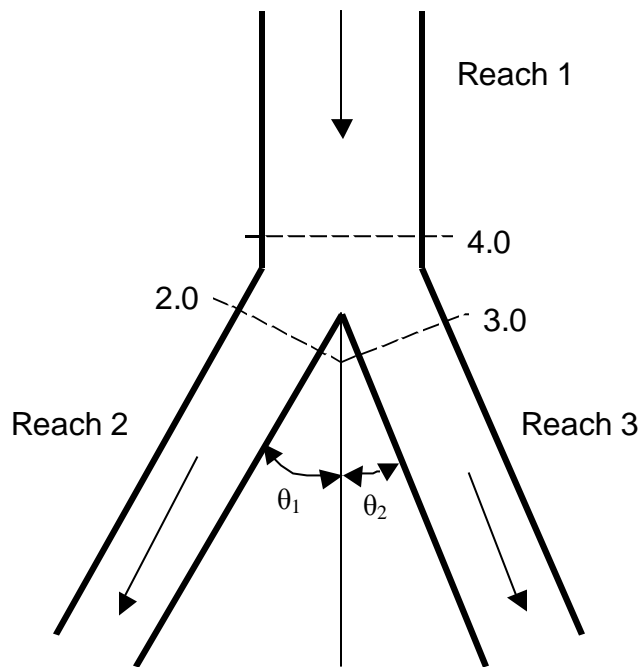
Figure 4-10 Example Geometry for Applying the Momentum Equation

To a Flow Split Type of Junction

For the flow split shown in Figure 4-10, the momentum equation is written as follows:

$$SF_4 = SF_2 \cos\theta_1 + F_{f_{4-2}} - W_{x_{4-2}} + SF_3 \cos\theta_2 \; F_{f_{4-3}} - W_{x_{4-3}}$$
(4-10)

For subcritical flow, the water surface elevation is known at sections 2.0 and 3.0, and the water surface elevation at section 4.0 can be found by solving Equation 4-10. For supercritical flow, the water surface is known at section 4.0 only, and, therefore, the water surface elevations at sections 3.0 and 2.0 must be solved simultaneously. In order to solve Equation 4-10 for supercritical flow, it is assumed that the water surface elevations at sections 2.0 and 3.0 are equal.

Mixed flow regime computations for a flow split are handled in the same manner as the energy based solution, except the momentum equation (Equation 4-10) is used to solve for the water surface elevations across the junction.

Flow Distribution Calculations

The general cross section output shows the distribution of flow in three subdivisions of the cross section: left overbank, main channel, and the right overbank. Additional output, showing the distribution of flow for multiple subdivisions of the left and right overbanks, as well as the main channel, can be requested by the user.

The flow distribution output can be obtained by first defining the locations that the user would like to have this type of output. The user can either select specific locations or all locations in the model. Next, the number of slices for the flow distribution computations must be defined for the left overbank, main channel, and the right overbank. The user can define up to 45 total slices. Each flow element (left overbank, main channel, and right overbank) must have at least one slice. The user can change the number of slices used at each of the cross sections. The final step is to perform the normal profile calculations. During the computations, at each cross section where flow distribution is requested, the program will calculate the flow (discharge), area, wetted perimeter, percentage of conveyance, hydraulic depth, and average velocity for each of the user defined slices.   For further details on how to request and view flow distribution output, see Chapters 7 and 8 of the HEC-RAS User's manual.

The computations for the flow distribution are performed after the program has calculated a water surface elevation and energy by the normal methodology described in Chapter 2 of this manual. The flow distribution computations are performed as follows:

1. First, the water surface is computed in the normal manner of using the three flow subdivisions (left overbank, main channel, and right overbank), and balancing the energy equation.

2. Once a water surface elevation is computed, the program slices the cross section into the user defined flow distribution slices, and then computes an area, wetted perimeter, and hydraulic depth (area over top width) for each slice.

3. Using the originally computed energy slope (Sf), the cross section Manning's n values, the computed area and wetted perimeter for each slice, and Manning's equation, the program computes the conveyance and percentage of discharge for each of the slices.

4. The program sums up the computed conveyance for each of the slices. In general, the slice computed conveyance will not be the same as the originally computed conveyance (from the traditional methods for conveyance subdivision described in Chapter 2 of this manual). Normally, as a cross section is subdivided further and further, the computed conveyance, for a given water surface elevation, will increase.

5. In order to correct for the difference in computed conveyances, the program computes a ratio of the original total conveyance (from the normal calculations) divided by the total slice conveyance. This ratio is then applied

to each of the slices, in order to achieve the same conveyance as was originally computed.

6. The final step is to compute an average velocity for each slice. The average velocity is computed by taking the discharge and dividing by the area for each of the user defined slices.

An example of the flow distribution output is shown in Figure 4-11.

Figure 4-11 Output for the Flow Distribution Option.

In general, the results of the flow distribution computations should be used cautiously. Specifically, the velocities and percentages of discharge are based on the results of a one-dimensional hydraulic model. A true velocity and flow distribution varies vertically as well as horizontally. To achieve such detail, the user would need to use a three-dimensional hydraulic model, or go out and measure the flow distribution in the field. While the results for the flow distribution, provided by HEC-RAS, are better than the standard three subdivisions (left overbank, main channel, and right overbank) provided by the model, the values are still based on average estimates of the one-dimensional results. Also, the results obtained from the flow

distribution option can vary with the number of slices used for the computations. In general, it is better to use as few slices as possible.

Split Flow Optimization

This feature is for Steady Flow Analyses only. The HEC-RAS software has the capability to optimize flow splits at lateral weirs/spillways, hydraulic connections, storage areas, and stream junctions. This feature is available by selecting "Split Flow Optimizations" from the "Options" menu of the Steady Flow Analysis" window.   When this option is selected, a window will appear as shown below.
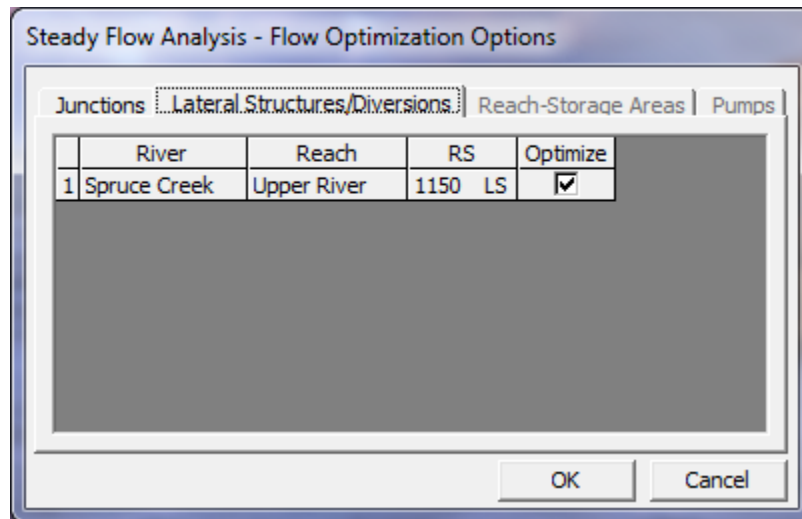
Figure 4-12 Split Flow Optimization Window

When the split flow optimization is turned on, the program will calculate a water surface profile with the first assumed flows. From the computed profile, new flows are calculated for the hydraulic structures and junctions and the profile is re-run. This process continues until the calculated and assumed flows match within a given tolerance. For more information on split flow optimization, please review Example 15 of the Applications Guide.

Pressurized Pipe Flow

HEC-RAS has the ability to model pressurized pipe flow for both steady flow and unsteady flow analyses. Pipes (other than culverts through a roadway, which are handled with the culvert hydraulics routines) can be modeled by using cross sections (to represent the bottom half of the pipe/tunnel) with the Lid option to represent the top of the pipe. An example plot of cross sections with a lid is shown in Figure 4-13.
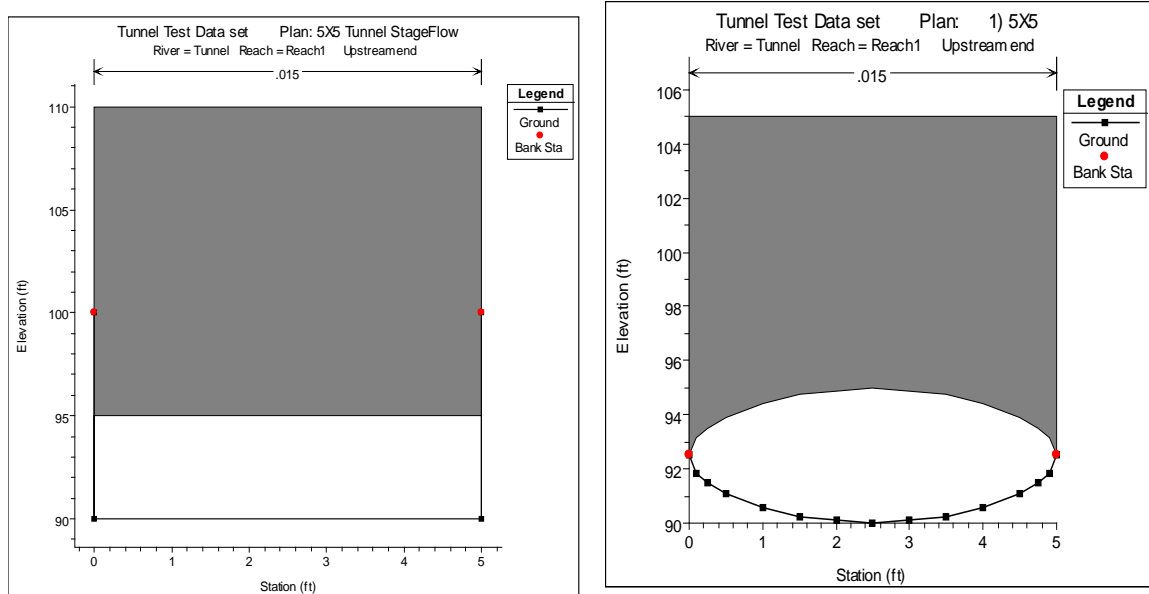
Figure 4-13 Example Cross Sections with Lids

Steady Flow Hydraulics. For a steady flow analyses the program solves the energy equation, just as it normally would for any cross section. The only difference is that the area and wetted perimeter are limited to the open area between the cross section bottom and lid. When the program computes a water surface greater than the top of the open conduit, the water surface line is representative of the hydraulic gradeline. The flow area and wetted perimeter are still being computed from the available open area, but the balance of the energy equation requires the computation to use the hydraulic gradeline instead of the water surface elevation in order to achieve a balance of energy. An example of this is shown in Figure 4-14.
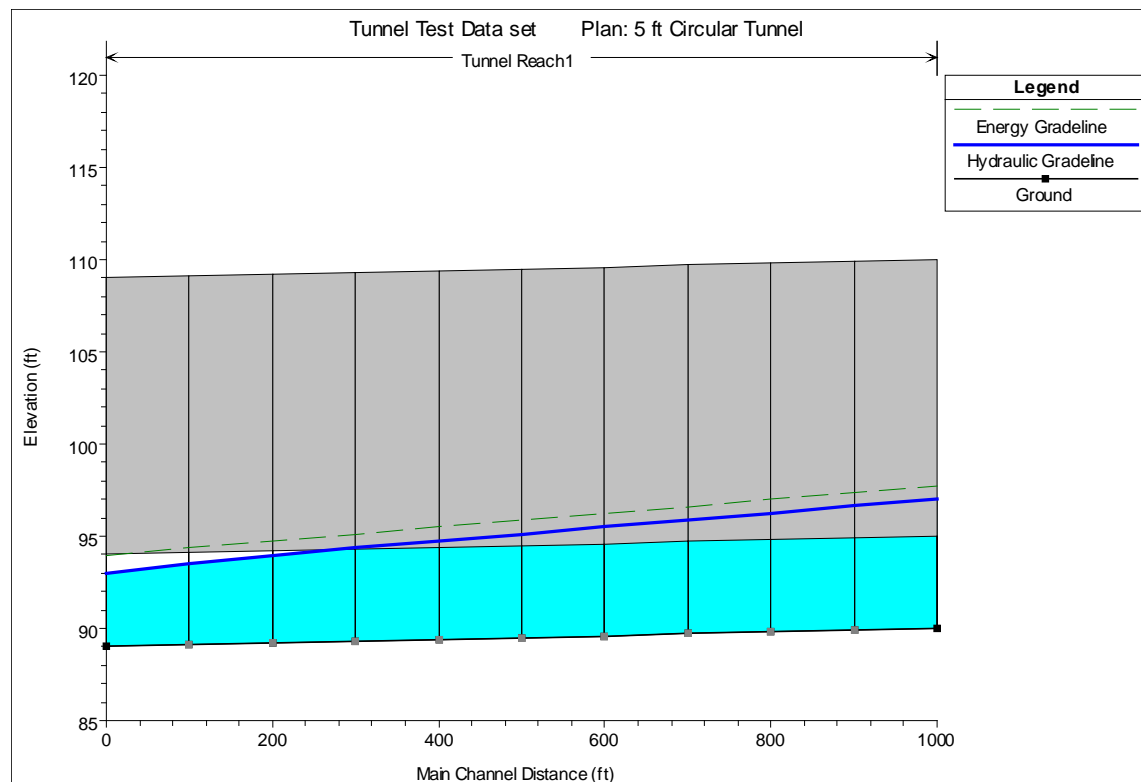
Figure 4-14 Water Surface Profile with Hydraulic Gradeline and Energy

For steady flow hydraulics, the user is not required to turn on any special option to get this to work. Just simply add the lid to any cross sections and this will happen when the energy equation is solved. **Note: If the user does not make the top of the lid high enough, and the hydraulic gradeline (water surface elevation) goes above the top of the lid, the program will use the area above the lid as available flow area.**

Unsteady Flow Hydraulics. For unsteady flow hydraulic computations, the modeling of pressurized conduit flow requires the use of Priessmann Slot theory. Closed conduits can experience both open channel flow and pressure flow within the same pipe. Generally, pressure flow is most often analyzed using waterhammer equations, which are presented below for a circular pipe (Streeter and Wylie, 1979).

Momentum:

$$V\frac{\partial V}{\partial x} + \frac{\partial V}{\partial t} + \frac{1}{\rho}\frac{\partial h}{\partial x} + g\sin\theta + \frac{fV|V|}{2D} = 0 \qquad (4\text{-}11)$$

Continuity:

$$\frac{1}{\rho}\left(V\frac{\partial h}{\partial x}+\frac{\partial h}{\partial t}\right)+a^2\frac{\partial V}{\partial x}=0 \tag{4-12}$$

Where:	V	=	Velocity
	h	=	piezometric head
	ρ	=	fluid density
	g	=	gravity
	θ	=	bed slope
	f	=	Darcy-Weisbach friction factor
	D	=	Pipe diameter
	t	=	time
	x	=	distance

These hyperbolic partial differential equations describe the translation of pressure waves through an elastic medium. Impulses travel at a rate given by the characteristic directions:

$$\frac{dx}{dt}=V\pm a \tag{4-13}$$

Because the wave celerity **a** is on the order of 1000 times larger than the water velocity **V**, the advective terms in equations 14-11 and 14-12 are often dropped and the characteristic directions become (Streeter and Wylie, 1979):

$$\frac{dx}{dt}=\pm a \tag{4-14}$$

For pressure flow, the celerity of an acoustic wave (sound wave) with a correction for elasticity of the conduit material is:

$$a=\left[\frac{\gamma}{g}\left(\frac{1}{K}+\frac{D\,c_1}{E\,e}\right)\right]^{-0.5} \tag{4-15}$$

Where:	γ	=	specific weight of water
	K	=	bulk modulus of elasticity of water
	D	=	Conduit diameter

e	=	conduit thickness
c_1	=	conduit support parameter, typically 0.91
E	=	Young's modulus of elasticity

If the conduit is buried or bored through rock, **e** is large and the elasticity correction becomes insignificant, hence:

$$a = \left(g \, \frac{K}{\gamma} \right)^{0.5}$$

(4-16)

If the bulk modulus of elasticity K is 43.2 x 10^6 lbs/ft², then the celerity a = 4721 ft/s.

The shallow water equations, can be written using velocity V and depth h as the dependent variables.

Momentum:

$$\frac{\partial V}{\partial t} + V \frac{\partial V}{\partial x} + g \frac{\partial h}{\partial x} + g \left(S_f - S_0 \right) = 0$$

(4-17)

Continuity:

$$T_w \frac{\partial h}{\partial t} + V T_w \frac{\partial h}{\partial x} + A \frac{\partial V}{\partial x} = 0$$

(4-18)

Where:	A	=	the cross-sectional area
	T_w	=	Top width of the flow

Like the water hammer equations, these equations are hyperbolic partial differential equations for which the impulses travel at a rate given by characteristic directions:

$$\frac{dx}{dt} = V \pm c$$

(4-19)

In the above equation, c is the celerity of a gravity wave. The celerity of a gravity wave is:

$$c = \sqrt{gD}$$

(4-20)

Where: c   =   the wave celerity

                   D   =   the hydraulic depth, A/T_w

Equations 4-16 and 4-20 are identical except for the values of the wave celerities. Recognizing this fact, Priessmann (Cunge et al., 1980) suggested that pressure waves can be approximated by the shallow water equations if the celerity **c** is set to the acoustic celerity. Priessmann proposed the insertion of a slot of constant width and infinite height above the top of the conduit (Figure 4-15).
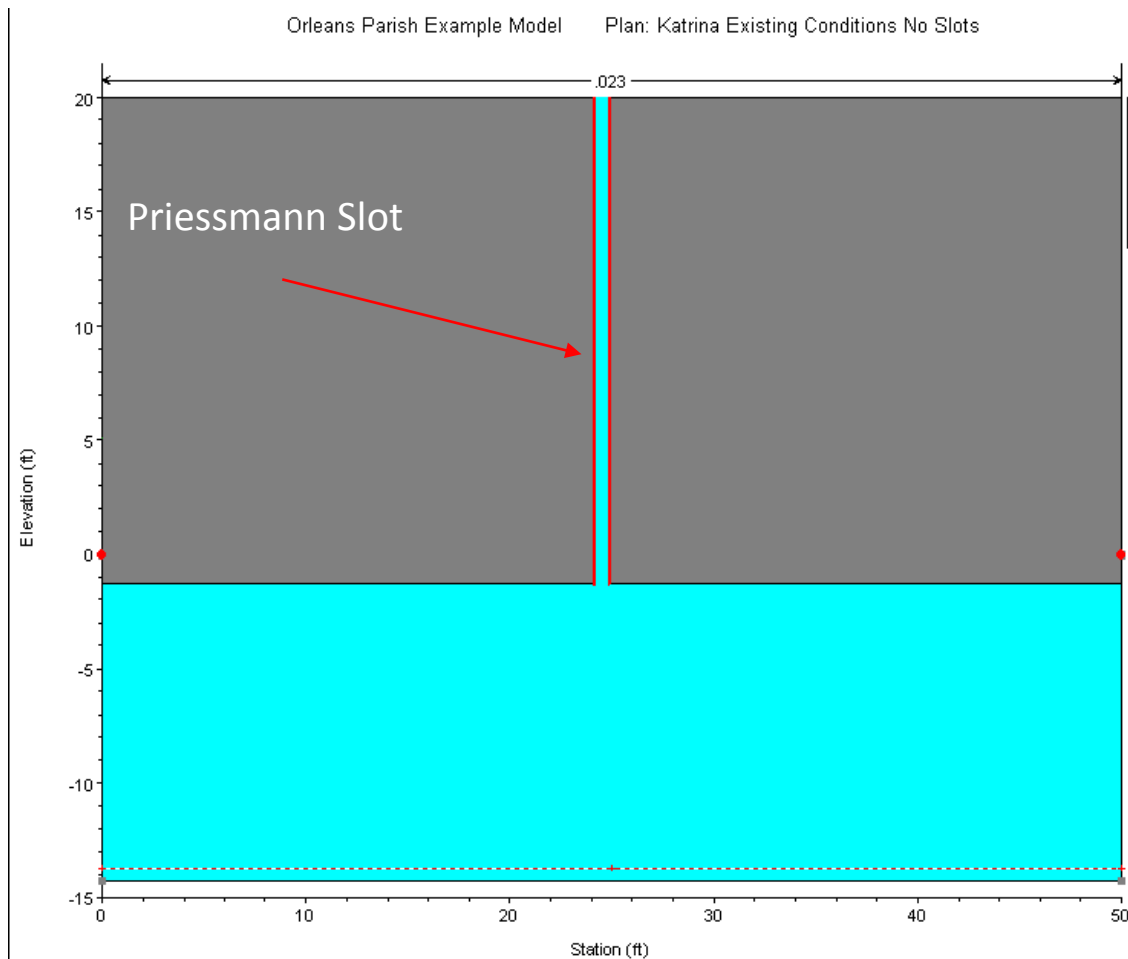
Figure 4-15 Box shaped Pipe with Priessmann Slot.

The width of the slot is determined by equating the wave celerity of a gravity wave (equation 14-20) to the acoustic wave celerity (14-16) and solving for the top width:

$$T_w = \frac{A\gamma}{K} \tag{4-21}$$

In which A is the full flow area of the pipe (not including the slot). Thus the wave celerity of a gravity wave , when the water surface is in the slot, is equivalent to that of an acoustic wave. The procedure has great utility in that both open channel flow and pressure flow can be solved with the same equation set in the same model. The penalty in accuracy is a very slight attenuation due to the increase in area associated with the slot. However, because the total slot area at a head of 200 ft is 2.98 x 10^{-4} times the area, the increase in storage is negligible.

Within HEC-RAS the user can model any shape of pipe by entering the bottom half as a cross section and the top half as the lid. The Priessmann slot method is an option that must be turned on for each cross section that has a lid. To learn how to turn this option on in the User Interface, please review the section called "Modeling Pressurized Pipe Flow" in Chapter 6 of the HEC-RAS User's manual.

During the unsteady flow calculations, as flow transitions from open channel flow to pressure flow, there can be a significant drop in conveyance as the water hits the top of the pipe and pressurizes. This is due to the large increase in wetted perimeter (friction) with little increase in flow area. Thus, the computed conveyance will drop as the water hits the top of the pipe. This drop in conveyance can cause an instability in the numerical solution as flow transitions from open channel flow to pressure flow. Because of this, the conveyance curves computed by HEC-RAS are cut off at the conveyance associated with a full flowing pipe, rather than going up to the theoretical maximum conveyance (right before the pipe pressurizes) and then coming back down to the full flowing pipe value (see Figure 14-16).
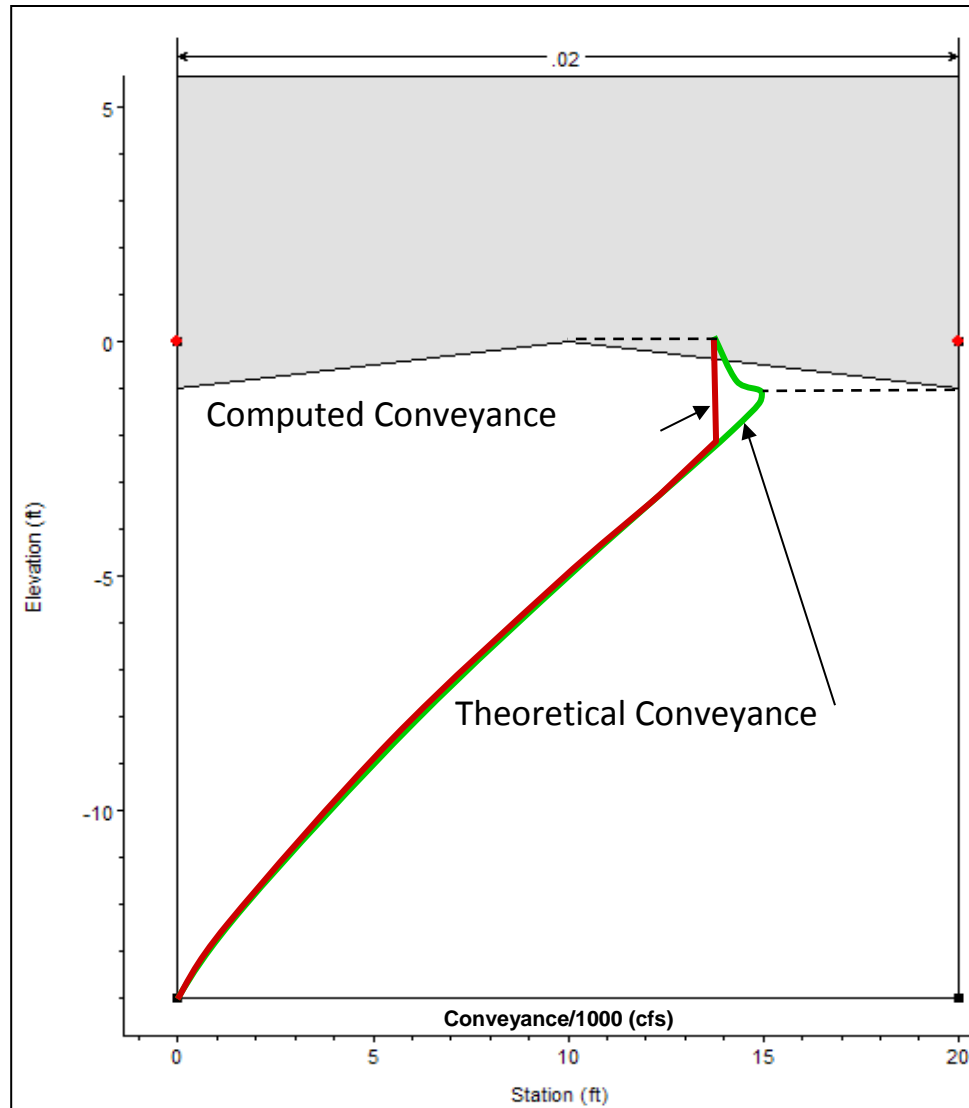
Figure 14-16 Theoretical and Computed Conveyance

Estimating Ungaged Area Inflows

Estimating ungaged inflow is a new feature for HEC-RAS version 4.0. In order to use this option, a given reach must have an upstream hydrograph boundary, a downstream hydrograph boundary, and one or more additional internal boundaries. The internal boundary (or boundaries) is typically a stream gage location. An estimate of the ungaged inflow can be made between the upstream boundary and the gage (or between two gages). The ungaged inflow is estimated by creating a Double Boundary Condition(s) (DBC) at the location of the gage(s) (the UNET program referred to this as a Null Internal Boundary Condition), and breaking the given reach up into one or more "routing reaches." A routing reach is a section of river between two gages, or between a gage and the upstream boundary.

The ungaged inflow is optimized to reproduce either a stage hydrograph or a flow hydrograph at the DBC station. When optimizing the stage hydrograph, the reproduction of flow is secondary, being dependent on the calibration of the model. Similarly, when optimizing the flow hydrograph, the reproduction of stage is secondary, also being dependent on the calibration of the model. Optimizing stage is generally used for flood forecast modeling, where stage accuracy is the primary goal. Optimizing flow is used whenever the observed flow record must be maintained, such as a period of record frequency analysis. In either case, the ungaged inflow compensates for all the errors in the measurement of stage and flow, for systematic changes in roughness and geometry that may not be included in the model, and any other errors in calibration, data, or the numerical solution. Hence, great care should be exercised when using this feature.

In order to compute the ungaged inflow, the user should start with a calibrated HEC-RAS river model. In addition, the user will have to specify: observed internal hydrographs (stage or stage and flow); the location and distribution of the ungaged flows; maximum number of ungaged flow iterations; tolerances; simultaneous or sequential optimization; ungaged hydrograph time interval; and optional maximum and minimum ungaged inflow. (This is covered in detail below.) After the data has been entered, HEC-RAS can compute the ungaged inflow in a single program execution (the program will automatically lag the inflows and rerun the model). The final ungaged lateral inflow hydrograph(s) will be output to DSS. The results can be viewed from inside HEC-RAS, or used with any other DSS compatible program.

Theory

The DBC is inserted between two identical cross-sections that are separated by a small distance (HEC-RAS creates the identical cross-section automatically). Given the small distance, the DBC assumes that the stage and flow at the two cross-sections should be the same; hence, if the upstream cross-section is number j, then

$$Z_j^n = Z_{j+1}^n$$
$$Q_j^n = Q_{j+1}^n \qquad (4\text{-}22)$$

in which Z is the stage and Q is the flow.

When optimizing stage, the river reach is effectively broken into two routing reaches. The stage hydrograph is used as the new downstream boundary for the upstream reach and the stage hydrograph is used as the new upstream boundary for the downstream reach; cross-sections j and $j+1$ are the downstream and upstream boundaries respectively.

When optimizing flow, the flow hydrograph is applied as the upstream boundary at cross-section $j+1$ and serves as the upstream boundary of the downstream reach. The stage hydrograph is still applied at cross-section j and serves as the downstream boundary of the upstream reach.

After running the model, the flow at j is the routed flow from upstream. Since the ungaged inflow is unknown and not entered, the flow at j is missing the ungaged inflow. For the downstream reach, the flow at $j+1$ contains the ungaged inflow. If the flow at $j+1$ is computed from a stage boundary condition, the flow is generated by the hydrodynamics and the geometry of the reach downstream. The ungaged inflow is the difference between the flow hydrographs at j and the flow at $j+1$,

$$Q_U^1 = Q_{j+1}^n - Q_j^n \tag{4-23}$$

in which Q_U^1 is the ungaged inflow for iteration 1.

The ungaged inflow enters between the upstream boundary of the upstream reach and cross-section j, the downstream boundary. To use the ungaged inflow in a model, the program lags the flow backward in time and inserts it in the model as point and/or uniform lateral inflow(s). Point inflow occurs at known ungaged tributaries and the remainder is uniform inflow. The user can delineate any number of point inflows and uniform lateral inflows. The distribution of flow between the inflows must be specified (often this is based on drainage area) and the user must also enter the lag time for each inflow.

The DBC is best used at principal gage locations where the stage or flow records are the most accurate. Generally, these locations are the USGS (U. S. Geological Survey) gaging stations. If a reach includes k interior gages, inserting DBC at each of the gages creates k routing reaches. For example, for the Missouri River between Rulo, Nebraska and St. Charles, Missouri, DBC's are inserted at the USGS gages at St. Joseph, Kansas City, Waverly, Boonville, and Hermann, breaking the model into five routing reaches. Ungaged inflow cannot be optimized between Hermann and St. Charles because St. Charles is a stage gage in the backwater of the Mississippi River.

Optimization of Ungaged Inflow

Ungaged inflow is automatically optimized by the program by successively applying ungaged inflow to the upstream reach. The initial estimate of ungaged inflow is computed using equation 2 and ungaged inflow is successively corrected using:

$$Q_U^k = Q_U^{k-1} + \left(Q_{j+1}^n - Q_j^n\right) \tag{4-24}$$

This iterative procedure usually requires three to five iterations to converge. The user can set the maximum number of iterations.

For a free flowing river, such as the Missouri River, the ungaged inflow can be optimized for the routing reaches simultaneously, since, the flow computation at j+1 is not affected by the ungaged inflow downstream. This procedure is called simultaneous optimization.

For flat streams, when a stage hydrograph is applied, backwater from downstream of the DBC will affect the convergence of the ungaged inflow for the upstream reach. For instance, the flow at cross-section j+1 is computed from the stage hydrograph. If cross-section j+1 is influenced by backwater, the flow changes with the degree of backwater. Hence, the flow at j+1 changes as ungaged inflow is applied downstream, and the optimization of ungaged inflow begins to oscillate. The computed flow at cross-section j+1 is dependent on the ungaged inflow downstream. Generally, this problem occurs on streams with a gradient less than 0.2 feet per mile. Optimizing the routing reaches one routing reach at a time can eliminate this problem. This procedure is called sequential optimization.

Another example is the Illinois River from Lockport to Grafton. Ungaged inflow optimization reaches extend from Lockport to Marseilles TW; Marseilles TW to Kingston Mines; and Kingston Mines to Meredosia. The DBC stations at Marseilles TW and Kingston Mines are influenced by backwater. Meredosia is not affected because ungaged inflow is not optimized downstream. Ungaged inflow from Lockport to Marseilles TW is optimized first, without ungaged inflow in the Marseilles TW to Kingston Mines reach.   Ungaged inflow is then optimized from Marseilles TW to Kingston Mines with the ungaged inflow from Lockport to Marseilles TW. The process is repeated until the ungaged inflow for both reaches converge.

The user can decide whether to use simultaneous or sequential optimization. However, when ungaged inflow is optimized simultaneously, the routed flow hydrograph at cross-section j will have an error. This error can be significant. Sequential optimization corrects these errors as the optimization moves downstream. Therefore, even after simultaneous optimization, the program will still do a sequential optimization to correct the residual errors.

Simultaneous Optimization of Independent Reaches

The steps in simultaneous optimization follows:

1) Observed stage hydrographs and flow hydrographs (if optimizing to flow) are applied at the DBC stations.

2) The model is run.

3) Ungaged inflow is computed upstream of the DBC stations, using equation 2.

4) The ungaged inflow is distributed as point and uniform lateral inflow and lagged backward in time.

5) The program reruns the model.

6) The ungaged inflow is corrected using equation 3.

7) Computed flow is compared at the DBC stations at cross-section j and j+1. If convergence is satisfactory, the simultaneous iteration is concluded. Go to step 9.

8) Iteration continues with step 4.

9) One pass of sequential iteration is performed to correct errors.

Sequential Optimization

The steps in sequential optimization follows:

1) An observed stage hydrograph and a flow hydrographs (if optimizing to flow) are applied at the at the first DBC station. No observed hydrographs are applied at downstream stations.

2) The model is run.

3) Ungaged inflow is calculated for the first reach using equation 2.

4) The program reruns the model and ungaged inflow for the first reach is corrected using equation 3.

5) If the flow hydrographs at cross-sections j and j+1 have converged go to step 7.

6) Go to step 4.

7) Move to the next downstream DBC station. Remove observed hydrographs at all upstream DBC stations. Apply a stage hydrograph and a flow hydrograph (if optimizing to flow) to the DBC station. No observed hydrographs are applied to downstream stations.

8) The program reruns the model.

9) Ungaged inflow is calculated for the first reach using equation 2.

10) The program reruns the model and ungaged inflow for the first reach is corrected using equation 3.

11) If the flow hydrographs at cross-sections j and j+1 have converged go to step 13.

12) Go to step 10.

13) If the last DBC, the iteration is complete. Otherwise go to step 7.

The time interval for the ungaged inflow is based on the Hydrograph Output Interval (see the HEC-RAS Unsteady Flow Analysis editor). For instance, if the Hydrograph Output Interval is one hour, then the ungaged inflow will be computed as a series of hourly flows. The final ungaged inflow hydrograph will also be output to the DSS file at this same time interval. When determining the ungaged inflow, the program will average the flow over the given time interval. For hourly data, for example, the program will average the ungaged inflow for a half hour before and a half hour after the specified time—the 1:00 inflow is the average of the ungaged flow from 12:30 to 1:30.

Short time intervals may, in some instances, cause spikes and dips in the resulting hydrograph. For instance, a one hour time interval might bounce between a high and low flow value. In order to smooth this out, the user can set a time frame to average the flows over (i.e., smoothing window). For example, the user could choose a three hour smoothing window to go along with the one hour hydrograph interval. In this case, the flows will be computed each hour, but each computed flow will be the flow that is averaged from one and a half hours before the specified time until one and a half hours after the specified time.

The user can also enter a minimum and maximum ungaged inflow. This will put limits on the ungaged inflow and may be needed for stability and/or to maintain hydrologically reasonable answers.

The flow tolerance convergence is based on an average least squared difference. For each time step of the unsteady flow model, there is a difference between the computed flow and the known (observed) flow at the gage. This flow difference for each time step is squared and then summed for all of the time steps. The sum is then divided by the number of time steps and, finally, the square root is taken in order to determine an average flow difference over the entire simulation. The unknown inflow is considered to have converged if this flow difference is within the tolerance specified by the user.

CHAPTER 5

Modeling Bridges

HEC-RAS computes energy losses caused by structures such as bridges and culverts in three parts. One part consists of losses that occur in the reach immediately downstream from the structure, where an expansion of flow generally takes place. The second part is the losses at the structure itself, which can be modeled with several different methods. The third part consists of losses that occur in the reach immediately upstream of the structure, where the flow is generally contracting to get through the opening. This chapter discusses how bridges are modeled using HEC-RAS. Discussions include: general modeling guidelines; hydraulic computations through the bridge; selecting a bridge modeling approach; and unique bridge problems and suggested approaches.

Contents

■ General Modeling Guidelines

■ Hydraulic Computations Through the Bridge

■ Selecting a Bridge Modeling Approach

■ Unique Bridge Problems and Suggested Approaches

General Modeling Guidelines

Considerations for modeling the geometry of a reach of river in the vicinity of a bridge are essentially the same for any of the available bridge modeling approaches within HEC-RAS. Modeling guidelines are provided in this section for locating cross sections; defining ineffective flow areas; and evaluating contraction and expansion losses around bridges.

Cross Section Locations

The bridge routines utilize four user-defined cross sections in the computations of energy losses due to the structure. During the hydraulic computations, the program automatically formulates two additional cross sections inside of the bridge structure. A plan view of the basic cross section layout is shown in Figure 5-1. The cross sections in Figure 5-1 are labeled as river stations 1, 2, 3, and 4 for the purpose of discussion within this chapter. Whenever the user is performing water surface profile computations through a bridge (or any other hydraulic structure), additional cross sections should always be included both downstream and upstream of the bridge. This will prevent any user-entered boundary conditions from affecting the hydraulic results through the bridge.

Cross section 1 is located sufficiently downstream from the structure so that the flow is not affected by the structure (i.e., the flow has fully expanded). This distance (the expansion reach length, Le) should be determined by field investigation during high flows, however, is generally not likely that a large event will occur during the scope of your project. Therefore modelers must estimate this distance from known information. The expansion distance will vary depending upon the degree of constriction, the shape of the constriction, the magnitude of the flow, and the velocity of the flow.

Table 5-1 offers ranges of expansion ratios, which can be used for different degrees of constriction, different slopes, and different ratios of the overbank roughness to main channel roughness. Once an expansion ratio is selected, the distance to the downstream end of the expansion reach (the distance Le on Figure 5-1) is found by multiplying the expansion ratio by the average obstruction length (the average of the distances A to B and C to D from Figure 5-1). The average obstruction length is half of the total reduction in floodplain width caused by the two bridge approach embankments. In Table 5-1, b/B is the ratio of the bridge opening width to the total floodplain width, nob is the Manning n value for the overbank, nc is the n value for the main channel, and S is the longitudinal slope. The values in the interior of the table are the ranges of the expansion ratio. For each range, the higher value is typically associated with a higher discharge. The values shown in this table should be used as rough guidance for placing cross section 1, and determining the expansion reach length.

Table 5-1

Ranges of Expansion Ratios

		nob / nc = 1	nob / nc = 2	nob / nc = 4
b/B = 0.10	S = 1 ft/mile	1.4 – 3.6	1.3 – 3.0	1.2 – 2.1
	5 ft/mile	1.0 – 2.5	0.8 – 2.0	0.8 – 2.0
	10 ft/mile	1.0 – 2.2	0.8 – 2.0	0.8 – 2.0
b/B = 0.25	S = 1 ft/mile	1.6 – 3.0	1.4 – 2.5	1.2 – 2.0
	5 ft/mile	1.5 – 2.5	1.3 – 2.0	1.3 – 2.0
	10 ft/mile	1.5 – 2.0	1.3 – 2.0	1.3 – 2.0
b/B = 0.50	S = 1 ft/mile	1.4 – 2.6	1.3 – 1.9	1.2 – 1.4
	5 ft/mile	1.3 – 2.1	1.2 – 1.6	1.0 – 1.4
	10 ft/mile	1.3 – 2.0	1.2 – 1.5	1.0 – 1.4

Figure 5-1 Cross Section Locations at a Bridge

A detailed study of flow contraction and expansion zones has been completed by the Hydrologic Engineering Center entitled "Flow Transitions in Bridge Backwater Analysis" (RD-42, HEC, 1995). The purpose of this study was to provide better guidance to hydraulic engineers performing

water surface profile computations through bridges. Specifically the study focused on determining the expansion reach length, Le; the contraction reach length, Lc; the expansion energy loss coefficient, Ce; and the contraction energy loss coefficient, Cc. A summary of this research, and the final recommendations, can be found in Appendix B of this document.

The user should not allow the distance between cross section 1 and 2 to become so great that friction losses will not be adequately modeled. If the modeler thinks that the expansion reach will require a long distance, then intermediate cross sections should be placed within the expansion reach in order to adequately model friction losses. The ineffective flow option can be used to limit the effective flow area of the intermediate cross sections in the expansion reach.

Cross section 2 is located a short distance downstream from the bridge (i.e., commonly placed at the downstream toe of the road embankment). This cross section should represent the natural ground (main channel and floodplain) just downstream of the bridge or culvert. This section is normally located near the toe of the downstream road embankment. This cross section should **Not** be placed immediately downstream of the face of the bridge deck or the culvert opening (for example some people wrongly place this cross section 1.0 foot downstream of the bridge deck or culvert opening). Even if the bridge has no embankment, this cross section should be placed far enough from the downstream face of the bridge to allow enough distance for some flow expansion due to piers, or pressurized flow coming out of the bridge.

 Cross section 3 should be located a short distance upstream from the bridge (commonly placed at the upstream toe of the road embankment). The distance between cross section 3 and the bridge should only reflect the length required for the abrupt acceleration and contraction of the flow that occurs in the immediate area of the opening. Cross section 3 represents the natural ground of the channel and overbank area just upstream of the road embankment. This section is normally located near the toe of the upstream road embankment. This cross section should **Not** be placed immediately upstream of the bridge deck (for example some people wrongly place this cross section 1.0 foot upstream of the bridge deck). The bridge routines used between cross sections 2 and 3 account for the contraction losses that occur just upstream of the structure (entrance losses). Therefore, this cross section should be place just upstream of the area where the abrupt contraction of flow occurs to get into the bridge opening. This distance will vary with the size of the bridge opening.

Both cross sections 2 and 3 will have ineffective flow areas to either side of the bridge opening during low flow and pressure flow. In order to model only the effective flow areas at these two sections, the modeler should use the ineffective flow area option. This option is selected from the cross section data editor.

Cross section 4 is an upstream cross section where the flow lines are approximately parallel and the cross section is fully effective. In general, flow contractions occur over a shorter distance than flow expansions. The distance between cross section 3 and 4 (the contraction reach length, Lc) should generally be determined by field investigation during high flows. Traditionally, the Corps of Engineers guidance suggests locating the upstream cross section one times the average length of the side constriction caused by the structure abutments (the average of the distance from A to B and C to D on Figure 5-1). The contraction distance will vary

depending upon the degree of constriction, the shape of the constriction, the magnitude of the flow, and the velocity of the flow. As mentioned previously, the detailed study "Flow Transitions in Bridge Backwater Analysis" (RD-42, HEC, 1995) was performed to provide better guidance to hydraulic engineers performing water surface profile computations through bridges. A summary of this research, and the final recommendations, can be found in Appendix B of this document.

During the hydraulic computations, the program automatically formulates two additional cross sections inside of the bridge structure. The geometry inside of the bridge is a combination of the bounding cross sections (sections 2 and 3) and the bridge geometry. The bridge geometry consists of the bridge deck and roadway, sloping abutments if necessary, and any piers that may exist. The user can specify different bridge geometry for the upstream and downstream sides of the structure if necessary. Cross section 2 and the structure information on the downstream side of the bridge are used as the geometry just inside the structure at the downstream end. Cross section 3 and the upstream structure information are used as the bridge geometry just inside the structure at the upstream end. The user has the option to edit these internal bridge cross sections, in order to make adjustments to the geometry.

Defining Ineffective Flow Areas

A basic problem in defining the bridge data is the definition of ineffective flow areas near the bridge structure. Referring to Figure 5-1, the dashed lines represent the effective flow boundary for low flow and pressure flow conditions. Therefore, for cross sections 2 and 3, ineffective flow areas to either side of the bridge opening (along distance AB and CD) should not be included as part of the active flow area for low flow or pressure flow.

The bridge example shown in Figure 5-2 is a typical situation where the bridge spans the entire floodway and its abutments obstruct the natural floodplain. This is a similar situation as was shown in plan view in Figure 5-1. The cross section numbers and locations are the same as those discussed in the "Cross Section Locations" section of this chapter. The problem is to convert the natural ground profile at cross sections 2 and 3 from the cross section shown in part B to that shown in part C of Figure 5-2. The elimination of the ineffective overbank areas can be accomplished by redefining the geometry at cross sections 2 and 3 or by using the natural ground profile and requesting the program's ineffective area option to eliminate the use of the overbank area (as shown in part C of Figure 5-2). Also, for high flows (flows over topping the bridge deck), the area outside of the main bridge opening may no longer be ineffective, and will need to be included as active flow area. If the modeler chooses to redefine the cross section, a fixed boundary is used at the sides of the cross section to contain the flow, when in fact a solid boundary is not physically there. The use of the ineffective area option is more appropriate and it does not add wetted perimeter to the active flow boundary above the given ground profile.
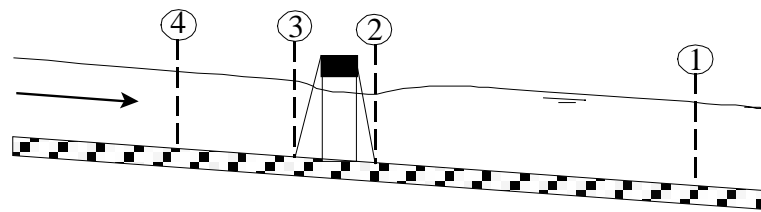
A. Channel Profile and cross section locations
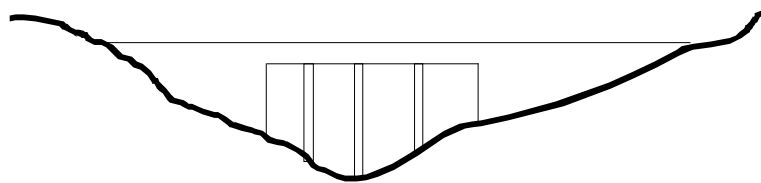
B. Bridge cross section on natural ground
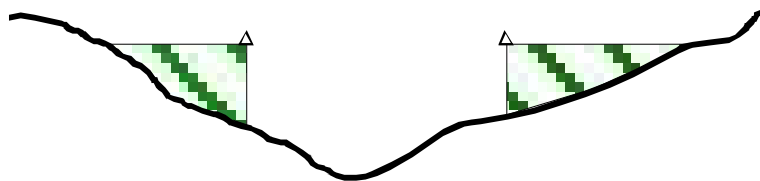
C. Portion of cross sections 2 & 3 that is ineffective for low flow

Figure 5-2 Cross Sections Near Bridges

The ineffective area option is used at sections 2 and 3 to keep all the active flow in the area of the bridge opening until the elevations associated with the left and/or right ineffective flow areas are exceeded by the computed water surface elevation. The program allows the stations and controlling elevations of the left and right ineffective flow areas to be specified by the user. Also, the stations of the ineffective flow areas do not have to coincide with stations of the ground profile, the program will interpolate the ground station.

The ineffective flow areas should be set at stations that will adequately describe the active flow area at cross sections 2 and 3. In general, these stations should be placed outside the edges of the bridge opening to allow for the contraction and expansion of flow that occurs in the immediate vicinity of the bridge. On the upstream side of the bridge (section 3) the flow is contracting rapidly. A practical method for placing the stations of the ineffective flow areas is to assume a 1:1 contraction rate in the immediate vicinity of the bridge. In other words, if cross section 3 is 10 feet from the upstream bridge face, the ineffective flow areas should be placed 10 feet away from each side of the bridge opening. On the downstream side of the bridge (section 2), a similar assumption can be applied. The active flow area on the downstream side of the bridge may be less than, equal to, or greater than the width of the bridge opening. As

flow converges into the bridge opening, depending on the abruptness of the abutments, the active flow area may constrict to be less than the bridge opening. As the flow passes through and out of the bridge it begins to expand. Because of this phenomenon, estimating the stationing of the ineffective flow areas at cross section 2 can be very difficult. In general, the user should make the active flow area equal to the width of the bridge opening or wider (to account for flow expanding), unless the bridge abutments are very abrupt (vertical wall abutments with no wing walls).

The elevations specified for ineffective flow should correspond to elevations where significant weir flow passes over the bridge. For the downstream cross section, the threshold water surface elevation for weir flow is not usually known on the initial run, so an estimate must be made. An elevation below the minimum top-of-road, such as an average between the low chord and minimum top-of-road, can be used as a first estimate.

Using the ineffective area option to define the ineffective flow areas allows the overbank areas to become effective as soon as the ineffective area elevations are exceeded. The assumption is that under weir flow conditions, the water can generally flow across the whole bridge length and the entire overbank in the vicinity of the bridge would be effectively carrying flow up to and over the bridge. If it is more reasonable to assume only part of the overbank is effective for carrying flow when the bridge is under weir flow, then the overbank n values can be increased to reduce the amount of conveyance in the overbank areas under weir flow conditions.

Cross section 3, just upstream from the bridge, is usually defined in the same manner as cross section 2. In many cases the cross sections are identical. The only difference generally is the stations and elevations to use for the ineffective area option. For the upstream cross section, the elevation should initially be set to the low point of the top-of-road. When this is done the user could possibly get a solution where the bridge hydraulics are computing weir flow, but the upstream water surface elevation comes out lower than the top of road. Both the weir flow and pressure flow equations are based on the energy grade line in the upstream cross section. Once an upstream energy is computed from the bridge hydraulics, the program tries to compute a water surface elevation in the upstream cross section that corresponds to that energy. Occasionally the program may get a water surface that is confined by the ineffective flow areas and lower than the minimum top of road. When this happens, the user should decrease the elevations of the upstream ineffective flow areas in order to get them to turn off. Once they turn off, the computed water surface elevation will be much closer to the computed energy gradeline (which is higher than the minimum high chord elevation).

Using the ineffective area option in the manner just described for the two cross sections on either side of the bridge provides for a constricted section when all of the flow is going under the bridge. When the water surface is higher than the control elevations used, the entire cross section is used. The program user should check the computed solutions on either side of the bridge section to ensure they are consistent with the type of flow. That is, for low flow or pressure flow solutions, the output should show the effective area restricted to the bridge opening. When the bridge output indicates weir flow, the solution should show that the entire cross section is effective. During overflow situations, the modeler should ensure that the overbank flow around the bridge is consistent with the weir flow.

Contraction and Expansion Losses

Losses due to contraction and expansion of flow between cross sections are determined during the standard step profile calculations. Manning's equation is used to calculate friction losses, and all other losses are described in terms of a coefficient times the absolute value of the change in velocity head between adjacent cross sections. When the velocity head increases in the downstream direction, a contraction coefficient is used; and when the velocity head decreases, an expansion coefficient is used.

As shown in Figure 5-1, the flow contraction occurs between cross sections 4 and 3, while the flow expansion occurs between sections 2 and 1. The contraction and expansion coefficients are used to compute energy losses associated with changes in the shape of river cross-sections (or effective flow areas). The loss due to expansion of flow is usually larger than the contraction loss, and losses from short abrupt transitions are larger than losses from gradual transitions. Typical values for contraction and expansion coefficients under subcritical flow conditions are shown in Table 5-2 below:

Table 5-2 Subcritical Flow Contraction and Expansion Coefficients

	Contraction	Expansion
No transition loss computed	0.0	0.0
Gradual transitions	0.1	0.3
Typical Bridge sections	0.3	0.5
Abrupt transitions	0.6	0.8

The maximum value for the contraction and expansion coefficient is 1.0. As mentioned previously, a detailed study was completed by the Hydrologic Engineering Center entitled "Flow Transitions in Bridge Backwater Analysis" (HEC, 1995). A summary of this research, as well as recommendations for contraction and expansion coefficients, can be found in Appendix B.

In general, contraction and expansion coefficients for supercritical flow should be lower than subcritical flow. For typical bridges that are under class C flow conditions (totally supercritical flow), the contraction and expansion coefficients should be around 0.03 and 0.05 respectively. For abrupt bridge transitions under class C flow, values of 0.05 and 0.1 may be more appropriate.

Hydraulic Computations through the Bridge

The bridge routines in HEC-RAS allow the modeler to analyze a bridge with several different methods without changing the bridge geometry. The bridge routines have the ability to model low flow (Class A, B, and C), low flow and weir flow (with adjustments for submergence on the

weir), pressure flow (orifice and sluice gate equations), pressure and weir flow, and highly submerged flows (the program will automatically switch to the energy equation when the flow over the road is highly submerged). This portion of the manual describes in detail how the program models each of these different flow types.

Low Flow Computations

Low flow exists when the flow going through the bridge opening is open channel flow (water surface below the highest point on the low chord of the bridge opening). For low flow computations, the program first uses the momentum equation to identify the class of flow. This is accomplished by first calculating the momentum at critical depth inside the bridge at the upstream and downstream ends. The end with the higher momentum (therefore most constricted section) will be the controlling section in the bridge. If the two sections are identical, the program selects the upstream bridge section as the controlling section. The momentum at critical depth in the controlling section is then compared to the momentum of the flow downstream of the bridge when performing a subcritical profile (upstream of the bridge for a supercritical profile). If the momentum downstream is greater than the critical depth momentum inside the bridge, the class of flow is considered to be completely subcritical (i.e., class A low flow). If the momentum downstream is less than the momentum at critical depth, in the controlling bridge section, then it is assumed that the constriction will cause the flow to pass through critical depth and a hydraulic jump will occur at some distance downstream (i.e., class B low flow). If the profile is completely supercritical through the bridge, then this is considered class C low flow.

Class A low flow. Class A low flow exists when the water surface through the bridge is completely subcritical (i.e., above critical depth). Energy losses through the expansion (sections 2 to 1) are calculated as friction losses and expansion losses. Friction losses are based on a weighted friction slope times a weighted reach length between sections 1 and 2. The weighted friction slope is based on one of the four available alternatives in the HEC-RAS, with the average-conveyance method being the default. This option is user selectable. The average length used in the calculation is based on a discharge-weighted reach length. Energy losses through the contraction (sections 3 to 4) are calculated as friction losses and contraction losses. Friction and contraction losses between sections 3 and 4 are calculated in the same way as friction and expansion losses between sections 1 and 2.

There are four methods available for computing losses through the bridge (sections 2 to 3):

> - Energy Equation (standard step method)
>
> - Momentum Balance
>
> - Yarnell Equation
>
> - FHWA WSPRO method

The user can select any or all of these methods to be computed. This allows the modeler to compare the answers from several techniques all in a single execution of the program. If more than one method is selected, the user must choose either a single method as the final solution

or direct the program to use the method that computes the greatest energy loss through the bridge as the final solution at section 3. Minimal results are available for all the methods computed, but detailed results are available for the method that is selected as the final answer. A detailed discussion of each method follows:

Energy Equation (standard step method):

The energy-based method treats a bridge in the same manner as a natural river cross-section, except the area of the bridge below the water surface is

subtracted from the total area, and the wetted perimeter is increased where the water is in contact with the bridge structure. As described previously, the program formulates two cross sections inside the bridge by combining the ground information of sections 2 and 3 with the bridge geometry. As shown in Figure 5-3, for the purposes of discussion, these cross sections will be referred to as sections BD (Bridge Downstream) and BU (Bridge Upstream).

The sequence of calculations starts with a standard step calculation from just downstream of the bridge (section 2) to just inside of the bridge (section BD) at the downstream end. The program then performs a standard step through the bridge (from section BD to section BU). The last calculation is to step out of the bridge (from section BU to section 3).
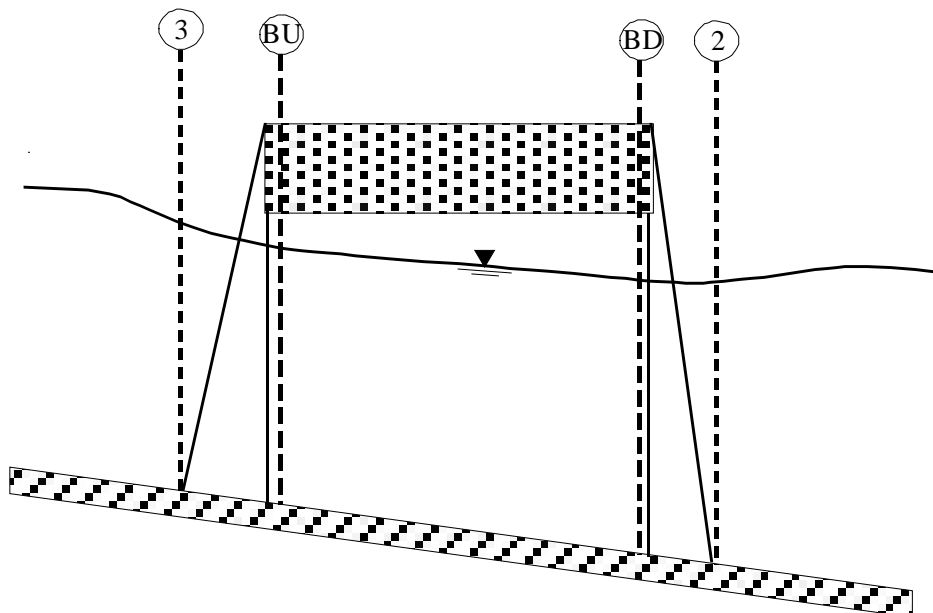
Figure 5-3 Cross Sections Near and Inside the Bridge

The energy-based method requires Manning's n values for friction losses and contraction and expansion coefficients for transition losses. The estimate of Manning's n values is well documented in many hydraulics text books, as well as several research studies. Basic guidance for estimating roughness coefficients is provided in Chapter 3 of this manual. Contraction and expansion coefficients are also provided in Chapter 3, as well as in earlier sections of this chapter. Detailed output is available for cross sections inside the bridge (sections BD and BU) as well as the user entered cross sections (sections 2 and 3).

Momentum Balance Method:

The momentum method is based on performing a momentum balance from cross section 2 to cross-section 3. The momentum balance is performed in three steps. The first step is to perform a momentum balance from cross section 2 to cross-section BD inside the bridge. The equation for this momentum balance is as follows:

$$A_{BD}\,\overline{Y}_{BD} + \frac{\beta_{BD}\,Q_{BD}^2}{g\,A_{BD}} = A_2\,\overline{Y}_2 + \frac{\beta_2\,Q_2^2}{g\,A_2} - A_{p_{BD}}\,\overline{Y}_{p_{BD}} + F_f - W_x \qquad (5\text{-}1)$$

Where: A_2, A_{BD} = Active flow area at section 2 and BD, respectively

$A_{P_{BD}}$ = Obstructed area of the pier on downstream side

$\overline{Y}_2, \overline{Y}_{BD}$ = Vertical distance from water surface to center of gravity of flow area A_2 and $A_{BD,}$ respectively

$\overline{Y}_{P_{BD}}$ = Vertical distance from water surface to center gravity of wetted pier area on downstream side

β_2, β_{BD} = Velocity weighting coefficients for momentum equation.

Q_2, Q_{BD} = Discharge

g = Gravitational acceleration

F_f = External force due to friction, per unit weight of water

W_x = Force due to weight of water n the direction of flow, per unit weight of water

The second step is a momentum balance from section BD to BU (see Figure 5-3). The equation for this step is as follows:

$$A_{BU} \overline{Y}_{BU} + \frac{\beta_{BU} Q_{BU}^2}{g A_{BU}} = A_{BD} \overline{Y}_{BD} + \frac{\beta_{BD} Q_{BD}^2}{g A_{BD}} + F_f - W_x \tag{5-2}$$

The final step is a momentum balance from section BU to section 3 (see Figure 5-3). The equation for this step is as follows:

$$A_3 \overline{Y}_3 + \frac{\beta_3 Q_3^2}{g A_3} = A_{BU} \overline{Y}_{BU} + \frac{\beta_{BU} Q_{BU}^2}{g A_{BU}} + A_{p_{BU}} \overline{Y}_{p_{BU}} + \frac{1}{2} C_D \frac{A_{p_{BU}} Q_3^2}{g A_3^2} + F_f - W_x$$

$$\tag{5-3}$$

Where: C_D = coefficient for flow going around the piers. Guidance on selecting drag coefficients can be found under Table 5-3 below.

The momentum balance method requires the use of roughness coefficients for the estimation of the friction force and a drag coefficient for the force of drag on piers. As mentioned previously, roughness coefficients are described in Chapter 3 of this manual. Drag coefficients are used to estimate the force due to the water moving around the piers, the separation of the flow, and the resulting wake that occurs downstream. Drag coefficients for various cylindrical shapes have been derived from experimental data (Lindsey, 1938). The following table shows some typical drag coefficients that can be used for piers:

Table 5-3

Typical drag coefficients for various pier shapes

Pier Shape	Drag Coefficient C_D
Circular pier	1.20
Elongated piers with semi-circular ends	1.33
Elliptical piers with 2:1 length to width	0.60
Elliptical piers with 4:1 length to width	0.32
Elliptical piers with 8:1 length to width	0.29
Square nose piers	2.00
Triangular nose with 30 degree angle	1.00
Triangular nose with 60 degree angle	1.39
Triangular nose with 90 degree angle	1.60
Triangular nose with 120 degree angle	1.72

The momentum method provides detailed output for the cross sections inside the bridge (BU and BD) as well as outside the bridge (2 and 3). The user has the option of turning the friction and weight force components off. The default is to include the friction force but not the weight component. The computation of the weight force is dependent upon computing a mean bed

slope through the bridge. Estimating a mean bed slope can be very difficult with irregular cross section data. A bad estimate of the bed slope can lead to large errors in the momentum solution. The user can turn this force on if they feel that the bed slope through the bridge is well behaved for their application.

During the momentum calculations, if the water surface (at sections BD and BU) comes into contact with the maximum low chord of the bridge, the momentum balance is assumed to be invalid and the results are not used.

Yarnell Equation:

The Yarnell equation is an empirical equation that is used to predict the change in water surface from just downstream of the bridge (section 2 of Figure 5-3) to just upstream of the bridge (section 3). The equation is based on approximately 2600 lab experiments in which the researchers varied the shape of the piers, the width, the length, the angle, and the flow rate. The Yarnell equation is as follows (Yarnell, 1934):

$$H_{3-2} = 2K(K + 10\omega - 0.6)(\alpha + 15\alpha^4)\frac{V^2}{2g}$$ (5-4)

Where: H_{3-2} =   Drop in water surface elevation from section 3 to 2

K =   Yarnell's pier shape coefficients

ω =   Ratio of velocity head to depth at section 2

α =   Obstructed area of the piers divided by the total unobstructed area at section 2

V_2 =   Velocity downstream at section 2

The computed upstream water surface elevation (section 3) is simply the downstream water surface elevation plus H3-2. With the upstream water surface known the program computes the corresponding velocity head and energy elevation for the upstream section (section 3). When the Yarnell method is used, hydraulic information is only provided at cross sections 2 and 3 (no information is provided for sections BU and BD).

The Yarnell equation is sensitive to the pier shape (K coefficient), the pier obstructed area, and the velocity of the water. The method is not sensitive to the shape of the bridge opening, the shape of the abutments, or the width of the bridge. Because of these limitations, the Yarnell method should only be used at bridges where the majority of the energy losses are associated with the piers. When Yarnell's equation is used for computing the change in water surface through the bridge, the user must supply the Yarnell pier shape coefficient, K. The following table gives values for Yarnell's pier coefficient, K, for various pier shapes:

Table 5-4

Yarnell's pier coefficient, K, for various pier shapes

Pier Shape	Yarnell K Coefficient
Semi-circular nose and tail	0.90
Twin-cylinder piers with connecting diaphragm	0.95
Twin-cylinder piers without diaphragm	1.05
90 degree triangular nose and tail	1.05
Square nose and tail	1.25
Ten pile trestle bent	2.50

FHWA WSPRO Method:

The low flow hydraulic computations of the Federal Highway Administration's (FHWA) WSPRO computer program, has been adapted as an option for low flow hydraulics in HEC-RAS. The WSPRO methodology had to be modified slightly in order to fit into the HEC-RAS concept of cross-section locations around and through a bridge.

The WSPRO method computes the water surface profile through a bridge by solving the energy equation. The method is an iterative solution performed from the exit cross section (1) to the approach cross-section (4). The energy balance is performed in steps from the exit section (1) to the cross section just downstream of the bridge (2); from just downstream of the bridge (2) to inside of the bridge at the downstream end (BD); from inside of the bridge at the downstream end (BD) to inside of the bridge at the upstream end (BU); From inside of the bridge at the upstream end (BU) to just upstream of the bridge (3); and from just upstream of the bridge (3) to the approach section (4). A general energy balance equation from the exit section to the approach section can be written as follows:

$$h_4 + \frac{a_4 V_4^2}{2g} = h_1 + \frac{a_1 V_1^2}{2g} + h_f + h_e \tag{5-5}$$

Where: h_1 = Water surface elevation at section 1

V_1 = Velocity at section 1

h_4 = Water surface elevation at section 4

V_4 = Velocity at section 4

h_L = Energy losses from section 4 to 1

The incremental energy losses from section 4 to 1 are calculated as follows:

From Section 1 to 2

Losses from section 1 to section 2 are based on friction losses and an expansion loss. Friction losses are calculated using the geometric mean friction slope times the flow weighted distance between sections 1 and 2. The following equation is used for friction losses from 1 to 2:

$$h_{f_{1-2}} = \frac{BQ^2}{K_2 K_1}$$

(5-6)

Where B is the flow weighted distance between sections 1 and 2, and K1 and K2 are the total conveyance at sections 1 and 2 respectively. The expansion loss from section 2 to section 1 is computed by the following equation:

$$h_e = \frac{Q^2}{2gA_1^2}\left[2\beta_1 - a_1 - 2\beta_2\left(\frac{A_1}{A_2}\right) + a_2\left(\frac{A_1}{A_2}\right)^2\right]$$

(5-7)

Where α and β are energy and momentum correction factors for non-uniform flow. a_1 and β₁ are computed as follows:

$$a_1 = \frac{\sum\left(K_i^3/A_i^2\right)}{K_T^3/A_T^2}$$

(5-8)

$$\beta_1 = \frac{\sum\left(K_i^2/A_1\right)}{K_T^2/A_T}$$

(5-9)

a_2 and β_2 are related to the bridge geometry and are defined as follows:

$$a_2 = \frac{1}{C^2}$$

(5-10)

$$\beta_2 = \frac{1}{C}$$

(5-11)

where C is an empirical discharge coefficient for the bridge, which was originally developed as part of the Contracted Opening method by Kindswater, Carter, and Tracy (USGS, 1953), and subsequently modified by Matthai (USGS, 1968). The computation of the discharge coefficient, C, is explained in detail in appendix D of this manual.

From Section 2 to 3

Losses from section 2 to section 3 are based on friction losses only. The energy balance is performed in three steps: from section 2 to BD; BD to BU; and BU to 3. Friction losses are calculated using the geometric mean friction slope times the flow weighted distance between sections. The following equation is used for friction losses from BD to BU:

$$h_{f(BU-BD)} = \frac{L_B Q^2}{K_{BU} K_{BD}}$$

(5-12)

Where K_{BU} and K_{BD} are the total conveyance at sections BU and BD respectively, and L_B is the length through the bridge. Similar equations are used for the friction losses from section 2 to BD and BU to 3.

From Section 3 to 4

Energy losses from section 3 to 4 are based on friction losses only. The equation for computing the friction loss is as follows:

$$h_{f(3-4\_)} = \frac{L_{av} Q^2}{K_3 K_4}$$

(5-13)

Where L_{av} is the effective flow length in the approach reach, and K_3 and K_4 are the total conveyances at sections 3 and 4. The effective flow length is computed as the average length of 20 equal conveyance stream tubes (FHWA, 1986). The computation of the effective flow length by the stream tube method is explained in appendix D of this manual.

Class B low flow. Class B low flow can exist for either subcritical or supercritical profiles. For either profile, class B flow occurs when the profile passes through critical depth in the bridge constriction. For a **subcritical profile**, the momentum equation is used to compute an upstream water surface (section 3 of Figure 5-3) above critical depth and a downstream water surface (section 2) below critical depth. For a **supercritical profile**, the bridge is acting as a control and is causing the upstream water surface elevation to be above critical depth. Momentum is used to calculate an upstream water surface above critical depth and a downstream water surface below critical depth. If for some reason the momentum equation fails to converge on an answer during the class B flow computations, the program will automatically switch to an energy-based method for calculating the class B profile through the bridge.

Whenever class B flow is found to exist, the user should run the program in a mixed flow regime mode.   If the user is running a mixed flow regime profile the program will proceed with backwater calculations upstream, and later with forewater calculations downstream from the bridge. Also, any hydraulic jumps that may occur upstream and downstream of the bridge can be located if they exist.

Class C low flow. Class C low flow exists when the water surface through the bridge is completely supercritical. The program can use either the energy equation or the momentum equation to compute the water surface through the bridge for this class of flow.

High Flow Computations

The HEC-RAS program has the ability to compute high flows (flows that come into contact with the maximum low chord of the bridge deck) by either the Energy equation (standard step method) or by using separate hydraulic equations for pressure and/or weir flow. The two methodologies are explained below.

Energy Equation (standard step method). The energy-based method is applied to high flows in the same manner as it is applied to low flows. Computations are based on balancing the energy equation in three steps through the bridge. Energy losses are based on friction and contraction and expansion losses. Output from this method is available at the cross sections inside the bridge as well as outside.

As mentioned previously, friction losses are based on the use of Manning's equation. Guidance for selecting Manning's n values is provided in Chapter 3 of this manual. Contraction and expansion losses are based on a coefficient times the change in velocity head. Guidance on the selection of contraction and expansion coefficients has also been provided in Chapter 3, as well as previous sections of this chapter.

The energy-based method performs all computations as though they are open channel flow. At the cross sections inside the bridge, the area obstructed by the bridge piers, abutments, and deck is subtracted from the flow area and additional wetted perimeter is added. Occasionally the resulting water surfaces inside the bridge (at sections BU and BD) can be computed at elevations that would be inside of the bridge deck. The water surfaces inside of the bridge reflect the hydraulic grade line elevations, not necessarily the actual water surface elevations. Additionally, the active flow area is limited to the open bridge area.

Pressure and Weir Flow Method. A second approach for the computation of high flows is to utilize separate hydraulic equations to compute the flow as pressure and/or weir flow. The two types of flow are presented below.

Pressure Flow Computations:

Pressure flow occurs when the flow comes into contact with the low chord of the bridge. Once the flow comes into contact with the upstream side of the bridge, a backwater occurs and orifice flow is established. The program will handle two cases of orifice flow; the first is when only the upstream side of the bridge is in contact with the water; and the second is when the bridge opening is flowing completely full. The HEC-RAS program will automatically select the appropriate equation, depending upon the flow situation. For the first case (see Figure 5-4), a sluice gate type of equation is used (FHWA, 1978):

$$Q = C_d A_{BU} \sqrt{2g} \left[Y_3 - \frac{Z}{2} + \frac{a_3 V_3^2}{2g} \right]^{1/2}$$

(5-14)

Where: Q = Total discharge through the bridge opening

  C_d = Coefficients of discharge for pressure flow

A_{BU} = Net area of the bridge opening at section BU

Y_3 = Hydraulic depth at section 3

Z = Vertical distance from maximum bridge low chord to the mean river bed elevation at section BU

The discharge coefficient C_d, can vary depending upon the depth of water upstream. Values for C_d range from 0.27 to 0.5, with a typical value of 0.5 commonly used in practice. The user can enter a fixed value for this coefficient or the program will compute one based on the amount that the inlet is submerged. A diagram relating Cd to Y_3/Z is shown in Figure 5-5.
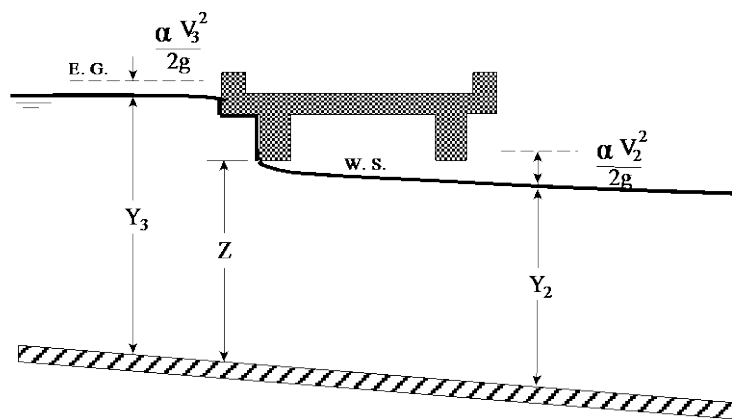
Figure 5-4 Example of a bridge under sluice gate type of pressure flow

Coefficient of Discharge
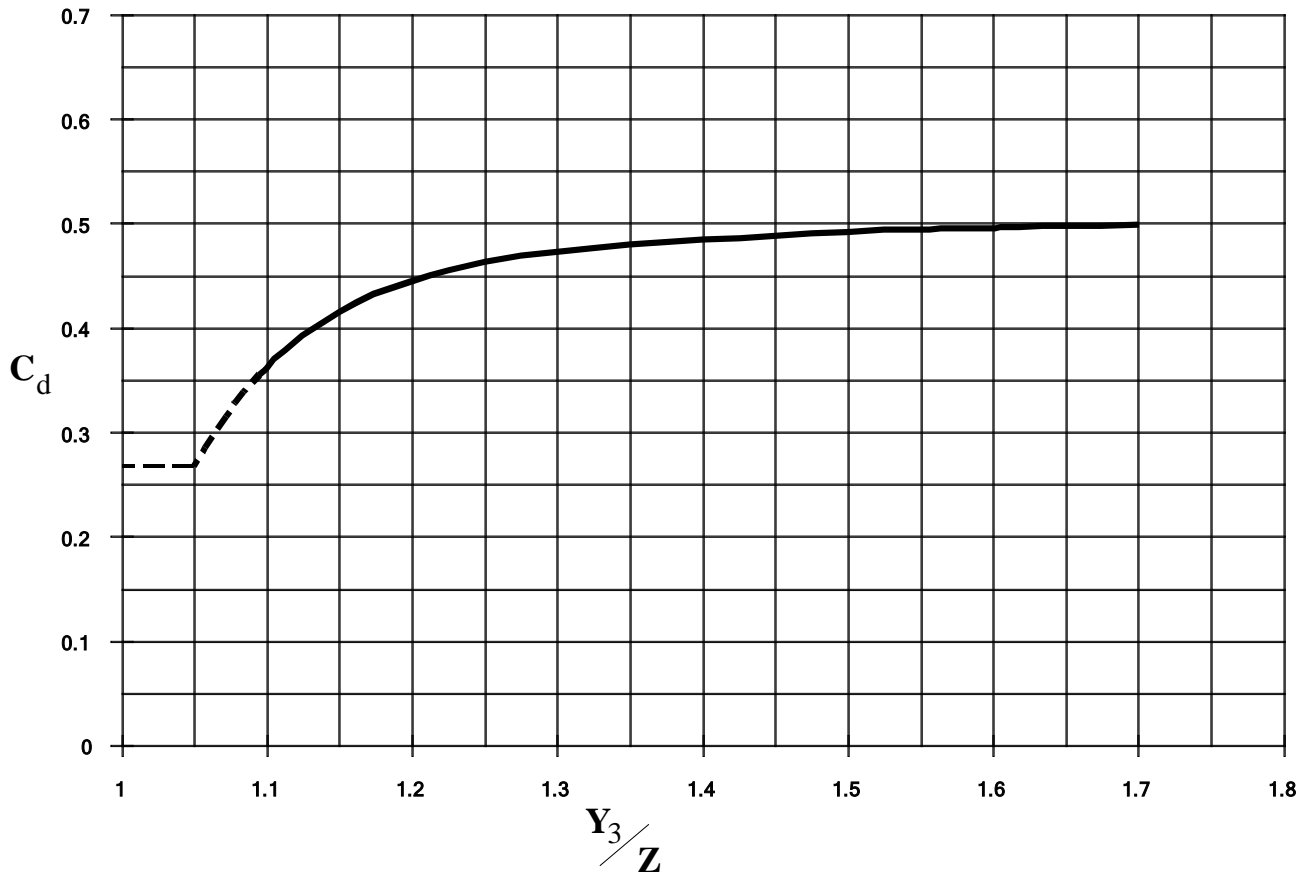
Figure 5-5 Coefficient of discharge for sluice gate type flow

As shown in Figure 5-5, the limiting value of Y_3/Z is 1.1. There is a transition zone somewhere between Y_3/Z = 1.0 and 1.1 where free surface flow changes to orifice flow. The type of flow in this range is unpredictable, and equation 5-14 is not applicable.

In the second case, when both the upstream and downstream side of the bridge are submerged, the standard full flowing orifice equation is used (see Figure 5-6). This equation is as follows:

$$Q = CA\sqrt{2gH} \tag{5-15}$$

Where: *C* = Coefficient of discharge for fully submerged pressure flow. Typical value of C is 0.8.

   H = The difference between the energy gradient elevation upstream and the water surface elevation downstream.

   A = Net area of the bridge opening.
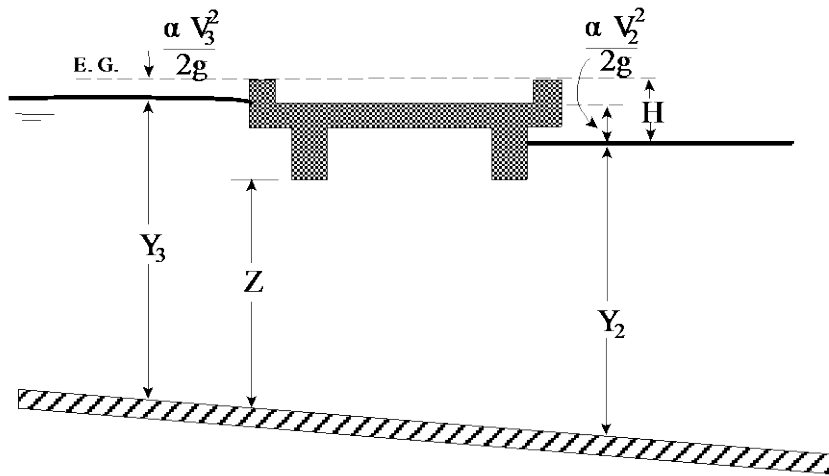
Figure 5-6 Example of a bridge under fully submerged pressure flow

Typical values for the discharge coefficient C range from 0.7 to 0.9, with a value of 0.8 commonly used for most bridges. The user must enter a value for C whenever the pressure flow method is selected. The discharge coefficient C can be related to the total loss coefficient, which comes from the form of the orifice equation that is used in the HEC-2 computer program (HEC, 1991):

$$Q = A\sqrt{\frac{2gH}{K}}$$ (5-16)

Where: K = Total loss coefficient

The conversion from K to C is as follows:

$$C = \sqrt{\frac{1}{K}}$$ (5-17)

The program will begin checking for the possibility of pressure flow when the computed low flow energy grade line is above the maximum low chord elevation at the upstream side of the bridge. Once pressure flow is computed, the pressure flow answer is compared to the low flow answer, the higher of the two is used. The user has the option to tell the program to use the water surface, instead of energy, to trigger the pressure flow calculation.

Weir Flow Computations:

Flow over the bridge, and the roadway approaching the bridge, is calculated using the standard weir equation (see Figure 5-7):

$$Q = CLH^{3/2}$$ (5-18)

Where: Q = Total flow over the weir

C = Coefficients pf discharge for weir flow

L = Effective length of the weir

H = Difference between energy upstream and road crest.
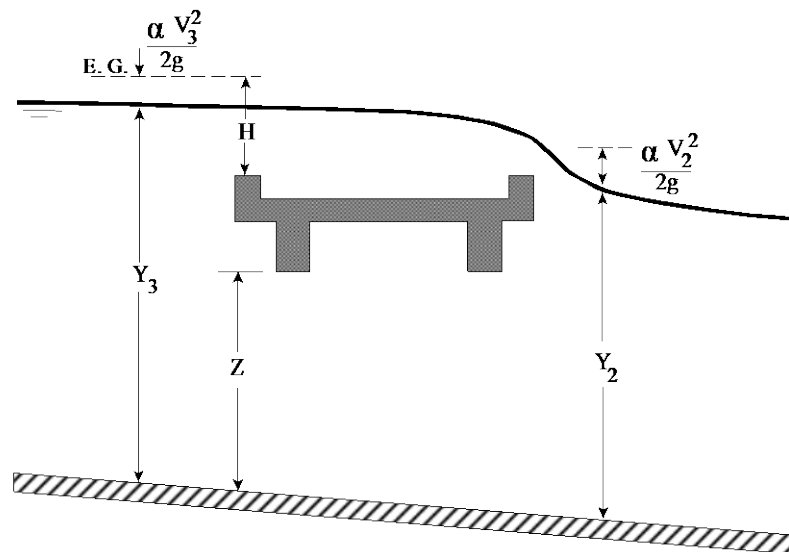
Figure 5-7 Example bridge with pressure and weir flow

The approach velocity is included by using the energy grade line elevation in lieu of the upstream water surface elevation for computing the head, H.

Under free flow conditions (discharge independent of tailwater) the coefficient of discharge C, ranges from 2.5 to 3.1 (1.38 - 1.71 metric) for broad-crested weirs depending primarily upon the gross head on the crest (C increases with head). Increased resistance to flow caused by obstructions such as trash on bridge railings, curbs, and other barriers would decrease the value of C.

Tables of weir coefficients, C, are given for broad-crested weirs in King's Handbook (King, 1963), with the value of C varying with measured head H and breadth of weir. For rectangular weirs with a breadth of 15 feet and a H of 1 foot or more, the given value is 2.63 (1.45 for metric). Trapezoidal shaped weirs generally have a larger coefficient with typical values ranging from 2.7 to 3.08 (1.49 to 1.70 for metric).

"Hydraulics of Bridge Waterways" (FHWA, 1978) provides a curve of C versus the head on the roadway. The roadway section is shown as a trapezoid and the coefficient rapidly changes from 2.9 for a very small H to 3.03 for H = 0.6 feet. From there, the curve levels off near a value of 3.05 (1.69 for metric).

With very little prototype data available, it seems the assumption of a rectangular weir for flow over the bridge deck (assuming the bridge can withstand the forces) and a coefficient of 2.6 (1.44 for metric) would be reasonable. If the weir flow is over the roadway approaches to the bridge, a value of 3.0 (1.66 for metric) would be consistent with available data. If weir flow occurs as a combination of bridge and roadway overflow, then an average coefficient (weighted by weir length) could be used.

For high tailwater elevations, the program will automatically reduce the amount of weir flow to account for submergence on the weir. Submergence is defined as the depth of water above the minimum weir elevation on the downstream side (section 2) divided by the height of the energy gradeline above the minimum weir elevation on the upstream side (section 3). The reduction of weir flow is accomplished by reducing the weir coefficient based on the amount of submergence. Submergence corrections are based on a trapezoidal weir shape or optionally an ogee spillway shape. The total weir flow is computed by subdividing the weir crest into segments, computing L, H, a submergence correction, and a Q for each section, then summing the incremental discharges. The submergence correction for a trapezoidal weir shape is from "Hydraulics of Bridge Waterways" (Bradley, 1978). Figure 5-8 shows the relationship between the percentage of submergence and the flow reduction factor.

When the weir becomes highly submerged the program will automatically switch to calculating the upstream water surface by the energy equation (standard step backwater) instead of using the pressure and weir flow equations. The criteria for when the program switches to energy based calculations is user controllable. A default maximum submergence is set to 0.95 (95 percent).
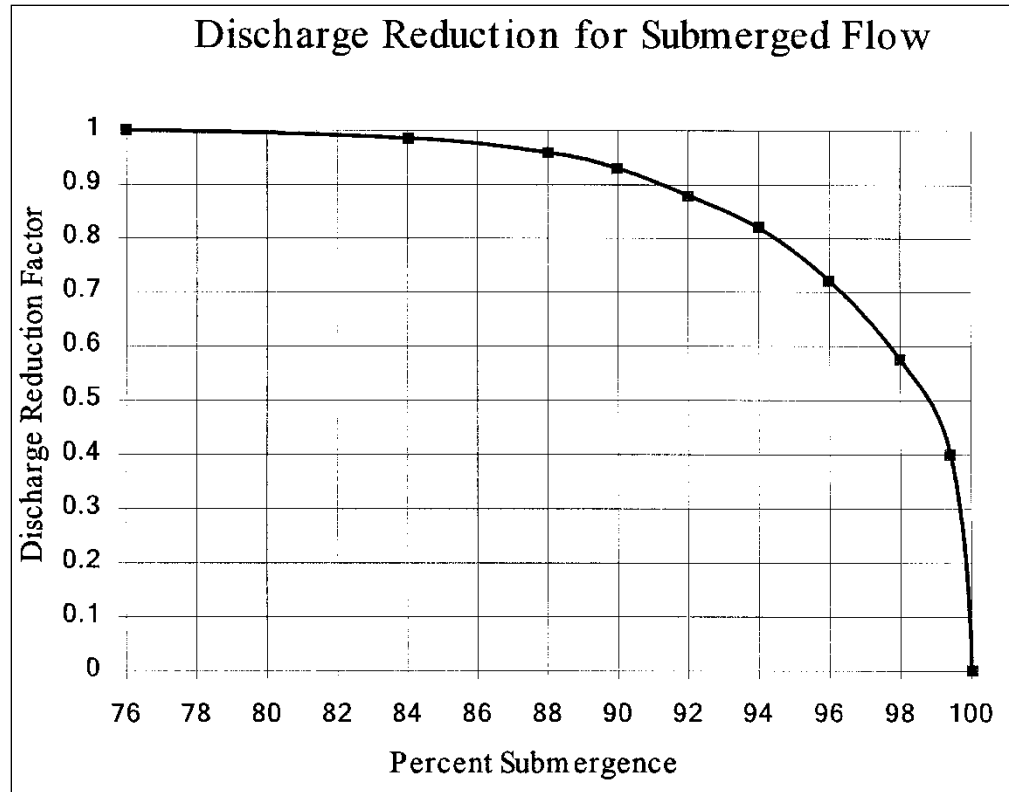
Figure 5-8 Factor for reducing weir flow for submergence

Combination Flow

Sometimes combinations of low flow or pressure flow occur with weir flow. In these cases, an iterative procedure is used to determine the amount of each type of flow. The program continues to iterate until both the low flow method (or pressure flow) and the weir flow method have the same energy (within a specified tolerance) upstream of the bridge (section 3). The combination of low flow and weir flow can only be computed with the energy and Yarnell low flow method.

Selecting a Bridge Modeling Approach

There are several choices available to the user when selecting methods for computing the water surface profile through a bridge. For low flow (water surface is below the maximum low chord of the bridge deck), the user can select any or all of the four available methods. For high flows, the user must choose between either the energy based method or the pressure and weir flow approach. The choice of methods should be considered carefully. The following discussion provides some basic guidelines on selecting the appropriate methods for various situations.

Low Flow Methods

For low flow conditions (water surface below the highest point on the low chord of the bridge opening), the Energy and Momentum methods are the most physically based, and in general are applicable to the widest range of bridges and flow situations. Both methods account for friction losses and changes in geometry through the bridge. The energy method accounts for additional losses due to flow transitions and turbulence through the use of contraction and expansion losses. However, the energy method does not account for losses associated with the shape of the piers and abutments. The momentum method can account for additional losses due to pier drag. One draw back of the momentum method is that the weight force is computed with an average bed slope through the bridge. The computation of this bed slope can be very difficult for natural cross sections.

The FHWA WSPRO method was originally developed for bridge crossings that constrict wide flood plains with heavily vegetated overbank areas. The method is an energy-based solution with some empirical attributes (the expansion loss equation in the WSPRO method utilizes an empirical discharge coefficient). However, the expansion loss is computed with an idealized equation in which the C coefficient is empirically derived.

The Yarnell equation is an empirical formula. Yarnell developed his equation from 2600 lab experiments in which he varied pier shape, width, length, angle, and flow rate. His experiments were run with rectangular and trapezoidal channel shapes, but no overbank areas. When applying the Yarnell equation, the user should ensure that the problem is within the range of data that the method was developed for. Additionally, the Yarnell method should only be applied to channels with uniform sections through the bridge (no everbank areas upstream and downstream) and where pers are the primary obstruction to the flow.

The following examples are some typical cases where the various low flow methods might be used:

1.   In cases where the bridge piers are a small obstruction to the flow, and friction losses are the predominate consideration, the energy based method, the momentum method, and the WSPRO method should give the best answers.

2.   In cases where pier losses and friction losses are both predominant, the momentum method should be the most applicable. But the energy and WSPRO methods can be used.

3.   Whenever the flow passes through critical depth within the vicinity of the bridge, both the momentum and energy methods are capable of modeling this type of flow transition. The Yarnell and WSPRO methods are for subcritical flow only.

4.   For supercritical flow, both the energy and the momentum method can be used. The momentum-based method may be better at locations that have a substantial amount of pier impact and drag losses. The Yarnell equation and the WSPRO method are only applicable to subcritical flow situations.

5.   For bridges in which the piers are the dominant contributor to energy losses and the change in water surface, either the momentum method or the Yarnell equation would be most applicable. However, the Yarnell equation is only applicable to Class A low flow.

6.   For long culverts under low flow conditions, the energy based standard step method is the most suitable approach. Several sections can be taken through the culvert to model changes in grade or shape or to model a very long culvert. This approach also has the benefit of providing detailed answers at several locations within the culvert, which is not possible with the culvert routines in HEC-RAS. However, if the culvert flows full, or if it is controlled by inlet conditions, the culvert routines would be the best approach. For a detailed discussion of the culvert routines within HEC-RAS, see Chapter 6 of this manual.

High Flow Methods

For high flows (flows that come into contact with the maximum low chord of the bridge deck), the program has two methods available to the user: the pressure and weir flow method and the energy-based method. The following examples are some typical cases where the various high flow methods might be used.

1.   When the bridge deck is a small obstruction to the flow, and the bridge opening is not acting like a pressurized orifice, the energy based method should be used.

2.   When the bridge deck and road embankment are a large obstruction to the flow, and a backwater is created due to the constriction of the flow, the pressure and weir method should be used.

3.   When the bridge and/or road embankment is overtopped, and the water going over top of the bridge is not highly submerged by the downstream tailwater, the pressure and weir method should be used. The pressure and weir method will automatically switch to the energy method if the bridge becomes 95 percent submerged. The user can change the percent submergence at which the program will switch from

the pressure and weir method to the energy method. This is accomplished from the Deck/Roadway editor in the Bridge/Culvert Data editor.

4.   When the bridge is highly submerged, and flow over the road is not acting like weir flow, the energy-based method should be used.

Unique Bridge Problems and Suggested Approaches

Many bridges are more complex than the simple examples presented in the previous sections. The following discussion is intended to show how HEC-RAS can be used to calculate profiles for more complex bridge crossings. The discussion here will be an extension of the previous discussions and will address only those aspects that have not been discussed previously.

Perched Bridges

A perched bridge is one for which the road approaching the bridge is at the floodplain ground level, and only in the immediate area of the bridge does the road rise above ground level to span the watercourse (Figure 5-9). A typical flood-flow situation with this type of bridge is low flow under the bridge and overbank flow around the bridge. Because the road approaching the bridge is usually not much higher than the surrounding ground, the assumption of weir flow is often not justified. A solution based on the energy method (standard step calculations) would be better than a solution based on weir flow with correction for submergence. Therefore, this type of bridge should generally be modeled using the energy-based method, especially when a large percentage of the total discharge is in the overbank areas.
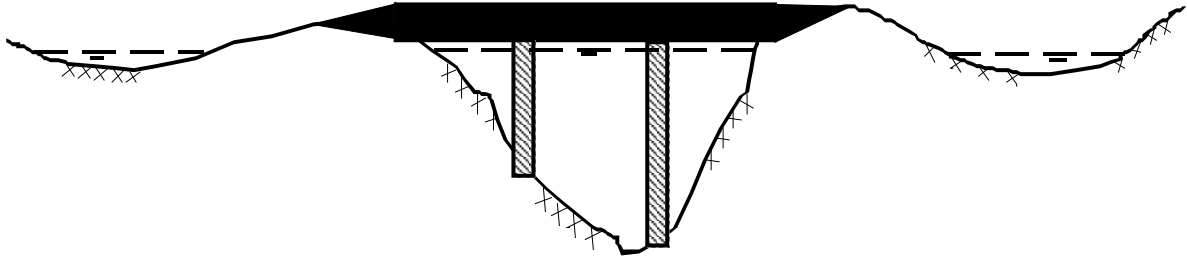
Figure 5-9 Perched Bridge Example

Low Water Bridges

A low water bridge (Figure 5-10) is designed to carry only low flows under the bridge. Flood flows are carried over the bridge and road. When modeling this bridge for flood flows, the anticipated solution is a combination of pressure and weir flow. However, with most of the flow over the top of the bridge, the correction for submergence may introduce considerable error. If the tailwater is going to be high, it may be better to use the energy-based method.
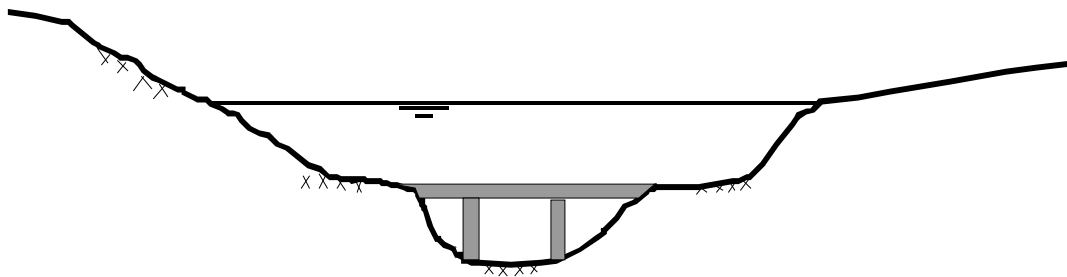
Figure 5-10 Low Water Bridge Example

Bridges on a Skew

Skewed bridge crossings (Figure 5-11) are generally handled by making adjustments to the bridge dimensions to define an equivalent cross section perpendicular to the flow lines. The

bridge information, and cross sections that bound the bridge, can be adjusted from the bridge editor. An option called Skew Bridge/Culvert is available from the bridge/culvert editor.

In the publication "Hydraulics of Bridge Waterways" (Bradley, 1978) the effect of skew on low flow is discussed. In model testing, skewed crossings with angles up to 20 degrees showed no objectionable flow patterns. For increasing angles, flow efficiency decreased. A graph illustrating the impact of skew indicates that using the projected length is adequate for angles up to 30 degrees for small flow contractions. **Warning: the skew angle is based on comparing the angle of the flow as it goes through the bridge, with a line perpendicular to the cross sections bounding the bridge.** The user should not base the skew angle on the direction of the flow upstream of the bridge.   When a bridge is highly skewed, most likely the flow will turn somewhat before it goes through the bridge opening. So the effective area of the opening is actually larger than if you assume an angle based on the upstream approach section.
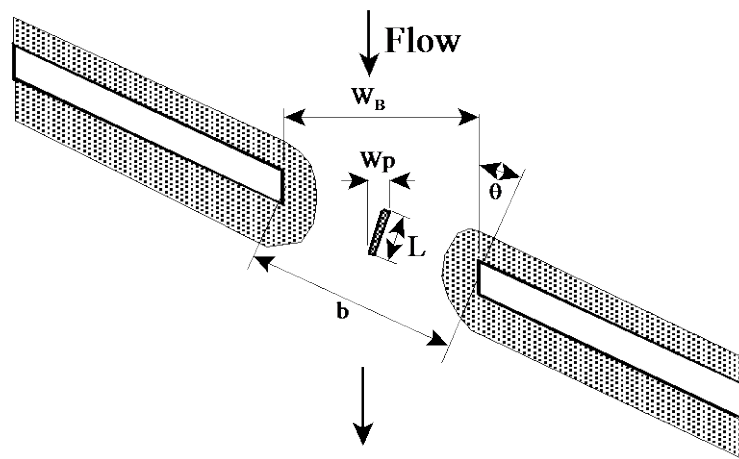
Figure 5-11 Example Bridge on a Skew

For the example shown in figure 5-11, the projected width of the bridge opening, perpendicular to the flow lines, will be computed with the following equation:

$$W_B = \cos\theta * b \qquad\qquad (5\text{-}19)$$

Where: W_B = Projected width of the bridge opening, perpendicular to the flow lines

B   = The length of the bridge opening as measured along the skewed road crossing

Θ   = The bridge skew angle in degrees. This angle is with respect to the flow going through the bridge opening and a line perpendicular to the bridge cross sections.

The pier information must also be adjusted to account for the skew of the bridge. HEC-RAS assumes the piers are continuous, as shown in Figure 5-11, thus the following equation will be applied to get the projected width of the piers, perpendicular to the flow lines:

$$W_p = \sin\theta * L + \cos\theta * w_p \qquad\qquad (5\text{-}20)$$

Where: W_p = The projected width of the pier, perpendicular to the flow lines

L   = The actual length of the pier

w_p = The actual width of the pier

Parallel Bridges

With the construction of divided highways, a common modeling problem involves parallel bridges (Figure 5-12). For new highways, these bridges are often identical structures. The hydraulic loss through the two structures has been shown to be between one and two times the loss for one bridge [Bradley, 1978]. The model results [Bradley, 1978] indicate the loss for two bridges ranging from 1.3 to 1.55 times the loss for one bridge crossing, over the range of bridge spacing's tested. Presumably if the two bridges were far enough apart, the losses for the two bridges would equal twice the loss for one. If the parallel bridges are very close to each other, and the flow will not be able to expand between the bridges, the bridges can be modeled as a single bridge. If there is enough distance between the bridge, in which the flow has room to expand and contract, the bridges should be modeled as two separate bridges. If both bridges are modeled, care should be exercised in depicting the expansion and contraction of flow between the bridges. Expansion and contraction rates should be based on the same procedures as single bridges.
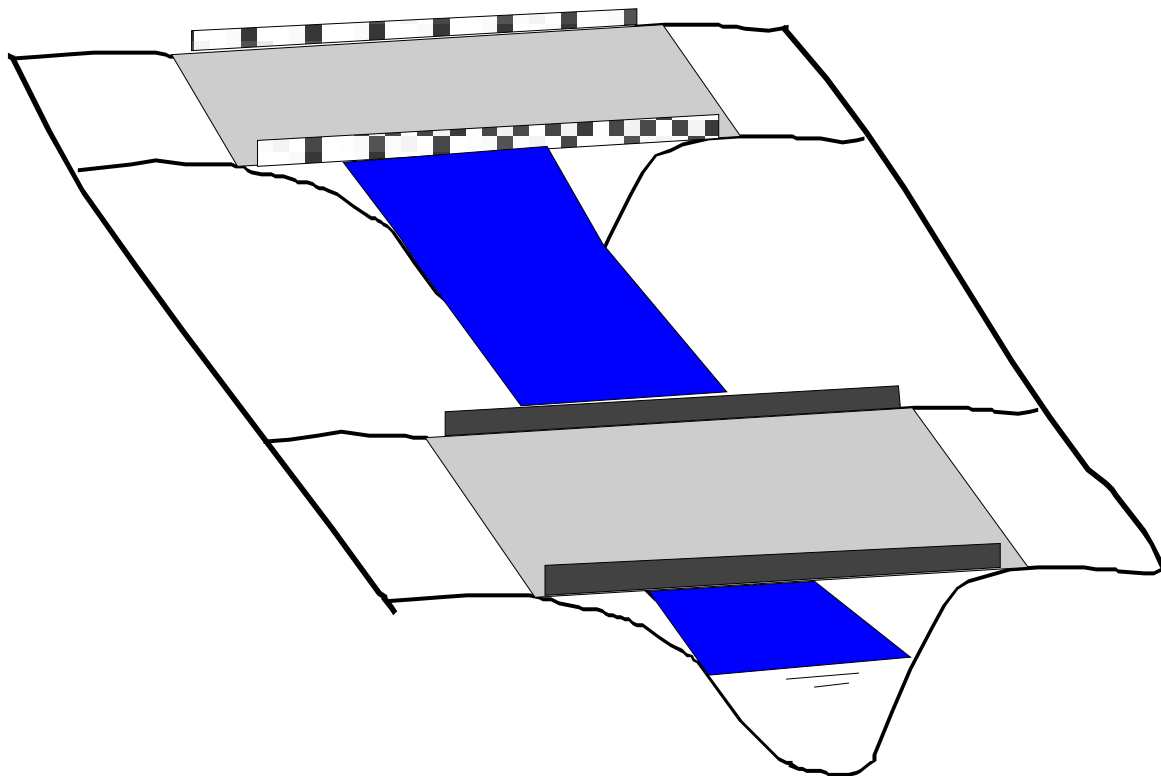
Figure 5-12 Parallel Bridge Example

Multiple Bridge Opening

Some bridges (Figure 5-13) have more than one opening for flood flow, especially over a very wide floodplain. Multiple culverts, bridges with side relief openings, and separate bridges over a divided channel are all examples of multiple opening problems. With more than one bridge opening, and possible different control elevations, the problem can be very complicated. HEC-RAS can handle multiple bridge and/or culvert openings. Detailed discussions on how to model multiple bridge and/or culvert openings is covered under Chapter 7 of the HEC-RAS Hydraulic Reference manual and Chapter 6 of the User's manual.
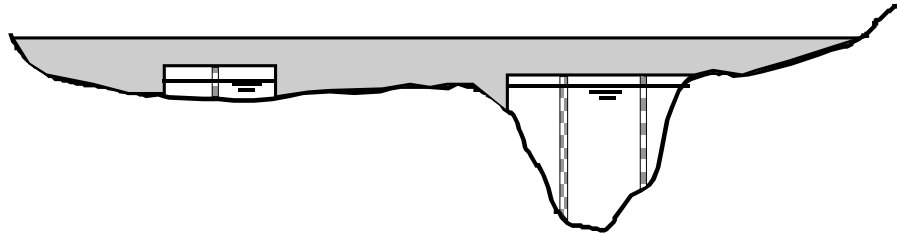
Figure 5-13 Example Multiple Bridge Opening

Modeling Floating Pier Debris

Trash, trees, and other debris may accumulate on the upstream side of a pier. During high flow events, this debris may block a significant portion of the bridge opening. In order to account for this effect, a pier debris option has been added to HEC-RAS.

The pier debris option blocks out a rectangular shaped area in front of the given pier. The user enters the height and the width of the given block. The program then adjusts the area and wetted perimeter of the bridge opening to account for the pier debris. The rectangular block is centered on the centerline of the upstream pier. The pier debris is assumed to float at the top of the water surface. That is, the top of the rectangular block is set at the same elevation as the water surface. For instance, assume a bridge opening that has a pier that is six feet wide with a centerline station of 100 feet, the elevation of water inside of the bridge is ten feet, and that the user wants to model pier debris that sticks out two feet past either side of the pier and is [vertically] four feet high. The user would enter a pier debris rectangle that is 10 feet wide (six feet for the pier plus two feet for the left side and two feet for the right side) and 4 feet high. The pier debris would block out the flow that is between stations 95 and 105 and between an elevation of six and ten feet (from an elevation of six feet to the top of the water surface).

The pier debris does not form until the given pier has flow. If the bottom of the pier is above the water surface, then there is no area or wetted perimeter adjustment for that pier. However, if the water surface is above the top of the pier, the debris is assumed to lodge underneath the bridge, where the top of the pier intersects the bottom of the bridge deck. It is assumed that the debris entirely blocks the flow and that the debris is physically part of the pier. (The Yarnell

and momentum bridge methods require the area of the pier, and pier debris is included in these calculations.)

The program physically changes the geometry of the bridge in order to model the pier debris. This is done to ensure that there is no double accounting of area or wetted perimeter. For instance, pier debris that extends past the abutment, or into the ground, or that overlaps the pier debris of an adjacent pier is ignored.

Shown in Figure 5-14 is the pier editor with the pier debris option turned on. Note that there is a check box to turn the floating debris option for this pier. Two additional fields must be filled out, the height and overall width of the pier debris. Additionally, there is a button that the user can use to set the entered height and width for the first pier as being the height and width of debris that will be used for all piers at this bridge location. Otherwise, the debris data can be defined separately for every pier.
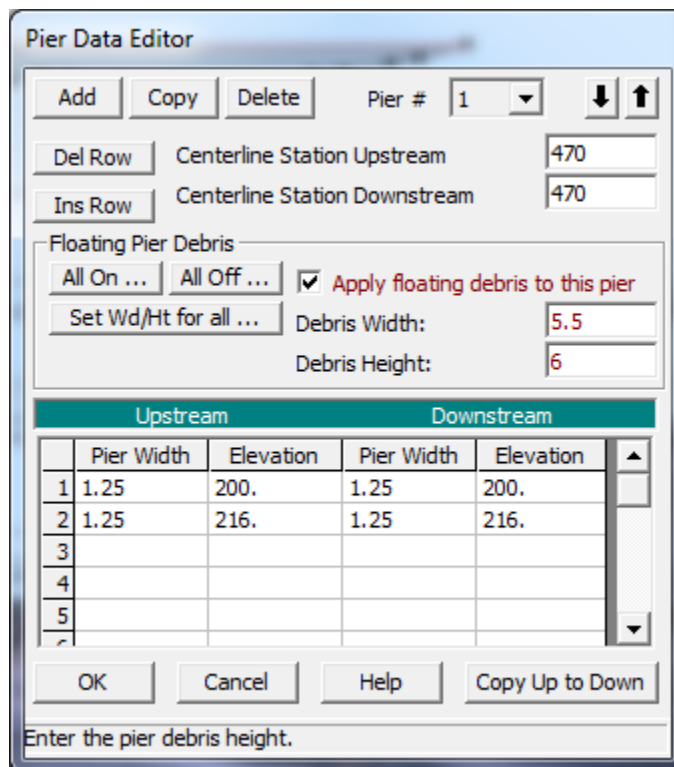
Figure 5-14 Pier Editor With Floating Debris Option

After the user has run the computational program with the pier debris option turned on, the pier debris will then be displayed on the cross section plots of the upstream side of the bridge (this is the cross sections with the labels "BR U," for inside of the bridge at the upstream end). An example cross-section plot with pier debris is shown in Figure 5-15.

CHAPTER 6

Modeling Culverts

HEC-RAS computes energy losses, caused by structures such as culverts, in three parts. The first part consists of losses that occur in the reach immediately downstream from the structure, where an expansion of flow takes place. The second part consists of losses that occur as flow travels into, through, and out of the culvert. The last part consists of losses that occur in the reach immediately upstream from the structure, where the flow is contracting towards the opening of the culvert.

HEC-RAS has the ability to model single culverts; multiple identical culverts; and multiple non-identical culverts.

This chapter discusses how culverts are modeled within HEC-RAS. Discussions include: general modeling guidelines; how the hydraulic computations through the culvert are performed; and what data are required and how to select the various coefficients.

Contents

■ General Modeling Guidelines

■ Culvert Hydraulics

■ Culvert Data and Coefficients

General Modeling Guidelines

The culvert routines in HEC-RAS are similar to the bridge routines, except that the Federal Highway Administration's (FHWA, 1985) standard equations for culvert hydraulics are used to compute inlet control losses at the structure. Outlet control is computed by balancing the energy equation from downstream of the culvert to upstream of the culvert. The HEC-RAS culvert routines are also capable of reproducing all 6 of the USGS flow classifications for culverts, outlined in their report "Measurements of Peak Discharge at Culverts by Indirect Methods", (USGS, 1976). Figure 6-1 illustrates a typical box culvert road crossing. As shown, the culvert is similar to a bridge in many ways. The walls and roof of the culvert correspond to the abutments and low chord of the bridge, respectively.
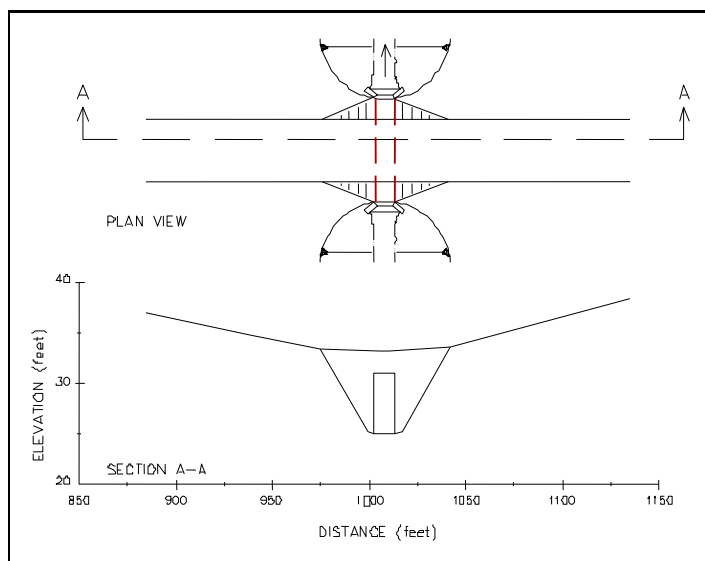
Figure 6-1 Typical Culvert Road Crossing

Because of the similarities between culverts and other types of bridges, culverts are modeled in a similar manner to bridges. The layout of cross sections, the use of the ineffective areas, the selection of loss coefficients, and most other aspects of bridge analysis apply to culverts as well.

Types of Culverts

HEC-RAS has the ability to model nine of the most commonly used culvert shapes. These shapes include: circular; box (rectangular); arch; pipe arch; low profile arch; high profile arch; elliptical (horizontal and vertical); semi-circular, and Con/Span culverts (Figure 6-2). The program has the ability to model up to ten different culvert types (any change in shape, slope, roughness, or chart and scale number requires the user to enter a new culvert type) at any given culvert crossing. For a given culvert type, the number of identical barrels is limited to 25.
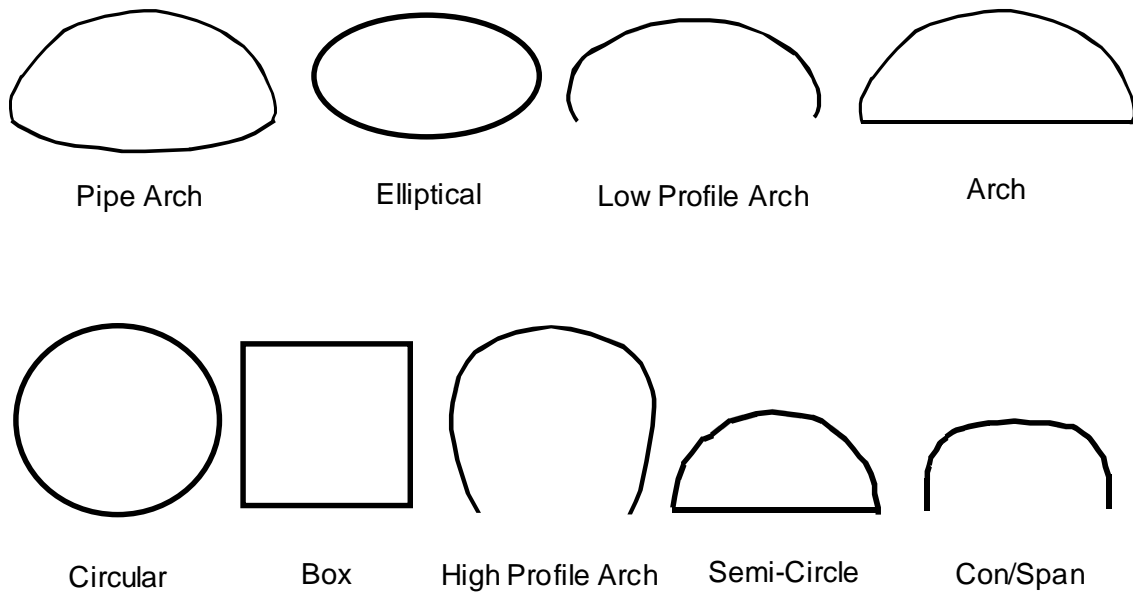
Figure 6-2 Commonly used culvert shapes

Cross Section Locations

The culvert routines in HEC-RAS require the same cross sections as the bridge routines. Four cross sections are required for a complete culvert model. This total includes one cross section sufficiently downstream from the culvert such that flow is not affected by the culvert, one at the downstream end of the culvert, one at the upstream end of the culvert, and one cross section located far enough upstream that the culvert again has no effect on the flow. Note, the cross sections at the two ends of the culvert represent the channel outside of the culvert. Separate culvert data will be used to create cross sections inside of the culvert. Figure 6-3 illustrates the cross sections required for a culvert model. The cross sections are labeled 1, 2, 3, and 4 for the purpose of discussion within this chapter. Whenever the user is computing a water surface profile through a culvert (or any other hydraulic structure), additional cross sections should always be included both upstream and downstream of the structure. This will prevent any user-entered boundary conditions from affecting the hydraulic results through the culvert.

Cross Section 1 of Culvert Model. Cross Section 1 for a culvert model should be located at a point where flow has fully expanded from its constricted top width caused by the culvert constriction. The cross section spacing downstream of the culvert can be based on the criterion stated under the bridge modeling chapter (See Chapter 5, "Modeling Bridges" for a more complete discussion of cross section locations). The entire area of Cross Section 1 is usually considered to be effective in conveying flow.
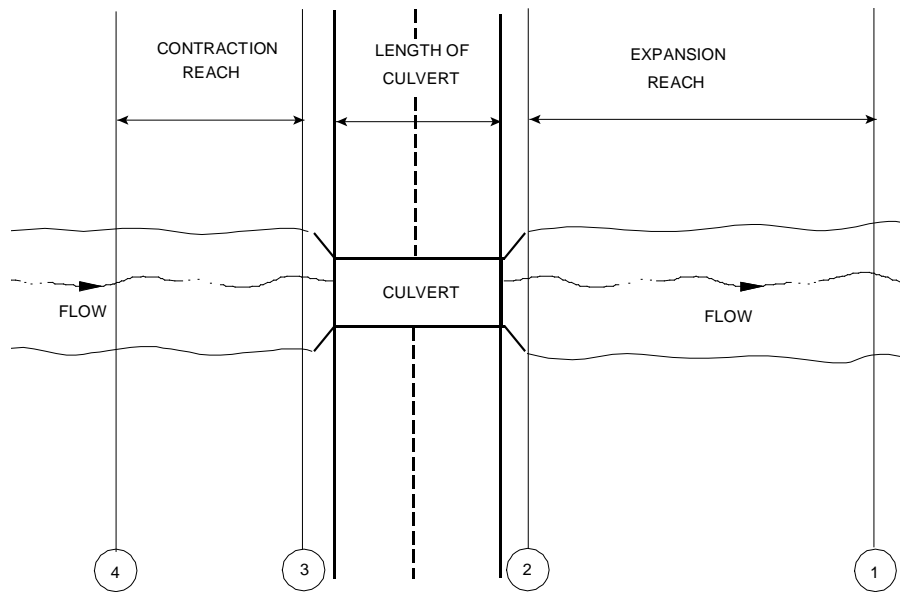
Figure 6-3 Cross Section Layout for Culvert Method

Cross Section 2 of Culvert Model. Cross Section 2 of a culvert model is located a short distance downstream from the culvert exit. This distance should represent the short distance that is required for the abrupt transition of the flow from the culvert to the channel. Cross section 2 does not include any of the culvert structure or embankments, but represents the physical shape of the channel just downstream of the culvert. The shape and location of this cross section is entered separately from the Bridge and Culvert editor in the user interface (cross section editor).

The HEC-RAS ineffective area option is used to restrict the effective flow area of Cross Section 2 to the flow area around or near the edges of the culverts, until flow overtops the roadway. The ineffective flow areas are used to represent the correct amount of active flow area just downstream of the culvert. Because the flow will begin to expand as it exits the culvert, the active flow area at Section 2 is generally wider than the width of the culvert opening. The width of the active flow area will depend upon how far downstream Cross Section 2 is from the culvert exit. In general, a reasonable assumption would be to assume a 1.5:1 expansion rate over this short distance. With this assumption, if Cross Section 2 were 6 feet from the culvert exit, then the active flow area at Section 2 should be 8 feet wider than the culvert opening (4 feet on each side of the culvert) Figure 6-4 illustrates Cross Section 2 of a typical culvert model with a box culvert. As indicated, the cross section data does not define the culvert shape for the culvert model. On Figure 6-4, the channel bank locations are indicated by small circles, and the stations and elevations of the ineffective flow areas are indicated by triangles.

Cross Sections 1 and 2 are located so as to create a channel reach downstream of the culvert in which the HEC-RAS program can accurately compute the friction losses and expansion losses downstream of the culvert.
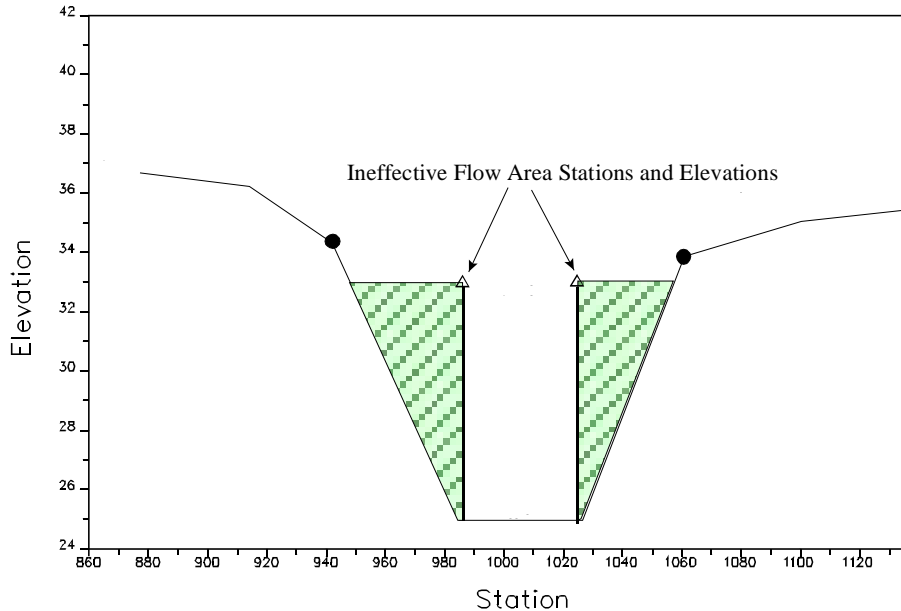
Figure 6-4 Cross Section 2 of Culvert Model

Cross Section 3 of Culvert Model. Cross Section 3 of a culvert model is located a short distance upstream of the culvert entrance, and represents the physical configuration of the upstream channel. This cross section should be far enough upstream from the culvert face, such that the abrupt contraction of flow has room to occur. Also, the culvert routines take into account an entrance loss in all of the calculations. This entrance loss requires some distance to occur over. The culvert method uses a combination of a bridge deck, Cross Sections 2 and 3, and culvert data, to describe the culvert or culverts and the roadway embankment. The culvert data, which is used to describe the roadway embankment and culvert openings, is located at a river station between Cross Sections 2 and 3.

The HEC-RAS ineffective area option is used to restrict the effective flow area of Cross Section 3 until the flow overtops the roadway. The ineffective flow area is used to represent the correct amount of active flow area just upstream of the culvert. Because the flow is contracting rapidly as it enters the culvert, the active flow area at Section 3 is generally wider than the width of the culvert opening. The width of the active flow area will depend upon how far upstream Cross Section 3 is placed from the culvert entrance. In general, a reasonable assumption would be to assume a 1:1 contraction rate over this short distance. With this assumption, if Cross Section 3 were 5 feet from the culvert entrance, then the active flow area at Section 3 should be 10 feet wider than the culvert opening (5 feet on each side of the culvert).   Figure 6-5 illustrates Cross

Section 3 of a typical culvert model for a box culvert, including the roadway profile defined by the bridge deck/roadway editor, and the culvert shape defined in the culvert editor. As indicated, the ground profile does not define the culvert shape for the culvert model. On Figure 6-5, the channel bank locations are indicated by small circles and the stations and elevations of ineffective area control are indicated by triangles.
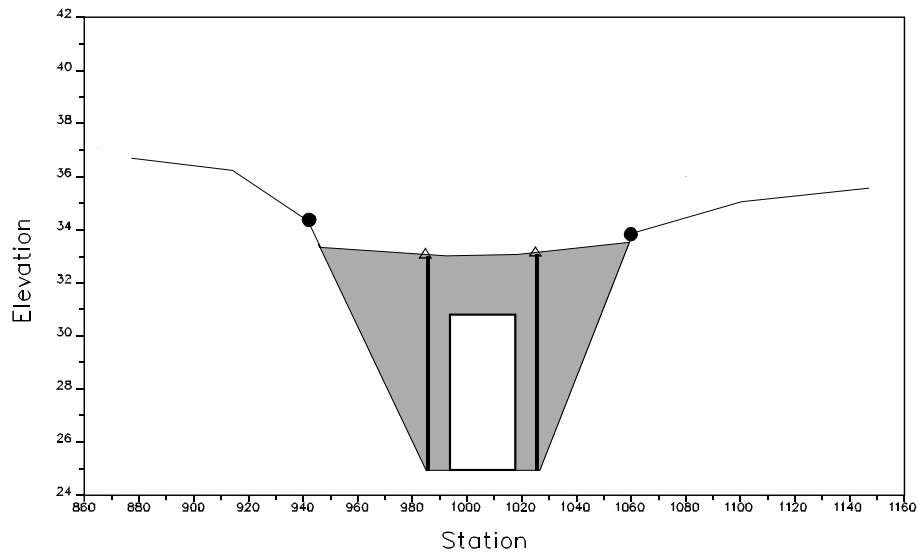
Figure 6-5 Cross Section 3 of the Culvert Model

Cross Section 4 of Culvert Model. The final cross section in the culvert model is located at a point where flow has not yet begun to contract from its unrestrained top width upstream of the culvert to its constricted top width near the culvert. This distance is normally determined assuming a one to one contraction of flow. In other words, the average rate at which flow can contract to pass through the culvert opening is assumed to be one foot laterally for every one foot traveled in the downstream direction. More detailed information on the placement of cross sections can be found in Chapter 5, "Modeling Bridges." The entire area of Cross Section 4 is usually considered to be effective in conveying flow.

Expansion and Contraction Coefficients

User-defined coefficients are required to compute head losses due to the contraction and expansion of flows upstream and downstream of a culvert. These losses are computed by multiplying an expansion or contraction coefficient by the absolute difference in velocity head between two cross sections.

If the velocity head increases in the downstream direction, a contraction coefficient is applied. When the velocity head decreases in the downstream direction, an expansion coefficient is used. Recommended values for the expansion and contraction coefficients have been given in Chapter 3 of this manual (table 3-2). As indicated by the tabulated values, the expansion of

flow causes more energy loss than the contraction. Also, energy losses increase with the abruptness of the transition. For culverts with abrupt flow transitions, the contraction and expansion loss coefficients should be increased to account for additional energy losses.

Limitations of the Culvert Routines in HEC-RAS

The HEC-RAS routines are limited to culverts that are considered to be constant in shape, flow rate, and bottom slope.

Culvert Hydraulics

This section introduces the basic concepts of culvert hydraulics, which are used in the HEC-RAS culvert routines.

Introduction to Culvert Terminology

A culvert is a relatively short length of closed conduit, which connects two open channel segments or bodies of water. Two of the most common types of culverts are: circular pipe culverts, which are circular in cross section, and box culverts, which are rectangular in cross section. Figure 6-6 shows an illustration of circular pipe and box culverts. In addition to box and pipe culverts, HEC-RAS has the ability to model arch; pipe arch; low profile arch; high profile arch; elliptical; semi-circular; and ConSpan culvert shapes.
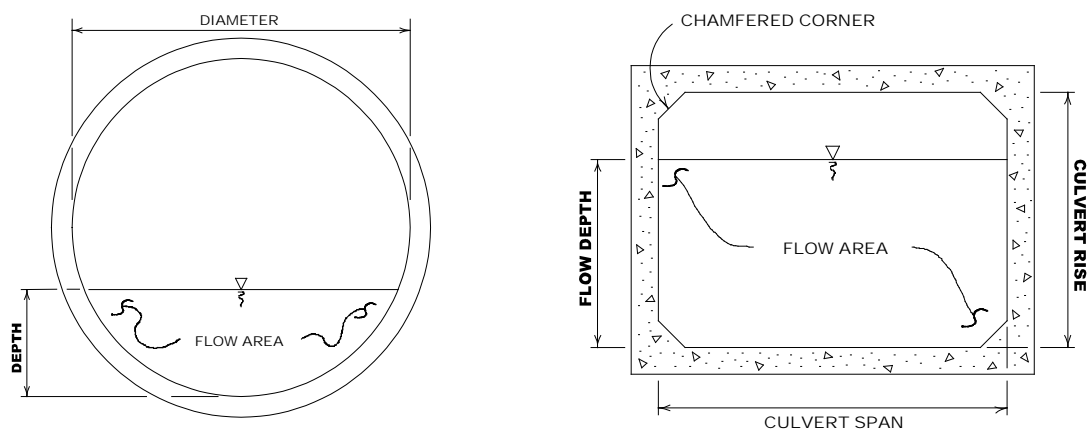
Figure 6-6 Cross section of a circular pipe and box culvert, respectively

Culverts are made up of an **entrance** where water flows into the culvert, a **barrel**, which is the closed conduit portion of the culvert, and an **exit**, where the water flows out of the culvert (see Figure 6-7). The total flow capacity of a culvert depends upon the characteristics of the entrance as well as the culvert barrel and exit.

The **Tailwater** at a culvert is the depth of water on the exit or downstream side of the culvert, as measured from the downstream invert of the culvert (shown as **TW** on Figure 6-7). The **invert** is the lowest point on the inside of the culvert at a particular cross section. The tailwater depth depends on the flow rate and hydraulic conditions downstream of the culvert.

Headwater (HW on Figure 6-7) is the depth from the culvert inlet invert to the energy grade line, for the cross section just upstream of the culvert (Section 3). The Headwater represents the amount of energy head required to pass a given flow through the culvert.

The **Upstream Water Surface** (WSU on Figure 6-7) is the depth of water on the entrance or upstream side of the culvert (Section 3), as measured from the upstream invert of Cross Section 3.

The **Total Energy** at any location is equal to the elevation of the invert plus the specific energy (depth of water + velocity heady) at that location. All of the culvert computations within HEC-RAS compute the total energy for the upstream end of the culvert. The upstream water surface (WSU) is then obtained by placing that energy into the upstream cross section and computing the water surface that corresponds to that energy for the given flow rate.
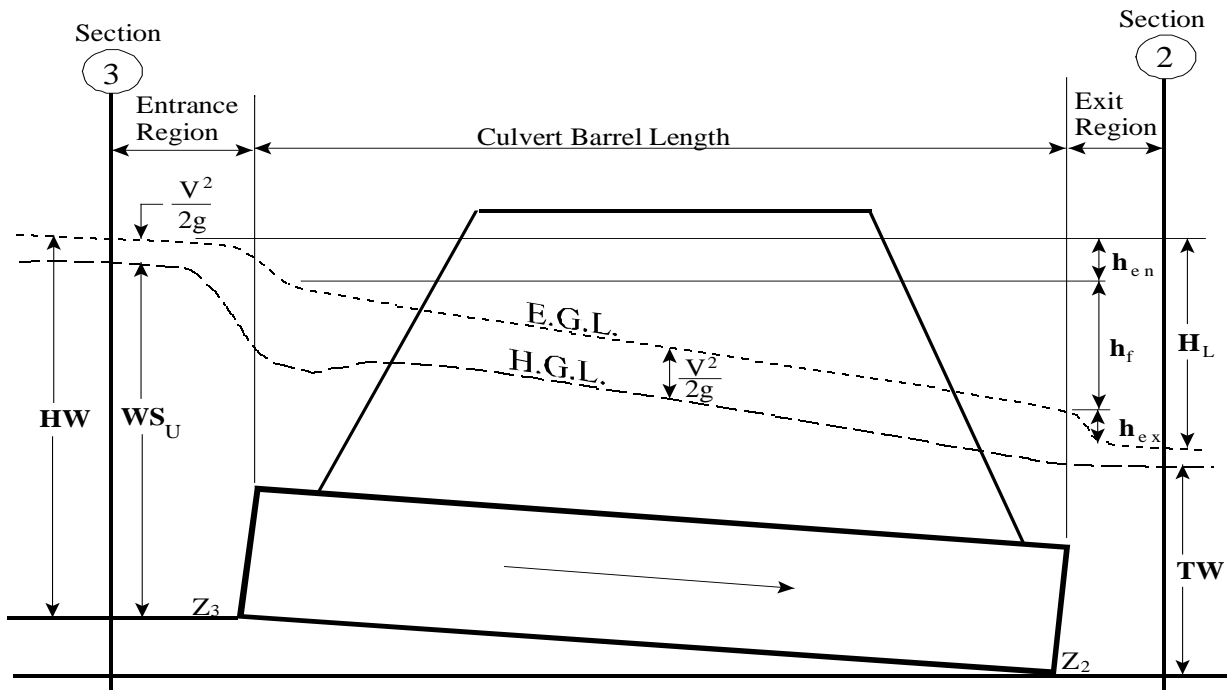
Figure 6-7 Full flowing culvert with energy and hydraulic grade lines

Flow Analysis for Culverts

The analysis of flow in culverts is quite complicated. It is common to use the concepts of "inlet control" and "outlet control" to simplify the analysis. **Inlet control** flow occurs when the flow capacity of the culvert entrance is less than the flow capacity of the culvert barrel. The control section of a culvert operating under inlet control is located just inside the entrance of the culvert. The water surface passes through critical depth at or near this location, and the flow regime immediately downstream is supercritical. For inlet control, the required upstream energy is computed by assuming that the culvert inlet acts as a sluice gate or as a weir. Therefore, the inlet control capacity depends primarily on the geometry of the culvert entrance. **Outlet control** flow occurs when the culvert flow capacity is limited by downstream conditions (high tailwater) or by the flow carrying capacity of the culvert barrel. The HEC-RAS culvert routines compute the upstream energy required to produce a given flow rate through the culvert for inlet control conditions and for outlet control conditions (Figure 6-8). In general, the higher upstream energy "controls" and determines the type of flow in the culvert for a given flow rate and tailwater condition (however, this is not always true). For outlet control, the required upstream energy is computed by performing an energy balance from the downstream section to the upstream section.   The HEC-RAS culvert routines consider entrance losses,

friction losses in the culvert barrel, and exit losses at the outlet in computing the outlet control headwater of the culvert.
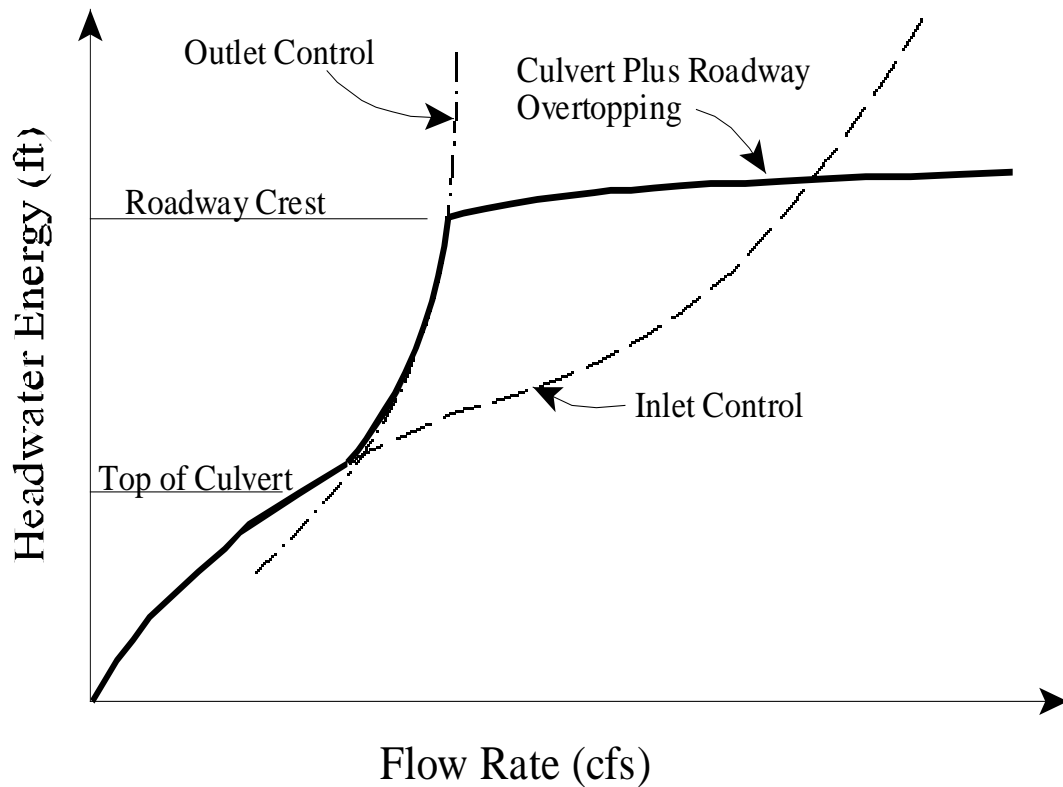
Figure 6-8 Culvert performance curve with roadway overtopping

During the computations, if the inlet control answer comes out higher than the outlet control answer, the program will perform some additional computations to evaluate if the inlet control answer can actually persist through the culvert without pressurizing the culvert barrel. The assumption of inlet control is that the flow passes through critical depth near the culvert inlet and transitions into supercritical flow. If the flow persists as low flow through the length of the culvert barrel, then inlet control is assumed to be valid. If the flow goes through a hydraulic jump inside the barrel, and fully develops the entire area of the culvert, it is assumed that this condition will cause the pipe to pressurize over the entire length of the culvert barrel and thus act more like an orifice type of flow. If this occurs, then the outlet control answer (under the assumption of a full flowing barrel) is used instead of the inlet control answer.

Computing Inlet Control Headwater

For inlet control conditions, the capacity of the culvert is limited by the capacity of the culvert opening, rather than by conditions farther downstream. Extensive laboratory tests by the National Bureau of Standards, the Bureau of Public Roads, and other entities resulted in a series of equations, which describe the inlet control headwater under various conditions. These equations form the basis of the FHWA inlet control nomographs shown in the "Hydraulic Design of Highway Culverts" publication [FHWA, 1985]. The FHWA inlet control equations are used by the HEC-RAS culvert routines in computing the upstream energy. The inlet control equations were developed for submerged and unsubmerged inlet conditions. These equations are:

Unsubmerged Inlet:

$$\frac{HW_i}{D} = \frac{H_c}{D} + K \left[\frac{Q}{AD^{0.5}} \right]^M - 0.5S \qquad (6\text{-}1)$$

$$\frac{HW_i}{D} = K \left[\frac{Q}{AD^{0.5}} \right]^M \qquad (6\text{-}2)$$

Submerged Inlet:

$$\frac{HW_i}{D} = c \left[\frac{Q}{AD^{0.5}} \right]^2 + Y - 0.5S \qquad (6\text{-}3)$$

Where: HW_i = Headwater energy depth above the invert of the culvert inlet, feet

D   = Interior height of the culvert barrel, feet

H_c = Specific head at critical depth (dc + Vc2/2g), feet

Q   = Discharge through the culvert, cfs.

A   = Full cross sectional area of the culvert barrel, feet2

S   = Culvert barrel slope, feet/feet

K,M,c ,Y   = Equation constants, which vary depending on culvert shape and entrance conditions

Note that there are two forms of the unsubmerged inlet equation. The first form (equation 6-1) is more correct from a theoretical standpoint, but form two (equation 6-2) is easier to apply and is the only documented form of equation for some of the culvert types. Both forms of the equations are used in the HEC-RAS software, depending on the type of culvert.

The nomographs in the FHWA report are considered to be accurate to within about 10 percent in determining the required inlet control headwater [FHWA, 1985]. The nomographs were computed assuming a culvert slope of 0.02 feet per foot (2 percent). For different culvert slopes, the nomographs are less accurate because inlet control headwater changes with slope. However, the culvert routines in HEC-RAS consider the slope in computing the inlet control energy. Therefore, the culvert routines in HEC-RAS should be more accurate than the nomographs, especially for slopes other than 0.02 feet per foot.

Computing Outlet Control Headwater

For outlet control flow, the required upstream energy to pass the given flow must be computed considering several conditions within the culvert and downstream of the culvert. Figure 6-9 illustrates the logic of the outlet control computations. HEC-RAS use's Bernoulli's equation in order to compute the change in energy through the culvert under outlet control conditions. The outlet control computations are energy based. The equation used by the program is the following:

$$Z_3 + Y_3 + \frac{a_3 V_3^2}{2g} = Z_2 + Y_2 + \frac{a_2 V_2^2}{2g} + H_L \qquad (6\text{-}4)$$

Where: Z_3 = Upstream invert elevation of the culvert

       Y_3 = The depth of water above the upstream culvert inlet

       V_3 = The average velocity upstream of the culvert

       a_3 = The velocity weighting coefficient upstream of the culvert

       g = The acceleration of gravity

       Z_2 = Downstream invert elevation of the culvert

       Y_2 = The depth of water above the downstream culvert inlet

       V_2 = The average velocity downstream of the culvert

       a_2 = The velocity weighting coefficient downstream of the culvert

       H_L = Total energy loss through the culvert (from section 2 to 3
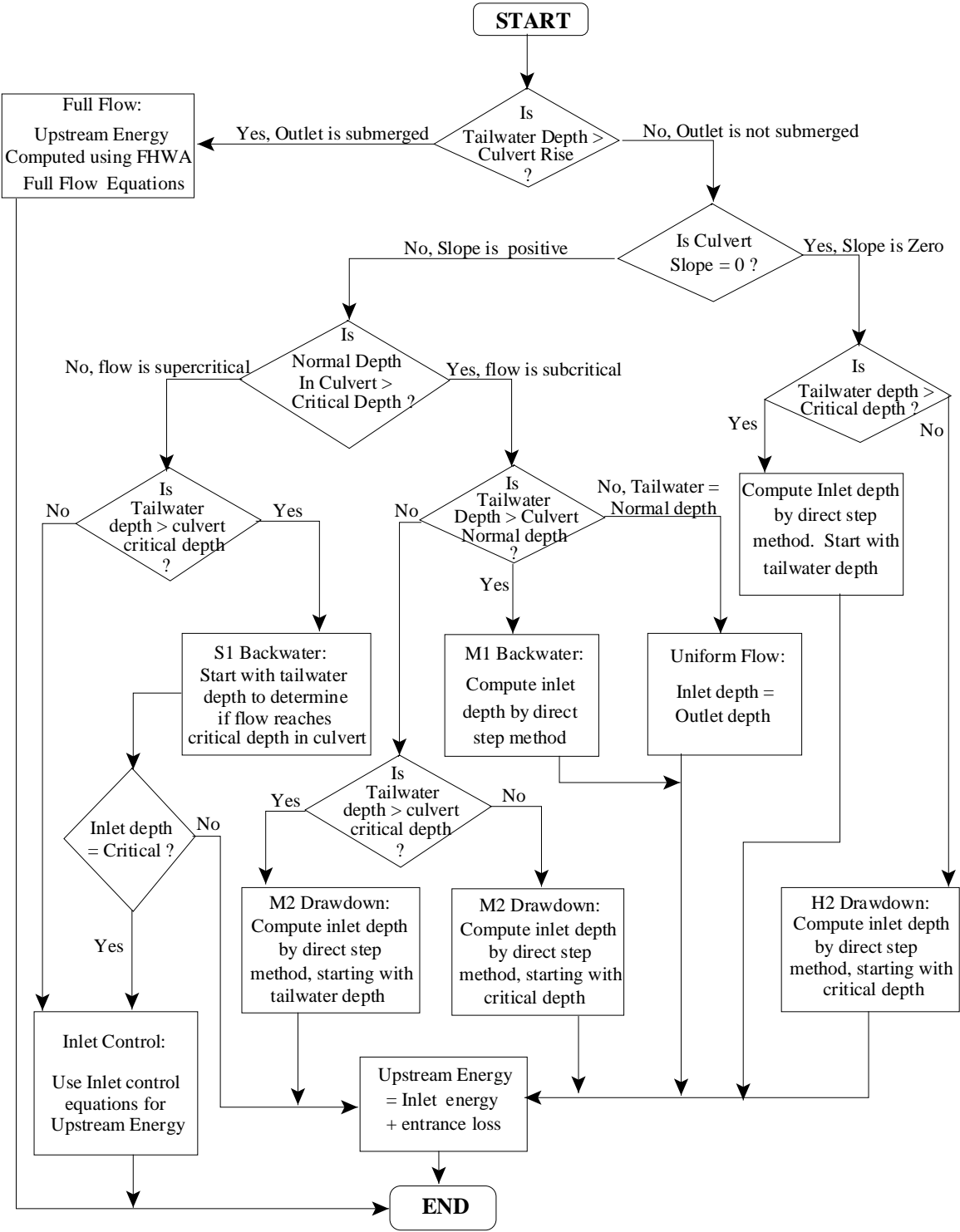
Figure 6-9 Flow Chart for Outlet Control Computations

FHWA Full Flow Equations

For culverts flowing full, the total head loss, or energy loss, through the culvert is measured in feet (or meters). The head loss, HL, is computed using the following formula:

$$H_L = h_{en} + h_f + h_{ex}$$ (6-5)

Where: h_{en} = entrance loss (feet or meters)

h_f = friction loss (feet or meters)

h_{ex} = exit loss (feet or more)

The friction loss in the culvert is computed using Manning's formula, which is expressed as follows:

$$h_f = L\left(\frac{Qn}{1.486AR^{2/3}}\right)^2$$ (6-6)

Where: h_f = friction loss (feet)

L = culvert length (feet)

Q = flow rate in the culvert (cfs)

n = Manning's roughness coefficient

A = area of flow (square feet)

R = hydraulic radius (feet)

The exit energy loss is computed as a coefficient times the change in velocity head from just inside the culvert, at the downstream end, to outside of the culvert at the downstream end. The entrance loss is computed as a coefficient times the absolute velocity head of the flow inside the culvert at the upstream end. The exit and entrance loss coefficients are described in the next section of this chapter.

Direct Step Water Surface Profile Computations

For culverts flowing partially full, the water surface profile in the culvert is computed using the direct step method. This method is very efficient, because no iterations are required to determine the flow depth for each step. The water surface profile is computed for small increments of depth (usually between 0.01 and 0.05 feet). If the flow depth equals the height of the culvert before the profile reaches the upstream end of the culvert, the friction loss through the remainder of the culvert is computed assuming full flow.

The first step in the direct step method is to compute the exit loss and establish a starting water surface inside the culvert. If the tailwater depth is below critical depth inside the culvert, then the starting condition inside the culvert is assumed to be critical depth. If the tailwater depth is greater than critical depth in the culvert, then an energy balance is performed from the downstream cross section to inside of the culvert. This energy balance evaluates the change in energy by the following equation.

$$Z_c + Y_c + \frac{a_c V_c^2}{2g} = Z_2 + Y_2 + \frac{a_2 V_2^2}{2g} + H_{ex} \qquad (6\text{-}7)$$

Where: Z_C = Elevation of the culvert invert at the dpwnstream end

     Y_C = Depth of flow inside culvert at downstream end

     V_C = Velocity inside the culvert at downstream end

     Z_2 = Invert elevation of the cross section downstream of culvert (Cross Section 2 from Figure 6-7)

     Y_2 = Depth of water at Cross Section 2

     V_2 = Average velocity of flow at Section 2

Once a water surface is computed inside the culvert at the downstream end, the next step is to perform the direct step backwater calculations through the culvert. The direct step backwater calculations will continue until a water surface and energy are obtained inside the culvert at the upstream end. The final step is to add an entrance loss to the computed energy to obtain the upstream energy outside of the culvert at Section 3 (Figure 6-7). The water surface outside the culvert is then obtained by computing the water surface at Section 3 that corresponds to the calculated energy for the given flow rate.

Normal Depth of Flow in the Culvert

Normal depth is the depth at which uniform flow will occur in an open channel. In other words, for a uniform channel of infinite length, carrying a constant flow rate, flow in the channel would be at a constant depth at all points along the channel, and this would be the normal depth.

Normal depth often represents a good approximation of the actual depth of flow within a channel segment. The program computes normal depth using an iterative approach to arrive at a value, which satisfies Manning's equation:

$$Q = \frac{1.486}{n} AR^{2/3} S_f^{1/2} \qquad\qquad (6\text{-}8)$$

Where: Q = flow rate in the channel (cfs)

     n = Manning's roughness coefficient

     A = area of flow (square feet)

     R = hydraulic radius (feet)

     S_f = slope of energy grade line (feet per foot)

If the normal depth is greater than the culvert rise (from invert to top of the culvert), the program sets the normal depth equal to the culvert rise.

Critical Depth of Flow in the Culvert

Critical depth occurs when the flow in a channel has a minimum specific energy. **Specific energy** refers to the sum of the depth of flow and the velocity head. Critical depth depends on the channel shape and flow rate.

The depth of flow at the culvert outlet is assumed to be equal to critical depth for culverts operating under outlet control with low tailwater. Critical depth may also influence the inlet control headwater for unsubmerged conditions.

The culvert routines compute critical depth in the culvert by an iterative procedure, which arrives at a value satisfying the following equation:

$$\frac{Q^2}{g} = \frac{A^3}{T} \qquad\qquad (6\text{-}9)$$

Where: Q = flow rate in the channel (cfs)

g = acceleration due to gravity (32.2 ft/sec^2)

A = cross-sectional area of flow (square feet)

T = Top width of flow (feet)

Critical depth for box culverts can be solved directly with the following equation [AISI, 1980]:

$$y_c = \sqrt[3]{\frac{q^2}{g}} \qquad\qquad (6\text{-}10)$$

Where: y_c = critical depth (feet)

q = unit discharge per linear foot of width (cfs/ft)

g = acceleration due to gravity (32.2 ft/sec^2)

Horizontal and Adverse Culvert Slopes

The culvert routines also allow for horizontal and adverse culvert slopes. The primary difference is that normal depth is not computed for a horizontal or adverse culvert. Outlet control is either computed by the direct step method for an unsubmerged outlet or the full flow equation for a submerged outlet.

Weir Flow

The first solution through the culvert is under the assumption that all of the flow is going through the culvert barrels. Once a final upstream energy is obtained, the program checks to see if the energy elevation is greater than the minimum elevation for weir flow to occur. If the computed energy is less than the minimum elevation for weir flow, then the solution is final. If the computed energy is greater than the minimum elevation for weir flow, the program performs an iterative procedure to determine the amount of flow over the weir and through the culverts. During this iterative procedure, the program recalculates both inlet and outlet control culvert solutions for each estimate of the culvert flow. In general the higher of the two is used for the culvert portion of the solution, unless the program feels that inlet control cannot be maintained. The program will continue to iterate until it finds a flow split that produces the same upstream energy (within the error tolerance) for both weir and culvert flow.

Supercritical and Mixed Flow Regime Inside of Culvert

The culvert routines allow for supercritical and mixed flow regimes inside the culvert barrel. During outlet control computations, the program first makes a subcritical flow pass through the culvert, from downstream to upstream. If the culvert barrel is on a steep slope, the program may default to critical depth inside of the culvert barrel. If this occurs, a supercritical forewater calculation is made from upstream to downstream, starting with the assumption of critical depth at the culvert inlet. During the forewater calculations, the program is continually

checking the specific force of the flow, and comparing it to the specific force of the flow from the subcritical flow pass. If the specific force of the subcritical flow is larger than the supercritical answer, the program assumes that a hydraulic jump will occur at that location. Otherwise, a supercritical flow profile is calculated all the way through and out of the culvert barrel.

For inlet control, it is assumed that the water surface passes through critical depth near the upstream end of the barrel. The first step is to find the "Vena Contracta" water surface and location. As flow passes through critical depth at the upstream end of the barrel, it goes into the supercritical flow regime. The most constricted depth that is achieved will depend on the barrel entrance shape and the flow rate. The program uses an empirical equation to estimate the location and depth of the Vena Contracta (supercritical) water surface elevation. Once this depth and location are estimated, hydraulic forewater computations are performed to get the water surface profile through the barrel. The program will evaluate and compute a hydraulic jump if either the downstream tailwater is controlling, or if the slope of the barrel is flat enough and long enough that a jump would occur due to barrel control. If a hydraulic jump occurs, and that jump produces a water surface that will fill the barrel, it is assumed that any air pocket in the barrel would burp out and that outflow control will ultimately dictate the upstream energy and water surface elevation.

Multiple Manning's n Values Inside of Culvert

This version of HEC-RAS allows the user to enter two Manning's n values inside of the culvert, one for the top and sides, and a second for the culvert bottom. The user defines the depth inside the culvert to which the bottom n value is applied. This feature can be used to simulate culverts that have a natural stream bottom, or a culvert that has the bottom portion rougher than the top, or if something has been placed in the bottom of the culvert for fish passage. An example of this is shown in Figure 6-10.
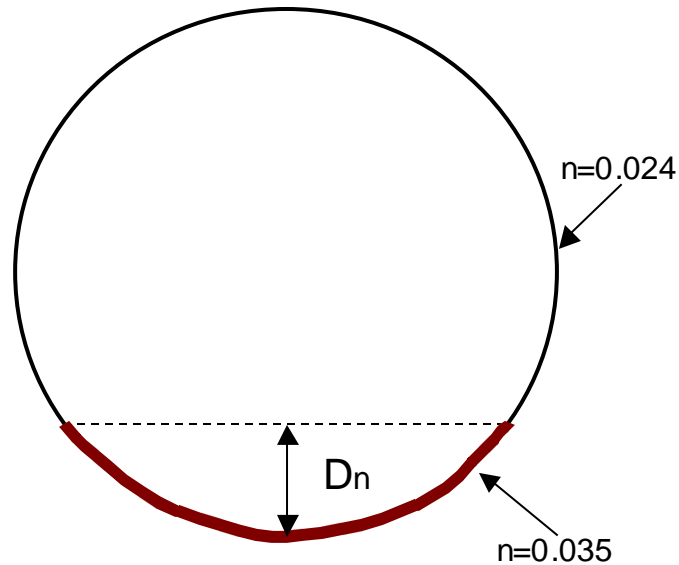
Figure 6-10 Culvert With Multiple Manning's n Values

When multiple Manning's n values are applied to a culvert, the computational program will use the bottom n value until the water surface goes above the specified bottom n value. When the water surface goes above the bottom n value depth the program calculates a composite n value for the culvert as a whole. This composite n value is based on an equation from Chow's book on Open Channel Hydraulics (Chow, 1959) and is the same equation we use for computing a composite n value in open channel flow (see equation 2- 6, from chapter 2 of this manual).

Partially Filled or Buried Culverts

This version of HEC-RAS allows the user to fill in a portion of the culvert from the bottom. This option can be applied to any of the culvert shapes. The user is only required to specify the depth to which the culvert bottom is filled in. An example of this is shown in figure 6-11. The user can also specify a different Manning's n value for the blocked portion of the culvert (the bottom), versus the remainder of the culvert. The user must specify the depth to apply the bottom n value as being equal to the depth of the filled portion of the culvert.
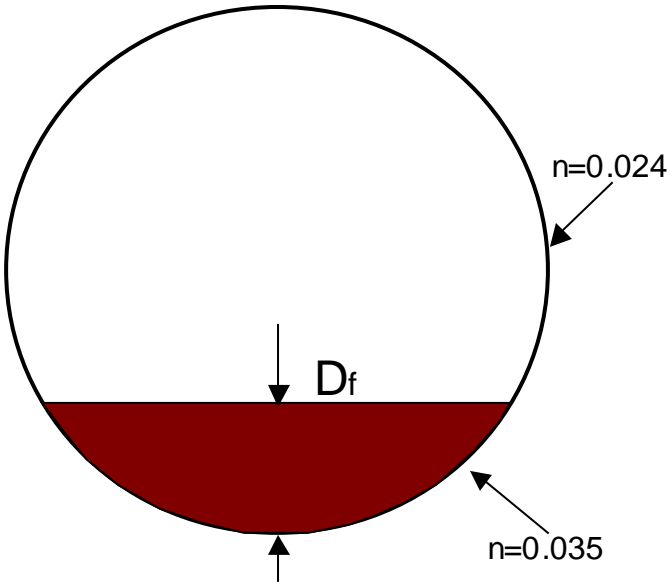
Figure 6-11 Partially Filled or Buried Culverts

Comparison to the USGS Culvert Procedures

Many people have asked how the HEC-RAS culvert routines compare to the USGS culvert procedures outlined in the publication "Measurement of Peak Discharge at Culverts by Indirect Methods" (Bodhaine, 1978), and if the HEC-RAS software would give the same or similar answers to their culvert analysis program (CAP). To prove that HEC-RAS could handle all 6 flow types outlined in the USGS publication, we put models together to replicate 8 of the example data sets in the back of the USGS publication mentioned above. HEC-RAS was able to compute similar upstream water surface elevations, as reported in the USGS publication, for all of the example data sets except number 8. However, we believe the reported result for example problem number 8 is questionable. This will be explained in more detail below. The 8 examples were put together in HEC-RAS by entering the culvert geometry, and all other properties provided in the publication.

Here is a table of the HEC-RAS and USGS answers for the 8 example problems:

Example Number	Flow Rate Q (cfs)	USGS Water Surface (ft)	HEC-RAS Water Surface (ft)	HEC-RAS Flow Classification	USGS Flow Classification
1	729	12.00	11.89	Inlet	1
2	530	10.00	10.68	Inlet	1
3	268	6.00	6.00	Outlet	2
4	523	8.19	8.88	Outlet	2
5	251	6.00	5.94	Outlet	3
6	125	7.00	7.17	Outlet	4
7	120	8.00	8.14	Inlet	5
8*	209	8.00	11.00	Inlet	6

***Note**: We think the answer shown in the USGS publication, for example number 8, questionable. Here is why:

Example 8 is for a circular concrete culvert that is 4.0 feet in diameter. The Manning's n is 0.012, and the culvert has a beveled entrance. The resulting flow rate computed in the example is 209 cfs. The culvert invert is set at an elevation of 1.0 ft at the upstream end, and the top of the culvert is at 5.0 feet inside elevation at the upstream end.

> The Culvert Area is A = 12.5664 sq. ft.
>
> Therefore V = Q/A = 209/12.5664 = 16.63 ft/s inside the culvert at the upstream end.
>
> The velocity head is $V^2/2g = (16.63)^2/ (2\times32.3) = 4.3$ feet of velocity head.

Therefore, the energy at the upstream inside end of the barrel must be at least 5.0 + 4.3 = 9.3 feet of energy head. The energy upstream, outside of the barrel, will be this energy plus an entrance losses to get the flow into the barrel, plus friction losses. Therefore the upstream energy will be greater than 9.3 feet. HEC-RAS computed an upstream energy of 11.0 feet, which we believe is more correct than the 8.00 feet reported in example 8 in the USGS report.

The USGS results of 8.0 feet is based on the assumption of this culvert acting as a Syphon for this particular flow rate. The HEC-RAS computations did not fill the barrel, so we do not think the culvert will act as a Syphon. If the culvert were to act like a Syphon, then the answer would be closer to the USGS culvert routines answer.

Additionally HEC-RAS was able to reproduce all six of the USGS flow classification types. For Type 6, the example 8 problem did not flow as a full barrel for HEC-RAS. However, we took the same data set and lowered the upstream invert to an elevation of 0.0 feet, which put the culvert on a horizontal slope. HEC-RAS did compute that the flow was following the USGS Type 6 classification for this culvert.

We have therefore concluded that HEC-RAS can handle all 6 of the USGS Culvert flow classifications, and can reproduce the results of the CAP program within a reasonable tolerance (Except for example 8, which is in not been resolved at this time). It is also believed that most of the differences in the results are due to the fact they the two programs use different: empirical coefficients entrance losses; friction slope computations (therefore different friction losses); and exit losses.

Culvert Data and Coefficients

This section describes the basic data that are required for each culvert. Discussions include how to estimate the various coefficients that are required in order to perform inlet control, outlet control, and weir flow analyses. The culvert data are entered on the Culvert Data Editor in the user interface. Discussions about the culvert data editor can be found in Chapter 6 of the HEC-RAS User's Manual.

Culvert Shape and Size

The shape of the culvert is defined by picking one of the nine available shapes. These shapes include: circular; box (rectangular); arch; pipe arch; elliptical; high profile arch; low profile arch; semi-circular; and ConSpan. The size of the culvert is defined by entering a rise and span. The rise refers to the maximum inside height of the culvert, while the span represents the maximum inside width. Both the circular and semi-circular culverts are defined by entering a diameter.

The inside height (rise) of a culvert opening is important not only in determining the total flow area of the culvert, but also in determining whether the headwater and tailwater elevations are adequate to submerge the inlet or outlet of the culvert. Most box culverts have **chamfered** corners on the inside, as indicated in Figure 6-6. The chamfers are ignored by the culvert routines in computing the cross-sectional area of the culvert opening. Some manufacturers' literature contains the true cross-sectional area for each size of box culvert, considering the reduction in area caused by the chamfered corners. If you wish to consider the loss in area due to the chamfers, then you should reduce the span of the culvert. You should not reduce the rise of the culvert, because the program uses the culvert rise to determine the submergence of the culvert entrance and outlet.

All of the arch culverts (arch, pipe arch, low profile arch, high profile arch, and ConSpan arch) within HEC-RAS have pre-defined sizes. However, the user can specify any size they want. When a size is entered that is not one of the pre-defined sizes, the program interpolates the hydraulic properties of the culvert from tables (except for ConSpan culverts).

HEC-RAS has 9 predefined Conspan arches. Conspan arches are composed of two vertical walls and an arch. Each predefined span has a predefined arch height, for example the 12 ft arch has an arch height of 3.07 ft. For the 12 span, any rise greater than 3.07 ft can be made by adding vertical wall below the arch, when a rise is entered less than the arch height, the arch must be modified as discussed below.   RAS has the ability to produce a culvert shape for rise and span combinations not in the predefined list. The following is a list of the pre-defined ConSpan sizes.

Predefined Spans	Arch Heights
12	3.00
14	3.00
16	3.53
20	4.13
24	4.93
28	5.76
32	6.51
36	7.39
42	9.19

If a span is requested that is not in the list of predefined shapes, then one is interpolated geometrically from the bounding predefined shapes. The plot below shows an interpolated 21 ft arch from 20 and 24 predefined arches.
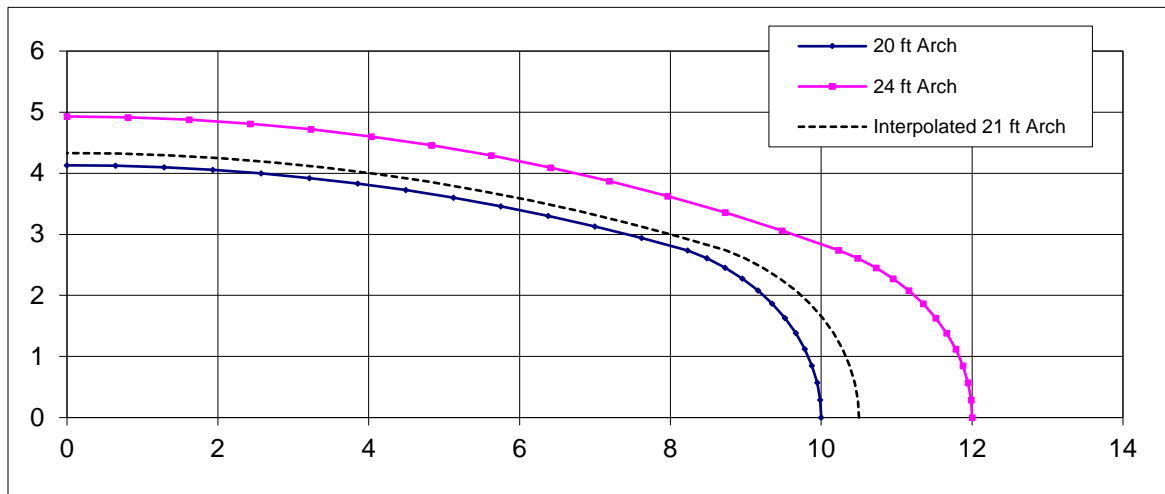
Figure 6-12 Geometric Interpolation of ConSpan Culvert for Non-Standard Widths (Span)

If the span is less that the smallest predefined arch, then the smallest arch is scaled to the requested span, similarly, if a span is entered larger than the largest predefined arch, then the largest arch is scaled to the requested span.

If a rise is entered that is less that the predefined arch rise, then the vertical ordinates of the arch are scaled down to the requested arch rise and no vertical segments are added. In the plot below, a 20 ft span was requested with a 3 ft rise.   The arch height of the 20 ft span is 4.13 feet so all the vertical distances were multiplied by 3 / 4.13.
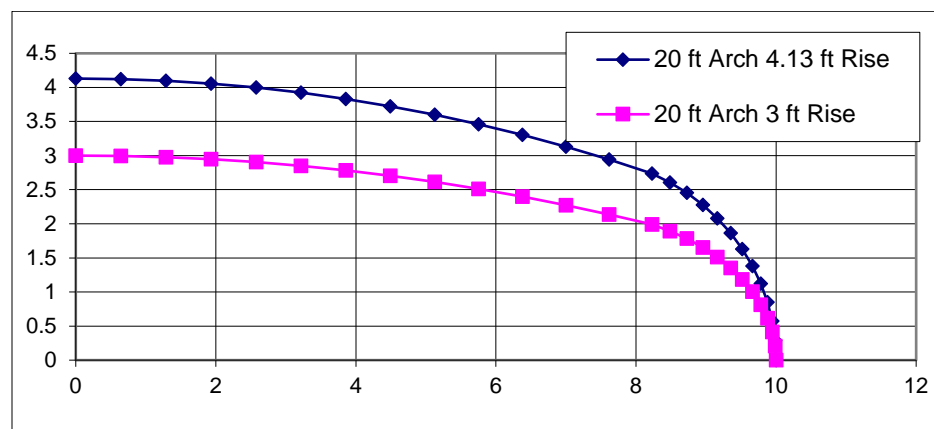
Figure 6-13 Geometric Interpolation of the ConSpan Culvert for Non-Standard Rise.

Culvert Length

The culvert length is measured in feet (or meters) along the center-line of the culvert. The culvert length is used to determine the friction loss in the culvert barrel and the slope of the culvert.

Number of Identical Barrels

The user can specify up to 25 identical barrels. To use the identical barrel option, all of the culverts must be identical; they must have the same cross-sectional shape and size, chart and scale number, length, entrance and exit loss coefficients, upstream and downstream invert elevations, and roughness coefficients. If more than one barrel is specified, the program automatically divides the flow rate equally among the culvert barrels and then analyzes only a single culvert barrel. The hydraulics of each barrel is assumed to be exactly the same as the one analyzed.

Manning's Roughness Coefficient

The Manning's roughness coefficients must be entered for each culvert type. HEC-RAS uses Manning's equation to compute friction losses in the culvert barrel, as described in the section entitled "Culvert Hydraulics" of this chapter. Suggested values for Manning's n-value are listed in Table 6-1 and Table 6-2, and in many hydraulics reference books. Roughness coefficients should be adjusted according to individual judgment of the culvert condition.

Entrance Loss Coefficient

Entrance losses are computed as a function of the velocity head inside the culvert at the upstream end. The entrance loss for the culvert is computed as:

$$h_{en} = k_{en} \frac{V_{en}^2}{2g}$$
(6-11)

Where: h_{en} = Energy loss due to the entrance

k_{en} = Entrance loss coefficient

V_{en} = Flow velocity inside the culvert at the entrance

g = Acceleration due to gravity

The velocity head is multiplied by the **entrance loss coefficient** to estimate the amount of energy lost as flow enters the culvert. A higher value for the coefficient gives a higher head loss. Entrance loss coefficients are shown in Tables 6-3, 6-4, and 6-5. These coefficients were taken from the Federal Highway Administration's "Hydraulic Design of Highway Culverts" manual (FHWA, 1985). Table 6-3 indicates that values of the entrance loss coefficient range from 0.2 to about 0.9 for pipe-arch and pipe culverts. As shown in Table 6-4, entrance losses can vary from about 0.2 to about 0.7 times the velocity head for box culverts. For a sharp-edged culvert entrance with no rounding, 0.5 is recommended. For a well-rounded entrance, 0.2 is appropriate. Table 6-5 list entrance loss coefficients for ConSpan culverts.

Note: Entrance loss coefficients should be calibrated whenever possible. The Tables shown in this document for entrance loss coefficients are guidelines and not absolutes.

Table 6-1 Manning's "n" for Closed Conduits Flowing Partly Full

Type of Channel and Description	Minimum	Normal	Maximum
Brass, smooth:	0.009	0.010	0.013
Steel:			
Lockbar and welded	0.010	0.012	0.014
Riveted and spiral	0.013	0.016	0.017
Cast Iron:			
Coated	0.010	0.013	0.014
Uncoated	0.011	0.014	0.016
Wrought Iron:			
Black	0.012	0.014	0.015
Galvanized	0.013	0.016	0.017
Corrugated Metal:			
Subdrain	0.017	0.019	0.021
Storm Drain	0.021	0.024	0.030
Lucite:	0.008	0.009	0.010
Glass:	0.009	0.010	0.013
Cement:			
Neat, surface	0.010	0.011	0.013
Mortar	0.011	0.013	0.015
Concrete:			
Culvert, straight and free of debris	0.010	0.011	0.013
Culvert with bends, connections, and some debris	0.011	0.013	0.014
Finished	0.011	0.012	0.014
Sewer with manholes, inlet, etc., straight	0.013	0.015	0.017
Unfinished, steel form	0.012	0.013	0.014
Unfinished, smooth wood form	0.012	0.014	0.016
Unfinished, rough wood form	0.015	0.017	0.020
Wood:			
Stave	0.010	0.012	0.014
Laminated, treated	0.015	0.017	0.020
Clay:			
Common drainage tile	0.011	0.013	0.017
Vitrified sewer	0.011	0.014	0.017
Vitrified sewer with manholes, inlet, etc.	0.013	0.015	0.017
Vitrified Subdrain with open joint	0.014	0.016	0.018
Brickwork:			
Glazed	0.011	0.013	0.015
Lined with cement mortar	0.012	0.015	0.017
Sanitary sewers coated with sewage slime with bends and connections	0.012	0.013	0.016
Paved invert, sewer, smooth bottom	0.016	0.019	0.020
Rubble masonry, cemented	0.018	0.025	0.030

[Chow, 1959]

Table 6-2 Manning's "n" for Corrugated Metal Pipe

Type of Pipe and Diameter	Unpaved	25% Paved	Fully Paved
Annular 2.67 x 2 in. (all diameters) **Helical 1.50 x 1/4 in.:**	0.024	0.021	0.021
8 inch diameter	0.012		
10 inch diameter	0.014		
Helical 2.67 x 2 inc.:			
12 inch diameter	0.011		
18 inch diameter	0.014		
24 inch diameter	0.016	0.015	0.012
36 inch diameter	0.019	0.017	0.012
48 inch diameter	0.020	0.020	0.012
60 inch diameter	0.021	0.019	0.012
Annular 3 x 1 in. (all diameters)	0.027	0.023	0.012
Helical 3 x 1 in.:			
48 inch diameter	0.023	0.020	0.012
54 inch diameter	0.023	0.020	0.012
60 inch diameter	0.024	0.021	0.012
66 inch diameter	0.025	0.022	0.012
72 inch diameter	0.026	0.022	0.012
78 inch & larger	0.027	0.023	0.012
Corrugations 6 x 2 in.:			
60 inch diameter	0.033	0.028	
72 inch diameter	0.032	0.027	
120 inch diameter	0.030	0.026	
180 inch diameter	0.028	0.024	

[AISI, 1980]

Table 6-3 Entrance Loss Coefficient for Pipe Culverts

Type of Structure and Design of Entrance	Coefficient, k_{en}
Concrete Pipe Projecting from Fill (no headwall):	
Socket end of pipe	0.2
Square cut end of pipe	0.5
Concrete Pipe with Headwall or Headwall and Wingwalls:	
Socket end of pipe (grooved end)	0.2
Square cut end of pipe	0.5
Rounded entrance, with rounding radius = 1/12 of diameter	0.2
Concrete Pipe:	
Mitered to conform to fill slope	0.7
End section conformed to fill slope	0.5
Beveled edges, 33.7 or 45 degree bevels	0.2
Side slope tapered inlet	0.2
Corrugated Metal Pipe or Pipe-Arch:	
Projected from fill (no headwall)	0.9
Headwall or headwall and wingwalls square edge	0.5
Mitered to conform to fill slope	0.7
End section conformed to fill slope	0.5
Beveled edges, 33.7 or 45 degree bevels	0.2
Side slope tapered inlet	0.2

Table 6-4 Entrance Loss Coefficient for Reinforced Concrete Box Culverts

Type of Structure and Design of Entrance	Coefficient, k_{en}
Headwall Parallel to Embankment (no wingwalls):	
Square-edged on three edges	0.5
Three edges rounded to radius of 1/12 barrel dimension	0.2
Wingwalls at 30 to 75 degrees to Barrel:	
Square-edge at crown	0.4
Top corner rounded to radius of 1/12 barrel dimension	0.2
Wingwalls at 10 to 25 degrees to Barrel:	
Square-edge at crown	0.5
Wingwalls parallel (extension of sides):	
Square-edge at crown	0.7
Side or slope tapered inlet	0.2

Table 6-5 Entrance Loss Coefficients For ConSpan Culverts

Type of Entrance	Coefficient, k_{en}
Extended wingwalls 0 degrees	0.5
45 degree wingwalls	0.3
Straight Headwall	0.4

Exit Loss Coefficient

Exit losses are computed as a coefficient times the change in velocity head from just inside the culvert, at the downstream end, to the cross section just downstream of the culvert. The equation for computing exit losses is as follows:

$$h_{ex} = k_{ex} \left(\frac{a_{ex} V_{ex}^2}{2g} - \frac{a_2 V_2^2}{2g} \right) \tag{6-12}$$

Where: h_{ex} = Energy loss due to exit

k_{ex} = Exit loss coefficient

V_{ex} = Velocity inside of culvert at exit

V_2 = Velocity outside of culvert at downstream cross   section

For a sudden expansion of flow, such as in a typical culvert, the exit loss coefficient (kex) is normally set to 1.0 (FHWA, 1985). In general, exit loss coefficients can vary between 0.3 and 1.0. The exit loss coefficient should be reduced as the transition becomes less abrupt.

FHWA Chart and Scale Numbers

The FHWA chart and scale numbers are required input data. The FHWA chart number and scale number refer to a series of nomographs published by the Bureau of Public Roads (now called the Federal Highway Administration) in 1965 [BPR, 1965], which allowed the inlet control headwater to be computed for different types of culverts operating under a wide range of flow conditions. These nomographs and others constructed using the original methods were republished [FHWA, 1985]. The tables in this chapter are copies of the information from the 1985 FHWA publication.

Each of the FHWA charts has from two to four separate scales representing different culvert entrance designs. The appropriate FHWA chart number and scale number should be chosen according to the type of culvert and culvert entrance. Table 6-6 may be used for guidance in selecting the FHWA chart number and scale number.

Chart numbers 1, 2, and 3 apply only to pipe culverts. Similarly, chart numbers 8, 9, 10, 11, 12, and 13 apply only to box culverts. The HEC-RAS program checks the chart number to assure that it is appropriate for the type of culvert being analyzed. HEC-RAS also checks the value of the Scale Number to assure that it is available for the given chart number. For example, a scale number of 4 would be available for chart 11, but not for chart 12.

Figures 6-14 through 6-23 can be used as guidance in determining which chart and scale numbers to select for various types of culvert inlets.
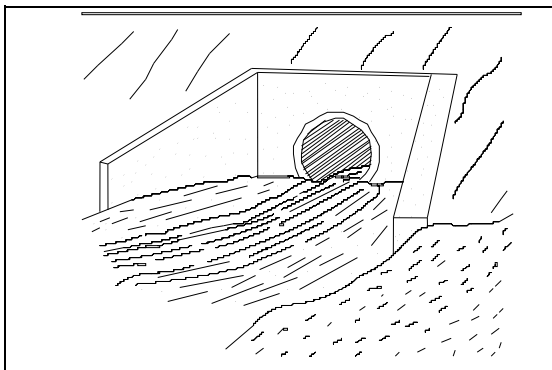
Figure 6-14

Culvert Inlet with Hardwall and Wingwalls
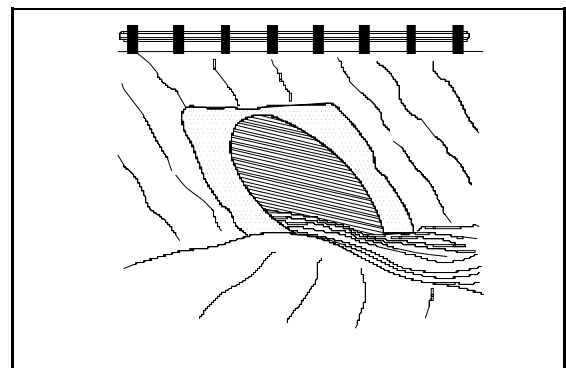
Figure 6-15

Culvert Inlet Mitered to Conform to Slope

Table 6-6 FHWA Chart and Scale Numbers for Culverts

Chart Number	Scale Number	Description
1		**Concrete Pipe Culvert**
	1	Square edge entrance with headwall (See Figure 6-10)
	2	Groove end entrance with headwall (See Figure 6-10)
	3	Groove end entrance, pipe projecting from fill (See Figure 6-12)
2		**Corrugated Metal Pipe Culvert**
	1	Headwall (See Figure 6-10)
	2	Mitered to conform to slope (See Figure 6-11)
	3	Pipe projecting from fill (See Figure 6-12)
3		**Concrete Pipe Culvert; Beveled Ring Entrance (See Figure 6-13)**
	1(A)	Small bevel: b/D = 0.042; a/D = 0.063; c/D = 0.042; d/D = 0.083
	2(B)	Large bevel; b/D = 0.083; a/D = 0.125; c/D = 0.042; d/D = 0.125
8		**Box Culvert with Flared Wingwalls (See Figure 6-14)**
	1	Wingwalls flared 30 to 75 degrees
	2	Wingwalls flared 90 or 15 degrees
	3	Wingwalls flared 0 degrees (sides extended straight)
9		**Box Culvert with Flared Wingwalls and Inlet Top Edge Bevel (See Figure 6-15)**
	1	Wingwall flared 45 degrees; inlet top edge bevel = 0.043D
	2	Wingwall flared 18 to 33.7 degrees; inlet top edge bevel = 0.083D
10		**Box Culvert; 90-degree Headwall; Chamfered or Beveled Inlet Edges (See Figure 6-16)**
	1	Inlet edges chamfered 3/4-inch
	2	Inlet edges beveled 2-in/ft at 45 degrees (1:1)
	3	Inlet edges beveled 1-in/ft at 33.7 degrees (1:1.5)
11		**Box Culvert; Skewed Headwall; Chamfered or Beveled Inlet Edges (See Figure 6-17)**
	1	Headwall skewed 45 degrees; inlet edges chamfered 3/4-inch
	2	Headwall skewed 30 degrees; inlet edges chamfered 3/4-inch
	3	Headwall skewed 15 degrees; inlet edges chamfered 3/4-inch
	4	Headwall skewed 10 to 45 degrees; inlet edges beveled
12		**Box Culvert; Non-Offset Flared Wingwalls; 3/4-inch Chamfer at Top of Inlet (See Figure 6-18)**
	1	Wingwalls flared 45 degrees (1:1); inlet not skewed
	2	Wingwalls flared 18.4 degrees (3:1); inlet not skewed
	3	Wingwalls flared 18.4 degrees (3:1); inlet skewed 30 degrees
13		**Box Culvert; Offset Flared Wingwalls; Beveled Edge at Top of Inlet (See Figure 6-19)**
	1	Wingwalls flared 45 degrees (1:1); inlet top edge bevel = 0.042D
	2	Wingwalls flared 33.7 degrees (1.5:1); inlet top edge bevel = 0.083D
	3	Wingwalls flared 18.4 degrees (3:1); inlet top edge bevel = 0.083D
16-19		**Corrugated Metal Box Culvert**
	1	90 degree headwall
	2	Thick wall Projecting
	3	Thin wall projecting
29		**Horizontal Ellipse; Concrete**
	1	Square edge with headwall
	2	Grooved end with headwall
	3	Grooved end projecting
30		**Vertical Ellipse; Concrete**
	1	Square edge with headwall
	2	Grooved end with headwall
	3	Grooved end projecting
34		**Pipe Arch; 18" Corner Radius; Corrugated Metal**
	1	90 Degree headwall
	2	Mitered to slope
	3	Projecting

Table 6-6 (Continued) FHWA Chart and Scale Numbers for Culverts

Chart Number	Scale Number	Description
35		**Pipe Arch; 18" Corner Radius; Corrugated Metal**
	1	Projecting
	2	No bevels
	3	33.7 degree bevels
36		**Pipe Arch; 31" Corner Radius; Corrugated Metal**
	1	Projecting
	2	No bevels
	3	33.7 degree bevels
41-43		**Arch; low-profile arch; high-profile arch; semi circle; Corrugated Metal**
	1	90 degree headwall
	2	Mitered to slope
	3	Thin wall projecting
55		**Circular Culvert**
	1	Smooth tapered inlet throat
	2	Rough tapered inlet throat
56		**Elliptical Inlet Face**
	1	Tapered inlet; Beveled edges
	2	Tapered inlet; Square edges
	3	Tapered inlet; Thin edge projecting
57		**Rectangular**
	1	Tapered inlet throat
58		**Rectangular Concrete**
	1	Side tapered; Less favorable edges
	2	Side tapered; More favorable edges
59		**Rectangular Concrete**
	1	Slope tapered; Less favorable edges
	2	Slope tapered; More favorable edges
60		**ConSpan Span/Rise Approximately 2:1**
	1	0 degree wingwall angle
	2	45 degree wingwall angle
	3	90 degree wingwall angle
61		**ConSpan Span/Rise Approximately 4:1**
	1	0 degree wingwall angle
	2	45 degree wingwall angle
	3	90 degree wingwall angle

Figure 6-16 Culvert Inlet Projecting from Fill
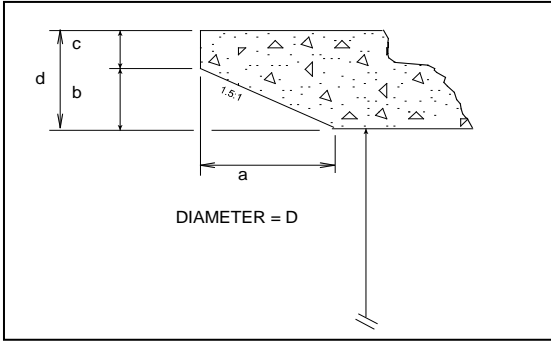
Figure 6-17 Culvert Inlet with Beveled Ring Entrance
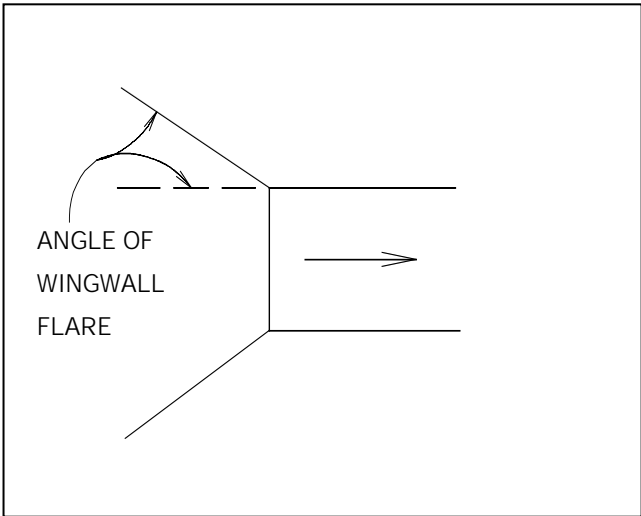
Figure 6-18 Flared Wingwalls (Chart 8)
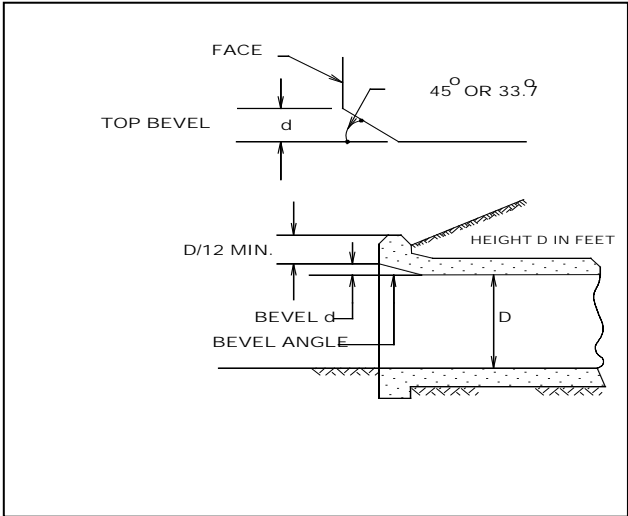
Figure 6-19 Inlet Top Edge Bevel (Chart 9)
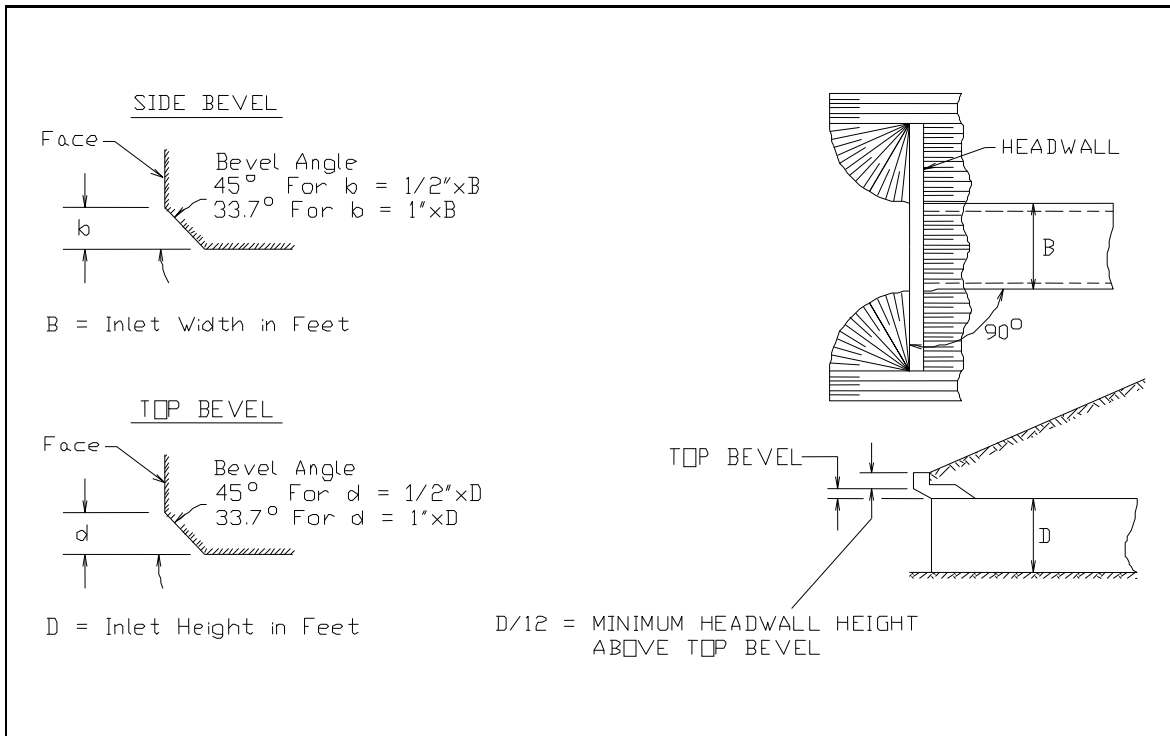
Figure 6-20 Inlet Side and Top Edge Bevel with Ninety Degree Headwall (Chart 10)
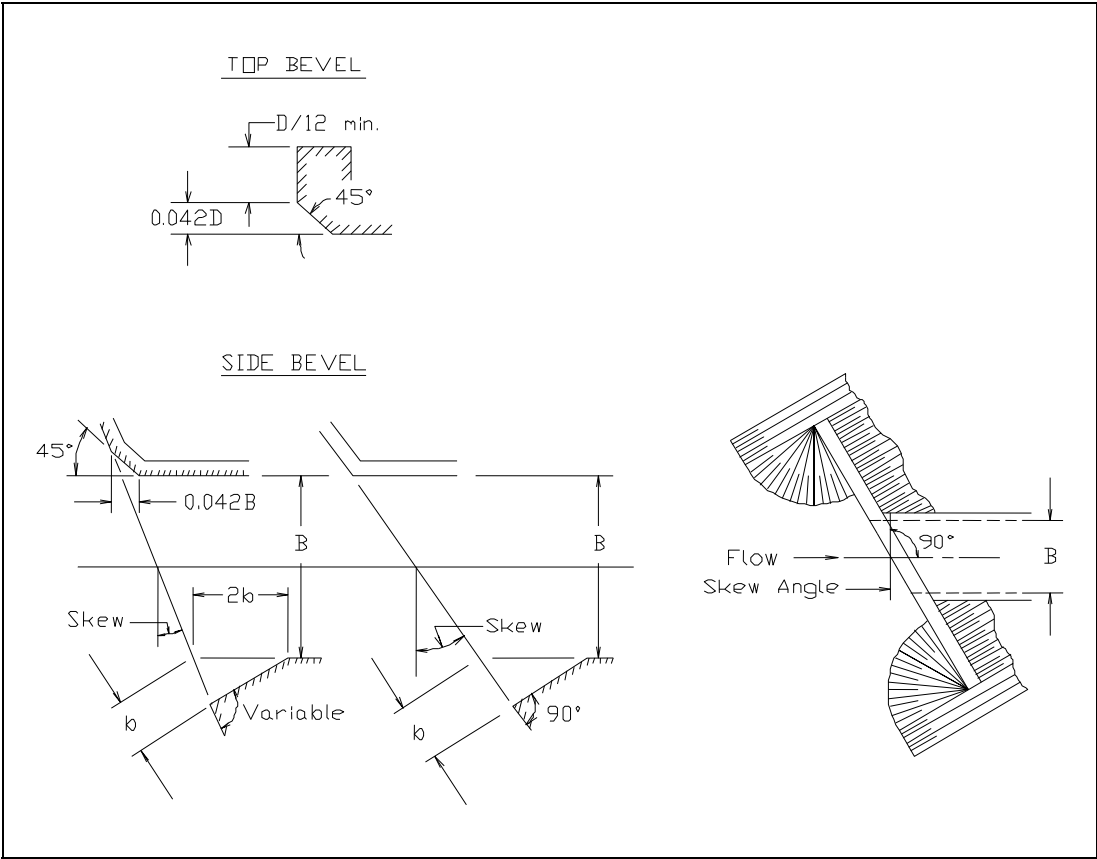
Figure 6-21 Inlet Side and Top Edge Bevel with Skewed Headwall (Chart 11)
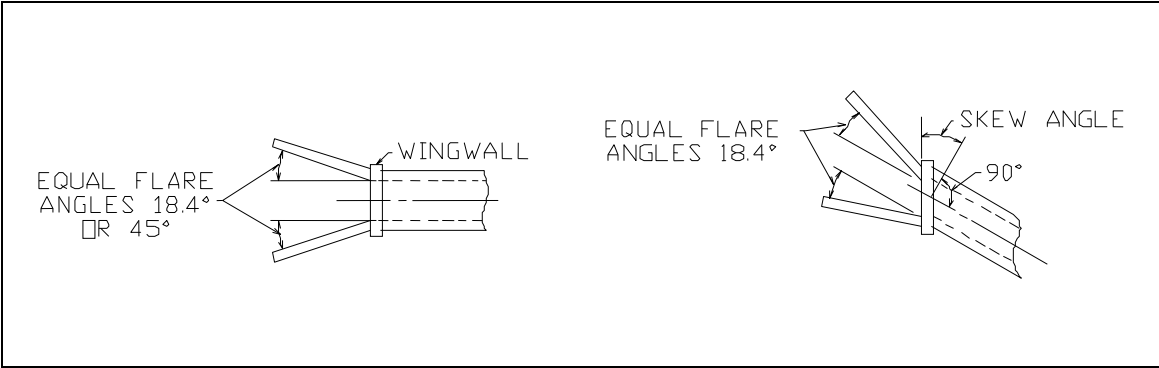
Figure 6-22 Non-Offset Flared Wingwalls (Chart 12)
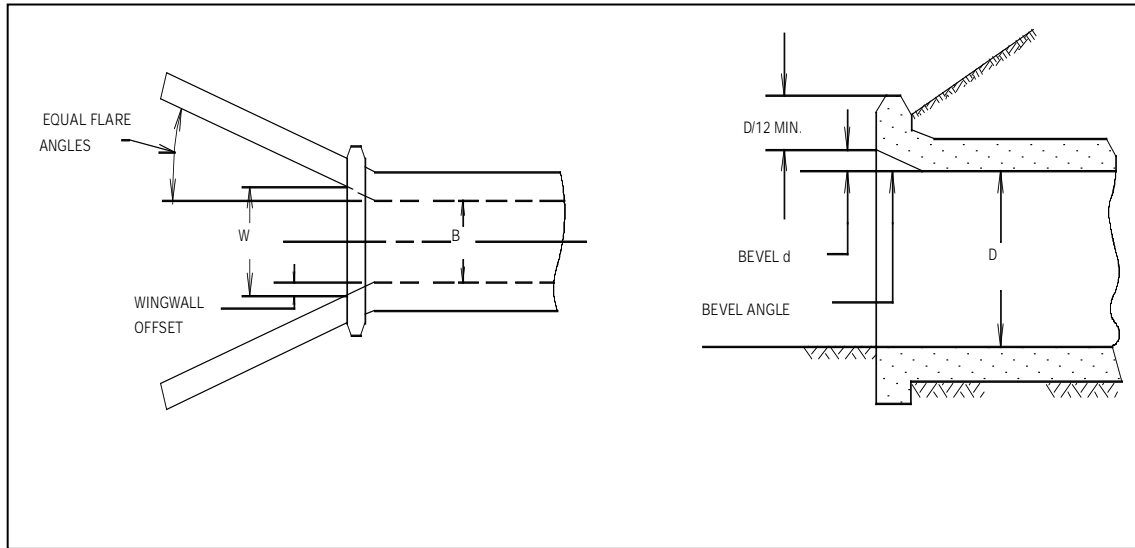
Figure 6-23 Offset Flared Wingwalls (Chart 13)

Culvert Invert Elevations

The culvert flow-line slope is the average drop in elevation per foot of length along the culvert. For example, if the culvert flow-line drops 1 foot in a length of 100 feet, then the culvert flow-line slope is 0.01 feet per foot. Culvert flow-line slopes are sometimes expressed in percent. A slope of 0.01 feet per foot is the same as a one percent slope.

The culvert slope is computed from the upstream invert elevation, the downstream invert elevation, and the culvert length. The following equation is used to compute the culvert slope:

$$S = \frac{ELCHU - ELCHD}{\sqrt{CULCLN^2 - (ELCHU - ELCHD)^2}} \qquad (6\text{-}13)$$

Where: $ELCHU$ = Elevation of the culvert invert upstream

$ELCHD$ = Elevation of the culvert invert downstream

$CULVLN$ = Length of the culvert

The slope of the culvert is used by the program to compute the normal depth of flow in the culvert under outlet control conditions.

Weir Flow Coefficient

Weir flow over a roadway is computed in the culvert routines using exactly the same methods used in the HEC-RAS bridge routines. The standard weir equation is used:

$$Q = CLH^{3/2} \qquad\qquad (6\text{-}14)$$

Where: Q = flow rate

        C = weir flow coefficient

        L = weir length

        H = weir energy head

For flow over a typical bridge deck, a weir coefficient of 2.6 is recommended. A weir coefficient of 3.0 is recommended for flow over elevated roadway approach embankments. More detailed information on weir discharge coefficients and how weirs are modeled in HEC-RAS may be found in Chapter 5 of this manual, "Modeling Bridges." Also, information on how to enter a bridge deck and weir coefficients can be found in Chapter 6 of the HEC-RAS User's Manual, "Editing and Entering Geometric Data."

CHAPTER 7

Modeling Multiple Bridge and/or Culvert Openings

The HEC-RAS program has the ability to model multiple bridge and/or culvert openings at a single location. A common example of this type of situation is a bridge opening over the main stream and a relief bridge (or group of culverts) in the overbank area. The HEC-RAS program is capable of modeling up to seven opening types at any one location.

Contents
■ General Modeling Guidelines

■ Multiple Opening Approach

■ Divided Flow Approach

General Modeling Guidelines

Occasionally you may need to model a river crossing that cannot be modeled adequately as a single bridge opening or culvert group. This often occurs in wide floodplain areas where there is a bridge opening over the main river channel, and a relief bridge or group of culverts in the overbank areas. There are two ways you can model this type of problem within HEC-RAS. The first method is to use the multiple opening capability in HEC-RAS, which is discussed in detail in the following section. A second method is to model the two openings as divided flow. This method would require the user to define the flow path for each opening as a separate reach. This option is discussed in the last section of this chapter.

Multiple Opening Approach

The multiple opening features in HEC-RAS allow users to model complex bridge and/or culvert crossings within a one dimensional flow framework. HEC-RAS has the ability to model three types of openings: Bridges; Culvert Groups (a group of culverts is considered to be a single opening); and Conveyance Areas (an area where water will flow as open channel flow, other than a bridge or culvert opening). Up to seven openings can be defined at any one river crossing. The HEC-RAS multiple opening methodology is limited to subcritical flow profiles. The program can also be run in mixed flow regime mode, but only a subcritical profile will be calculated in the area of the multiple opening. An example of a multiple opening is shown in Figure 7-1.

As shown in Figure 7-1, the example river crossing has been defined as three openings, labeled as #1, #2, and #3. Opening #1 represents a Conveyance Area, opening #2 is a Bridge opening, and opening #3 is a Culvert Group.

The approach used in HEC-RAS is to evaluate each opening as a separate entity. An iterative solution is applied, in which an initial flow distribution between openings is assumed. The water surface profile and energy gradient are calculated through each opening. The computed upstream energies for each opening are compared to see if they are within a specified tolerance (the difference between the opening with the highest energy and the opening with the lowest energy must be less than the tolerance). If the difference in energies is not less than the tolerance, the program makes a new estimate of the flow distribution through the openings and repeats the process. This iterative technique continues until either a solution that is within the tolerance is achieved, or a predefined maximum number of iterations is reached (the default maximum is 30).

Reach: Easy Creek Riv.Sta.: 5
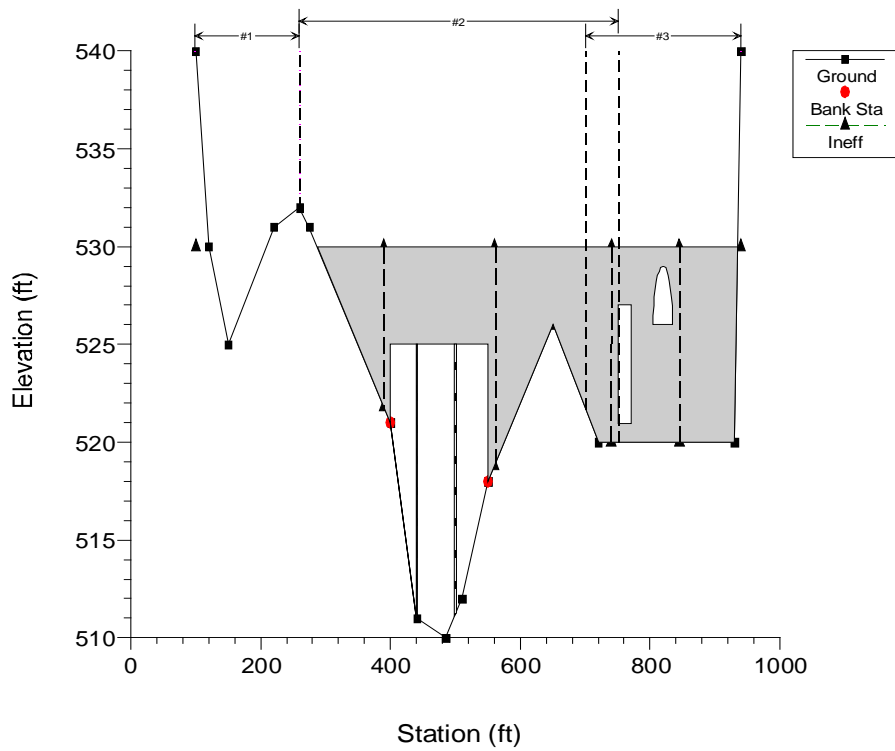
Figure 7-1 Example Multiple Opening River Crossing

The distribution of flow requires the establishment of flow boundaries both upstream and downstream of the openings. The flow boundaries represent the point at which flow separates between openings. These flow boundaries are referred to as "Stagnation Points" (the term "stagnation points" will be used from this point on when referring to the flow separation boundaries). A plan view of a multiple opening is shown in Figure 7-2.
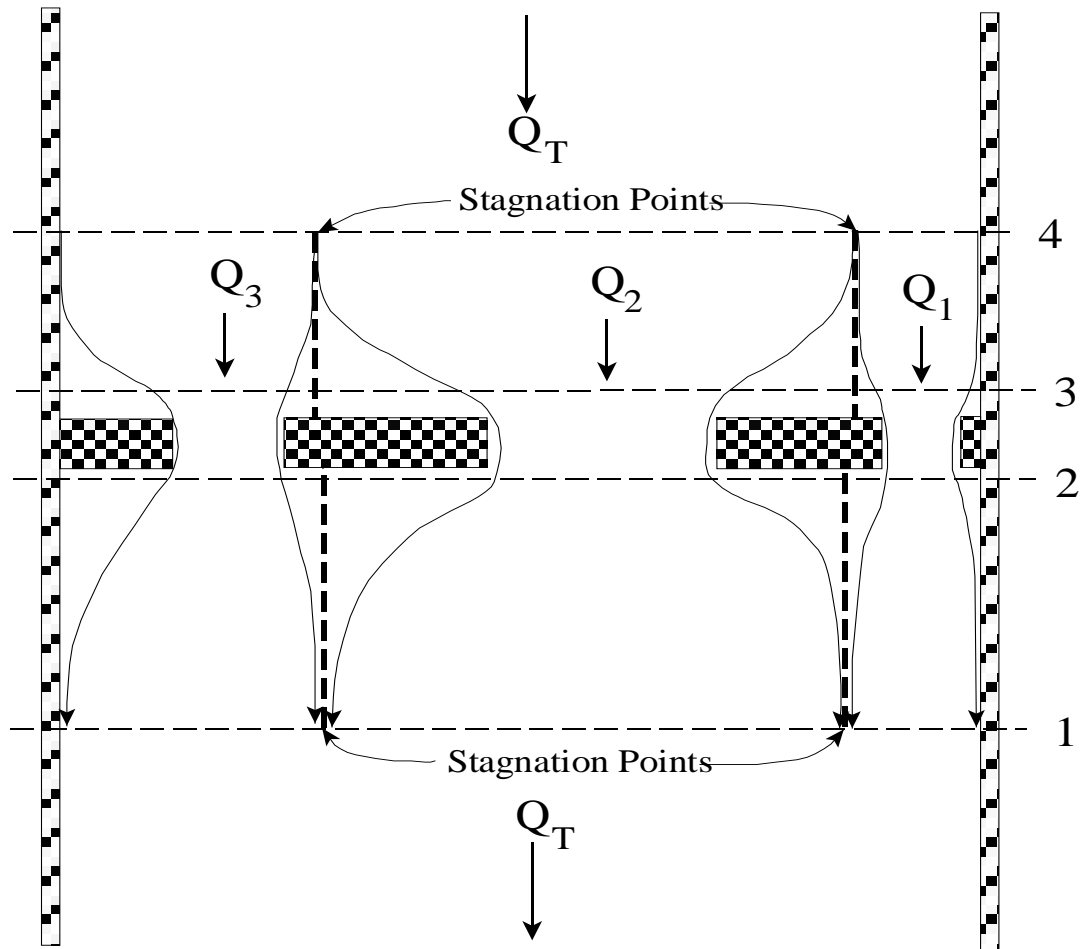
Figure 7-2 Plan view of a Multiple Opening Problem

Locating the Stagnation Points

The user has the option of fixing the stagnation point locations or allowing the program to solve for them within user defined limits. In general, it is better to let the program solve for the stagnation points, because it provides the best flow distribution and computed water surfaces. Also, allowing the stagnation points to migrate can be important when evaluating several different flow profiles in the same model. Conversely though, if the range in which the stagnation points are allowed to migrate is very large, the program may have difficulties in converging to a solution. Whenever this occurs, the user should either reduce the range over which the stagnation points can migrate or fix their location.

Within HEC-RAS, stagnation points are allowed to migrate between any bridge openings and/or culvert groups. However, if the user defines a conveyance area opening, the stagnation point between this type of opening and any other must be a fixed location. Also, conveyance area openings are limited to the left and right ends of the cross section.

Computational Procedure for Multiple Openings

HEC-RAS uses an iterative procedure for solving the multiple opening problem. The following approach is used when performing a multiple opening computation:

1. The program makes a first guess at the upstream water surface by setting it equal to the computed energy on the downstream side of the river crossing.

2. The assumed water surface is projected onto the upstream side of the bridge. A flow distribution is computed based on the percent of flow area in each opening.

3. Once a flow distribution is estimated, the stagnation points are calculated based on the upstream cross section. The assumed water surface is put into the upstream section. The hydraulic properties are calculated based on the assumed water surface and flow distribution. Stagnation points are located by apportioning the conveyance in the upstream cross section, so that the percentage of conveyance for each section is equal to the percentage of flow allocated to each opening.

4. The stagnation points in the downstream cross section (section just downstream of the river crossing) are located in the same manner.

5. Once a flow distribution is assumed, and the upstream and downstream stagnation points are set, the program calculates the water surface profiles through each opening, using the assumed flow.

6. After the program has computed the upstream energy for each opening, a comparison is made between the energies to see if a balance has been achieved (i.e., the difference between the highest and lowest computed energy is less than a predefined tolerance). If the energies are not within the tolerance, the program computes an average energy by using a flow weighting for each opening.

7. The average energy computed in step 6 is used to estimate the new flow distribution. This estimate of the flow distribution is based on adjusting the flow in each opening proportional to the percentage that the computed energy for that opening is from the weighted average energy. An opening with a computed energy higher than the weighted mean will have its flow reduced, while an opening with a computed energy that is lower than the weighted mean will have its flow increased. Once the flow for all the openings is adjusted, a continuity

check is made to ensure that the sum of the flows in all the openings is equal to the total flow. If this is not true, the flow in each opening is adjusted to ensure that the sum of flows is equal to the total flow.

8. Steps 3 through 7 continue until either a balance in energy is reached or the program gets to the fifth iteration. If the program gets to the fifth iteration, then the program switches to a different iterating method. In the second iteration method, the program formulates a flow versus upstream energy curve for each opening. The rating curve is based on the first four iterations. The rating curves are combined to get a total flow verses energy curve for the entire crossing. A new upstream energy guess is based on entering this curve with the total flow and interpolating an energy. Once a new energy is estimated, the program goes back to the individual opening curves with this energy and interpolates a flow for each opening. With this new flow distribution the program computes the water surface and energy profiles for each opening. If all the energies are within the tolerance, the calculation procedure is finished. If it is not within the tolerance the rating curves are updated with the new computed points, and the process continues. This iteration procedure continues until either a solution within the tolerance is achieved, or the program reaches the maximum number of iterations. The tolerance for balancing the energies between openings is 5 times the normal cross section water surface tolerance (0.05 feet or 0.015 meters). The default number of iterations for the multiple opening solutions scheme is 1.5 times the normal cross section maximum (the default is 30).

9. Once a solution is achieved, the program places the mean computed energy into the upstream cross section and computes a corresponding water surface for the entire cross section. In general, this water surface will differ from the water surfaces computed from the individual openings. This mean energy and water surface are reported as the final solution at the upstream section. User=s can obtain the results of the computed energies and water surfaces for each opening through the cross section specific output table, as well as the multiple opening profile type of table.

Limitations of the Multiple Opening Approach

The multiple opening method within HEC-RAS is a one-dimensional flow approach to a complex hydraulic problem. The methodology has the following limitations: the energy grade line is assumed to be constant upstream and downstream of the multiple opening crossing; the stagnation points are not allowed to migrate past the edge of an adjacent opening; and the stagnation points between a conveyance area and any other type of opening must be fixed (i.e. can not float). The model is limited to a maximum of seven openings. There can only be up to two conveyance type openings, and these openings must be located at the far left and right ends of the cross sections. Given these limitations, if you have a multiple opening crossing in which the water surface and energy vary significantly between openings, then this methodology may not be the most appropriate approach. An alternative to the multiple opening approach is the divided flow approach. This method is discussed below.

Divided Flow Approach

An alternative approach for solving a multiple opening problem is to model the flow paths of each opening as a separate river reach. This approach is more time consuming, and requires the user to have a greater understanding of how the flow will separate between openings. The benefit of using this approach is that varying water surfaces and energies can be obtained between openings. An example of a divided flow application is shown in Figure 7-3.

In the example shown in Figure 7-3, high ground exist between the two openings (both upstream and downstream). Under low flow conditions, there are two separate and distinct channels. Under high flow conditions the ground between the openings may be submerged, and the water surface continuous across both openings. To model this as a divided flow the user must create two separate river reaches around the high ground and through the openings. Cross sections 2 through 8 must be divided at what the user believes is the appropriate stagnation points for each cross section. This can be accomplished in several ways. The cross sections could be physically split into two, or the user could use the same cross sections in both reaches. If the same cross sections are used, the user must block out the area of each cross section (using the ineffective flow option) that is not part of the flow path for that particular reach. In other words, if you were modeling the left flow path, you would block out everything to the right of the stagnation points. For the reach that represents the right flow path, everything to the left of the stagnation points would be blocked out.
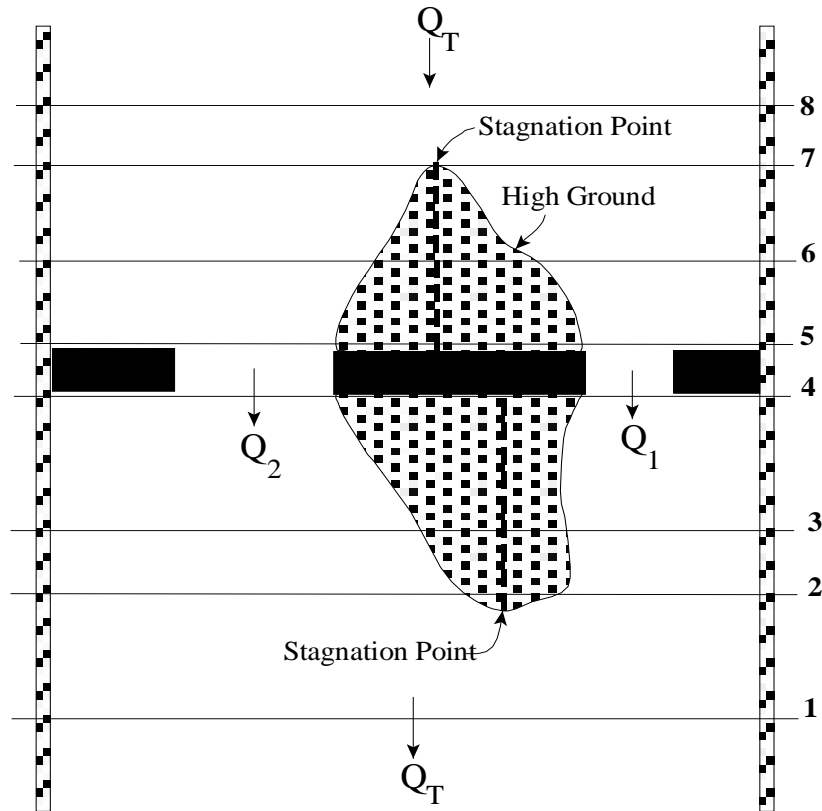
Figure 7-3 Example of a Divided Flow Problem

When modeling a divided flow, you must define how much flow is going through each reach. The current version of HEC-RAS can optimize the flow split. The user makes a first guess at the flow distribution, and then runs the model with the split flow optimization option turned on. The program uses an iterative procedure to calculate the correct flow in each reach. More information on split flow optimization can be found in chapter 7 of the User's Manual, chapter 4 of the Hydraulic Reference Manual, and Example 15 of the Applications Guide.

CHAPTER 8

Modeling Gated Spillways, Weirs and Drop Structures

This version of HEC-RAS allows the user to model inline structures, such as gated spillways, overflow weirs, drop structures, as well as lateral structures.   HEC-RAS has the ability to model radial gates (often called tainter gates), vertical lift gates (sluice gates), or overflow gates. The spillway crest of the gates can be modeled as either an ogee shape, broad crested weir, or a sharp crested weir shape. In addition to the gate openings, the user can also define a separate uncontrolled overflow weir.

This chapter describes the general modeling guidelines for using the gated spillway and weir capability within HEC-RAS, as well as the hydraulic equations used. Information on modeling drop structures with HEC-RAS is also provided. For information on how to enter gated spillway and weir data, as well as viewing gated spillway and weir results, see Chapter 6 and Chapter 8 of the HEC-RAS User's Manual, respectively.

Contents
■ General Modeling Guidelines

■ Hydraulic Computations through Gated Spillways

■ Uncontrolled Overflow Weirs

■ Modeling Lateral Structures

■ Drop Structures

General Modeling Guidelines

The gated spillway and weir option within HEC-RAS can be used to model inline (structures across the main stream) or lateral (structures along the side of the stream) weirs, gated spillways, or a combination of both. An example of a dam with a gated spillways and overflow weir is shown in Figure 8-1.
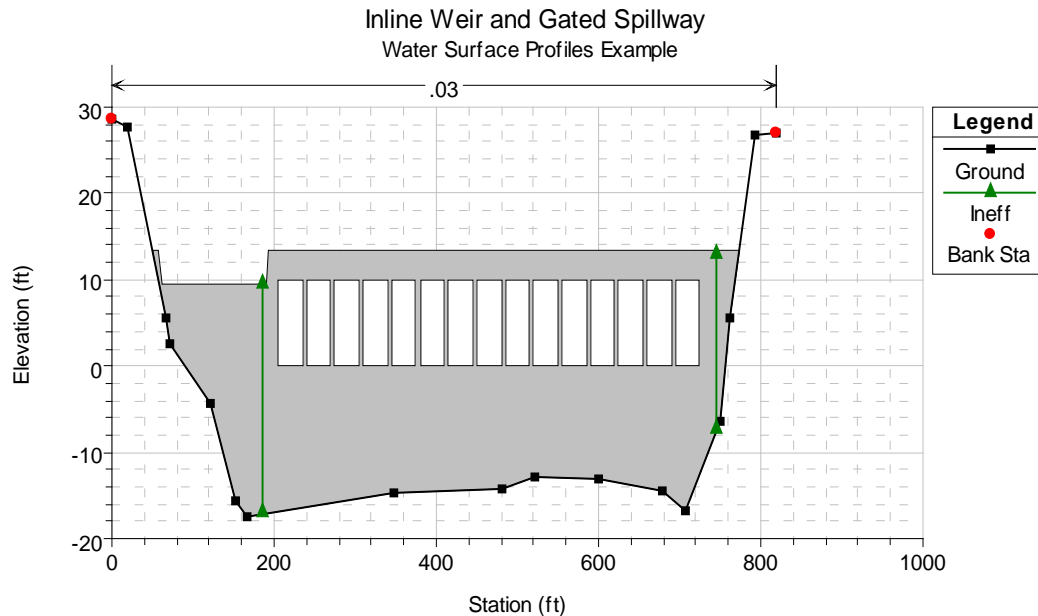
Figure 8-1 Example of Inline Gated Spillway and Weir

In the example shown in Figure 8-1 there are 15 identical gate openings and the entire top of the embankment is specified as an overflow weir.

Gated Spillways within HEC-RAS can be modeled as radial gates (often called tainter gates), vertical lift gates (sluice gates), overflow gates (open to the air or closed top), or a family of user defined rating curves. The equations used to model the gate openings can handle both submerged and unsubmerged conditions at the inlet and outlet of the gates. If the gates are opened far enough, such that unsubmerged conditions exist at the upstream end, the program automatically switches to a weir flow equation to calculate the hydraulics of the flow. The spillway crest through the gate openings can be specified as either an ogee crest shape, broad crested , or sharp crested. The program has the ability to calculate both free flowing and submerged weir flow through the gate openings. Figure 8-2 is a diagram of sluice and radial gate types with different spillway crests.

Sluice Gate

Radial Gate

Broad Crested Spillway

Ogee Spillway Crest
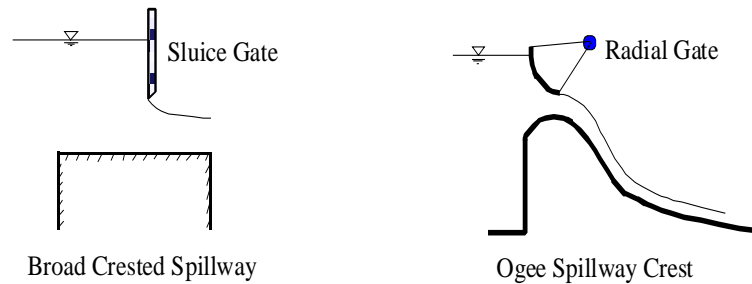
Figure 8-2 Example Sluice and Radial Gates

Up to 10 gate groups can be entered into the program at any one river crossing. Each gate group can have up to 25 identical gate openings. Identical gate openings must be the same gate type; size; elevation; and have identical gate coefficients. If anything about the gates is different, except their physical location across the stream, the gates must be entered as separate gate groups.

The overflow weir capability can be used by itself or in conjunction with the gated spillway option (as well as the other outlet types available in Inline and Lateral structures). The overflow weir is entered as a series of station and elevation points across the stream, which allows for complicated weir shapes. The user must specify if the weir is broad crested, ogee shape, or sharp crested. The software has the ability to account for submergence due to the downstream tailwater. Additionally, if the weir has an ogee shaped crest, the program can calculate the appropriate weir coefficient for a given design head. The weir coefficient will automatically be decreased or increased when the actual head is lower or higher than the design head.

Cross Section Locations

The inline weir and gated spillway routines in HEC-RAS require the same cross sections as the bridge and culvert routines. Four cross sections in the vicinity of the hydraulic structure are required for a complete model, two upstream and two downstream. In general, there should always be additional cross sections downstream from any structure (bridge, culvert, weir, etc...), such that the user entered downstream boundary condition does not affect the hydraulics of flow through the structure. In order to simplify the discussion of cross sections around the inline weir and gated spillway structure, only the four cross sections in the vicinity will be discussed. These four cross sections include: one cross section sufficiently downstream such that the flow is fully expanded; one at the downstream end of the structure (representing the tailwater location); one at the upstream end of the structure (representing the headwater location); and one cross section located far enough upstream at the point in which the flow begins to contract. Note, the cross sections that bound the structure represent the channel geometry outside of the embankment. Figure 8-3 illustrates the cross sections required for an inline weir and gated spillway model.
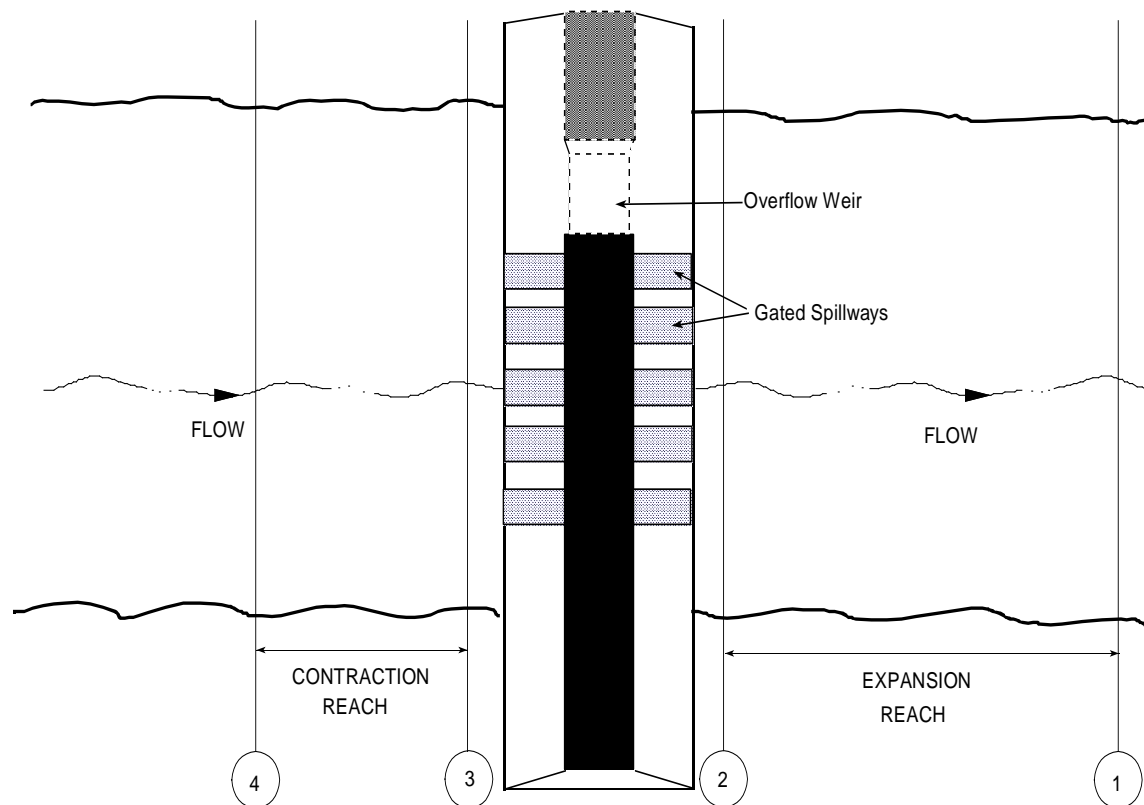
Figure 8-3 Cross Section Layout for Inline Gated Spillways and Weirs

Cross Section 1. Cross Section 1 for a weir and/or gated spillway should be located at a point where flow has fully expanded from its constricted top width caused by the constriction. The entire area of Cross Section 1 is usually considered to be effective in conveying flow.

Cross Section 2. Cross Section 2 is located a short distance downstream from the structure. The computed water surface at this cross section will represent the tailwater elevation of the weir and the gated spillways. This cross section should not include any of the structure or embankment, but represents the physical shape of the channel just downstream of the structure. The shape and location of this cross section is entered separately from the Inline Weir and Gated Spillway data (from the cross section editor).

The HEC-RAS ineffective area option is used to restrict the effective flow area of Cross Section 2 to the flow area around or near the edges of the gated spillways, until flow overtops the overflow weir and/or embankment. The ineffective flow areas are used to represent the correct amount of active flow area just downstream of the structure. Establishing the correct amount of effective flow area is very important in computing an accurate tailwater elevation at Cross Section 2. Because the flow will begin to expand as it exits the gated spillways, the active flow area at Section 2 is generally wider than the width of the gate openings. The width of the active flow area will depend upon how far downstream Cross Section 2 is from the structure. In general, a reasonable assumption would be to assume a 1:1 expansion rate over this short distance. Figure 8-4 illustrates Cross Section 2 of a typical inline weir and gated spillway model.

On Figure 8-4, the channel bank locations are indicated by small circles and the stations and elevations of the ineffective flow areas are indicated by triangles.

Cross Sections 1 and 2 are located so as to create a channel reach downstream of the structure in which the HEC-RAS program can accurately compute the friction losses and expansion losses that occur as the flow fully expands.
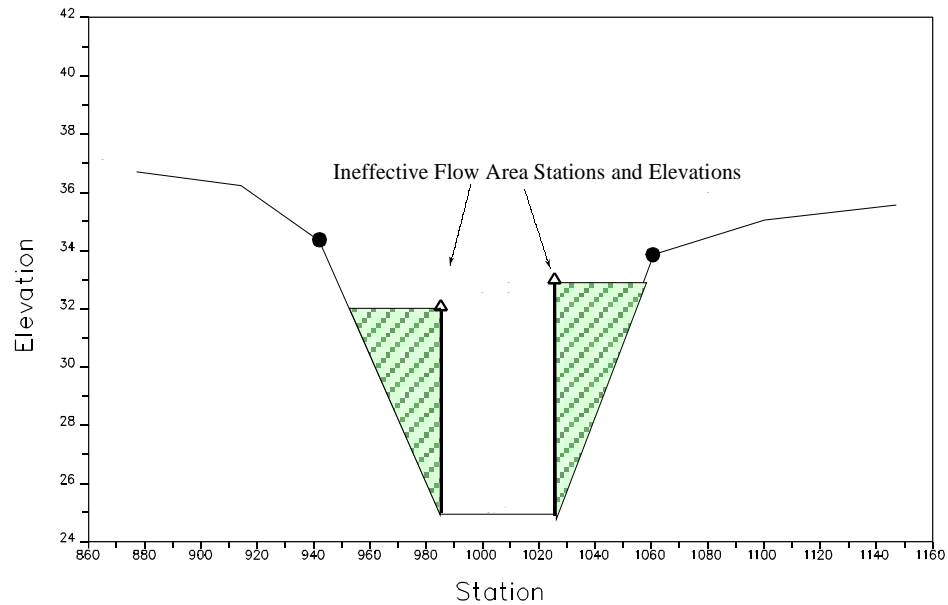
Figure 8-4 Section 2 of Inline Gated Spillway and Weir Model

Cross Section 3. Cross Section 3 of an inline weir and gated spillway model is located a short distance upstream of the embankment, and represents the physical configuration of the upstream channel. The water surface computed at this cross section represents the upstream headwater for the overflow weir and the gated spillways. The software uses a combination of the deck/road embankment data, Cross Section 3, and the gated spillway data, to describe the hydraulic structure and the roadway embankment. The inline weir and gated spillway data are located at a river station between Cross Section 2 and Cross Section 3.

The HEC-RAS ineffective area option is used to restrict the effective flow area of Cross Section 3 until the flow overtops the roadway. The ineffective flow area is used to represent the correct amount of active flow area just upstream of the structure. Because the flow is contracting rapidly as it enters the gate openings, the active flow area at Section 3 is generally wider than the width of the gates. The width of the active flow area will depend upon how far upstream Cross Section 3 is placed from the structure. In general, a reasonable assumption would be to assume a 1:1 contraction rate over this short distance. Figure 8-5 illustrates Cross Section 3 for a typical model, including the embankment profile and the gated spillways. On Figure 8-5, the channel bank locations are indicated by small circles, and the stations and elevations of ineffective areas are indicated by triangles.
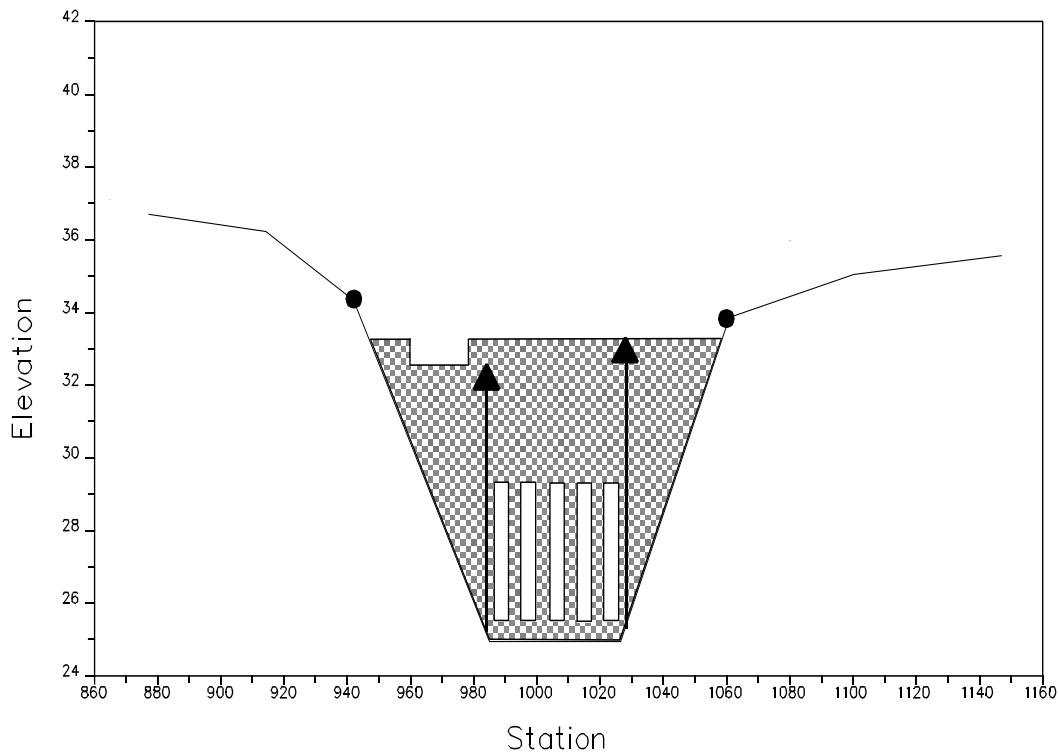
Figure 8-5 Cross Section 3 of Inline Gated Spillway and Weir

Cross Section 4. The final cross section in the inline weir and gated spillway model is located at a point where flow has not yet begun to contract from its unrestrained top width upstream of the structure. This distance is normally determined assuming a one to one contraction of flow. In other words, the average rate at which flow can contract to pass through the gate openings is assumed to be one foot laterally for every one foot traveled in the downstream direction. The entire area of Cross Section 4 is usually considered to be effective in conveying flow.

Expansion and Contraction Coefficients

User-defined coefficients are required to compute head losses due to the contraction and expansion of flows upstream and downstream of an inline weir and gated spillway structure. These losses are computed by multiplying an expansion or contraction coefficient by the absolute difference in velocity head between two cross sections.

If the velocity head increases in the downstream direction, a contraction coefficient is applied. When the velocity head decreases in the downstream direction, an expansion coefficient is used.   Recommended values for the expansion and contraction coefficients have been given in Chapter 3 of this manual (Table 3-2).   As indicated by the tabulated values, the expansion of flow causes more energy loss than the contraction. Also, energy losses increase with the abruptness of the transition.

Hydraulic Computations through Gated Spillways

As mentioned previously, the program is capable of modeling radial gates (often called tainter gates), vertical lift gates (sluice gates), and overflow gates. The equations used to model the gate openings can handle both submerged and unsubmerged conditions at the inlet and the outlet of the gates. When the gates are opened to an elevation greater than the upstream water surface elevation, the program automatically switches to modeling the flow through the gates as weir flow. When the upstream water surface is greater than or equal to 1.25 times the height of the gate opening (with respect to the gate's spillway crest), the gate flow equations are applied. When the upstream water surface is between 1.0 and 1.25 times the gate opening, the flow is in a zone of transition between weir flow and gate flow. The program computes the upstream head with both equations and then calculates a linear weighted average of the two values (this is an iterative process to obtain the final headwater elevation for a flow in the transition range). When the upstream water surface is equal to or less than 1.0 times the gate opening, then the flow through the gate opening is calculated as weir flow.

Radial Gates

An example radial gate with an ogee spillway crest is shown in Figure 8-6.
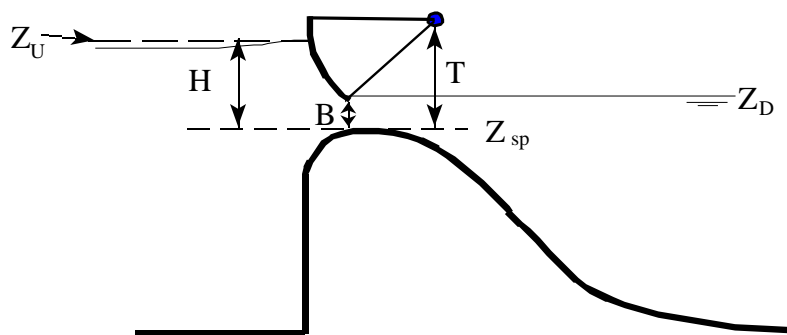
Figure 8-6 Example Radial Gate with an Ogee Spillway Crest

The flow through the gate is considered to be "Free Flow" when the downstream tailwater elevation (Z_D) is not high enough to cause an increase in the upstream headwater elevation for a given flow rate. The equation used for a Radial gate under free flow conditions is as follows:

$$Q = C\sqrt{2g}\, W\, T^{TE}\, B^{BE}\, H^{HE} \qquad\qquad (8\text{-}1)$$

Where: Q   = Flow rate in cfs

        C   = Discharge coefficient (typically ranges from 0.6 - 0.8)

        W   = Width of the gated spillway in feet

        T   = Trunnion height (from spillway crest to trunnion pivot point)

        TE   = Trunnion height exponent, typically about 0.16 (default 0.0)

        B   = Height of gate opening in feet

        BE   = Gate opening exponent, typically about 0.72 (default 1.0)

        H   = Upstream Energy Head above the spillway crest Z_U - Z_{sp}

        HE   = Head exponent, typically about 0.62 (default 0.5)

        Z_U = Elevation of the upstream energy grade line

        Z_D = Elevation of the downstream water surface

        Z_{sp} = Elevation of the spillway crest through the gate

Note: The default values for the equation, reduce the form of the equation down to a simple form. User's may need to calibrate the exponents to match observed data through a specific radial gate.

When the downstream tailwater increases to the point at which the gate is no longer flowing freely (downstream submergence is causing a greater upstream headwater for a given flow), the program switches to the following form of the equation:

$$Q = C\sqrt{2g}\, W\, T^{TE}\, B^{BE}\, (3H)^{HE} \qquad\qquad (8\text{-}2)$$

       where: H   = Z_U - Z_D

Submergence begins to occur when the tailwater depth divided by the headwater energy depth above the spillway, is greater than 0.67. Equation 8-2 is used to transition between free flow and fully submerged flow. This transition is set up so the program will gradually change to the fully submerged Orifice equation when the gates reach a submergence of 0.80. The fully submerged Orifice equation is shown below:

$$Q = CA\sqrt{2gH}$$

(8-3)

Where: A   = Area of the gate opening.

        H   = Z_U - Z_D

        C   = Discharge coefficient (typically 0.8)

Sluice Gate

An example sluice gate with a broad crest is shown in Figure 8-7.
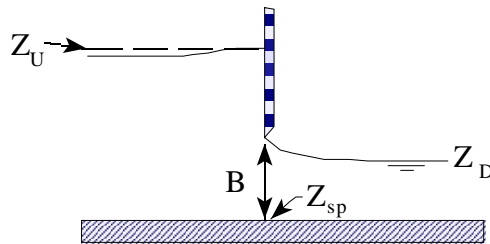
Figure 8-7 Example Sluice Gate with Broad Crested Spillway

The equation for a free flowing sluice gate is as follows:

$$Q = CWB\sqrt{2gH}$$

(8-4)

Where: H   = Upstream energy head above the spillway crest (Z_U - Z_{sp})

            C   = Coefficient of discharge, typically 0.5 to 0.7

When the downstream tailwater increases to the point at which the gate is no longer flowing freely (downstream submergence is causing a greater upstream headwater for a given flow), the program switches to the following form of the equation:

$$Q = CWB\sqrt{2g3H}$$

(8-5)

Where: H   = Z_U - Z_D

Submergence begins to occur when the tailwater depth above the spillway divided by the headwater energy above the spillway is greater than 0.67. Equation 8-5 is used to transition between free flow and fully submerged flow. This transition is set up so the program will gradually change to the fully submerged Orifice equation (Equation 8-3) when the gates reach a submergence of 0.80.

Overflow Gates

Overflow gates represent a gate in which the bottom of the gate opening moves up and down. Overflow gates can be completely open to the air at the top, or the top can be closed off. An example of an overflow gate is shown below in Figure 8-8.
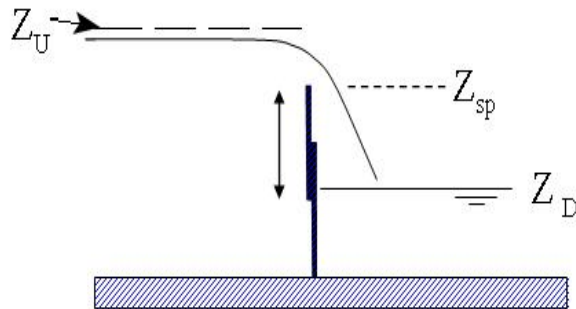
Figure 8-8 Example Overflow Gate

Overflow gates are generally modeled with the standard weir equation:

$$Q = CLH^{3/2}$$

(8-6)

where: C = Weir flow coefficient, typical values will range from 2.6 to 4.0 depending upon the shape of the spillway crest (i.e., broad crested, ogee shaped, or sharp crested). Most overflow spillways tend to be sharp crested, so a value of 3.2 is typical.

L = Length of the spillway crest.

H = Upstream energy head above the spillway crest.

For overflow gates in which the Sharp Crested spillway crest shape is selected, the user has the option of using the standard weir equation, The Rehbock equation (Henderson, 1966), or the Kindsvater and Carter equation (1957).

Low Flow through the Gates

When the upstream water surface is equal to or less than the top of the gate opening, the program calculates the flow through the gates as weir flow. An example of low flow through a gated structure is shown in Figure 8-9.
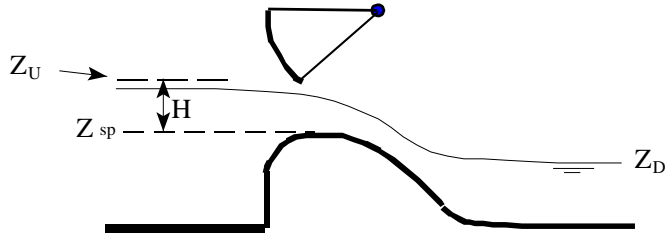
Figure 8-9 Example Radial Gate Under Low Flow Conditions

The standard weir equation used for this calculation is shown below:

$$Q = C L H^{3/2}$$

(8-7)

where: C = Weir flow coefficient, typical values will range from 2.6 to 4.1 depending upon the shape of the spillway crest (i.e., broad crested, ogee shaped, or sharp crested).

L = Length of the spillway crest.

H = Upstream energy head above the spillway crest.

The user can specify either a broad crested, ogee, or sharp crested weir shape for the spillway crest of the gate. If the crest of the spillway is ogee shaped, the weir coefficient will be automatically adjusted when the upstream energy head is higher or lower than a user specified design head. The adjustment is based on the curve shown in Figure 8-10 (Bureau of Reclamation, 1977). The curve provides ratios for the discharge coefficient, based on the ratio of the actual head to the design head of the spillway. In Figure 8-10, H_e is the upstream energy head; H_o is the design head; C_o is the coefficient of discharge at the design head; and C is the coefficient of discharge for an energy head other than the design head.
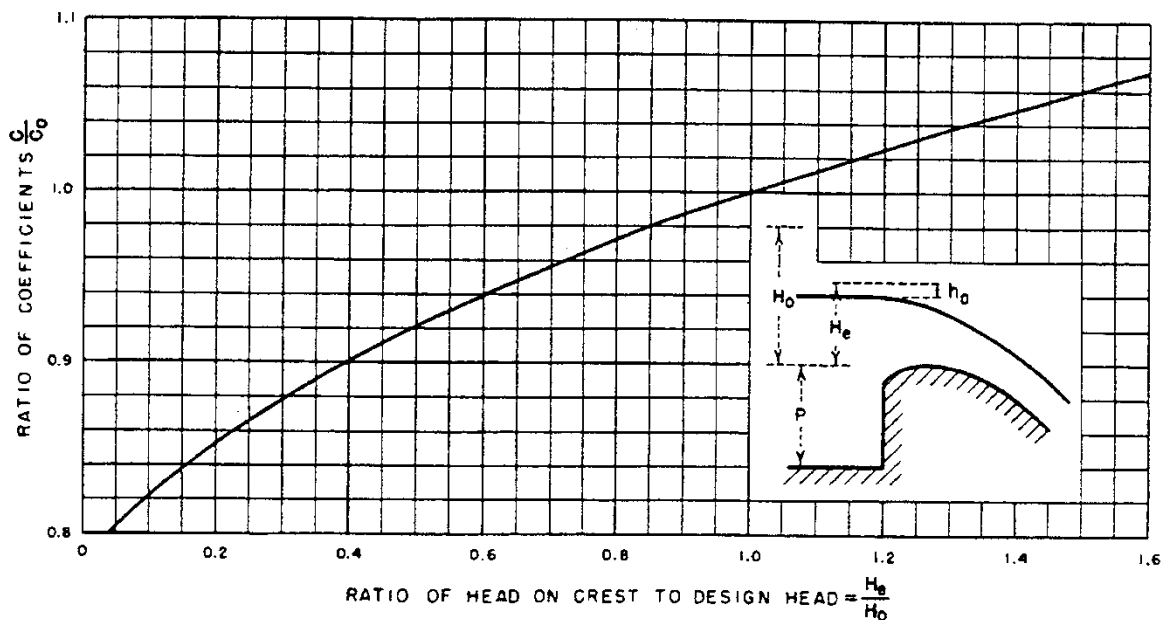
Figure 8-10 Flow Coefficient for Other Than Design Head

Submerged Weir Flow through the Gates

The program automatically accounts for submergence on the weir when the tailwater is high enough to slow down the flow. Submergence is defined as the depth of water above the weir on the downstream side divided by the headwater energy depth of water above the weir on the upstream side. As the degree of submergence increases, the program reduces the weir flow coefficient. Submergence corrections are based on the shape of the spillway crest (broad crested, ogee shaped weir, or sharp crested). If the spillway is a broad crested shape, then the same submergence curve that is used for flow over a roadway at a bridge (Figure 5-8) is used. If the spillway crest is ogee shaped, a submergence curve from the USACE EM 1110-2-1603 (Plate 3-5, A-A) is used. If the spillway crest is sharp crested, then the Villemonte equation (Villemonte, 1947) is used to compute the flow reduction coefficient.

Uncontrolled Overflow Weirs

In addition to the gate openings, the user can define an uncontrolled overflow weir at the same river crossing. The weir could represent an emergency spillway or the entire top of the structure and embankment. Weir flow is computed using the standard weir equation (Equation 8-6). The uncontrolled overflow weir can be specified as either a broad crested, ogee shaped, or sharp crested. The selection of a weir shape does not limit the modeling of other weir shapes. The limiting factor is what is entered for the weir coefficient. So the user can model other than the three listed weir shapes, by simply entering an appropriate weir coefficient. The selection of a weir shape does, however, fix how the program will calculate submerged weir flow.

Additionally, if the weir is ogee shaped, the program will allow for fluctuations in the discharge coefficient to account for upstream energy heads that are either higher or lower than the design head (Figure 8-10).

For weir flow in which the Sharp Crested spillway crest shape is selected, the user has the option of using the standard weir equation, the Rehbock equation (Henderson, 1966), or the Kindsvater and Carter equation (1957). If the standard weir equation is selected, the user must enter a weir coefficient. If either the Rehbock or the Kindsvater and Carter equation are selected, then the weir coefficient will automatically be calculated.

The following table is a list of typical weir coefficients for various shapes of weir crests:

Table 8-1 Typical Overflow Weir Coefficients

Weir Crest Shape	*Typical Coefficient Range*
Broad Crested	2.6 - 3.1
Ogee Crested	3.2 – 4.1
Sharp Crested	3.1 – 3.3

Submerged Weir Flow

The program automatically accounts for submergence on the weir when the tailwater is high enough to slow down the flow. Submergence is defined as the depth of water above the weir on the downstream side divided by the headwater energy depth of water above the weir on the upstream side. As the degree of submergence increases, the program reduces the weir flow coefficient. Submergence corrections are based on the shape of the spillway crest (broad crested, ogee shaped weir, or sharp crested). If the spillway is a broad crested shape, then the same submergence curve that is used for flow over a roadway at a bridge (Figure 5-8) is used. If the spillway crest is ogee shaped, a submergence curve from the USACE EM 1110-2-1603 (Plate 3-5, A-A) is used. If the spillway is sharp crested, then the Villemonte equation (Villemonte, 1947) is used to compute the flow reduction coefficient.

Modeling Lateral Structures

HEC-RAS has the ability to model lateral weirs, gated spillways, culverts, and user entered rating curves. The modeler can insert a lateral weir only, or a separate gated spillway structure, or any combination of the four types. An example diagram of a lateral structure is shown in Figure 8-11.
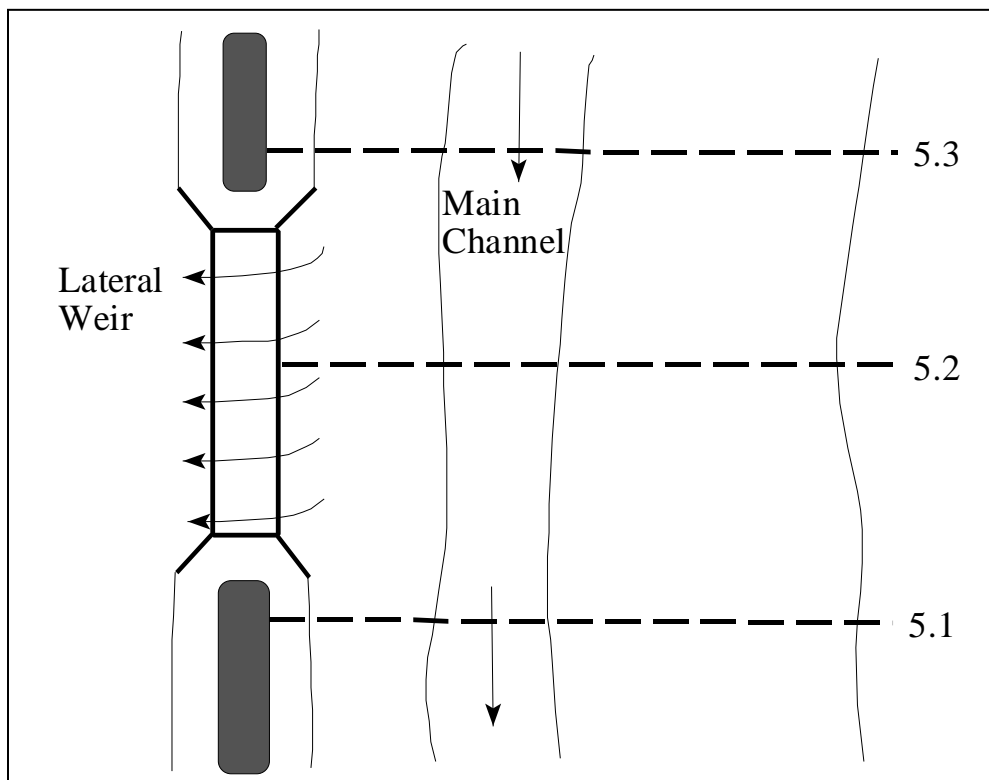
Figure 8-11 Plan View of an Example Lateral Weir

At a minimum there must be a cross section upstream of and a cross section downstream of the lateral structure. The upstream cross section can either be right at the beginning of the structure, or it can be a short distance upstream. The downstream cross section can be right at the downstream end of the structure or it can be a short distance downstream. The user can have any number of additional cross sections in the middle of the structure.

If there are gated openings in the structure, the hydraulic computations for lateral gated spillways are exactly the same as those described previously for inline gated spillways. The only difference is that the headwater energy is computed separately for each gate, based on its centerline location along the stream. The headwater energy for each gate is interpolated linearly between computed points at each cross section. Culvert hydraulics are modeled the same way as described in Chapter 6 of this document. The user has the additional option of defining a flap gate, which can be used to limit flow through a culvert to one direction only.

An example lateral structure is shown in Figure 8-12 as a profile view.
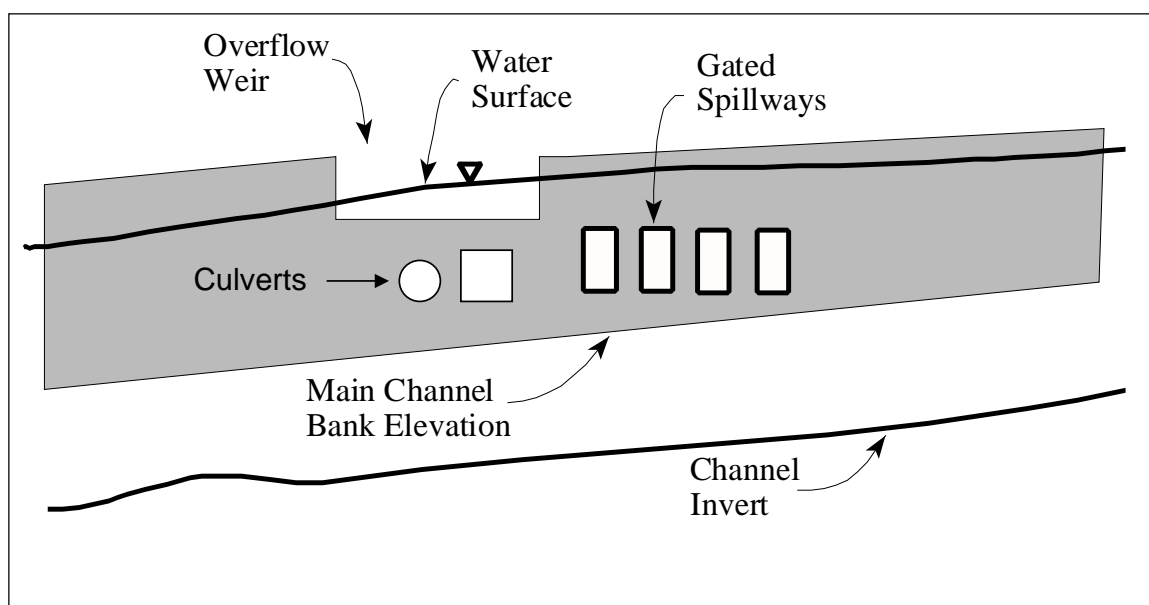
Figure 8-12 Example Lateral Weir and Gated Spillway

As shown in Figure 8-12, the water surface across the weir has a slope to it. Additionally, the weir itself could be on a slope. Because of this, an equation for weir flow with a sloping water surface and weir sill had to be derived. Shown in Figure 8-13 is a sloping weir segment with a sloping water surface. The equation for a sloping line representing the water surface and the weir segment are shown. The constants a_{ws} and a_w represent the slope of the water surface and the weir segment, respectively, while the variable C_{ws} and C_w are constants representing the initial elevations.
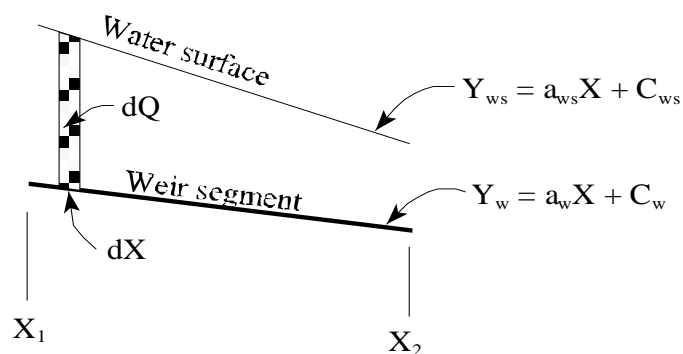
Figure 8-13 Sloping Weir Segment and Water Surface

The standard weir equation (8-6) assumes that the weir is parallel with the water surface (i.e. that the depth of water is constant from one end of the weir segment to the other). The

following general equation is derived for a sloping weir and water surface by integrating the standard weir equation:

$$dQ = C(y_{ws} - y_w)^{3/2} \, dx \tag{8-8}$$

$$dQ = C(a_{ws} x + C_{ws} - a_w x - C_w)^{3/2} \, dx \tag{8-9}$$

$$dQ = C((a_{ws} - a_w)x + C_{ws} - C_w)^{3/2} \, dx \tag{8-10}$$

Assuming: $a_1 = a_{ws} - a_w$ and $C_1 = C_{ws} - C_w$

$$\int_{x_1}^{x_2} dQ = C \int_{x_1}^{x_2} (a_1 x + C_1)^{3/2} \, dx = \frac{2C}{5a_1}(a_1 x + C_1)^{5/2} \,]_{x_1}^{x_2} \tag{8-11}$$

$$Q_{x_1 - x_2} = \frac{2C}{5a_1}((a_1 x_2 + C_1)^{5/2} - (a_1 x_1 + C_1)^{5/2}) \tag{8-12}$$

The above equation is valid as long as a_1 is not zero. When a_1 is zero, this implies that the water surface and the weir segment are parallel. When this is true, the original weir equation (equation 8-6) is used.

Within HEC-RAS, flow over a lateral weir can be computed from either the energy grade line or the water surface elevation. The standard weir equation is derived with the upstream energy head being based on the distance from the weir sill to the upstream energy grade line. The water surface elevation is the default for a lateral weir in HEC-RAS. However, the user has the option of instructing the program to use the energy elevation when computing the head term of the weir equation. The water surface is the most appropriate when the weir is located close to the main channel. In this situation the energy due to the velocity head is in the downstream direction, and not over the top of the lateral weir. Therefore, the computation of the energy head over the lateral weir is best depicted by using the water surface of the flow in the channel.

The predecessor to HEC-RAS (HEC-2 program) also used the water surface elevation as the default for lateral weir calculations. This is an important point to remember when comparing results between HEC-RAS and HEC-2. However, both programs allow the user to select either the energy grade line or the water surface elevation for this calculation.

Hager's Lateral Weir Equation

HEC-RAS has the option for using Hager's weir equation for lateral weirs. The equation is the same as the standard weir equation, except the weir discharge coefficient is computed automatically based on physical and hydraulic properties. Hager's equation for the lateral discharge coefficient is (Hager, W. H., 1987):

$$C = \frac{3}{5} C_0 \sqrt{g} \left[\frac{1-W}{3-2y-W} \right]^{0.5} \left\{ 1 - (\beta + S_0) \left[\frac{3(1-y)}{y-W} \right]^{0.5} \right\} \tag{8-13}$$

Where:

$$W = \frac{h_w}{H_t + h_w} \qquad y = \frac{H + h_w}{H_t + h_w} \qquad C_0 = Function(weir\ shape)$$

H	=	Height of the water surface above the weir
h_w	=	Height of the weir above the ground
H_t	=	Height of the energy grade line above the weir
S_0	=	Average main channel bed slope
β	=	main channel contraction angle in radians (zero if the weir is parallel to

the main channel).
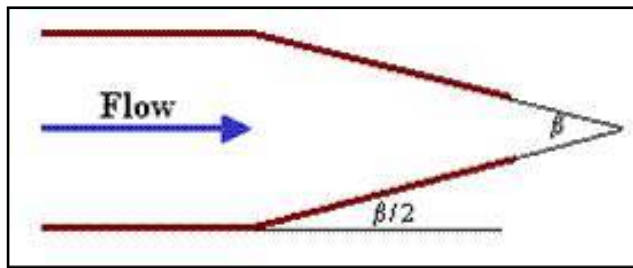
C_0	=	Base Discharge coefficient. $C_0 = 1.0$ for a sharp crested weir. $C_0 = 8/7$ for a zero height weir.

For a broad crested weir (*b* = weir width):

$$C_0 = 1 - \frac{2}{9\left[1+\left(\dfrac{H_t}{b}\right)^4\right]}$$

For round or ogee crested weirs (*r* = weir radius):

$$C_0 = \frac{\sqrt{3}}{2}\left[1+\frac{\dfrac{22}{81}\left(\dfrac{H_t}{r}\right)^2}{1+\dfrac{1}{2}\left(\dfrac{H_t}{r}\right)^2}\right]$$

Drop Structures

Drop structures can be modeled with the inline weir option or as a series of cross sections. If you are just interested in getting the water surface upstream and downstream of the drop structure, then the inline weir option would probably be the most appropriate (as described in a previous section of this chapter). However, if you want to compute a more detailed profile upstream of and through the drop, then you will need to model it as a series of cross sections.

When modeling a drop structure as a series of cross sections, the most important thing is to have enough cross sections at the correct locations. Cross sections need to be closely spaced where the water surface and velocity are changing rapidly (i.e. just upstream and downstream of the drop). An example of a drop structure is shown in Figure 8-14.
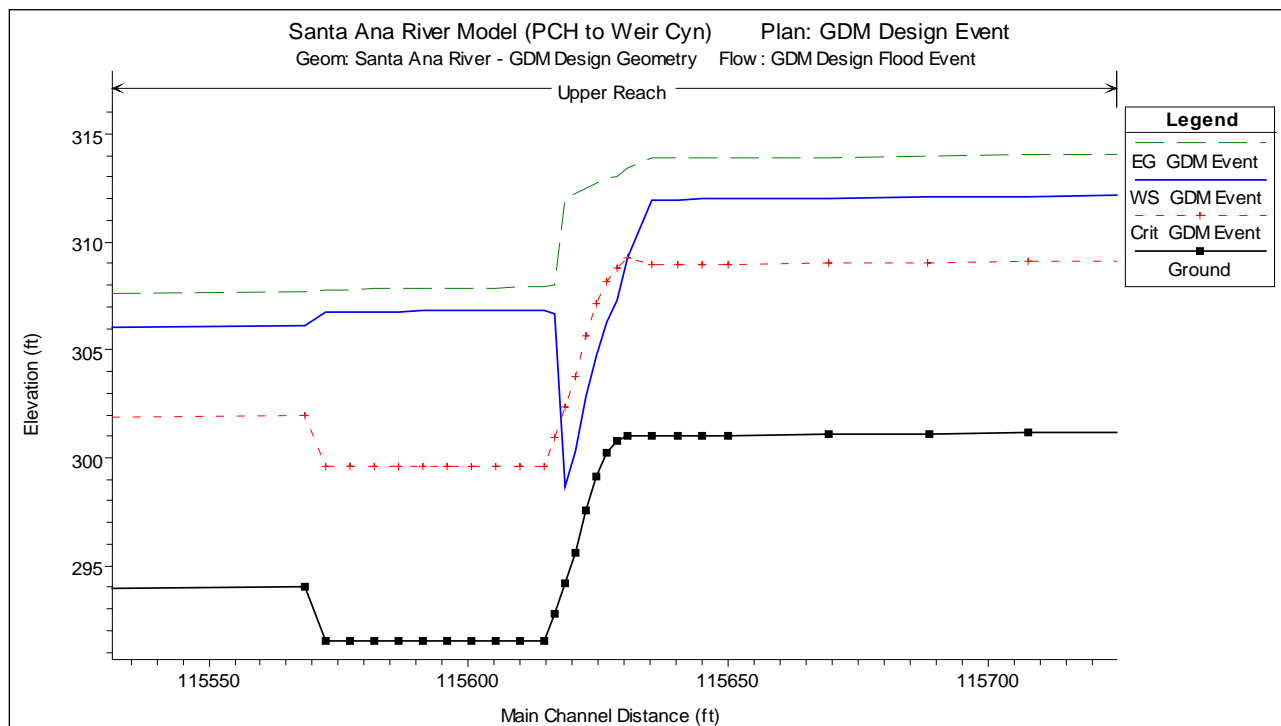
Figure 8-14 Drop Structure Modeled With Cross Sections

As shown in Figure 8-14, the spacing between cross sections should decrease as you get closer to the drop structure (cross sections are located at each square shown on the ground profile). Additionally, if the drop itself is on a slope, then additional cross sections should be placed along the sloping drop in order to model the transition from subcritical to supercritical flow. Several cross sections should also be placed in the stilling basin (location of energy dissipaters) in order to correctly locate where the hydraulic jump will occur (i.e. the hydraulic jump could occur on the slope of the drop, or it may occur inside of the stilling basin). Manning's n values should be increased inside of the stilling basin to represent the increased roughness due to the energy dissipater blocks.

In order to evaluate this method of modeling drop structures, a comparison was made between a physical model study and an HEC-RAS model of the drop structure. During the design phase of improvements to the Santa Ana River, the Waterways Experiment Station (WES) was contracted to study the drop structures and make recommendations. The results of this study were reported in General Design for Replacement of or Modifications to the Lower Santa Ana River Drop Structures, Orange County, California (Technical Report HL-94-4, April 1994, USACE). Over 50 different designs were tested in 1:25 scale flume models and 1:40 scale full width models. The designs evaluated existing structures, modifying original structures and replacing them with entirely new designs. The drop structure design used in the Santa Ana River is similar to one referred to as Type 10 in the report. An HEC-RAS model was developed to model the Type 10 drop structure and the model results were compared to the flume results.

The geometry for the HEC-RAS model was developed from the following design diagram in the WES report (Figure 8-15).
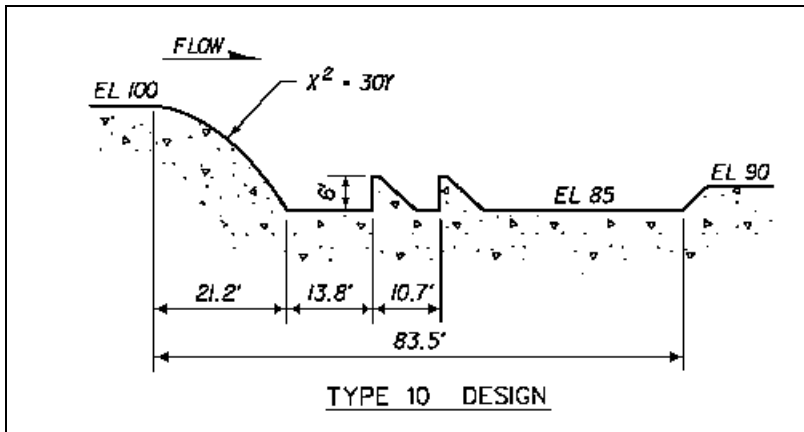
Figure 8-85 WES Report Plate 13.

The total reach in the model was 350 feet, 150 upstream of the crest of the drop structure and 200 feet below the crest. The cross sections were rectangular, with the following spacing used in the HEC-RAS model:

Location	Reach Lengths
Upstream of drop structure:	10 feet
Over the drop:	2 feet
Inside the stilling basin:	10 feet
Downstream of structure:	10 feet

The expansion and contraction coefficients were set to 0.3 and 0.1 respectively. Two Manning's n values were used in the HEC-RAS model of the flume. Inside the stilling basin where the bottom elevation was 85 feet, the Manning's n values were set to 0.05. In all other cross

sections the Manning's n values were set to 0.03. The higher n value was used in the stilling basin to account for the additional energy loss due to the rows of baffles that exist in the flume but were not added into the cross sections data of HEC-RAS.

The original data from the flume experiments were obtained from the Waterways Experiment Station and entered in HEC-RAS as observed data. The results of the HEC-RAS model are compared in profile to the observed water surface elevations from the flume study in Figure 8-15. These results show that HEC-RAS was able to adequately model the drop structure, both upstream and downstream of the crest.

Some differences occur right at the crest and through the hydraulic jump. The differences at the crest are due to the fact that the energy equation will always show the flow passing through critical depth at the top of the crest. Whereas, in the field it has been shown that the flow passes through critical depth at a distance upstream of 3-4 times critical depth. However, as shown in Figure 8-15, a short distance upstream of the crest the HEC-RAS program converges to the same depth as the observed data. HEC-RAS correctly obtained the maximum upstream water surface is the most important part of modeling the drop structure.

Downstream of the drop, the flow is supercritical and then goes through a hydraulic jump. The flume data shows the jump occurring over a distance of 50 to 60 feet with a lot of turbulence. The HEC-RAS model cannot predict how long of a distance it will take for the jump to occur, but it can predict where the jump will begin. The HEC-RAS model will always show the jump occurring between two adjacent cross sections. The HEC-RAS model shows the higher water surface inside of the stilling basin and then going down below the stilling basin. The model shows all of this as a fairly smooth transition, whereas it is actually a turbulent transition with the water surface bouncing up and down. In general, the results from the HEC-RAS model are very good at predicting the stages upstream, inside, and downstream of the drop structure.
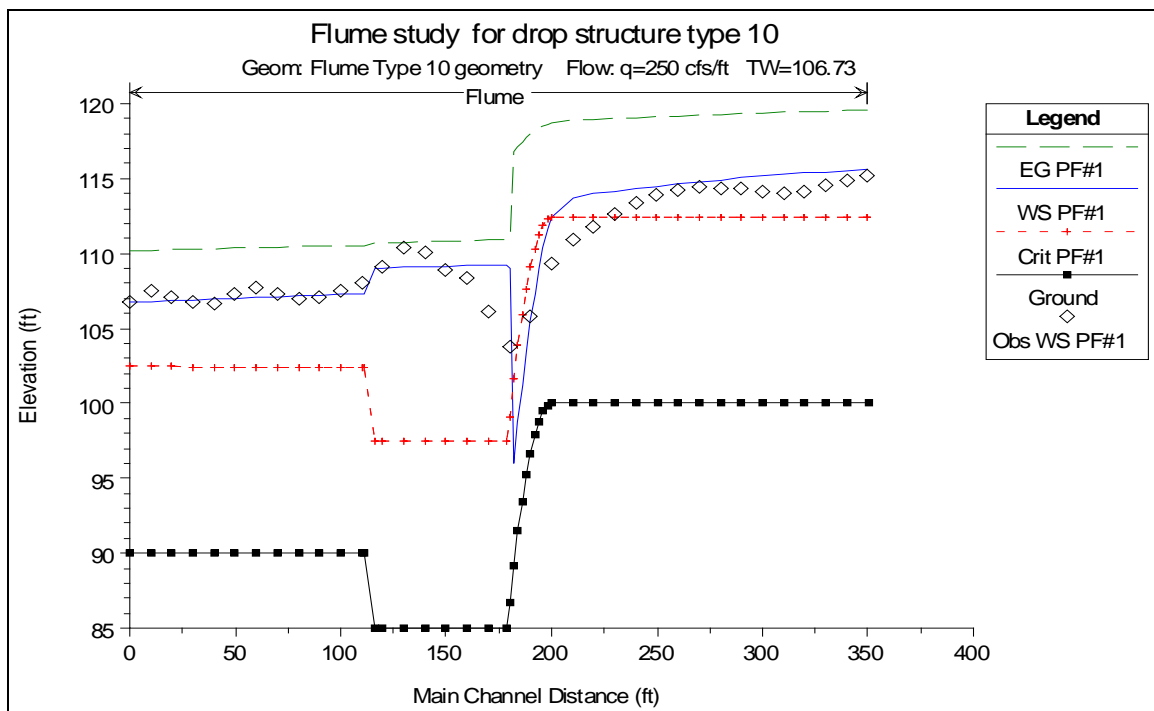
Figure 8-9 Comparison between Flume Data and HEC-RAS for a Drop Structure

CHAPTER 9

Floodplain Encroachment Calculations

The evaluation of the impact of floodplain encroachments on water surface profiles can be of substantial interest to planners, land developers, and engineers. It is also a significant aspect of flood insurance studies. HEC-RAS contains five optional methods for specifying floodplain encroachments within a steady flow analysis. This chapter describes the computational details of each of the five encroachment methods, as well as special considerations for encroachments at bridges, culverts, and multiple openings. Discussions are also provided on a general modeling approach for performing an encroachment analysis.

For information on how to enter encroachment data, how to perform the encroachment calculations, and viewing encroachment results, see Chapter 9 of the HEC-RAS user's manual.

Contents

■ Introduction

■ Encroachment Methods

■ Bridge, Culvert, and Multiple Opening Encroachments

■ General Modeling Guidelines

Introduction

The HEC-RAS floodway procedure for steady flow analyses is based on calculating a natural profile (existing conditions geometry) as the first profile in a multiple profile run. Other profiles in a run are calculated using various encroachment options, as desired. Before performing an encroachment analysis, the user should have developed a model of the existing river system. This model should be calibrated to the fullest extent that is possible. Verification that the model is adequately modeling the river system is an extremely important step before attempting to perform an encroachment analysis.

Encroachment Methods

HEC-RAS contains five optional methods for specifying floodplain encroachments. Each method is illustrated in the following paragraphs.

Encroachment Method 1

With encroachment method 1 the user specifies the exact locations of the encroachment stations for each individual cross section. The encroachment stations can also be specified differently for each profile. An example of encroachment method 1 is shown in Figure 9-1.
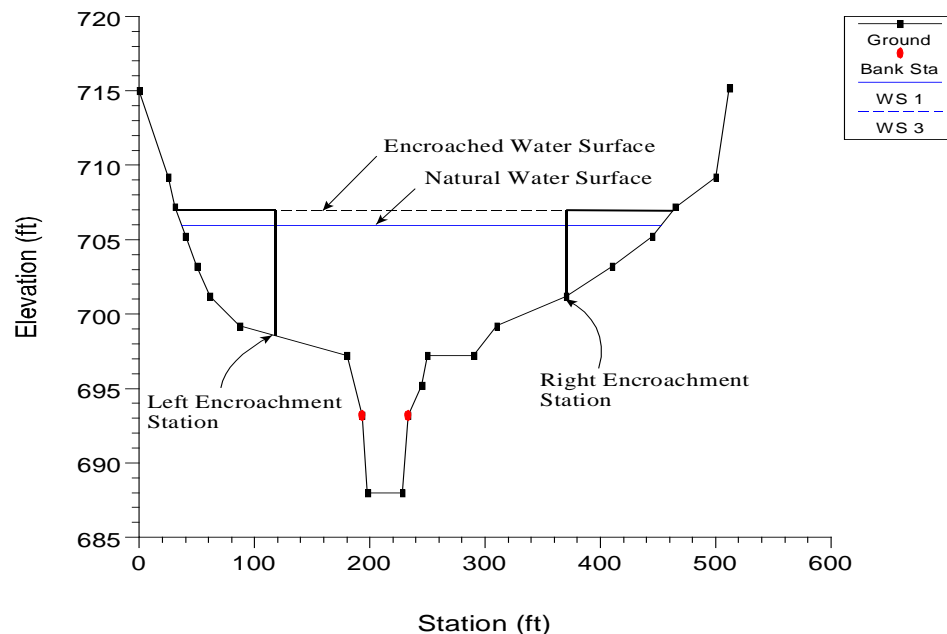
Figure 9-1 Example of Encroachment Method 1

Encroachment Method 2

Method 2 utilizes a fixed top width. The top width can be specified separately for each cross section. The left and right encroachment stations are made equal distance from the centerline of the channel, which is halfway between the left and right bank stations. If the user specified top width would end up with an encroachment inside the channel, the program sets that encroachment (left and/or right) to the channel bank station. An example of encroachment method 2 is shown in Figure 9-2.

HEC-RAS also allows the user to establish a left and right offset. The left and right offset is used to establish a buffer zone around the main channel for further limiting the amount of the encroachments. For example, if a user established a right offset of 5 feet and a left offset of 10 feet, the model will limit all encroachments to 5 feet from the right bank station and 10 feet from the left bank station. If a user entered top width would end up inside of an offset, the program will set the encroachment at the offset stationing.
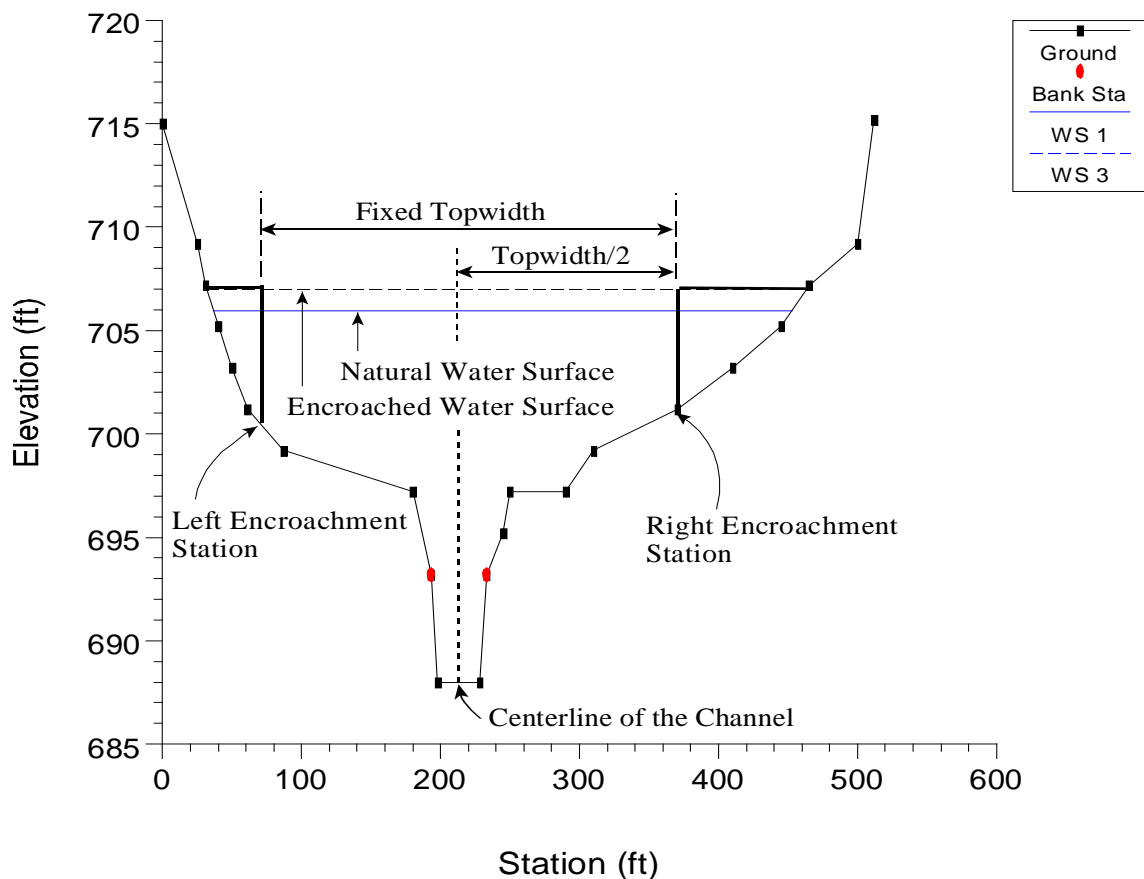
Figure 9-2 Example of Encroachment Method 2

Encroachment Method 3

Method 3 calculates encroachment stations for a specified percent reduction in the conveyance (%K Reduction) of the natural profile for each cross section. One-half of the conveyance is eliminated on each side of the cross section (if possible). The computed encroachments cannot infringe on the main channel or any user specified encroachment offsets. If one-half of the conveyance exceeds either overbank conveyance, the program will attempt to make up the difference on the other side. If the percent reduction in cross section conveyance cannot be accommodated by both overbank areas combined, the encroachment stations are made equal to the stations of left and right channel banks (or the offset stations, if specified). An example of encroachment method 3 is shown in Figure 9-3.
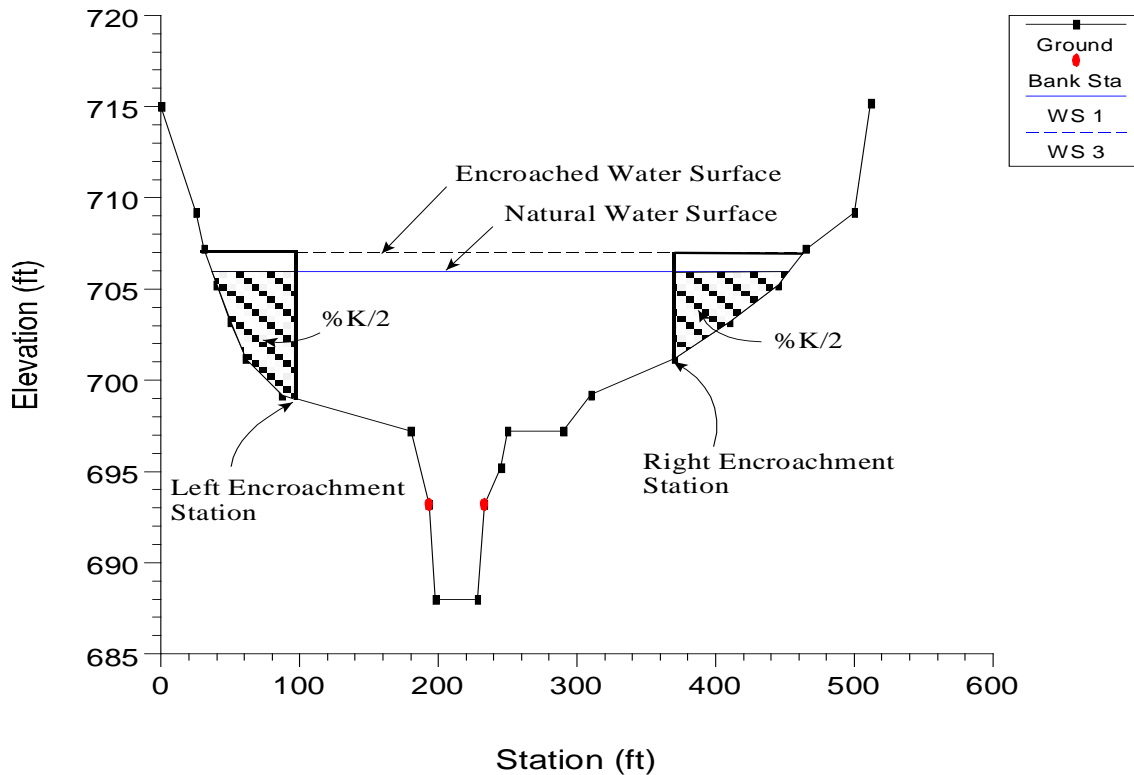
Figure 9-3 Example of Encroachment Method 3

Encroachment Method 3 requires that the first profile (of a multiple profile run) must be a natural (un-encroached) profile. Subsequent profiles (profiles 2-15) of a multiple profile run may be utilized for Method 3 encroachments. The percentage of reduction in conveyance can be changed for any cross section. A value of 10 percent for the second profile would indicate that 10 percent of the conveyance based on the natural profile (first profile) will be eliminated - 5 percent from each overbank. Equal conveyance reduction is the default.

An alternate scheme to **equal** conveyance reduction is conveyance reduction in **proportion** to the distribution of natural overbank conveyance. For instance, if the natural cross section had twice as much conveyance in the left overbank as in the right overbank, a 10 percent conveyance reduction value would reduce 6.7 percent from the left overbank and 3.3 percent from the right overbank.

Encroachment Method 4

Method 4 computes encroachment stations so that conveyance within the encroached cross section (at some higher elevation) is equal to the conveyance of the natural cross section at the natural water level. This higher elevation is specified as a fixed amount (target increase) above the natural (e.g., 100 year) profile. The encroachment stations are determined so that an equal loss of conveyance (at the higher elevation) occurs on each overbank, if possible. If half of the loss cannot be obtained in one overbank, the difference will be made up, if possible, in the other overbank, except that encroachments will not be allowed to fall within the main channel.

A target increase of 1.0 indicates that a 1 foot rise will be used to determine the encroachments based on equal conveyance. An alternate scheme to **equal** conveyance reduction is to reduce conveyance in **proportion** to the distribution of natural overbank conveyance. See Method 3 for an explanation of this. A key difference between Method 4 and Method 3 is that the reduction in conveyance is based on the higher water surface (target water surface) for Method 4, while Method 3 uses the lower water surface (natural water surface). An example of a Method 4 encroachment is shown in Figure 9-4.
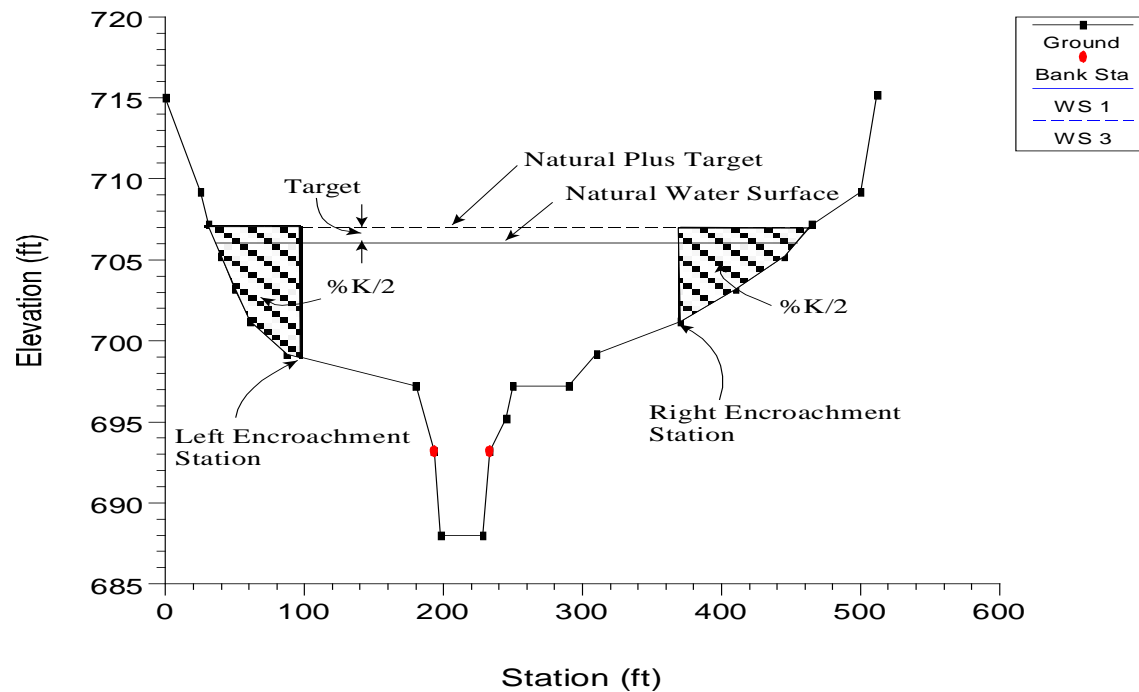
Figure 9-4 Example of Encroachment Method 4

Encroachment Method 5

Method 5 operates much like Method 4 except that an optimization scheme is used to obtain the target difference in water surface elevation between natural and encroached conditions. A maximum of 20 trials is allowed in attempting a solution. Equal conveyance reduction is attempted in each overbank, unless this is not possible (i.e., the encroachment goes all the way into the bank station before the target is met). The input data for method 5 consists of a target water surface increase and a target energy increase. The program objective is to match the target water surface without exceeding the target energy. If this is not possible, the program will then try to find the encroachments that match the target energy. If no target energy is entered, the program will keep encroaching until the water surface target is met. If only a target energy is entered, the program will keep encroaching until the target energy is met. If neither of the criteria is met after 20 trials, the program will take the best answer from all the trials and use it as the final result. The target water surface and energy can be changed at any cross section, like Methods 1 through 4. An example of method 5 is shown in Figure 9-5.
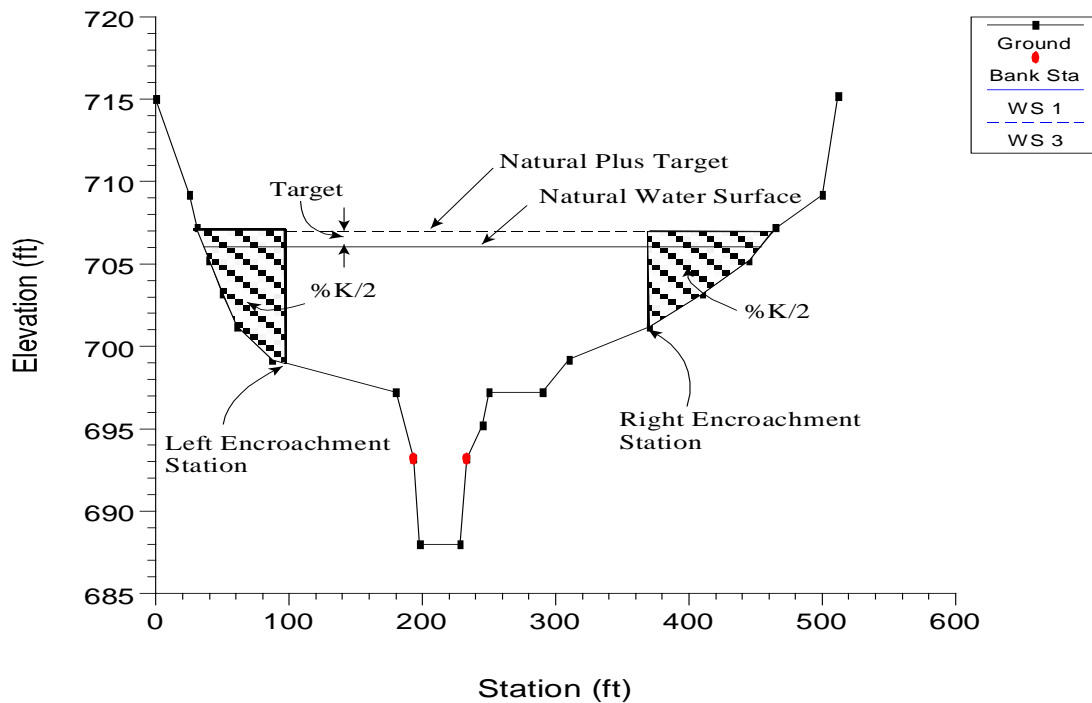
Figure 9-5 Example of Encroachment Method 5

Bridge, Culvert, and Multiple Opening Encroachments

In general, the default methodology for encroachments at bridges, culverts, and multiple openings, is to use the downstream computed encroachments through the structure, and at the cross section just upstream of the structure (the program does this automatically). There are a few exceptions to this rule.

First, when using Method 1, the user can enter separate encroachment stations downstream of the structure and upstream of the structure. The encroachments inside the structure will be based on what is entered outside (i.e. the encroachment inside the structure on the downstream side is based on the encroachment outside the structure on the downstream side. The upstream inside encroachment is based on what the user places for the cross section upstream and outside of the bridge)..

Second, for encroachment methods 2 through 5, the program will allow for separate encroachment calculations at a bridge, when using the energy based bridge computation method. For all other bridge computation methods (Momentum, Yarnell, WSPRO, Pressure Flow, Pressure and Weir Flow, and Low Flow and Weir Flow) the program will use the computed downstream encroachments through the bridge and at the cross section just upstream (as long as the cross section stationing is consistent from downstream to upstream of the bridge).

At a culvert crossing or a multiple opening, when using encroachment methods 2 through 5, the program will always use the computed downstream encroachments through the structure and just upstream of the structure. The only way to override this is to use Method 1 encroachments.

Also, encroachments can be turned off at any bridge, culvert, or multiple opening.

General Modeling Guidelines

The HEC-RAS floodway procedure is based on calculating a natural profile (no encroachments) as the first profile of a multiple profile run. Subsequent profiles are calculated with the various encroachment options available in the program.

In general, when performing a floodway analysis, encroachment methods 4 and 5 are normally used to get a first cut at the encroachment stations. Recognizing that the initial floodway computations may provide changes in water surface elevations greater, or less, than the "target" increase, initial computer runs are usually made with several "target" values. The initial computer results should then be analyzed for increases in water surface elevations, changes in velocities, changes in top width, and other parameters. Also, plotting the results with the X-Y-Z perspective plot, or onto a topographic map, is recommended. From these initial results, new estimates can be made and tried.

The increase in water surface elevation will frequently exceed the "target" used to compute the conveyance reduction and encroachment stations for the section. That is why several target increase values are generally used in the initial floodway computations.

After a few initial runs, the encroachment stations should become more defined. Because portions of several computed profiles may be used, additional runs with method 4 or 5 should be made with varying targets along the stream. The final computer runs are usually made with encroachment Method 1 defining the specific encroachment stations at each cross section. Additional runs are often made with Method 1, allowing the user to adjust encroachment stations at specific cross sections to further define the floodway.

While the floodway analysis generally focuses on the change in water surface elevation, it is important to remember that the floodway must be consistent with local development plans and provide reasonable hydraulic transitions through the study reach. Sometimes the computed floodway solution, which provides computed water surfaces at or near the target maximum, may be unreasonable when transferred to the map of the actual study reach. If this occurs, the user may need to change some of the encroachment stations, based on the visual inspection of the topographic map. The floodway computations should be re-run with the new encroachment stations to ensure that the target maximum is not exceeded.

CHAPTER 10

Estimating Scour at Bridges

The computation of scour at bridges within HEC-RAS is based upon the methods outlined in Hydraulic Engineering Circular No. 18 (HEC No. 18, FHWA, 2001). Before performing a scour analysis with the HEC-RAS software, the engineer should thoroughly review the procedures outlined in that report. This chapter presents the methods and equations for computing contraction scour and local scour at piers and abutments. Most of the material in this chapter was taken directly from the HEC No. 18 publication (FHWA, 2001).

NOTE: HEC-RAS has not been updated to the Federal Highways latest procedures documented in HEC No. 18, Evaluating Scour at Bridges (FHWA, April 2012). Therefore some differences may arise in computed results for certain flow regimes.

For information on how to enter bridge scour data into HEC-RAS, to perform the bridge scour computations, and to view the bridge scour results, see Chapter 11 of the HEC-RAS user's manual.

Contents

■ General Modeling Guidelines

■ Computing Contraction Scour

■ Computing Local Scour at Piers

■ Computing Local Scour at Abutments

■ Total Scour Depths at Bridge Piers and Abutments

General Modeling Guidelines

In order to perform a bridge scour analysis, the user must first develop a hydraulic model of the river reach containing the bridge to be analyzed. This model should include several cross sections downstream from the bridge, such that any user defined downstream boundary condition does not affect the hydraulic results inside and just upstream of the bridge. The model should also include several cross sections upstream of the bridge, in order to evaluate the long-term effects of the bridge on the water surface profile upstream.

The hydraulic modeling of the bridge should be based on the procedures outlined in Chapter 5 of this manual. If observed data are available, the model should be calibrated to the fullest extent possible. Once the hydraulic model has been calibrated (if observed data are available), the modeler can enter the design events to be used for the scour analysis. In general, the design event for a scour analysis is usually the 100 year (1 percent chance) event. In addition to this event, it is recommended that a 500 year (0.2 percent chance) event also be used to evaluate the bridge foundation under a super-flood condition.

After performing the water surface profile calculations for the design events, the bridge scour can then be evaluated. The total scour at a highway crossing is comprised of three components: long-term aggradation or degradation; contraction scour; and local scour at piers and abutments. The scour computations in the HEC-RAS software allow the user to compute contraction scour and local scour at piers and abutments. The current version of the HEC-RAS software does not allow the user to evaluate long-term aggradation and degradation. Long term aggradation and degradation should be evaluated before performing the bridge scour analysis. Procedures for performing this type of analysis are outlined in the HEC No. 18 report, and are beyond the scope of this discussion. The remaining discussions in this chapter are limited to the computation of contraction scour and local pier and abutment scour.

Computing Contraction Scour

Contraction scour occurs when the flow area of a stream is reduced by a natural contraction or a bridge constricting the flow. At a bridge crossing, many factors can contribute to the occurrence of contraction scour. These factors may include: the main channel naturally contracts as it approaches the bridge opening; the road embankments at the approach to the bridge cause all or a portion of the overbank flow to be forced into the main channel; the bridge abutments are projecting into the main channel; the bridge piers are blocking a significant portion of the flow area; and a drop in the downstream tailwater which causes increased velocities inside the bridge. There are two forms of contraction scour that can occur depending on how much bed material is already being transported upstream of the bridge contraction reach. The two types of contraction scour are called live-bed contraction scour and clear-water contraction scour. Live-bed contraction scour occurs when bed material is already being transported into the contracted bridge section from upstream of the approach section (before the contraction reach). Clear-water contraction scour occurs when the bed material sediment transport in the uncontracted approach section is negligible or less than the carrying capacity of the flow.

Contraction Scour Conditions

Four conditions (cases) of contraction scour are commonly encountered:

Case 1. Involves overbank flow on a floodplain being forced back to the main channel by the approaches to the bridge. Case 1 conditions include:

    a.   The river channel width becomes narrower either due to the bridge abutments projecting into the channel or the bridge being located at a narrowing reach of the river.

    b.   No contraction of the main channel, but the overbank flow area is completely obstructed by the road embankments.

    c.   Abutments are set back away from the main channel.

Case 2. Flow is confined to the main channel (i.e., there is no overbank flow). The normal river channel width becomes narrower due to the bridge itself or the bridge site is located at a narrowing reach of the river.

Case 3. A relief bridge in the overbank area with little or no bed material transport in the overbank area (i.e., clear-water scour).

Case 4. A relief bridge over a secondary stream in the overbank area with bed material transport (similar to case one).

Determination of Live-Bed or Clear-Water Contraction Scour

To determine if the flow upstream is transporting bed material (i.e., live-bed contraction scour), the program calculates the critical velocity for beginning of motion Vc (for the D50 size of bed material) and compares it with the mean velocity V of the flow in the main channel or overbank area upstream of the bridge at the approach section. If the critical velocity of the bed material is greater than the mean velocity at the approach section (Vc > V), then clear-water contraction scour is assumed. If the critical velocity of the bed material is less than the mean velocity at the approach section (Vc < V), then live-bed contraction scour is assumed. The user has the option of forcing the program to calculate contraction scour by the live-bed or clear-water contraction scour equation, regardless of the results from the comparison. To calculate the critical velocity, the following equation by Laursen (1963) is used:

$$V_c = K_u \, y_1^{1/6} \, D_{50}^{1/3}$$

    (10-1)

    Where: V_c =   Critical velocity above which material of size D50 and smaller will be transported, ft/s (m/s)

        y_1 =   Average depth of flow in the main channel or overbank area at the approach section, ft (m)

        D_{50} =   Bed material particle size in a mixture of which 50% are smaller, ft (m)

$$K_u \quad = \quad 11.17 \text{ (English Units), } 6.19 \text{ (S.I. Units)}$$

Live-Bed Contraction Scour

The HEC No. 18 publication recommends using a modified version of Laursen's (1960) live-bed scour equation:

$$y_2 = y_1 \left[\frac{Q_2}{Q_1} \right]^{6/7} \left[\frac{W_1}{W_2} \right]^{K_1}$$

(10-2)

$$y_s = y_2 - y_0$$

(10-3)

Where: y_s = Average depth of contraction scour in feet (m).

y_2 = Average depth after scour in the contracted section, feet (m). This is taken as the section inside the bridge at the upstream end in HEC-RAS (section BU).

y_1 = Average depth in the main channel or floodplain at the approach section, feet (m).

y_0 = Average depth in the main channel or floodplain at the contracted section before scour, feet (m).

Q_1 = Flow in the main channel or floodplain at the approach section, which is transporting sediment, cfs (m3/s).

Q_2 = Flow in the main channel or floodplain at the contracted section, which is transporting sediment, cfs (m3/s).

W_1 = Bottom width in the main channel or floodplain at the approach section, feet (m). This is approximated as the top width of the active flow area in HEC-RAS.

W_2 = Bottom width of the main channel or floodplain at the contracted section less pier widths, feet (m). This is approximated as the top width of the active flow area.

k_1 = Exponent for mode of bed material transport.

V* /ω	k1	Mode of Bed Material Transport
< 0.50	0.59	Mostly contact bed material discharge
0.50 to 2.0	0.64	Some suspended bed material discharge
> 2.0	0.69	Mostly suspended bed material discharge

V*	=	$(g\, y_1\, S_1)^{1/2}$, shear velocity in the main channel or floodplain at the approach section, ft/s (m/s).
ω	=	Fall velocity of bed material based on D50, ft/s (m/s).
g	=	Acceleration of gravity, ft/s2 (m/s2).
S_1	=	Slope of the energy grade line at the approach section, ft/ft (m/m).

Clear-Water Contraction Scour

The recommended clear-water contraction scour equation by the HEC No. 18 publication is an equation based on research from Laursen (1963):

$$y_2 = \left[\frac{Q_2^2}{C\, D_m^{2/3}\, W_2^2} \right]^{3/7}$$

(10-4)

$$y_s = y_2 - y_0$$

(10-5)

Where D_m =	Diameter of the smallest non-transportable particle in the bed material (1.25 D50) in the contracted section, feet (m).
D_{50} =	Median diameter of the bed material, feet (m).
C =	130 for English units (40 for metric).

Note: If the bridge opening has overbank area, then a separate contraction scour computation is made for the main channel and each of the overbanks.

Computing Local Scour at Piers

Pier scour occurs due to the acceleration of flow around the pier and the formation of flow vortices (known as the horseshoe vortex). The horseshoe vortex removes material from the base of the pier, creating a scour hole. As the depth of scour increases, the magnitude of the horshoe vortex decreases, thereby reducing the rate at which material is removed from the scour hole. Eventually an equilibrium between bed material inflow and outflow is reached, and the scour hole ceases to grow.

The factors that affect the depth of local scour at a pier are: velocity of the flow just upstream of the pier; depth of flow; width of the pier; length of the pier if skewed to the flow; size and

gradation of bed material; angle of attack of approach flow; shape of the pier; bed configuration; and the formation of ice jams and debris.

The HEC No. 18 report recommends the use of the Colorado State University (CSU) equation (Richardson, 1990) for the computation of pier scour under both live-bed and clear-water conditions. The CSU equation is the default equation in the HEC-RAS software. In addition to the CSU equation, an equation developed by Dr. David Froehlich (1991) has also been added as an alternative pier scour equation. The Froehlich equation is not recommended in the HEC No. 18 report, but has been shown to compare well with observed data.

Computing Pier Scour With The CSU Equation

The CSU equation predicts maximum pier scour depths for both live-bed and clear-water pier scour. The equation is:

$$y_s = 2.0 \, K_1 \, K_2 \, K_3 \, K_4 \, a^{0.65} \, y_1^{0.35} \, Fr_1^{0.43}$$

(10-6)

Where: y_s = Depth of scour in feet (m)

K_1 = Correction factor for pier nose shape

K_2 = Correction factor for angle of attack of flow

K_3 = Correction factor for bed condition

K_4 = Correction factor for armoring of bed material

a = Pier width in feet (m)

y_1 = Flow depth directly upstream of the pier in feet (m). This is taken from the flow distribution output for the cross section just upstream from the bridge.

Fr_1 = Froude Number directly upstream of the pier. This is taken from the flow distribution output for the cross section just upstream from the bridge.

Note: For round nose piers aligned with the flow, the maximum scour depth is limited as follows:

$y_s \leq$ 2.4 times the pier width (a) for $Fr_1 \leq 0.8$

$y_s \leq$ 3.0 times the pier width (a) for $Fr_1 > 0.8$

An optional correction factor, Kw for wide piers in shallow water can be applied to the CSU equation.

$$K_w = 2.58 \left(\frac{y}{a} \right)^{0.34} F^{0.65}$$

for V/V$_c$ < 1

$$K_w = 1.0 \left(\frac{y}{a} \right)^{0.13} F^{0.25}$$

for $V/V_c \geq 1$

Because this correction factor was developed based on limited flume data, it is not automatically accounted for in HEC-RAS. The user, however, can manually apply this factor to the computed scour depth, or can combine it with one of the user-entered correction factors (K_1 through K_4). See section 6.3 of HEC-18.

The correction factor for pier nose shape, K_1, is given in Table 10-1 below:

Table 10-1 Correction Factor, K1, for Pier Nose Shape

Shape of Pier Nose	K₁
(a) Square nose	1.1
(b) Round nose	1.0
(c) Circular cylinder	1.0
(d) Group of cylinders	1.0
(e) Sharp nose (triangular)	0.9

The correction factor for angle of attack of the flow, K2, is calculated in the program with the following equation:

$$K_2 = \left(\cos\theta + \frac{L}{a} \sin\theta \right)^{0.65}$$

(10-7)

Where: L   =   Length of the pier along the flow line, feet (m)

       θ   =   Angle of attack of the flow, with respect to the pier

Note: If L/a is larger than 12, the program uses L/a = 12 as a maximum in equation 10-7. If the angle of attack is greater than 5 degrees, K_2 dominates and K_1 should be set to 1.0 (the software does this automatically).

The correction factor for bed condition, K_3, is shown in table 10-2.

Table 10-2 Increase in Equilibrium Pier Scour Depth, K_3, For Bed Condition

Bed Condition	Dune Height H feet	K_3
Clear-Water Scour	N/A	1.1
Plane Bed and Antidune Flow	N/A	1.1
Small Dunes	$10 > H \geqslant 2$	1.1
Medium Dunes	$30 > H \geq 10$	1.1 to 1.2
Large Dunes	$H \geq 30$	1.3

The correction factor K_4 decreases scour depths for armoring of the scour hole for bed materials that have a D_{50} equal to or larger than 0.007 feet (0.002 m) and a D_{95} equal to or larger than 0.066 feet (0.020 m). The correction factor results from recent research by A. Molinas at CSU, which showed that when the velocity (V_1) is less than the critical velocity (Vc_{90}) of the D_{90} size of the bed material, and there is a gradation in sizes in the bed material, the D90 will limit the scour depth. The equation developed by J. S. Jones from analysis of the data is:

$$K_4 = 0.4(V_R)^{0.15}$$

(10-8)

Where:

$$V_R = \left[\frac{V_1 - V_{i50}}{V_{c50} - V_{i95}} \right]$$

(10-9)

$$V_{i50} = 0.645 \left[\frac{D_{50}}{a} \right]^{0.053} V_{c50}$$

(10-10)

$$V_{i95} = 0.645 \left[\frac{D_{95}}{a} \right]^{0.053} V_{c95}$$

V_R = Velocity ratio

V_1 = Average velocity in the main channel or overbank area at the cross section just upstream of the bridge, ft/s (m/s)

V_{i50} = Approach velocity required to initiate scour at the pier for grain size D50, ft/s (m/s)

V_{i95} = Approach velocity required to initiate scour at the pier for grain size D95, ft/s (m/s)

V_{c50} = Critical velocity for D50 bed material size, ft/s (m/s)

V_{c95} = Critical velocity for D95 bed material size, ft/s (m/s)

a = Pier width, ft (m)

$$V_{c50} = K_u \ y^{1/6} \ D_{50}^{1/3}$$
(10-11)

$$V_{c95} = K_u \ y^{1/6} \ D_{95}^{1/3}$$

Where: y = The depth of water just upstream of the pier, ft (m)

K_u = 11.17 (English Units), 6.19 (S.I. Units)

Limiting K_4 values and bed material size are given in Table 10-3.

Table 10-3 Limits for Bed Material Size and K_4 Values

Factor	Minimum Bed Material Size	Minimum K4 Value
K4	D50 ≥ 0.006 ft (0.002 m) D95≥0.06 ft (0.02 m)	0.4

Computing Pier Scour With The Froehlich Equation

A local pier scour equation developed by Dr. David Froehlich (Froehlich, 1991) has been added to the HEC-RAS software as an alternative to the CSU equation. This equation has been shown to compare well against observed data (FHWA, 1996). The equation is:

$$y_s = 0.32 \, \phi \, (a')^{0.62} \ y_1^{0.47} \ Fr_1^{0.22} \ D_{50}^{-0.09} + a$$
(10-12)

where: φ = Correction factor for pier nose shape: φ = 1.3 for square nose piers; φ = 1.0 for rounded nose piers; and φ = 0.7 for sharp nose (triangular) piers.

a′ = Projected pier width with respect to the direction of the flow, feet (m)

Note: This form of Froehlich's equation is use to predict maximum pier scour for design purposes. The addition of one pier width (+ a) is placed in the equation as a factor of safety. If the equation is to be used in an analysis mode (i.e. for predicting the scour of a particular event), Froehlich suggests dropping the addition of the pier width (+ a). The HEC-RAS program always includes the addition of the pier width (+ a) when computing pier scour. The pier scour from this equation is limited to a maximum in the same manner as the CSU equation. Maximum scour ys ≤□2.4 times the pier width (a) for Fr1 ≤□0.8, and ys ≤□3.0 times the pier width (a) for Fr1 > 0.8.

Computing Local Scour at Abutments

Local scour occurs at abutments when the abutment obstructs the flow. The obstruction of the flow forms a horizontal vortex starting at the upstream end of the abutment and running along the toe of the abutment, and forms a vertical wake vortex at the downstream end of the abutment.

The HEC No. 18 report recommends two equations for the computation of live-bed abutment scour. When the wetted embankment length (L□) divided by the approach flow depth (y1) is greater than 25, the HEC No. 18 report suggests using the HIRE equation (Richardson, 1990). When the wetted embankment length divided by the approach depth is less than or equal to 25, the HEC No. 18 report suggests using an equation by Froehlich (Froehlich, 1989).

The HIRE Equation

The HIRE equation is based on field data of scour at the end of spurs in the Mississippi River (obtained by the USACE). The HIRE equation is:

$$y_s = 4 \, y_1 \left(\frac{K_1}{0.55} \right) K_2 \, Fr_1^{0.33}$$

(10-13)

where: y_s = Scour depth in feet (m)

y_1 = Depth of flow at the toe of the abutment on the overbank or in the main channel, ft (m), taken at the cross section just upstream of the bridge.

K_1 = Correction factor for abutment shape, Table 10-4

K_2 = Correction factor for angle of attack (θ) of flow with abutment. θ = 90 when abutments are perpendicular to the flow, θ < 90 if embankment points downstream, and θ > 90 if embankment points upstream. $K_2 = (\theta/90)^{0.13}$

Fr_1 = Froude number based on velocity and depth adjacent and just upstream of the abutment toe

Table 10-4 Correction Factor for Abutment Shape, K_1

Description	K1
Vertical-wall Abutment	1.00
Vertical-wall Abutment with wing walls	0.82
Spill-through Abutment	0.55

The correction factor, K_2, for angle of attack can be taken from Figure 10-1.
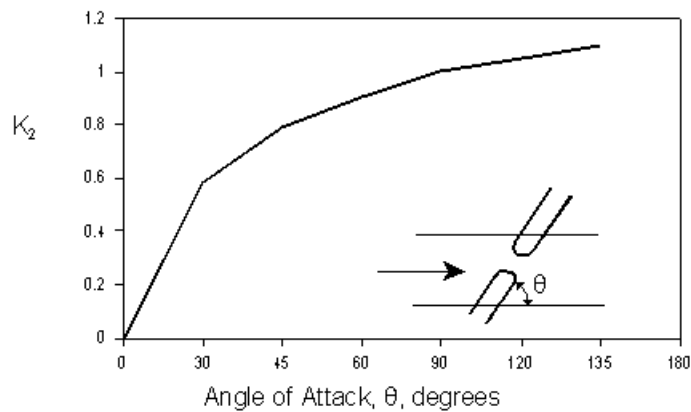
Figure 10-1 Correction Factor for Abutment Skew, K_2

Froehlich's Equation

Froehlich analyzed 170 live-bed scour measurements in laboratory flumes by regression analysis to obtain the following equation:

$$y_s = 2.27\, K_1\, K_2\, (L')^{0.43}\, y_a^{0.57}\, Fr^{0.61} + y_a$$

(10-14)

where: y_s = Scour depth in feet (m)

K_1 = Correction factor for abutment shape, Table 10-4

K_2 = Correction factor for angle of attack (θ) of flow with abutment. θ = 90 when abutments are perpendicular to the

flow, θ < 90 if embankment points downstream, and θ > 90 if

embankment points upstream (Figure 10-1). $K_2 = (\theta/90)^{0.13}$

L′ = Length of abutment (embankment) projected normal to flow, ft (m)

y_a = Average depth of flow on the floodplain at the approach section, ft (m)

Fr = Froude number of the floodplain flow at the approach section, Fr = $V_e /(gy_a)^{1/2}$

V_e = Average velocity of the approach flow $V_e = Q_e /A_e$ ft/s

Q_e = Flow obstructed by the abutment and embankment at the approach section, cfs (m^3/s)

Ae = Flow area of the approach section obstructed by the abutment and embankment, ft^2 (m^2)

Note: The above form of the Froehlich equation is for design purposes. The addition of the average depth at the approach section, y_a, was added to the equation in order to envelope 98 percent of the data. If the equation is to be used in an analysis mode (i.e. for predicting the scour of a particular event), Froehlich suggests dropping the addition of the approach depth (+ y_a). The HEC-RAS program always calculates the abutment scour with the (+y_a) included in the equation.

Clear-Water Scour at Abutments

Clear-water scour can be calculated with equation 9-13 or 9-14 for live-bed scour because clear-water scour equations potentially decrease scour at abutments due to the presence of coarser material. This decrease is unsubstantiated by field data.

Total Scour Depths Inside The Bridge

The total depth of scour is a combination of long-term bed elevation changes, contraction scour, and local scour at each individual pier and abutment. Once the scour is computed, the HEC-RAS software automatically plots the scour at the upstream bridge cross section. An example plot is shown in Figure 10-2 below.
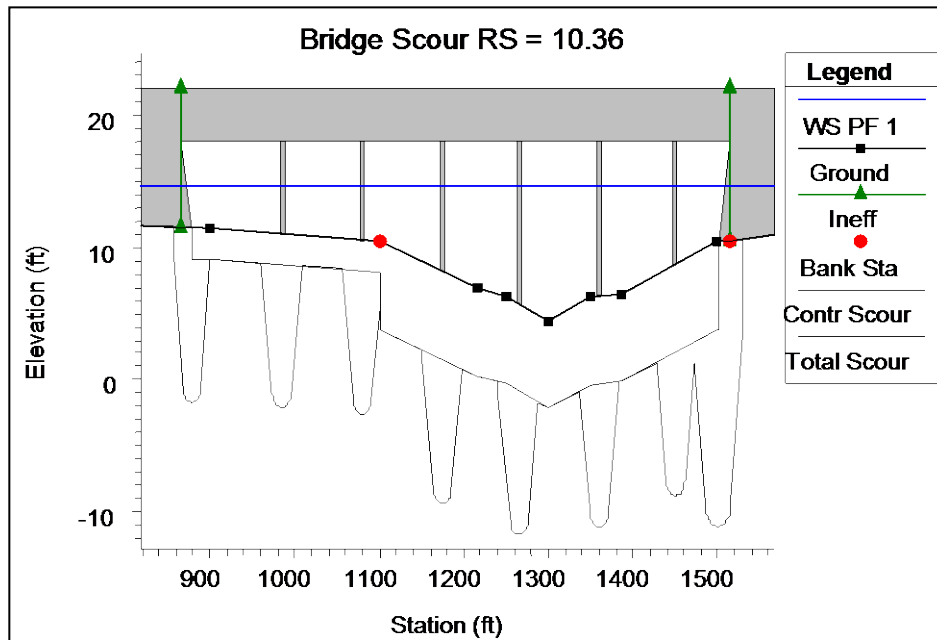
Figure 10-2 Graphic of Contraction and Total Scour at a Bridge

As shown in Figure 10-2, the program plots both contraction scour and total local scour. The contraction scour is plotted as a separate line below the existing conditions cross section data. The local pier and abutment scour are added to the contraction scour, and then plotted as total scour depths. The topwidth of the local scour hole around a pier is computed as 2.0 ys to each side of the pier. Therefore, the total topwidth of the scour hole at a pier is plotted as (4.0 ys + a). The topwidth of the local scour hole at abutments is plotted as 2.0 ys around each side of the abutment toe. Therefore, the total topwidth of the scour hole at abutments is plotted as 4.0 ys.

CHAPTER 11

Modeling Ice-covered Rivers

HEC-RAS allows the user to model ice-covered channels at two levels. The first level is an ice cover with known geometry. In this case, the user specifies the ice cover thickness and roughness at each cross section. Different ice cover thicknesses and roughness can be specified for the main channel and for each overbank and both can vary along the channel. The second level is a wide-river ice jam. In this case, the ice jam thickness is determined at each section by balancing the forces on it. The ice jam can be confined to the main channel or can include both the main channel and the overbanks. The material properties of the wide-river jam can be selected by the user and can vary from cross section to cross section. The user can specify the hydraulic roughness of the ice jam or HEC-RAS will estimate the hydraulic roughness on the basis of empirical data.

This chapter describes the general guidelines for modeling ice-covered channels with HEC-RAS. It contains background material and the equations used. For information on how to enter ice cover data and to view results, see Chapter 6 and Chapter 8 of the HEC-RAS User's Manual.

Contents

■ Modeling Ice Covers with Known Geometry

■ Modeling Wide-River Ice Jams

Modeling Ice Covers with Known Geometry

Ice covers are common on rivers during the cold winter months and they form in a variety of ways. The actual ways in which an ice cover forms depend on the channel flow conditions and the amount and type of ice generated. In most cases, river ice covers float in hydrostatic equilibrium because they react both elastically and plastically (the plastic response is termed creep) to changes in water level. The thickness and roughness of ice covers can vary significantly along the channel and even across the channel. A stationary, floating ice cover creates an additional fixed boundary with an associated hydraulic roughness. An ice cover also makes a portion of the channel cross sectional area unavailable for flow. The net result is generally to reduce the channel conveyance, largely by increasing the wetted perimeter and reducing the hydraulic radius of a channel, but also by modifying the effective channel roughness and reducing the channel flow area.

The conveyance of a channel or any subdivision of an ice-covered channel, Ki, can be estimated using Manning's equation:

$$K_i = \frac{1.486}{n_c} A_i R_i^{2/3}$$

(11-1)

Where: n_c =   the composite roughness.

       A_i =   the flow area beneath the ice cover.

       R_i =   the hydraulic roughness modified to account for the presence of ice.

The composite roughness of an ice-covered river channel can be estimated using the Belokon-Sabaneev formula as:

$$n_c = \left(\frac{n_b^{3/2} + n_i^{3/2}}{2} \right)^{2/3}$$

(11-2)

Where: n_b =   the bed Manning's roughness value.

       n_i =   the ice Manning's roughness value.

The hydraulic radius of an ice-covered channel is found as:

$$R_i = \frac{A_i}{P_b + B_i}$$

(11-3)

Where: P_b = the wetted perimeter associated with the channel bottom and side slopes

Bi   = the width of the underside of the ice cover

It is interesting to estimate the influence that an ice cover can have on the channel conveyance. For example, if a channel is roughly rectangular in shape and much wider than it is deep, then its hydraulic radius will be cut approximately in half by the presence of an ice cover. Assuming the flow area remains constant, we see that the addition of an ice cover, whose roughness is equivalent to the beds, results in a reduction of conveyance of 37%.

Separate ice thickness and roughness can be entered for the main channel and each overbank, providing the user with the ability to have three separate ice thicknesses and ice roughness at each cross section. The ice thickness in the main channel and each overbank can also be set to zero. The ice cover geometry can change from section to section along the channel. The suggested range of Manning's n values for river ice covers is listed in Table 11- 1.

The amount of a floating ice cover that is beneath the water surface is determined by the relative densities of ice and water. The ratio of the two densities is called the specific gravity of the ice. In general, the density of fresh water ice is about 1.78 slugs per cubic foot (the density of water is about 1.94 slugs per cubic foot), which corresponds to a specific gravity of 0.916. The actual density of a river ice cover will vary, depending on the amount of unfrozen water and the number and size of air bubbles incorporated into the ice. Accurate measurements of ice density are tedious, although possible. They generally tell us that the density of freshwater ice does not vary significantly from its nominal value of 0.916. In any case the user can specify a different density if necessary.

Table 11-1 Suggested Range of Manning's n Values for Ice Covered Rivers

Type of Ice	Condition	Manning's n value
Sheet ice	Smooth	0.008 to 0.012
	Rippled ice	0.01 to 0.03
	Fragmented single layer	0.015 to 0.025
Frazil ice	New 1 to 3 ft thick	0.01 to 0.03
	3 to 5 ft thick	0.03 to 0.06
	Aged	0.01 to 0.02

The suggested range of Manning's n values for a single layer of ice

The suggested range of Manning's n values for ice jams

Thickness	Manning's n values		
ft	Loose frazil	Frozen frazil	Sheet ice
0.3	-	-	0.015
1.0	0.01	0.013	0.04
1.7	0.01	0.02	0.05
2.3	0.02	0.03	0.06
3.3	0.03	0.04	0.08
5.0	0.03	0.06	0.09
6.5	0.04	0.07	0.09
10.0	0.05	0.08	0.10
16.5	0.06	0.09	-

Modeling Wide-River Ice Jams

The wide river ice jam is probably the most common type of river ice jam. In this type, all stresses acting on the jam are ultimately transmitted to the channel banks. The stresses are estimated using the ice jam force balance equation:

$$\frac{d(\overline{\sigma}_x t)}{dx} + \frac{2\tau_b t}{B} = \rho' g S_w t + \tau_i$$

(11-4)

where: $\overline{\sigma}_x$ = the longitudinal stress (along stream direction)

t = the accumulation thickness

τ_b = the shear resistance of the banks

B = the accumulation width

ρ' = the ice density

g = the acceleration of gravity

S_w = the water surface slope

τ_i = the shear stress applied to the underside of the ice by the flowing water

This equation balances changes in the longitudinal stress in the ice cover and the stress acting on the banks with the two external forces acting on the jam: the gravitational force attributable to the slope of the water surface and the shear stress of the flowing water on the jam underside.

Two assumptions are implicit in this force balance equation: that $\overline{\sigma_x}$, t, and τ_i are constant across the width, and that none of the longitudinal stress is transferred to the channel banks through changes in stream width, or horizontal bends in the plan form of the river. In addition, the stresses acting on the jam can be related to the mean vertical stress using the passive pressure concept from soil mechanics, and the mean vertical stress results only from the hydrostatics forces acting in the vertical direction. In the present case, we also assume that there is no cohesion between individual pieces of ice (reasonable assumption for ice jams formed during river ice breakup). A complete discussion of the granular approximation can be found elsewhere (Beltaos 1996).

In this light, the vertical stress, $\overline{\sigma_z}$, is:

$$\overline{\sigma}_z = \gamma_e\, t \qquad\qquad (11\text{-}5)$$

Where:

$$\gamma_e = 0.5\,\rho'\, g\,(1-s)(1-e) \qquad\qquad (11\text{-}6)$$

> Where: e = the ice jam porosity (assumed to be the same above and below the water surface)
>
> s = the specific gravity of ice

The longitudinal stress is then:

$$\overline{\sigma}_x = k_x\,\overline{\sigma}_z \qquad\qquad (11\text{-}7)$$

Where:

$$k_x = \tan^2\left(45 + \frac{\varphi}{2}\right) \qquad\qquad (11\text{-}8)$$

φ = the angle of internal friction of the ice jam

The lateral stress perpendicular to the banks can also be related to the longitudinal stress as

$$\overline{\sigma}_y = k_1\,\overline{\sigma}_x \qquad\qquad (11\text{-}9)$$

Where: k_1 = the coefficient of lateral thrust

Finally, the shear stress acting on the bank can be related to the lateral stress:

$$\tau_b = k_0 \,\overline{\sigma}_y$$

(11-10)

Where:

$$k_0 = \tan \varphi$$

(11-11)

Using the above expressions, we can restate the ice jam force balance as:

$$\frac{dt}{dx} = \frac{1}{2 k_x \gamma_e} \left[\rho' g \, S_w + \frac{\tau_i}{t} \right] - \frac{k_0 \, k_1 \, t}{B} = F$$

(11-12)

Where: F   = a shorthand description of the force balance equation

To evaluate the force balance equation, the under-ice shear stress must be estimated. The under-ice shear stress is:

$$\tau_i = \rho \, g \, R_{ic} \, S_f$$

(11-13)

Where: R_{ic} = the hydraulic radius associated with the ice cover

S_f = the friction slope of the flow

R_{ic} can be estimated as:

$$R_{ic} = \left(\frac{n_i}{n_c} \right)^{1.5} R_i$$

(11-14)

The hydraulic roughness of an ice jam can be estimated using the empirical relationships derived from the data of Nezhikovsky (1964). For ice accumulations found in wide river ice jams that are greater than 1.5 ft thick, Manning's n value can be estimated as:

$$n_i = 0.069 \, H^{-0.23} \, t_i^{0.40}$$

(11-15)

and for accumulations less than 1.5 ft thick

$$n_i = 0.0593 \, H^{-0.23} \, t_i^{0.77}$$

(11-16)

Where: H   = the total water depth

t_i = the accumulation thickness

Solution Procedure

The ice jam force balance equation is solved using an approach analogous to the standard step method. In this, the ice thickness at each cross section is found, starting from a known ice thickness at the upstream end of the ice jam. The ice thickness at the next downstream section is assumed and the value of F found. The ice jam thickness at this downstream cross section, t_{ds}, is then computed as:

$$t_{ds} = t_{us} + \overline{F} \, L$$

(11-17)

Where: t_{us} = the thickness at the upstream section

L = the distance between sections

$$\overline{F} = \frac{F_{us} + F_{ds}}{2}$$

And (11-18)

The assumed value and computed value of tds are then compared. The new assumed value of the downstream ice jam thickness set equal to the old assumed value plus 33% of the difference between the assumed and computed value. This "local relaxation" is necessary to ensure that the ice jam calculations converge smoothly to a fixed value at each cross section. A maximum of 25 iterations is allowed for convergence. The above steps are repeated until the values converge to within 0.1 ft (0.03 m) or to a user defined tolerance.

After the ice thickness is calculated at a section, the following tests are made:

The ice thickness cannot completely block the river cross section. At least 1.0 ft must remain between the bottom of the ice and the minimum elevation in the channel available for flow.

The water velocity beneath the ice cover must be less than 5 fps (1.5 m/s) or a user defined maximum velocity. If the flow velocity beneath the ice jam at a section is greater than this, the ice thickness is reduced to produce a flow velocity of approximately 5 fps or the user defined maximum water velocity.

The ice jam thickness cannot be less than the thickness supplied by the user. If the calculated ice thickness is less than this value, it is set equal to the user supplied thickness.

It is necessary to solve the force balance equation and the energy equation (eq. 2-1) simultaneously for the wide river ice jam. However, difficulties arise because the energy equation is solved using the standard step method, starting from the downstream end of the channel and proceeding upstream, while the force balance equation is solved starting from the

upstream end and proceeding downstream. The energy equation can only be solved in the upstream direction because ice covers and wide river jams exist only under conditions of subcritical flow. To overcome this incompatibility and to solve both the energy and the ice jam force balance equations, the following solution scheme was adopted.

A first guess of the ice jam thickness is provided by the user to start this scheme. The energy equation is then solved using the standard step method starting at the downstream end. Next, the ice jam force balance equation is solved from the upstream to the downstream end of the channel. The energy equation and ice jam force balance equation are solved alternately until the ice jam thickness and water surface elevations converge to fixed values at each cross section. This is "global convergence."

Global convergence occurs when the water surface elevation at any cross section changes less than 0.06 ft, or a user supplied tolerance, and the ice jam thickness at any section changes less than 0.1 ft, or a user supplied tolerance, between successive solutions of the ice jam force balance equation. A total of 50 iterations (or a user defined maximum number) are allowed for convergence. Between iterations of the energy equation, the ice jam thickness at each section is allowed to vary by only 25% of the calculated change. This "global relaxation" is necessary to ensure that the entire water surface profile converges smoothly to a final profile.

CHAPTER 12

Stable Channel Design Functions

The stable channel design functions are based upon the methods used in the SAM Hydraulic Design Package for Channels, developed by the U.S. Army Corps of Engineers Waterways Experiment Station. This chapter presents the methods and equations used for designing stable channels, including channel geometry, and sediment transport capacity.

Much of the material in this chapter directly references the SAM Hydraulic Design Package for Channels User's Guide (USACE, 1998) and EM 1110-2-1601. There have been a number of alterations to the general approach used in SAM in order to expand its capabilities and to fit within the framework of HEC-RAS. For information on how to enter data for stable channel design and sediment transport capacity analysis, and how to view results, see Chapter 15 of the HEC-RAS user's manual.

Contents
- Uniform Flow Computations

- Stable Channel Design

- Sediment Transport Capacity

Uniform Flow Computations

For preliminary channel sizing and analysis for a given cross section, a uniform flow editor is available in HEC-RAS. The uniform flow editor solves the steady-state, Manning's equation for uniform flow. The five parameters that make up the Manning's equation are channel depth, width, slope, discharge, and roughness.

$$Q=f(A, R, S, n) \tag{12-1}$$

Where: Q   = Discharge

      A   = Cross sectional area

      R   = Hydraulic radius

      S   = Energy slope

      n   = Manning's n value

When an irregularly shaped cross section is subdivided into a number of subareas, a unique solution for depth can be found. And further, when a regular trapezoidal shaped section is used, a unique solution for the bottom width of the channel can be found if the channel side slopes are provided. The dependant variables A, and R, can then be expressed in the Manning equation in terms of depth, width and side slope as follows:

$$Q=f(Y, W, z, S, n) \tag{12-2}$$

Where: Y   = Depth

      W   = Bottom width

      z   = Channel side slope

By providing four of the five parameters, HEC-RAS will solve the fifth for a given cross section. When solving for width, some normalization must be applied to a cross section to obtain a unique solution, therefore a trapezoidal or compound trapezoidal section with up to three templates must be used for this situation.

Cross Section Subdivision for Conveyance Calculations

In the uniform flow computations, the HEC-RAS default Conveyance Subdivision Method is used to determine total conveyance. Subareas are broken up by roughness value break points and then each subarea's conveyance is calculated using Manning's equation. Conveyances are then combined for the left overbank, the right overbank, and the main channel and then further summed to obtain the total cross section conveyance. Refer to Chapter 2 for more detail.

Bed Roughness Functions

Because Manning's n values are typically used in HEC-RAS, the uniform flow feature allows for the use of a number of different roughness equations to solve for n. HEC-RAS allows the user to apply any of these equations at any area within a cross section, however, the applicability of each equation should be noted prior to selection.   The following bed roughness equations are available:

- Manning Equation

- Keulegan Equation

- Strickler Equation

- Limerinos Equation

- Brownlie Equation

- Soil Conservation Service Equations for Grass Lined Channels

The Manning equation is the basis for the solution of uniform flow in HEC-RAS.

$$Q = \frac{1.486}{n} A R^{2/3} S^{1/2}$$

(12-3)

Roughness values solved for using other roughness equations are converted to Manning's n values for use in the computations. One n value or a range of n values is prescribed across the cross section and then the Manning's equation is used to solve for the desired parameter.

Manning Equation:

When choosing the Manning equation method, one n value or a range of n values is prescribed across the cross section and then the Manning's equation is used to solve for the desired parameter.

Keulegan Equation:

The Keulegan (1938) equation is applicable for rigid boundary channel design. Flow is classified according to three types: hydraulically smooth, hydraulically rough, or a transitional zone between smooth and rough. To solve the Keulegan equation, a Nikaradse equivalent sand roughness value, ks must be provided. Values for ks typically range from 1d90 for large stones to 3d90 for sand and gravel with bed forms, where d90 is the representative grain size in which 90% of all particles in the bed are smaller. However, ks values are highly variable and depend also on the types of bed forms, the overall grain distribution, the particle shape factor, and other physical properties. Therefore, unless there is specific data related to the ks value for a given cross section of a river, it is recommended that one of the other roughness equations be chosen. If the discharge, area, hydraulic radius, and slope are known, a ks value can be

calculated and then used in the solution of additional discharges, depths, slopes, or widths. EM 1110-2-1601 has a table of suggested ks values for concrete-lined channels.

Van Rijn (1993) defines the three boundary-zone flow regimes as follows:

Hydraulically smooth flow is defined as flow in which the bed roughness elements are much smaller than the thickness of the viscous sublayer and do not affect the velocity distribution (Figure 12-1). This is found when

$$\frac{u_* k_s}{v} \leq 5 \tag{12-4}$$

Where: u_* = current related bed shear velocity

   v = kinematic viscosity coefficient

   k_s = equivalent sand roughness value

Hydraulically rough flow is defined as flow in which a viscous sublayer does not exist and the velocity distribution is not dependent on the viscosity of the fluid (Figure 12-1). This is found when

$$\frac{u_* k_s}{v} \geq 70 \tag{12-5}$$

Transitional flow is where the velocity distribution is affected by viscosity as well as by the bottom roughness.

$$5 < \frac{u_* k_s}{v} < 70 \tag{12-6}$$
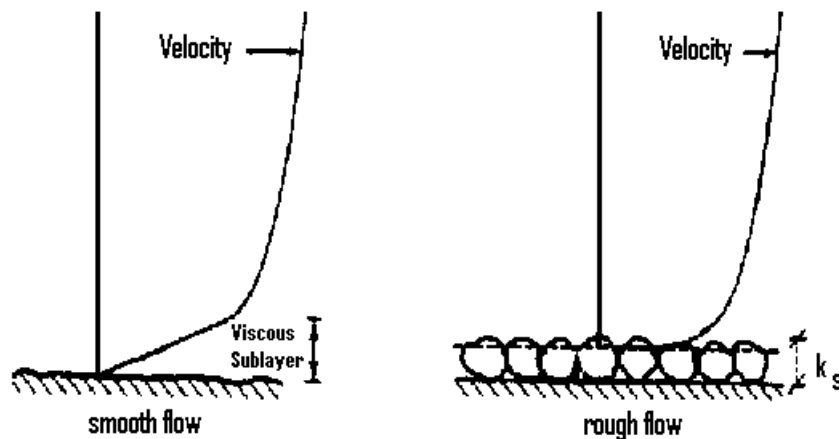
Figure 12-1 Velocity Distribution in Smooth and Rough Flow (Van Rijn, 1993)

The equation for fully rough flow is

$$C = 32.6 \log_{10}\left(\frac{12.2R}{k_s}\right) \tag{12-7}$$

Where: C = Chezy roughness coefficient

R = Hydraulic radius

And for fully smooth flow

$$C = 32.6 \log_{10}\left(\frac{5.2R_n}{C}\right) \tag{12-8}$$

Where R_n = Reynolds number

Iwagaki (Chow, 1959) found from experimental data that the coefficients 12.2 and 5.1 actually vary with the Froude number. He reasoned that as the Froude number increases, the stability of the free surface diminishes, creating more resistance in the open channel. According to Iwagaki, for fully rough flow, the coefficient 12.2 should be replaced by

$$10^{\frac{A_r\sqrt{g}}{32.6}} \qquad\qquad \text{to get} \qquad C = 32.6\log_{10}\left[10^{\frac{A_r\sqrt{g}}{32.6}}\left(\frac{R}{k_s}\right)\right]$$

(12-9)

Where: A_r = Coefficient for rough flow that varies with Froude number.

$$A_r = -27.058\log_{10}(F+9) + 34.289 \tag{12-10}$$

Where: F = Froude number

For fully smooth flow the coefficient 5.2 should be replaced by

$$\frac{\sqrt{g}}{4}10^{\frac{A_r\sqrt{g}}{32.6}} \quad \text{to get} \quad C = 32.6\log_{10}\left[10^{\frac{A_r\sqrt{g}}{32.6}}\left(\frac{\sqrt{g}R}{4C}\right)\right] \tag{12-11}$$

Where: A_s = Coefficient for smooth flow that varies with Froude number

$$As = -24.739\log_{10}(F+10) + 29.349$$
(12-12)

When the flow is in the transitional regime, the Chezy coefficient is just a combination of the equations for smooth and rough flow.

$$C = -32.6\log_{10}\left[\frac{k_s}{R10^{\frac{A_r\sqrt{g}}{32.6}}} + \frac{4C}{\sqrt{g}R_n10^{\frac{A_r\sqrt{g}}{32.6}}}\right]$$ (12-13)

It should be noted that the data used to develop these equations had Froude numbers ranging from 0.2 to 8.0. Also, the Keulegan method should not be used when the relative roughness (R/k$_s$) is less than 3. This indicates extremely rough flow, which does not follow the logarithmic velocity distribution from which Keulegan's method is based. HEC-RAS uses equation 12-13 for uniform flow computations when the Keulegan method is selected. When the flow is fully rough, the relative roughness term of the equation becomes dominant and the viscous effects (R$_n$) are relatively small. When the flow is fully smooth, the sublayer viscous effects become dominant and the relative roughness term drops out.

Once the Chezy coefficient is determined, it is converted to a Manning's n value for use in the Manning equation from the following expression:

$$n = \frac{1.486}{C}R^{1/6}$$ (U.S. Customary Units)   (12-14)

$$n = \frac{1}{C}R^{1/6}$$ (S.I. Units)

Strickler Equation

When comparing the relative roughness to a so-called Strickler function, it is found that over a wide range of relative roughness, the variation of the Strickler function, $\phi R / k_s$ is small (Chow, 1959). Because of this relationship, a constant value for the Strickler function can be used to calculate an n value. Strickler assumed this constant value to be 0.0342 when k_s and *R* are given in feet and when the Nikaradse k_s value is given as the d$_{50}$ of the bed sediment. Research at WES (Maynard, 1991) has produced different results when the Strickler function is applied to riprap-lined beds. In this case ks is the bed sediment d90 and the value applied to the Strickler function should depend on the type of calculations when designing channels. For velocity and stone sized calculations, the Strickler function should be 0.0342. For discharge capacity calculations, 0.038 should be used. The following expression converts k_s to an n value.

$$n = \phi\frac{R}{k_s}k_s^{1/6}$$ (12-15)

Where: k_s = Nikaradse equivalent sand roughness, ft or m, =d50 for natural channels and d90 for riprap-lined channels.

$\phi R / k_s$ =   Strickler function = 0.0342 for natural channels

=   0.0342 for velocity and stone size calculations in riprap design.

=   0.038 for discharge calculations in riprap design

Limerinos Equation

Larger grain sizes from coarse sands to cobbles were used by Limerinos (1970) to develop an n-value predictor based on Hydraulic roughness and particle sediment size for mobile bed streams. This method can only be applied to the grain-related upper flow regime, which includes plane bed, antidunes, and chutes and pools. Sand bed streams are applicable provided that the bed form is plane bed (Burkham and Dawdy, 1976). Whether a channel is in upper, lower, or the transitional bed form regime is a function of the localized, or Grain-related Froude Number which is defined as the following:

$$F_g = \frac{V}{\sqrt{(s_s - 1)gd_{50}}}$$
(12-16)

Where: F_g = Grain-related Froude number

V = Average channel velocity

s_s = Specific Gravity of sediments particles

If the bed slope is greater than 0.006, flow is always considered to be in the upper regime. Otherwise, upper and lower regime can be defined as follows

$$F_g > \frac{1.74}{S^{1/3}}$$ Grain-related upper Regime Flow

(12-17)

$$F_g \leq \frac{1.74}{S^{1/3}}$$ Grain-related lower Regime Flow

Where: S   = Bed Slope

The n-value predictor as defined by Limerinos is:

$$n = \frac{0.0929R^{1/6}}{1.16 + 2.0\log_{10}\left(\dfrac{R}{d_{84}}\right)}$$
(12-18)

Where: R   = Hydraulic Radius

d_{84} = the particle size for which 84% of all sediments are smaller

It is important that the Limerinos method be chosen with care. The data ranges at which it applies are relatively small and limited to coarse sands to cobbles in upper regime flow. A particular advantage with the Limerinos method is its apparent accounting for bed form roughness losses. As a consequence, n values computed using Limerinos will normally be significantly higher than those found using Strickler. Burkham and Dawdy showed that the range of relative roughness of the Limerios method is between 600 and 10,000.

<u>Brownlie Equation</u>

Brownlie (1983) developed a method for use with bed forms in both the upper and lower regime. In this method the Strickler function is multiplied by a bed-form roughness, which is a function of the hydraulic radius, the bed slope and the sediment gradation. The resulting equations for lower and upper regime are:

$$n = \left[1.6940 \left(\frac{R}{d_{50}} \right)^{0.1374} S^{0.1112} \sigma^{0.1605} \right] 0.034 (d_{50})^{0.167} \text{ (Lower Regime)}$$

(12-19)

$$n = \left[1.0213 \left(\frac{R}{d_{50}} \right)^{0.0662} S^{0.0395} \sigma^{0.1282} \right] 0.034 (d_{50})^{0.167} \text{ (Upper Regime)}$$

Where: σ = the geometric standard deviation of the sediment mixture

$$\sigma = 0.5 \left(\frac{d_{84} + d_{50}}{d_{50} + d_{16}} \right)$$

(12-20)

In actuality, the transition between the upper and lower regimes does not occur at one point, but rather over a range of hydraulic radii. Within this range, there are actually two valid solutions (a lower and an upper regime solution) because the transition is initiated at different discharges depending on whether the occurrence is on the rising end or falling end of the hydrograph. HEC-RAS will solve for both and when there are two solutions, a message box will appear that requests the user to select which regime to solve for. A general rule of thumb is to use the upper regime for the rising end of the hydrograph and the lower regime for the falling end of the hydrograph (Figure 12-2).

Pigeon Roost Creek
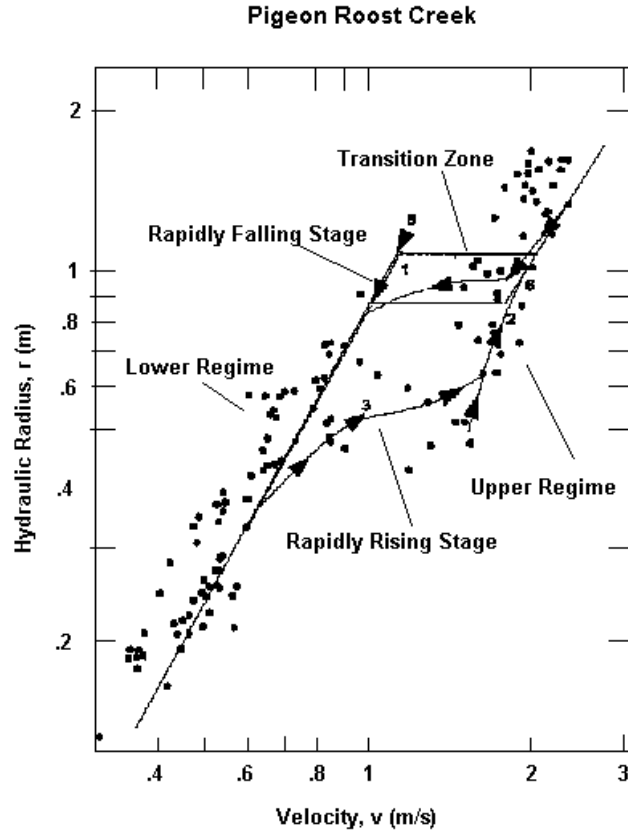
Figure 12-2 Example: Velocity vs. Hydraulic Radius in a Mobile Bed Stream (California Institute of Technology)
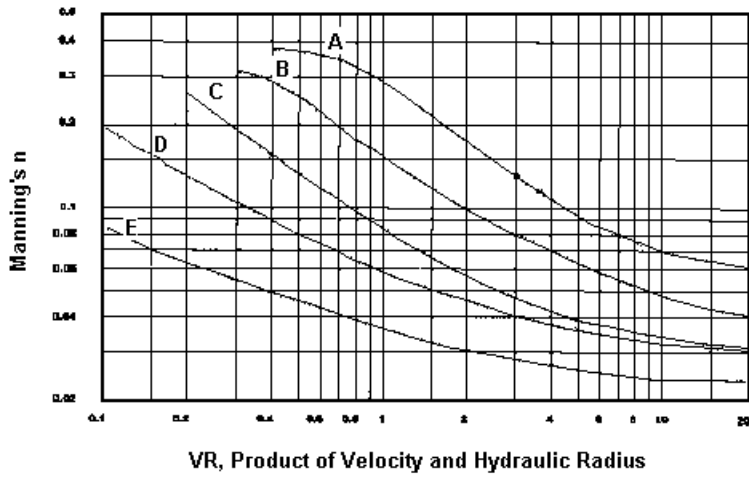
Figure 12-3 SCS Grass Cover n-value Curves (US Dept. of Agriculture, 1954)

Table 12-1 Characteristics of Grass Cover

Grass Type	Cover	Condition
A	Weeping lovegrass……………… Yellow bluestem Ischaemum……	Excellent Stand, tall (average 30 in) Excellent stand, tall (average 36 in)
B	Kudzu…………………………… Bermudagrass…………………… Native grass mixture (little bluestem, blue grama, other long and short Midwest grasses) Weeping lovegrass……………… Lespedeza serices……………… Alfalfa…………………………… Weeping lovegrass……………… Kudzu…………………………… Blue grama………………………	Very dense growth, uncut Good stand, tall (average 12 in) Good stand, unmowed Good stand, tall (average 24 in) Good stand, not weedy, tall (average 19 in) Good stand, uncut (average 11 in) Good stand, mowed (average 13 in) Dense growth, uncut Good stand, uncut (average 13 in)
C	Crabgrass………………………... Bermudagrass…………………… Common lespedeza……………… Grass-legume mixture—summer (orchard grass, redtop, Italian ryegrass and common lespedeza) Centipedegrass…………………... Kentucky bluegrass………………	Fair stand, uncut (10 to 48 in) Good stand, mowed Good stand, uncut (average 11 in) Good stand, uncut (6 to 8 in) Very dense cover (average 6 in) Good stand headed (6 to 12 in)
D	Bermudagrass…………………… Common lespedeza……………… Buffalograss…………………….. Grass-legume mixture—fall, spring (orchard grass, redtop, Italian ryegrass and common lespedeza) Lespedeza serices………………	Good stand, cut to 2.5 in height Excellent stand, uncut (average 4.5 in) Good stand, uncut (3 to 6 in) Good stand, uncut (4 to 5 in) After cutting to 2 in height; very good stand before cutting
E	Bermudagrass…………………… Bermudagrass……………………	Good stand, cut to 1.5 in height Burned stubble

Soil Conservation Service Grass Cover

The Soil Conservation Service (SCS, US Department of Agriculture, 1954) has developed five curves that define the respective roughness as a function of the product of velocity and hydraulic radius. Each curve, A through E, represents a different type of grass cover, all of which are presented in Table 12-1. The ranges over which these curves apply can be seen in Figure 12-3.

Selection of Roughness Equation

Each of the roughness equations described above have limitations to their applicability. Selection of one or more methods should be chosen based on stream characteristics with knowledge of the development of the chosen method(s) to better determine the appropriate roughness values to use. For example, vegetation roughness and bank angle typically do not permit the movement of bed load along the face of the banks, therefore bed roughness

predictors such as Limerinos and Brownlie should not be used at those locations in the cross section. For this reason, HEC-RAS only allows the user to define one sediment gradation, which should be applied to the main channel bed only. In addition, the equations used to solve for Manning's n values are typically based on a representative grain diameter and hydraulic parameters. Other roughness affects such as vegetation, temperature, planform, etc., are not accounted for. The following table (Table 12-2) gives a general idea of the limitations and applicabilities of each roughness predictor.

Table 12-2 Data Range and Applicabilities of Roughness Predictors

Equation	Data Range	Applicability
Mannings	Typically .01<n<.5	All. However, n-values do not have the ability to directly vary with Hydraulic Radius
Keulegan	Froude number 0.2<F<8.0	In streams where the relative roughness value, R/ks >= 3
Strickler	R/ks >=1	Natural channels for uniform flow computations.
Limerinos	1.5mm<d84<250mm 0.2<n<0.10 1ft<R<6ft 600<R/ks<10,000	Coarse sand to large cobbles. Only upper regime flow. Mobile beds. Main channel bed only.
Brownlie		Upper, lower, and transitional regimes. Mobile beds. Main channel bed only.
SCS Grass Curves	0.1 to 0.4<VR<20	Grass cover. See Table 12-1

Stable Channel Design

Three approaches can be used in HEC-RAS for stable channel design. They are the Copeland, Regime, and Tractive Force methods. The Copeland method uses an analytical approach to solve stable channel design variables of depth, width, and slope. Stability is achieved when the sediment inflow to a particular reach equals the sediment outflow. The Regime method is purely empirical, and, within HEC-RAS, uses equations developed by Blench (1975). The Regime method defines a channel as being stable when there is no net annual scour or deposition in the design reach. The Tractive Force method is an analytical scheme that defines channel stability as no appreciable bed load movement. It is important to know the characteristics of the design stream to determine which approach will work best. Each of these approaches stem from work done previously in conditions with somewhat limited validity ranges.

Copeland Method

The Copeland Method for stable channel design was developed by Dr. Ronald Copeland at the Waterways Experiment Station for use in the SAM software package (Copeland, 1994). This approach is primarily analytical on a foundation of empirically-derived equations and it uses the sediment discharge and flow depth prediction methods of Brownlie (1981) to ultimately solve for stable depth and slope, for a given channel bottom width for trapezoidal cross sections. This method assumes bed load movement occurs above the bed, not the banks, and separates hydraulic roughness into bed and bank components.

To determine the level of stability of the design channel, an inflowing sediment discharge must be established. This can be done simply by entering the upstream sediment concentration, or by entering a supply reach bottom width and slope and allowing the program to calculate the sediment discharge. Sediment concentration is given by the following:

$$C = 9022(F_g - F_{go})^{1.978} S^{0.6601} \left(\frac{R_b}{d_{50}} \right)^{-0.3301}$$

(12-21)

Where: C = Sediment concentration over the bed, in ppm

F_g = Grain-related Froude number

F_{go} = Critical grain-related Froude number

S = Slope

R_b = Bed hydraulic radius

d_{50} = Median grain size

$$F_g = \frac{V}{\sqrt{(s_s - 1)g d_{50}}}$$

(12-22)

Where: V = Average channel velocity (this method assumes the average velocity for the total cross section is representative of the average velocity in each sub section).

s_s = Specific Gravity of sediment particles.

$$F_{go} = \frac{4.596\tau_{*o}^{0.5293}}{S^{0.1405}\sigma^{0.1606}}$$ (12-23)

$$\tau_{*o} = 0.22Y + 0.06(10)^{-7.7Y}$$ (12-24)

$$Y = \left(\sqrt{s_s - 1}\ R_g\right)^{-0.6}$$ (12-25)

$$R_g = \sqrt{\frac{gd_{50}^3}{v}}$$ (12-26)

$$\sigma = \frac{1}{2}\left(\frac{d_{84}}{d_{50}} + \frac{d_{50}}{d_{16}}\right)$$ (12-27)

Where: τ_{*o} = Critical shear stress

Rg = Grain Reynolds Number

V = Kinematic viscosity

σ = Sediment gradation coefficient

Brownlie uses the above regression equations to equate critical shear from Shield's diagram with critical Froude number, which can ultimately be used to represent a critical velocity by substituting Fgo into equation 12-22.

For the case where the Grain-related Froude Number is less than or equal to the Critical Grain-related Froude Number, the sediment concentration, C, will automatically be returned as zero, indicating no sediment bed movement.

Once the inflowing sediment concentration over the bed is determined, the total sediment concentration for the entire channel is used to size stable channel dimensions for various channel bottom widths. To do this, Brownlie's resistance equations are used:

$$R_b = 0.2836 d_{50} q_*^{0.6248} S^{-0.2877} \sigma^{0.08013} \text{, for Upper Regime}$$

(12-28)

$$R_b = 0.3724 d_{50} q_*^{0.6539} S^{-0.2542} \sigma^{0.1050} \text{, for Lower Regime}$$

Where: q_* = dimensionless unit discharge

σ = sediment gradation coefficie

$$q_* = \frac{VD}{\sqrt{g d_{50}^3}}$$

(12-29)

Upper or lower transport regime is determined using the relationship expressed in equation 12-17. However, if the Grain-related Froude Number is within 0.8 to 1.25 of 1.74/S1/3, then it is considered to be in the transitional regime. Currently, a definition for a function describing the transitional transport regime is not available. The user has the choice of applying either the upper or lower regime equations in this circumstance. In the lower regime, the bed form can be composed of ribbons or ridges, ripples, dunes, bars, or simply a flat bed with transportation mostly as bed load. The transitional regime consists of washed-out dunes and sand waves, with particles transported mostly by suspension. The upper regime develops symmetrical sand waves in subcritical flow and plane bed and/or anti dunes for supercritical flow. Particles are almost entirely in suspension. If a transitional regime is realized in one or more of the solutions, recompute the stable channel dimensions using the other transport regime and compare results. Typically the upper regime is found on the rising end of a flood wave and the lower regime is found on the falling end. It is suggested that the more conservative results be used for design if the regime is not known.

Because the roughness of the side slopes is accounted for in this solution method, an assumption has to be made as to their hydraulic parameters. It is assumed that the average velocity over the side slopes is equal to the average channel velocity. With that,

$$R_s = \left(\frac{V n_s}{1.486 S^{0.5}} \right)$$

(12-30)

and the channel area, A, can be determined by

$$A = R_b P_b + R_s P_s$$

(12-31)

Where: R_s = Hydraulic radius of the side slopes

n_s = Manning's n value of the side slopes

P_s = Wetted perimeter of the side slopes

R_b = Hydraulic radius of the bed

P_b = Bed width.

The bed roughness is calculated using Brownlie's roughness predictor (Equation 12-19).

The user can enter a median channel width to bracket the desired results or this value can be left empty, in which case, HEC-RAS will automatically compute a median channel width from the following regime equation, which is proposed in EM 1110-2-1418:

$$B = 2.0Q^{0.5}$$

<div align="right">(12-32)</div>

Using the median channel width, HEC-RAS determines 19 other channel widths at increments of 0.1B. Stable channel geometry is then solved for each channel width. A stability curve can be analyzed by plotting the array of base widths and their corresponding stable slopes within HEC-RAS by pressing the "Stability Curve" command button after computations have been run. As shown in Figure 12-4, it is easy to see for what slope/width channel geometries degradation, aggradation, or stabilization can be expected.   It is important to note that the further away from the stability curve, the more aggradation of degradation can be expected. A second-order Lagrangian interpolation scheme is used to find the minimum stream power solution that will transport the inflowing sediment load.
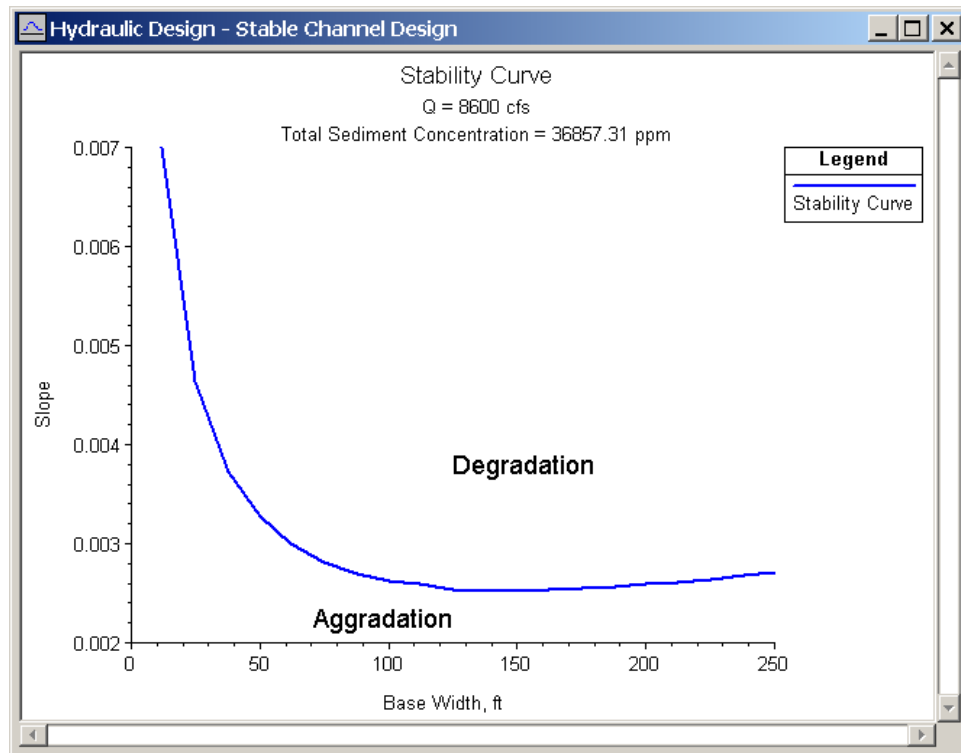
Figure 12-4 Stability Curve

The use of k values to define roughness on the side slopes is permitted for the Copeland Method. HEC-RAS simply converts the k value to an associated Manning's n value using Strickler's equation (Equation 12-15) with a value of 0.039 for the Strickler function, as suggested by Copeland. The bank roughness should be an accurate representation of everything that contributes to roughness on the banks. This includes channel irregularities,

variations of channel cross-section shape, channel sinuosity, and vegetation. It is important to run the computations using a range of roughness values to test the sensitivity. Because, in this method, all sediment transport is assumed to occur over the bed, and not over the banks, flow distribution is very important for accuracy. This is accounted for in the bank steepness and roughness. For maximum transport, use a very steep bank with low roughness.

Sound judgment must be used when selecting the appropriate design discharge for performing a stability analysis. To date, no generally accepted discharge for stable channel design is agreed upon, therefore the use of a range of discharges is recommended. Suggested design discharges that may represent the channel forming discharge are:

- 2-year frequency flood (perennial streams)

- 10-year frequency flood (ephemeral streams)

- Bankfull discharge

- Effective discharge (Q that carries the most bed load sediment)

Selection of the design discharge should be made after considering the general physical characteristics of the stream, the temporal characteristics of the stream, what is the desired outcome (channel stabilization?), and any other applicable factor. It would be wise to run the calculations using a range of discharges as well as sediment inflows for a sensitivity analysis to understand how the channel reacts to different sediment and water inflow events.

As in the SAM package, HEC-RAS calculates a range of widths and slopes, and their unique solution for depth. This makes it possible to easily analyze or design stable channels. If a given slope is desired, the channel width through that reach can be adjusted to a value on the stability curve. Likewise, if a particular channel width is desired, the channel slope can be adjusted to achieve stability. If, for a given width, the slope is greater than the input valley slope, which is the maximum possible slope for the channel invert, this creates a sediment trap, which is indicate by the results. However, if the slope is less than the valley slope, the stability curve can be used to aid in adding sinuosity or the spacing of drop structures.

Because the Brownlie equations were developed from an analysis of field and laboratory data, there are limits of applicability that should be adhered to. At the least, the user needs to be aware if the limits are being exceeded. Table 12-3 presents the ranges of selected parameters of field and laboratory data used in Brownlie's research.

Table 12-3 Data Range and Applicabilities of Copeland Method

	Velocity (fps)		**Depth (ft)**		**Slope x 10^3**		**d_{50} x 10^{-3} (ft)**		**Conc. (ppm)**	
	Min	Max	Min	Max	Min	Max	Min	Max	Min	Max
Lab	0.73	6.61	0.11	1.91	0.269	16.950	0.28	4.42	10.95	39263
Field	1.20	7.95	0.35	56.7	0.010	1.799	0.28	4.72	11.70	5830

In addition, Brownlie suggests input data be restricted to the following:

Table 12-4 Suggested Input Restrictions for Copeland Method

Parameter	Symbol	Restiction	Reason
Median Grain Size (ft x 10^{-3})	d_{50}	$0.203 < d_{50} < 6.56$	Sand only
Geometric Standard Deviation of Bed Particles	σ_g	$\sigma_g < 5$	Eliminate bimodal grain distributions
Width to Depth Ratio	B/D	$B/D > 4$	Reduce sidewall effects
Relative Roughness	R_b/d_{50}	$R_b/d_{50} > 100$	Eliminate shallow water effects
Concentration (ppm)	C	$C > 10$	Accuracy problems associated with low concentration

Regime Method

The regime method for stable channel design originated from irrigation design studies in Pakistan and India, and is based on a set of empirically derived equations, which typically solve for depth, width, and slope as a function of discharge and grain size.

$$D, B, S = f(Q, d_{50}) \tag{12-33}$$

Where: D = Depth

B = Channel width

S = Slope

Q = Discharge

D_{50} = median grain size.

To be considered in regime, or equilibrium, transport of sediments is allowed as long as there is no net annual scour or deposition in the channel. The regime method is applicable to large-scale irrigation systems with a wide range of discharges of silts and find sands. Because regime equations are purely empirical and based on field observations, the regime method can only be used within its validity range (Van Rijn, 1993).

The Blench Regime Method (Blench, 1970) is used in HEC-RAS. These equations are intended to be used with channels that have sand beds. In addition to the typical independent variables of

discharge and grain size, the Blench method requires an inflowing sediment concentration and some information about the bank composition.   The three regime equations are:

$$B = \left(\frac{F_B Q}{F_S}\right)^{0.5}$$

(12-34)

$$D = \left(\frac{F_S Q}{F_B^2}\right)^{\frac{1}{3}}$$

(12-35)

$$S = \frac{F_B^{0.875}}{\frac{3.63g}{v^{0.25}} B^{0.25} D^{0.125} \left(1 + \frac{C}{2330}\right)}$$

(12-36)

Where: D = Channel depth

B = Channel width

S = Channel slope

Q = Channel forming discharge

d_{50} = Median grain size of bed material

C = Bed material sediment concentration

v = Kinematic viscosity

F_B = Bed factor

F_S = Side factor

The bed factor can be determined by the following equation:

$$F_B = 1.9\sqrt{d_{50}}$$

(12-37)

Blench suggests the following values be used for the side factor:

- $F_S = 0.1$, for friable banks
- $F_S = 0.2$, for silty, clayey, loamey banks
- $F_S = 0.3$, for tough clayey banks

The Blench regime method is applicable only to straight reaches with beds of silt to fine sand. In addition, Blench suggests that the regime equations be applied only under the following circumstances:

- Sides behave as if hydraulically smooth (i.e. friction due only to viscous forces).

- Bed width exceeds three times the depth.

- Side slopes are consistent with those of a cohesive nature.

- Discharges are steady.

- Sediment load is steady.

- Bed load is non-cohesive, and moves in dune formation.

- Subcritical flow.

- Sediment size is small compared with the depth of water.

- Regime has been achieved by the channel.

These circumstances seem very confining, and in reality, no one channel or canal can claim to behave strictly in this manner. However, if the channel can be adequately approximated by these conditions, without deviating significantly from its true nature, the regime equations may be applicable. At a minimum, the Blench Regime method is a quick way of obtaining "ball-park" figures for results.

Tractive Force Method

Essentially an analytical stable design method, the tractive force approach utilizes a critical shear stress to define when initiation of motion begins, the point at which the channel becomes unstable. In HEC-RAS, this concept is followed to allow the user to solve for two dependant variables when two others are given. The dependant variables are depth, width, slope, and a representative grain size (either d50 or d75, depending on the solution method selected). For example, width and grain size can be entered, and HEC-RAS will solve for depth and slope.

The tractive force can be defined as the force that is resisted by friction force and, while in equilibrium, is equal and opposite in magnitude and direction. It is also called shear stress or drag force and can be represented as:

$$\tau_o = \gamma R S$$

(12-38)

Where: τ_o = Tractive force per unit wetted area

      γ = Unit weight of water

      R = Hydraulic radius

      S = Slope

For very wide channels (B/D > 10), equation 12-38 is very representative of the shearing force felt on the bed. Because $\boxed{d}$ is the average tractive force over the wetted area, the shear distribution becomes more non-uniform as the channel becomes narrower and more trapezoidal. As a result, the maximum tractive force is actually less than that predicted by equation 12-38 by some reduction factor. In addition, the channel walls, due to their inclination, have an even greater reduction effect on the maximum tractive force felt on the side slopes. For typical trapezoidal sections, it has been determined experimentally by Lane (1953) that the adjustment factor for both the bed and side slopes is largely dependent on the width to depth ratio and the side slope angle. Figure 12-5 presents the curves used to determine the adjustment factors for both the bed and side slopes.

The channel is considered stable if the tractive force at any given location in the cross section is less than the critical shear force. There are currently three methods for determining the critical shear stress in HEC-RAS. They are the Lane, Shields, and user-entered methods.

Lane Method:

Lane conducted experiments on canals in the San Luis Valley of Colorado to develop a method for predicting the critical shear stress. The canals tested were stable, straight, and regular in section, with a wide range of coarse particle sizes from about 0.3 inches to 3 inches in diameter. The results
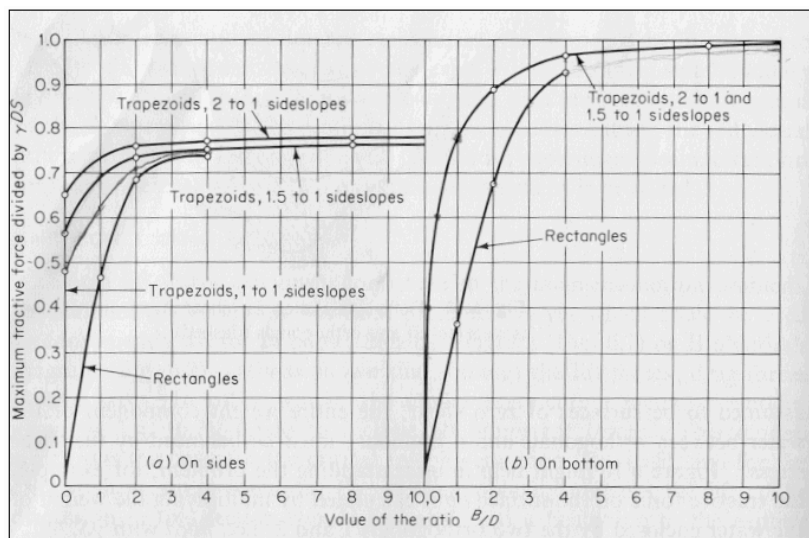
Figure 12-5 Maximum Shear Stress in a Channel (Lane, 1953)

indicated that the critical shear stress was more or less linearly related to the diameter of the particle as follows:

$$\tau_{cr} = 0.4d_{75}$$

(12-39)

The particle size, d75(inches) was used because Lane noticed that throughout the experiments, the smaller particles were consistently shielded by the larger ones. By using a particle size in

which only 25% of the particles were larger by weight, the initiation of motion was better represented.

The Shields method has historically been much more widely used to determine the initiation of motion. Shields (1936) developed a relationship between the shear Reynolds number, Re* and the critical mobility parameter, θcr from a wide range of experimental data. Shield's diagram is presented in Figure 12-6. The Shear Reynolds number is a representation of the ratio of inertial forces to viscous forces at the bed and is given as:

$$\mathbf{Re}_* = \frac{u_* d}{\nu} \tag{12-40}$$

Where: u_* = Shear velocity, which is a representation of the intensity of turbulent fluctuations in the boundary layer.

d = Representative particle size (d_{50} is used in HEC-RAS)

ν = Kinematic viscosity

$$u_* = \sqrt{gDS} \tag{12-41}$$

Where: D = Water depth

S = Channel slope

The critical mobility parameter is also known as the dimensionless shear stress and is given as:

$$\theta_{cr} = \frac{\tau_{cr}}{(\gamma_s - \gamma)d} \tag{12-42}$$

Where: γ_s = Unit weight of the particles

γ = Unit weight of water

From reviewing Shield's diagram, a number of things become clear. First, it is evident that the critical mobility parameter never drops below about 0.03. If the specific gravity of the sediments and the unit weight of water are assumed to be 2.65 and 62.4 lb/ft3, respectively, then the critical shear stress in lb/ft2 is never less than about 3 times the particle diameter (in feet). Also, if the shear Reynolds number exceeds about 450, the viscous forces in the sublayer no
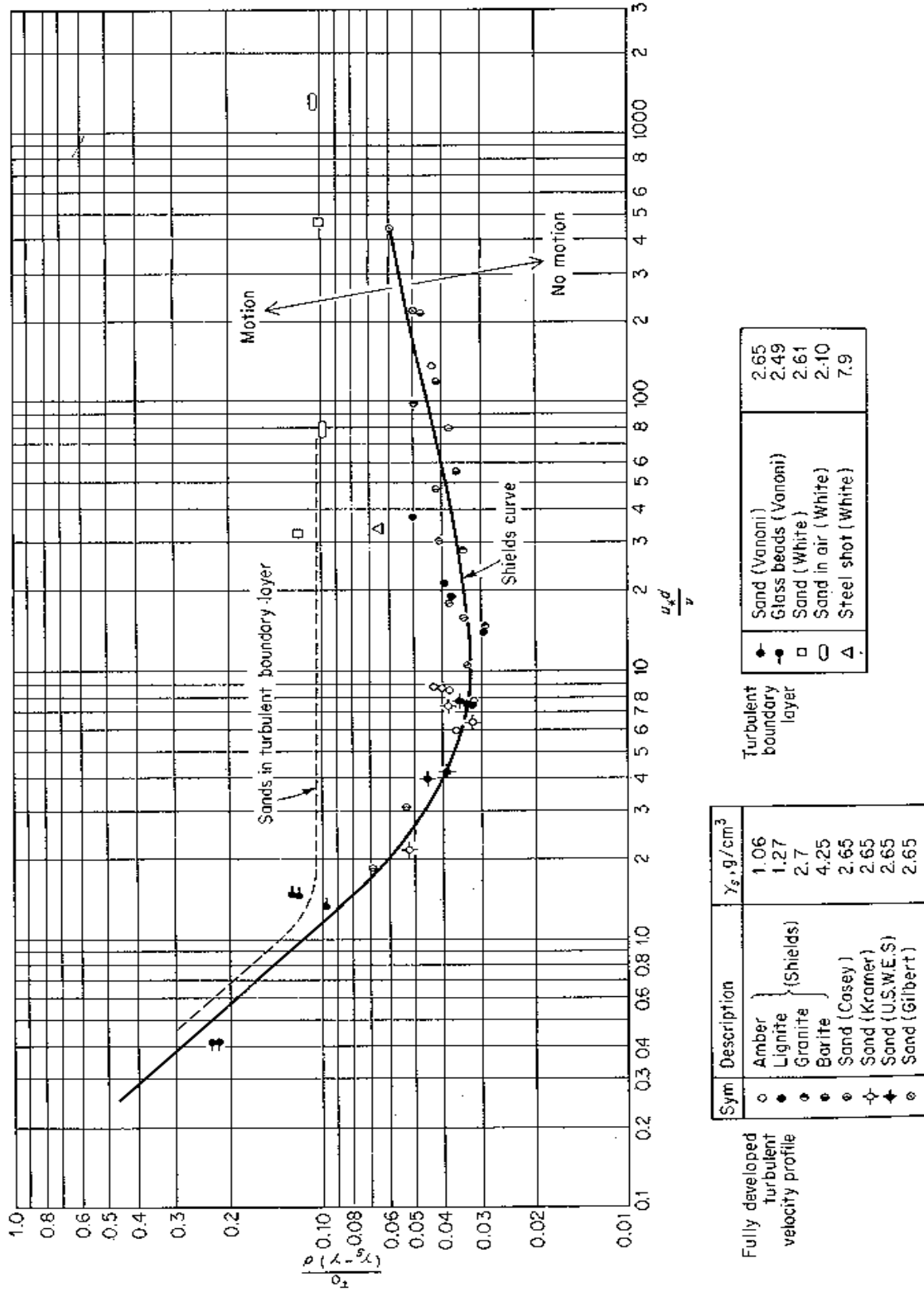
Figure 12-6 Shield's Diagram, Graf (1971)

longer have an effect on the shearing force and the Shield's curve levels off with a critical mobility parameter of about 0.055. At this point, the critical shear stress is purely a function of the particle characteristics (size, weight). Likewise, when the shear Reynolds number drops below about 2.0, the inertial forces in the sublayer are negligible and the critical shear stress becomes linearly related to the particle characteristics and the inverse of the viscosity. However, in most natural stream conditions, the shear Reynolds number is high and inertial forces are dominant. HEC-RAS, however, will solve for the critical mobility parameter throughout the full range of Shield's diagram.

A third solution option provided in HEC-RAS allows the user to enter in a value for the critical mobility parameter. This option is given due to the wide range of research on initiation of motion and the varying definitions of what exactly initiation of motion means. Although the Shield's curve is meant to represent the initiation of motion, more recent research indicates that this curve more accurately represents permanent grain movement at all locations of the bed. This can be quite different from the shearing required to initiate motion of one or a few particles. Figure 12-7 presents the Shield's curve overlain on seven qualitative curves developed by Delft Hydraulics (1972) describing particle movement. It is evident that the critical shear stress found with Shield's curve can be as much as twice the value required to cause occasional particle movement at some locations.

Because of the variety of opinions on this matter, the user is able to supply HEC-RAS with his/her own value for the critical mobility parameter. This value should be selected such that it represents not only the type of conditions present, but also the type of results desired (i.e. is the design based on permanent particle movement, infrequent particle movement, no particle movement, total suspension, etc?). Many curves present the critical shear stress as the dependent parameter in the initiation of motion curves. A collection of these types of curves is shown in Figure 12-8. **It is important for the user to know that the value entered into RAS must be in the form of the Critical Mobility Parameter, or dimensionless shear stress shown as equation 12-42.**

In HEC-RAS, a reduction factor is applied to the critical shear stress on the side slopes to account for the greater effect of gravity on the particle stability.

$$\tau_{cr,s} = k_\alpha \tau_{cr}$$

(12-43)

Where: $\tau_{cr,s}$ = Critical shear stress on the side slope

τ_{cr} = Critical shear stress on the bed

k_α = Reduction factor

* measured
1 occasional particle movement at some locations
2 frequent particle movement at some locations
3 frequent particle movement at many locations
4 frequent particle movement at nearly all locations
5 frequent particle movement at all locations
6 permanent particle movement at all locations
7 general transport (initiation of ripples)
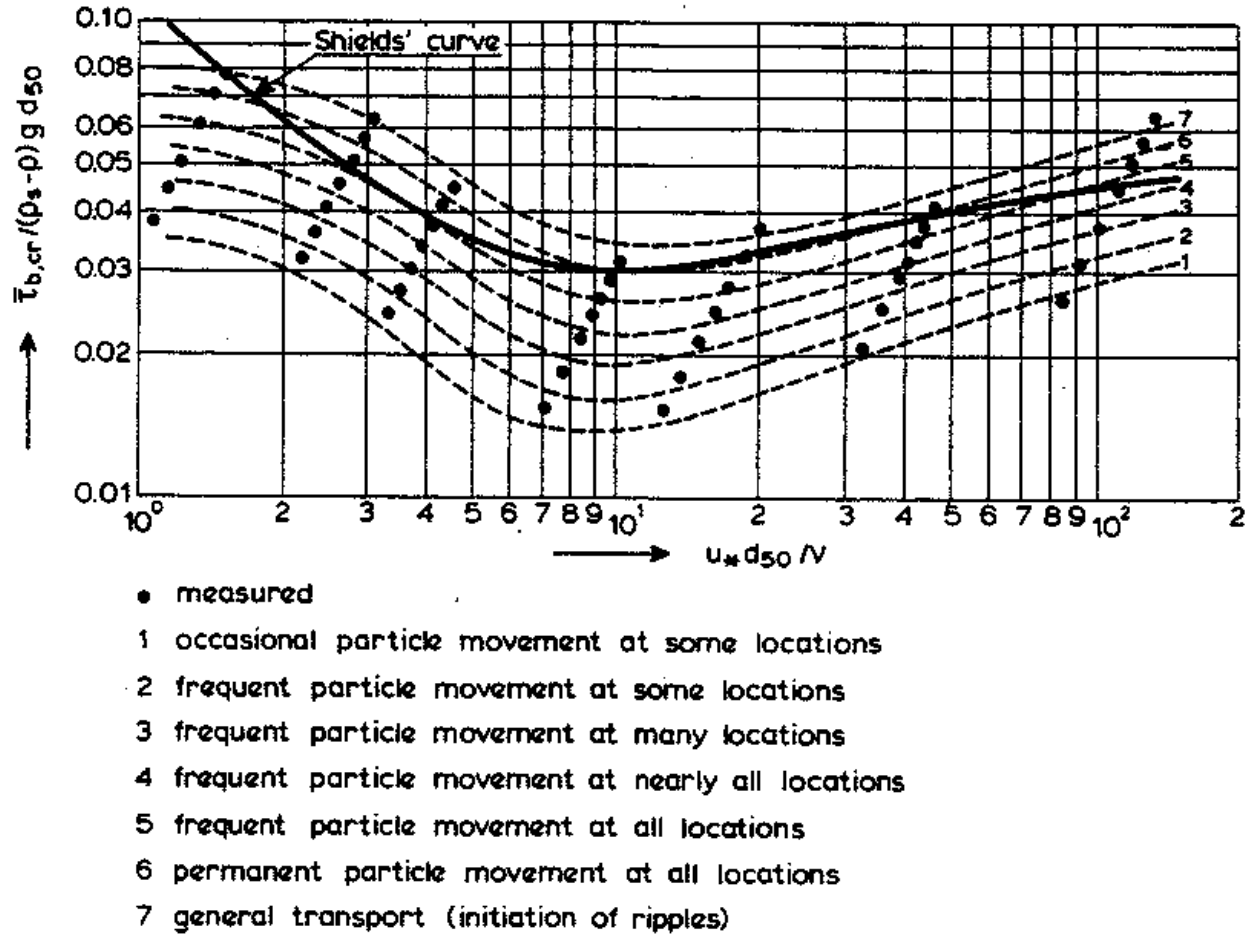
Figure 12-7 Initiation of Motion and Suspension for a Current Over a Plane Bed (Delft Hydraulics, 1972)

$$k_\alpha = \cos\alpha \sqrt{1 - \frac{\tan^2\alpha}{\tan^2\phi}} \qquad\qquad (12\text{-}44)$$

Where: α = Angle of the side slope, in degrees

   ϕ = Angle of repose of the sediment, in degrees

   and $\phi > \alpha$

The angle of repose of the sediment particles must be entered by the user for the bed and both of the side slopes. Lane provides a diagram that suggests values for angles of repose for different grain sizes and angularities (Figure 12-9).

HEC-RAS allows the user to solve for two dependant variables when two others are provided. The computations equate the critical shear stress with the actual shear stress to solve the first variable and then uses Manning's equation to solve the second variable. If the particle size is to be computed by HEC-RAS, one or all of the particle sizes (bed, left side slope, or right side slope) can be solved for, along with one other variable (depth, slope, or width). The equation RAS uses to determine the two unknown variables depends on the two unknown variables selected. Particle size is always determined using tractive force (i.e. equating critical shear with actual shear). The following table (Table 12-5) indicates which variable is solved by which method. This is helpful to know, in order to make sense of the results.
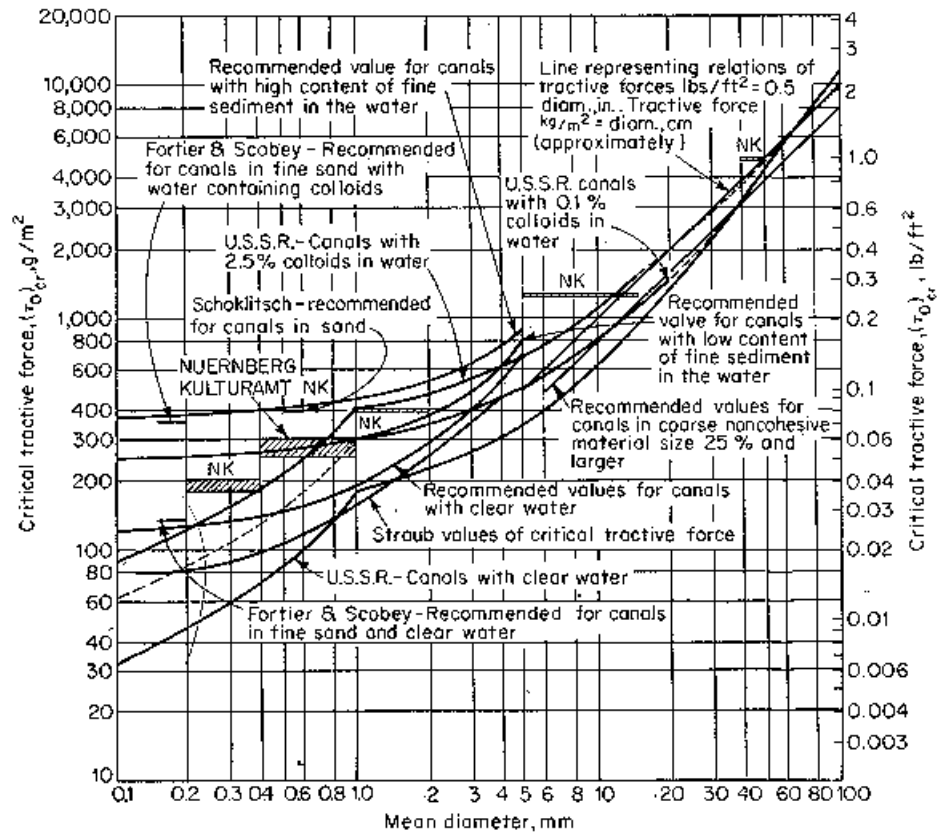
Figure 12-8 Critical shear stress as a function of grain diameter (Lane, 1953)

For example, assume depth and width are to be solved for. If a large diameter grain size is used, a high value for allowable depth will be returned by the tractive force equations. Then because this depth is high, Manning's equation will return a very low value for width, sometimes unrealistic. Be aware that the value for width is the value to achieve uniform flow based on the maximum allowable depth for a stable cross section. The variables "width" and "maximum depth" in the above statement can be replaced with any of the four dependant variables in accordance with the equation priorities as shown in Table 12-5.
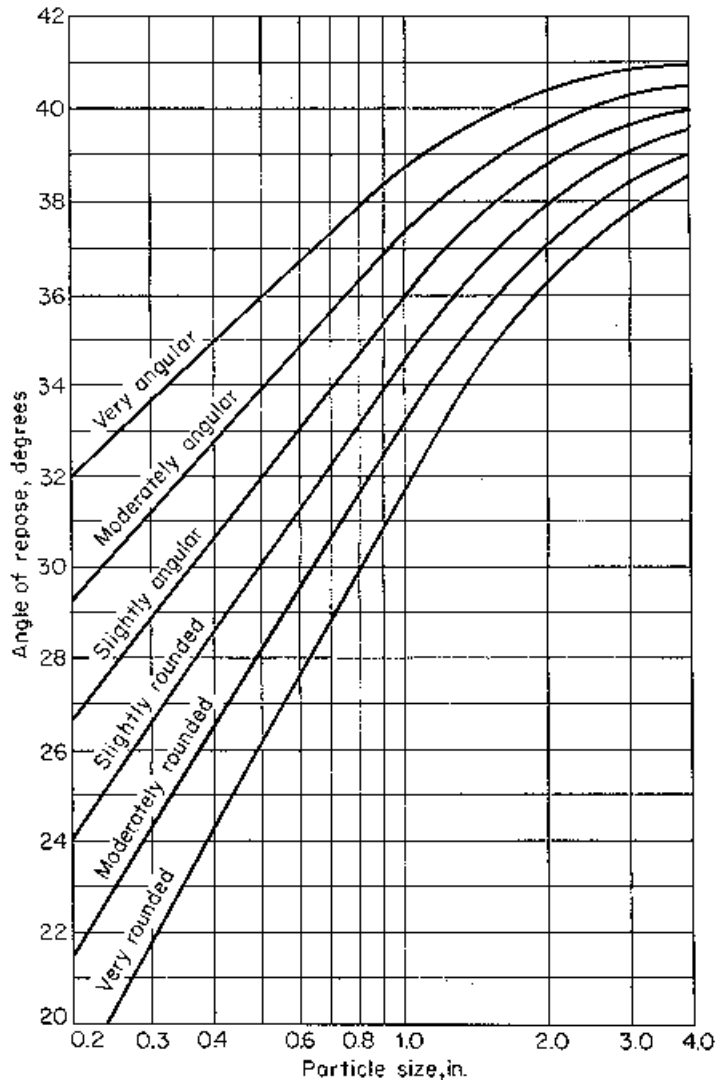
Figure 12-9 Angle of Repose for Non-Cohesive Material (Lane, 1953)

The result of this solution technique can create an apparent inconsistency that the user must be aware of. If width and slope are solved for, slope will be determined by tractive force and width will be determined by Mannings. Now if the resulting width is used to solve for slope and particle size, the particle size will be different from what was used in the first solution. This is because when particle size and slope are solved for, particle size is first solved for using tractive force, then slope is solved using Mannings.   Because true uniform flow conditions are rarely found on river reaches, be sure that the tractive force method is the equation solving the variable you are most interested in.

For more information on all three stable channel design methods presented herein, refer to the referenced literature.

Table 12-5 Solution Priorities for Tractive Force Method

Unknown Variables	Tractive Force	Mannings
d, D	Min d	D
d, B	Min d	B
d, S	Min d	S
D, B	Max D	B
D, S	Max D	S
B, S	Max S	B

Where: d   = particle size (d_{50} for Shields, d_{75} for Lane)

       D   = Depth

       B   = Width

       S   = Slope

Sediment Transport Capacity

The sediment transport capacity function in HEC-RAS has the capability of predicting transport capacity for non-cohesive sediment at one or more cross sections based on existing hydraulic parameters and known bed sediment properties. It does not take into account sediment inflow, erosion, or deposition in the computations. Classically, the sediment transport capacity is comprised of both bed load and suspended load, both of which can be accounted for in the various sediment transport predictors available in HEC-RAS. Results can be used to develop sediment discharge rating curves, which help to understand and predict the fluvial processes found in natural rivers and streams.

Background

Transported sediment is comprised of bed load, suspended load, and wash load. Van Rijn (1993) defines them as:

<u>Suspended load</u>: That part of the total sediment transport which is maintained in suspension by turbulence in the flowing water for considerable periods of time without contact with the streambed. It moves with practically the same velocity as that of the flowing water.

<u>Bed load</u>: The sediment in almost continuous contact with the bed, carried forward by rolling, sliding, or hopping.

<u>Wash load</u>: That part of the suspended load which is composed of particle sizes smaller than those found in appreciable quantities in the bed material. It is in near-permanent suspension and, therefore, is transported through the stream without deposition. The discharge of the wash load through a reach depends only on the rate with which these particles become available in the catchment area and not on the transport capacity of the flow.

Because wash load volume is purely a function of the upstream catchment and not the study reach, it is ignored in the sediment transport computations. However, a particle size considered wash load at one cross section in a reach, may become suspended load at a downstream section, and eventually may become bed load. Therefore, it is important to account for the wash load in a system-wide sediment analysis.

The initiation of motion of particles in the bed depends on the hydraulic characteristics in the near-bed region. Therefore, flow characteristics in that region are of primary importance. Since determining the actual velocity at the bed level is difficult, particularly with 1-D model results, shear stress has become the more prevalent, though not exclusive, way of determining the point of incipient motion. Shear stress at the bed is represented by the following:

$$\tau_b = \gamma RS \qquad\qquad (12\text{-}45)$$

Where: τ_b = Bed shear stress

      γ = Unit weight of water

       R   = Hydraulic radius

       S   = Energy slope

Another factor that plays an important role in the initiation and continued suspension of particles is the turbulent fluctuations at the bed level. A measure of the turbulent fluctuations near the bed can be represented by the current-related bed shear velocity:

$$u_* = \sqrt{\frac{\tau_b}{\rho}} \qquad \text{or} \qquad u_* = \sqrt{gRS} \qquad (12\text{-}46)$$

Where: u*   = Current-related bed shear velocity

Additionally, the size, shape, roughness characteristics, and fall velocity of the representative particles in the stream have a significant influence on their ability to be set into motion, to remain suspended, and to be transported. The particle size is frequently represented by the median particle diameter (dm). For convenience, the shape is typically represented as a perfect sphere, but sometimes can be accounted for by a shape factor, and the roughness is a function of the particle size.

In general, a typical sediment transport equation for multiple grain size classes can be represented as follows:

$$g_{si} = f\left(D, V, S, B, d, \rho, \rho_s, sf, d_i, p_i, T\right) \qquad (12\text{-}47)$$

Where: g_{si} = Sediment transport rate of size class i

      D   = Depth of flow

      V   = Average channel velocity

      S   = Energy slope

      B   = Effective channel width

      d   = Representative particle diameter

      ρ = Density of water

      ρ_s = Density of sediment particles

      sf   = Particle shape factor

      d_i = Geometric mean diameter of particles in size class i

      p_i = Fraction of particle size class i in the bed.

      T   = Temperature of water

Not all of the transport equations will use all of the above parameters. Typically one or more correction factors (not listed) are used to adapt the basic formulae to transport measurements. Refer to the respective references for more detail.

Fall Velocity

The suspension of a sediment particle is initiated once the bed-level shear velocity approaches the same magnitude as the fall velocity of that particle. The particle will remain in suspension as long as the vertical components of the bed-level turbulence exceed that of the fall velocity. Therefore, the determination of suspended sediment transport relies heavily on the particle fall velocity.

Within HEC-RAS, the method for computing fall velocity can be selected by the user. Three methods are available and they include Toffaleti (1968), Van Rijn (1993), and Rubey (1933). Additionally, the default can be chosen in which case the fall velocity used in the development of the respective sediment transport function will be used in RAS. Typically, the default fall velocity method should be used, to remain consistent with the development of the sediment transport function, however, if the user has specific information regarding the validity of one method over the other for a particular combination of sediment and hydraulic properties, computing with that method is valid. The shape factor (sf) is more important for medium sands and larger. Toffaleti used a sf of 0.9, while Van Rijn developed his equations for a sf of 0.7. Natural sand typically has a sf of about 0.7. The user is encouraged to research the specific fall velocity method prior to selection.

$$sf = \frac{c}{\sqrt{ab}} \qquad (12\text{-}48)$$

Where: a = Length of particle along the longest axis perpendicular to the other two axes.

b = Length of particle along the intermediate axis perpendicular to other two axes.

c = Length of particle along the short axis perpendicular to other two axes.

<u>Toffaleti</u>: (Toffaleti, 1968). Toffaleti presents a table of fall velocities with a shape factor of 0.9 and specific gravity of 2.65. Different fall velocities are given for a range of temperatures and grain sizes, broken up into American Geophysical Union standard grain size classes from Very Fine Sand (VFS) to Medium Gravel (MG). Toffaleti's fall velocities are presented in Table 12-6.

<u>Van Rijn</u>: (Van Rijn, 1993). Van Rijn approximated the US Inter-agency Committee on Water Resources' (IACWR) curves for fall velocity using non-spherical particles with a shape factor of 0.7 in water with a temperature of 20oC. Three equations are used, depending on the particle size:

$$\omega = \frac{(s-1)gd}{18\nu} \quad 0.001 < d \le 0.1 \text{ mm} \qquad (12\text{-}49)$$

$$\omega = \frac{10v}{d}\left[\left(1 + \frac{0.01(s-1)gd^3}{v^2}\right)^{0.5} - 1\right] \qquad\qquad 0.1 < d < 1 \text{ mm}$$

(12-50)

$$\omega = 1.1\left[(s-1)gd\right]^{0.5} \qquad\qquad d \geq 1 \text{ mm} \qquad\qquad (12\text{-}51)$$

Where: ω = Particle fall velocity

     v = Kinematic viscosity

     s = Specific gravity of particles

     d = Particle diameter

Table 12-6 Fall Velocity (Toffaleti, 1968)

Sand Grain Settling Velocity Versus Temperature, SP.G. 2.65, Shape Factor 0.9

TEMP °F	VFS	FS	MS	CS	VCS	VFG	FG	MG	TEMP °F	VFS	FS	MS	CS	VCS	VFG	FG	MG
35	.013	.045	.130	.305	.590	1.00	1.41	1.95	65	.021	.065	.165	.354	.640	1.00	1.41	1.95
36	.013	.045	.131	.307	.592	1.00	1.41	1.95	66	.021	.066	.166	.356	.641	1.00	1.41	1.95
37	.013	.046	.132	.310	.594	1.00	1.41	1.95	67	.021	.067	.167	.357	.643	1.00	1.41	1.95
38	.014	.047	.133	.312	.596	1.00	1.41	1.95	68	.022	.067	.168	.359	.644	1.00	1.41	1.95
39	.014	.047	.135	.314	.598	1.00	1.41	1.95	69	.022	.068	.170	.360	.646	1.00	1.41	1.95
40	.014	.048	.136	.316	.600	1.00	1.41	1.95	70	.022	.069	.171	.361	.647	1.00	1.41	1.95
41	.015	.049	.137	.318	.602	1.00	1.41	1.95	71	.022	.070	.172	.362	.649	1.00	1.41	1.95
42	.015	.050	.138	.320	.604	1.00	1.41	1.95	72	.023	.071	.173	.363	.650	1.00	1.41	1.95
43	.015	.051	.140	.321	.606	1.00	1.41	1.95	73	.023	.071	.175	.364	.652	1.00	1.41	1.95
44	.016	.051	.141	.322	.608	1.00	1.41	1.95	74	.023	.072	.176	.365	.653	1.00	1.41	1.95
45	.016	.052	.142	.323	.609	1.00	1.41	1.95	75	.024	.072	.177	.365	.655	1.00	1.41	1.95
46	.016	.053	.143	.325	.610	1.00	1.41	1.95	76	.024	.073	.178	.367	.656	1.00	1.41	1.95
47	.016	.053	.144	.326	.612	1.00	1.41	1.95	77	.024	.073	.180	.368	.657	1.00	1.41	1.95
48	.017	.054	.145	.328	.614	1.00	1.41	1.95	78	.024	.074	.181	.370	.658	1.00	1.41	1.95
49	.017	.055	.146	.330	.616	1.00	1.41	1.95	79	.025	.074	.182	.371	.659	1.00	1.41	1.95
50	.017	.055	.147	.331	.618	1.00	1.41	1.95	80	.025	.075	.183	.373	.660	1.00	1.41	1.95
51	.018	.056	.148	.333	.620	1.00	1.41	1.95	81	.025	.075	.184	.375	.661	1.00	1.41	1.95
52	.018	.057	.150	.334	.621	1.00	1.41	1.95	82	.025	.076	.185	.376	.662	1.00	1.41	1.95
53	.018	.057	.151	.336	.623	1.00	1.41	1.95	83	.025	.077	.186	.378	.663	1.00	1.41	1.95
54	.018	.058	.152	.338	.624	1.00	1.41	1.95	84	.026	.077	.187	.380	.664	1.00	1.41	1.95
55	.018	.059	.153	.340	.626	1.00	1.41	1.95	85	.026	.078	.188	.381	.665	1.00	1.41	1.95
56	.019	.059	.154	.341	.627	1.00	1.41	1.95	86	.026	.078	.190	.383	.666	1.00	1.41	1.95
57	.019	.060	.155	.343	.629	1.00	1.41	1.95	87	.026	.079	.192	.385	.667	1.00	1.41	1.95
58	.019	.061	.156	.344	.630	1.00	1.41	1.95	88	.027	.079	.194	.386	.668	1.00	1.41	1.95
59	.019	.061	.157	.346	.632	1.00	1.41	1.95	89	.027	.080	.195	.388	.669	1.00	1.41	1.95
60	.020	.062	.158	.347	.633	1.00	1.41	1.95	90	.027	.080	.196	.390	.670	1.00	1.41	1.95
61	.020	.063	.160	.349	.635	1.00	1.41	1.95	91	.028	.081	.197	.391	.671	1.00	1.41	1.95
62	.020	.063	.161	.350	.636	1.00	1.41	1.95	92	.028	.081	.198	.392	.672	1.00	1.41	1.95
63	.020	.064	.162	.351	.638	1.00	1.41	1.95	93	.028	.082	.199	.393	.673	1.00	1.41	1.95
64	.021	.065	.163	.353	.639	1.00	1.41	1.95	94	.028	.082	.200	.394	.674	1.00	1.41	1.95

Rubey: (Rubey, 1933). Rubey developed an analytical relationship between the fluid, sediment properties, and the fall velocity based on the combination of Stoke's law (for fine particles subject only to viscous resistance) and an impact formula (for large particles outside the Stoke's region). This equation has been shown to be adequate for silt, sand, and gravel grains. Rubey suggested that particles of the shape of crushed quartz grains, with a specific gravity of around 2.65, are best applicable to the equation. Some of the more cubic, or uniformly shaped particles tested, tended to fall faster than the equation predicted. Tests were conducted in water with a temperature of 16o Celsius.

$$\omega = F_1\sqrt{(s-1)gd_s} \tag{12-52}$$

in which $F_1 = \sqrt{\dfrac{2}{3} + \dfrac{36v^2}{gd^3(s-1)}} - \sqrt{\dfrac{36v^2}{gd^3(s-1)}}$ (12-53)

Correction for Fine Sediment

The viscosity of a fluid has a significant affect on the fall velocity of a particle within that fluid. In clear water, the kinematic viscosity is on the order of 1 X 10-5 ft2/s, however, when a high concentration of fine sediment, particularly clay particles, is present, the viscosity will increase, in much the same way as when the water temperature is reduced. Colby (1964) proposed an adjustment factor to account for high concentration of fines, as well as temperature, which is shown in Figure 12-10.

HEC-RAS provides and field for the user to enter the concentration of fine sediments. This is an optional field, and, if left blank, bypasses the Colby adjustment factor calculations. Concentration magnitudes are entered in parts per million (ppm).

Sediment Gradation

Sediment transport rates are computed for the prescribed hydraulic and sediment parameters for each representative grain size. Transport capacity is determined for each grain size as if that particular grain size made up 100% of the bed material. The transport capacity for that size group is then multiplied by the fraction of the total sediment that that size represents. The fractional transport capacities for all sizes are summed for the total sediment transport capacity.

$$g_s = \sum_{i=1}^{n} g_{si} p_i \qquad (12\text{-}54)$$

Where: g_s = Total sediment transport

      g_{si} = Sediment transport for size class i

      p_i = Fraction of size class i in the sediment

      n = Number of size classes represented in the gradation
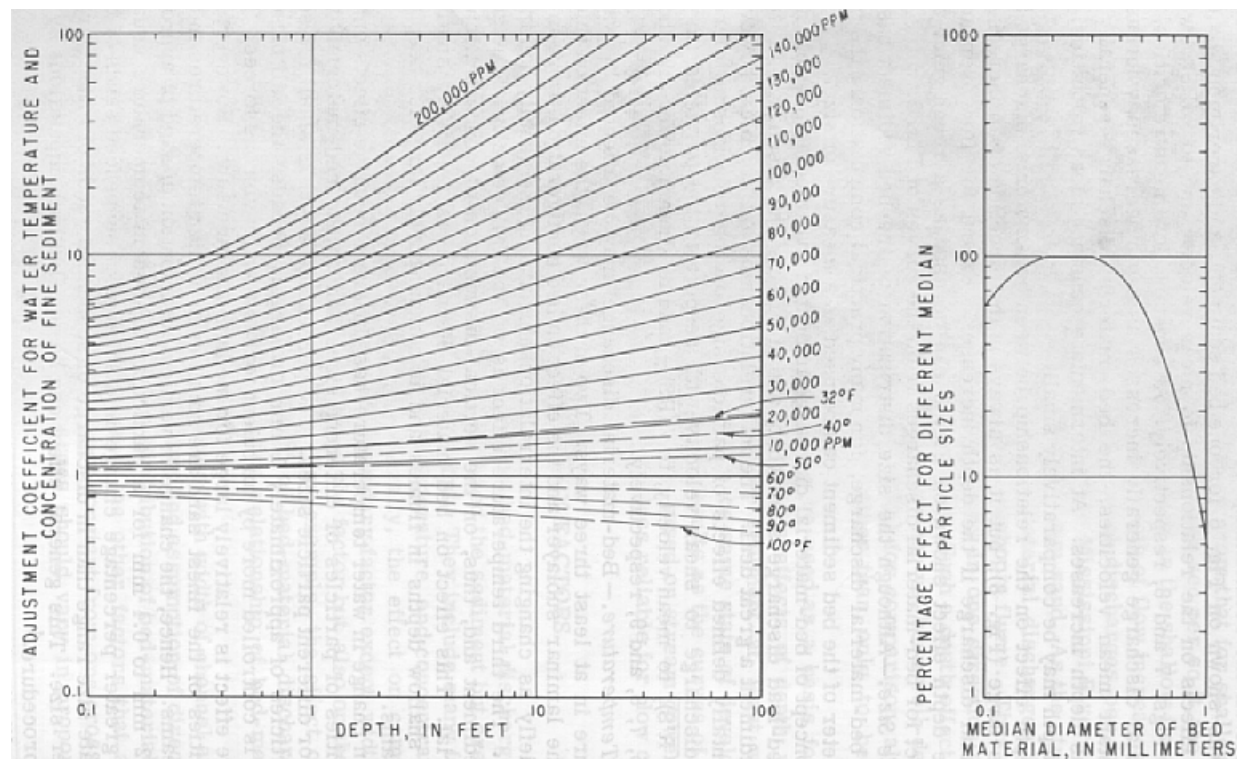
Figure 12-10 Adjustment Factor for Concentration of Fine Sediment (Colby, 1964)

The user enters gradation information as particle sizes with an associated percentage value that indicates the amount of material within the sediment mixture that is finer by volume (percent finer). HEC-RAS then interpolates logarithmically to determine a representative percent finer for the standard grade class sizes. The standard grade class sizes are based on the American Geophysical Union (AGU) classification scale shown in Table 12-6.

If a maximum particle diameter is not entered (i.e. d100), HEC-RAS will automatically assign the 100% finer value to the next greater standard grain size from the largest particle diameter established by the user. For example, if the largest particle diameter is entered as 1.6 mm with a percent finer value of 84%, then the maximum grain size will be automatically assigned to 2.0 mm with 100% of the particles finer than that. On the low end, if the user does not establish a zero percent finer particle diameter (i.e. d0), then the smallest standard grain size range (0.002 – 0.004 mm) is assigned zero percent. Because the ultra-fine sized sediment has a tendency to produce inaccurate results for certain transport functions, it is important that the user realize the extrapolation used in this instance. To avoid the automatic extrapolation on the fine-side of the gradation curve, simply enter in a particle diameter with an associated "percent finer" value of zero.

Table 12-7 Grain Size Classification of Sediment Material American Geophysical Union

Sediment Material	Grain Diameter Range(mm)	Geometric Median Diameter (mm)
Clay	0.002-0.004	0.003
Very Fine Silt	0.004-0.008	0.006
Fine Silt	0.008-0.016	0.011
Medium Silt	0.016-0.032	0.023
Coarse Silt	0.032-0.0625	0.045
Very Fine Sand	0.0625-0.125	0.088
Fine Sand	0.125-0.250	0.177
Medium Sand	0.250-0.5	0.354
Coarse Sand	0.5-1.0	0.707
Very Coarse Sand	1-2	1.41
Very Fine Gravel	2-4	2.83
Fine Gravel	4-8	5.66
Medium Gravel	8-16	11.3
Coarse Gravel	16-32	22.6
Very Coarse Gravel	32-64	45.3
Small Cobbles	64-128	90.5
Large Cobbles	128-256	181
Small Boulders	256-512	362
Medium Boulders	512-1024	724
Large Boulders	1024-2048	1448

If the user enters in one or more particle sizes that are less than the smallest standard grain size diameter (0.002 mm), HEC-RAS will automatically lump all of that sediment into the smallest standard grain size range (Clay, 0.002 to 0.004 mm). This is done so that all of the sediment in the gradation curve will be accounted for volumetrically.

The rate of transport is extremely sensitive to the grain size distribution, particularly on the finer side, and should be chosen carefully. The application of grain size particles smaller than the designated range of applicability for a given function can lead to extremely high, and unreasonable sediment transport rates. For this reason, RAS provides an option to not compute sediment transport rates for grain sizes outside the range of applicability on the low end. This is done by going to the options menu and selecting "No" under the menu item "Compute for Small Grains Outside Applicable Range". Still, the user should check unreasonable results for all given parameter ranges (Table 12-7). (Note: the low end of applicable grain size for Laursen was chosen as that used in the field research.) The selection of a representative sediment sampling is described in EM 1110-2-4000.

Hydraulic Parameters

The hydraulic parameters used to compute sediment transport capacity are taken from the output of steady or unsteady flow runs. The user is required only to indicate for which profile the sediment transport computations will be made for each sediment reach. HEC-RAS automatically retrieves the required hydraulic input parameters, depending on which sediment

transport function has been selected. Therefore, steady, or unsteady flow computations must be run before sediment capacity computations can be performed.   The hydraulic parameters are retrieved from the steady output computations for the left overbank, main channel, and right overbank, as defined by the sediment bank stations. The total sediment transport for the cross section is then the sum of the three sub-sections.

Because different sediment transport functions were developed differently with a wide range of independent variables, HEC-RAS gives the user the option to select how depth and width are to be computed. The HEC-6 method converts everything to an effective depth and width by the following equations:

$$EFD = \frac{\sum_{i=1}^{n} D_{avg} a_i D_{avg}^{\frac{2}{3}}}{\sum_{i=1}^{n} a_i D_{avg}^{\frac{2}{3}}} \qquad\qquad EFW = \frac{\sum_{i=1}^{n} a_i D_{avg}^{\frac{2}{3}}}{EFD^{\frac{5}{3}}} \qquad (12\text{-}55/6)$$

Where: *EFD*   = Effective depth

   EFW   = Effective width

   a_i = Area of subsection i

   D_{avg} = Average depth of sub section i

   n   = Number of subsections

However, many of the sediment transport functions were developed using hydraulic radius and top width, or an average depth and top width. For this reason, HEC-RAS allows the user to designate which depth/width method to use. If the default selection is chosen, then the method consistent with the development of the chosen function will be used. For irregular cross section shapes, RAS uses the effective depth/effective width or hydraulic radius/top width as the default. Also available for use is the hydraulic depth, which is used to represent the average depth and is simply the total area of the section divided by the top width. RAS computes these depth/width parameters for the left overbank, main channel, and right overbank, as designated by the bed load stations.

Bed Load Stations

By default, the channel bank stations are used to separate the left overbank, main channel, and right overbank for sediment transport computations. However, this may not necessarily represent the sediment distribution across the cross section. Therefore, HEC-RAS allows the

user to designate bed load stations to separate the three channels based on sediment properties.

Output

HEC-RAS provides the option of viewing results in sediment rating curves and profile plots. The rating curve plot presents the sediment transport capacity vs. the river discharge and can be plotted for one or more cross sections. The profile plot presents the sediment transport capacity along the stream length for one or more sediment reaches.

Both types of plots allow have a number of dropdown boxes that allow the user to specify what is required for plotting. For example, by default, the total sediment transport rate is given for each cross section when a plot is opened. However, the user can view just the sediment transport of a single grain size or can compare sediment transport capacities of two or more grain sizes. Additionally, the user has the ability to view the overbanks and main channel separately as well as each transport function.

Sediment Transport Functions

Because different sediment transport functions were developed under different conditions, a wide range of results can be expected from one function to the other. Therefore it is important to verify the accuracy of sediment prediction to an appreciable amount of measured data from either the study stream or a stream with similar characteristics. It is very important to understand the processes used in the development of the functions in order to be confident of its applicability to a given stream.

Typically, sediment transport functions predict rates of sediment transport from a given set of steady-state hydraulic parameters and sediment properties. Some functions compute bed-load transport, and some compute bed-material load, which is the total load minus the wash load (total transport of particles found in the bed). In sand-bed streams with high transport rates, it is common for the suspended load to be orders of magnitude higher than that found in gravel-bed or cobbled streams. It is therefore important to use a transport predictor that includes suspended sediment for such a case.

The following sediment transport functions are available in HEC-RAS:

- Ackers-White

- Engelund-Hansen

- Laursen

- Meyer-Peter Müller

- Toffaleti

- Yang

These functions were selected based on their validity and collective range of applicability. All of these functions, except for Meyer-Peter Müller, are compared extensively by Yang and Schenggan (1991) over a wide range of sediment and hydraulic conditions. Results varied, depending on the conditions applied. The Meyer-Peter Müller and the bed-load portion of the Toffaleti function were compared with each other by Amin and Murphy (1981). They concluded that Toffaleti bed-load procedure was sufficiently accurate for their test stream, whereby, Meyer-Peter Müller was not useful for sand-bed channels at or near incipient motion.   The ranges of input parameters used in the development of each function are shown in Table 12-7. Where available, these ranges are taken from those presented in the SAM package user's manual (Waterways Experiment Station, 1998) and are based on the developer's stated ranges when presented in their original papers. The ranges provided for Engelund and Hansen are taken from the database (Guy, et al, 1966) primarily used in that function's development.   The parameter ranges presented are not limiting, in that frequently a sediment transport function will perform well outside the listed range. For example, Engelund-Hansen was developed with flume research only, and has been historically applied successfully outside its development range. The parameter ranges are presented as a guideline only.

A short description of the development and applicability of each function follows.   It is strongly recommended that a review of the respective author's initial presentation of their function be undertaken prior to its use, as well as a review of "comparison" papers such as those referenced in the preceding paragraph. References are included in Appendix A. Sample solutions for the following sediment transport methods are presented in Appendix E.

Table 12-8 Range of input values for sediment transport functions (Sam User's Manual, 1998)

Function	d	d_m	s	V	D	S	W	T
Ackers-White (*flume*)	0.04 - 7.0	NA	1.0 - 2.7	0.07 - 7.1	0.01 - 1.4	0.00006 - 0.037	0.23 - 4.0	46 - 89
Englund-Hansen (*flume*)	NA	0.19 - 0.93	NA	0.65 – 6.34	0.19 – 1.33	0.000055 – 0.019	NA	45 - 93
Laursen (*field*)	NA	0.08– 0.7	NA	0.068 – 7.8	0.67 – 54	0.0000021 – 0.0018	63 – 3640	32 - 93
Laursen (*flume*)	NA	0.011 - 29	NA	0.7 - 9.4	0.03 – 3.6	0.00025 – 0.025	0.25 – 6.6	46 - 83
Meyer-Peter Muller (*flume*)	0.4 – 29	NA	1.25 – 4.0	1.2 – 9.4	0.03 – 3.9	0.0004 – 0.02	0.5 – 6.6	NA
Tofaletti (*field*)	0.062 – 4.0	0.095 – 0.76	NA	0.7 - 7.8	0.07 – 56.7 (R)	0.000002 – 0.0011	63 - 3640	32 – 93
Tofaletti (*flume*)	0.062 – 4.0	0.45 – 0.91	NA	0.7 - 6.3	0.07 – 1.1 (R)	0.00014 – 0.019	0.8 – 8	40 - 93
Yang (*field-sand*)	0.15 – 1.7	NA	NA	0.8 - 6.4	0.04 – 50	0.000043 – 0.028	0.44 – 1750	32 - 94
Yang (*field-gravel*)	2.5 – 7.0	NA	NA	1.4 - 5.1	0.08 – 0.72	0.0012 – 0.029	0.44 – 1750	32 - 94

Where: d   = Overall particle diameter, mm

   d_m = Median particle diameter, mm

   s   = Sediment specific gravity

   V   = Average channel velocity, fps

   D   = Channel depth, ft

   S   = Energy gradient

   W   = Channel width, ft

   T   = Water temperature, ^{o}F

   (R)   = Hydraulic Radius, ft

   NA   = Data not available

Ackers-White: The Ackers-White transport function is a total load function developed under the assumption that fine sediment transport is best related to the turbulent fluctuations in the water column and coarse sediment transport is best related to the net grain shear with the mean velocity used as the representative variable. The transport function was developed in terms of particle size, mobility, and transport.

A dimensionless size parameter is used to distinguish between the fine, transitionary, and coarse sediment sizes. Under typical conditions, fine sediments are silts less than 0.04 mm, and coarse sediments are sands greater than 2.5 mm. Since the relationships developed by Ackers-White are applicable only to non-cohesive sands greater than 0.04 mm, only transitionary and coarse sediments apply.   Original experiments were conducted with coarse grains up to 4 mm, however the applicability range was extended to 7 mm.

This function is based on over 1000 flume experiments using uniform or near-uniform sediments with flume depths up to 0.4 m. A range of bed configurations was used, including plane, rippled, and dune forms, however the equations do not apply to upper phase transport (e.g. anti-dunes) with Froude numbers in excess of 0.8.

The general transport equation for the Ackers-White function for a single grain size is represented by:

$$X = \frac{G_{gr} s d_s}{D\left(\dfrac{u_*}{V}\right)^n} \qquad \text{and} \qquad G_{gr} = C\left(\frac{F_{gr}}{A} - 1\right) \qquad (12\text{-}57/8)$$

Where: *X*   = Sediment concentration, in parts per part

G_{gr}	= Sediment transport parameter	
s	= Specific gravity of sediments	
d_s	= Mean particle diameter	
D	= Effective depth	
u_*	= Shear velocity	
V	= Average channel velocity	
n	= Transition exponent, depending on sediment size	
C	= Coefficient	
F_{gr}	= Sediment mobility parameter	
A	= Critical sediment mobility parameter	

A hiding adjustment factor was developed for the Ackers-White method by Profitt and Sutherland (1983), and is included in RAS as an option. The hiding factor is an adjustment to include the effects of a masking of the fluid properties felt by smaller particles due to shielding by larger particles. This is typically a factor when the gradation has a relatively large range of particle sizes and would tend to reduce the rate of sediment transport in the smaller grade classes.

Engelund-Hansen: The Engelund-Hansen function is a total load predictor which gives adequate results for sandy rivers with substantial suspended load. It is based on flume data with sediment sizes between 0.19 and 0.93 mm. It has been extensively tested, and found to be fairly consistent with field data.

The general transport equation for the Engelund-Hansen function is represented by:

$$g_s = 0.05\gamma_s V^2 \sqrt{\frac{d_{50}}{g\left(\frac{\gamma_s}{\gamma}-1\right)}}\left[\frac{\tau_o}{(\gamma_s - \gamma)d_{50}}\right]^{3/2} \qquad (12\text{-}59)$$

Where: g_s = Unit sediment transport

γ = Unit wt of water

γ_s = Unit wt of solid particles

V = Average channel velocity

τ_o = Bed level shear stress

d_{50} = Particle size of which 50% is smaller

Laursen: The Laursen method is a total sediment load predictor, derived from a combination of qualitative analysis, original experiments, and supplementary data. Transport of sediments is primarily defined based on the hydraulic characteristics of mean channel velocity, depth of flow, energy gradient, and on the sediment characteristics of gradation and fall velocity. Contributions by Copeland (Copeland, 1989) extend the range of applicability to gravel-sized sediments. The range of applicability is 0.011 to 29 mm, median particle diameter.

The general transport equation for the Laursen (Copeland) function for a single grain size is represented by:

$$C_m = 0.01\gamma\left(\frac{d_s}{D}\right)^{7/6}\left(\frac{\tau_o^{'}}{\tau_c}-1\right)f\left(\frac{u_*}{\omega}\right)$$

(12-60)

Where: C_m = Sediment discharge concentration, in weight/volume

G = Unit weight of water

d_s = Mean particle diameter

D = Effective depth of flow

$\tau_o^{'}$ = Bed shear stress due to grain resistance

τ_c = Critical bed shear stress

$f\left(\frac{u_*}{\omega}\right)$ =   Function of the ratio of shear velocity to fall velocity as defined in

Laursen's Figure 14 (Laursen, 1958).

Meyer-Peter Müller: The Meyer-Peter Müller bed load transport function is based primarily on experimental data and has been extensively tested and used for rivers with relatively coarse sediment. The transport rate is proportional to the difference between the mean shear stress acting on the grain and the critical shear stress.

Applicable particle sizes range from 0.4 to 29 mm with a sediment specific gravity range of 1.25 to in excess of 4.0.   This method can be used for well-graded sediments and flow conditions that produce other-than-plane bed forms. The Darcy-Weisbach friction factor is used to define bed resistance. Results may be questionable near the threshold of incipient motion for sand bed channels as demonstrated by Amin and Murphy (1981).

The general transport equation for the Meyer-Peter Müller function is represented by:

$$\left(\frac{k_r}{k_r^{'}}\right)^{3/2} \gamma RS = 0.047(\gamma_s - \gamma)d_m + 0.25\left(\frac{\gamma}{g}\right)^{1/3}\left(\frac{\gamma_s - \gamma}{\gamma_s}\right)^{2/3} g_s^{2/3} \qquad (12\text{-}61)$$

Where: g_s = Unit sediment transport rate in weight/time/unit width

       k_r = A roughness coefficient

       $k_r^{'}$ = A roughness coefficient based on grains

       γ = Unit weight of water

       γ_s = Unit weight of the sediment

       g = Acceleration of gravity

       d_m = Median particle diameter

       R = Hydraulic radius

       S = Energy gradient

Toffaleti: The Toffaleti method is a modified-Einstein total load function that breaks the suspended load distribution into vertical zones, replicating two-dimensional sediment movement. Four zones are used to define the sediment distribution. They are the upper zone, the middle zone, the lower zone and the bed zone. Sediment transport is calculated independently for each zone and the summed to arrive at total sediment transport.

This method was developed using an exhaustive collection of both flume and field data. The flume experiments used sediment particles with mean diameters ranging from 0.3 to 0.93 mm, however successful applications of the Toffaleti method suggests that mean particle diameters as low as 0.095 mm are acceptable.

The general transport equations for the Toffaleti function for a single grain size is represented by:

$$g_{ssL} = M \frac{\left(\dfrac{R}{11.24}\right)^{1+n_v-0.756z} - (2d_m)^{1+n_v-0.756z}}{1 + n_v - 0.756z} \quad \text{(lower zone)} \qquad (12\text{-}62)$$

$$g_{ssM} = M \frac{\left(\dfrac{R}{11.24}\right)^{0.244z} \left[\left(\dfrac{R}{2.5}\right)^{1+n_v-z} - \left(\dfrac{R}{11.24}\right)^{1+n_v-z}\right]}{1+n_v-z} \quad \text{(middle zone)} \tag{12-63}$$

$$g_{ssU} = M \frac{\left(\dfrac{R}{11.24}\right)^{0.244z} \left(\dfrac{R}{2.5}\right)^{0.5z} \left[R^{1+n_v-1.5z} - \left(\dfrac{R}{2.5}\right)^{1+n_v-1.5z}\right]}{1+n_v-1.5z} \quad \text{(upper zone)} \tag{12-64}$$

$$g_{sb} = M(2d_m)^{1+n_v-0.756z} \quad \text{(bed zone)} \tag{12-65}$$

$$M = 43.2C_L(1+n_v)VR^{0.756z-n_v}$$
(12-66)

$$g_s = g_{ssL} + g_{ssM} + g_{ssU} + g_{sb} \tag{12-67}$$

Where: g_{ssL} =   Suspended sediment transport in the lower zone, in tons/day/ft

g_{ssM} =   Suspended sediment transport in the middle zone, in tons/day/ft

g_{ssU} =   Suspended sediment transport in the upper zone, in tons/day/ft

g_{sb} =   Bed load sediment transport in tons/day/ft

g_s =   Total sediment transport in tons/day/ft

M =   Sediment concentration parameter

C_L =   Sediment concentration in the lower zone

R =   Hydraulic radius

d_m =   Median particle diameter

z =   Exponent describing the relationship between the sediment and hydraulic characteristics

n_v =   Temperature exponent

Yang: Yang's method (1973) is developed under the premise that unit stream power is the dominant factor in the determination of total sediment concentration. The research is supported by data obtained in both flume experiments and field data under a wide range conditions found in alluvial channels. Principally, the sediment size range is between 0.062 and 7.0 mm with total sediment concentration ranging from 10 ppm to 585,000 ppm. Channel widths range from 0.44 to1746 ft, depths from 0.037 to 49.4 ft, water temperature from 0o to 34.3o Celsius, average channel velocity from 0.75 to 6.45 fps, and slopes from 0.000043 to 0.029.

Yang (1984) expanded the applicability of his function to include gravel-sized sediments. The general transport equations for sand and gravel using the Yang function for a single grain size is represented by:

$$
\log C_t = 5.435 - 0.286 \log \frac{\omega d_m}{v} - 0.457 \log \frac{u_*}{\omega} +
$$

$$
\left(1.799 - 0.409 \log \frac{\omega d_m}{v} - 0.314 \log \frac{u_*}{\omega} \right) \log \left(\frac{VS}{\omega} - \frac{V_{cr}S}{\omega} \right)
$$

for sand $d_m < 2mm$ (12-68)

$$
\log C_t = 6.681 - 0.633 \log \frac{\omega d_m}{v} - 4.816 \log \frac{u_*}{\omega} +
$$

$$
\left(2.784 - 0.305 \log \frac{\omega d_m}{v} - 0.282 \log \frac{u_*}{\omega} \right) \log \left(\frac{VS}{\omega} - \frac{V_{cr}S}{\omega} \right)
$$

for gravel $d_m \geq 2mm$ (12-69)

Where: C_t = Total sediment concentration

       ω = Particle fall velocity

       d_m = Median particle diameter

       v = Kinematic viscosity

       u^* = Shear velocity

       V = Average channel velocity

       S   = Energy gradient

CHAPTER 13

Sediment Modeling

Sediment transport modeling is notoriously difficult. Sediment data are uncertain and transport theory is empirical and highly sensitive to a broad array of physical variables and model parameters which are difficult to measure and estimate. However, with good data, a skilled modeler can use a calibrated sediment model to predict regional, long term trends that can inform planning decisions and evaluate project alternatives. HEC-RAS includes mobile boundary, sediment transport modeling capabilities which route sediment and adjust channel cross sections in response to sediment dynamics. This chapter describes the theory and assumptions used for this analysis.

Sediment Hydrodynamics

Sediment transport models require hydraulic parameters. Therefore, HEC-RAS computes hydraulics each time step before it routs sediment or updates cross sections. HEC-RAS 5.0 couples sediment transport computations with either quasi-unsteady hydraulics or unsteady hydraulics. The User's Manual offers pros and cons of both approaches. Unsteady flow is not unique to sediment studies. HEC-RAS can simulate unsteady flow without sediment data and Chapter 2 documents the unsteady equations in detail.

Quasi-unsteady hydraulics, on the other hand, are only used for sediment studies. Therefore, the quasi-unsteady approach is described below.

Quasi-Unsteady Flow

The quasi-unsteady flow model simplifies hydrodynamics, representing a continuous hydrograph with a series of discrete steady flow profiles. HEC-RAS keeps flow constant for each flow record, computing transport over flow record duration. The steady flow profiles are more stable than the matrix solution of the unsteady Saint-Venant equations, but approximating a hydrograph with a series of steady flows does not conserve flow or explicitly account for volume.

The quasi-unsteady flow model has divides time into three time step. HEC-RAS divides each discrete steady flow profile (**Flow Duration**), over which HEC-RAS holds flow constant, into **Computational Increments**, which are the hydraulic and sediment transport time step. HEC-RAS updates the hydraulics and cross sections every **Computational Increment**, but further subdivides this time step into **Bed Mixing Time Steps**, updated bed gradation accounting for each bed layer several times each **Computational Increment**.

Duration

The Duration is the coarsest time step. HEC-RAS assumes that flow, stage, temperature, or sediment are constant over the Duration (Figure 13 1). For example, enter daily flow data (e.g. from a USGS day) with twenty-four hour Flow Durations.

Computational Increment

The **Computational Increment** is the primary quasi-unsteady hydraulic and sediment time step. The **Computation Increment** usually subdivides the **Duration** (Figure 13-1), though it can be equal (but not larger) to the duration. While flow remains constant over the entire flow duration, HEC-RAS updates the bed geometry and hydrodynamics after each computational increment. If cross sections change, particularly if they change rapidly, sediment sensitive hydraulic parameters can change even if the flow does not.

Model stability can be sensitive to the **Computation Increment**, because HEC-RAS assumes that hydraulics and bed geometry are constant. If the bed changes rapidly, large computation increments decouple the feedbacks between sediment and hydraulic processes, leading to unreasonable deposition or erosion, which can cause the model to crash. If HEC-RAS computes erratic bed change, experiment with **Computation Increment** sensitivity.

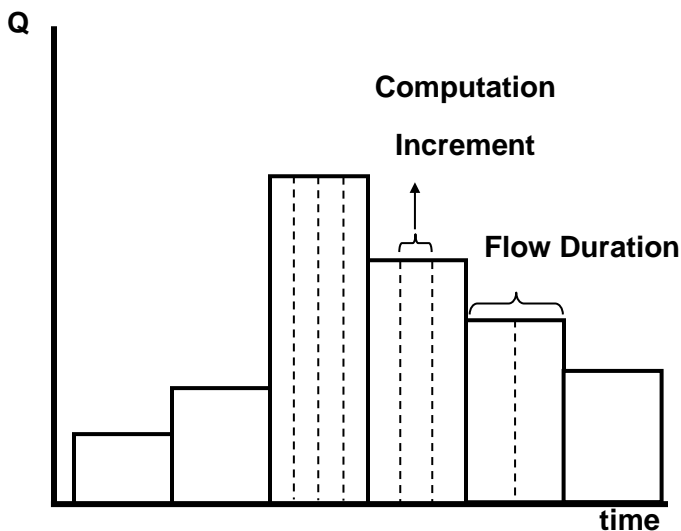

Figure 13-1. A Quasi-Unsteady Flow Series with time step.

Bed Mixing Time Step

Finally, HEC-RAS also subdivides Computational Increments into the bed mixing time step (sometimes called the SPI parameter). Bed gradation can evolve very quickly, so HEC-RAS updates the bed gradation accounting (running the bed sorting and armoring routines) several times during each computation increment.

HEC-RAS holds hydraulic parameters and cross section elevation constant over all mixing time step in a computation increment throughout the **Computation Increment**. However, the model updates the composition of the bed mixing layers (e.g. the active, cover and/or inactive layers) at the **Mixing Time Step**, revising the grain class accounting in these layers several times between hydraulic and sediment capacity computations. The vertical gradational profile changes response to the deposition or erosion even though the bed does not change until the end of the **Computation Increment**. Tighter accounting of bed gradation affects transport. HEC-RAS computes transport capacity base on the active layer gradation, so while the hydraulics (and transport potential, see below) remain constant throughout the **Computation Increment**, transport capacity can change between **Bed Mixing Time Steps**.

Sediment Continuity

The HEC-RAS sediment routing routines solve the sediment continuity equation also known as the Exner equation:

$$(1 - \lambda_p) B \frac{\partial \eta}{\partial t} = -\frac{\partial Q_s}{\partial x}$$

where:

B	= channel width
η	= channel elevation
λ_p	= active layer porosity
t	= time
x	= distance
Q_s	= transported sediment load

Like most continuity equations, the Exner equation simply states that the difference between sediment entering and leaving a control volume must be stored or removed from storage. The unique feature of the Exner equation is that sediment storage is stored in the bed in a multi-phase mixture with water, requiring porosity to translate mass change into volume change. The Exner equation translates the difference between inflowing and outflowing loads into bed change, eroding or depositing sediment.

HEC-RAS solves the sediment continuity equation by computing a sediment transport capacity for control volume (Q_{s-out}) associated with each cross section, comparing it to the sediment supply (Q_{s-in}) entering the control volume from the upstream control volume or loacal sources (e.g. lateral sediment loads). If capacity is greater than supply, HEC-RAS satisfies the deficit by eroding bed sediments. If supply exceeds capacity, HEC-RAS deposits the sediment surplus.

Computing Transport Capacity

The right hand side of the continuity equation, the sediment gradient across the control volume, compares the sediment inflow with the sediment outflow. Sediment inflow is simply the sediment entering the control volume from the upstream control volume(s) and any local

sources (lateral sediment inflows). Computing the sediment leaving the control volume is more difficult, a measure of the sediment mass the water can move, which is a complex function of the hydrodynamics and sediment properties. **Sediment transport capacity** is a measure of the control volume competence to pass sediment, computing the maximum sediment it can transport by grain class.

Grain Classes

HEC-RAS divides the sediment material into multiple grain classes. Default grain classes sub-divide the range of transportable material, (0.002 mm to 2048 mm) into 20 grain classes or bins, each including adjacent, non-overlapping fractions of the grain size spectrum.   Default grain classes follow a standard log base 2 scale where the upper bound of each class is twice its lower bound, the upper bound of the smaller, adjacent class. The gain class represents all particles they contain with a single, representative grain size. HEC-RAS uses the geometric mean of the grain class to represent the grain size for each bin. Grain boundaries (and labels) are editable.

Sediment Transport Potential

Sediment **transport potential** is the transportable mass of a *particular* grain class in response to cross channel hydraulic parameters. HEC-RAS computes **transport potential** for each grain class with one of a number of sediment transport equations available in the program.

The sediment transport equations are empirical equations or algorithms that translate hydrodynamics into transport. However, most of these equations were developed for a single representative grain size.

To apply these equations to sediment mixtures, with multiple discrete grain classes, HEC-RAS computes **transport potential**, allying the transport function independently to each grain class present in the system, as if it were the only grain class in the system. Later **transport potential** is prorated by the prevalence of the grain class, to compute the **transport capacity** (see discussion below), which is the transport used in the Exner equation. But first HEC-RAS applies the transport function to each available grain class *independently*, computing a **transport potential** for each.

HEC-RAS includes eight sediment transport potential functions. Since sediment transport is sensitive to so many variables, transport potentials computed by the different equations can vary by orders of magnitude, depending on how the material and hydrodynamics compare to the parameters over which the transport function was developed. As much as possible, select a transport function developed for similar gradations and hydraulic parameters as the project reach. Appendix E in this document include the actual equations and algorithms. This section includes brief, qualitative notes on the use, applicability, and sensitivity of each equation.

Ackers and White

Ackers and White (1973) is a total load function, developed from flume data for relatively uniform gradations ranging from sand to fine gravels. Ackers and White derived the equation

dimensional analysis and did not include a grain shear partition. They fit coefficients to the equation based on experiments that included a range of bed configurations including ripples, dunes, and plane bed conditions.

Engelund-Hansen

Engelund-Hansen (1967) is a total load transport equation, developed from flume data, using relatively uniform sand sizes between 0.19 mm and 0.93 mm. England Hansen is the simplest transport equation, an explicit function of channel velocity, bed shear (not even excess shear), and the d_{50} of the material. Application should be restricted to sand systems.

Laursen-Copeland

Laursen (1968) is also a total load function, initially based on flume equations, later expanded by Madden to include the Arkansas River data. It is a basic function of excess shear and a ratio of the shear velocity to the fall velocity. Later, Copeland (1989) generalized the equation for gravel transport, making it applicable graded beds.

Laursen parameterized this equation with material that extended slightly into the silt range. Recent work at Colorado State (Watson, personal communication) demonstrated that the Laursen equation outperforms other transport functions in the very fine sand and very coarse silt range.

Meyer-Peter Müller

The Meyer-Peter and Müller (MPM) equation (1948) was one of the earliest equations developed and is still one of the most widely used. It is a simple excess shear relationship. MPM is strictly a bedload equation developed from flume experiments of sand and gravel under plane bed conditions. The MPM experiments mostly examined uniform gravel, making the transport function MPM most applicable in gravel systems. MPM tends to under predict transport of finer materials.

HEC-RAS uses the version of MPM from Vanoni (1975), ASCE Manual 54, the version used in HEC 6. This version includes a form drag correction (the RKR parameter, based on the roughness element ratio, $(K_b'/K_r)^{1.5}$, computed from the Darcy –Weisbach bed fiction factor). The form drag correction isolates grain shear, computing transport based on the bed shear component acting only on the particles. The form drag correction should be unnecessary in plane-bed conditions, so some versions of MPM exclude it. Wong and Parker (2006) demonstrate that using MPM without the form drag correction over-predicts bed load transport.

Therefore, HEC-RAS offers the Wong Parker correction to MPM based on their 2006 paper. The Wong Parker correction changes MPM in *two* ways. First, it sets the form drag correction to unity (RKR=1), effectively removing it from the equation. Second, it sets the MPM coefficients to those Wong and Parker (2006) computed using the *plane-bed* data sets from the original MPM analysis recasting:

$$q_b^* = 8(\tau^* - \tau_c^*)^{3/2} \quad , \quad \tau_c^* = 0.047$$

as

$$q_b^* = 3.97\,(\tau^* - \tau_c^*)^{3/2} \quad , \quad \tau_c^* = 0.0495$$

Where: q_b^* is the Einstein bedload number (correlated with bedload), τ^* is the Shield's stress which is compared to, τ_c^* which is the 'critical' Shields stress.

The effects of these changes can push transport higher or lower than MPM based on the magnitude of the form drag correction. Removing the form drag correction can increase transport (if it was computing a partition) and changing the coefficients decreases transport.

Wong and Parker (2006) based their work on the *plane-bed* data sets MPM analyzed, those without appreciable bed forms. Therefore, their correction is directly applicable only to lower-regime plane-bed conditions.

Toffaleti

Toffaleti (1968) is a total load function developed primarily for sand sized particles, which followed the basic principles of the Einstein approach, replacing some of the empirical assumptions. Toffaleti is usually applied to 'large rivers', since most of the data used to develop it were from large, suspended load systems. The function is not driven by excess shear velocity or bed shear. Instead, it describes the relationship between sediment, hydraulics, and water temperature with a set of regressions.

Toffaleti breaks the water column down into vertical zones and computes the concentration of each zone with a simple approximation of a Rouse concentration profile. HEC-RAS can output transport for each zone separately, approximating the vertical concentration profile. The USACE has applied the function successfully to large systems like the Mississippi, Arkansas, Sacramento, and the Atchafalaya Rivers. However, it performs particularly poorly for gravel size particles. HEC-RAS 5.0 included a combined Toffaleti-MPM function to mitigate this limitation.

Additionally, the Toffaleti equation uses two different grain sizes, a d_{50} and a d_{65}, in an attempt to quantify transport dependence on the gradational deviation from the mean. This made more sense when the equation was used to compute the transport of the bulk gradational material. When HEC-RAS applies it to the individual grain classes, it will use the d_{50} and d_{65} for the given grain class, stretching the original intent of the d_{65} parameter a bit.

Yang

Yang (1973, 1984) is a total load transport equation which bases transport on Stream Power, the product of velocity and shear stress. The function was developed and tested over a variety of flume and field data. The equation includes two separate relations for sand and gravel transport. Yang tends to be very sensitive to stream velocity, and it is more sensitive to fall velocity than most.

Wilcock

Wilcock and Crowe (2003) is a bedload equation designed for graded beds containing both sand and gravel. It is a surface transport method based on the theory that transport is primarily dependent on the material in direct contact with the flow. It was developed based on the surface gradations of flumes and rivers. Therefore, the bed gradations should reflect the bed surface properties. Always use this function with the **Active Layer** bed mixing method and consider defining separate active layer gradations to reflect the cover layer.

Wilcock and Crowe include features that account for grain class inter-dependence. By computing each grain class separately, HEC-RAS assumes that transport in each grain class is independent of the prevalence or behavior of other grain classes. The last two decades of graded sediment transport research suggests that gravel and cobbles affect sand transport and visa versa. Wilcock and Crowe quantify grain class dependence with hiding and sand dependent gravel transport equations:

<u>Hiding</u>: Wiclcock and Crow computes the influence of gravel and cobble on sand with a hiding function. The hiding function reduces the transport potential of smaller particles, because sand nestles between larger gravel clasts, which reduces the bed shear it experiences.

<u>Sand Dependent Gravel Transport</u>: Wilcock and Crowe's also quantified the effect of sand content on gravel transport. While coarse clasts reduce the shear on and transport of fine particles, gravel transport increases with sand content. As sand content increases it 'lubricates' the bed, decreasing the framework integrity, depositing in between interlocking grave-on-gravel contacts. Sand also makes gravel clasts more 'prone', allowing bed shear to act on more of the gravel particle, particularly a dislodged gravel particle, already transporting over a 'sand ribbon.'

Wilcock and Crowe compute a dimensionless reference shear for the substrate which is a function of the sand content of the bed surface:

$$\tau_{rm}^* = 0.021 + 0.015 \cdot e^{-20 \cdot FS}$$

Where τ_{rm}^* is the reference shear stress and FS is the sand content in percent. As the sand content increases: the reference shear decreases, increasing the excess bed shear, and the total transport. The Wilcock equation is very sensitive to this sand content parameter. It tends to be most appropriate for bimodal systems that include significant gravel and sand components.

Transport Capacity

Once HEC-RAS computes **transport potential**, applying the transport equation to each grain class, (i.e. as if the system was composed of 100% of that grain class) the model must translate that into the actual grain class transport, as a function of the composition of the sediment mixture. The **transport capacity** prorates the **transport potential**, reducing the transport of each grain class based on its prevalence in the bed.

The **transport capacity** for each grain class is the **transport potential** multiplied by the percentage of that grain class in the bed. Therefore, the total transport capacity is:

$$T_c = \sum_{j=1}^{n} \beta_j T_j$$

Where: T_c is Total transport capacity, n is the number of grain size classes, B_j is the percentage of the active layer composed of material in grain size class "j", and T_j is the Transport potential computed for the material in grain class "j". Partitioning capacity based on the gradation of the active layer is a classic assumption based Einstein's (1950), who proposed sediment discharge of a size class is proportional to the fractional abundance of that size class in the bed (Vanoni, 1975).

Once HEC-RAS computes a **transport capacity** for each grin class it balances the continuity equation for each grain class separately. Total capacity is not used anywhere in the program. Then the model compares computed capacity to supply for each grain class and calculates a sediment surplus or deficit by grain class.

Continuity Limiters

The continuity equation compares the transport capacity to the supply (i.e. inflowing sediment load) for each grain class for each time step. If the capacity exceeds the supply HEC-RAS computes a sediment deficit. If the supply exceeds capacity the model computes a sediment surplus. In general, the model converts surplus into deposition and deficit into erosion. However, HEC-RAS applies some physical constraints to the continuity equation, checking if computed deficit or surplus can actually erode or deposit. HEC-RAS models these constraints with three basic limiters: a temporal deposition limiter, a temporal erosion limiter, and the sorting and armoring algorithms that provide an additional constraint on erosion.

Temporal Deposition Limiter

The temporal constraint on deposition is the limiter based on the simplest and most robust theory. Fall velocity controls how fast particles can drop out of the water column and deposit. By comparing the vertical distance a particle has to travel to reach the bed surface and the vertical distance a particle can travels in a time step (fall velocity * time), HEC-RAS computes the percentage of a sediment surplus can actually deposit in a given control volume in a given time step. The model computes a **deposition efficiency coefficient** for each grain class (i):

$$C_d = \frac{V_s(i) \cdot \Delta t}{D_e(i)}$$
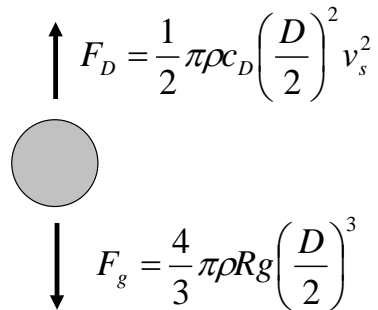
Where: C_d is the deposition efficiency coefficient, $V_s(i)$ is the fall velocity for the grain class, Δt is the time step, and D_e is the effective depth of the water column over which the grain class is transported.

The coefficient is a fraction, which will reduce deposition if the product of the fall velocity and the time step is less than the effective depth. If the time and fall velocity are sufficient for the grain class to fall the entire effective depth (i.e. the numerator is greater than the denominator),

all of the surplus sediment deposits. This ratio requires two parameters (in addition to the time step, which HEC-RAS provides automatically): fall velocity and the effective transport depth.

Fall Velocity

Most fall velocity derivations start with balancing the gravitational force and the drag force on a particle falling through the water column. The free body diagram is included in Figure 13-2.

$$F_D = \frac{1}{2} \pi \rho c_D \left(\frac{D}{2} \right)^2 v_s^2$$

$$F_g = \frac{4}{3} \pi \rho R g \left(\frac{D}{2} \right)^3$$

Figure 13-2. Free body diagram used for computing fall velocity.

However, the resulting equation is circular because fall velocity is function of the drag coefficient C_D, which is a function of the Reynolds number, which is itself a function of fall velocity. This self-referential quality of the force balance requires either an approximation of the drag coefficient/Reynolds number or an iterative solution. The fall velocity options in HEC-RAS are detailed in Chapter 12, pages 12-30 to 12-32, but a few brief comments on how each of these methods attempts to solve this equation (fall velocity dependence on fall velocity) are given below.

Rubey assumes a Reynolds number to derive a simple, analytical function for fall velocity. Toffaleti developed empirical, fall velocity curves that, based on experimental data, which HEC-RAS reads and interpolates directly. Van Rijn uses Rubey as an initial guess and then computed a new fall velocity from experimental curves based on the Reynolds number computed from the initial guess. Finally, Report 12 is an iterative solution that uses the same curves as Van Rijn but uses the computed fall velocity to compute a new Reynolds number and continues to iterate until the assumed fall velocity matches the computed within an acceptable tolerance.

Fall velocity is also dependent upon particle shape. The aspect ratio of a particle can cause both the driving and resisting forces in Figure 13-2 to diverge from their simple spherical derivation. All of the equations assume a shape factor or build one into their experimental curve. Only Report 12 is flexible enough to compute fall velocity as a function of shape factor. Therefore, HEC-RAS exposes shape factor as a user input variable but only uses it if the Report 12 method is selected.

Effective Transporting Depth

The deposition limiter works by comparing how far a particle can fall in a time step versus the distance available for it to travel. The fall velocity computes how far the particle can fall in a time step, but the temporal limiter equation also requires an average vertical distance that the

grain class can fall. That distance depends on the concentration profile of the grain class in the flow field (i.e. sediment is not uniformly distributed in the water column).

Rouse (1963) developed the classic concentration profile theory (Figure 13-3). The Rouse number z is higher for larger particles and lower for higher shear velocities. Smaller particles and higher shears distribute suspended particles over more of the water column. Grain classes with higher Rouse numbers have to fall farther to deposit.

Figure 13-3. Rouse concentration profiles.

Toffaleti (1968) subdivided the \water column into four zones, computing transport separately for each zone (Figure 13-4). HEC-RAS uses these zones as a (coarse) integration of vertical concentration profiles. HEC-RAS adopts these four zones as the effective transporting depth for different grain sizes, assuming that the grain class is evenly mixed and in equilibrium in the zone. The model distributes grain classes smaller than fine sand throughout the entire water column (Effective Depth = 1). The model distributes fine sand over the middle, lower, and bed zone which compose the lower 40% of the water column. All coarser particles (≥Medium Sand) transport relatively close to the bed, in the lower zone and bed zone, the deepest 9%of the water column.
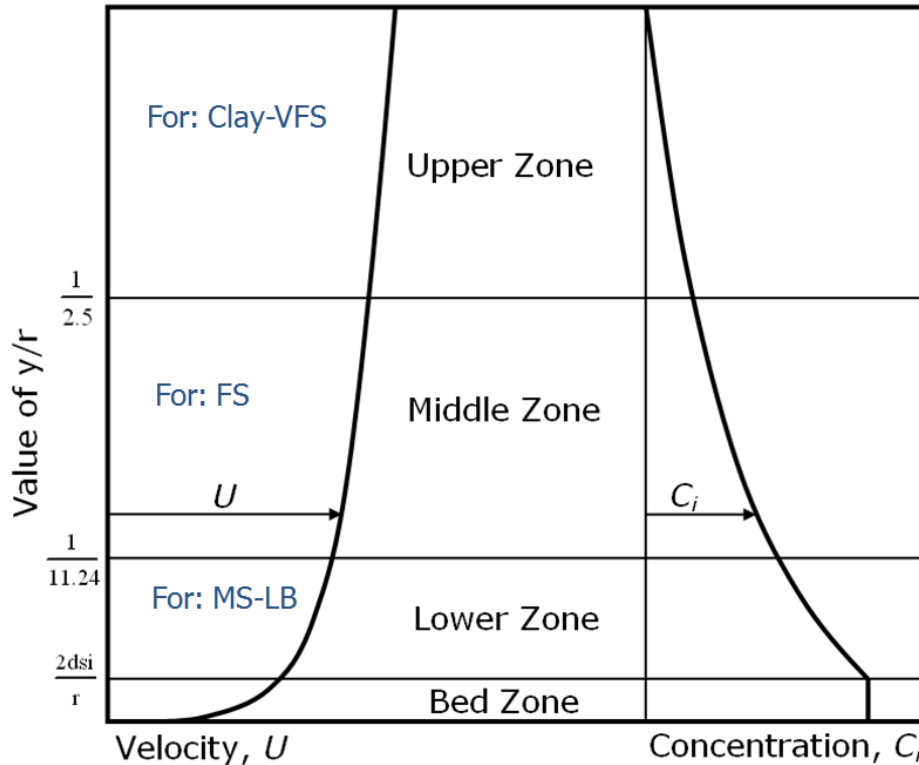
Figure 13-4. Toffaleti's zones for computing transport (after Vanoni, 1954)

This approach has limitations. It distributes sediment evenly throughout the zone at the beginning of each time step. This assumption simplifies the concentration gradients depicted in Figure 13-3. Additionally, assuming the effective depth (based on the transporting depth) is on only a function of grain size ignores the Rouse dependence on shear velocity. Finally, the algorithm mixes the transporting zone fully at the beginning of each time step, retaining no memory of how far material settled in the previous time step. Despite the limitations, however, the temporal deposition limiter improves the continuity approach, limiting the deposition with physical process.

Temporal Erosion Limiter

Like deposition, erosion is also a temporal process. Physical processes delay erosion, potentially limiting the continuity surplus to a smaller erosion mass. Therefore, erosion also requires a temporal limiter. Unfortunately, the physical processes that delay erosion are more diverse, site specific, and difficult to quantify than those that limit deposition. The equations used are more empirical and generally less accurate.

HEC-RAS adopted its erosion limitation equation from HEC 6. It is similar to 'Characteristic Flow Length' principles, but predates them. The governing assumption, based on undocumented flume experiments, is that an unarmored reach requires thirty times the water depth for erosion to fulfill the capacity. This assumption is reflected in the equation for the entrainment coefficient:

$$C_e = 1.368 - e^{-\left(\frac{L}{30 \cdot D}\right)}$$

Where: C_e is the entrainment coefficient, D is flow depth, and L is length of control volume. This equation produces the relationship between the entrainment coefficient and length/depth ratios in Figure 13-5. HEC-RAS multiplies the sediment deficit by this entrainment coefficient to calculate erosion.
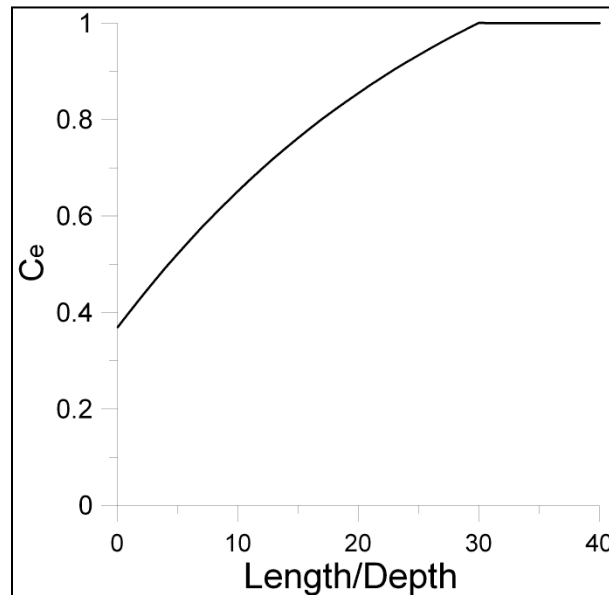
Figure 13-5. The calculated entrainment coefficients for a range of control volume length to depth ratios.

If the length exceeds the flow depth by thirty times or more, the entrainment coefficient goes to one and HEC-RAS erodes the full deficit. In the lower limit, as the length approaches the depth, the second term of the C_e equation goes to 1 leaving a minimum entrainment coefficient of 0.368. Therefore, the program will always allow at least 36.8% of the deficit to erode.

Sorting and Armoring

Erosion can also be supply limited. In many well graded rivers, a coarse armor layers forms on top of a subsurface layer, composed of the representative reach gradation. Rivers form these coarse armor layers by static or dynamic armoring (Parker, 2008). Static armoring comes from differential transport of finer materials, where finer particles transport, leaving the coarse particles behind until the immobile coarse particles armor the bed, precluding future erosion. Static armoring processes often dominate downstream of dams, where attenuated flow regimes are competent to move finer particles but not coarser particles. Dynamic armoring can also form armor layers in systems where large flows are competent to move all grain classes. Dynamic armoring forms coarse cover layers while all grain classes are mobile because equilibrium transport of graded material requires over representing coarse particles at the surface, compensating for their lower transportability by increasing their availability (Parker, 2008).

In either case, armor layers decrease total transport because the surface particles available for transport tend to be coarser and more difficult to move. This is also a physical limiter on the transport capacity.

HEC-RAS includes three algorithms to simulate bed sorting and armoring. All three algorithms divide the bed into an active layer and an inactive layer. The active layer is a surface layer that represents actively transporting material (or material that could be transported). The active layer gradation evolves independently and material is moved between it and the parent material in the inactive layer below it. HEC-RAS computes transport capacity based on the gradation of the active layer, not the entire bed.
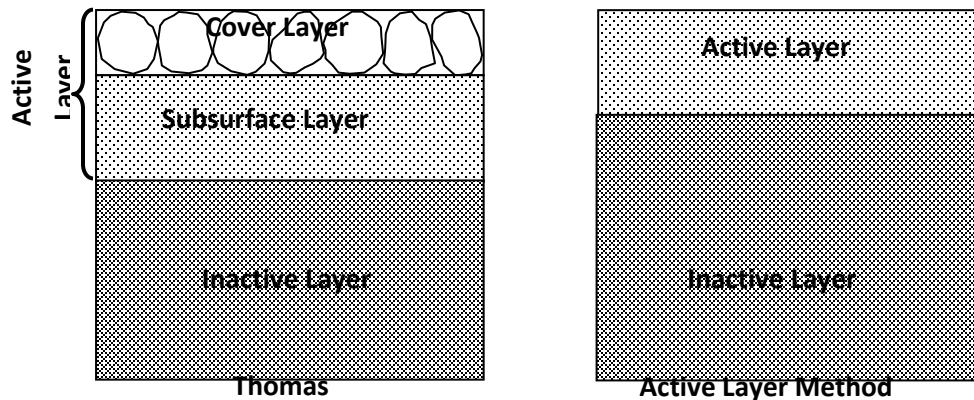
Figure 13-6. Schematic of the mixing layers in HEC-RAS' sorting and armoring methods.

Thomas Mixing Method (Exner 5)

The **Thomas** method (formerly Exner 5) is the default sorting and armoring method in HEC-RAS. This is a three layer bed mixing algorithm (Figure 13-6), which was designed to account for the influences of static armoring. Tony Thomas developed this method (Thomas, 1982), which was the default method in HEC-6. It subdivides the active layer into a cover layer and a subsurface layer, allowing a thin cover layer to coarsen and regulate erosion, while maintaining the more broadly graded active layer. HEC-RAS computes transport capacity computation based on the gradation of the entire active layer, which includes the combined cover and subsurface layers. Sediment deposits into and erode from the cover layer. Thomas developed this mixing algorithm based on the photograph in Figure 13-8 and the data in Harrison (1950).

If finer grain classes erode faster than coarser glasses (relative to their abundance) the cover layer coarsens, regulating the sediment that transport capacity can remove from the active layer. HEC-RAS can erode a grain class long as it is available in the cover layer. But once the model strips a grain class from the cover layer it will try to satisfy the grain class transport capacity with subsurface layer sediment. The cover layer can reduce or preclude erosion from the subsurface layer, leaving capacity unfulfilled.
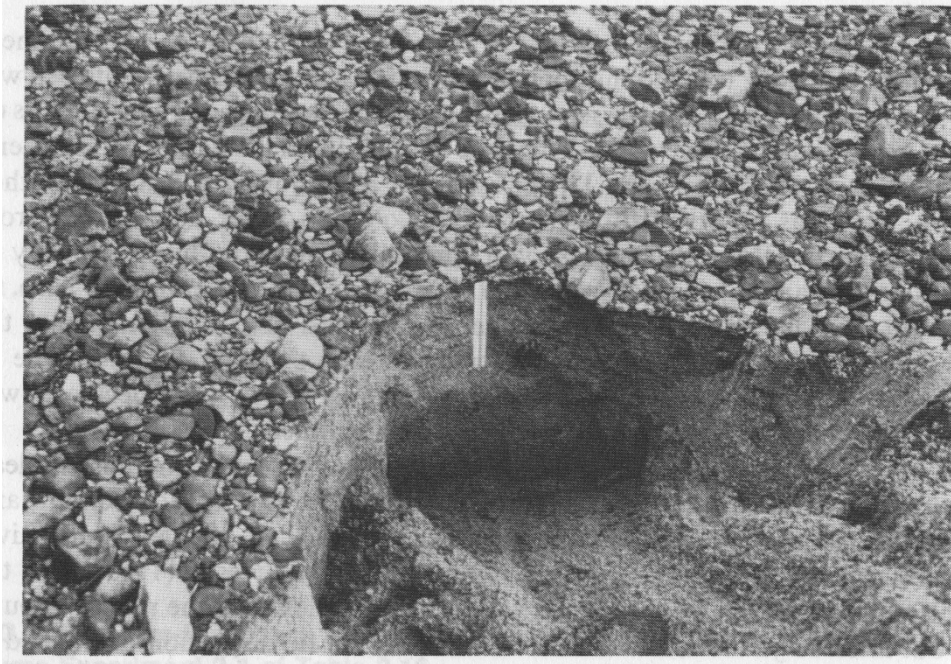
Figure 13-7. Static Armor layer below Fort Randall Dam (Livsey, 1963)

The Copeland (1992) method followed the basic approach and architecture of the Thomas method made a few critical changes. The discussion that follows generally applies to both methods, then the algorithm elements particular to Copeland are discussed in the next section.

Active Layer and Equilibrium Depth:

The Thomas method computes the Active Layer (cover layer + subsurface layer) at the beginning of each time step by computing the **Equilibrium Depth** (D_{eq}). Equilibrium Depth is the smallest water depth at which surface sediment does not move, where hydraulic forces are too small to move bed particles. Alternately, it is the maximum potential scour depth. Then it adjusts the active layer to the equilibrium depth (Figure 13-8).
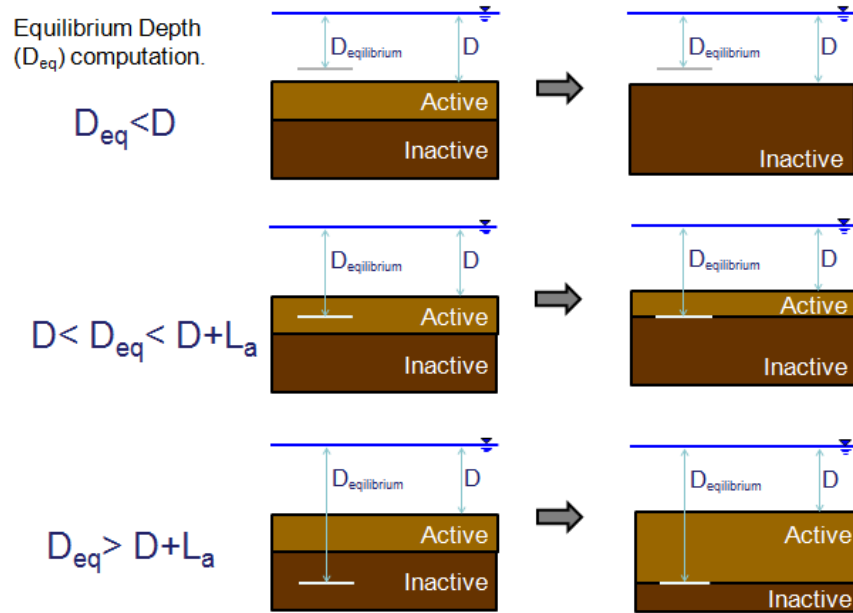
Figure 13-8: Active layer adjustment to the equilibrium depth for three conditions: equilibrium depth less than water depth (top), equilibrium depth within the current active layer (middle), and equilibrium depth deeper than current active layer (after Copeland, 1992).

Equilibrium Depth (D_{eq}) is based on a relationship between hydraulic energy, bed roughness and sediment transport intensity. The Thomas method combines Manning's equation for flow velocity, Strickler's equation for grain roughness, and Einstein's Transport Intensity equation to compute equilibrium depth:

Manning's Equation

$$V = \frac{1.49}{n} R^{\frac{2}{3}} S_f^{\frac{1}{2}}$$

Strickler's Roughness Equation

$$n = \frac{d^{\frac{1}{6}}}{29.3}$$

Einstein's Transport Intensity Equation

$$\Psi = \frac{\rho_s - \rho_w}{\rho_w} \cdot \frac{d}{D \cdot S_f}$$

Where:

    V = Velocity
    R = Hydraulic Radius
    S_f = Friction Slope

n = Manning's n value

d = representative particle size

ρ_s = grain density

ρ_w = water density

D = Depth

The Einstein Equation assumes particle erosion when the transportability $\Psi \geq 30$. Submerged particle density $(\rho_s - \rho_w / \rho_w)$ is 1.65. Substitution reduces the Einstein's Transport Intensity equation to:

$$S_f = \frac{d}{18.18D}$$

HEC-RAS solves these three equations for unit water discharge by replacing the sub-sectional hydraulic radius in the Manning equation with the panel depth, D, and the n-value with Strickler's equation such that:

$$q = \frac{1.49}{\left(\frac{d^{\frac{1}{6}}}{29.3} \right)} \cdot D^{\frac{5}{3}} \cdot \left(\frac{d}{18.18D} \right)^{\frac{1}{2}}$$

Or

$$q = 10.21 \cdot D^{\frac{7}{6}} \cdot d_i^{\frac{1}{3}}$$

Where: q = water discharge in cfs per ft of width

di = the particle diameter and

D = is the depth that does not transport the grain class, or the equilibrium depth D_{eq}.

Solving for D_{eq} yields:

$$D_{eq} = \left(\frac{q}{10.21 \cdot d_i^{\frac{1}{3}}} \right)^{\frac{6}{7}}$$

Where: D_e = Equilibrium depth for particle size, i

The Thomas method solves the equilibrium depth equation for each grain class, and sets the active layer thickness to the larges, which is the maximum possible scour.

<u>Splitting the Active Layer</u>: Cover and Subsurface Layers

Thomas' main innovation was dividing the active layer into two sub layers: a **cover layer** and a **subsurface layer**. The algorithm computes transport capacity based on the entire active layer, but he cover layer coarsens independently and regulates erosion from the rest of the active layer (the subsurface layer).

At the beginning of the bed mixing stage, HEC-RAS computes a new active layer thickness – based on the equilibrium depth. HEC-RAS carries the cover layer over from the previous time step but re-creates the sub-surface layer each time based on the new active layer thickness computed by equilibrium depth.

Equivalent Particle Diameter: The Thomas function (and the Copeland method after it) computes cover layer armoring based on an **equivalent particle diameter** principle. This **equivalent particle diameter** can be difficult to conceptualize, but is central to understanding the algorithm.

The **equivalent particle diameter (d_{eq})** converts the mass of each grain class into an equivalent *thickness*, expressed as a fraction or multiple of the grain class diameter. For example, if the large (grey) grain class in Figure 13-9 were spread evenly over the control volume, it would form a layer approximately half the particle diameter thick (half an equivalent particle diameter or $0.5d_{eq}$). Likewise, if the medium (brown) grain class in the cover layer (Figure 13-9) would form a layer approximately 40% of its diameter thick if spread evenly over the entire control volume ($d_{eq}=0.4$). The **equivalent particle diameter** converts the cover layer mass of each grain class into a thickness, normalized to the grain class diameter.
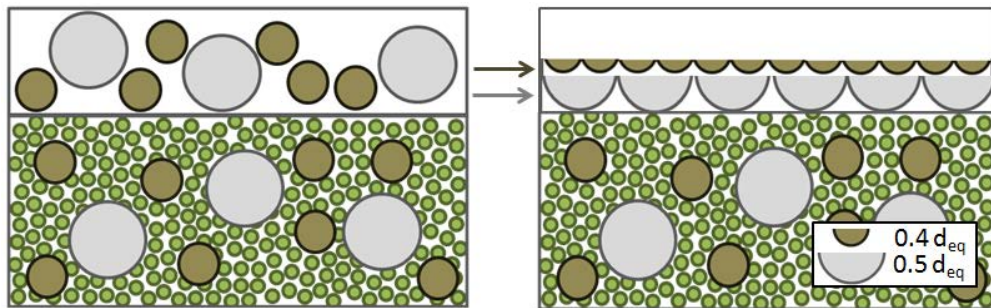
Figure 13-9: Example, idealized, three grain class cover and subsurface layer demonstrating the equivalent particle size principle

Armoring Ratio: The Thomas and Copeland methods both use the equivalent particle diameter to compute an ***Armor Ratio***. The Armor Ratio is a coefficient between 0 and 1, which reduces the sediment deficit HEC-RAS will erode from the sub-surface layer, if the cover layer includes enough coarser material.

The Thomas algorithm has five basic steps:

1. Compute Sediment Deficit by Grain Class: First HEC-RAS computes transport capacity for each grain class and compares it to supply. If capacity exceeds supply, it tries to erode the deficit from the bed.

2. Remove the Grain Class Mass from the Cover Layer: If the cover layer contains the enough of the grain class, HEC-RAS removes the entire deficit from the cover layer. If the cover layer does not have enough of the grain class to satisfy the deficit, HEC-RAS removes all of the grain class from the cover layer, and then tries to remove the balance from the sub-surface layer.

3. Sum the Equivalent Particle Diameters of all coarser grain classes in the cover layer: Before HEC-RAS removes any sediment from the sub-surface layer, it computes the equivalent particle diameter of every *coarser* grain class in the cover layer, and then sums them.

    For example, in the simplified substrate in Figure 13-9, if HEC-RAS tried to remove the smallest grain class (green), it would sum the equivalent diameter of the two coarser grain classes. HEC-RAS uses the sum of the equivalent grain diameters for cover layer grain classes, coarser than the eroding grain class (Σd_{eq}=0.9 in Figure 13-9) to compute armor layer regulation (i.e. reduce the amount of deficit the model can erode from the sub-surface layer).

4. Compute an Armoring Ratio: The Thomas method computes an armor ratio from the cumulative coarser equivalent diameter according to the relationship in Figure 13-10. This relationship interpolates between a low bound, where the cover layer has no effect on erosion and an upper bound where the armor layer totally prevents erosion from the subsurface layer.
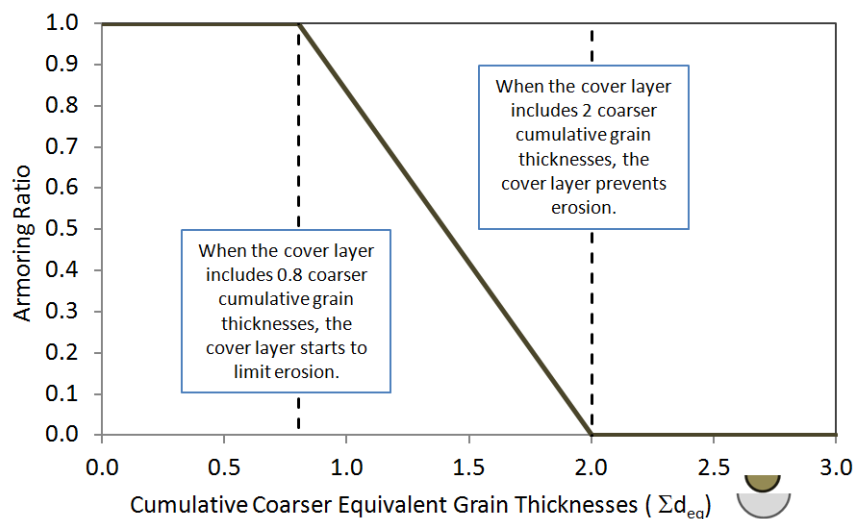
Figure 13-10: Armor ratio relationship used in the Thomas method.

Low Bound: If there is less than one total cumulative equivalent diameter of coarser material in the cover layer (Σd_{eq}<1), then the cover

layer can't be continuous. For $\Sigma d_{eq}<0.8$, 20% of the subsurface layer is exposed. At this thickness, the method assumes the cover layer has too many gaps to regulate the subsurface layer. The Thomas method does not reduce erosion for this case.

High Bound: On the other extreme, if the sum of the equivalent grain diameters of coarser grain classes is greater than 2 ($\Sigma d_{eq}>2$) the cover layer will not allow any erosion of that grain class from the sub surface layer. This end point comes from broad empirical evidence that flow cannot 'suction' fine sediment through more than two grain diameters of immobile armored layer.

The Thomas method interpolates linearly between these end points:

No Armoring (Armor Ratio = 1 →erosion =deficit) for $\Sigma d_{eq}<0.8$

and

No Erosion (Armor Ratio = 0 → erosion =0) for $\Sigma d_{eq}>2$.

5. <u>Erode the grain class from the sub-surface layer, reducing the deficit by the Armor Ratio</u>: HEC-RAS multiplies the sediment deficit for each grain class by the armor ratio such reducing erosion for each grain class (i) according to the expression:

$$\text{Erosion}_{(i)} = \text{Armor Ratio}_{(i)} * \text{Sediment Deficit}_{(i)}$$

For the example in Figure 13-9, where $\Sigma d_{eq}=0.9$, the Thomas method returns an armor ratio of 0.91, and HEC-RAS would remove 91% of the deficit of the fines grain class from the subsurface layer.

<u>Cover Layer Reset</u>: Destruction or Burial

The cover layer evolves during the simulation, coarsening or fining in response to capacity and upstream load. However, there are two situations which cause the cover layer to 'reset,' which introduce bed gradation non-linearity. Understanding these processes will help interpret bed gradation results.

<u>Cover Layer Destruction</u>: The cover layer can erode until it is too thin to regulate the bed. At that point, the Thomas method resets the layer, mixing it with the rest of the active layer, and cutting a new, thicker cover layer from the mixed active layer bed material.

At the beginning of *each* computation time step, HEC-RAS computes the **stratification weight** of the cover layer.   The **stratification weight** is simply the combined **equivalent particle diameter** of *all* grain classes in the cover layer. If the stratification weight, the total cumulative equivalent particle diameter is less than 0.5, HEC-RAS destroys the cover layer. Thomas based the 0.5 threshold on Harrison's (1950) experiments, which demonstrated that equilibrium sediment transport dropped when 40% of the bed surface was covered in his flume experiments.

Cover layer destruction can generate gradation results that are difficult to interpret, like those in Figure 13-11. This model eroded monotonically, and the capacity was high enough that the cover layer periodically slowed erosion but never stopped it. Therefore, as the bed eroded, the cover layer periodically coarsened, but as it coarsened it also thinned. When the cover layer thinned to less than 0.5 d_{eq}s, it reset, instantly fining as it adopted the gradation of the parent material. So, while the cover layer algorithm can form a static armor layer and keep the model from over-predicting erosion in graded sediment systems, cover layer dynamics also make it difficult to track gradation temporally or longitudinally (Gibson and Pridal, 2015).
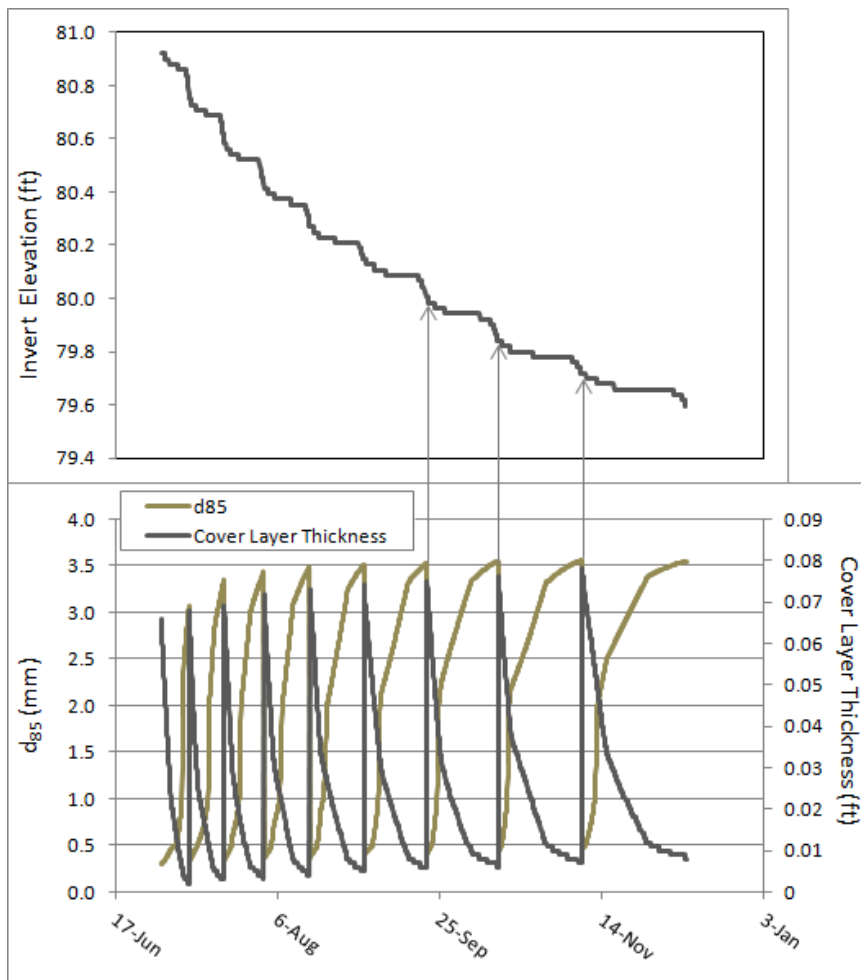
Figure 13-11: Degrading bed computed with the Thomas method which coarsens, thins and resets, never completely armoring. The periodic armor layer resets causes gradational oscillations.

Cover Layer Burial: HEC-RAS also resets the cover layer if deposition buries it. If the cover layer grows to 2 ft thick, the Thomas method assumes that the cover layer no longer exists as a distinct stratagraphic layer, and mixes the bed, resetting the cover layer with sediment from the mixed substrate. This feature is helpful in rapidly changing environments that alternate

between deposition and armoring erosion, but can also introduce non-linear shifts in the gradation output.

The HEC-6 User's Manual includes more discussion on this mixing method, calling it Method 2 (p. 25)

Copeland Mixing Method (Exner 7)

The Thomas method was developed for coarse, well graded systems. It was initially developed for the Snake River, then generalized for other systems. But it tended to overpredict armoring, and, therefore, underpredict erosion on finer systems (USACE, 1993, Thomas, 2010). Copeland (1992) adjusted the method, to make it more applicable to sand beds. The Copeland method follows the Thomas method in concept and approach. It subdivides the active layer into cover and subsurface layers, allowing the gradation of the former to regulate erosion from the later. The Copeland method adds a "bed source" layer, but is still, practically, a three layer method, like the Thomas method. It computes an **armor ratio** based on the **equivalent particle diameters** of coarser grain classes. But the Copeland method changes some of the equations and assumptions, and generally allows more scour, making it popular for large, sand bed rivers.

There are three main differences between the Copeland and Thomas methods:

1. The Copeland method doesn't compute active layer thickness with the **equilibrium depth** concept. Instead it starts at the maximum or 2 d90 or 15% of the water depth.
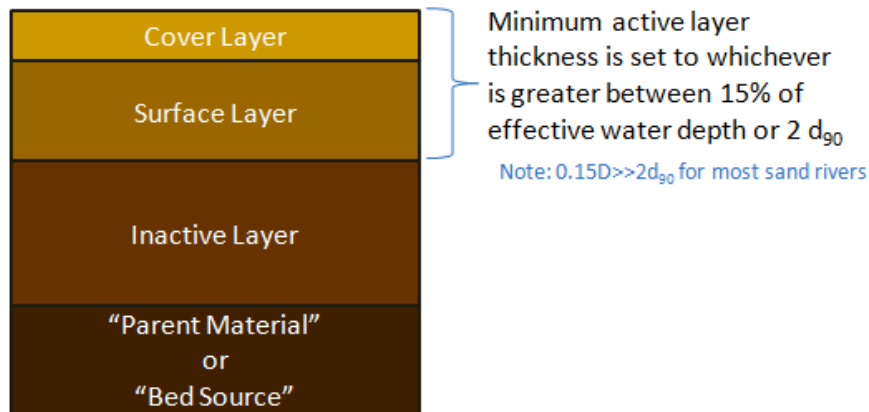
Figure 13-12: Schematic of the Copeland (1992) method.

2. The Copleand method replaces the linear interpolation between $0.8 < \Sigma d_{eq} < 2$ (from Figure 13-10) with a polynomial.

$AR = -0.026*(\Sigma d_{eq})^3 + 0.28*(\Sigma d_{eq})^2 - 1.07*(\Sigma d_{eq}) + 1.40$

This relationship has the same basic trend as the Thomas relationship but (Figure 13-13) starts armoring at a smaller Σd_{eq} ($0.4 < \Sigma d_{eq}$, following the Harrison observation) but not fully preventing subsurface erosion until Σd_{eq} is much higer ($\Sigma d_{eq} > 4$).

3. The cover layer is limited to a maximum thickness of $3d_{90}$. However, burial does not reset the cover layer.
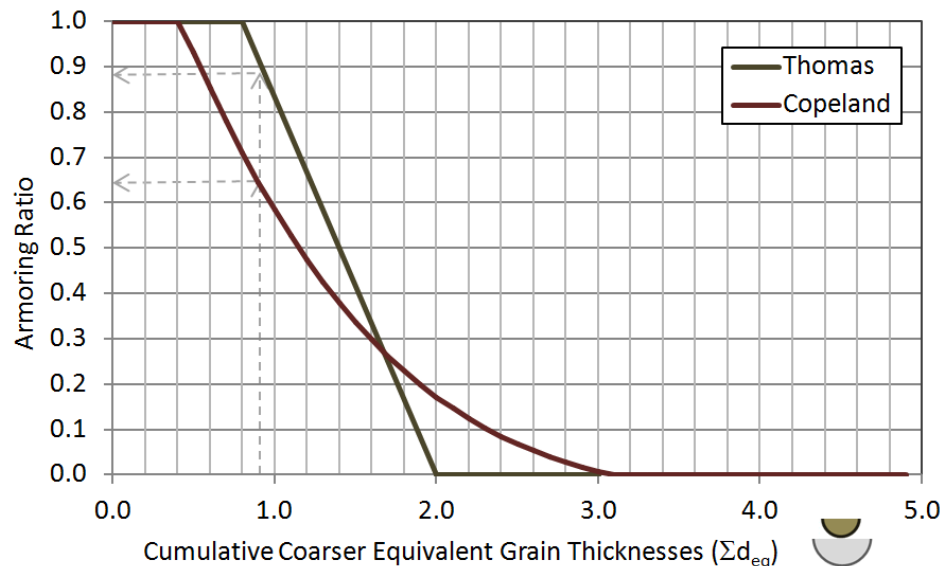
Figure 13-13: Armor ratio equations for the Thomas and Copeland armoring methods.

The main differences between the Thomas and Copeland methods are summarized in Table 13-1.

Table 13-1: Differences Between the Thomas and Copeland Armoring Methods.

Thomas (Ex 5)	Copeland (Ex 7)
Active Layer (L_a) thickness based on Equilibrium Depth (D_{eq})	Active Layer (L_a) thickness based on 15% of Water Depth or $3d_{90}$.
Linear Armor Ratio	Polynomial Armor Ratio.
Armors more rapidly, ↓ erosion	Armors more gradually, ↑ erosion

Active Layer Mixing Method

The Thomas and Copeland methods are sophisticated, multi-layer approaches to bed mixing and armoring. They are also complicated, doing a lot of math behind the scenes, providing results that can be difficult to interpret. Because HEC-RAS computes transport capacity for each grain class independently, these methods limit erosion while computing transport that reflects the subsurface gradation, which is generally observed in rivers.

However, a simplified two-layer active layer method (Figure 13-6) is also included in HEC-RAS. A simple active layer approach has obvious disadvantages including less vertical resolution and no explicit armoring factor. Use it with caution. However, it is a more intuitive and transparent

method, it can form a coarse or fine active layer, and, with an appropriate exchange increment, it may be preferable in some cases for modeling mobile armor systems (Gibson and Piper, 2007).

Hirano (1971) is often credited with introducing the "active layer" approach for sediment transport modeling, though HEC was doing similar work at the same time. This approach divides the substrate into an active (mixing or surface) layer, available for transport, and an inactive layer that has no influence on the computations for a given time step.

As the bed aggrades and degrades the sediment passes the active layer resets to a specified thickness (e.g. the d_{90}), and the layers pass material between them. If the bed erodes, the inactive layer sends sediment, an "**exchange increment**" to the active layer, to restore it. If the bed deposits, the active layer resizes and sends an **exchange increment** to the inactive layer.

The gradational composition of the erosion exchange increment is straight forward. The material the inactive layer sends to the active layer has the gradation of the inactive layer, and is mixed with the active layer sediment.

The depositional case is more complicated because the deposited material has a different gradation than the active layer. Three basic options have been proposed.

1. Mixed active Layer/Deposition Gradation. Adds the deposited material to the active layer, mix them, and send an exchange increment with the fully mixed gradation to the inactive layer. This method assumes the depositing material and the active layer are mixing fully at tight temporal scales.

2. Ambient Active Layer Gradation: Remove the exchange increment from the active layer and send it to the inactive layer first, then add the deposited material to the active layer and mix them. This method assumes static stratigraphy, that the deepest material, which would have the active layer gradation, would become inactive.

3. Deposited Material Gradation: Early work on dynamic armoring recognized that actively transporting channels maintain an armor layer even in depositional environments. But the previous two methods would cause depositing beds to fine, burying the cover layer (Parker *et al.* 1991a,b). So this method sends the deposited material directly to the inactive layer. This maintains a coarse cover layer, but does not allow any gradational evolution in the active layer.

Toro-Escobar *et al* (1996) tested these hypotheses and found that the was not composed entirely of the active layer or bed load gradations, but it also wasn't proportional (e.g. fully mixed). They found that method 3 was closer to their observations than method 2, but was not sufficient. So they proposed a depositional exchange increment during deposition was composed of 30% active layer material and 70% deposited material. This maintains a coarse cover layer better than methods 1 and 2 above, but also allows gradational evolution.

HEC-RAS follows this approach, passing depositional exchange increments to the inactive layer that are 30% active layer material and 70% depositional material. For example, if HEC-RAS deposited 10 tons of material in a time step (assuming the active layer remained the same thickness) it would transfer 3 tons from the active layer to the inactive layer and add 7 tons of the deposited material directly to the inactive layer. It would then mix the remaining 3 tons of the deposited material into the active layer.

Surface Based Transport Equations and the Active Layer Method: The Thomas and Copeland methods subdivide the active layer to address competing principles in sediment transport:

> 1. Transporting sediment generally has the same gradation as the subsurface layer, so transport capacity must be computed based on subsurface gradations.
>
> 2. The cover layer regulates erosion.

These bed mixing and armoring algorithms allow HEC-RAS to attribute the transport potential of classic transport functions based on subsurface gradations, computing transport capacity based on these gradations, without over predicting erosion.

In the years since these algorithms were developed, a different conceptual approach to graded bed transport has emerged: surface based transport functions. Parker (XXX) suggested that basing transport functions on surface gradations automatically account for dynamic armoring processes.

Wilcock and Crowe (2003), which is included in HEC-RAS, is a **surface based** equation in this tradition. It accounts for inter-particle interactions like hiding and sand-dependent gravel transport explicitly, but builds the armor layer regulation into the equation implicitly, by basing transport on armor layer gradations. Therefore, when using the Wilcock and Crowe (2003) equation in HEC-RAS, always use the active layer Mixing algorithm. Using Thomas or Copeland with a surface based transport equation double counts armoring and miss-matches conceptual frameworks.

Bed Roughness Predictors

Hydraulic computations are sensitive to bed roughness.   Bed roughness is a dynamic property and changes in response to sediment dynamics. If a fine pulse covers a coarse substrate, bed roughness will drop.   As flow increases on sand rivers, bed form amplitude increases, increasing bed roughness, until the river passes into a plane bed regime which results in substantial drops in n-values.

Mobile bed sediment models simulate changes in bed gradation, which the model can use to compute roughness, computing feedbacks between sediment transport and bed roughness. HEC-RAS includes three **bed roughness predictors**, equations and algorism that compute manning's-n from hydraulics and sediment properties, including: Limerinos, Brownlie, and Van Rijn. The **bed roughnes predictors**, compute new manning's n values each time step, as the bed

gradation and cross section evolve, which the program uses to compute hydraulics in the next computational increment.

Limerinos: The Limerinos equation computes bed roughness based on grain roughness. It is primarily applicable to channels without active bed forms, where grain roughness is the primary source of bed roughness. It is the simplest equation, computing bed roughness as a function of the hydraulic radius (R) of the channel and the d_{84} particle size (the partial size diameter two standard deviations above the mean):

$$n = \frac{0.0926\,R^{1/6}}{1.16 + 2.0\log\left(\dfrac{R}{d_{84}}\right)}$$

Brownlie: The Brownlie (1983) computes bed roughness in sand beds where form roughness (bed roughness from bed forms) is much more important than grain roughness. The Brownlie method computes bed roughness base on the median particle size (d_{50}), the hydraulic radius (R), the bed slope (S), and the geometric standard deviation of the mixture (σ). Because the Brownlie method is based on bed form mechanics it can shift between upper and lower regime relationships, causing non-linear changes in n-value:

Upper Regime:

$$n = \left[1.6940\left(\frac{R}{d_{50}}\right)^{0.1374} S^{0.1112}\sigma^{0.1605}\right]0.034\left(d_{50}\right)^{0.167}$$

Lower Regime:

$$n = \left[1.0213\left(\frac{R}{d_{50}}\right)^{0.0662} S^{0.0395}\sigma^{0.1282}\right]0.034\left(d_{50}\right)^{0.167}$$

Where R is the channel hydraulic radius in ft, d_{50} is the meidian particle size in ft, σ is the geometric standard deviation of sediment mixture: $\sigma = 0.5\left(\frac{d_{84}}{d_{50}} + \frac{d_{50}}{d_{16}}\right)$.

Brownlie defined S as the bed slope, HEC-RAS approximates this variable with the energy slope computed at the cross section.

To determine which equation to apply, HEC-RAS uses the Brownlie criteria to identify the regime.

If S>0.006, HEC-RAS always assumes the system is in the upper regime. Otherwise, Brownlie computes an empirical parameter $F_g{}'$

$$F_g' = \frac{1.74}{S^{1/3}}$$

which can be compared to the grain Froude number F_g:

$$F_g = \frac{V}{\sqrt{(S_s - 1)\, g\, d_{50}}}$$

(where V is the flow velocity, g is the gravitational constant and S_s is specific gravity of sediment particles).

HEC-RAS selects the lower regime flow if $F_g \leq F_g'$ and upper regime if $F_g \geq F_g'$. An example application of Brownlie in HEC-RAS, for a sand pulse arriving at a gravel cross section, is included in Figure 13-14.
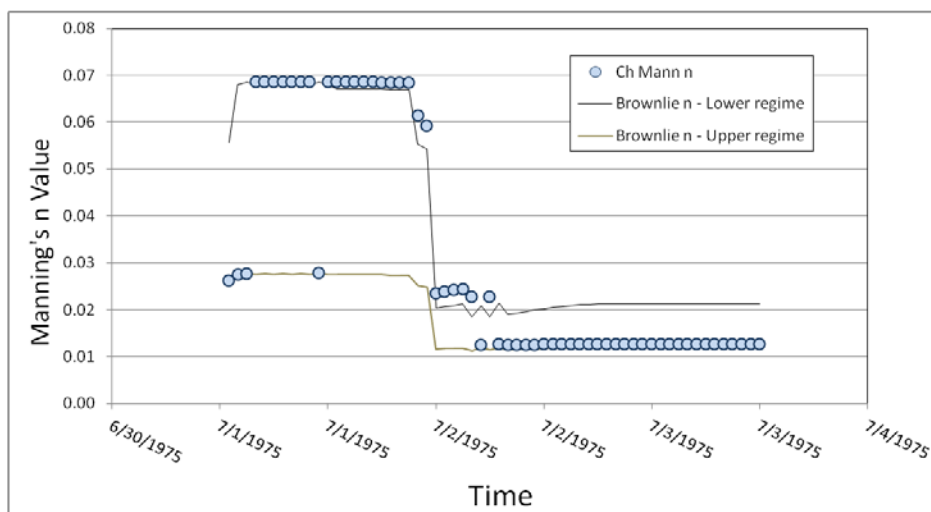
Figure 13-14: Bed roughness time series computed by Brownlie (in HEC-RAS) as a sand pulse passes through the cross section. First, when the sand pulse arrives at 7/2, the n value drops based on the gradation but stays lower regime. Eventually, the hydraulics change and it drops again, as the bed forms shift to upper regime.

<u>*van Rijn*</u>: van Rijn *(1984)* is a more recent method based on the flume and field data, and it has a good predictive ability in the dune and plane bed regimes. Van Rijn computes bed forms dimensions and the equivalent bed roughness. It estimates a Chezy-coefficient, which HEC-RAS converts into a Manning n, from bed roughness from flow, sediment transport parameters. The van Rijn method computes four key dimensionless parameters to estimate bed-form roughness.

1. <u>Particle Parameter</u>:

$$d_* = d_{50}[\frac{(s-1)g}{v^2}]^{1/3}$$

Where d_{50} is the median particle size (ft), s is the specific gravity ratio ($s = \frac{\rho_s}{\rho}$), where ρ_s is sediment density, and ρ is the fluid density, g is gravitational acceleration and v is kinematic viscosity.

2. <u>Transport Stage Parameter</u>:

$$T = \frac{(u_*')^2 - (u_{*,cr})^2}{(u_{*,cr})^2}$$

Which u_*' is grain bed-shear velocity:

$$u_*' = \frac{g^{0.5}}{C'}\bar{u}$$

where $\bar{u}$ is mean flow velocity, C' is the Chezy-coefficient.

$$C' = 18\log(\frac{12\,R}{3d_{90}})$$

where R is the hydraulic radius of the bed, $u_{*,cr}$ is the critical Sheild's parameter

$$u_{*,cr} = \sqrt{\frac{\tau_{cr}}{\rho}},$$

where τ_{cr} is the critical shear stress, and it is expressed as $\tau_{cr} = \tau_c^* \rho R g d_{50}$, and the dimensionless critical shear is computed with the equation

$$\tau_c^* = 0.5\,[0.22\,Re_p^{-0.6} + 0.06 * 10^{(-7.7\,Re_p^{-0.6})}],$$

where $R = \frac{\rho_s - \rho}{\rho}$, and $Re_p = \frac{\sqrt{gRD}\,D}{v}$, and ρ is the fluid density.

3. <u>Bed-form dimensional parameters</u>: The Bed-form parameter computes the bed form dimensions which the algorithm uses in the roughness computation:

$$\frac{\Delta}{h} = 0.11\,[\frac{d_{50}}{h}]\,\,[1 - e^{-0.5\,T}][25 - T]$$

$$\frac{\Delta}{\lambda} = 0.015\,[\frac{d_{50}}{h}]\,\,[1 - e^{-0.5\,T}][25 - T]$$

and it computes a ratio of the bed form height to the wavelength:

$$\psi = \frac{\Delta}{\lambda}$$

Where Δ is bed-form height, λ is bed-form length and is expressed as $\lambda = 7.3\,h$, and h represents flow depth. If $T \leq 0$ and $T \geq 25$, bed would be considered almost plane, and C' calculated in step 2 will be used as Chezy-coeffiient in step 4 for further calculation. ψ is bed-form steepness.

4. <u>Equivalent roughness of bed forms</u>: Finally, the algorithm uses the bed form height and height-to-wavelength ratio to compute a bed roughness.

$$k_s = 3d_{90} + 1.1\Delta[1 - e^{-25\psi}]$$

Van Rijn computes a Chezy-coefficient from the bed roughness:

$$C = 18 \log\left(\frac{12\,R}{k_s}\right)$$

HEC-RAS converts the Chezy coefficient to a Manning's n (in English units) with the equation:

$$n = 1.49\,\frac{R^{1/6}}{C}$$

An example roughness time series, using van Rijn (in HEC-RAS unsteady sediment transport) for a sand delta rapidly prograding into a gravel cross section, is included in Figure 13-15.
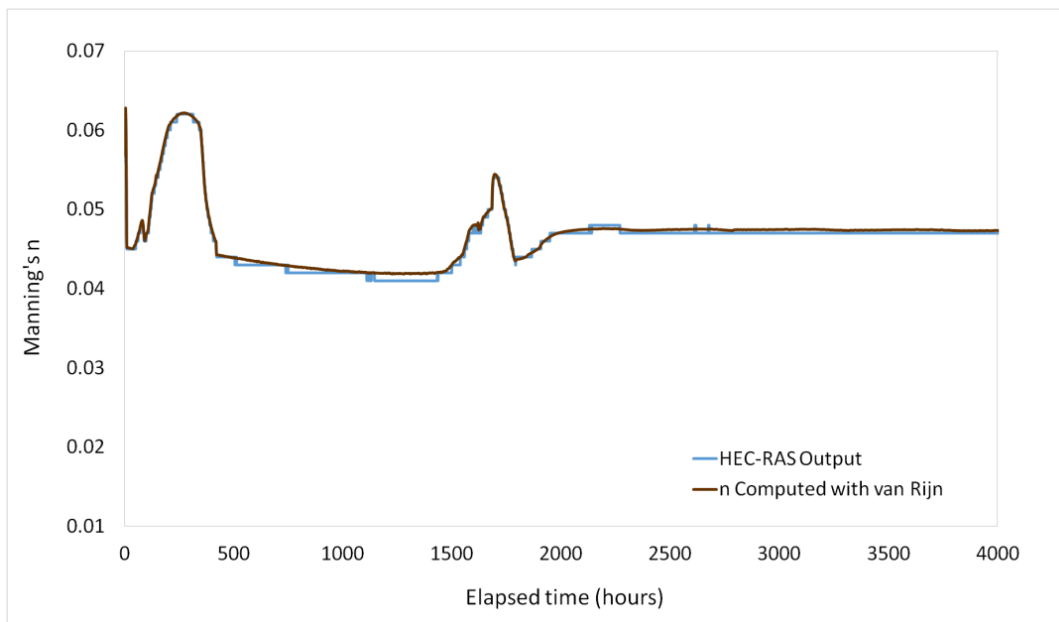
Figure 13-15: Bed roughness times series computed with HEC-RAS using the van Rijn predictor, compared to external computations.

Bed Change

Once HEC-RAS computes sediment surplus or deficit and applies the limiters, it computes a final mass to erode or deposit from the control volume. HEC-RAS adds or removes mass by adjusting the cross section station/elevation points.
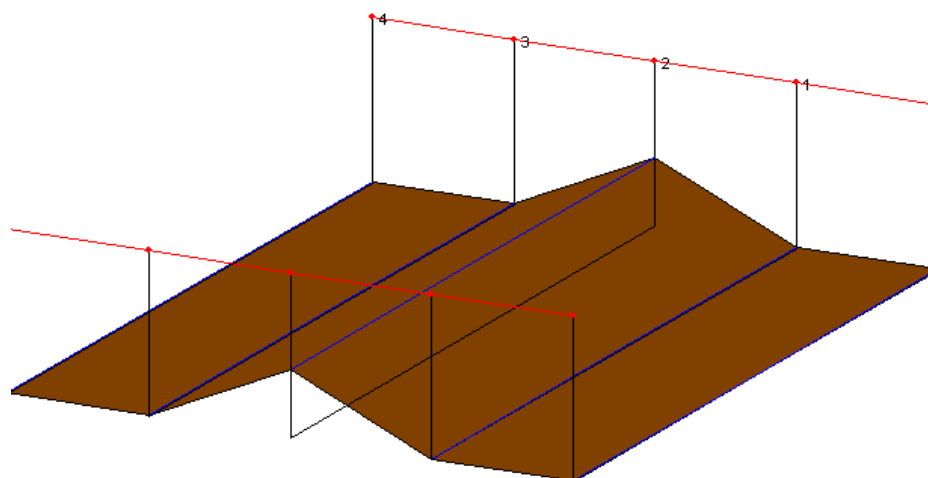
Figure 13-16. "Wedge" used to distribute erosion or deposition volume longitudinally over the control volume.

The model converts mass to volume and spreads the volume change upstream and downstream from the cross section in a "wedge", to determine the area change at the cross section. An exaggerated bed change is shown at river station 2, in Figure 13-16. HEC-RAS then converts the area change into cross section change.

Veneer Method

By default, HEC-RAS uses the "veneer method" to change cross sections. The veneer method changes all of the wetted nodes within the movable bed limits the same vertical distance. Currently the only method available for translating erosion or deposition into changes in the cross section shape is to deposit or erode each wetted, movable cross section station/elevation point equally. Following these guidelines, an example of a cross section update for erosional or depositional cases is included in Figure 13-17. The points that move are both within the erodible bed limits and beneath the water surface elevation. For the erosion case, a duplicate point is generated if the mobile bed limit is wet.
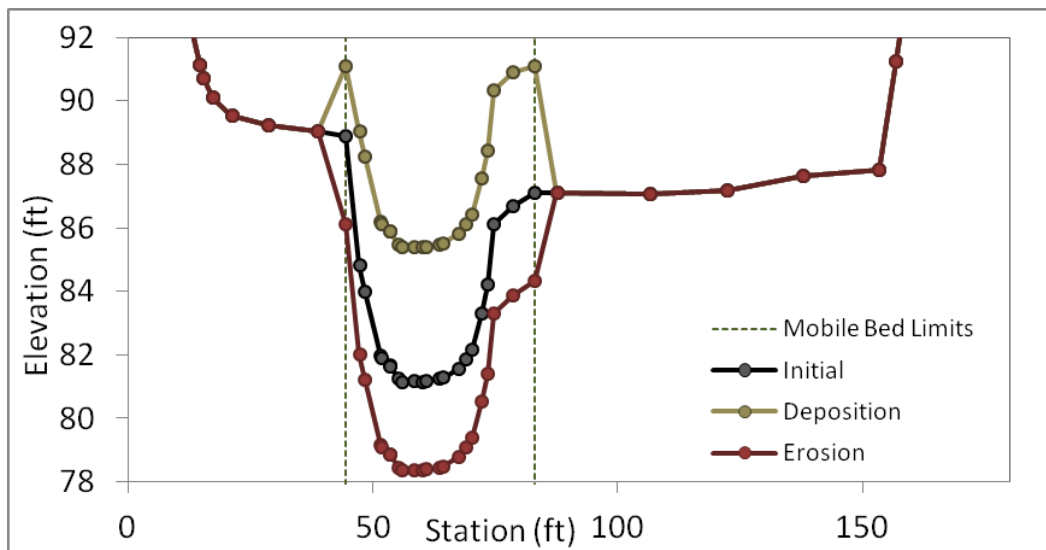
Figure 13-17: Example of veneer method, the standard bed change approach. HEC-RAS raises or lowers all wet nodes within (and including) the movable bed limits the same increment to reflect deposited or eroded mass.

HEC-RAS will not erode any node included in an ineffective flow area regardless of the bed change method or where the erodible bed limits are placed. Water velocity in an ineffective flow area is, by definition, zero. Therefore scour cannot occur at the cross section points in an ineffective flow area. However HEC-RAS will allow deposition in ineffective flow areas.

There are a couple of exceptions to these basic rules however. First, an alternate method which allows overbank deposition is available. This option handles erosion in precisely the same way as the default method, confining erosion to the movable bed limits. For the depositional case, however, HEC-RAS distributes bed change equally between all of the wetted points regardless of whether they are between the erodible bed limits or not (Figure 13-18). The principle behind this method is that eroding velocities or shears are limited to the channel, but deposition can occur in the floodplain where slowly moving water allows material to settle out.

Finally, HEC-RAS includes a depositional method that preferentially deposits in deeper parts of the cross section (Figure 13-19). This method can be useful in reservoirs, particularly in the prograding delta, where sand fills the channel. However, use it with care. Shear is often highest where the water is deepest, so depth dependent deposition requires low energy-high supply conditions.
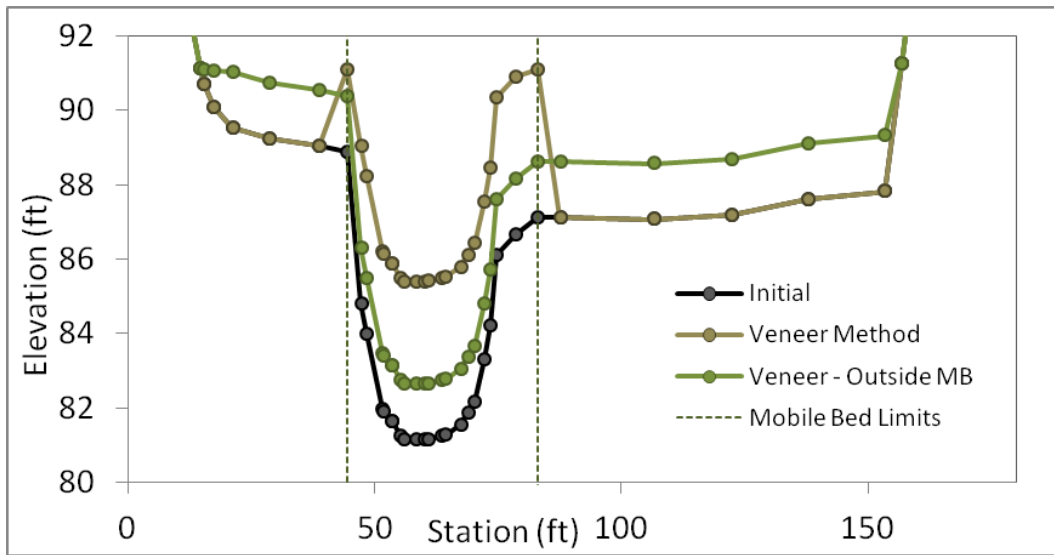
Figure 13-18: Deposition with the basic veneer method and the overbank deposition method.
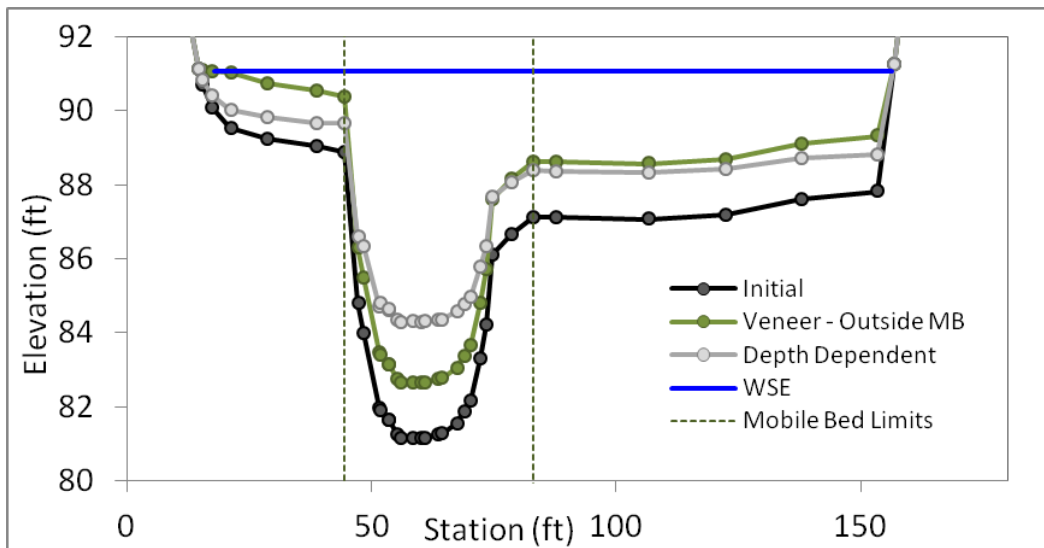
Figure 13-19: Alternate bed change method that confines erosion to the erodible limits but allows deposition at any wetted node.

Cohesive Transport

Most of the sediment transport equations were developed with sand and/or gravel data. Therefore, most silt and all clay particles are outside of the range of applicability of the sediment transport functions implemented in HEC-RAS. In most systems, these particles are *wash load,* material only found in the bed in trace amounts, because transport capacity always exceeds supply. Some modelers will just ignore fines as *throughput load*, arguing that if fines never interact with the bed in the model reach, the model is insensitive to them and they add unnecessary complexity and parameters to the model. However, sometimes fines must be modeled explicitly. In reservoirs and other backwater or low energy zones, silt and clay can

deposit and clay lined channels, both natural and engineered, can erode, causing local and downstream problems.

Fine sediment transport is further complicated by electrostatic and electrochemical forces. These particles are not just outside of the empirical range of the equations, but they often erode and deposit by fundamentally different processes. These forces cause fine particles, particularly clay, to flocculate and "stick" to the bed surface, so that fine erosion and deposition are often not primarily functions of sediment size. These process make fine deposition and erosion fundamentally different than the cohesionless sand and gravel transport.

HEC-RAS considers the smallest five grain classes 'fine sediment.' HEC-RAS applies the **cohesive method** selected to these grain classes. In the default grain classes, these five grain classes are the clay and silt classes, and are all finer than 0.625 mm. If the user edits these, the cohesive methods will still apply to the first five grain classes, regardless of their size. However, if more than 20% of the active layer is cohesive, then the model considers the sediment 'matrix supported,' assuming cohesive sediment is abundant enough to fill the voids and regulate the erosion rate of all particles.

HEC-RAS includes three cohesive methods: applying the standard transport equations, or two different implementations of the Krone and Partheniades approach.

Standard Transport Equations

The default option for silt and clay simply applies the selected transport function for the fine material as well. The transport equation will extrapolate well outside its derived range and usually compute enormous (often unreasonable) transport potentials. These transport potentials should not be considered remotely representative. They can be useful, however, to model fine sediment as wash load. With huge transport potentials, even a tiny amount of silt and clay in the active layer will produce essentially unlimited sediment transport capacity. This method can route fine wash load through the system, treating fine material as throughput load.

Krone and Parthenaides Methods

If the model objectives and systems morphology make cohesive erosion and deposition important, however, the standard transport equations are not sufficient. The Krone and Parthenaides equations are simpler than the cohesionless transport functions, building much of the predictive power into several, site specific parameters.

Earlier versions of HEC-RAS included a version of the Krone and Parthenaides cohesive approach. This approach differed from the algorithm implemented in HEC 6 and, subsequently HEC 6T. Both are defensible, taking alternate approaches applying the Parthenades scour relationship to a mixed bed. Therefore, the original HEC-RAS algorithm was retained but the HEC 6T algorithm was added as an option. Both methods apply the Krone and Parthenadeis equations to compute deposition and erosion rates in the same way.

HEC-RAS uses either the Krone equation to compute deposition or the Parthenades equations to compute erosion, and selects between them based on the bed shear stress. Two user defined

shear thresholds define three cohesive transport conditions: Deposition, Particle Erosion, and Mass Erosion. The user defined thresholds are:

τ_c: Critical shear threshold for particle erosion

τ_m: Critical shear threshold for mass erosion

where $\tau_c \leq \tau_m$. HEC-RAS computes a bed shear stress (τ_b) for each cross section and compares it to these two thresholds, determining the appropriate cohesive process, and applying the appropriate equation (Figure 13-9).
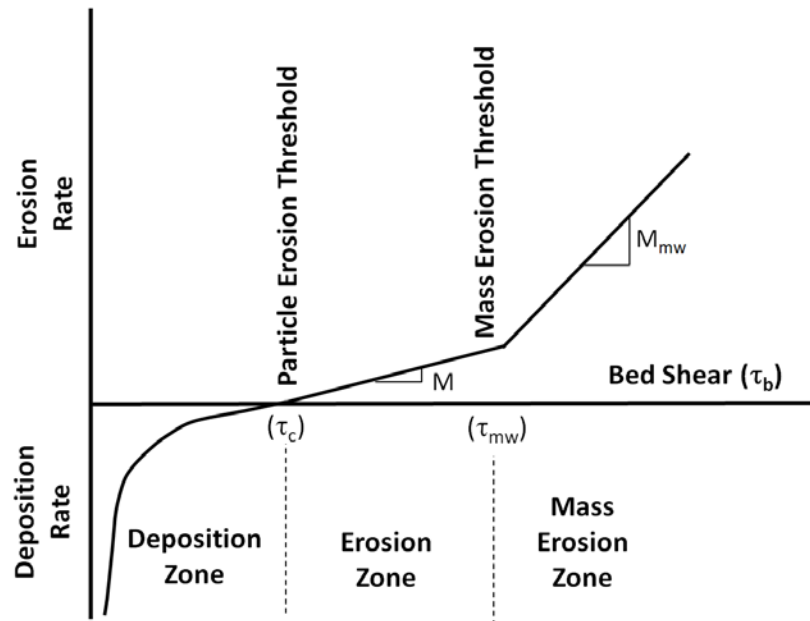
Figure 13-20. Schematic of cohesive sedimentation zones and processes as a function of shear.

Previous models often included a fourth zone, an equilibrium zone, which neither eroded nor deposited. This approach subdivided τ_c into deposision τ_d and erosion τ_e shears. In the intermediate zone between these ($\tau_d < \tau_b < \tau_e$) binding forces exceeded the erosion forces, but turbulence was sufficient to keep transported particles in suspension. This approach computed no bed change if bed shears fell in this equilibrium zone. More recent work has caused this concept to fall out of favor (Sanford and Halka, 1993). Therefore, HEC-RAS uses a single critical shear threshold (τ_c), above which particles erode and below which they deposit.

Deposition

HEC-RAS deposits cohesive sediment based on Krone (1962). Krone's observed that suspended sediment decreased logarithmically, in his experiments, for concentrations less than 300 mg/l, quantifying the deposition rate with the equation:

$$\left(\frac{dC}{dt}\right)_d = -\left(1 - \frac{\tau_b}{\tau_c}\right)\frac{V_s C}{y}$$

where: C = sediment concentration
t = time
τ_b = bed shear stress
τ_c = critical shear stress for deposition
Vs = fall velocity
y = water depth (Effective Depth in HEC-6)

This equation yields an exponential depositon relationship, where the deposition rate increases non-linearly as bed shear drops farther below the critical shear:

$$\int\frac{dC}{C} = \int -\left(1 - \frac{\tau_b}{\tau_c}\right)\frac{V_s}{y}dt \to C = C_o e^{\left(-\left(1-\frac{\tau_b}{\tau_c}\right)\frac{V_s t}{y}\right)}$$

Because of the logarithmic assumption the Krone equation only requires one empirical coefficient, the critical shear (τ_c).

If the calculated bed shear (τ_b) is less than the critical erosion shear (τ_c) HEC-RAS will deposit transporting cohesive sediment based on this equation. The equation is not applicable for shear stresses greater than the depositional threshold.

As Krone (1962) recognized, the cohesive deposition rate is also dependent on the flocculation rate, which is a function of the sediment concentration and the water chemistry. Many sophisticated coupled flocculation-deposition models account for these processes. However, HEC-RAS does not attempt to compute flocculation. Therefore, the grain size distribution should reflect the distribution of flocculants rather than discrete grains, even though standard particle sized distribution methods tend to report the latter.

Erosion

Erosion is more difficult to compute than deposition. The cohesive erosion equations are far more empirical. HEC-RAS computes cohesive erosion based on Parthenaides (1962). Parthenaides (1962) argued that the force resisting erosion is mainly electrostatic in nature, since the average electrochemical force exerted on a clay particle is a million times greater than the average weight of the particle. Therefore, cohesive erosion is not based on particle size, but an empirical 'erodibility' that accounts for the other binding processes.

Parthenaides (1962) modeled cohesive erosion rates as a pair of linear functions of bed shear. When bed shear exceeds critical shear, particle erosion begins as the shear stress removes individual 'particles' or flocs are removed. This particle erosion rate increases, approximately, a linear function of shear.

However, if bed shear gets high enough, it begins to remove clods from the bed, introducing a non-linear inflection point (τ_{mw} in Figure 13-20) in the erosion rate. This has historically been called 'mass wasting' or 'mass erosion.' The terminology is ambiguous but HEC-RAS retained it for continuity. Erosion rate above the mass erosion threshold is also linear, but increases as a function of shear at a different (usually higher) slope (Figure 13-21).

Particle Erosion ($\tau_c < \tau < \tau_m$)

According to the Parthenaides equation (1965):

$$\left(\frac{dm}{dt} \right)_e = M\left(\frac{\tau_b}{\tau_c} - 1 \right)$$

> where: m = mass of material in the water column
> t = time
> τ_b = bed shear stress
> τ_c = critical shear stress for erosion
> M = empirical erosion rate for particle scour

> Therefore:

$$\int dm = \int M\left(\frac{\tau_b}{\tau_c} - 1 \right) dt \rightarrow m = M\left(\frac{\tau_b}{\tau_c} - 1 \right) t + m_o$$
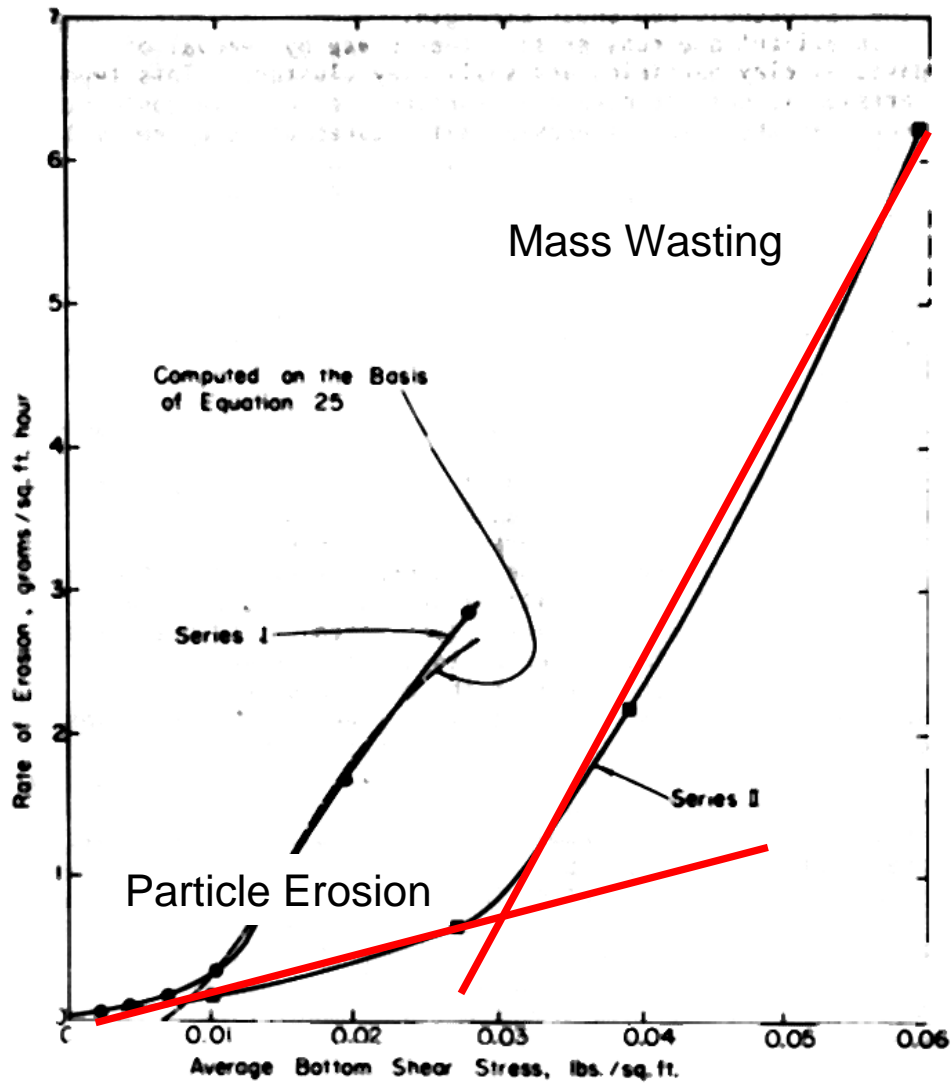
Figure 13-21. Shear stress - rate of erosion relationship from Partheniades (1965).

This equation essentially interpolates cohesive erosion between the lower and upper end of the particle erosion zone, based on an empirical, linear, user specified coefficient, the **Erodibility Coefficient (M)**.

Mass Erosion ($\tau_m < \tau$)

Beyond the mass erosion threshold, the cohesive algorithm extrapolates erosion rates from the maximum computed particle erosion rate, with a similar linear extrapolation, based on a new **Mass Erosion Erodibility Coefficient M$_{MW}$**.

More recent work on cohesive erodibility suggests that the erosion rate may be an exponential or polynomial function of shear. HEC-RAS approximates that with a piece-wise linear model.

Estimating Cohesive Thresholds and Rates

Applying the Partheniades method successfully requires estimating the shear thresholds and the erosion rates well. These parameters are site specific and can differ by five orders of magnitude between sites. Even within the same reach, τ_c, τ_{mw}, M, and M_{mw} can vary significantly between samples or at different depths. Therefore, the parameters can be determined experimentally (e.g. with a SEDFLUME apparatus) or are calibration parameters, adjusted to replicate measured bed change. These parameters cannot be estimated *a priori. Briaud et al.* (2001) summarize the situation well:

"Today, no widely accepted correlation could be found (between cohesive erodibility and bulk soil parameters) after extensive literature reviews. If a correlation is likely to exist on one hand, and if it has not been found after forty years of effort on the other hand, the correlation must be complex…Considering all the problems associated with correlations, a direct measurement with the (erodibility testing) is favored." Briaud *et al*. (2001) *Journal of Geotechnical and Geoenvironmental Engineering*

Others concur:
"With the vast number of factors involved in the determination of the erodibility of cohesive soils, it becomes necessary to test cohesive soils for critical shear stress for erosion and deposition rather than using soil properties for predicting threshold values or using methods similar to those for coarse sediments." Huang et al. (2006) Erosion and Sedimentation Manual

"Unfortunately, the erodibility of cohesive sediment cannot be predicted on the basis of environmental parameters. As a consequence, researchers have developed various test apparatus to empirically measure sediment erodibility." Ravens (2007) *ASCE Journal of Hydraulic Engineering*

The cohesive literature is full of pronouncements that these parameters must either be measured or calibrated including: Roberts et al. (1998), McNeil et al (1996), Jepsen et al., (1997), Hanson (1996), Julian and Torres (2006), Hansen and Simon (2001), Kapen et al. (2007), Sanford and Maa (2001). Therefore, HEC-RAS does not include default parameters.

In the absence of robust calibration data, the Parthenaides method requires experimental data for reliable results. The SEDFLUME is the most common apparatus used to measure the cohesive parameters, usually computing parameters from Shelby tube samples. This device pushes a core of the cohesive bed material through the bottom of the flume. The Corp's sediment lab in ERDC, and several universities, can perform these experiments. ERDC's has a portable SEDFLUME that can deploy to a project site, avoiding sample disturbance during transport.

CHAPTER 14

Performing a Dam Break Study with HEC-RAS

The development of any hydraulic model requires an accurate representation of the terrain data and the hydrologic inputs used as boundary conditions. Additionally, appropriate model parameters for terrain roughness and hydraulic structures must be estimated and then calibrated in order to have confidence in the model results. As these guidelines are focused on the development and use of unsteady flow models for dam break studies, discussions of basic data requirements, hydraulic parameter estimates, and model calibration/validation are not discussed. The HEC-RAS User's Manuals (HEC, 2015) contain information describing model input, data requirements, parameter estimation, and model calibration.

This section of the guidelines presents hydraulic modeling aspects that are unique to performing a dam break analysis. Topics include: inflow flood routing through a reservoir; estimating dam breach parameters; recommended approach; example application; and downstream routing/modeling issues.

Inflow Flood Routing a Through Reservoir

HEC-RAS can be used to route an inflowing flood hydrograph through a reservoir with any of the following three methods: one-dimensional (1D) unsteady flow routing (full Saint Venant equations); two-dimensional (2D) unsteady flow routing (Full Saint Venant equations or Diffusion wave equations); or with level pool routing. In general, full unsteady flow routing (1D or 2D) will be more accurate for both the with and without breach scenarios. This method can capture the water surface slope through the pool as the inflowing hydrograph arrives, as well as the change in water surface slope that occurs during a breach of the dam. Reservoirs with long narrow pools will exhibit greater water surface slope upstream of the dam than reservoirs that are wide and short. Therefore, the most accurate modeling technique to capture pool elevations and outflows of long narrow reservoirs is full dynamic wave (unsteady flow) routing. For wide and short reservoirs, level pool routing may be appropriate.

Several items must be taken into account before choosing the appropriate flood routing technique for a given study:

- In situations where the population at risk and any damage centers are far enough downstream, differences in peak outflow and the shape of the

breach hydrograph may not be significant by the time the flood wave reaches the downstream locations. Two hydrographs that have the same volume, but different peak flows and shape, will tend to converge as they are routed downstream through the river and floodplain. In this situation, the reservoir can be modeled with either full unsteady flow routing or level pool routing.

▪ The ability to acquire accurate cross section data through the pool can be problematic. Detailed bathymetric surveys may be required to accurately describe the elevation-volume relationship of the reservoir pool. If detailed bathymetric data are not available, and full unsteady-flow routing is still desired, cross section data can be modified to match the published elevation-volume curve of the reservoir pool. This can be accomplished by running a series of steady flow profiles from the dam to the upstream end of the pool, using a small flow and varying the downstream starting condition for different pool elevations. HEC-RAS will compute the volume under each profile. The elevation-volume curve computed by HEC-RAS can then be compared to the published curve. Start with the lowest elevations. If the computed volume does not match the published volume, the cross sections should be modified to increase or decrease the volume required. The Channel Design/Modification Editor in HEC-RAS may prove very useful for this task.

▪ Capturing the full reservoir volume upstream of the dam will require the modeler to extend cross sections far enough upstream, such that the invert elevation of the most upstream cross section is higher than the highest elevation that will be modeled in the dam during the largest event. Rough guidance would be to add a few feet to the top of the dam, and then extend the model upstream far enough so that the most upstream cross sections invert is higher than that elevation.

▪ If there are significant numbers of tributaries, or some large tributaries upstream of the dam that enter the pool directly, then storage volume due to backwater up the tributaries must be accounted for as well as their inflows. Tributaries can be modeled in several manners. One option is to model all of the significant tributaries as separate river reaches, using cross sections. A second option is to model the tributaries as storage areas, and connect those storage areas to the main pool with a lateral structure (weir). This will allow water to back up into the tributary as a

level pool of water, thus accounting for its volume. A third option is to extend the reservoir cross sections up the tributaries and define that portion of the reservoir cross section as an ineffective flow area.

The differences between level pool routing and full unsteady flow routing through a reservoir can be very difficult to quantify. In order to decide if level pool routing is adequate, it is helpful to estimate the potential error in the peak flow of the routed outflow hydrograph, due to the use of level pool routing. Dr. Danny Fread (National Weather Service) performed several numerical experiments in which he compared both full dynamic wave routing to level pool routing (Fread, 2006). From these experiments he developed a set of equations and a graph that can be used to estimate the error in using level pool routing for a given reservoir and flood event. The graph and equations are shown below in Figure 14-1 (Fread, 2006).
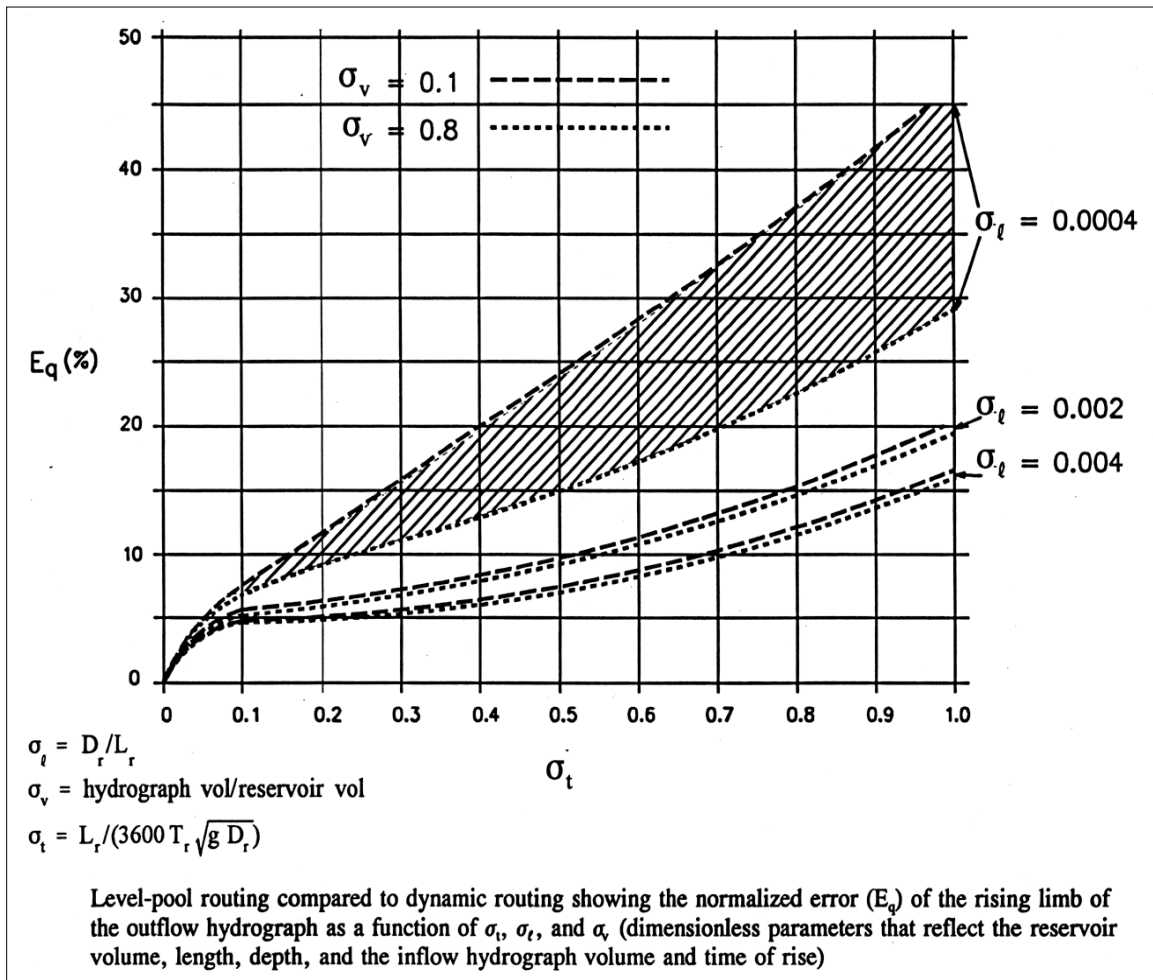
Figure 14-1. Error in level pool routing compared to full dynamic wave routing.

Where: D_r = the average depth of water in the reservoir (ft). Approximated as Dmax/2

   L_r = The length of the reservoir pool in feet

   T_r = The time of rise if the inflowing hydrograph in hours

In order to use Figure 14-1, the user must calculate σ_l, σ_v, and σ_t. Once these three parameters are calculated, a percent error in the rising limb/peak flow of the outflow hydrograph can be estimated. This error represents the difference in the answers between using level pool routing and full dynamic wave routing.

Full Dynamic Wave Routing

As discussed previously, full dynamic wave (unsteady flow) routing through the reservoir pool is the most accurate methodology and therefore should be performed for dam break analyses of Corps dams whenever practical. To model the reservoir using full dynamic wave routing with HEC-RAS, the user can either model the pool with 1D cross sections throughout the entire reservoir, as would be done for a normal river reach, or the reservoir pool could be modeled as a single 2D Flow Area. The dam is modeled with the Inline Structure option in HEC-RAS. An example plot of modeling the pool with 1D cross sections is shown in Figure 14-2.
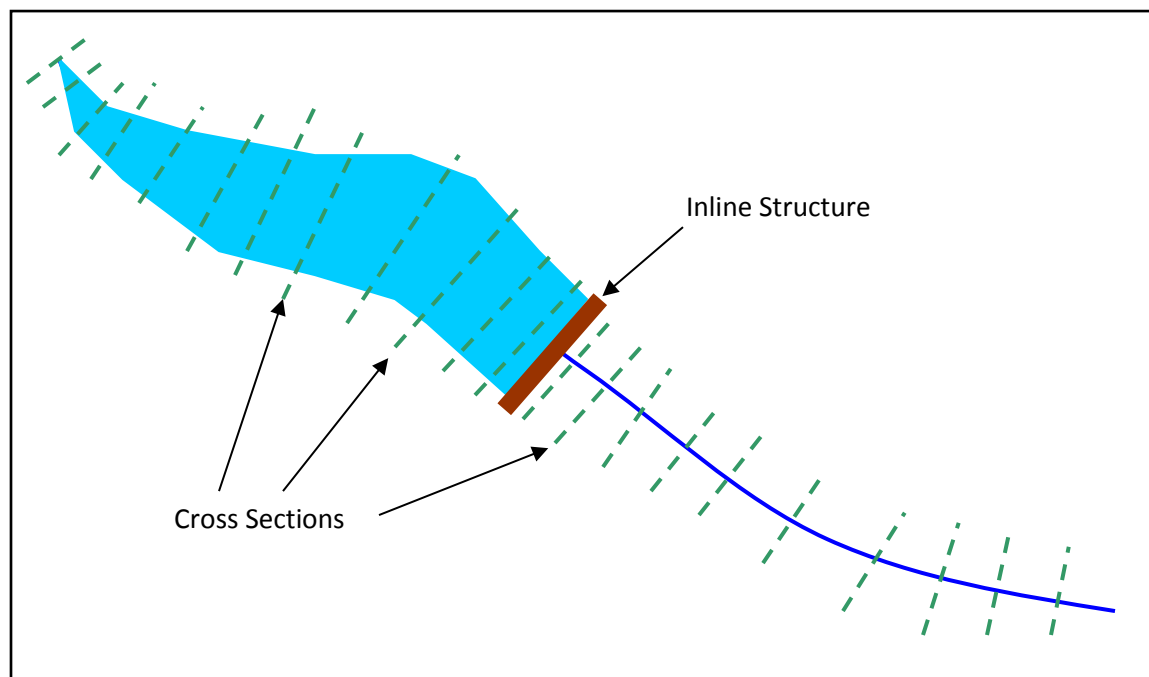
Figure 14-2. Cross section layout for full dynamic routing through a reservoir

The inflow hydrographs (computed with HEC-HMS) can be entered as boundary conditions at the upper most cross section (flow hydrograph), and at any of the cross sections within the reservoir pool (lateral inflow hydrographs).

When modeling the pool with cross sections, the engineer should be aware that after a dam breach occurs, the upper reach will no longer be fully inundated from the reservoir pool, thus acting more like a normal river reach. If the inflowing hydrograph recedes to a very low flow at the tail of the event, there could be some potential model instabilities resulting from the combination of a low flow and irregular channel geometry. One way around this is to increase the base flow on the recession of the upstream hydrographs. Another approach is to smooth out any major irregularities in the channel invert for the cross sections upstream of the dam. Sometimes, the combination of these two suggestions may be necessary to keep a stable solution above the dam for the tail end of the hydrograph.

If the reservoir pool is modeled with a 2D flow area, then the 2D cells can go completely dry without any model stability issues when they dry out.

Level Pool Routing

If it is not possible, necessary, or reasonable to perform full dynamic wave routing though the reservoir, or if the presumed difference between level pool routing and dynamic routing is small, then level pool routing can be performed with HEC-RAS. To model a reservoir using level pool routing in HEC-RAS, the pool area is modeled with a Storage Area (HEC-RAS option for modeling any area with level pool routing). That storage area is connected to a downstream river reach, and that river reach must have a cross section that is inside of the reservoir pool. The first cross section in the reach is tied to the storage area by the fact that they will always have the same water surface elevation during the computations. The dam is modeled as an inline structure, which requires one cross section upstream of the inline structure. However, the cross section upstream of the inline structure is tied to the inline structure boundary condition, and it cannot be the first cross section of the reach. Because of this limitation in HEC-RAS, the result is that the model must have two cross sections upstream of the inline structure: one cross section for the connection to the storage area, and the second cross section for the inline structure boundary condition. Both of the upstream cross sections should be representative of the reservoir area immediately upstream of the dam. The distance between these two cross sections should be short (10 to 20 ft), so that the storage volume between the two cross sections is small. An example diagram of modeling the reservoir with a storage area in HEC-RAS is shown in Figure 14-3.
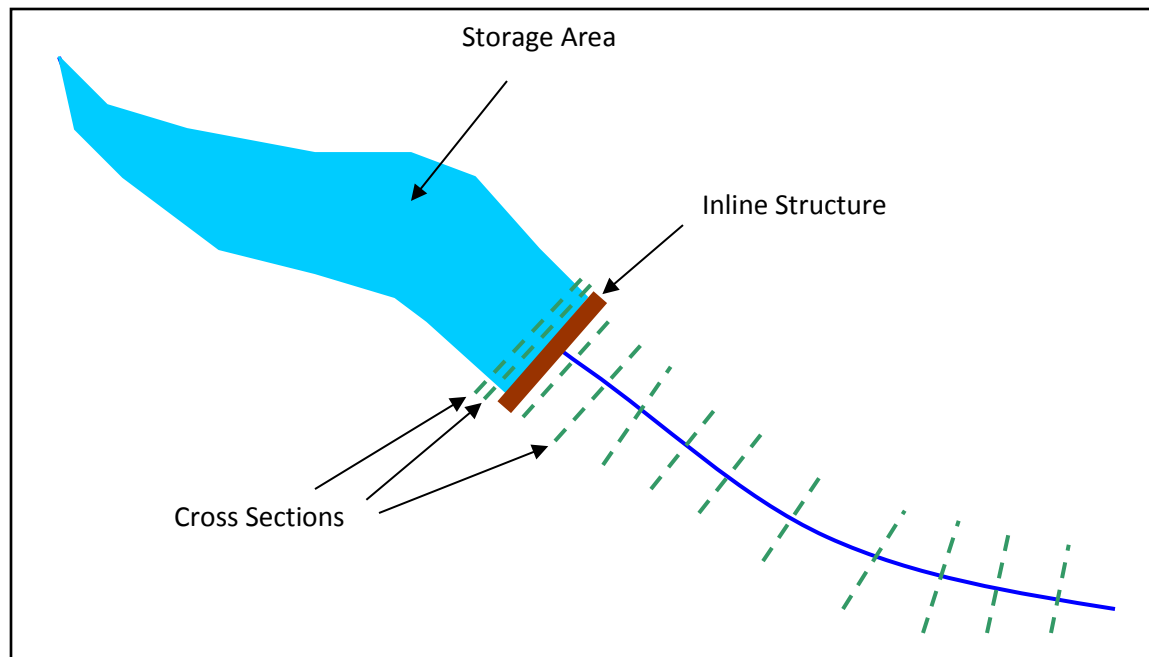
Figure 14-3. Storage area and cross section layout for level pool routing

The engineer must enter an elevation-volume curve as part of the storage-area data describing the reservoir. The minimum elevation of the two upstream cross sections should be roughly equal to the minimum elevation specified for the storage area in order to prevent any instability once the storage area is emptied.

When a dam break is modeled, the breach discharge will be computed by using the same equations as the full dynamic wave method. The only difference is that the water supplied to the dam will come from the storage area, and the storage area elevation will drop as a level pool as water flows out of the breach. As noted above, when a rapidly forming breach occurs, the water surface upstream of the dam will often have a significant slope to it. With the level pool routing method, the water surface in the reservoir is always horizontal. This may or may not produce significant differences in the outflow hydrograph, depending on many factors as outlined in this Section.

Estimating Dam Breach Parameters

The estimation of a dam breach location, dimensions, and development time are crucial in any assessment of the potential risk from a dam. This is especially true in a risk assessment where dams will be ranked based on the potential for loss of life and property damage. The breach parameters will directly affect the estimate of the peak flow coming out of the dam, as well as any possible warning time available to downstream locations. Unfortunately, the breach location, size, and formation time, are often the most uncertain pieces of information in a dam failure analysis.

When performing a dam breach analysis, one must first estimate the characteristics of the breach. Once the breaching characteristics are estimated, then HEC-RAS can be used to compute the outflow hydrograph from the breach and perform the downstream routing.

The breach dimensions and development time must be estimated for every failure scenario that will be evaluated. This requirement includes different failure modes as well as different hydrologic events. The breach parameters associated with a PMF hydrologic event will be greatly different than the breach parameters for a sunny day failure at a normal pool elevation. Therefore, for each combination of pool elevation (hydrologic event) and failure scenario, a corresponding set of breach parameters must be developed.

A dam's potential breach characteristics can be estimated in several ways, including: comparative analysis (comparing your dam to historical failures of dams of similar size, materials, and water volume); regression equations (equations developed from historical dam failures in order to estimate peak outflow or breach size and development time); and physically based computer models (computer programs that attempt to model the physical breaching process by using sediment transport/erosion equations, soil mechanics, and principles of hydraulics). All of these methods are viable techniques for estimating breach characteristics. However, each of these methods has strengths and weaknesses and should be considered as a way of "estimating" the parameters and not utilized as absolute values.

In addition to the methods described above, site specific information, structural, and geotechnical analyses should be used to refine and support the estimates of the breach parameters for each failure scenario/hydrologic event. Historic breach information, regression equations, and physically based computer models all have limitations that must be well understood when they are applied. In any dam safety study it is important to consider a range of parameter estimates for the breach size and development time for each failure scenario/event, and then perform a sensitivity analysis of the breach parameters to identify their effect on the outflow hydrograph, downstream stages and flows, and warning time to any population at risk.

This section of the manual will cover causes and types of dam failures; estimating breach parameters; recommended approach; and an example application.

As with many aspects of dam failure modeling in risk assessment studies, the level of effort in estimating breach parameters should be consistent with the type of risk assessment. In general, the level of effort and detail will increase from dams that are classified as Low Hazard dams, to dams that are classified as High Hazard dams.

Causes and Types of Dam Failures

Historically, all types of dams have experienced failures due to one or more types of event/loading. However, by far the majority of dam failures that have occurred have been earthen dams, caused by some level of flood. The types of dams that are commonly built and found in the field are:

- Earthen embankment/rockfill

- Concrete arch and multi arch

- Concrete gravity

- Buttress (combination of concrete gravity and arch dam)

- Steel, timber, and composite materials

There are many mechanisms that can be the driving force of a dam failure. The following is a list of mechanisms that can cause dam failures:

- Flood event

- Piping/seepage (internal and underneath the dam)

- Land slide

- Earthquake

- Foundation failure

- Equipment failure/malfunction (gates, etc…)

- Structural failure

- Upstream dam failure

- Rapid drawdown of pool

- Sabotage

- Planned removal

Given the different mechanisms that cause dam failures, there can be several possible ways a dam may fail for a given driving force/mechanism. Table 14-1 shows a list of dam types versus possible modes of failure (Costa, 1985, and Atallah, 2002).

Table 14-1. Possible failure modes for various dam types.

Failure Mode	Earthen/ Embankment	Concrete Gravity	Concrete Arch	Concrete Buttress	Concrete Multi-Arch
Overtopping	X	X	X	X	X
Piping/Seepage	X	X	X	X	X
Foundation Defects	X	X	X	X	X
Sliding	X	X		X	
Overturning		X	X		
Cracking	X	X	X	X	X
Equipment failure	X	X	X	X	X

Costa (1985) reports that of all dam failures as of 1985, 34% were caused by overtopping, 30% due to foundation defects, 28% from piping and seepage, and 8% from other modes of failure. Costa (1985) also reports that for earth/embankment dams only, 35% have failed due to overtopping, 38% from piping and seepage, 21% from foundation defects; and 6% from other failure modes.

Estimating Breach Parameters

The estimation of the breach location, size, and development time are crucial in order to make an accurate estimate of the outflow hydrographs and downstream inundation. However, these parameters are some of the most uncertain in the entire analysis. The HEC-RAS software requires the user to enter the following information to describe a dam breach:

Failure Location: centerline stationing of the breach in the dam

Failure Mode: overtopping or piping

Shape: bottom elevation, bottom width, left and right side slopes H:V

Time: critical breach development time

Trigger Mechanism: pool elevation, pool elevation + duration, or clock time

Weir and Piping Coefficients: weir coefficients are used to compute overtopping/weir flow, and an orifice coefficient is used to compute piping/pressure flow.

Failure Location: The breach failure location is based on many factors (type and shape of dam, failure type, mode, and driving force of the failure). In general, one should consider all factors about the dam, including any historical knowledge of seepage and foundation problems, and place the breach location in the most probable location for each failure type. The geotechnical engineer should be involved in determining the appropriate placement of the breach.

Failure Mode: While HEC-RAS hydraulic computations are limited to overtopping and piping failure modes, all of the other failure modes can still be simulated with one of these two methods. The failure mode is the mechanism for starting and growing the breach. Overtopping failures start at the top of the dam and grow to maximum extents, while a piping failure mode can start at any elevation/location and grow to the maximum extents. The ultimate breach size and breach formation time are much more critical in the estimation of the outflow hydrograph, than the actual failure initiation mode.

Critical Breach Development Time: HEC-RAS requires the user to enter what is called the "critical breach development time." The critical breach development time for HEC-RAS can be described as follows:

Overtopping Failure: The HEC-RAS breach start time is considered to be when the erosion process has migrated to the upstream face of the dam (this is the start of a breach for HEC-RAS). This is the point at which the outflow from the dam will start to increase due to the breach. This condition is depicted in Figures 14-4C through 4D below. The end of the breach development time for HEC-RAS is when the breach is fully formed and significant erosion has stopped (Figure 14-4E). The breach development ending time should not include the time to completely drain the reservoir pool.

Piping Failure: The HEC-RAS breach starting time for a piping failure is considered to be when a significant amount of flow and material are coming out of the piping failure hole. The breach ending time is considered to be when the breach is, for the most part, fully formed (significant erosion has stopped, not the time until the reservoir pool is emptied).

The estimation of the critical breach development time must be done outside of the HEC-RAS software and entered as input data. Descriptions on how to estimate this time are given below.

Breach Weir and Piping Flow Coefficients: Weir and piping coefficients must be entered by the user in HEC-RAS. These coefficients directly affect the magnitude of the peak outflow hydrograph for any given breach. Unfortunately, exact knowledge of the magnitude of these coefficients for a dam failure (overtopping or piping failure) is not known. In order to estimate the weir and piping flow coefficients, it is necessary to understand the basic failure process. The following is a generalized description of the breach process for an overtopping failure of an earthen dam. This description may not be true for all earthen dams, as the breach process is a function of many parameters, such as: height of the dam; volume of water behind the dam (including the inflowing hydrograph); materials that the dam is constructed of; depth and

duration of overtopping; outer protective cover on the downstream and upstream side of the embankment; etc…

In general, during an overtopping failure of an earthen dam, a headcut erosion process will first start on the downstream side of the dam embankment (Figure 14-4A). While water is going over the dam crest, the dam crest acts like a broad-crested weir. The headcut will erode back towards the center of the dam and widen over time (Figure 14-4B). As the headcut begins to cut into the dam crest, the weir crest length will become shorter, and the appropriate weir coefficient will trend towards a sharp-crested weir value (Figure 14-4C). The time for breach initiation used in HEC-RAS is shortly after what is depicted in Figure 14-4C. When the headcut reaches the upstream side of the dam crest, a mass failure of the upstream crest may occur, and the hydraulic control section will act very much like a sharp-crested weir (Figure 14-4D). The headcut will continue to erode upstream through the dam embankment, as well as erode down through the dam and widen at the same time (Figure 14-4E). During this process, the appropriate weir coefficient will begin to trend back towards a broad-crested weir coefficient. As the downward cut reaches the natural river bed elevation, and the breach is more in a widening phase, the appropriate weir coefficient is more in the range of a broad-crested weir value.
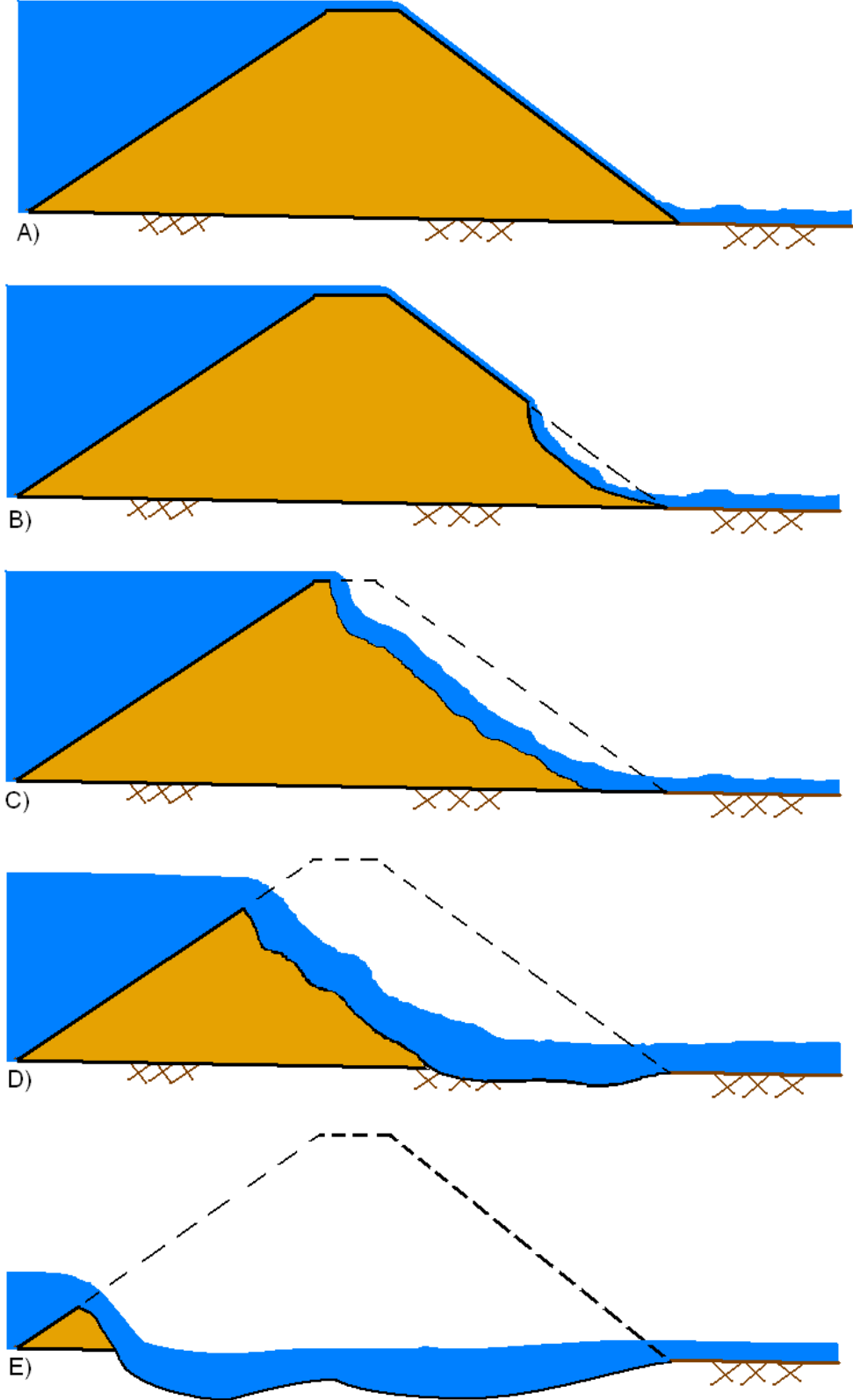
Figure 14-4. Example breach process for an overtopping failure

A general description of a piping failure is as follows. Water is seeping through the dam at a significant enough rate, such that it is internally eroding material and transporting it out of the dam. As the material is eroded, a larger hole is formed, thus able to carry more water and erode more material (Figure 14-5A). The movement of water through the dam during this process is modeled as a pressurized orifice type of flow. During the piping flow process, erosion and headcutting will begin to occur on the downstream side of the dam (Figure 14-5B) as a result of flow exiting the pipe. As the piping hole grows larger, material above the hole will begin to slough off and fall into the moving water (Figure 14-5C). The headcutting and material sloughing processes will continue to move back towards the upstream side of the dam, while the piping hole continues to grow simultaneously (Figure 14-5D). If the piping hole is large enough, the weight of the material above the hole may be too great to be maintained, and a mass caving of material will occur. This will result in a large rise in the outflow through the breach and will accelerate the breaching process. Also at this point, the hydraulics of the flow transitions from a pressure/orifice type flow to an open air weir type flow. The headcutting and erosion process then continues back through the dam, as well as downward (Figure 14-5E). Additionally, the breach will be widening. Depending on the volume of water behind the dam, the breach may continue to cut down and widen until the natural channel bed is reached. Then the breach will go into a widening phase.
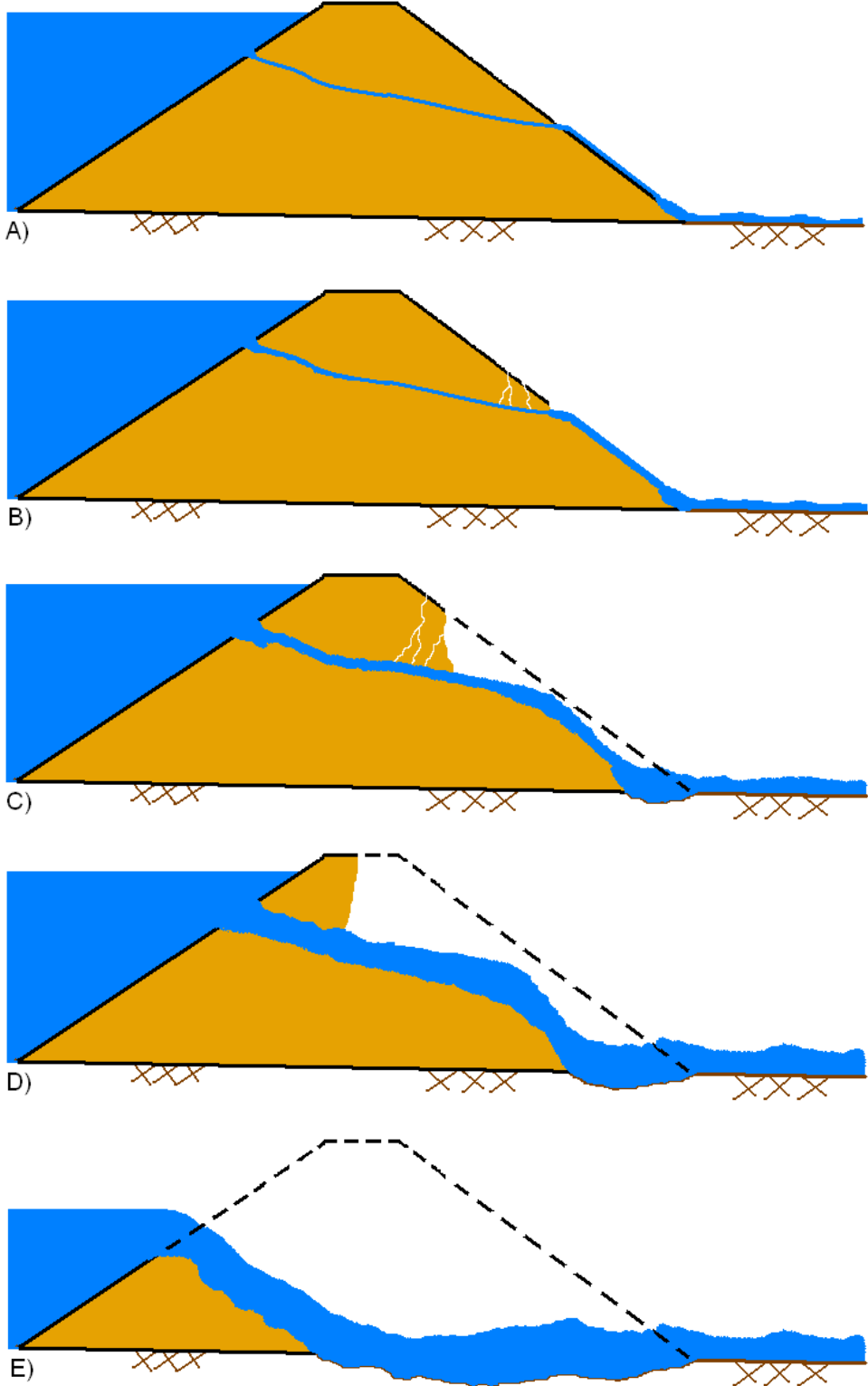
Figure 14-5. Example breach process for a piping failure

As you can imagine from the description of the breach processes described above, as well as other factors and complications that may occur in the real world, estimating these parameters can be difficult. Currently in computer programs such as HEC-RAS, the user is only allowed to enter a single value for the breach weir coefficient and for the piping coefficient. Because the estimate of the peak flow is so important in this process, one should try to estimate these coefficients based on the phase of the breach process in which they think the largest flows will most likely occur. For example, earthen dams with medium to very large storage volumes upstream, will most likely have failed all the way down to the natural stream bed elevation, and be in the breach widening phase when the peak outflow occurs. This would suggest using a weir coefficient that is typical of a broad-crested weir with a long crest length (i.e. C = 2.6). However, for dams with a relatively low volume of water in comparison to the height of the dam, the peak flow may occur during the phase of the breach in which the breach is still cutting down through the dam. For this case, a weir coefficient typical of a sharp-crested weir would be more appropriate (i.e. C = 3.2). Other factors to consider are the material types of the dam. Dams that have a clay core, and are generally constructed of clay material, will tend to have a much more pronounced headcut process. While dams that are more in the sand and gravel range will have a less pronounced headcut process. This may lead to using higher weir coefficients for a clay dam (i.e. C=3.2, sharp-crested weir) versus a gravel/sand dam (i.e. C=2.6, broad-crested weir).

During a piping failure breach, the rate of water flowing through the dam is modeled with an orifice pressure flow equation. This equation also requires a discharge coefficient, which is a measure of how efficiently the flow can get into the pipe orifice. Because a piping failure is not a hydraulically designed opening, it is assumed that the entrance is not very efficient. Recommended values for the piping/pressure flow coefficients are in the range of 0.5 to 0.6.

Guidelines for selecting breach weir and piping flow coefficients are provided in Table 14-2.

Table 14-2. Dam breach weir and piping coefficients

Dam Type	Overflow/Weir Coefficients	Piping/Pressure Flow Coefficients
Earthen Clay or Clay Core	2.6 – 3.3	0.5 – 0.6
Earthen Sand and gravel	2.6 – 3.0	0.5 – 0.6
Concrete Arch	3.1 – 3.3	0.5 – 0.6
Concrete Gravity	2.6 – 3.0	0.5 – 0.6

Breach Shape Definitions. For the purposes of these guidelines, the physical description of the breach will consist of the height of the breach, breach width, and side slopes in H:V. These values represent the maximum breach size. A diagram describing the breach is shown in Figure 14-6 below.
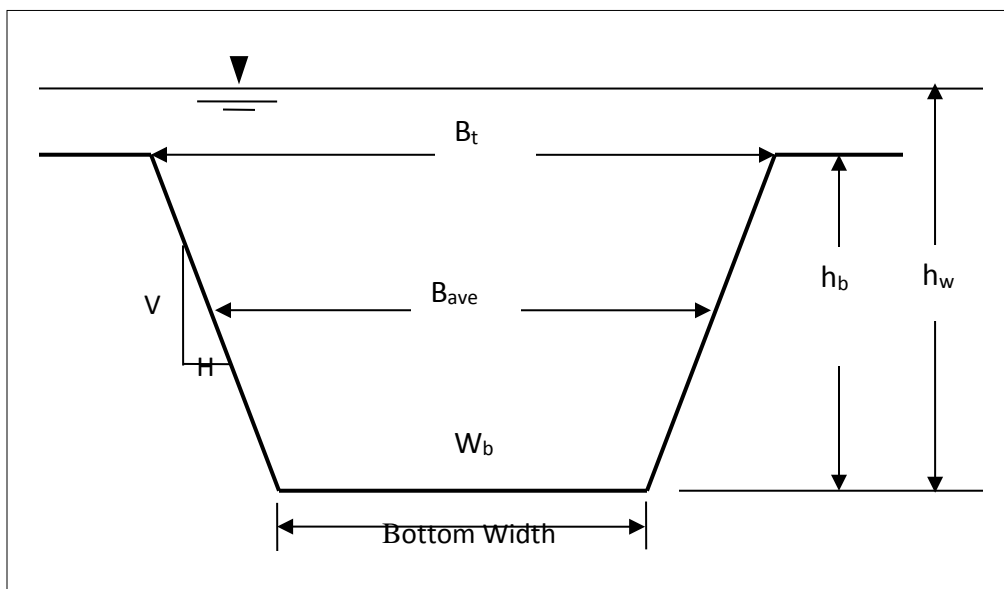
Figure 14-6. Description of the breach parameters

The breach width is described as the average breach width (B_{ave}) in many equations, while HEC-RAS requires the breach bottom width (W_b) for input. The breach height (h_b) is the vertical extent from the top of the dam to the average invert elevation of the breach. Many publications and equations also use the height of the water (h_w), which is the vertical extent from the maximum water surface to the invert elevation of the breach. The side slopes are expressed in units of distance horizontal to every one unit in the vertical (H: 1V).

The breach dimensions, as well as the breach formation time must be estimated outside of the HEC-RAS software, and entered into the program. Many case studies have been performed on data from historic dam failures, leading to guidelines, regression equations, and computer modeling methodologies for prediction of the dam breach size and time. One of the most comprehensive summaries of the literature on historic dam failures is a Bureau of Reclamation report written by Tony Wahl titled "Prediction of Embankment Dam Breach Parameters" (Wahl, 1998). This report discusses all types of dams, however it focuses on earthen/embankment dams for the discussion of estimating breach parameters. Much of what is presented in this section was extracted from that report. Guidelines for breach parameters for concrete (arch, gravity, buttress, etc), steel, timber, and other types of structures, are very sparse, and are limited to simple ranges.

Federal Agency Guidelines. Many federal agencies have published guidelines in the form of possible ranges of values for breach width, side slopes, and development time. Table 14-3 below summarizes some of these guidelines.

Table 14-3. Ranges of possible values for breach characteristics.

Dam Type	Average Breach Width B_{ave}	Horizontal Component of Breach Side Slope (H) H:1V	Failure Time t_f (hrs)	Agency
Earthen/ Rockfill	(0.5 to 3.0) x HD	0 to 1.0	0.5 to 4.0	COE 1980
	(1.0 to 5.0) x HD	0 to 1.0	0.1 to 1.0	FERC
	(2.0 to 5.0) x HD	0 to 1.0 (slightly larger)	0.1 to 1.0	NWS
	(0.5 to 5.0) x HD*	0 to 1.0	0.1 to 4.0*	COE 2007
Concrete Gravity	Multiple Monoliths	Vertical	0.1 to 0.5	COE 1980
	Usually ≤ 0.5 L	Vertical	0.1 to 0.3	FERC
	Usually ≤ 0.5 L	Vertical	0.1 to 0.2	NWS
	Multiple Monoliths	Vertical	0.1 to 0.5	COE 2007
Concrete Arch	Entire Dam	Valley wall slope	≤ 0.1	COE 1980
	Entire Dam	0 to valley walls	≤ 0.1	FERC
	(0.8 x L) to L	0 to valley walls	≤ 0.1	NWS
	(0.8 x L) to L	0 to valley walls	≤ 0.1	COE 2007
Slag/ Refuse	(0.8 x L) to L	1.0 to 2.0	0.1 to 0.3	FERC
	(0.8 x L) to L		≤ 0.1	NWS

Where: HD = Height of the Dam.

L   = Length of the Dam crest.

*Note: Dams that have very large volumes of water, and have long dam crest lengths, will continue to erode for long durations (i.e. as long as a significant amount of water is flowing through the breach), and may therefore have longer breach widths and times than what is shown in Table 14-3.

The guidelines shown in Table 14-3 should be used as minimum and maximum bounds for estimating breach parameters. More specific ways to estimate breach characteristics are addressed below.

Regression Equations. Several researchers have developed regression equations for the dimensions of the breach (width, side slopes, volume eroded, etc…), as well as the failure time. These equations were derived from data for earthen, earthen with impervious core (i.e. clay, concrete, etc…), and rockfill dams, and therefore do not directly apply to concrete dams or earthen dams with concrete cores. The report by Wahl (1998) describes several equations that can be used for estimating breach parameters. Summarized in Figure 14-7 are the regression equations developed to predict breach dimensions and failure time from the USBR report (Wahl, 1998).

Table 2. — Breach parameter relations based on dam-failure case studies.
For explanations of symbols see the *Notation* section at the end of this report.

Reference	Number of Case Studies	Relations Proposed (S.I. units, meters, m³/s, hours)
Johnson and Illes (1976)		$0.5h_d \leq B \leq 3h_d$ for earthfill dams
Singh and Snorrason (1982, 1984)	20	$2h_d \leq B \leq 5h_d$ $0.15 \text{ m} \leq d_{ovtop} \leq 0.61 \text{ m}$ $0.25 \text{ hr} \leq t_f \leq 1.0 \text{ hr}$
MacDonald and Langridge-Monopolis (1984)	42	Earthfill dams: $V_{er} = 0.0261(V_{out}*h_w)^{0.769}$ [best-fit] $t_f = 0.0179(V_{er})^{0.364}$ [upper envelope] Non-earthfill dams: $V_{er} = 0.00348(V_{out}*h_w)^{0.852}$ [best fit]
FERC (1987)		B is normally 2-4 times h_d B can range from 1-5 times h_d $Z = 0.25$ to 1.0 [engineered, compacted dams] $Z = 1$ to 2 [non-engineered, slag or refuse dams] $t_f = 0.1-1$ hours [engineered, compacted earth dam] $t_f = 0.1-0.5$ hours [non-engineered, poorly compacted]
Froehlich (1987)	43	$\overline{B}^* = 0.47K_o\left(S^*\right)^{0.25}$ $K_o = 1.4$ overtopping; 1.0 otherwise $Z = 0.75K_c\,(h_w^*)^{1.57}\,(\overline{W}^*)^{0.73}$ $K_c = 0.6$ with corewall; 1.0 without a corewall $t_f^* = 79(S^*)^{0.47}$
Reclamation (1988)		$B = (3)h_w$ $t_f = (0.011)B$
Singh and Scarlatos (1988)	52	Breach geometry and time of failure tendencies B_{top}/B_{bottom} averages 1.29
Von Thun and Gillette (1990)	57	B, Z, t_f guidance (see discussion)
Dewey and Gillette (1993)	57	Breach initiation model; B, Z, t_f guidance
Froehlich (1995b)	63	$\overline{B} = 0.1803K_o V_w^{0.32} h_b^{0.19}$ $t_f = 0.00254 V_w^{0.53} h_b^{(-0.90)}$ $K_o = 1.4$ for overtopping; 1.0 otherwise

Figure 14-7. Summary of regression equations for breach size and failure time (Wahl 1998).

Since the report by Wahl, additional regression equations have been developed to estimate breach width and breach development time. In general, several of the regression equations should be used to make estimates of the breach dimensions and failure time. These estimates should then be used to perform a sensitivity analysis, as discussed later in this chapter. The user should try to pick regression equations that were developed with data that is representative of the study dam. In many cases this may not be possible, due to the fact that most of the historic dam failures for earthen dams have occurred on smaller structures. In fact, out of the 108 historic dam breaches listed in the USBR report (Wahl, 1998), only 13 of the dams are over 100 ft (30.5 m) high and only 5 of the dams had a storage volume greater than 100,000 acre-feet ($123.4\text{x}10^6$ m^3) at the time of failure. Additionally, most of the regression equations were developed from a smaller subset of this data (20 to 50 dams), and the dams included in the analysis are a mixture of homogenous earthen dams and zoned earthen dams (dams with clay cores, or varying materials). Therefore, the use of any of the regression equations should be done with caution, especially when applying them to larger dams that are outside the range of data for which the equations were developed. The use of regression equations for situations outside of the range of the data they for which were developed for may lead to unrealistic breach dimensions and development times.

The following regression equations have been used for several dam safety studies found in the literature (except the Xu and Zhang equations, which are presented because of their wide range of historical data values), and are presented in greater detail in this chapter:

- Froehlich (1995a)

- Froehlich (2008)

- MacDonald and Langridge-Monopolis (1984)

- Von Thun and Gillette (1990)

- Xu and Zhang (2009)

These regression equations have been used on several dam break studies and have been found to give a reasonable range of values for earthen, zoned earthen, earthen with a core wall (i.e. clay), and rockfill dams. The following is a brief discussion of each equation set.

Froehlich (1995a):

Froehlich utilized 63 earthen, zoned earthen, earthen with a core wall (i.e. clay), and rockfill data sets to develop a set of equations to predict average breach width, side slopes, and failure time. The data that Froehlich used for his regression analysis had the following ranges:

Height of the dams: 3.66 – 92.96 m (12 – 305 ft) with 90% < 30 m, and 76% < 15 m

Volume of water at breach time: 0.0130 – 660.0 m^3 x 10^6 (11 - 535,000 acre-ft) with 87% < 25.0 m^3 x 10^6, and 76% < 15.0 m^3 x 10^6

Froehlich's regression equations for average breach width and failure time are:

$$B_{ave} = 0.1803\ K_o\ V_w^{0.32}\ h_b^{0.19}$$

$$t_f = 0.00254\ V_w^{0.53}\ h_b^{-0.90}$$

Where: B_{ave} =   Average breach width (m)

      K_o =   Constant (1.4 for overtopping failures, 1.0 for piping)

      V_w =   Reservoir volume at time of failure (m^3)

      h_b =   Height of the final breach (m)

      t_f =   Breach formation time (hrs).

Froehlich states that the average side slopes should be:

      1.4H:1V Overtopping failures

      0.9H:1V Otherwise (i.e. piping/seepage)

While not clearly stated in Froehlich's paper, the height of the breach is normally calculated by assuming the breach goes from the top of the dam all the way down to the natural ground elevation at the breach location.

Froehlich (2008):

In 2008 Dr. Froehlich updated his breach equations based on the addition of new data. Dr. Froehlich utilized 74 earthen, zoned earthen, earthen with a core wall (i.e. clay), and rockfill data sets to develop a set of equations to predict average breach width, side slopes, and failure time. The data that Froehlich used for his regression analysis had the following ranges:

Height of the dams: 3.05 – 92.96 m (10 – 305 ft) with 93% < 30 m, and 81% < 15 m

Volume of water at breach time: 0.0139 – 660.0 m^3 x 10^6 (11.3 - 535,000 acre-ft) with 86% < 25.0 m^3 x 10^6, and 82% < 15.0 m^3 x 10^6

Froehlich's regression equations for average breach width and failure time are:

$$B_{ave} = 0.27 \ K_o \ V_w^{0.32} \ h_b^{0.04}$$

$$t_f = 63.2 \sqrt{\frac{V_w}{gh_b^2}}$$

Where: B_{ave} =   Average Breach Width (m)

            K_o =   Constant (1.3 for overtopping failures, 1.0 for piping)

     V_w =   Reservoir volume at time of failure (m^3)

     h_b =   Height of the final breach (m)

     g   =   Gravitational acceleration (9.80665 m/s^2)

     t_f =   Breach formation time (Seconds).

Froehlich's 2008 paper states that the average side slopes should be:

     1.0 H:1V   Overtopping failures

     0.7 H:1V   Otherwise (i.e. piping/seepage)

While not clearly stated in Froehlich's paper, the height of the breach is normally calculated by assuming the breach goes from the top of the dam all the way down to the natural ground elevation at the breach location.

MacDonald and Langridge – Monopolis (1984):

MacDonald and Langridge-Monopolis utilized 42 data sets (predominantly earthfill, earthfill with a clay core, and rockfill) to develop a relationship for what they call the "Breach Formation Factor." The Breach Formation Factor is a product of the volume of water coming out of the dam and the height of water above the dam. They then related the breach formation factor to the volume of material eroded from the dam's embankment. The data that MacDonald and Langridge-Monopolis used for their regression analysis had the following ranges:

Height of the dams: 4.27 – 92.96 m (14 – 305 ft) with 76% < 30 m, and 57% < 15 m

Breach Outflow Volume: 0.0037 – 660.0 m^3 x 10^6 (3 - 535,000 acre-ft) with 79% < 25.0 m^3 x 10^6, and 69% < 15.0 m^3 x 10^6

The following is the MacDonald and Langridge-Monopolis equation for volume of material eroded and breach formation time, as reported by Wahl (1998):

For earthfill dams:

$$V_{eroded} = 0.0261 \left(V_{out} * h_w\right)^{0.769}$$

$$t_f = 0.0179 \left(V_{eroded}\right)^{0.364}$$

For earthfill with clay core or rockfill dams:

$$V_{eroded} = 0.00348 \left(V_{out} * h_w\right)^{0.852}$$

Where: V_{eroded} =   Volume of material eroded from the dam embankment (m^3)

V_{out} =   Volume of water that passes through the breach (m^3). i.e. storage volume at time of breach plus volume of inflow after breach begins, minus any spillway and gate flow after breach begins.

h_w =   Depth of water above the bottom of the breach (m).

t_f =   Breach formation time (hrs).

The V_{out} parameter is not exactly known before performing the breach analysis, as it is the volume of water that passes through the breach (not including flow from gates, spillways, and overtopping of the dam away from the breach area). A good first estimate is the volume of water in the reservoir at the time the breach initiates. Once a set of parameters are estimated, and a breach analysis is performed, the user should go back and try to make a better estimate of

the actual volume of water that passes through the breach. Then recalculate the parameters with that volume. The recalculation of the volume makes the method iterative. The actual breach dimensions are a function of the volume eroded. The MacDonald and Langridge-Monopolis paper states that the breach should be trapezoidal with side slopes of 0.5H:1V. The breach size is computed by assuming the breach erodes vertically to the bottom of the dam and it erodes horizontally until the maximum amount of material has been eroded or the abutments of the dam have been reached. The base width of the breach can be computed from the dam geometry with the following equation (State of Washington, 1992):

$$W_b = \frac{V_{eroded} - h_b^2 \, (CZ_b + h_b Z_b Z_3 / 3)}{h_b (C + h_b Z_3 / 2)}$$

Where:
W_b	=	Bottom width of the breach (m)
h_b	=	Height from the top of the dam to bottom of breach (m)
C	=	Crest width of the top of dam (m)
Z_3	=	$Z_1 + Z_2$
Z_1	=	Average slope (Z_1:1) of the upstream face of dam.
Z_2	=	Average slope (Z_2:1) of the upstream face of dam.
Z_b	=	Side slopes of the breach (Z_b:1), 0.5 for the MacDonald method.

Note: The MacDonald and Langridge-Monopolis paper states that the equation for the breach formation time is an envelope of the data from the earthfill dams. An envelope equation implies that the equation will tend to give high estimates (too long) of the actual breach time (for homogenous earthfill dams). Wahl's study states this method will over predict times in some cases, while many equations will under predict.

Von Thun and Gillette (1990):

Von Thun and Gillette used 57 dams from both the Froehlich (1987) paper and the MacDonald and Langridge-Monopolis (1984) paper to develop their methodology. The method proposes to use breach side slopes of 1.0H:1.0V, except for dams with cohesive soils, where side slopes

should be on the order of 0.5H:1V to 0.33H:1V. The data that Von Thun and Gillette used for their regression analysis had the following ranges:

Height of the dams: 3.66 – 92.96 m (12 – 305 ft) with 89% < 30 m, and 75% < 15 m

Volume of water at breach time: 0.027 – 660.0 m^3 x 10^6 (22 - 535,000 acre-ft) with 89% < 25.0 m^3 x 10^6, and 84% < 15.0 m^3 x 10^6

The Von Thun and Gillette equation for average breach width is:

$$B_{ave} = 2.5\ h_w + C_b$$

Where: B_{ave} = Average breach width (m)

h_w = Depth of water above the bottom of the breach (m)

C_b = Coefficient, which is a function of reservoir size, see table below.

Reservoir Size, m^3	C_b, meters	Reservoir Size, acre-feet	C_b, feet
< 1.23*10^6	6.1	< 1,000	20
1.23*10^6 - 6.17*10^6	18.3	1,000-5,000	60
6.17*10^6 - 1.23*10^7	42.7	5,000-10,000	140
> 1.23*10^7	54.9	>10,000	180

Von Thun and Gillette developed two different sets of equations for the breach development time. The first set of equations shows breach development time as a function of water depth above the breach bottom:

$$t_f = 0.02\ h_w + 0.25 \qquad \text{(erosion resistant)}$$

$$t_f = 0.015\ h_w \qquad \text{(easily erodible)}$$

Where: t_f = Breach formation time (hrs).

h_w = Depth of water above the bottom of the breach (m).

The second set of equations shows breach development time as a function of water depth above the bottom of the breach and average breach width:

$$t_f = \frac{B_{ave}}{4\,h_w} \qquad \text{(erosion resistant)}$$

$$t_f = \frac{B_{ave}}{4\,h_w + 61.0} \qquad \text{(easily erodible)}$$

Where: B_{ave} =   Average breach width (m)

Note that Von Thun and Gillette's breach formation time equations are presented for both "erosion resistant" and "easily erodible" dams. Their paper states: "It is suggested that these limits be viewed as upper and lower bounds corresponding respectively to well-constructed dams of erosion resistant materials and poorly-constructed dams of easily eroded materials".

Xu and Zhang (2009):

In 2009 a paper was published by Y. Xu and L.M. Zhang in the Journal of Geotechnical and Geo-Environmental Engineering.   The database gathered by Xu and Zang contained 182 earth and rockfill dams from the United States and China, with nearly 50% of the dams greater than 15 meters in height. However, their final equations are based on a much smaller subset of these dams due to missing data. Their paper shows details for 75 dams that were composed of homogeneous earth fill, zoned-filled, dams with core walls, and concrete faced dams. Their final equation for the average breach width is based on 45 dam failures, and their equation for the time of failure is based on only 28 dam failures.

The data that Xu and Zhang used for their regression analysis had the following ranges:

Height of the dams: 3.2 – 92.96 m (10 – 305 ft) with 78% < 30 m, and 58% < 15 m

Volume of water at breach time: 0.105 – 660.0 m^3 x 10^6 (11.3 - 535,000 acre-ft) with 80% < 25.0 m^3 x 10^6, and 67% < 15.0 m^3 x 10^6

Xu and Zhang's regression equation for average breach width is:

$$\frac{B_{ave}}{h_b} = 0.787 \left(\frac{h_d}{h_r} \right)^{0.133} \left(\frac{V_w^{1/3}}{h_w} \right)^{0.652} e^{B_3}$$

Where: B_{ave} =   Average breach width (m)

        V_w =   Reservoir volume at time of failure (m^3)

        h_b =   Height of the final breach (m)

        h_d =   Height of the dam (m)

        h_r =   15 meters, which is considered to be a reference height for distinguishing large dams from small dams.

        h_w =   Height of the water above the breach bottom elevation at time of breach (m).

        B_3 =   b3+b4+b5 Coefficient that is a function of dam properties.

        b_3 =   -0.041, 0.026, and -0.226 for dams with corewalls, concrete faced dams, and homogeneous/zoned-fill dams, respectively.

        b_4 =   0.149 and -0.389 for overtopping and seepage/piping, respectively.

b_5 =   0.291, -0.14, and -0.391 for high, medium, and low dam erodibility, respectively.

The Xu and Zhang paper does not provide estimates for side slopes directly. Instead, they provide an equation to estimate the Top Width of the breach, which can then be used with the average breach width, to compute the corresponding side slopes. Here is their equation for the breach top width:

$$\frac{B_t}{h_b} = 1.062 \left(\frac{h_d}{h_r}\right)^{0.092} \left(\frac{V_w^{1/3}}{h_w}\right)^{0.508} e^{B_2}$$

Where: B_t =   Breach top width (m)

B_2 =   b3+b4+b5 Coefficient that's is a function of Dam Properties

b_3 =   0.061, 0.088, and -0.089 for dams with corewalls, concrete faced dams, and homogeneous/zoned-fill dams, respectively.

b_4 =   0.299 and -0.239 for overtopping and seepage/piping, respectively.

b_5 =   0.411, -0.062, and -0.289 for high, medium, and low dam erodibility, respectively.

Breach side slopes can be computed with the following equation:

$$Z = \frac{B_t - B_w}{h_b}$$

Important Note: the data Xu and Zhang used in the development of the equation for breach development time includes more of the initial erosion period and post erosion period than what is generally used in HEC-RAS for the critical breach development time. In general, this equation will produce breach development times that are greater than the other four equations described above. Because of this fact, the Xu Zhang equation for breach development time should not be used in HEC-RAS. However, it is shown here for completeness of their method:

$$\frac{T_f}{T_r} = 0.304 \left(\frac{h_d}{h_r} \right)^{0.707} \left(\frac{V_w^{1/3}}{h_w} \right)^{1.228} e^{B_5}$$

Where: T_f =   Breach Formation time (hrs)

T_r =   1 hour (unit duration)

V_w =   Reservoir volume at time of failure (m^3)

h_d =   Height of the dam (m)

h_r =   15 meters, which is considered to be a reference height for distinguishing large dams from small dams.

h_w =   Height of the water above the breach bottom elevation at time of breach (m)

B_5 =   b3+b4+b5 Coefficient that is a function of dam properties

b_3 =   -0.327, -0.674, and -0.189 for dams with corewalls, concrete faced dams, and homogeneous/zoned-fill dams, respectively.

b_4 =   -0.579 and -0.611 for overtopping and seepage/piping, respectively.

b_5 =   -1.205, -0.564, and 0.579 for high, medium, and low dam erodibility, respectively.

While not clearly stated in the Xu and Zhang paper, the height of the breach is normally calculated by assuming the breach goes from the top of the dam all the way down to the natural ground elevation at the breach location.

Simplified Physical Breaching Method

The **Simplified Physical** breaching method allows the user to enter velocity versus breach down-cutting and breach widening relationships, which are then used dynamically to figure out the breach progression versus the actual velocity being computed through the breach, on a time step by time step basis. The main data requirement differences between this method and the **User Entered Data** breach method, are the following:

Max Possible Bottom Width – This field is now used to enter a maximum possible breach bottom width. This does not mean the entered value will be the final breach bottom width; it is really being used to limit the breach bottom width growth to this amount. The actual bottom width will be dependent on the velocity verses erosion rate data entered, and the hydraulics of flow through the breach. This field is used to prevent breaches from growing larger than this user set upper limit during the run.

Min Possible Bottom Elev – This field is used to put a limit on how far down the breach can erode during the breaching process. This value is not necessarily the final breach bottom elevation; it is a user entered limiter (i.e. the breach cannot go below this elevation). The final breach elevation will be dependent on the velocity verses erosion rate data entered, and the hydraulics of flow through the breach.

Starting Notch Width or Initial Piping Diameter – If the Overtopping Failure mode is selected, the user will be asked to enter a starting notch width. The software will use this width at the top of the dam to compute a velocity. From the velocity it will get a down cutting erosion rate (based on user entered data), which will be used to start the erosion process. If a Piping Failure mode is selected, the user must enter an initial piping diameter. Once the breach is triggered to start, this initial hole will show up immediately. A velocity will be computed through it, then the down cutting and widening process will begin based in user entered erosion rate data.

Mass Wasting Feature – This option allows the user to put a hole in the dam or the levee at the beginning of the breach, in a very short amount of time. This option would probably most often be used in a levee evaluation, in which a section of the levee may give way (Mass Wasting), then that initial hole would continue to erode and widen based on the erosion process. The required data for this option is a width for the mass wasting hole; duration in hours that this mass wasting occurs over (this would normally be a short amount of time); and the final bottom elevation of the initial mass wasting hole (It is assumed that the hole is open all the way to the top of the levee or dam if this option is used).

Velocity vs. Downcutting and Widening Erosion Rates. When using the **Simplified Physical** breaching option, the user is required to enter velocity versus downcutting erosion rates, as well as velocity versus erosion widening rates. An example of the required data input for this method is shown below in Figure 14-8.

14-8. *HEC-RAS Simplified Physical Breach Option*

As shown in Figure 14-8 above, the user is required to enter velocity versus downcutting erosion rates and velocity versus erosion widening rates. This data is often very difficult to come by. Users will need to consult with geotechnical engineers to come up with reasonable estimates of this data for their specific levee or dam. Another way to estimate this information is to try to derive it by simulating a historic levee or dam breach, and adjusting the velocity versus erosion rate data until the model simulates the correct breach width and time. This is obviously an iterative process, and may require the user to perform this at multiple locations to see if there is a consistent set of erosion rates that will provide a reasonable model for simulating levee breaches (or dams) in your geographical area.   We realize that this data is not readily available for any specific levee or dam. The hope is that over time we will be able to develop guidelines for these erosion rates based on analyzing historical levee and dam breaches. Additionally, users can try to back into a set of erosion rates in order to reproduce historic levee breaches in their area, then use these relationships to analyze potential future levee breaches.

Physically-Based Breach Computer Models. Several computer models have been developed that attempt to model the breach process using sediment transport theories, soil slope stability, and hydraulics. Wahl (1998) summarized some of these models in his report

"Prediction of Embankment Dam Breach Parameters." A table from Wahl's (1998) report, which summarizes the physically based computer models he reviewed is shown in Table 14-4 below.

Table 14-4. Physically-based embankment dam breach computer models.

Model and Year	Sediment Transport	Breach Morphology	Parameters	Other Features
Cristofano (1965)	Empirical formula	Constant breach width	Angle of repose, others	
Harris and Wagner (1967) BRDAM (Brown and Rogers, 1977)	Schoklitsch formula	Parabolic breach shape	Breach dimensions, sediment	
Lou (1981); Ponce and Tsivoglou (1981)	Meyer-Peter and Müller formula	Regime type relation	Critical shear stress, sediment	Tailwater effects
BREACH (Fread, 1988)	Meyer-Peter and Müller modified by Smart	Rectangular, triangular, or trapezoidal	Critical shear, sediment	Tailwater effects, dry slope stability
BEED (Singh and Scarlatos, 1985)	Einstein-Brown formula	Rectangular or trapezoidal	Sediment, others	Tailwater effects, saturated slope stability
FLOW SIM 1 and FLOW SIM 2 (Bodine, undated)	Linear predetermined erosion; Schoklitsch formula option	Rectangular, triangular, or trapezoidal	Breach dimensions, sediment	

In general, all of the models listed in Table 14-4 rely on the use of bed-load sediment transport equations, which were developed for riverine sediment transport processes. The use of these models should be viewed as an additional way of "estimating" the breach dimensions and breach development time.

Of all the models listed in Table 14-4, the BREACH model developed by Dr. Danny Fread (1988) has been used the most for estimating dam breach parameters. Dr. Fread's model can be used for constructed earthen dams as well as landslide formed dams. The model can handle forming breaches from either overtopping or piping/seepage failure modes. The software uses weir and orifice equations for the hydraulic computation of flow rates. The Meyer-Peter and Muller sediment transport equation is used to compute transport capacity of the breach flow. Breach enlargement is governed by the rate of erosion, as well as the collapse of material from slope failures. The software can handle up to three material layers (inner core, outer portion of the dam, and a thin layer along the downstream face). The material properties that must be described are: internal friction angle; cohesive strength, grain size of the material (D50), unit weight, porosity, ratio of D90 to D30, and Manning's *n*. This software has been tested on a limited number of data sets, but has produced reasonable results.

Additional research on the erosion process of earthen embankments that are overtopped is being conducted in the US as well as Europe. The Agricultural Research Service (ARS) has been testing earthen embankment failures at sizes ranging from small scale laboratory models to near prototype scale dams (up to 7 ft high) for several years (Hanson, et al. 2003, Hassan, et al. 2004). Similar tests have been performed in Norway for earthen dams, 5 to 6 meters high, constructed of rock, clay, and glacial moraine (Vaskinn, et al., 2004). The hope is that this research work will lead to the development of improved computer models of the breach process. A dam safety interest group made up of US Government agencies (USBR, ARS, USACE), private industry, and Canadian and European research partners is currently evaluating new technologies for simulating the breach process. The goal of this effort is to develop computer simulation programs that can model the dam breach process by progressive erosion for earthen dams initiated by either overtopping flow or seepage. Computer models that are currently being evaluated are: WINDAM (Temple, et. Al. 2006.); HR-BREACH (Mohammed et. Al., 2002. HR Wallingford); and FIREBIRD (Wang and Kahawita, 2006. Ecole Polytechnique de Montreal, Canada).   Table 14-5 below is a summary of these models capabilities (Tony L. Wahl, 2009):

Table 14-5. Summary of Erosion Process Models Currently Under Development.

Model and Year	Embankment Types	Failure Modes	Erosion Processes
WINDAM	Homogeneous with varying levels of cohesiveness	Overtopping	Headcut formation on downstream face, deepening, and upstream advancement; lateral widening
HR-BREACH	Homogeneous cohesive, or simple composite embankments with noncohesive zones, surface protection (grass or rock), and cohesive cores	Overtopping Piping	Variety of sediment transport/erosion equations and multiple methods of application. Discrete breach growth using bending, shear, sliding and overturning failure of soil masses.
FIREBIRD	Homogeneous cohesive or noncohesive	Overtopping	Coupled equations for hydraulics and sediment transport.

Peak Flow Equations and Envelope Curves. Several researchers have developed peak flow regression equations from historic dam failure data. The peak flow equations were derived from data for earthen, zoned earthen, earthen with impervious core (i.e. clay, concrete, etc…) and rockfill dams only, and do not apply to concrete dams. In general, the peak flow equations should be used for comparison purposes.

Once a breach hydrograph is computed from HEC-RAS, the computed peak flow from the models can be compared to these regression equations as a test for reasonableness. However, one should use great caution when comparing results from these equations to model predictions. First, the user should go back to the original paper for each equation and evaluate the data sets and assumptions that were used to develop that equation. Many of the equations were developed from limited data sets, and most were for smaller dams. Also, when using these equations to compare against model results, the event being studied can have a significant impact on the model result's peak flow. For example, studies being performed with Probable Maximum Flood (PMF) inflows may have larger computed peak outflows than what will be predicted by some of the peak flow equations. This is due to the fact that none of the historic data sets were experiencing a PMF level flood when they failed.

Shown below is a summary of some of the peak flow equations that have been developed from historic dam failures:

- Bureau of Reclamation (1982):
  $Q = 19.1(h_w)^{1.85}$ (envelope equation)

- MacDonald and Langridge-Monopolis (1984):
  $Q = 1.154(V_w h_w)^{0.412}$
  $Q = 3.85(V_w h_w)^{0.411}$ (envelope equation)

- Froehlich (1995b):
  $Q = 0.607 V_w^{0.295} h_w^{1.24}$

- Xu and Zhang (2009):

$$\frac{Q}{\sqrt{g V_w^{5/3}}} = 0.175 \left(\frac{h_d}{h_r}\right)^{0.199} \left(\frac{V_w^{1/3}}{h_w}\right)^{-1.274} e^{B_4}$$

- Kirkpatrick (1977):
  $Q = 1.268(h_w + 0.3)^{1.24}$

- SCS (1981):
  $Q = 16.6 h_w^{1.85}$

- Hagen (1982):
  $Q = 0.54(S\ h_d)^{0.5}$

- Singh and Snorrason (1984):
  $Q = 13.4(h_d)^{1.89}$
  $Q = 1.776(S)^{0.47}$

- Costa (1985):
  $Q = 1.122(S)^{0.57}$
  $Q = 0.981(S\ h_d)^{0.42}$
  $Q = 2.634(S\ h_d)^{0.44}$ (envelope equation)

- Evans (1986):
  $Q = 0.72 V_w^{0.53}$

- Walder and O'Connor (1997): Q estimated by computational and graphical method using relative erodibility of dam and volume of reservoir.

Note: All equations are in metric form.

Where: Q = Peak breach outflow (m^3/s)

  h_w = Depth of water above the breach invert at time of breach (m)

  V_w = Volume of water above breach invert at time of failure (m^3)

  S = Reservoir storage for water surface elevation at breach time (m^3)

  h_d = Height of dam (m)

  h_r = 15 meters, which is considered to be a reference height for distinguishing large dams from small dams.

  B_4 = b3+b4+b5 Coefficients that are a function of Dam Properties

  b_3 = -0.503, -0.591, and -0.649 for dams with corewalls, concrete faced dams, and homogeneous/zoned-fill dams, respectively.

  b_4 = -0.705 and -1.039 for overtopping and seepage/piping, respectively.

  b_5 = -0.007, -0.375, and -1.362 for high, medium, and low dam erodibility, respectively.

In addition to the peak flow equations, one can also compare computed model peak outflows to envelope curves of historic failures. One such curve is shown in Figure 14-9 (HEC, 1980).
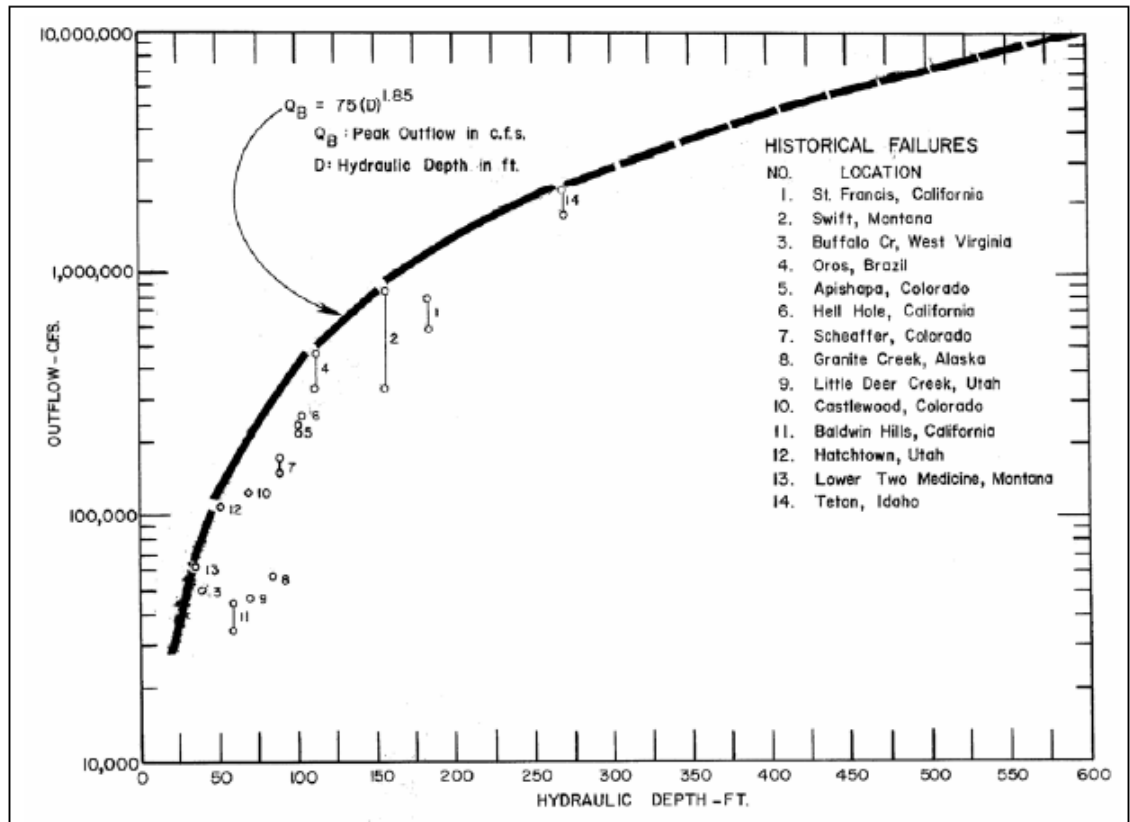
Figure 14-9. Envelope of experienced outflow rates from breached dams

When comparing computed results to the envelope curve shown in Figure 14-9, keep in mind that this envelope curve was developed from only 14 data sets, and may not be a true upper bound of peak flow versus hydraulic depth.

Site Specific Data and Engineering Analysis. Site specific information about the dam should always be collected and evaluated. Site specific information that may be useful in this type of analysis includes: materials/soil properties used in building the dam; whether or not the dam includes an impervious core/filter; material used for impervious core/filter; embankment protection materials (rock, concrete, grass, etc…); embankment slopes of the dam; historic seepage information; known foundation or abutment problems; known problems/issues with gates and spillways; etc…

Whenever possible a geotechnical analysis of the dam should be performed. Geotechnical evaluations can be useful in the selection of dam breach parameters. Specifically, geotechnical analyses can be used to estimate appropriate breach side slopes based on soil material properties. Additionally, a geotechnical analysis can be used to make a qualitative assessment of the breach parameters estimated by the various methods described above (historic comparisons, regression equations, and physically based model results).

Consideration of structural features such as spillway gates should also be considered for determination of the appropriate breach geometry for failure modes involving gate malfunction, blockage, or loss of the structure.

Recommended Approach

In general, several methods should be used to predict a range of breach sizes and failure times for each failure mode/hydrologic event. It is recommended that the modeler select several regression equations to estimate breach parameter values. Care must be taken when selecting regression equations, such that the equations are appropriate for the dam being investigated. Regression equations that have been used for earthen, zoned earth, earth with a clay core, and rockfill dams are: Froehlich (1995a), Froehlich (2008), MacDonald and Langridge-Monopolis (1984), Von Thun and Gillette (1990), and Xu and Zhang (2009). If the dam under investigation is outside the range of data used in the development of the regression equations, resulting breach parameter estimates should be scrutinized closely for reasonableness. **Note:** Never mix and match breach parameters from multiple regression equations. In other words, use the average breach width and time of failure from the same equation set. Do not use a breach width from one equation set and a time of failure from another. The breach widths and times are interrelated, as they are derived from a specific data set.

In addition to the regression equations, physically based computer models should also be utilized if appropriate for the level of study (NWS-BREACH, WinDAM, and HR-BREACH models are currently recommended). Whenever possible, geotechnical analyses of the dam should be used to assist in estimating the breach parameters (i.e. side slopes of the breach), or at least used as a qualitative assessment of the estimates. Additionally, breach parameter estimates should be compared to the government agency ranges provided in Table 14-3. If values are outside the recommended ranges, those estimates may need to be adjusted, unless there is compelling physical evidence that the values are appropriate. This will lead to a range of values for the breach size and failure times. A sensitivity analysis of breach parameters and times should be performed by running all of the parameter estimates within the HEC-RAS model.

Each set of breach parameters and failure times will produce a different outflow hydrograph. However, once these hydrographs are routed downstream, they will tend to converge towards each other. There are two main reasons for this convergence: (1) the total volume of water in each of the different hydrographs is basically the same (being the stored water behind the dam at the time of failure, plus whatever inflow occurs); (2) as the hydrographs move downstream, a sharp hydrograph will attenuate much more quickly than a flat hydrograph. Hydrographs from different assumed breach

parameters can converge to produce similar peak flow and stage in a surprisingly short distance. An example flow versus time plot from a study performed with HEC-RAS is shown in Figure 14-10. However these differences could be huge for Loss of Life calculations if a population at risk is immediately downstream of the dam.
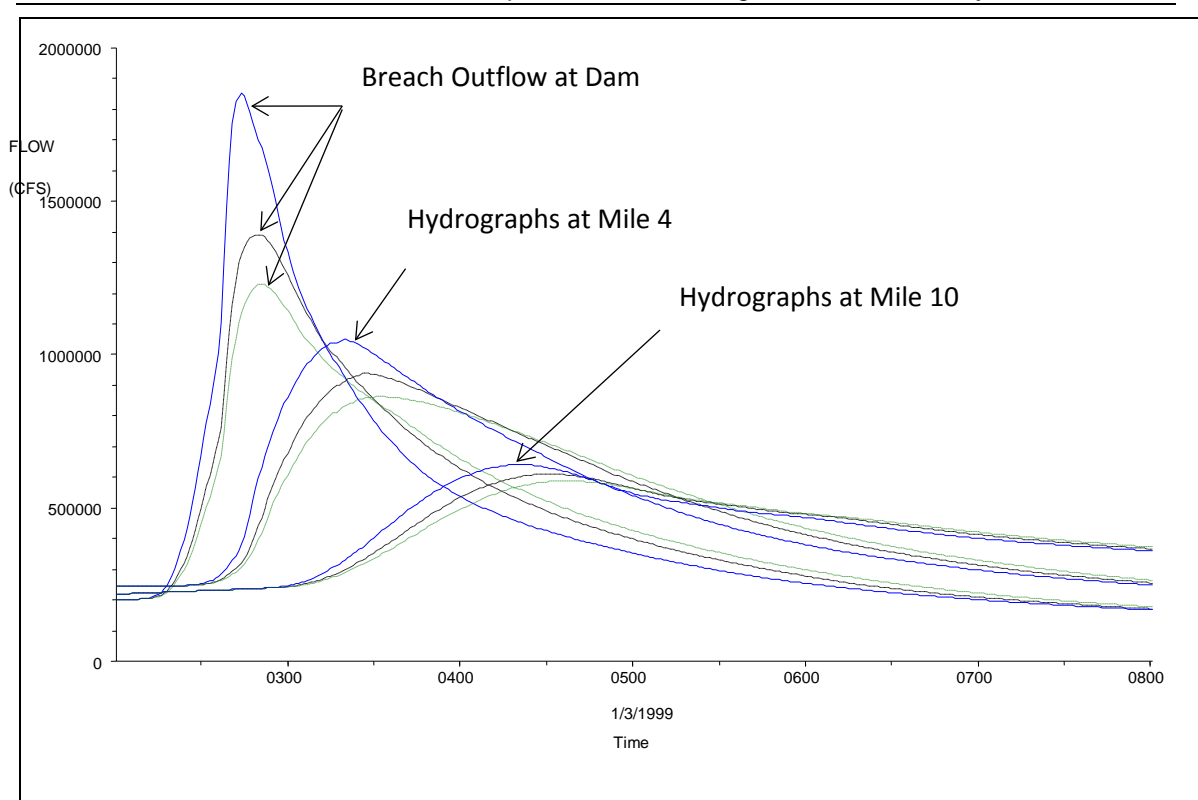
14-11. Dam break flood wave progression downstream

In the example shown in Figure 14-10, three different sets of breach parameters were used for the same model. The hydrographs coming out of the dam are very different in magnitude of peak flow, but they have the same volume of water. In this example, as the hydrographs move downstream they have substantially converged within four miles and are almost the same peak flow by mile 10. The rate at which the hydrographs will converge is dependent on many factors: steepness in the rise of the outflow hydrograph, volume of the outflow hydrograph, slope of the downstream reach, roughness of the downstream reach, available storage in the downstream floodplain, etc… The user will need to route all of the breach outflow hydrographs downstream through the entire study area in order to fully evaluate the affect of the breach parameters on the resulting flood hydrographs and inundation levels.

For a risk assessment study, the user must select the set of breach parameters that are considered to be most likely for each event/pool elevation. This will require engineering judgment. If all of the breach estimates, for a given event/pool elevation, end up converging to the same flow and stage before getting to any population at risk and potential damage areas, then the selection of a final set of breach parameters should not affect the computations and a simple mean value should be used. However, if the various sets of breach parameters produce significantly different flow and stage values at downstream locations (population at risk locations and potential damage zones), then engineering judgment will need to be used to pick a set of values that are considered most likely. Conservatively high or low values should not be used, as this will bias the overall results.

Once a final set of breach parameters is selected for a given event/failure mode, the computed peak outflow from the breach can be compared to some of the peak flow equations as a check of reasonableness. Keep in mind the limitations of the peak flow equations, as discussed in the Peak Flow Regression Equations section above.

Another check for reasonableness should be done by evaluating the breach flow and velocities through the breach, during the breach formation process. This can be accomplished by reviewing the detailed output for the inline structure (Dam) and reviewing the flow rate and velocities going through the breach. This output is provided on the HEC-RAS detailed output table for the Inline Structure. There are two things to check for here:

1) if the model reaches the full breach development time and size, and there are still very high flow rates and velocities going through the breach, then this is a sign that either your breach is too small, or your development time is to short (unless there are some physical constraints limiting the size of the breach).

2) if the flow rate and the velocities through the breach become very small before the breach has reached its full size and development time, then this is an indicator that your breach size may be too large, or your breach time may be too long. Additional factors affecting this could be your breach progression curve and the hydraulic coefficients (weir and piping) you used. When you get into the situation described above in either scenario 1 or 2, the breach size and development time should be re-evaluated to improve the estimates for that particular structure.

The level of effort in estimating breach parameters should be consistent with the type of risk assessment. In general, the level of effort and detail will increase from Type 1 (Low Hazard Potential) through Type 3 (High Hazard Potential). For Type 1 analyses a basic estimate of breach parameters consistent with the range of values in Table 14-3 could be appropriate. Type 2 (Significant Hazard Potential) and Type 3 analyses will typically require a greater level of detail and accuracy incorporating most if not all of the methods provided in this Section.

Example Application

In order to demonstrate how to estimate breach parameters, an example application for a fictitious dam is provided below. The event being evaluated in the example is a PMF scale event. This process for developing breach parameters needs to be performed for each failure mode/event (fully modeled hydrologic event or pool elevation for sunny day failures). The following is the necessary information required about a dam in order to develop breach parameter estimates as outlined in these guidelines.

Reservoir Data:

Important Pool Elevations	Elevation (m)	Volume (m³)
Stream Bed	1678.0	0.0
Multipurpose Pool	1692.1	15.81×10^6
Top of Flood Control	1710.0	151.64×10^6
Top of Dam	1720.9	327.01×10^6
PMF Max Water Surface	1722.26	357.98×10^6

Dam Embankment Data:

Crest Length:	4360 m
Crest Width:	9.15 m
Maximum Height above river bed:	42.9 m
Average Upstream Embankment slope:	3.3H:1V
Average Downstream Embankment slope:	3.3H:1V
Embankment Material:	Rolled earth, zoned
Embankment Core:	Impervious core, clay
Upstream slope Protection:	18" riprap
Downstream slope protection:	Topsoil and grass

Regression Equations:

For this example, the Froehlich (1995b), Froehlich (2008), MacDonald and Langridge-Monopolis (1984), Von Thun and Gillette (1990), and Xu Zhang (2009) regression equations for predicting breach size and development time were used. This dam is within the range of the data used to develop these regression equations, therefore the equations are considered to be an appropriate methodology for estimating the breach parameters. During the PMF event for this dam it is overtopped by 1.36 meters. The mode of failure for this example will be assumed as an overtopping failure. The failure location is assumed to be at the main channel centerline. The breach bottom elevation is assumed to be at an elevation of 1678 m (invert of the main channel). The water surface elevation at the initiation of the breach will be at an elevation of 1722.26 m (max pool for PMF event). The following are the calculations for each method.

Froehlich (1995a):

$$B_{ave} = 0.1803 \ K_o \ V_w^{0.32} \ h_b^{0.19}$$

$$B_{ave} = 0.1803 \ (1.4) \ (357.98 \times 10^6)^{0.32} \ (42.9)^{0.19}$$

B_{ave} = 281.5 m

$$t_f = 0.00254 \ V_w^{0.53} \ h_b^{-0.90}$$

$$t_f = 0.00254 \ (357.98 \times 10^6)^{0.53} \ (42.9)^{-0.90}$$

t_f = 2.95 hrs

The Froehlich (1995a) method assumes a side slope of 1.4H:1V for an overtopping breach. Given the breach height of 42.9 meters, this yields a bottom width for the breach of **W_b = 221.4 m**.

Froehlich (2008):

$$B_{ave} = 0.27 \ K_o \ V_w^{0.32} \ h_b^{0.04}$$

$$B_{ave} = 0.27 \ (1.3) \ (357.98 \times 10^6)^{0.32} \ (42.9)^{0.04}$$

B_{ave} = 222.76 m

$$t_f = 63.2 \ (\ V_w \ /(gh_b^2))^{0.5}$$

$$t_f = 63.2 \ (357.98 \times 10^6 \ /(9.80665 \times (42.9)^2))^{0.5}$$

t_f = 2.47 hrs

The Froehlich (2008) method assumes a side slope of 1.0H:1V for an overtopping breach. Given the breach height of 42.9 meters, this yields a bottom width for the breach of **W_b = 179.86 m**.

MacDonald and Langridge-Monopolis[*]:

The MacDonald and Langridge-Monopolis equation for an earthfill dam with a clay core is:

$$V_{eroded} = 0.00348 \ (V_{out} * h_w)^{0.852}$$

Since the outflow volume through the breach is unknown before performing the analysis, a good starting estimate is the volume of water in the dam at the peak stage of the event.

$$V_{eroded} = 0.00348 \ (357.98 \text{x} 10^6 * 44.26)^{0.852}$$

$$V_{eroded} = 1.70556 \text{x} 10^6 \ m^3 \text{ of material}$$

To compute the bottom width of the breach, the method says to use side slopes of 0.5H:1V. The user must also estimate an average side slope for both the upstream and downstream embankment of the dam. For this example average side slopes of 3.3H:1V were used for both upstream and downstream. Then using the bottom width equation (State of Washington, 1992):

$$W_b = \frac{V_{eroded} - h_b^2 \ (CZ_b + h_b Z_b Z_3 / 3)}{h_b (C + h_b Z_3 / 2)}$$

$$W_b = (1.70556 \text{x} 10^6 - 42.9^2(9.15*0.5 + 42.9*0.5*6.6/3))/(42.9(9.15 + 42.9*6.6/2))$$

W_b = 249.0 m

$t_f = 0.0179 \ (V_{eroded})^{0.364}$

$t_f = 0.0179 \ (1.70556 \text{x} 10^6)^{0.364}$

t_f = 3.32 hrs

*Note: Once an actual breach hydrograph is computed with the MacDonald and Langridge-Monopolis parameters, the volume of water coming out of the breach should be calculated, and the parameters should be re-estimated using that volume of water for V_{out}.

Von Thun and Gillette:

The Von Thun and Gillette equation for the breach average width is:

B_{ave} = 2.5 * h_w + C_b

B_{ave} = 2.5 * 44.26 + 54.9

B_{ave} = 165.6 m

Von Thun and Gillette suggest using breach side slopes of 0.5H:1V for earthen dams with a clay core. Given the dam height of 42.9 meter, the Breach bottom width will be **W_b = 144.2 m.**

Von Thun and Gillette show two equations for predicting the breach failure time. One equation is a function of the depth of water only, while the other is a function of depth of water and the computed average breach width. Both equations are used below.

t_f = 0.02 * h_w + 0.25 $\qquad\qquad$ t_f = B_{ave}/(4*h_w)

t_f = 0.02 * 44.26 + 0.25 $\qquad$ t_f = 166/(4*44.26)

t_f = 1.14 hrs $\qquad\qquad\qquad$ **t_f = 0.94 hrs**

Both of the Von Thun and Gillette equations yield similar answers for the breach time. Reviewing the Von Thun and Gillette paper showed that the data they used in their experiments were mostly earthen embankments with slightly cohesive materials. Given that the example dam we are studying has an engineered clay core, the longer time estimate is probably more appropriate. Therefore the selected failure time is **t_f = 1.14 hrs.**

Xu and Zhang (2009):

The Xu and Zhang equation for the breach average width is:

$$\frac{B_{ave}}{h_b} = 0.787 \left(\frac{h_d}{h_r} \right)^{0.133} \left(\frac{V_w^{1/3}}{h_w} \right)^{0.652} e^{B_3}$$

B_{ave} = (42.9)(0.787)(42.9/15)$^{0.133}$((357.98x10^6)$^{1/3}$/44.26)$^{0.652}$ e$^{-0.283}$

B_{ave} = 178.67 m

$$\frac{B_t}{h_b} = 1.062 \left(\frac{h_d}{h_r} \right)^{0.092} \left(\frac{V_w^{1/3}}{h_w} \right)^{0.508} e^{B_2}$$

$B_t = (42.9)(1.062)(42.9/15)^{0.092}((357.98\text{x}10^6)^{1/3}/44.26)^{0.508} \; e^{0.071}$

$B_t = 220.64$ m

Based on the computation of B_{ave} and B_t above, the breach bottom width for this method is **$W_b = 136.7$** and the side slopes are **Z = 0.98H:1V.**

The breach development time from the Xu and Zhang equation is as follows:

$$\frac{T_f}{T_r} = 0.304 \left(\frac{\text{h}_\text{d}}{\text{h}_\text{r}}\right)^{0.707} \left(\frac{V_w^{1/3}}{h_w}\right)^{1.228} e^{B_5}$$

$T_f = (1.0)(0.304)(42.9/15)^{0.707}((357.98\text{x}10^6)^{1/3}/44.26)^{1.228} \; e^{-0.327}$

$T_f = 13.92$ Hrs*

*Note: Please see note about the Xu Zhang method over estimating the breach time under the method description above.

Physically-Based Breach Computer Models:

For this example, Dr. Fread's NWS-BREACH model was the only physically based breach model run to make an estimate of breach parameters. The physical dimensions of the dam, the soil properties, and the hydrologic event data were entered into the BREACH model. The results from the BREACH model for this example are:

Breach Bottom Width W_b	**238 m**
Breach Side Slopes	**0.9H:1V**
Breach Failure Time t_f	**4.2 hrs**

Summary Results for Breach Parameters:

Shown in Table 14-6 is a summary of the breach parameters computed from the regression equations and the NWS-BREACH model.

Table 14-6. Summary of breach parameter estimates

Method	Breach Bottom Width (meters)	Breach Side Slopes (H:1V)	Breach Failure Time (hours)
Froehlich (1995a)	221.4	1.4	2.95
Froehlich (2008)	179.9	1.0	2.47
MacDonald and Langridge-Monopolis	249.0	0.5	3.32
Von Thun and Gillette	144.2	0.5	1.14
Xu and Zhang (2009)	136.7	0.98	13.92*
NWS-BREACH Computer Model	238	0.9	4.2

*Note: The data Xu and Zhang used in the development of their equation for breach development time includes more of the initial erosion period and post erosion period than what is generally used in HEC-RAS for the critical breach development time. In general, this equation will produce breach development times that are greater than the other four equations described above. Because of this fact, the Xu and Zhang equation for breach development time should not be used in HEC-RAS.

From here, all six sets of parameters should be entered into the HEC-RAS software and run as separate breach plans. This will result in six different breach outflow hydrographs. However,

once the hydrographs are routed downstream, they will begin to converge towards each other. The selection of a final set of breach parameters for this event should be based on guidance provided above in the "Recommended Approach" section of this document.

Downstream Flood Routing/Modeling Issues

The modeling of a dam break flood wave is one of the most difficult unsteady flow problems to solve. Previous discussions in this document have focused on modeling the reservoir pool, modeling the dam itself, and estimating breach parameters to be used in computing the breach outflow hydrograph. However, the most difficult part of performing a dam safety study is routing the dam break flood wave downstream.

Within HEC-RAS, the user can model the downstream area in the following manner: as a combination of 1D streams and storage areas; a combination of 1D streams, storage areas, and 2D flow areas; or as a single 2D flow area. There are many things that the hydraulic modeler must consider to get an accurate estimate of the downstream flood stages and flows. The following is a list of things that should be considered when developing an unsteady flow model for a dam break application. Most of these issues are concerns for 1D river reach modeling with cross sections.

- Cross Section Spacing and Hydraulic Properties
- Computational Time Step
- Manning's Roughness Coefficients
- Downstream Storage, Tributaries, and Levees
- Modeling Bridge and Culvert Crossings
- Modeling Steep Streams
- Drops in the Bed Profile
- Initial Conditions (Low Flow)
- Downstream Boundary Conditions

Cross Section Spacing and Hydraulic Properties

Cross-sectional cut lines should be created to capture the entire extent of flooding anticipated by the dam break scenario. As in any hydraulic modeling study, cross sections must be laid out to accurately describe the channel and floodplain geometry. Cross sections are laid out perpendicular to the anticipated flow lines of both the channel and the floodplain, during high flow conditions. There must be enough cross sections to describe the following: contractions and expansions of the channel and/or floodplain; changes in bed slope; changes in roughness; and significant changes in discharge. Cross sections also need to be added immediately upstream and downstream of: tributary inflow locations; dams and other inline structures (weirs, drop structures, or natural drops in the bed profile); bridge and culvert crossings; levees and other types of lateral hydraulic structures. An example of a cross section layout is shown in Figure 14-11 below.
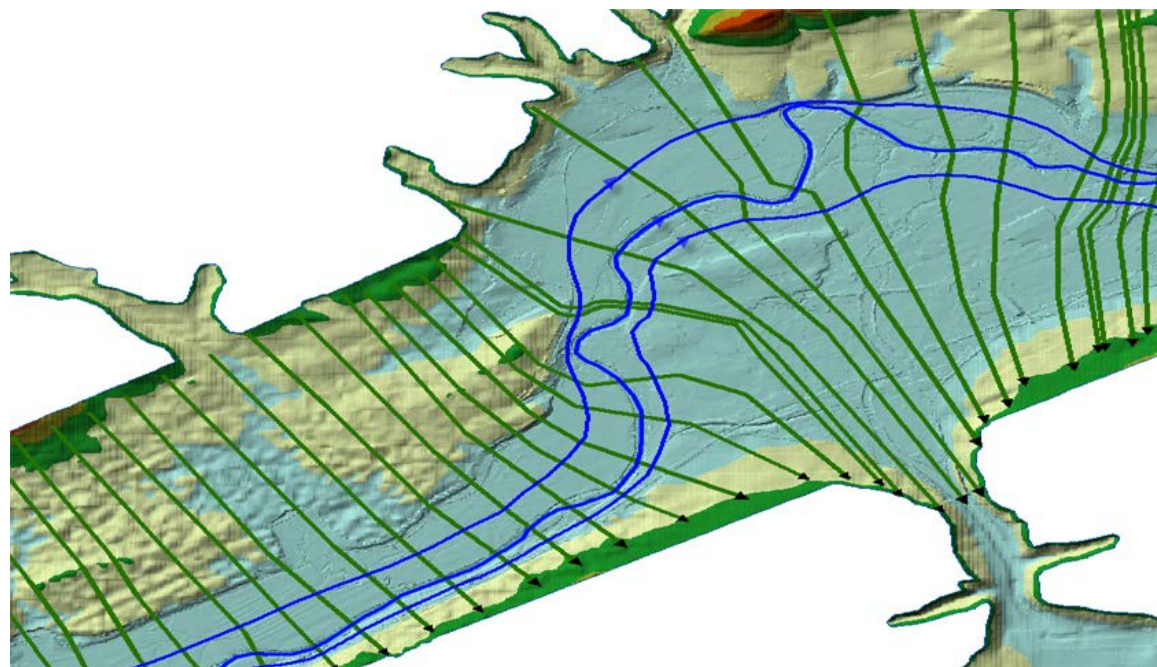
Figure 14-12. Example Cross Section Layout.

In addition to describing the physical changes and hydraulic structures within the channel and floodplain, there are also numerical considerations for adding or removing cross sections.

Cross Sections Spaced Too Far Apart. In general, cross sections spaced too far apart will cause additional numerical diffusion of the floodwave, due to the derivatives with respect to distance being averaged over too long of a distance. See an example of artificial numerical diffusion in Figure 14-12. Figure 14-12 shows an upstream inflow hydrograph and two downstream hydrographs after they have been routed through the river system. In this example, the channel is a rectangular channel on a constant slope, with a constant Manning's roughness. The only change in the example is the cross section spacing.

Additionally, when cross sections are spaced far apart, and the changes in hydraulic properties are great, the solution can become unstable.   Instability can occur when the distance between cross sections is so great that the Courant number becomes much greater than 1.0, and numerical errors grow to the point of the model becoming unstable. Another way to say this is that the cross section spacing is not commensurate with the hydrograph being routed and the computational time step being used (i.e. the cross section spacing is much further than the flood wave can travel within the computational time step being used).
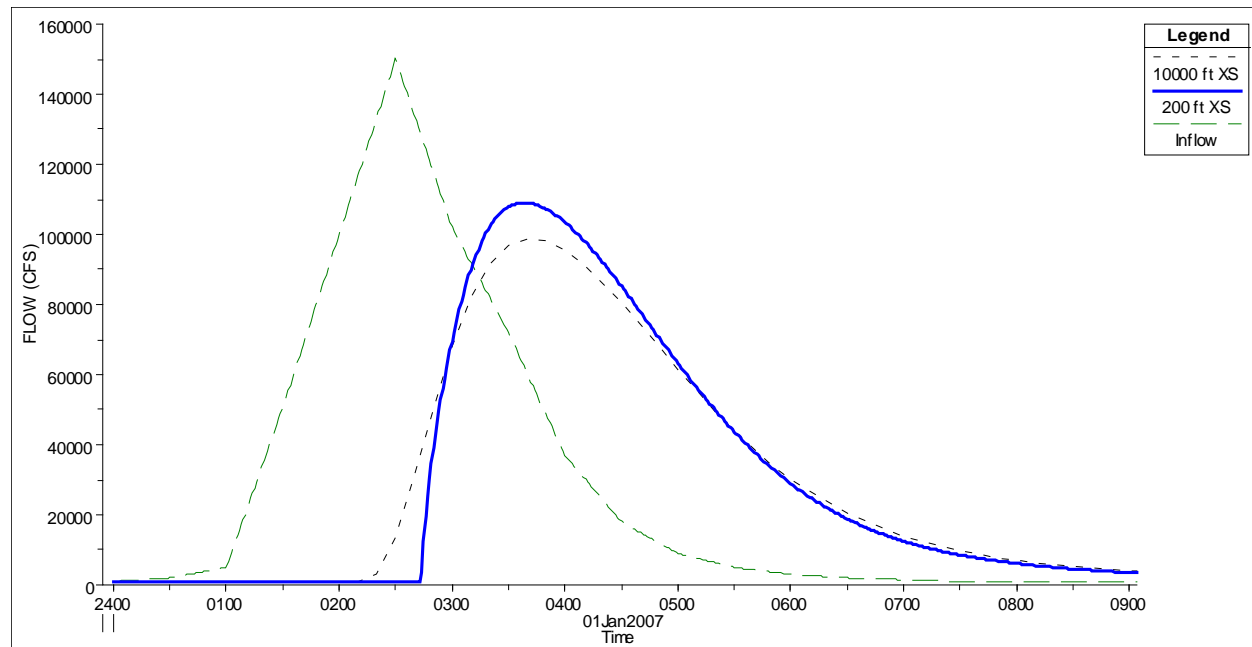
Figure 14-13. Numerical Error Due to Cross Section Spacing

Maximum Cross Section Spacing. A good starting point for estimating maximum cross section spacing are two empirically derived equations by Dr. Danny Fread (Fread, 1993) and P.G. Samuels (Samuels, 1989).   These two equations represent very different methods for coming up with spacing. The Samuels equation implies that smaller streams and steeper streams will require tighter cross section spacing. In general, the Samuels equation was derived for typical flood studies, in which the modeler is developing a steady state model for a typical floodplain study of the 2 yr through 100 yr events. For dambreak flood studies, the Samuels equation may be to strict, in that it requires much tighter cross section spacing than needed. Samuels' equation is as follows:

$$\Delta x \leq \frac{0.15D}{S_0}$$

Where: Δx =   the cross section spacing distance (ft)

       D =   the average main channel bankfull depth (ft)

       S_0 =   the bed slope (ft/ft)

Note: Samuels' equation was derived from data with slopes ranging from 2 - 50 ft/mi.

Dr. Fread's equation implies smaller streams and steeper hydrographs will require tighter cross sections. Fread's equation is one set of three conditions he presented in his paper for determining spacing. It is a theoretical derivation of spacing based on the inherent numerical

errors involved with linearizing the St. Venant equations into a four-point implicit finite-difference scheme. The other two involve a check of the change in cross sectional area from one cross section to the next, and the other accounts for changes in slope. Consequently, the spacing determined by Fread's equation may be too coarse, depending on the bed slope changes, the contraction and expansion characteristics and other non-linear data. Dr. Fread's equation is as follows:

$$\Delta x \le \frac{cT_r}{20}$$

Where: Δx   =   the cross section spacing distance (ft)

    C   =   the wave speed (ft/s)

T_r =   time of rise (from low flow to peak) of the hydrograph (seconds)

Samuels' and Dr. Fread's equations are rough estimates of cross section spacing - a good place to start. However, over time and practice, the modeler should be able to determine a good first estimate based on experience.

Cross Sections Too Close Together. If the cross sections are too close together, then the derivatives with respect to distance may be overestimated, especially on the rising side of the flood wave. This can cause the leading edge of the flood wave to over steepen, to the point at which the model may become unstable. An example of this is shown in Figure 14-13. In this example, the only change made to the model was that cross sections were interpolated at very short intervals (5 feet). If it is necessary to have cross sections at such short intervals, then much smaller time steps will need to be used in order for the numerical computations to solve the equations over such short distances. In general, for most dam break flood studies, cross sections should not be spaced at intervals closer than about 50 feet, unless you can use very small time steps (i.e. a few seconds or less). However, cross sections can be placed at closer distances at hydraulic structures, such as bridges/culverts, dams, and inline weirs, due to the fact that the model does not solve the unsteady flow equations through these structures. Rather it uses hydraulic equations specifically defined for those structures.
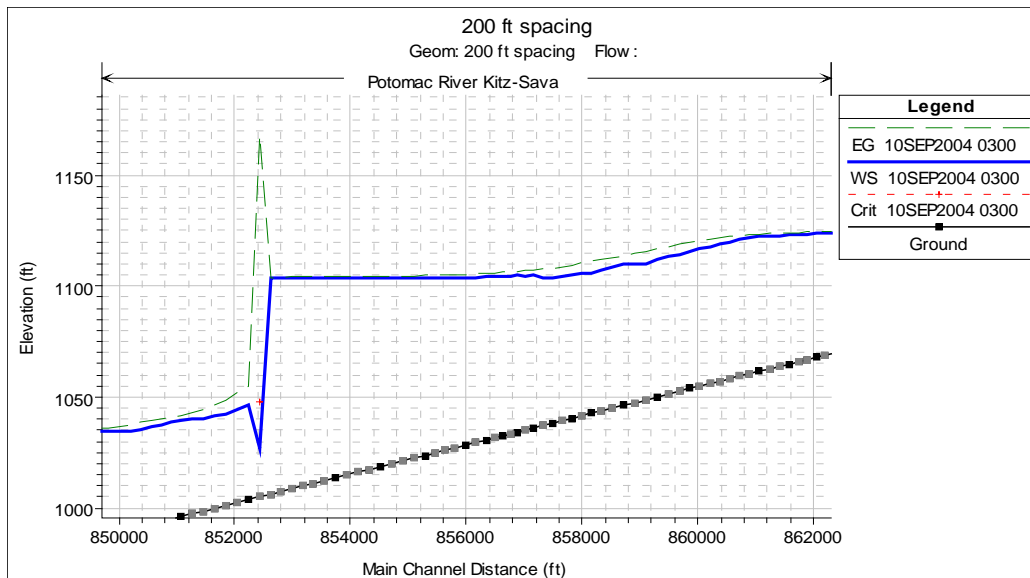
Figure 14-14. Example Model Instability due to Very Short Cross Section Spacing.

Computational Time Step

In the development of any unsteady flow model, stability and numerical accuracy can be improved by selecting a time step that satisfies the Courant condition. This is very important for a dam break model. Too large a time step will cause numerical diffusion (attenuation of the peak) and possibly model instability. Too small of a time step can lead to very long computation times, as well as possible model instability.

Too large of a time step: When the solution scheme solves the unsteady flow equations, derivatives are calculated with respect to distance and time. If the changes in hydraulic properties at a given cross section are changing rapidly with respect to time, too large of a time step may cause over estimation (too steep) of the time based derivatives, causing the calculations to become unstable. The solution to this problem in general is to decrease the time step. Even if the calculations do not go unstable, too large of a time step will cause numerical attenuation of the hydrograph that is not physically related. An example of a model with varying time steps is shown in Figure 14-14. In this example, all things in the model were exactly identical, except one run was done with a 1 minute time step (appropriate for this model), and the other was done with a 10 minute time step (too large for this model). As shown in Figure 14-13, the run with the 10 minute time step has a 10% lower peak flow, and the flood wave is much more spread out (diffused) than the run with the 1 minute time step.
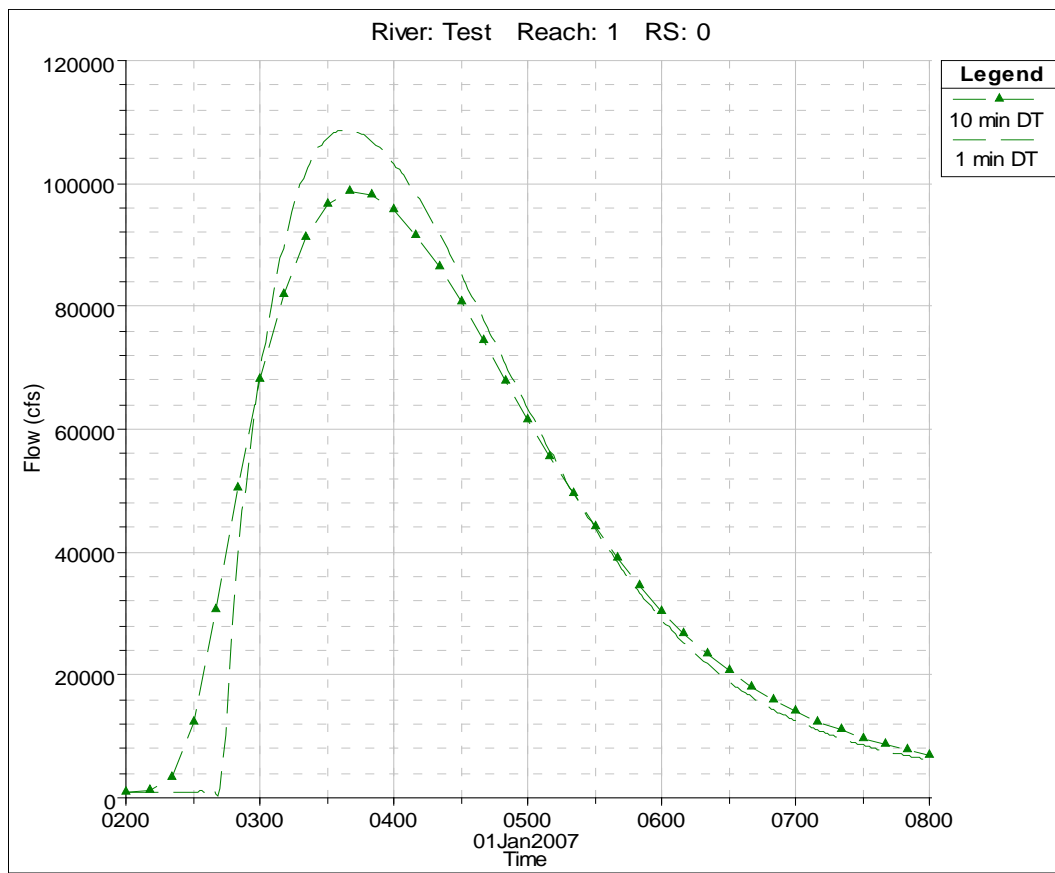
Figure 14-15. Example of Varying Computational Time Step.

Too Small of a Time Step. If a time step is selected that is much smaller than what the Courant Condition would suggest for a given flood wave, then model run times will be much longer than necessary, and this can also cause model stability problems. In general, a time step that is to small will cause the leading edge of the flood wave to steepen, possible to the point of oscillating and going unstable. Extremely small time steps (less than 0.1 seconds) can possibly cause round off errors when storing numbers in the computer, which in turn can lead to numerical errors which can grow over time.

Time Step Selection. As mentioned above, the best way to estimate a computational time step for HEC-RAS is to use the Courant Condition. This is especially important for dam break flood studies. The Courant Condition is the following:

$$C = \frac{V_w \, \Delta T}{\Delta X} \leq 1$$

and therefore, assuming a Courant number of 1 yields:

$$\Delta T \leq \frac{\Delta x}{V_w}$$

Where :C   =   Courant Number

ΔT   =   Time step in seconds

Δx   =   Distance step in feet

V_w =   Wave speed in ft/s

The flood wave speed is based on capturing the speed of the rising side of the flood wave as it propagates downstream. Flood wave speed is most accurately calculated in the area of the initial rise of the flood wave, where there is the largest change in discharge with respect to the change in cross sectional area (this is the leading edge of the dam break flood wave). The equation for calculating flood wave speed is:

$$V_w = \frac{dQ}{dA}$$

Where: V_w =   Flood wave speed in ft/s

dQ   =   The change in discharge over a short time interval ($Q_2 - Q_1$)

dA   =   The change in cross section area over a short time interval ($A_2 - A_1$)

Note: dQ/dA can be approximated by calculating the change in discharge and flow area at a single cross section over a single computational time step. This should be done while the flood wave's initial abrupt rise is occurring at that cross section.

For practical applications of the Courant Condition, the user can take maximum average velocity from HEC-RAS and multiply it by 1.5, to get a rough estimate of flood wave speed in natural cross sections.

For medium to large rivers the Courant Condition may yield time steps that are too restrictive (i.e. a larger time step could be used and still maintain accuracy and stability). A practical time step can be estimated as:

$$\Delta t \le \frac{Tr}{20}$$

However, treat this estimate as an upper limit. Remember that for dam break models, typical time steps are in the range of 1- 60 seconds due to the short time of rise and very fast flood wave velocities.

Manning's Roughness Coefficients

Roughness coefficients represent the resistance to flow in channels and floodplains. Roughness is usually presented in the form of a Manning's n value in HEC-RAS. There is extensive research and literature on methods to determine n values; however most of this work is representative of only main channels and not floodplains. Additionally, the literature on Manning's n values is for historically experienced floods, which are much lower than the flood resulting from a dam break. The actual selection of n values to be used for each dam assessment will require judgment by the engineer responsible for hydraulic model development.

A proper perspective is required before establishing a range of n values to be used in USACE risk assessment studies. The following general guidelines of factors that affect n value should be considered in developing representative values.

Base Surface Roughness: Base surface roughness is often represented by the size and shape of surface or channel and floodplain material that produces a friction effect on flow.

Stage and Discharge: The n value in most streams decreases with increase in stage and discharge. However, this is not always the case. If the channel bed is of lesser roughness than the channel banks, then the composite channel n values will increase with channel stage. Once the stage gets higher than the main channel banks, the roughness coefficient could begin to decrease. The main point here is that the variation of Manning's n with stage is site specific.

Obstructions: Objects constructed in the channel or in overbanks such as bridge piers or buildings can potentially cause increases in n value. It is especially difficult to estimate Manning's roughness coefficients to represent buildings in the floodplain, as there are many factors to consider: the area obstructed and the density of the buildings, direction of the flow in relation to the layout of the structures, roughness of all of the other boundaries, slope of the terrain, velocities of the flow, etc…

Irregularities: Irregularities are variations in cross-section size and shape along the floodplain. Irregularities are often caused by natural constrictions and expansions, sand deposition and scour holes, ridges, projecting points and depressions, and holes and humps on the channel bed. Gradual and uniform changes will generally not appreciably affect n value, whereas, areas that have lots of sharp channel irregularities will tend to have higher Manning's roughness coefficients.

Channel Alignment: Smooth curvature with large radius will generally not increase roughness values, whereas sharp curvature with severe meandering will increase the roughness.

Vegetation: Vegetation effects are dependent on height, density, distribution, and type of vegetation. Heavily treed areas can have a significant effect for dam failures. In general a lower average depth results in a higher n value. High velocities can potentially flatten the vegetation and result in lower n values.

Silting, Scouring, and Debris: Silting may change a very irregular channel into a comparatively uniform one and decrease n, and scouring may do the reverse. During a dam break flood wave, there will be a tremendous amount of scouring occurring, as well as lots of debris in the flow. The increased sediment load and debris will cause the flow to bulk up (increase in stage). One

way to account for this increased sediment load and debris is to increase the Manning's n values.

The resulting maximum water surface profile associated with the failure of a dam will often be much higher than any historically observed flood profile. In such cases, there is no historical based model data to calibrate to floods of this magnitude. It is therefore incumbent upon the engineer to determine reasonable roughness coefficients for flows and stages that will be higher than ever experienced. To gain a perspective on how each modeling parameter affects results, a bounding type sensitivity analysis can be performed regardless of the methods used to establish n values.

Historical regional knowledge of channels and floodplains should be used along with published guidelines in establishing a base level set of n values.   Guidelines for establishing base level Manning's n values can be found in Chapter 3 of this manual. The base level n values should be adjusted up or down based on factors addressed previously. Calibration to the largest historical events of record should be done whenever possible. Once adjusted roughness coefficients are established, uncertainty analyses should be performed by varying all values (two additional computational runs) by plus or minus 20%. In general, channel n values for risk assessment may be in the range of 0.025 to 0.075. The overbank n values may range between 0.05 and 0.15. Note that higher n values can be used in areas to allow for storage embayments with little to no conveyance.

Manning's n Values Immediately below Dam. Significant turbulence, sediment load and debris should be expected for the immediate reach downstream of a failed dam.   This is obvious when viewing the photo of the Teton Dam failure shown in Figure 14-15. Because HEC-RAS does not directly account for high volumes of sediment in the flow, and the extreme turbulence in the water surface caused by the breach, it is often a good idea to increase the Manning's n values just downstream of the dam. The increased sediment and turbulence will cause higher water surfaces to occur.   The only way to mimic this is by increasing the roughness coefficients. Proper modification and variation of n values is one of the many uncertainties in dam failure modeling. An accurate assessment can be confidently attained only after previous knowledge of a particular dam failure event. A reasonable modeling approach may be to assume double the normal n value directly downstream of the dam and transition to normal roughness coefficients where failure induced turbulence, sediment load, and debris transport are expected to recede.

Figure 14-16. Significant Turbulence and Sediment load during the Teton Dam Failure

Roughness Coefficients for Steep Streams. Many dams are located in mountainous regions, where the slopes of the stream are significantly steep. It is very common to underestimate Manning's n values for steep terrain. Underestimation of the roughness coefficients can cause water surface elevations to be too low, increased velocities, and possibly even supercritical flow. In addition to this, abrupt changes in n values or underestimation of n values can cause the model to go unstable. Dr. Robert Jarrett (Jarrett, 1984) collected some extensive field data on steep streams (slopes greater than 0.002 ft/ft) in the Rocky Mountains. Dr. Jarrett measured cross sectional shape, flow rates, and water surface elevations at 21 locations for a total of 75 events. From this data he performed a regression analysis and developed an equation to estimate the Manning's roughness coefficient of the main channel. Here is his equation:

$$n = 0.39 S^{0.38} R^{-0.16}$$

Where: n = Manning's roughness coefficient of the main channel

S = Energy Slope (slope of the energy grade line, ft/ft)

R = Hydraulic Radius of the main channel (ft).

While Dr. Jarrett's equation is not necessarily applicable to all locations, it is often a useful check for reasonableness of the Manning's n values in steep terrain.

Downstream Storage, Tributaries, and Levees

Accounting for downstream storage in the floodplain below the dam is crucial in order to get a reasonable estimate of the flood wave propagation and attenuation as it moves downstream.

General floodplain storage (areas that get wet but have little to no velocity) can often be modeled as part of the normal cross section by using ineffective flow areas. If a portion of a cross section is wet, but it will have a very low velocity, using a high Manning's n values is another approach to modeling that area of the cross section.

Modeling Tributaries. Tributaries that come into the main river downstream may have flow reversals during the passing of the flood wave. Significant size tributaries need to be accounted for, since they may represent a large amount of storage volume taken out of the flood wave. Further, the resultant inundation maps will need to include the flooding extent up the tributaries. These factors require scrutiny when developing geometric data for HEC-RAS and can be addressed in four different ways when laying out data for tributaries. A tributary may be modeled using: (1) a separate river reach, (2) a 2D flow area, (3) a storage area, or (4) an extension of the main river cross sections.

The most comprehensive way to model the effects of a tributary to the main river is to model the tributary with cross sections or a 2D flow area. If the computed water surface along the tributary results in a sloped water surface, then modeling the tributary as a separate river reach is the preferred modeling method. Tributaries that have significant inflows to the overall flood hydrograph are strong candidates to be modeled as separate 1D reaches, or part of a 2D flow area that is being used to model the downstream area.

When adding a tributary to the main stem of a river, it is important to differentiate between the contributing area of the main stem cross sections versus the contributing area of the tributary cross sections. At the stream junction, if flow from the two reaches will mix, a decision will need to be made as to the line that represents the separation point of the tributary and the main stem flows. Cross sections from one reach should end just where the cross sections of the other reach begin, to insure complete inundation mapping. Cross sections should not overlap. Figure

14-16 depicts a tributary included in the model as a separate reach. As shown in Figure 14-16, the user must identify the point at which to end the main stem cross sections and begin the tributary cross sections.
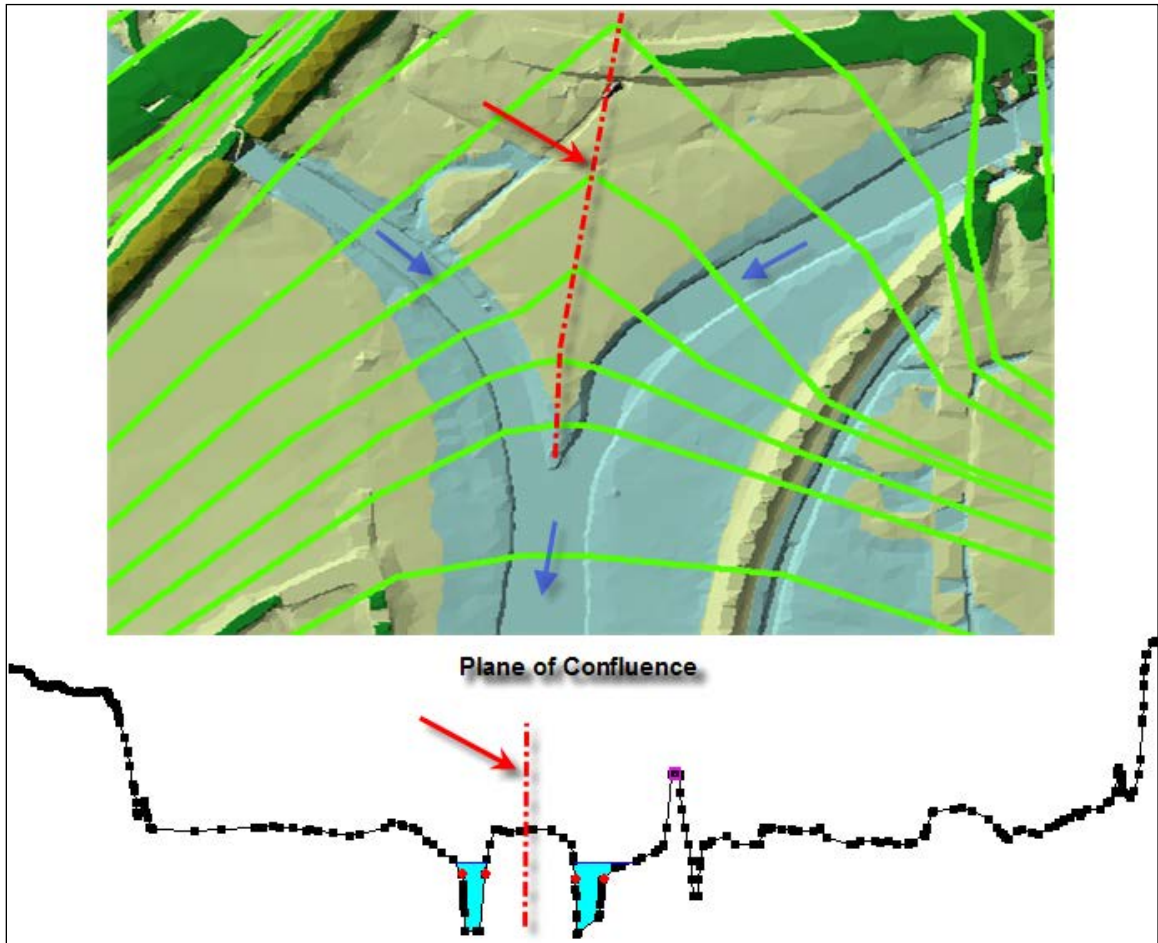
Figure 14-17. Cross section layout for a tributary coming into a main stem river.

The next best option for accounting for tributary storage, is to model the tributary as a storage area, and connect the storage area to the main river with a lateral structure. The lateral structure can be a weir, in which the weir geometry is represented with a cross section from the tributary. This will allow water from the flood wave to back up and fill the storage area as a level pool of water. An example of modeling tributaries with storage areas and lateral structures is shown in Figure 14-17.
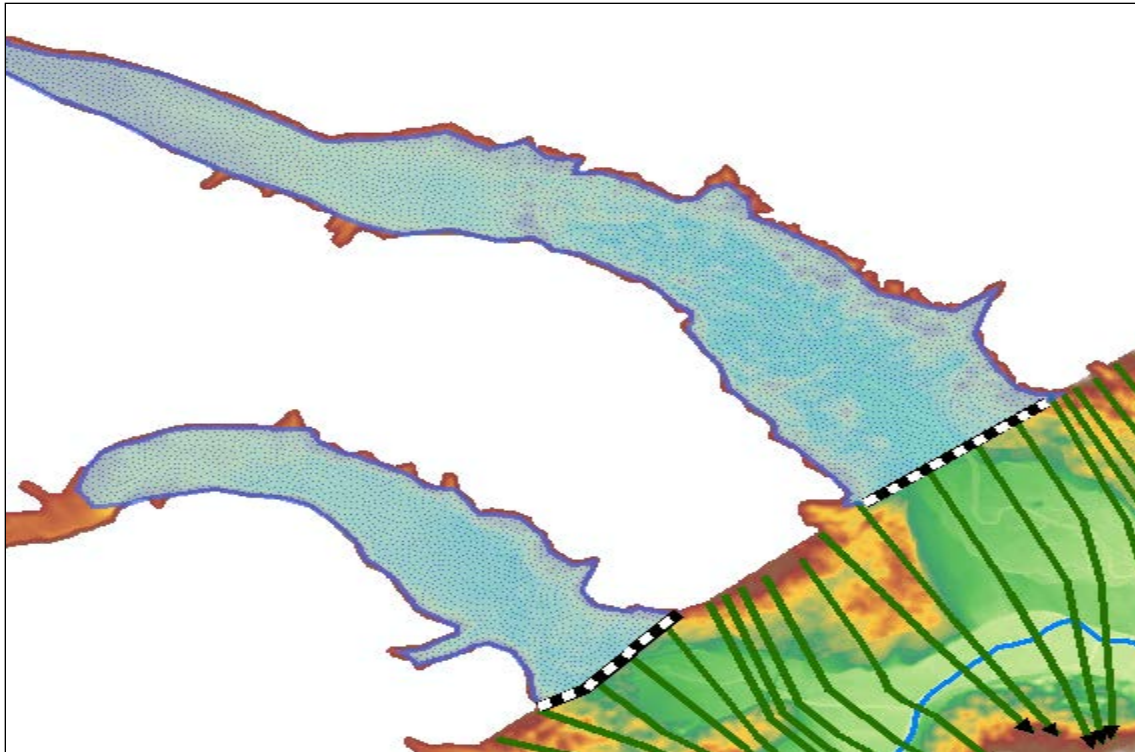
Figure 14-18. Example of using storage areas and lateral weirs to account for flow reversals up tributaries.

The third option is to extend the normal cross sections up into the tributary, and use ineffective flow areas for that portion of the cross sections. This option is depicted in Figure 14-18. This is the least accurate of these three approaches, and should only be used for very short tributaries in which you are just trying to capture the available storage for which the flood wave could back into. This is not a recommended approach for a tributary of significant size, or in which the tributary would have a sloping water surface elevation. Additionally, when storage is modelled as part of the cross section, it has the same water surface elevation as the cross section, and it is available to put water into instantaneously and take water out of instantaneously.
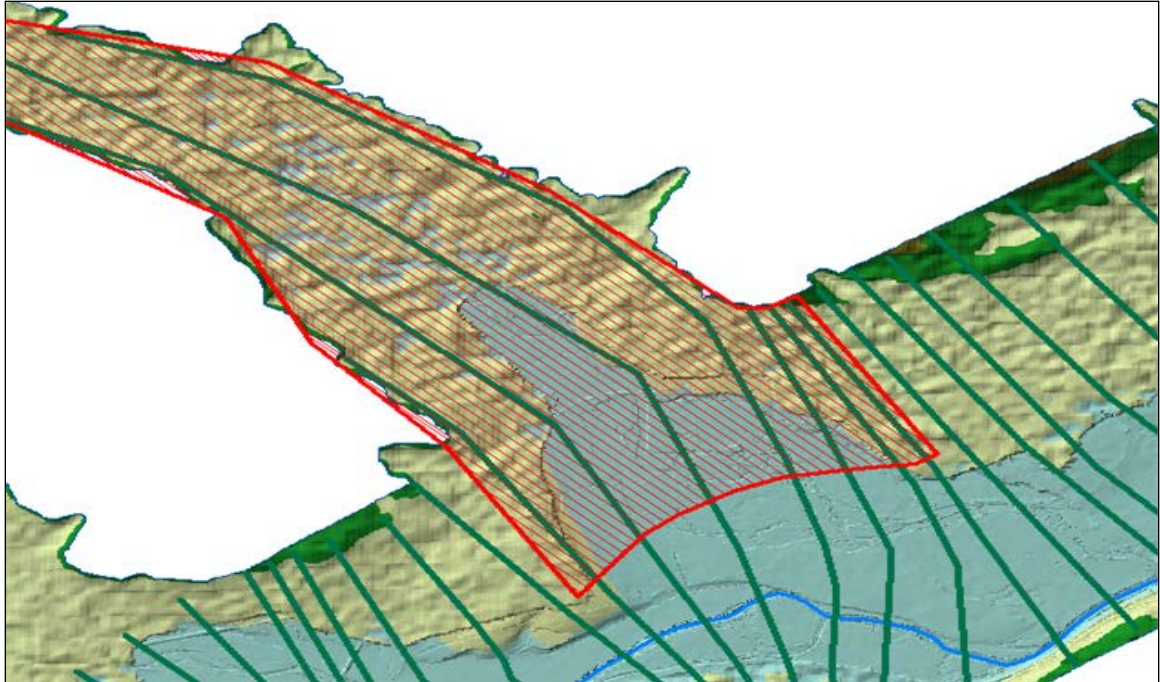
Figure 14-19. Tributary storage modeled as cross section ineffective flow areas.

Modeling Levees and Major Roads. Downstream levees and major roads, that normally prevent water from getting into protected areas, must also be considered. In general it is best to model the area behind the levees separately as a 2D flow area, a storage area, a series of interconnected storage areas, or another routing reach. The details of modeling an area behind a levee will depend on the terrain and details of the interior area. A lateral structure (weir) should be used to model the top of the levees and major roads. Using a lateral structure to model a levee in HEC-RAS allows the model to evaluate levee overtopping, breaching, and the filling of the interior area separate from the main river and floodplain. An example of modeling a levee and protected area with a single storage area is shown in Figure 14-19.
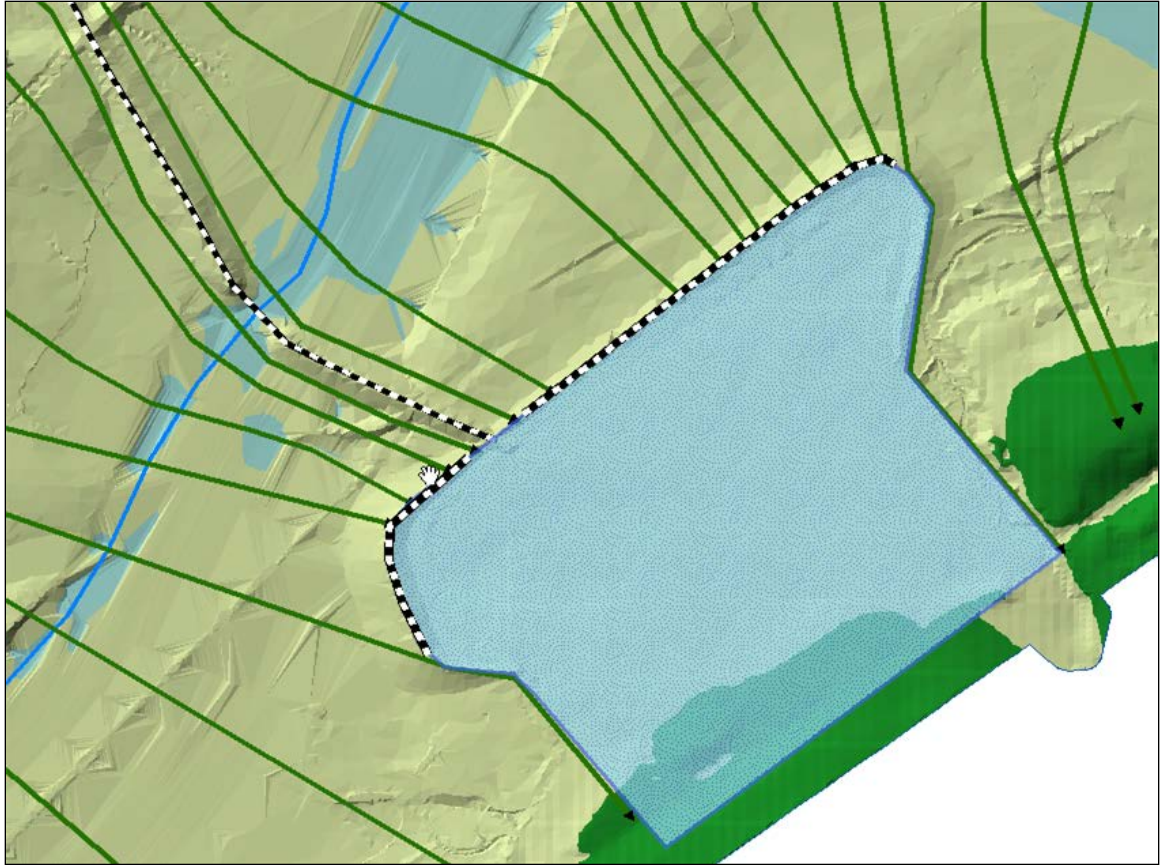
Figure 14-19. Example of using lateral structures and a storage area to model a protected area.

If a levee or road is only a small obstruction to the flow, such that it will be completely overwhelmed during the routing of the dam break flood wave, then it may be better to model that levee/road as part of the general cross sections. This means using cross sections to model both the interior and exterior area around the levee, and using the HEC-RAS cross section levee option to keep flow in the river side of the levee until the levee is overtopped. This should only be done for small levees/roads, in which the area behind these levees is not a significant area/storage volume. An example of this type of modeling is shown in Figure 14-20.
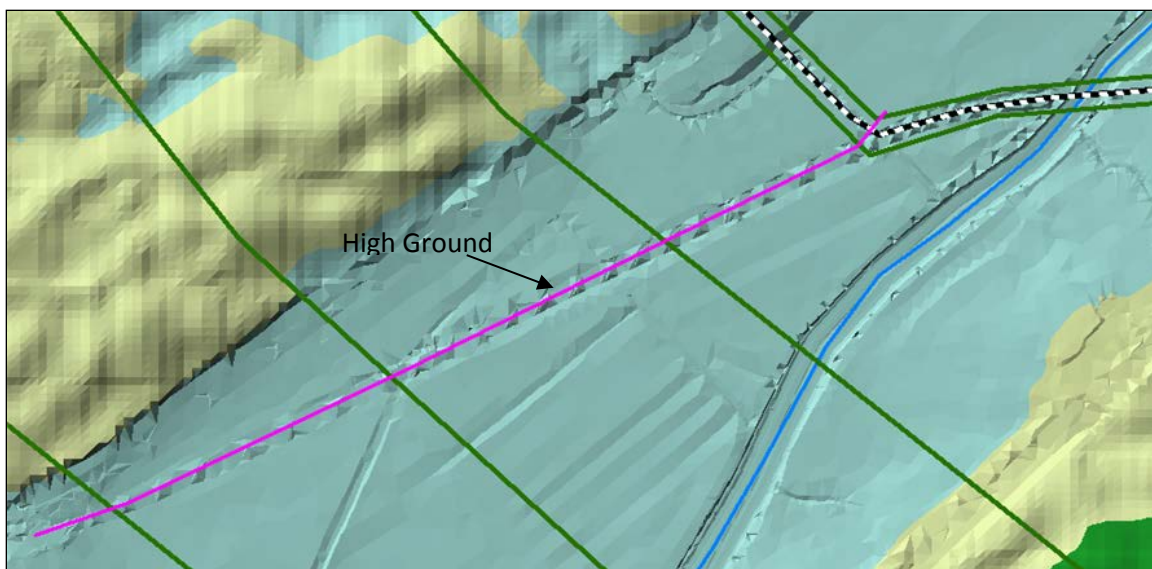
Figure 14-20. High ground (road or levee) represented as part of the cross sections.

Modeling Bridge and Culvert Crossings

Bridges and culvert crossings can often be a source of model instability problems in a dam break study. Many downstream bridges will be overtopped, and may even be washed away. If it is almost certain that a downstream bridge/Culvert will be washed away, then it probably does not need to be included in the model. Additionally, if a structure is so high above the stream that the water surface will not hit the low chord of the bridge deck (which may be the case for very large highway bridges that are far downstream from the dam), then that bridge will also not need to be modeled. However, if the road embankment, and the bridge/culvert will cause a backwater (i.e. a significant rise in the water surface), then it should be included in order to obtain the correct stages upstream of the structure and the increased storage behind the structure. If the impact of the structure is unknown, then in general it should be modeled. Then once the model is up and running, the structure could be evaluated for both its impact on the water surface and whether or not it is expected to remain in place due to the forces placed on it during the event.

Bridge/culvert crossings are a common source of model stability problems when performing a dam break analysis. Many bridges will be overtopped during such an event. Many of those bridges may in fact be washed out during such an event. A common problem at bridges/culverts is the extreme rapid rise in stages when flow hits the low chord of the bridge deck or the top of the culvert. Modelers need to check the computed family of rating curves closely and make sure they are reasonable. One solution to this problem is to use smaller time steps, such that the rate of rise in the water surface is smaller for a given time step. Modelers may also need to change hydraulic coefficients to get curves that have more reasonable transitions.

Just as with cross sections, HEC-RAS pre-processes bridges/culverts into a family of rating curves. Users must ensure that these curves go high enough to capture all possible water

surface elevations and flows. An additional source of instability can arise when the curves do not go high enough, and the program extrapolates from the last two points in the curve. This extrapolation can cause problems when it is not consistent with the cross section geometry upstream and downstream of the structure. The extrapolation is basically assuming that the changes in conveyance, area, and other hydraulic parameters are linear with respect to increased stage. However, these hydraulic properties are very non-linear. Therefore the extrapolation can cause the unsteady flow equations to be difficult to solve. An example bridge crossing and set of preprocessed curves is shown in Figure 14-21.
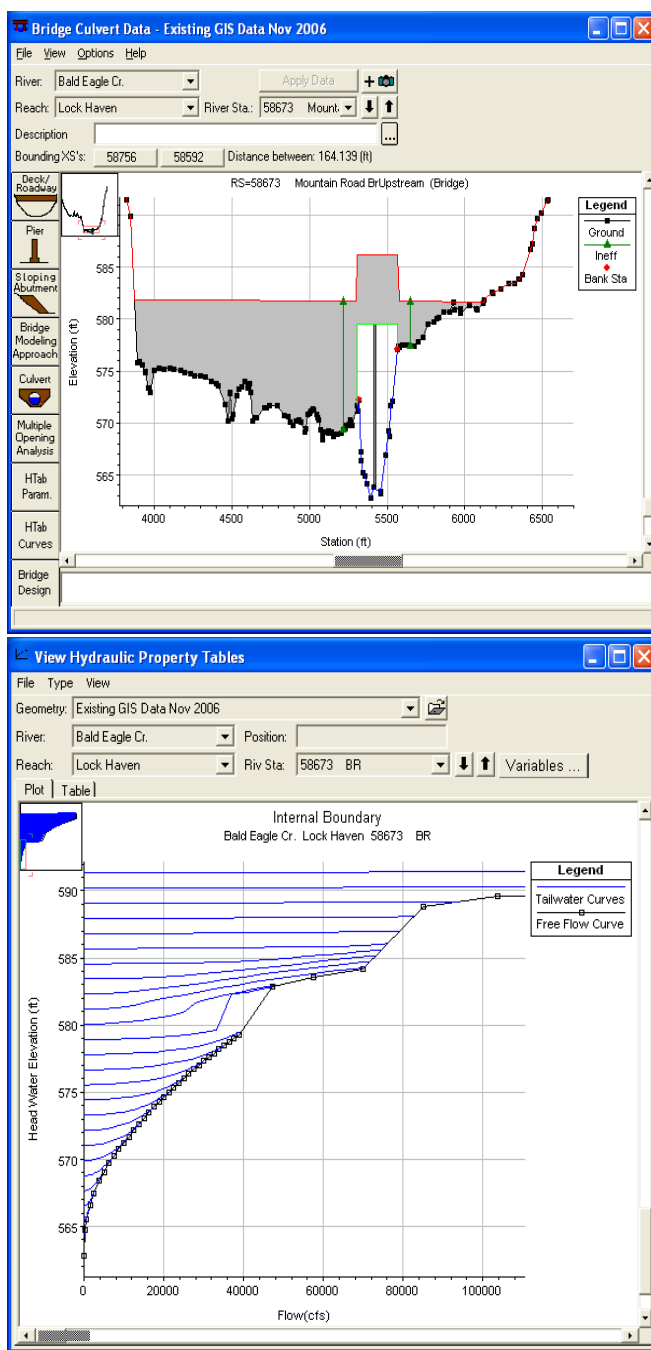
Figure 14-21. Example Bridge with Pre-Processed Bridge Curves.

Modeling Steep Streams

Steep streams are very difficult to model with an unsteady flow model in general. Modeling a dam break flood wave through a steep stream system is even more difficult. Steep streams tend to have very high velocities and rapid changes in depth, area, and velocity, which make it more challenging to obtain a stable model solution through these areas.

The default solution methodology for the 1D unsteady flow routing option within HEC-RAS is generally for gradually varied flow. Areas of rapidly varied flow, such as flow profiles transitioning from subcritical to supercritical flow, and hydraulic jumps, tend to cause the 1D solution scheme to have difficulties in remaining stable. Additionally, the assumption of a hydrostatic flow distribution may not be valid. As Froude number approaches 1.0 (critical depth), the inertial terms of the St. Venant equations and their derivatives tend to cause model instabilities (generally in rapid flow areas the derivatives are over estimated). However, the HEC-RAS software does have an option to run the 1D solution scheme in a mixed flow regime mode, which allows it to solve through these types of flow transitions.

Manning's n Values. If you are running the software in the default mode (mixed flow option not turned on), and if the program goes down to critical depth at a cross section, the changes in area, depth, and velocity are very high. This sharp increase in the water surface slope will often cause the program to overestimate the depth at the next cross section upstream, and possibly underestimate the depth at the next cross section downstream (or even the one that went to critical depth the previous time step). One solution to this problem is to increase the Manning's n value in the area where the program is first going to critical depth and in the steeper portions of the reach. This will force the solution to a subcritical answer and allow it to continue with the run. It is common for people to underestimate the magnitude of the Manning's roughness coefficient for steep streams. Additionally, it is common to have pool and riffle sequences in steep streams. In a pool and riffle sequence, Manning's n values will often be higher in the steeper riffle areas, and lower in the flatter pool areas. This level of detail for modifying Manning's n values is often not done, and can be a contributor to the instability of the model.

Mixed Flow Regime Option. If you feel that the true water surface should go to critical depth, or even to an extended supercritical flow regime, then the mixed flow regime option should be turned on when using 1D river reaches to model steep areas. In order to solve the stability problem for a mixed flow regime system, Dr. Danny Fread (Fread, 1986) developed a methodology called the "Local Partial Inertia Technique" (LPI). The LPI method has been adapted to HEC-RAS as an option for solving mixed flow regime problems when using the unsteady flow analysis portion of HEC-RAS. This methodology applies a reduction factor to the two inertia terms in the momentum equation as the Froude number goes towards a user defined threshold.

The default values for the methodology are FT = 1.0 (Froude number threshold) and m = 4 (exponent). When the Froude number is greater than the threshold value, the factor is set to zero. The user can change both the Froude number threshold and the exponent. As you increase the value of both the threshold and the exponent, you decrease stability but increase accuracy. As you decrease the value of the threshold and/or the exponent, you increase stability but decrease accuracy. To learn more about the Mixed Flow Regime option in HEC-RAS, please see the HEC-RAS User's Manual.

Increased Base Flow. Another solution to the problem of flow going from subcritical to supercritical flow, and back again, is to increase the base flow in the hydrographs, as well as the

base flows used for computing the initial conditions. Increased base flow will often dampen out any water surfaces going towards or through critical depth due to low flows that are in a pool riffle sequence.

Modified Puls Routing. HEC-RAS has an option that will allow the user to define any portion of a model to be solved with the Modified Puls routing method instead of the full unsteady flow equations. This allows the user to define problem areas, such as very steep reaches, as Modified Puls routing reaches. A Modified Puls routing reach can be defined at the upstream end of a HEC-RAS river reach, at the downstream end, in the middle of a reach, or even defined for the entire reach. The computations are performed in conjunction with the unsteady flow equations on a time step by time step basis. Additionally, reaches that are defined as Modified Puls reaches can contain bridges, culverts, and even lateral structures. The hydraulics of these structure types are accounted for during the Modified Puls routing. To use this option, please review the HEC-RAS User's Manual.

2D Flow Areas. The new 2D Flow Area option in HEC-RAS allows user to model areas with either the Full Saint Venant equations in two-dimensions, or the Diffusion Wave form of the equations in two-dimensions. The new 2D solver uses a finite volume solution algorithm, which can handle subcritical, supercritical, and mixed flow regime (including hydraulic jumps), much more robustly then the current 1D finite difference solution scheme. This makes it very easy to use 2D flow areas to model steep streams.

Drops in the bed Profile

Significant drops in the bed profile can also be a source of model stability problems, especially at low flows. Significant drops in the elevation of the channel bed can cause flow to pass through critical depth and results in an unstable model solution. An example of this type of problem is shown in Figure 14-22.
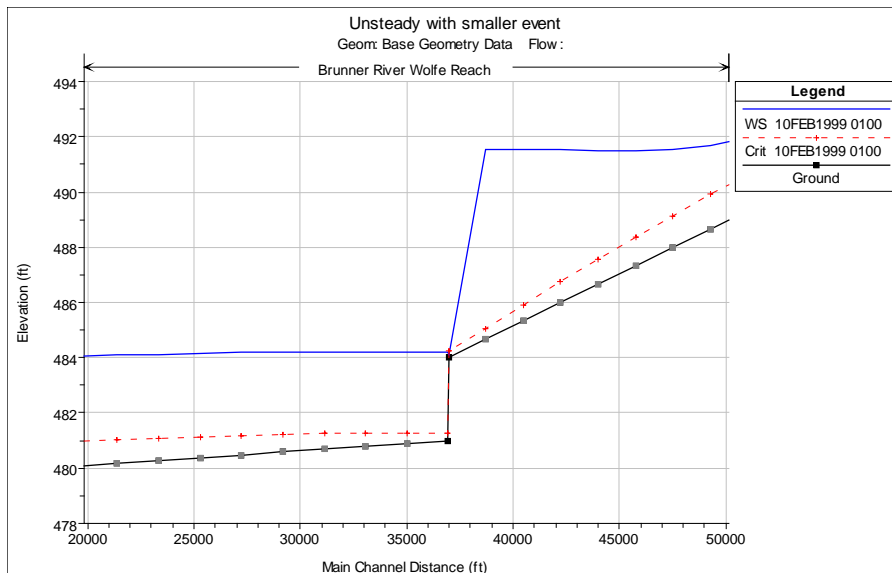
Figure 14-22. Model Instability due to a Drop in the Bed Profile.

If the drop is very small, then usually an increase in base flow will drown out the drop, thus preventing the model from passing through critical depth. If the drop is significant, then it should be modeled with an inline structure using a weir profile at the top of the drop. This will allow the model to use a weir equation for calculating the upstream water surface for a given flow, rather than using the unsteady flow equations. This produces a much more stable model, as the program does not have to model the flow passing through critical depth with the unsteady flow equations. HEC-RAS automatically handles submergence on the weir, so this is not a problem. An additional solution to this problem is to use the cross section rating curve option at the top of the drop, which causes the program to interpolate the water surface from the rating curve, rather than solving the unsteady flow equations through the drop in the bed profile.

Initial Conditions and Low Flow

Initial Conditions. In order for the unsteady flow model to run, the user must establish the initial conditions in the entire system. This means that it must have a flow and a stage at every cross section, as well as a stage in every storage area/2D flow area (storage areas and 2D flow areas can start dry). The most common way to establish the initial conditions is for the user to enter a set of initial flows for all the reaches, and the software performs a steady flow backwater profile to get the corresponding stages. The initial condition flows entered by the user must be consistent with all of the boundary condition flows at time zero (the start of the unsteady flow run).

Initial reservoir elevations and gate settings must also be consistent with the initial condition flows, such that the flow computed out of the reservoir at the first time step is consistent with what the user entered to perform the initial conditions profile (Figure 14-23). If the user enters

a low flow for the initial conditions backwater profile, and then at the first unsteady flow time step the program calculates a much larger flow coming out of the reservoir (due to gate settings and initial reservoir stages), this can cause an instability in the area just below the dam.

Another possible source of initial conditions causing the model to go unstable right away, are the initial storage area elevations. It is up to the user to enter an initial storage area water surface elevation for all storage areas, even if it is to start out dry (water surface is set to the lowest elevation of the storage area). When a storage area is hydraulically connected to a river reach (this is normally done with a lateral structure), and the initial water surface in the river reach is at an elevation that will cause a flow interaction with a storage area (water surface is above the lateral structure weir profile, or culverts, or gates), then that storage area needs to have an initial water surface elevation set equal to the computed initial stage in the river. If the storage area is set much higher or lower than the elevation of the river section it is connected to, then a large discharge may be computed at the hydraulic structure that connects them. This large discharge across the lateral structure will either take a lot of flow from the river (if the river stage is higher than the storage area), or it will have a large inflow into the river (if the storage area stage is much higher than the connected river stage). Either of these two cases can cause the model to become unstable at the initial start of the unsteady flow computations. By setting the storage area elevations to the same as the initial water surface of the cross section to which it is connected, then the computed flow across the lateral structure will be close to zero. Shown in Figure 14-23 are two lateral structures, which are connected to storage areas. The initial condition water surface elevation is higher than the downstream lateral structure. Therefore, the storage area connected to this structure must be set to the initial condition water surface elevation in this area. Because the initial water surface is lower than the most upstream lateral structure, the water surface elevation for that connected storage area can be set to dry, or whatever elevation is appropriate below the minimum elevation of the lateral structure.
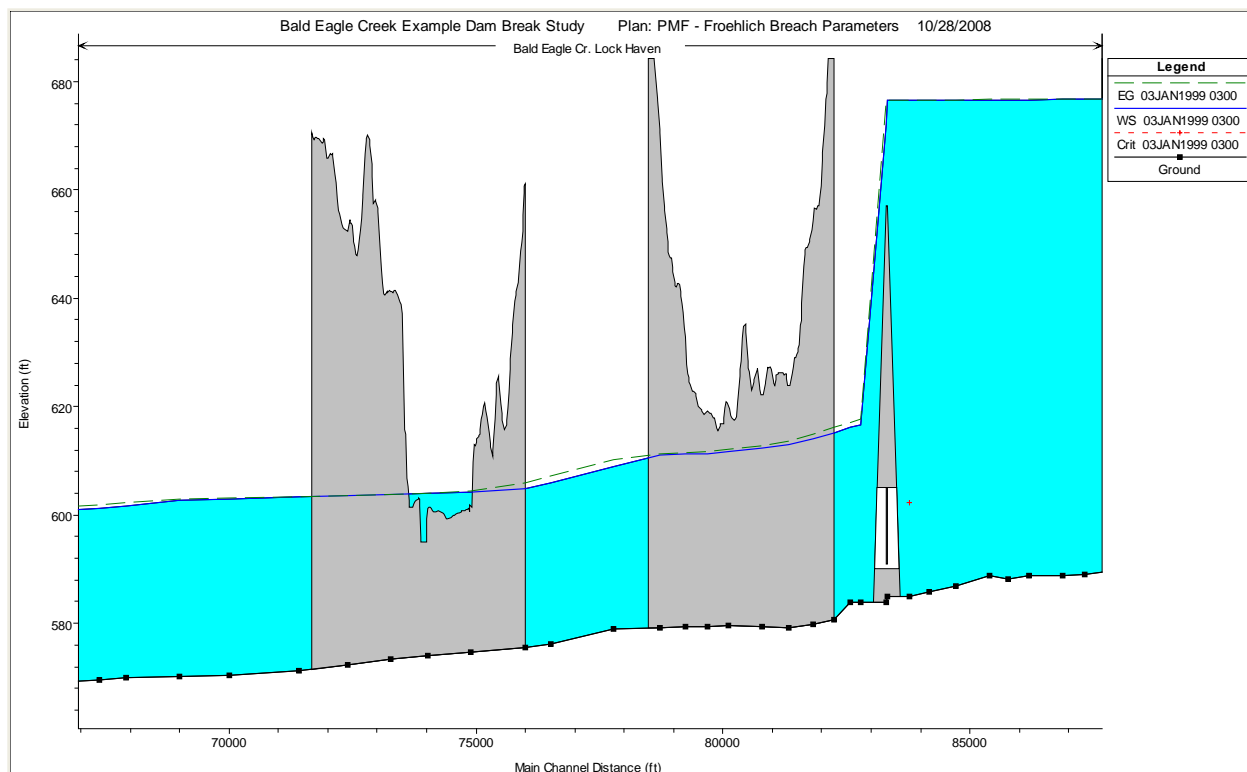
Figure 14-23. Example of Initial Conditions for a Reservoir and Lateral Structures connected to Storage Areas.

Low Flow Conditions. Low flows can often be very difficult to model with an unsteady flow model. Medium to steeper slope streams will often have a pool and riffle sequence at low flow, and the water surface will generally pass through critical depth at the upper end of the riffle (bottom of the pool). In addition to this, the depths of water are very shallow. Once the flood wave begins the water surface will change quickly, and there will be a large change in depth with respect to distance and time. The leading edge of a dam break flood wave will be very steep, and can often be a source of model instability as it propagates down the river system. The finite difference solution to the equations will generally have the most trouble balancing during the initial dramatic rise at the beginning of the flood wave. The fact that the initial conditions may be very low flows and depths can make it even more difficult to solve the equations through those shallow and steep riffle regions.

There are several things the modeler can do to allow the program to solve the equations in a stable manner in low flow situations. The easiest solution is to increase the base flow for the initial conditions. This will provide a higher initial depth of water in general, and it may also drowned out the pool and riffle sequence. A general "rule of thumb" is to start out by trying a base flow around 1% of the peak flow that will be routed. Increase the base flow if necessary, but never go above 10% of the peak flow. If you artificially use a base flow that is 10% or more of the peak, the computed peak flow and stage will be higher than it would have been otherwise.

If you have increased the base flow to a reasonable level, and are still having model stability problems at the leading edge of the flood wave, then try adding a pilot channel for the reach in which the model is having stability issues. A pilot channel is an option in which will add some depth without adding much flow area or conveyance. The pilot channel is an option in HEC-RAS, and it is only used during low flow, once the cross sections get to some appreciable depth, the program automatically removes it from the cross section. To learn more about the use of pilot channels, please review the section on Pilot channels in Chapter 6 of the HEC-RAS User's Manual.

One other option that can help stabilize the model during the initial rise of the flood wave, is turning on the Mixed Flow Regime Option. This option drops the acceleration terms when the Froude number gets greater than a user defined threshold, which is often the case on the leading edge of the flood wave.

Downstream Boundary Conditions

Downstream boundary conditions are important for all hydraulic models, especially unsteady flow models. Downstream boundary conditions can often be a source of model error, as well as model instability. More often than not, the true stage for a given flow at the downstream end of our models is not known. Because of this we often use either Normal Depth (Manning's equation), or a rating curve computed from a steady flow model. The normal depth boundary condition requires the user to enter a single energy slope, which is then in turn used in Manning's equation to compute the downstream stage for any flow occurring. Occasionally this forced slope, or even a single valued rating curve can end up with stages that are not correct for the given flow at a given point on the flood hydrograph. In general, the best solution is to make sure that the downstream boundary condition is downstream from any of the locations in which stages are being used to compute damages or loss of life, such that the error in the water surface elevation at the boundary condition does not affect the area of interest.

Additionally, if a boundary condition is ill posed, this can be a source of model instability (i.e. rating curves with not enough points, or the user entered stages are too low for a given flow rate; and normal depth boundaries where the user has entered to steep of a slope for the energy gradeline). In other words, the downstream boundary condition may be causing abrupt drops or rises in the computed water surface near the location of the boundary condition. An example of what can happen when using a Normal Depth boundary condition, and entering too steep of an energy slope is shown in Figure 14-24. In this case, the steep energy slope caused the program to compute lower stages than appropriate for a given flow, which in turn caused the model to over steepen the flood wave at the downstream end of the model.
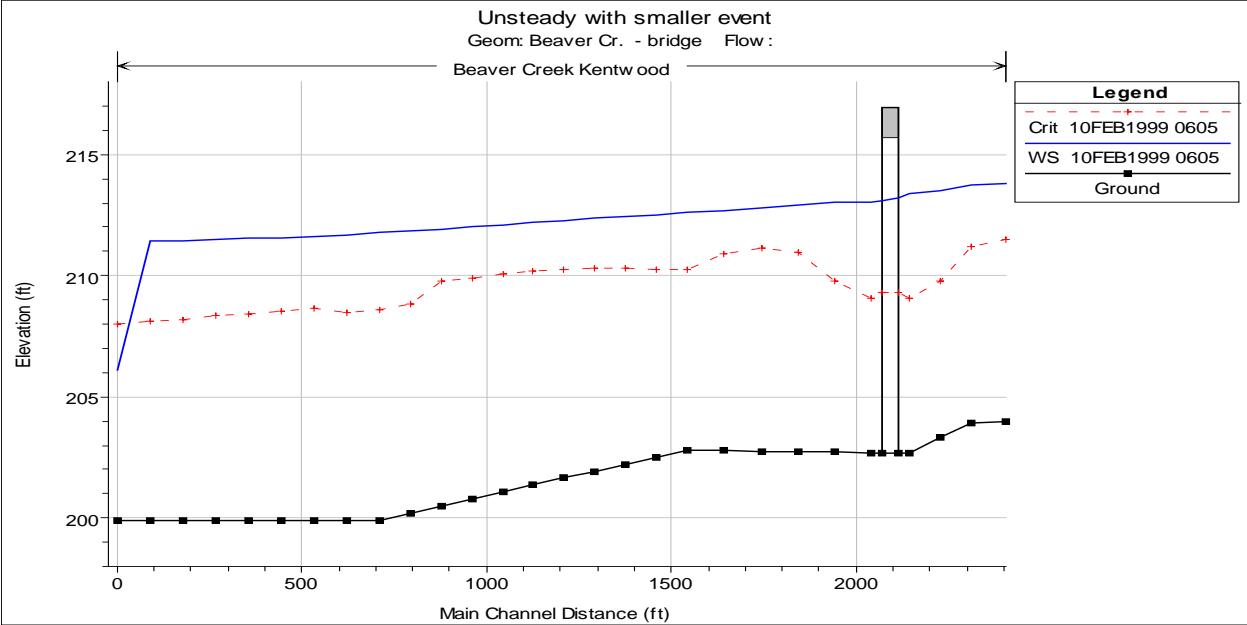
Figure 14-24. Example model error due to bad downstream boundary condition.

Using 2D Flow Areas for Dam Break Analyses

The latest version of HEC-RAS (5.0 or later) now has the ability to perform two-dimensional flow routing. For a dam break study, the user can model the downstream area entirely with 1D elements (Cross sections and storage areas); as a combination of 1D and 2D elements (cross sections, storage areas, and 2D flow areas); or the entire downstream area can be modeled as a 2D flow area.

2D flow areas can be directly connected to storage areas by using a hydraulic structure called a Storage Area/ 2D Flow Area Hydraulic Connector ("SA/2D Area Conn"). See the example below in Figure 14-25.
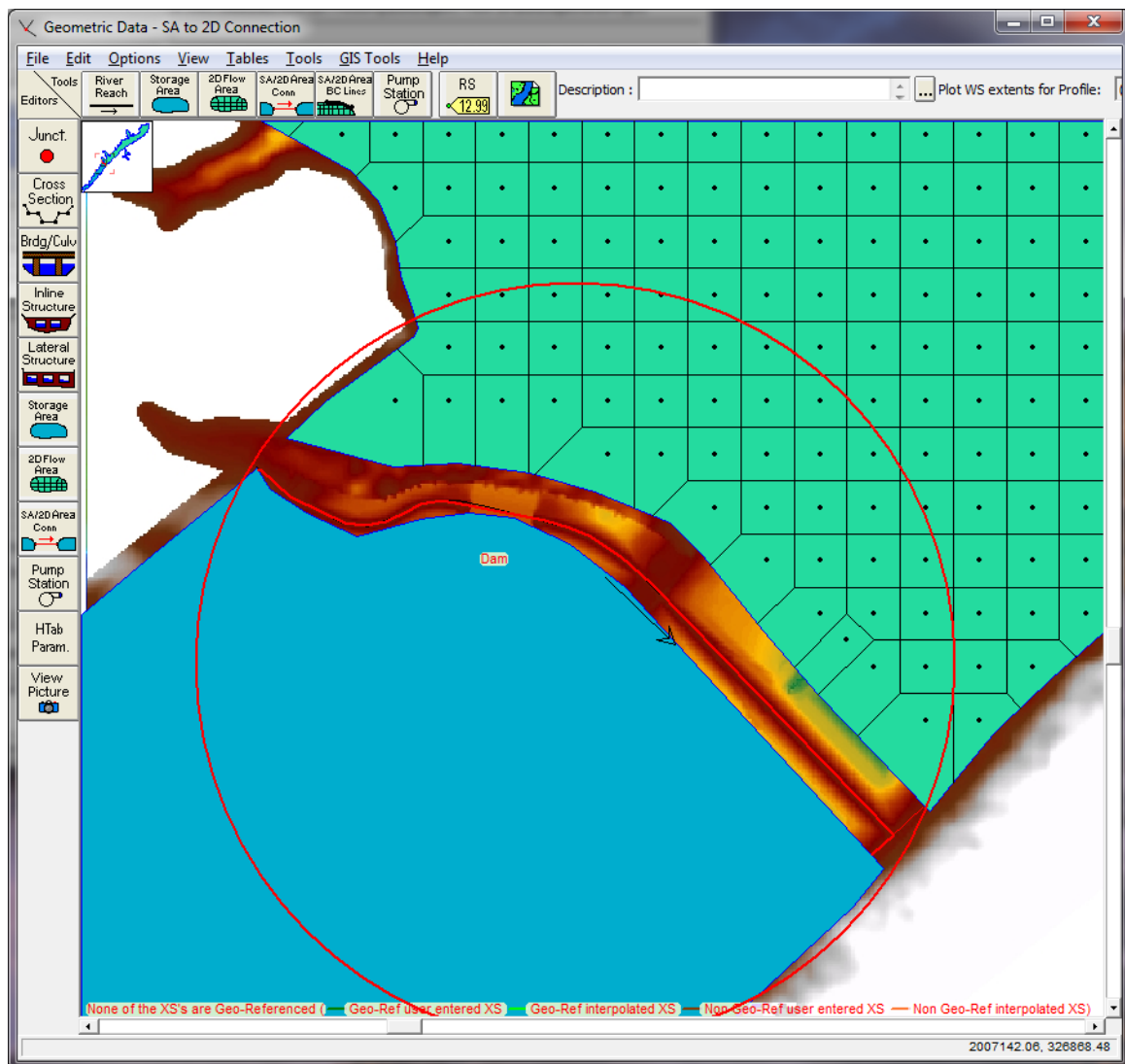
Figure 14-25. Example of a Storage Area connected to a 2D Flow Area.

In the example shown in Figure 14-25, the storage area is upstream of the 2D flow area, so the positive flow direction is from the storage area to the 2D flow area. So when defining the hydraulic structure that connects the two areas, the storage area will be considered the headwater side, and the 2D flow area will be considered the tailwater side. In the example shown in Figure 14-25, a storage area is being used to represent a reservoir pool. The hydraulic connection between the storage area and the 2D flow area is used to model the dam. The 2D flow area is being used to model the hydraulics of the flow downstream of the dam. Additionally, the user could model the reservoir pool with a 1D river reach, or a 2D flow area.

Using the approach shown in Figure 14-25, is a very quick way to get a dam break model up and running. However, modeling the downstream area with a 2D flow area, does not necessarily

make this a detailed model. Downstream areas will often have bridges, culverts, roads that are barriers to flow, levees protecting urban areas, etc… These types of areas require detailed modeling to get accurate answers, whether you are modeling them as 2D flow areas or 1D river reaches. Developing a detailed model for the downstream area requires detailed terrain, hydraulic structure information, and the time to model those areas correctly. If a 2D flow area is used, it still requires lots of work to make the computational mesh respect all of the barriers to flow (bridges, culverts, roads, levees, etc…). Developing a detailed computational mesh that respects all of the flow barriers, and includes all of the hydraulic structures is the most time consuming part of developing a model, but it is necessary to get good results downstream. If you do not take the time to do this, and you just throw in a 2D flow area with a nominal grid size, do not assume you have "accurate" results just because you are doing 2D modeling.

APPENDIX A

References

Ackers, P., and White, W.R. November 1973. "Sediment Transport: New Approach and Analysis," Journal of the Hydraulics Division, American Society of Civil Engineers, Vol. 99, No. HY 11, pp. 2040-2060.

Alonso, Santillana and Dawson. 2008. On the diffusive wave approximation of the shallow water equations. Euro. J. Appl. Math. 2008, Vol. 19.

American Iron and Steel Institute (AISI), 1980. Modern Sewer Design, Washington D.C.

American Society of Civil Engineers. 1977. "Sedimentation Engineering, "Vito A. Vanoni, ed., American Society of Civil Engineers Task Committee, American Society of Engineers, New York.

Amein, M. and Fang, C.S., 1970, "Implicit Flood Routing in Natural Channels," Journal of the Hydraulics Division, ASCE, Vol. 96, No. HY12, Proc. Paper 7773, pp. 2481-2500.

Amin, M.I., and Murphy, P.J. August 1981. "Two Bed-Load Formulas: An Evaluation," Journal of the Hydraulics Division, American Society of Civil Engineers, Vol. 107, No. HY8, pp. 961-972.

Arcement, G. J., Jr., and V. R. Schneider, 1989. "Guide for Selecting Manning's Roughness Coefficient for Natural Channels and Floodplains," U.S. Geological Survey, Water Supply Paper 2339, 38 p., Washington D.C.

Balzano. 1998. Evaluation of methods for numerical simulation of wetting and drying in shallow water flow models. Coastal Eng. 1998, 34.

Barkau, R.L., 1981, "Simulation of the Failure of Illinois River Levees," Memo to File, St. Louis District, Corps of Engineers, St. Louis, MO.

Barkau, R.L., 1982, "Simulation of the July 1981 Flood Along the Salt River," Report for CE695BV, Special Problems in Hydraulics, Department of Civil Engineering, Colorado State University, Ft. Collins, CO.

Barkau, R.L., 1985, "A Mathematical Model of Unsteady Flow Through a Dendritic Network," Ph.D. Dissertation, Department of Civil Engineering, Colorado State University, Ft. Collins, CO.

Barkau, Robert L., 1992. UNET, One-Dimensional Unsteady Flow Through a Full Network of Open Channels, Computer Program, St. Louis, MO.

Bathe, K. and Wilson, E.L., 1976, Numerical Methods in Finite Element Analysis, Prentice-Hall, Inc., Englewood Cliffs, NJ.

Briaud, J., Ting, C., Chen, H., Cao, Y., Han, S., and Kwak, K. (2001) "Erosion Functions Apparatus for Scour Rate Predictions," *Journal of Geotechnical and Geoenvironmental Engineering*, 106-113.

Brunner, Gary W., August 1994. "Improved Hydraulic Features of the HEC River Analysis System," presented at the ASCE Hydraulic engineering conference, Buffalo, NY

Brunner, Gary W. and John H. Hunt, 1995. A Comparison of the One-Dimensional Bridge Hydraulic Routines from: HEC-RAS, HEC-2, and WSPRO, Research Document No. 41, Hydrologic Engineering Center, U.S. Army Corps of Engineers, September 2009, Davis, CA.

Brunner, Gary W., June 1996. "HEC-RAS (River Analysis System)," presented at the ASCE North American Water and Environmental Congress, Anaheim, CA.

Brunner, Gary W., June 1996. "Computing Bridge Scour With HEC-RAS," presented at the ASCE North American Water and Environmental Congress, Anaheim, CA.

Brunner, Gary W., Mark R. Jensen, and Steven S. Piper, 2000. Unsteady Flow Routing with the Hydrologic Engineering Center River Analysis System (HEC-RAS), Watershed Management and Operations Management, ASCE, EWRI, June 2000, Fort Collins, CO.

Brunner, Gary W. and Mark E. Forest, 2002. Unsteady Flow Routing With HEC-RAS – Truckee River, Joint Federal Interagency Conference, April 2002, Las Vegas, NV

Brunner, Gary W., 2003. Dam and Levee Breaching With HEC-RAS, World Water & Environmental Resources Congress, ASCE, EWRI, June 2003, Philadelphia, PA.

Brunner, Gary W. and Stanford S. Gibson, 2005. Sediment Transport Modeling in HEC-RAS, World Environmental & Water Resources Congress, ASCE, EWRI, May 2005, Anchorage, AL.

Brunner, Gary W. and Cameron T. Ackerman, 2012. "HEC-RAS Modeling for Operation of the Birds Point - New Madrid Floodway, Mississippi River Flood of 2011", World Environmental & Water Resources Congress, ASCE, EWRI, May 2012, Albuquerque, NM.

Brunner, Gary W., 2014. Using HEC-RAS for Dam Break Studies, Training Document No. 39, Hydrologic Engineering Center, U.S. Army Corps of Engineers, August 2014, Davis, CA.

Brunner, Gary W., Steven S. Piper, Mark R. Jensen, and Ben Chacon, 2015. Combined 1D and 2D Hydraulic Modeling within HEC-RAS, World Environmental & Water Resources Congress, ASCE, EWRI, May 2015, Austin, TX.

Barnes, Harry H,, Jr., 1967. "Roughness Characteristics of Natural Channels," U.S. Geological Survey, Water Supply Paper 1849, Washington D.C.

Blench, T. , 1970, "Regime Theory Design of Canals with Sand Beds." Journal of the Irrigation and Drainage Division, ASCE, Vol. 96, No. IR2, Proc. Paper 7381, pp 205-213.

Bodhaine, G.L., 1982, "Measurement of Peak Discharge at Culverts by Indirect Methods," Techniques of Water Resources Investigations of the United States Geological Survey, Book 3, Chapter A3, U.S. Geological Survey, WA.

Bradley, J.N., 1978. Hydraulics of Bridge Waterways, Hydraulic Design Series No. 1, Federal Highway Administration, U.S. Department of Transportation, Second Edition, revised March 1978, Washington D.C.

Brownlie, William R., 1981 (Nov). "Prediction of Flow Depth and Sediment Discharge in Open Channels," Report No. KH-R-43A, California Institute of Technology, W.M Keck Laboratory of Hydraulics and Water Resources, Report No. KH-R-43A, November 1981. Pasadena, CA.

Brownlie, Williem R. 1983 (Jul). "Flow Depth in Sand Bed Channels." Journal of Hydraulic Engineering. American Society of Civil Engineers, Vol 109, No 7, pp 959-990.

Bureau of Public Roads (BPR), 1965. Hydraulic Charts for the Selection of Highway Culverts, Hydraulic Engineering Circular No. 5, U.S. Department of Commerce.

Bureau of Reclamation, 1977. Design of Small Dams, Water Resources Technical Publication, Washington D.C..

Burkham, Durl E. and David R. Dawdy. 1976. Resistance Equation.

Casulli and Stelling. 2010. Semi-implicit subgrid modelling of three dimensional free-surface flows. Int. J. Numer. Meth. Fluids. 2010.

Casulli. 2008. A high-resolution wetting and drying algorithm for free-surface hydrodynamics. Int. J. Numer. Meth. Fluids. 2008.

Casulli and Zanolli. 2005. High resolution methods for multidimensional advection-difusion problems in free surface hydrodynamics. Ocean Modelling. 2005, 10.

Casulli and Zanolli. 2002. Semi-implicit numerical modelling of nonhydrostatic free-surface flows for environmental problems. Math. Comp. Modelling. 2002, 36.

Casulli and Walters. 2000. An unstructured grid, three-dimensional model based on the shallow water equations. Int. J. Numer. Meth. Fluids. 2000, 32.

Casulli and Stelling. 1998. Numerical simulation of 3D quasi-hydrostatic free-surface flows. J. Hydraulic Eng. 1998.

Casulli. 1997. Numerical simulation of three-dimensional free surface flow in isopycnal co-ordinates. Int. J. Numer. Meth. Fluids. 1997, Vol. 25.

Casulli and Cattani. 1994. Stability, accuracy and efficiency of a semi-implicit method for three-dimensional shallow water flow. Computers Math. Applic. 1994, Vol. 27.

Casulli and Cheng. 1992. Semi-implicit finite difference methods for three dimensional shallow water flow. Int. J. Numer. Meth. Fluids. 1992, Vol. 15.

Casulli and Cheng. 1990. Stability analysis of Eulerian-Lagrangian methods for the one-dimensional shallow water equations. Appl. Math. Modelling. 1990, Vol. 14.

Casulli. 1990. Sami-implicit fiinite difference methods for the two-dimensional shallow water equations. J. Comp. Physics. 1990, 86.

Chanson, Hubert. 1999. "The Hydraulics of Open Channel Flow." John Wiley & Sons Inc., New York.

Chen, Y.H., 1973, "Mathematical Modeling of Water and Sediment Routing in Natural Channels," Ph.D. Dissertation, Department of Civil Engineering, Colorado State University, Ft. Collins, CO.

Chen, Y.H. and Simons, D.B., 1979, "A Mathematical Model of the Lower Chippewa River Network System," Report CER-79 DBS-YHC-58, Department of Civil Engineering, Colorado State University, Ft. Collins, CO.

Chow, V.T., 1959, Open Channel Hydraulics, McGraw-Hill Book Company, NY.

Colby, B.R. March 1964. "Practical Computations of Bed-Material Discharge," Journal of the Hydraulics Division, American Society of Civil Engineers, Vol 90, No. HY2, pp 217-246.

Copeland, Ronald R., and Thomas, William A. 1989. "Corte Madera Creek Sedimentation Study." Numerical Model Investigation. US Army Engineer Waterways Experiment Station, Vicksburg, MS. TR-HL-89-6

Copeland, R. R. and Thomas, W. A. (1992) "Dynamic Sorting and Armoring Algorithm in TABS-1 Numerical Sedimentation Model," *Proceedings, International Seminar on Grain Sorting*, Ascona, Swotzerland, Mitteilungen 117 der Versuchsanstalt für Wasserbau, Hydrologieund Gaziologie, ETH Zurich, pgs. 359-368.

Copeland, Ronald R. 1994 (Sep). "Application of Channel Stability Methods—Case Studies." US Army Engineer Waterways Experiment Station, Vicksburg, MS. TR-HL-94-11.

Cunge, J.A., Holly, F.M., and Verwey, A., 1980, Practical Aspects of Computational River Hydraulics, Pitman Advanced Publishing Program, Boston, MA.

Cowan, W.L., 1956. "Estimating Hydraulic Roughness Coefficients," Agricultural Engineering, Vol. 37, No. 7, pp 473-475.

Einstein, Hans A. 1950. "The Bed Load Function for Sediment Transportation in Open Channels," Technical Bulletin 1026, US Department of Agricultural, Soil Conservation Service, Washington, D.C.

Fasken, G.B., 1963. "Guide for Selecting Roughness Coefficient n Values for Channels," Soil Conservation Service, US department of Agriculture, 45 p.

Federal Emergency Management Agency, 1985. Flood Insurance Study Guidelines and Specifications for Study Contractors, FEMA 37, Washington D.C., September 1985.

Federal Highway Administration, 1984. "Guide for Selecting Manning's Roughness Coefficients for Natural Channels and Flood Plains," Report No. FHWA-TS-84-204, McLean, Virginia.

Federal Highway Administration, 1985. Hydraulic Design of Highway Culverts, Hydraulic Design Series No. 5, U.S. Department of Transportation, September 1985, Washington D.C..

Federal Highway Administration, 1986. Bridge Waterways Analysis Model: Research Report, Report No. FHWA/RD-86/108, July 1986, Washington D.C..

Federal Highway Administration, 1990. User's Manual for WSPRO - A Computer Model for Water Surface Profile Computations, Publication No. FHWA-IP-89-027, September 1990.

Federal Highway Administration, 1995. Evaluating Scour at Bridges, Federal Highway Administration, HEC No. 18, Publication No. FHWA-IP-90-017, 3rd Edition, November 1995, Washington D.C.

Federal Highway Administration, 1996. Channel Scour at Bridges in the United States, Publication No. FHWA-RD-95-184, August 1996, Washington D.C.

Fischer, et al. 1979. Mixing in Inland and Coastal Waters. 1979.

Fread, D.L., 1974, Numerical Properties of the Implicit Four Point Finite Difference Equations of Unsteady Flow," NOAA Technical Memorandum NWS Hydro-18, U.S. Department of Commerce, NOAA, NWS, Silver Spring, MD, 123pp.

Fread, D.L., 1976, "Theoretical Development of an Implicit Dynamic Routing Model," Hydrologic Research Laboratory, Office of Hydrology, U.S. Department of Commerce, NOAA, NWS, Silver Spring, MD., presented at Dynamic Routing Seminar, Lower Mississippi River Forecast Center, Slidell, LA., 13-17 Dec 1976.

French, R.H., 1985, Open-Channel Hydraulics, McGraw-Hill Book Company, New York.

Friazinov, 1970, "Solution Algorithm for Finite Difference Problems on Directed Graphs," Journal of Mathematics and Mathematical Physics, Vol. 10, No. 2, (in Russian).

Froehlich, D.C., 1989. Local Scour at Bridge Abutments, Proceedings of the 1989 National Conference on Hydraulic Engineering, ASCE, New Orleans, LA, pp. 13-18.

Froehlich, D.C., 1991. Analysis of Onsite Measurements of Scour at Piers, Proceedings of the ASCE National Hydraulic Engineering Conference, Colorado Springs, CO.

Gibson, S and Piper, S (2007) "Sensitivity and Applicability of Bed Mixing Algorithms" *EWRI ASCE Water Congress.*

Graf, Walter Hans. 1971. "Hydraulics of Sediment Transport." McGraw Hill, Inc.,

Hager, W. H., 1987. "Lateral Outflow Over Side Weirs", Journal of Hydraulic Engineering, ASCE, Vol. 113, No. 4, PP 491-504.

Ham, Pietrzak and Stelling. 2006. A streamline tracking algorithm for semi-Lagrangian advection schemes based on the analythic integration of the velocity field. J. Comp. Appl. Math. 2006, 192.

Hanson, G.J. (1996) "Investigating Soil Strength and Stress-Strain Indices to Characterize Erodibility," *Transactions of the American Society of Agricultural Engineers,* 39 (3), 883-890.

Hanson, G.J. and Simon, A. (2001) "Erodibility of Cohesive Streambeds in the Loess Area of the Midwestern USA," *Hydrologic Processes*, 15, 23-38.

Harrison, A.S. (1950) "Report on Special Investigation of Bed Sediment Segregation in a Degrading Bed," *California Institute of Engineering Research, 33(1).*

Hicks, D.M. and P.D. Mason, 1991. Roughness Characteristics of New Zealand Rivers, Water Resources Survey, DSIR Marine and Freshwater, New Zealand, June 1991.

Hirano, M (1971) "River Bed Degradation with Armoring," *Proceedings of Japan Society of Civil Engineers*, **195**, 55-65.

Hromadka, et al. 2010. Manning's equation and two dimensional flow analogs. J. Hydrology. 2010, 389.

Huang, J., Hilldale, R.C., Greiman, B. P. (2006) "Cohesive Sediment Transport," Erosion and Sedimentation Manual, U.S. Department of the Interior Bureau of Reclamation, 55p

Hydrologic Engineering Center, 1986. "Accuracy of Computed Water Surface Profiles," Research Document 26, U.S. Army Corps of Engineers, Davis CA.

Hydrologic Engineering Center, 1991. HEC-2, Water Surface Profiles, User's Manual, U.S. Army Corps of Engineers, Davis CA.

Hydrologic Engineering Center, August 1993. HEC-6 Generalized Computer Program. "Scour and Deposition in Rivers and Reservoirs," User's Manual. U.S. Army Corps of Engineers, Davis CA.

Hydrologic Engineering Center, 1994. HECDSS, User's Guide and Utility Programs Manual, U.S. Army Corps of Engineers, Davis CA.

Hydrologic Engineering Center, 1995. RD-41, A Comparison of the One-Dimensional Bridge Hydraulic Routines from: HEC-RAS, HEC-2, and WSPRO, U.S. Army Corps of Engineers, Davis CA., September 1995

Hydrologic Engineering Center, 1995. RD-42, Flow Transitions in Bridge Backwater Analysis, U.S. Army Corps of Engineers, Davis CA., September 1995

Hydrologic Engineering Center, 1997. UNET, One-Dimensional Unsteady Flow Through a Full Network of Open Channels, User's Manual, U.S. Army Corps of Engineers, Davis, CA.

Henderson, F.M., 1966, Open Channel Flow, Macmillan Publishing Co., Inc., NY, 523pp.

Iwagaki, Yuichi. 1954. "On the Law of Resistance to Turbulent Flow in Open Rough Channels," Proceedings of the 4th Japan National Congress for Applied Mechanics, pp 229-233.

Jansen, P.Ph. 1979. "Principles of River Engineering, the Non-Tidal Alluvial River." Delftse Uitgevers Maatsschappij, Delft, The Netherlands.

Jarrett, R.D., 1984. "Hydraulics of High Gradient Streams," A.S.C.E. Journal of Hydraulic Engineering, Vol. 110, No. 11, November 1984.

Keulegan, Garbis H. 1938. "Laws of Turbulent Flow in Open Channels," Research Paper RP 1151, National Bureau of Standards, Journal of Research, vol 21: PP 701-741.

Kindswater, C.E. and R.W. Carter 1957. "Discharge Characteristics of Rectangular Thin-Plate Weirs." J. Hyd. Div. ASCE, 83, No. HY6, pp 1453-1 to 35.

King, H.W. and E.F. Brater 1963. Handbook of Hydraulics, Fifth Edition, McGraw Hill Book Company, New York.

Knapen, A., Poesen, J., Govers, G., Gyssels, G., and Nachtergaele (2007) "Resistance of Soils to Concentrated Flow Erosion: A Review," *Earth-Science Review*, 80, 75-109.

Krol. 2009. Momentum exchange as a common physical background of a transparent and physically coherent description of transport phenomena. Turbulence, Heat and Mass Transfer. 2009, 6.

Krone, R. B. (1962) *Flume Studies of the Transport of Sediment in Estuarial Shoaling Processes*, Hydrologic Engineering Laboratory, University of California Berkley

Lamb, Crossley and Waller. 2008. A fast two-dimansional floodplain inundation model. Water Management. 2008, 162.

Lane, E.W., 1953, "Design of Stable Channels." American Society of Civil Engineers, Transactions, Paper number 2776, pp 1234-1261.

Laursen, Emmett M., 1958 (Feb). "Total Sediment Load of Streams," Journal of the Hydraulics Division, American Society of Civil Engineers, 84(HY1), 1530-1 to 1530-36.

Laursen, E.M., 1960. Scour at Bridge Crossings, ASCE Journal of Hydraulic Engineering, Vol. 89, No. HY 3.

Laursen, E.M., 1963. An Analysis of Relief Bridges, ASCE Journal of Hydraulic Engineering, Vol. 92, No. HY 3.

Leer. 1979. Towards the ultimate conservative difference scheme. A second-order sequel to Godunov's method. J. Comp. Physics. 1979, 32.

Liggett, J.A., and Cunge, J.A., 1975, "Numerical Methods of Solution of the Unsteady Flow Equations," in Unsteady Flow in Open Channels, edited by K. Mahmood and V. Yevjevich, Vol. I, Chapter 4, Water Resources Publications, Ft. Collins, CO.

Limerinos, J.T. 1970. "Determination of the Manning Coefficient from Measured Bed Roughness in Natural Channels," Geological Survey Water-Supply Paper 1898-B, Prepared in cooperation with the California Department of Water Resources, US Government Printing Office, Washington DC, 20402.

Lindsey, W.F., 1938. "Typical Drag Coefficients for Various Cylinders in Two Dimensional Flow," NACA Technical Report 619.

Livsey, Robert H. 1963. "Channel Armoring Below Fort Randall Dam" *Proceedings of the Federal Inter-Agency Sedimentation Conference*, Miscellaneous Publication No. 970. Agricultural Research Service, U.S. Department of Agriculture. p 469.

McNeil, J., Taylor, C., and Lick, W. (1996) "Measurements of Erosion of Undisputed Bottom Sediments with Depth, Journal of Hydraulic Engineering,122(6), 316-324

Meyer, et al. 2002. Generalized barycentric coordinates on irregular polygons. Journal of Graphics Tools. 2002, Vol. 7.

Parker, G. (2008) "Chapter 3: Transport of Gravel and Sediment Mixtures" *ASCE Manual of Practice 120* (in press)*.*

Parker, G. (1991) "Selective Sorting and Abrasion of River Gravel I: Theory," *ASCE Journal of Hydraulic Engineering*, **117(2)**, 131-149.

Parker, G. (1991) "Selective Sorting and Abrasion of River Gravel II: Applications," *ASCE Journal of Hydraulic Engineering*, **117(2)**, 131-149.

Parmakian, J., 1963, Waterhammer Analysis, Dover Publications, Inc., NY.

Partheniades E. 1962. *A Study of Erosion and Deposition of Cohesive Soils in Salt Water*. Berkeley PhD Dissertation.

Pathirana, et al. 2008. A simple 2-D inundation model for incorporating flood damage in urban drainage planning. Hydrol. Earth Syst. Sci. Discuss. 2008, 5.

Proffitt, G.T., and Sutherland, A.J. 1983. "Transport of Non-Uniform Sediments," Journal of Hydraulic Research, vol. 21, No. 1, pp. 33-43.

Raudkivi, Arved J. 1998. "Loose Boundary Hydraulics," A.A. Balkema, Rotterdam, pp 8-28.

Ravens, T. (2007) "Comparison of Two Techniques to Measure Sediment Erodibility in the Fox River, Wisconsin," Journal of Hydraulic Engineering, 133(1), 111-115.

Reed, J.R. and A.J. Wolfkill, 1976. "Evaluation of Friction Slope Models," River 76, Symposium on Inland Waterways for Navigation Flood Control and Water Diversions, Colorado State University, CO.

Richardson, E.V., D.B. Simons and P. Julien, 1990. Highways in the River Environment, FHWA-HI-90-016, Federal Highway Administration, U.S. Department of Transportation, Washington, D.C.

Roberts, J., Jepsen, R., Gotthard, D., Lick, W. (1998) "Effects of Particle Size and Bulk Density on Erosion of Quartz Particles, ASCE Journal of Hydraulic Engineering, 124(12), 1261-1267.

Russel, Takano and Abramopoulos. 1987. Comparison of horizontal difference schemes for the shallow water equations on a sphere. Short- and Medium-Range Numerical Weather Prediction. 1987.

Rouse, H. (1965) Engineering Hydraulics, John Wiley & Sons, Inc., 1950, fifth printing, pp. 828-829.

Rubey, W.W. 1933. "Settling Velocities of Gravel, Sand, and Silt Particles," American Journal of Science, 5th Series, Vol. 25, No 148, 1933, pp. 325-338.

Sanford, L. P. and Halka, J.P. (1993) "Assessing the Paradigm of Mutually Exclusive Erosion and Deposition of Mud, With Examples from Upper Chesapeake Bay," Marine Geology, 114: 37-57.

Sanford, L.P. and Maa, J.P. (2001) "A Unified Erosion Formulation for Fine Sediments," *Marine Geology,* 179, 9-23.

Santillana and Dawson. 2010. A local discontinuous Galerkin method for a doubly nonlinear diffusion equation arising in shallow water modeling. Comp. Meth. Appl. Mech. Eng. 2010, 199.

Santillana and Dawson. 2009. A numerical approach to study the properties of solutions of the diffusive wave approximation of the shallow water equations. Comput. Geosci. 2009.

Schaffranek, R.W., et al., 1981, "A Model for the Simulation of Flow in Singular and an Interconnected Network of Channels," Techniques of Water Resources Investigations, Chapter 3, U.S. Geological Survey, Reston, VA.

Schenk and Gärtner. 2006. On fast factorization pivoting methods for symmetric indefinite systems. Elec. Trans. Numer. Anal. 2006, 23.

Schenk and Gärtner. 2011. Parallel Sparse Direct and Multi-Recursive Iterative Linear Solvers: Pardiso User Guide Version 4.1.2. 2011.

Schenk and Gärtner. 2004. Solving unsymmetric sparse systems of linear equations with PARDISO. J. Future Generation Comp. Systems. 2004, 20(3).

Schenk, Bollhoefer and Roemer. 2008. On large-scale diagonalization techniques for the Anderson model of localization. SIAM Review. 2008, 50.

Schenk, Waechter and Hagermann. 2007. Matching-based preprocessing algorithms to the solution of saddle-point problems in large-scale nonconvex interior-point optimization. J. Comp. Optim. App. 2007, Vol. 36, 2-3.

Schlichting, Hermann. 1968. "Boundary-Layer Theory," Translated by J. Kestin. McGraw-Hill Book Company, New York, pp 578-586.

Shearman, J. O., 1990. User's Manual for WSPRO - A computer model for water surface profile computations, Federal Highway Administration, Publication No. FHWA-IP-89-027, 177 p.

Shames, I.H., 1962, Mechanics of Fluids, McGraw-Hill Book Company, NY.

Simons, Daryl B., and Senturk, Fuat. 1992. "Sediment Transport Technology." Water Resources Publications, Littleton, Colorado.

Smith, R.H., 1978, "Development of a Flood Routing Model for Small Meandering Rivers," Ph.D. Dissertation, Department of Civil Engineering, University of Missouri at Rolla, MO.

Stelczer, K. 1981. "Bed-Load Transport." Water Resources Publications, Littleton, Colorado.

Streeter, V.L. and Wylie, E.B., 1967, Hydraulic Transients, McGraw-Hill Book Company, NY.

Tayefi, et al. 2007. A comparison of one- and two-dimensional approaches to modelling flood innundation over complex upland floodplains. Hydrol. Processes. 2007, 21.

Thacker. 1981. Some exact solutions to the non-linear shallow-water wave equations. J. Fluid Mech. 1981, Vol. 107.

Thomas, W. A., (1982) "Mathematical modeling of sediment movement," Chapter 18 of Gravel Bed Rivers, Edited by R.D. Hey, J.C. Bathurst and C.R. Thorne, John Wiley & Sons Ltd, 487-508.

Thomas, W. A. (2010) *Sedimentation in Stream Networks (HEC 6T): User Manual*, 388p

Toffaleti, F.B. 1968. Technical Report No. 5. "A Procedure for Computation of Total River Sand Discharge and Detailed Distribution, Bed to Surface", Committee on Channel Stabilization, U.S. Army Corps of Engineers, November, 1968

Toro-Escobar, C. M., Parker, G., Paola, C. (1996) "Transfer Function for the Deposition of Poorly Sorted Gravel in Response to Streambed Aggradation," *Journal of Hydraulic Research*, **34(1)**, 35-53.

Tucci, C.E.M., 1978, "Hydraulic and Water Quality Model for a River Network," Ph.D. Dissertation, Department of Civil Engineering, Colorado State University, Ft. Collins, CO.

U.S. Army Corps of Engineers, 1965. Hydraulic Design of Spillways, EM 1110-2-1603, Plate 33.

U.S. Army Corps of Engineers, 1990. Hydraulic Design of Spillways, EM 1110-2-1603, US Army Corps of Engineers, Washington DC.

U.S. Army Corps of Engineers, 1993. HEC 6 Scour and Deposition in Rivers and Reservoirs: User Manual, 288p.

USACE, 1993, River Hydraulics, Engineer Manual 1110-2-1416, Headquarters, U.S. Army Corps of Engineers, Washington, DC, October 1993.

US Army Corps of Engineers. 1994. "Channel Stability Assessment for Flood Control Projects," EM 1110-2-1418, US Army Corps of Engineers, Washington DC.

US Army Corps of Engineers. 1994. "Engineering and Design – Hydraulic Design of Flood Control Channels," EM 1110-2-1601, US Army Corps of Engineers, Washington DC.

US Army Corps of Engineers, Waterways Experiment Station. 1998. "SAM Hydraulic Design Package for Channels User's Manual," Vicksburg, MS.

U.S. Bureau of Reclamation (USBR), 1985, Canal Radial Gate Structure Design for Arizona Canal System, WCPM 11.04.

U.S. Geological Survey, 1953. Computation of Peak Discharge at Contractions, Geological Survey Circular No. 284, Washington, D.C.

U.S. Geological Survey, 1968. Measurement of Peak Discharge at Width Contractions By Indirect Methods, Water Resources Investigation, Book 3, Chapter A4, Washington, D.C.

Vanoni V. A. (1975) *Sedimentation Engineering*, ASCE Manuals and Reports on Engineering Practice-No. 54, 745 p.

Van Rijn, Leo C. 1984. "Sediment Transport, Part I: Bed Load Transport," Journal of Hydraulic Engineering, American Society of Civil Engineers, Vol 110, No. 10, pp 1412-1430.

Van Rijn, Leo C. 1993. "Principles of Sediment Transport in Rivers, Estuaries, Coastal Seas and Oceans," International Institute for Infrastructural, Hydraulic, and Environmental Engineering, Delft, The Netherlands.

Versteeg and Malalasekera. 2007. An Introduction to Computational Fluid Dynamics: The Finite Volume Method. 2007.

Villemonte James R. 1947. "Submerged Weir Discharge Studies." Engineering New Record, December 15, 1947. pp 54 to 57.

Wang, Zhao and Fringer. 2011. Reconstruction of vector fields for semi-Lagrangian advection on unstructured, staggered grids. Ocean Modelling. 2011, 40.

Waterways Experiment Station (WES), 1973, Bridge Pier Losses, Section 010-6, Hydraulic Design Criteria, U.S. Army Corps of Engineers, Vicksburg, MS.

Wilcock, P. R.(2001) "Toward a Practical Method for Estimating Sediment-Transport Rates in Gravel Bed Rivers," *Earth Surface Processes and Landforms*, **26**, 1395–1408.

Wilcock, P. R. and Crowe, J. C. (2003) "Surface-based Transport Model for Mixed-Size Sediment" *ASCE Journal of Hydraulic Engineering*, **129(2)**, 120-128.

Wong, M., 2003, Does the bedload equation of Meyer-Peter and Müller fit its own data?, *Proceedings,* 30th Congress, International Association of Hydraulic Research, Thessaloniki, J.F.K. Competition Volume: 73-80.

Wong, M. and Parker, G., (2006) "Reanalysis and Correction of Bed-Load Relation of Meyer-Peter and Müller Using Their Own Database," *Journal of Hydraulic Engineering*, **132**(11), 1159-1168,

Yang, C.T. 1973. "Incipient Motion and Sediment Transport," Journal of the Hydraulics Division, American Society of Civil Engineers, Vol. 99, No HY10, October, 1973, pp 1679-1704.

Yang, C.T. 1984. "Unit Stream Power Equation for Gravel," Journal of the Hydraulics Division, American Society of Civil Engineers, Vol. 110, No. 12, December 1984, pp1783-1797.

Yang, C.T., Schenggan, Wan, 1991. "Comparison of Selected Bed-Material Load Formulas," Journal of Hydraulic Engineering, American Society of Civil Engineers, Vol 117, No. 8, August 1991, pp 973-989.

Yarnell, D.L., 1934. "Bridge Piers as Channel Obstructions," Technical Bulletin 442, U.S. Department of Agriculture, Washington D.C.

Yu and Lane. 2006. Urban fluvial flood modelling using a two-dimensional diffussion-wave treatment, part 1: mesh resolution effects. Hydrol. Processes. 2006, 20.

Yu and Lane. 2006. Urban fluvial flood modelling using a two-dimensional diffussion-wave treatment, part 2: development of a sub-grid-scale treatment. Hydrol. Processes. 2006, 20.

A P P E N D I X   B

Flow Transitions in Bridge Backwater Analysis

Bridges across floodplains may require special attention in one-dimensional hydraulic modeling if they cause severe contraction and expansion of the flow. The accurate prediction of the energy losses in the contraction reach upstream from the bridge and the expansion reach downstream from the bridge, using one-dimensional models, presents particular difficulty. Modeling these reaches requires the accurate evaluation of four parameters: the expansion reach length, Le; the contraction reach length, Lc; the expansion coefficient, Ce; and the contraction coefficient, Cc. Research was conducted at the Hydrologic Engineering Center to investigate these four parameters through the use of field data, two-dimensional hydraulic modeling, and one-dimensional modeling. The conclusions and recommendations from that study are reported in this appendix. For further information regarding this study, the reader should obtain a copy of Research Document 42 (HEC, 1995).
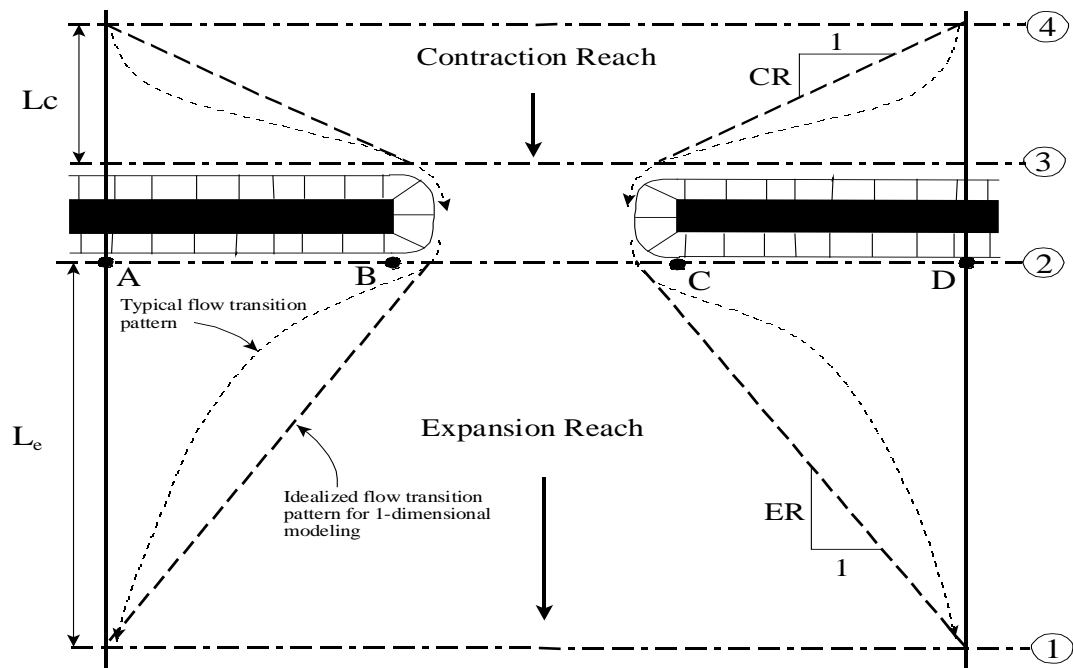
Figure B- 1 Typical Cross Section Layout for Bridge Modeling

The data used in this study consisted of 3 actual bridge sites and 76 idealized bridge sites. The field data had certain hydraulic characteristics in common. All had wide, heavily vegetated overbanks, with Manning's n values from 0.07 to 0.24, and slopes between 2.5 feet/mile and 8.0 feet/mile. To extend the scope and general applicability of the study, it was decided to create a large number of two-dimensional models (using RMA-2, King, 1994) of idealized floodplain and bridge geometries. Figure B-2 shows a typical cross section for the idealized cases. The overall floodplain width was constant at 1000 feet. The main channel n value was constant at 0.04. The other pertinent parameters were systematically varied as follows:

Bridge opening width, b = 100, 250, and 500 feet

Discharge,   Q = 5000, 10000, 20000, and 30000 cfs

Overbank Manning coef., n_{ob} =   0.04, 0.08, and 0.16

Bed slope, S =   1, 5, and 10 feet/mile
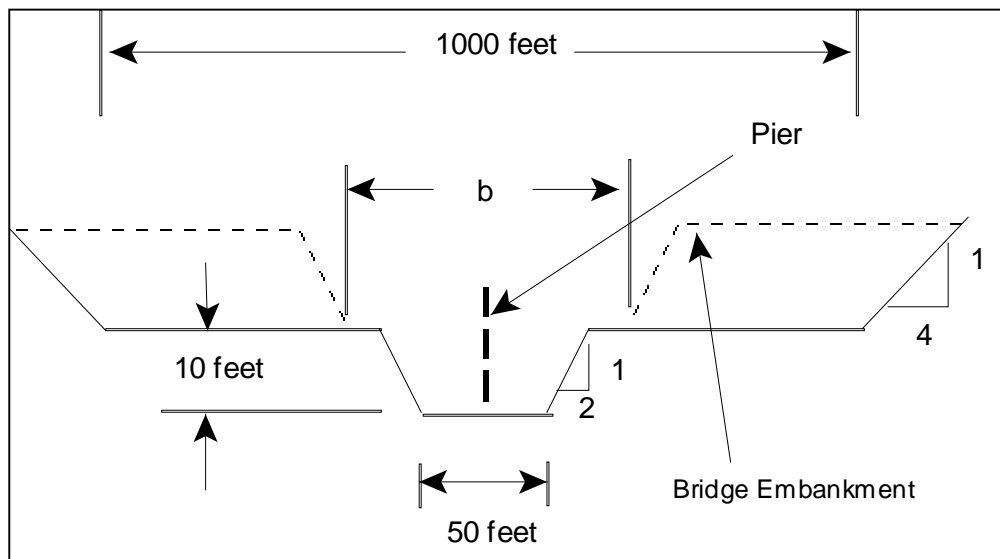
Figure B- 2 Idealized Case Cross Section

In addition to the systematic variation of these parameters, eleven additional cases were created which had vertical abutments rather than spill-through abutments, six cases were developed which had asymmetric rather than symmetric bridge obstructions, and four more cases were studied which were enlarged-scale and reduced-scale versions of four of the standard cases. A total of 97 idealized models were created.

Once the data were collected for all of the idealized models, they were analyzed with the aid of the statistical analysis program STATGRAPHICS (STSC, 1991). The goals of the statistical analysis were to compile summary statistics and develop regression relationships for the parameters of

interest where possible. Table B-1 lists the summary statistics for the four parameters of interest.

Table B-1 Summary Statistics

Variable	L_e	L_c	C_e	C_c
Sample size	76	76	76	76
Average	564 feet	386 feet	0.27	0.11
Median	510 feet	360 feet	0.30	0.10
Standard deviation	249 feet	86 feet	0.15	0.06
Minimum	260 feet	275 feet	0.10	0.10
Maximum	1600 feet	655 feet	0.65	0.50
Range	1340 feet	380 feet	0.55	0.40

The regression relationships were required to express Le, Lc, Ce, and Cc as functions of independent hydraulic variables which could be easily evaluated by the users of a one-dimensional model such as HEC-RAS. Some of the independent variables used in the regression analysis, such as discharge, slope, and roughness, had been set in defining each case. The other variables, such as Froude numbers, discharge distributions, velocities, depths, and conveyances, were evaluated from the HEC-RAS models, which had been developed for each case. The raw independent variables were then entered into a spreadsheet. In the spreadsheet other variables were created as ratios and multiples of some of the raw variables.

After the spreadsheet of independent variables was complete, it was saved as an ASCII text file, which was in turn converted into a STATGRAPHICS data file. Only the cases with symmetric openings and spill-through abutments were included in the regression analyses. Those cases which had asymmetric openings or vertical abutments, were later compared with the corresponding symmetric, spill-through cases.

Conclusions From The Study

The research has successfully provided valuable insight with regard to all four parameters of concern. Also, strong relationships between the expansion reach length, the contraction reach length and the expansion coefficient and the independent variables that affect them have emerged from the analysis of the idealized two-dimensional models. The insights gained and relationships determined from this study provide a basis for improved guidance in the bridge-related application of one-dimensional models such as HEC-RAS and HEC-2.

Expansion Reach Lengths (Le on Figure B-1)

Of all of the two-dimensional cases created for this study, which included a wide range of hydraulic and geometric conditions, none of the cases had an expansion ratio (ER on Figure B-1) as great as 4:1. Most of the cases had expansion ratios between 1:1 and 2:1. This indicates that a dogmatic use of the traditional 4:1 rule of thumb for the expansion ratio leads to a consistent over prediction of the energy losses in the expansion reach in most cases. The accompanying over prediction of the water surface elevation at the downstream face of the bridge may be conservative for flood stage prediction studies. For bridge scour studies, however, this overestimation of the tailwater elevation could in some circumstances lead to an underestimation of the scour potential.

The results from the two-dimensional flow models did not always indicate the presence of large-scale flow separations or eddy zones downstream of the bridge. Their presence corresponded with the larger values of Le. For many of the cases there was no significant separation evident in the results. In sensitivity tests, the presence or absence of eddy zones was not sensitive to the eddy viscosity coefficient value. Likewise, eddy viscosity settings did not have an appreciable effect on Le.

It was found that the ratio of the channel Froude number at Section 2 to that at Section 1 (Fc2/Fc1) correlated strongly with the length of the expansion reach. Regression equations were developed for both the expansion reach length and the expansion ratio. The equations are presented later in this appendix. Both equations are linear and contain terms involving the Froude number ratio and the discharge. The equation for expansion length also includes the average obstruction length in one term. To use these regression equations in the application of a one-dimensional model will usually require an iterative process since the hydraulic properties at Section 2 will not be known in advance. The effort involved in this process will not be large, however, because the method will usually converge rapidly.

The value of the Froude number ratio reflects important information about the relationship between the constricted flow and the normal flow conditions. It is in effect a measure of the degree of flow constriction since it compares the intensity of flow at the two locations. Since these Froude numbers are for the main channel only, the value of Fc1 also happens to reflect to some extent the distribution of flow between the overbanks and main channel.

There was no support from these investigations for the WSPRO concept of the expansion reach length being proportional to or equal to the bridge opening width.

Contraction Reach Lengths (Lc on Figure B-1)

While the apparent contraction ratios of the five field prototype cases were all below 1:1, the contraction ratios (CR on Figure B-1) for the idealized cases ranged from 0.7:1 to 2.3:1.   As with the expansion reach lengths, these values correlated strongly with the same Froude number ratio. A more important independent variable, however, is the decimal fraction of the total discharge conveyed in the overbanks (Qob/Q) at the approach section. A strong regression equation was developed for the contraction length and is presented later in this appendix.

Because the mean and median values of the contraction ratios were both around 1:1, there is some support from this study for the rule of thumb which suggests the use of a 1:1 contraction ratio. There is no support, however, for the concept of the contraction reach length being equal to or proportional to the bridge opening width.

Expansion Coefficients

Regression analysis for this parameter was only marginally successful. The resulting relationship is a function of the ratio of hydraulic depth in the overbank to that in the main channel for undisturbed conditions (evaluated at Section 1). Perhaps more interesting are the summary statistics, which indicate lower values for this coefficient than the traditional standard values for bridges.

Contraction Coefficients

Owing to the nature of this data (69 out of 76 cases had the minimum value of 0.10), a regression analysis was not fruitful. Like the expansion coefficients, the prevailing values are significantly lower than the standard recommended values.

Asymmetric Bridge Openings

For these data the averages of the reach length values for the two corresponding symmetric cases closely approximated the values determined for the asymmetric cases. When the regression equations for Le, ER, and Lc were applied to the asymmetric cases, the predicted values were near the observed values.   This indicates that the regression relationships for the transition reach lengths can also be applied to asymmetric cases (that is, most real-world cases).

Vertical-Abutment Cases

For these data there was no major effect on the transition lengths or the coefficients due to the use of vertical rather than spill-through abutments. The exceptions to this statement were three vertical-abutment cases in the narrow-opening class for which square corners were used. The square-cornered abutments were a deliberate attempt to model a very severe situation. Because the RMA-2 program, or any two-dimensional numerical model for that matter, is not well-formulated to handle such drastic boundary conditions, no general conclusions should be drawn from these cases about actual field sites having such a configuration.

Recommendations From The Study

The remainder of this appendix presents recommendations arising from the results documented in RD-42 (HEC, 1995). These recommendations are intended to provide the users of one-dimensional water surface profile programs, such as HEC-RAS, with guidance on modeling the flow transitions in bridge hydraulics problems.

In applying these recommendations, the modeler should always consider the range of hydraulic and geometric conditions included in the data. Wherever possible, the transition reach lengths used in the model should be validated by field observations of the site in question, preferably under conditions of high discharge. The evaluation of contraction and expansion coefficients should ideally be substantiated by site-specific calibration data, such as stage-discharge measurements just upstream of the bridge. The following recommendations are given in recognition of the fact that site-specific field information is often unavailable or very expensive to obtain.

Expansion Reach Lengths

In some types of studies, a high level of sophistication in the evaluation of the transition reach lengths is not justified. For such studies, and for a starting point in more detailed studies, Table B-2 offers ranges of expansion ratios, which can be used for different degrees of constriction, different slopes, and different ratios of overbank roughness to main channel roughness. Once an expansion ratio is selected, the distance to the downstream end of the expansion reach (the distance Le on Figure B-1) is found by multiplying the expansion ratio by the average obstruction length (the average of the distances A to B and C to D from Figure B-1). The average obstruction length is half of the total reduction in floodplain width caused by the two bridge approach embankments. In Table B-2, b/B is the ratio of the bridge opening width to the total floodplain width, nob is the Manning n value for the overbank, nc is the n value for the main channel, and S is the longitudinal slope. The values in the interior of the table are the ranges of the expansion ratio. For each range, the higher value is typically associated with a higher discharge.

Table B-2 Ranges of Expansion Ratios

		nob / nc = 1	nob / nc = 2	nob / nc = 4
b/B = 0.10	**S = 1 ft/mile**	1.4 – 3.6	1.3 – 3.0	1.2 – 2.1
	5 ft/mile	1.0 – 2.5	0.8 – 2.0	0.8 – 2.0
	10 ft/mile	1.0 – 2.2	0.8 – 2.0	0.8 – 2.0
b/B = 0.25	S = 1 ft/mile	1.6 – 3.0	1.4 – 2.5	1.2 – 2.0
	5 ft/mile	1.5 – 2.5	1.3 – 2.0	1.3 – 2.0
	10 ft/mile	1.5 – 2.0	1.3 – 2.0	1.3 – 2.0
b/B = 0.50	S = 1 ft/mile	1.4 – 2.6	1.3 – 1.9	1.2 – 1.4
	5 ft/mile	1.3 – 2.1	1.2 – 1.6	1.0 – 1.4
	10 ft/mile	1.3 – 2.0	1.2 – 1.5	1.0 – 1.4

The ranges in Table B-2, as well as the ranges of other parameters to be presented later in this appendix, capture the ranges of the idealized model data from this study. Another way of establishing reasonable ranges would be to compute statistical confidence limits (such as 95% confidence limits) for the regression equations. Confidence limits in multiple linear regression equations have a different value for every combination of values of the independent variables (Haan, 1977). The computation of these limits entails much more work and has a more restricted range of applicability than the corresponding limits for a regression, which is based on only one independent variable. The confidence limits were, therefore, not computed in this study.

Extrapolation of expansion ratios for constriction ratios, slopes or roughness ratios outside of the ranges used in this table should be done with care. The expansion ratio should not exceed 4:1, nor should it be less than 0.5:1 unless there is site-specific field information to substantiate such values. The ratio of overbank roughness to main-channel roughness provides information about the relative conveyances of the overbank and main channel. The user should note that in the data used to develop these recommendations, all cases had a main-channel n value of 0.04. For significantly higher or lower main-channel n values, the n value ratios will have a different meaning with respect to overbank roughness. It is impossible to determine from the data of this study whether this would introduce significant error in the use of these recommendations.

When modeling situations which are similar to those used in the regression analysis (floodplain widths near 1000 feet; bridge openings between 100 and 500 feet wide; flows ranging from 5000 to 30000 cfs; and slopes between one and ten feet per mile), the regression equation for the expansion reach length can be used with confidence. The equation developed for the expansion reach length is as follows:

$$L_e = -298 + 257\left(\frac{F_{c2}}{F_{c1}}\right) + 0.918\,\overline{L}_{obs} + 0.00479\,Q$$

(B-1)

Where: L_e = length of the expansion reach, in feet

F_{c2} = main channel Froude number at Section 2

F_{c1} = main channel Froude number at Section 1

L_{obs} = average length of obstruction caused by the two bridge approaches, in feet, and

Q = total discharge, cfs

When the width of the floodplain and the discharge are smaller than those of the regression data (1000 ft wide floodplain and 5000 cfs discharge), the expansion ratio can be estimated by

Equation B-2. The computed value should be checked against ranges in Table B-1. Equation B-2 is:

$$ER = \frac{L_e}{\overline{L_{obs}}} = 0.421 + 0.485\left(\frac{F_{c2}}{F_{c1}}\right) + 0.000018\,Q \qquad \text{(B-2)}$$

When the scale of the floodplain is significantly larger than that of the data, particularly when the discharge is much higher than 30,000 cfs, Equations B-1 and B-2 will overestimate the expansion reach length. Equation B-3 should be used in such cases, but again the resulting value should be checked against the ranges given in Table B-1:

$$ER = \frac{L_e}{\overline{L_{obs}}} = 0.489 + 0.608\left(\frac{F_{c2}}{F_{c1}}\right)$$

(B-3)

The depth at Section 2 is dependent upon the expansion reach length, and the Froude number at the same section is a function of the depth. This means that an iterative process is required to use the three equations above, as well as the equations presented later in this chapter for contraction reach lengths and expansion coefficients. It is recommended that the user start with an expansion ratio from Table B-1, locate Section 1 according to that expansion ratio, set the main channel and overbank reach lengths as appropriate, and limit the effective flow area at Section 2 to the approximate bridge opening width. The program should then be run and the main channel Froude numbers at Sections 2 and 1 read from the model output. Use these Froude number values to determine a new expansion length from the appropriate equation, move Section 1 as appropriate and recompute. Unless the geometry is changing rapidly in the vicinity of Section 1, no more than two iterations after the initial run should be required.

When the expansion ratio is large, say greater than 3:1, the resulting reach length may be so long as to require intermediate cross sections, which reflect the changing width of the effective flow area. These intermediate sections are necessary to reduce the reach lengths when they would otherwise be too long for the linear approximation of energy loss that is incorporated in the standard step method. These interpolated sections are easy to create in the HEC-RAS program, because it has a graphical cross section interpolation feature. The importance of interpolated sections in a given reach can be tested by first inserting one interpolated section and seeing the effect on the results. If the effect is significant, the subreaches should be subdivided into smaller units until the effect of further subdivision is inconsequential.

Contraction Reach Lengths

Ranges of contraction ratios (CR) for different conditions are presented in Table B-3.

These values should be used as starting values and for studies which do not justify a sophisticated evaluation of the contraction reach length. Note that this table does not differentiate the ranges on the basis of the degree of constriction. For each range the higher values are typically associated with higher discharges and the lower values with lower discharges.

	nob / nc = 1	nob / nc = 2	nob / nc = 4
S = 1 ft/mile	1.0 - 2.3	0.8 - 1.7	0.7 - 1.3
5 ft/mile	1.0 - 1.9	0.8 - 1.5	0.7 - 1.2
10 ft/mile	1.0 - 1.9	0.8 - 1.4	0.7 - 1.2

Table B-3 Ranges of Contraction Ratios (CR)

When the conditions are within or near those of the data, the contraction reach length regression equation (Equation B-4) may be used with confidence:

$$L_c = 263 + 38.8\left(\frac{F_{c2}}{F_{c1}}\right) + 257\left(\frac{Q_{ob}}{Q}\right)^2 - 58.7\left(\frac{n_{ob}}{n_c}\right)^{0.5} + 0.161\overline{L}_{obs}$$

(B-4)

Where: $\underline{L}_{obs}$ = average length of obstruction as described earlier in this chapter, in feet

Q_{ob} = the discharge conveyed by the two overbanks, in cfs, at the approach section (Section 4)

n_{ob} = the average Manning n value for the overbanks at Section 4, and

n_c = the average Manning n value for the main channel at Section 4

In cases where the floodplain scale and discharge are significantly larger or smaller than those that were used in developing the regression formulae, Equation B-4 should not be used. The recommended approach for estimating the contraction ratio at this time is to compute a value from Equation B-5 and check it against the values in Table B-3:

$$CR = 1.4 - 0.333\left(\frac{F_{c2}}{F_{c1}}\right) + 1.86\left(\frac{Q_{ob}}{Q}\right)^2 - 0.19\left(\frac{n_{ob}}{n_c}\right)^{0.5}$$

(B-5)

As with the expansion reach lengths, the modeler must use Equations B-4 and B-5 and the values from Table B-2 with extreme caution when the prototype is outside of the range of data used in this study. The contraction ratio should not exceed 2.5:1 nor should it be less than 0.3:1.

Expansion Coefficients

The analysis of the data with regard to the expansion coefficients did not yield a regression equation, which fit the data well. Equation B-6 was the best equation obtained for predicting the value of this coefficient:

$$C_e = -0.09 + 0.570\left(\frac{D_{ob}}{D_c}\right) + 0.075\left(\frac{F_{c2}}{F_{c1}}\right)$$

(B-6)

Where: D_{ob} =   hydraulic depth (flow area divided by top width) for the overbank at the fully- expanded flow section (Section 1), in feet, and

D_c =   hydraulic depth for the main channel at the fully-expanded flow section, in feet

It is recommended that the modeler use Equation B-6 to find an initial value, then perform a sensitivity analysis using values of the coefficient that are 0.2 higher and 0.2 lower than the value from Equation B-6. The plus or minus 0.2 range defines the 95% confidence band for Equation B-6 as a predictor within the domain of the regression data. If the difference in results between the two ends of this range is substantial, then the conservative value should be used. The expansion coefficient should not be higher than 0.80.

Contraction Coefficients

The data of this study did not lend itself to regression of the contraction coefficient values. For nearly all of the cases the value that was determined was 0.1, which was considered to be the minimum acceptable value. The following table presents recommended ranges of the contraction coefficient for various degrees of constriction, for use in the absence of calibration information.

Table B-4 Contraction Coefficient Values

Degree of Constriction	Recommended Contraction Coefficient
0.0 < b/B < 0.25	0.3 - 0.5
0.25 < b/B < 0.50	0.1 - 0.3
0.50 < b/B < 1.0	0.1

The preceding recommendations represent a substantial improvement over the guidance information that was previously available on the evaluation of transition reach lengths and coefficients. They are based on data, which, like all data, have a limited scope of direct application. Certain situations, such as highly skewed bridge crossings and bridges at locations of sharp curvature in the floodplain were not addressed by this study. Even so, these recommendations may be applicable to such situations if proper care is taken and good engineering judgment is employed.

A P P E N D I X   C

Computational Differences Between HEC-RAS and HEC-2

HEC-RAS is a completely new software product. None of the computational routines in the HEC-2 program were used in the HEC-RAS software. When HEC-RAS was being developed, a significant effort was spent on improving the computational capabilities over those in the HEC-2 program.   Because of this, there are computational differences between the two programs. This appendix describes all of the major areas in which computational differences can occur.

Cross Section Conveyance Calculations

Both HEC-RAS and HEC-2 utilize the Standard Step method for balancing the energy equation to compute a water surface for a cross section. A key element in the solution of the energy equation is the calculation of conveyance. The conveyance is used to determine friction losses between cross sections, the flow distribution at a cross section, and the velocity weighing coefficient alpha. The approach used in HEC-2 is to calculate conveyance between every coordinate point in the cross section overbanks (Figure C-1). The conveyance is then summed to get the total left overbank and right overbank values. HEC-2 does not subdivide the main channel for conveyance calculations. This method of computing overbank conveyance can lead to different amounts of total conveyance when additional points are added to the cross section, without actually changing the geometry.   The HEC-RAS program supports this method for calculating conveyance, but the default method is to make conveyance calculations only at n-value break points (Figure C-2).
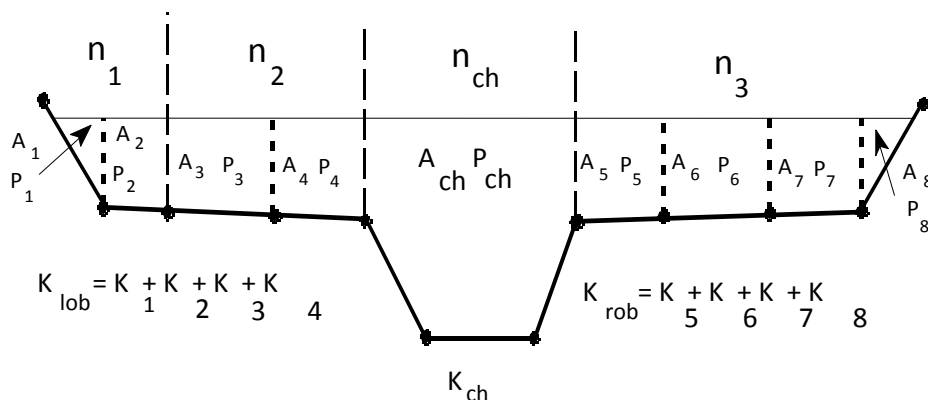
Figure C-1 HEC-2 Conveyance Subdivision
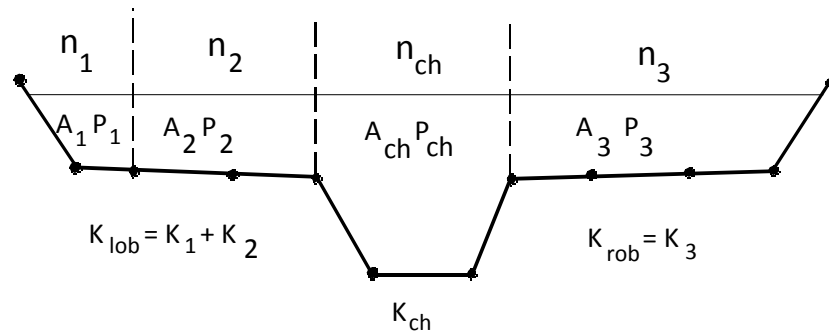
Figure C-2 HEC-RAS Default Conveyance Subdivision Method

Testing Using HEC-2 Conveyance Calculation Approach

Comparisons of HEC-RAS results with those from HEC-2 were performed using 97 data sets from the HEC profile accuracy study (HEC, 1986). Water surface profiles were computed for 10% and 1% chance floods using HEC-2 and HEC-RAS, both programs using the HEC-2 approach for computing overbank conveyance. Table C-1 shows the percentage, of approximately 2000 cross sections, within ±0.02 feet (±6 mm). For the 10% chance flood, 53 cross sections had difference greater than ±0.02 feet (±6 mm). For those sections, 62.2% were caused by differences in computation of critical depth and 34% resulted from propagation of the difference upstream. For the 1% chance flood, 88 sections had elevation differences over ±0.02 feet (6 mm), of which 60.2% resulted from critical depth and 36.4% from the upstream propagation of downstream differences. HEC-RAS uses 0.01 feet (3 mm) for the critical depth error criterion, while HEC-2 uses 2.5% of the depth of flow.

Table C- 1 Computed Water Surface Elevation Difference (HEC-RAS - HEC-2)

Difference (feet)	-0.02	-0.01	0.0	0.01	0.02	Total
10% Chance Flood	0.8%	11.2%	73.1%	11.2%	0.6%	96.9%
1% Chance Flood	2.0%	11.6%	70.1%	10.8%	1.3%	95.8%

Testing Using HEC-RAS and HEC-2 Approach

The two methods for computing conveyance will produce different answers whenever portions of the overbanks have ground sections with significant vertical slopes. In general, the HEC-RAS default approach will provide a lower total conveyance for the same elevation and, therefore, a higher computed water surface elevation. In order to test the significance of the two ways of computing conveyance, comparisons were performed using the same 97 data sets. Water surface profiles were computed for the 1% chance event using the two methods for computing conveyance in HEC-RAS. The results confirmed that the HEC-RAS default approach will generally produce a higher computed water surface elevation. Out of the 2048 cross section locations, 47.5% had computed water surface elevations within 0.10 feet (30.5 mm), 71% within 0.20 feet (61 mm), 94.4% within 0.40 feet (122 mm), 99.4% within 1.0 feet (305 mm), and one cross section had a difference of 2.75 feet (0.84 m). Because the differences tend to be in the same direction, some effects can be attributed to propagation.

The results from these comparisons do not show which method is more accurate, they only show differences. In general, it is felt that the HEC-RAS default method is more commensurate with the Manning equation and the concept of separate flow elements. The default method in HEC-RAS is also more consistent, in that the computed conveyance is based on the geometry, and not on how many points are used in the cross section. Further research, with observed water surface profiles, will be needed to make any final conclusions about the accuracy of the two methods.

Critical Depth Calculations

During the water surface profile calculations, each of the two programs may need to calculate critical depth at a cross section if any of the following conditions occur:

(1)   The supercritical flow regime has been specified by the user.

(2)   The calculation of critical depth has been requested by the user.

(3)   The current cross section is an external boundary cross section and critical depth must be determined to ensure the user-entered boundary condition is in the correct flow regime.

(4)   The Froude number check for a subcritical profile indicates that critical depth needs to be determined to verify the flow regime of the computed water surface elevation.

(5)   The program could not balance the energy equation within the specified tolerance before reaching the maximum number of iterations.

The HEC-RAS program has two methods for calculating critical depth: a "parabolic" method and a "secant" method. The HEC-2 program has one method, which is very similar to the HEC-RAS "parabolic" method. The parabolic method is computationally faster, but it is only able to locate a single minimum energy. For most cross sections there will only be one minimum on the total energy curve; therefore, the parabolic method has been set as the default method for HEC-RAS (the default method can be changed from the user interface). If the parabolic method is tried

and it does not converge, then the HEC-RAS program will automatically try the secant method. The HEC-RAS version of the parabolic method calculates critical depth to a numerical accuracy of 0.01 feet, while HEC-2's version of the parabolic method calculates critical depth to a numerical accuracy of 2.5 percent of the flow depth. This, in its self, can lead to small differences in the calculation of critical depth between the two programs.

In certain situations it is possible to have more than one minimum on the total energy curve. Multiple minimums are often associated with cross sections that have breaks in the total energy curve. These breaks can occur due to very wide and flat overbanks, as well as cross sections with levees and ineffective flow areas. When the parabolic method is used on a cross section that has multiple minimums on the total energy curve, the method will converge on the first minimum that it locates. This approach can lead to incorrect estimates of critical depth, in that the returned value for critical depth may be the top of a levee or an ineffective flow elevation. When this occurs in the HEC-RAS program, the software automatically switches to the secant method. The HEC-RAS secant method is capable of finding up to three minimums on the energy versus depth curve. Whenever more than one minimum energy is found, the program selects the lowest valid minimum energy (a minimum energy at the top of a levee or ineffective flow elevation is not considered a valid critical depth solution).

Given that HEC-RAS has the capability to find multiple critical depths, and detect possible invalid answers, the final critical depth solutions between HEC-2 and HEC-RAS could be quite different. In general the critical depth answer from the HEC-RAS program will always be more accurate than HEC-2.

Bridge Hydraulic Computations

A vast amount of effort has been spent on the development of the new bridge routines used in the HEC-RAS software. The bridge routines in HEC-RAS allow the modeler to analyze a bridge by several different methods with the same bridge geometry. The model utilizes four user defined cross sections in the computations of energy losses due to the structure. Cross sections are automatically formulated inside the bridge on an as need basis by combining the bridge geometry with the two cross sections that bound the structure.

The HEC-2 program requires the user to use one of two possible methods, the special bridge routine or the normal bridge routine. The data requirements for the two methods are different, and therefore the user must decide a prior which method to use.

Differences between the HEC-2 and HEC-RAS bridge routines will be addressed by discussing the two HEC-2 bridge methodologies separately.

HEC-2 Special Bridge Methodology

The largest computational differences will be found when comparing the HEC-2 special bridge routines to the equivalent HEC-RAS bridge methodologies. The following is a list of what is different between the two programs:

1.   The HEC-2 special bridge routines use a trapezoidal approximation for low flow calculations (Yarnell equation and class B flow check with the momentum equation). The HEC-RAS program uses the actual bridge opening geometry for all of the low flow methodologies.

2.   Also for low flow, the HEC-2 program uses a single pier (of equivalent width to the sum total width of all piers) placed in the middle of the trapezoid. In the HEC-RAS software, all of the piers are defined separately, and the hydraulic computations are performed by evaluating the water surface and impact on each pier individually. While this is more data for the user to enter, the results are much more physically based.

3.   For pressure flow calculations, HEC-2 requires the net flow area of the bridge opening. The HEC-RAS software calculates the area of the bridge opening from the bridge and cross section geometry. Because of the potential error involved in calculating the bridge opening area by hand, differences between the programs may occur for pressure flow calculations.

4.   The HEC-RAS software has two equations that can be used for pressure flow. The first equation is for a fully submerged condition (i.e. when both the upstream side and downstream side of the bridge is submerged). The fully submerged equation is also used in HEC-2. A second equation is available in HEC-RAS, which is automatically applied when only the upstream side of the bridge is submerged. This equation computes pressure flow as if the bridge opening were acting as a sluice gate. The HEC-2 program only has the fully submerged pressure flow equation. Therefore, when only the upstream side of the bridge is submerged, the two programs will compute different answers for pressure flow because they will be using different equations.

5.   When using the HEC-2 special bridge routines, it is not necessary for the user to specify low chord information in the bridge table (BT data). The bridge table information is only used for weir flow in HEC-2. When HEC-2 special bridge data is imported into HEC-RAS, the user must enter the low chord information in order to define the bridge opening. This is due to the fact that the trapezoidal approximation used in HEC-2 is not used in HEC-RAS, and therefore the opening must be completely defined.

6.   When entering bridge table (BT records) information in the HEC-2 special bridge method, the user had to enter stations that followed along the ground in the left overbank, then across the bridge deck/road embankment; and then along the ground of the right overbank. This was necessary in order for the left and right overbank area to be used in the weir flow calculations. In HEC-RAS this is not necessary. The bridge deck/roadway information only needs to reflect the additional blocked

out area that is not part of the ground. HEC-RAS will automatically merge the ground information and the high chord data of the bridge deck/roadway.

HEC-2 Normal Bridge Methodology

In general, when importing HEC-2 normal bridge data into HEC-RAS there should not be any problems. The program automatically selects the energy-based methods for low flow and high flow conditions, which is equivalent to the normal bridge method. The following is a list of possible differences that can occur.

1.   In HEC-2 pier information is either entered as part of the bridge table (BT data) or the ground information (GR data). If the user stays with the energy based methods in HEC-RAS the results should be about the same. If the user wishes to use either the Momentum or Yarnell methods for low flow, they must first delete the pier information from the BT or GR data, and then re-enter it as separate pier information in HEC-RAS. If this is not done, HEC-RAS will not know about the pier information, and will therefore incorrectly calculate the losses with either the Momentum or Yarnell methods.

2.   The HEC-2 Normal bridge method utilizes six cross sections. HEC-RAS uses only four cross sections in the vicinity of the bridge. The two cross sections inside the bridge are automatically formulated from the cross sections outside the bridge and the bridge geometry. In general, it is common for HEC-2 users to repeat cross sections through the bridge opening (i.e. the cross sections used inside the bridge were a repeat of the downstream section). If however, the HEC-2 user entered completely different cross sections inside the bridge than outside, the HEC-RAS software will add two additional cross sections just outside of the bridge, in order to get the correct geometry inside of the bridge. This however gives the HEC-RAS data set two more cross-sections than the original HEC-2 data set. The two cross sections are placed at zero distance from the bridge, but could still cause some additional losses due to contraction and expansion of flow. The user may want to make some adjustments to the data when this happens.

3.   In HEC-2 the stationing of the bridge table (BT Records) had to match stations on the ground (GR data). This is not required in HEC-RAS. The stationing of the data that makes up a bridge (ground, deck/roadway, piers, and abutments) does not have to match in any way, HEC-RAS will interpolate any points that it needs.

Culvert Hydraulic Computations

The culvert routines in HEC-RAS and HEC-2 were adapted from the Federal Highway Administrations Hydraulic Design of Highway Culverts publication, HDS No. 5 (FHWA, 1985). The following is a list of the differences between the two programs.

    1.   HEC-2 can only perform culvert calculations for box and circular culvert shapes. HEC-RAS can handle the following shapes: box; circular pipe; semi-circle; arch; pipe arch, vertical ellipse; horizontal ellipse; low profile arch; high profile arch; and ConSpan.

    2.   HEC-RAS also has the ability to mix the culvert shapes, sizes, and all other parameters at any single culvert crossing. In HEC-2 the user is limited to the same shape and size barrels.

    3.   HEC-RAS has the ability to use two roughness coefficients inside the culvert barrel (one for the top and sides, and one for the bottom). This allows for better modeling of culverts that have a natural bottom, or culverts that were designed for fish passage.

    4.   HEC-RAS allows the user to fill in a portion of a culvert. This allows users to model culverts that are buried.

Floodway Encroachment Calculations

The floodway encroachment capabilities in HEC-RAS were adapted from those found in HEC-2. For the most part, encroachment methods 1-3 in HEC-RAS are the same as methods 1-3 in HEC-2. The following is a list of the differences between the two programs.

    1.   HEC-RAS has an additional capability of allowing the user to specify a left and right encroachment offset. While in general the encroachments can go all the way up to the main channel bank stations, the offset establishes an additional buffer zone around the main channel bank stations for limiting the encroachments. The offset is applicable to methods 2-5 in HEC-RAS.

    2.   The logic of method 4 in HEC-RAS is the same as method 4 in HEC-2. The only difference is that the HEC-RAS method 4 will locate the final encroachment to an accuracy of 0.01 feet, while the HEC-2 method 4 uses a parabolic interpolation method between the existing cross section points. Since conveyance is non-linear with respect to the horizontal stationing, the interpolation in HEC-2 does not always find the encroachment station as accurately as HEC-RAS.

    3.   Method 5 in HEC-RAS is a combination of HEC-2's methods 5 and 6. The HEC-RAS method five can be used to optimize for a change in water

surface (HEC-2 method 5); a change in energy (HEC-2 method 6); or both parameters at the same time (new feature).

4.   At bridges and culverts, the default in HEC-RAS is to perform the encroachment, while in HEC-2 the default was not to perform the encroachment. Both programs have the ability to turn encroachments at bridges and culverts on or off.

5.   At bridges where the energy based modeling approach is being used (similar to HEC-2's normal bridge method), HEC-RAS will calculate the encroachment for each of the cross sections through the bridge individually. HEC-2 will take the encroachments calculated at the downstream side of the bridge and fix those encroachment stations the whole way through the bridge.

6.   In HEC-2, if the user specifies a fixed set of encroachments on the X3 record, this would override anything on the ET record. In HEC-RAS, when the data is imported the X3 record encroachment is converted into a blocked obstruction.   Therefore any additional encroachment information found on the ET record will be used in addition to the blocked obstruction.

New Computational Features in HEC-RAS

1.   HEC-RAS can perform sub-critical, supercritical, or mixed flow regime calculations all in a single execution of the program. The cross section order does not have to be reversed (as in HEC-2), the user simply presses a single button to select the computational flow regime. When in a mixed flow regime mode, HEC-RAS can also locate hydraulic jumps.

2.   HEC-RAS has the ability to perform multiple bridge and/or culvert openings at the same road crossing.

3.   At bridges, the user has the ability to use a momentum-based solution for class A, B, and C low flow. In HEC-2 the momentum equation was used for class B and C flow, and requires the trapezoidal approximation. The HEC-RAS momentum solution also takes into account friction and weight forces that HEC-2 does not.

4.   HEC-RAS can model single reaches, dendritic stream systems, or fully looped network systems. HEC-2 can only do single reaches and a limited number of tributaries (up two three stream orders).

5.   At stream junctions, HEC-RAS has the ability to perform the calculations with either an energy-based method or a momentum based method. HEC-2 only has the energy based method.

6.   HEC-RAS has the following new cross section properties not found in HEC-2: blocked ineffective flow areas; normal ineffective flow areas can be located at any station (in HEC-2 they are limited to the main channel bank stations); blocked obstructions; and specification of levees.

7.   In HEC-RAS the user can enter up to 500 points in a cross section. HEC-2 has a limit of 100.

8.   HEC-RAS has the ability to perform geometric cross section interpolation. HEC-2 interpolation is based on a ratio of the current cross section and a linear elevation adjustment.

9.   HEC-RAS has an improved flow distribution calculation routine. The new routine can subdivide the main channel as well as the overbanks, and the user has control over how many subdivisions are used. The HEC-2 flow distribution option is limited to the overbank areas and breaks at existing coordinate points.

A P P E N D I X   D

Computation of the WSPRO Discharge Coefficient and Effective Flow Length

This appendix documents how the effective flow length and discharge coefficient are computed for the WSPRO bridge hydraulics methodology in HEC-RAS. The effective flow length is used in the computation of friction losses from the cross section just upstream of the bridge (section 3) to the approach cross section (section 4). The coefficient of discharge is used in the expansion loss equation from sections 1 to 2. The information in this appendix was extracted directly from the Federal Highway Administrations Research Report entitled: "Bridge Waterways Analysis Model" (FHWA, 1986).

Effective Flow Length

Since friction losses are directly proportional to flow length, it becomes imperative to obtain the best possible estimate of flow length, especially for those cases where the friction loss is a significant component of the energy balance between two sections. For minor degrees of constriction, a straight line distance between cross sections is usually adequate. However, for more significant constrictions, this straight-line distance is representative of only that portion of the flow that is generally in direct line with the opening. Flow further away from the opening must flow not only downstream, but also across the valley to get to the opening, thus traveling much farther than the straight-line distance.

Schneider et al. (USGS, 1977) tabulated average streamline lengths for various approach section locations and various degrees of constriction. These results are not directly applicable in this model because they are derived for symmetric constrictions in channel reaches having uniform, homogeneous flow conveyance characteristics. Even if the exact-solution algorithms were developed for non-symmetric, non-homogeneous conditions, the computer resource requirements for an exact solution are too great to warrant inclusion in the model. Therefore, a simplified computational technique was developed and incorporated into the model to compute average streamline length.

Schneider et al., defined the optimum location of the approach section as:

$$L_{opt} = \frac{b}{\pi\left(1 - m'\right)}\phi \tag{D-1}$$

Where L_{opt} is the distance, in ft, between the approach section and the upstream face of the bridge opening, b is the bridge-opening width, and m' is the geometric contraction ratio computed by:

$$m' = 1 - \frac{b}{B} \tag{D-2}$$

Where B is the top width, in ft, of the approach section flow area. The Φ term in equation D-1 is computed by:

$$\phi = \frac{1}{2} \ln\left[\left(\sqrt{\frac{8}{\varepsilon^2} + 8} - \frac{3}{\varepsilon} - \varepsilon \right) \left(\sqrt{8 + 8\varepsilon^2} - 3\varepsilon - \frac{1}{\varepsilon} \right) \right] - \ln\left(\varepsilon - \frac{1}{\varepsilon} \right) \tag{D-3}$$

Where ε is computed by:

$$\varepsilon = 1 + \delta + \sqrt{\delta^2 + 2\delta} \tag{D-4}$$

With δ computed as:

$$\delta = \frac{2}{\tan^2\left[\left(1 - \frac{b}{2B} \right) \pi \right]} \tag{D-5}$$

L_{opt} is located in a zone of nearly one-dimensional flow, thus satisfying the basic requirements of the one-dimensional energy equation.

The simplified computational technique varies depending upon the relative magnitudes of Lopt and b. To introduce the technique, discussion is limited to the ideal situation of a symmetric constriction with uniform, homogeneous conveyance. For such conditions only one-half of the valley cross-section is required. This one-half section is divided into ten equal conveyance stream tubes between edge of water and the centerline at both the Lopt location and the upstream face of the bridge. Equal-conveyance stream tubes are equivalent to equal-flow stream tubes for one-dimensional flow. Figure D-1 illustrates a case with a small geometric contraction ratio. Lopt is less than b for lesser degrees of constriction. Since Lopt is located in a zone of nearly one-dimensional flow, the streamlines are essentially parallel between the approach section and the Lopt location. Between Lopt and the bridge opening the corresponding flow division points are connected with straight lines. The effective flow length used by the model is the average length of the ten equal-flow stream tubes computed by:
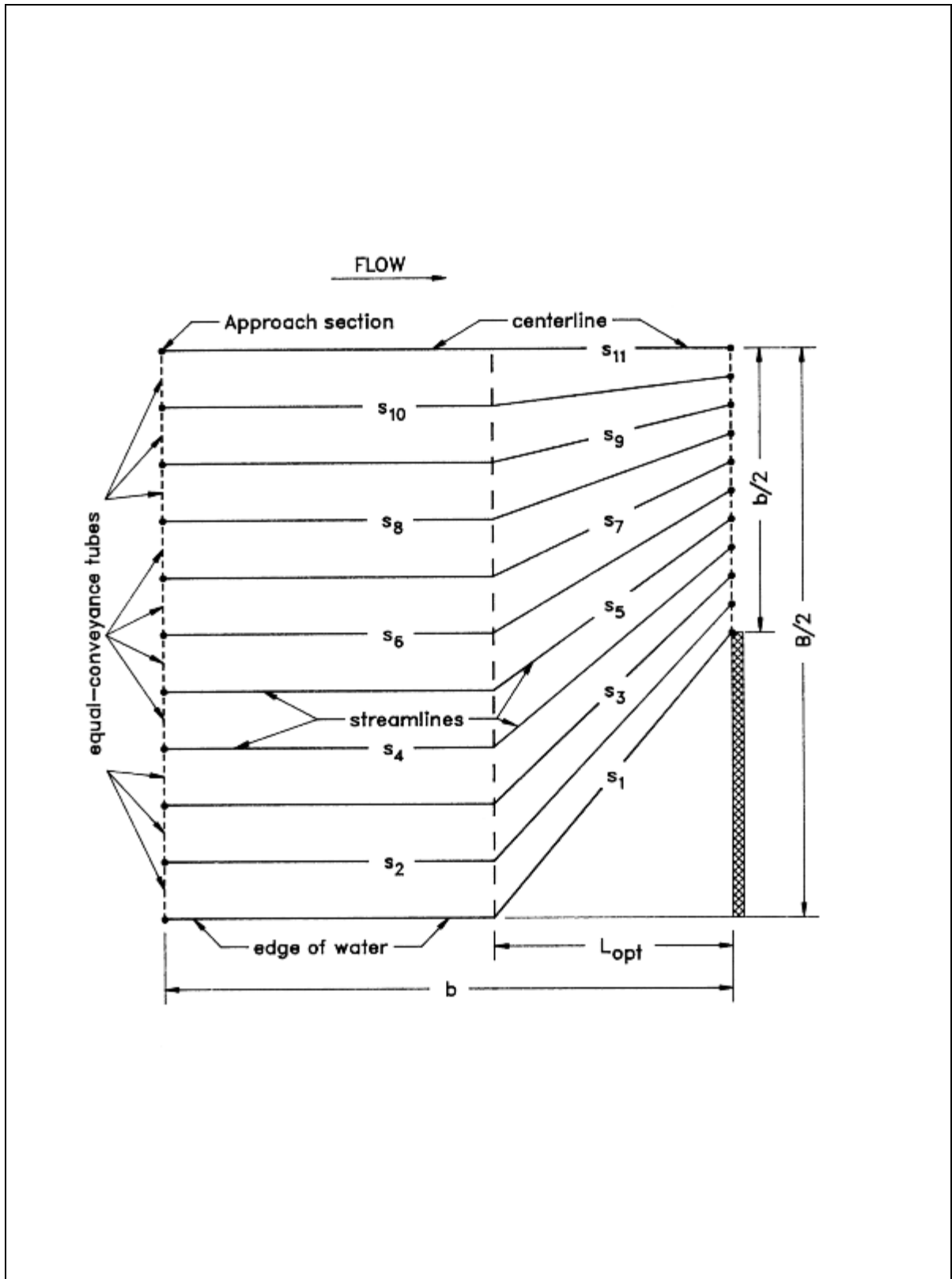
Figure D-1 Definition sketch of assumed streamlines for relatively low degree of contraction.

$$L_{av} = \frac{1}{10}\left[\sum_{i=2}^{10} S_i + \frac{(S_1 + S_{11})}{2}\right] \tag{D-5}$$

Where i indicates the streamline number and s is the individual streamline length. Although the straight-line pattern is a gross simplification of the actual curvilinear streamlines, the computed Lav values are less than 2 percent smaller than the exact solution for small geometric contraction ratios.

Figure D-2 illustrates a relatively high degree of geometric contraction. Simply connecting the flow division points of the Lopt and bridge sections does not result in representative lengths for those streamlines furthest away from the opening.

Therefore, a parabola is computed by the equation:

$$y^2 = 2b\left(x + \frac{b}{2}\right) \tag{D-6}$$

This parabola has its focus at the edge of water and its axis in the plane of the upstream face of the bridge. Positive x and y distances are measured from the edge of water towards the stream centerline and upstream from the plane of the bridge, respectively. For portions of the section where Lopt is upstream from this parabola, the parallel streamlines are projected to the parabola and then a straight line connects this projected point with the corresponding flow division point in the bridge opening. Flow division points of the Lopt section at or downstream from the parabola are connected directly to their corresponding flow division point for the bridge opening. Only the distances between the approach and the cross section just upstream of the bridge opening are used to compute Lav with equation D-5. This process generally produces results that are within 5 percent of the exact solution. For very severe constrictions (i.e., m' = 0.95), the differences are closer to 10 percent.

The non-uniform conveyance distribution in the approach reach is represented by defining the stream tubes on a conveyance basis. The model determines the horizontal stationing of 19 interior flow division points that subdivide both the Lopt and bridge sections into 20 tubes of equal conveyance. Asymmetric constrictions with nonuniform conveyances are analyzed by treating each half of the reach on either side of the conveyance midpoints separately, then averaging the results. Lav for each side provides the conveyance-weighted average streamline length. Figure D-3 illustrates a typical asymmetric, nonuniform conveyance situation.
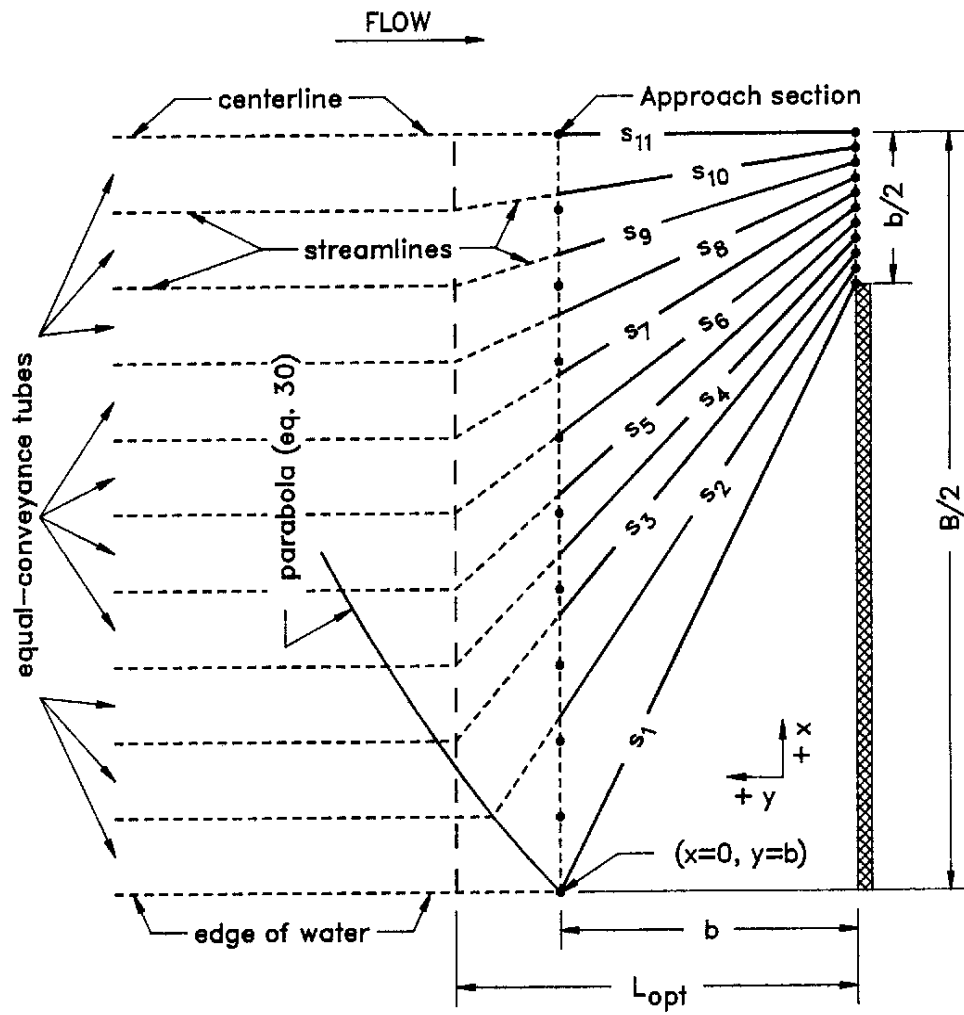
Figure D-2 Definition sketch of assumed streamlines for relatively high degrees of contraction.
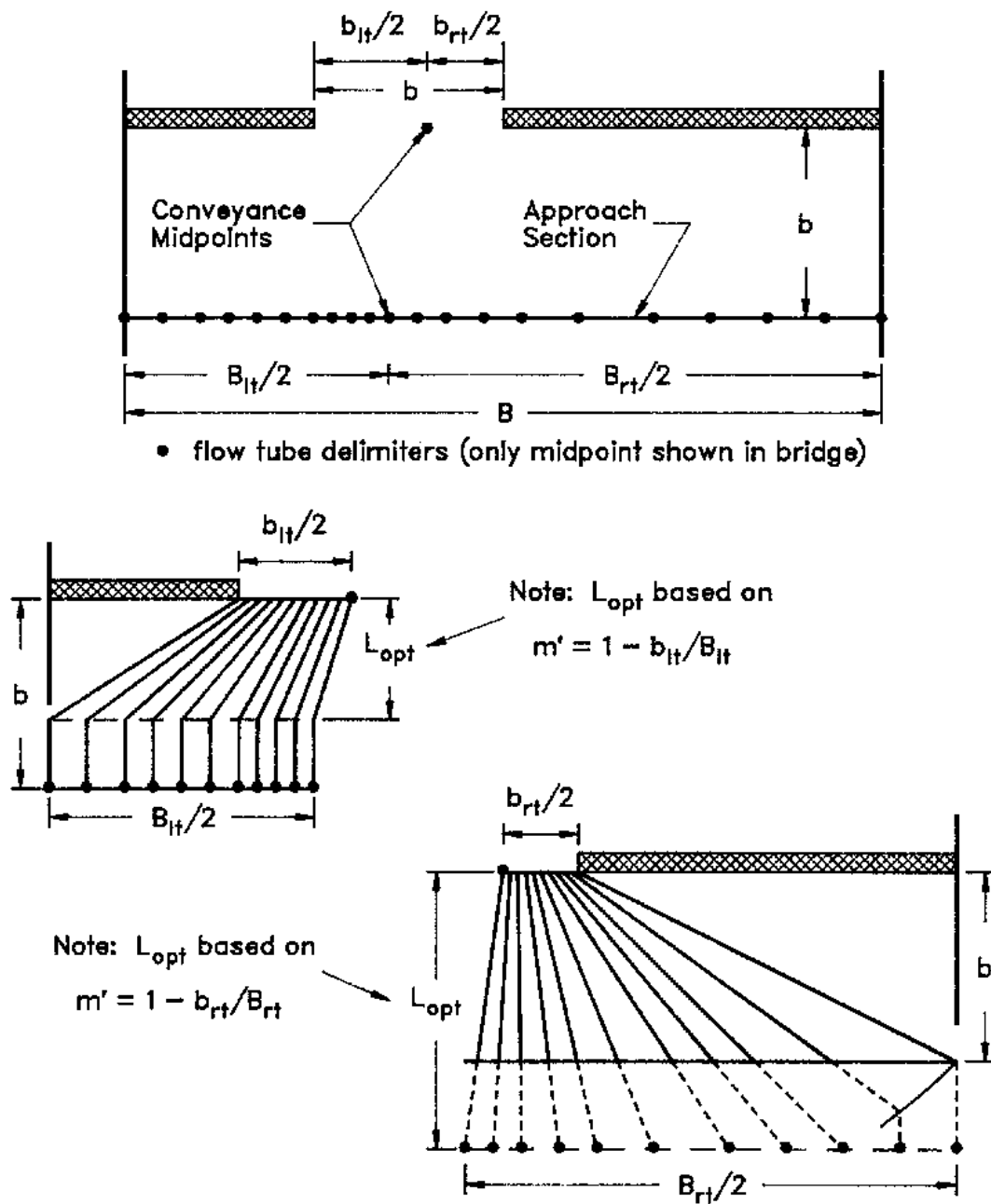
Figure D-3 Assumed flow pattern for a nonsymmetric constriction with nonhomogenous roughness distribution

Coefficient of Discharge

The coefficient of discharge, as defined by Matthai and used in this model, is a function of bridge geometry and flow characteristics. Matthai's report presents detailed instructions for computing the coefficient of discharge for the four most common types of bridge openings. It is not practical to reproduce that entire report herein, but the following paragraphs summarize the procedures as adapted to this model. All of the key figures from Matthai's report, the tabular values and equations used to determine the coefficient of discharge, and a discussion of the minor modifications made to Matthai's procedures are presented in this appendix. Bridge openings are classified as one of four different types depending upon characteristics of embankment and abutment geometry. Regardless of opening type, the first step is to determine a base coefficient of discharge, C', which is a function of (1) a channel contraction ratio and (2) a ratio of flow length through the bridge, L, to the bridge-opening width, b. The channel contraction ratio is

$$m = 1 - \frac{K_q}{K_1}$$ (D-7)

Where K_q is the conveyance of a portion of the approach section (based on projecting the bridge opening width up to the approach section) and K1 is the total conveyance of the approach section. The definition of the L and b terms for the length ratio depends upon the opening type. The definition sketches below define these terms for each opening type. The final coefficient of discharge, C, is computed by multiplying C' by a series of adjustment factors to account for variations in geometry and flow from the base conditions used to derive C'. The number of parameters for which adjustment factors are required depends partially upon the opening type. Following is a summary description of the opening types and the adjustment factors that are unique to each:

●   Type 1 openings have vertical embankments and vertical abutments with or without wingwalls. The discharge coefficient is adjusted for the Froude number (k_F) and also for wingwall width (k_w) if wingwalls are present or for entrance rounding (kr) if there are no wingwalls.

●   Type 2 openings have sloping embankments and vertical abutments and do not have wingwalls. The discharge coefficient is adjusted on the basis of the average depth of flow at the abutments (k_y).

●   Type 3 openings have sloping embankments with spillthrough abutments. The discharge coefficient is adjusted on the basis of entrance geometry (k_x).

●   Type 4 openings have sloping embankments, vertical abutments, and wingwalls. The discharge coefficient is adjusted depending upon the wingwall angle ($k\theta$).

In addition to the above adjustment factors, which are dependent upon opening type, there are adjustment factors for piers or piles (kj) and spur dikes (ka, kb, kd) that may be applied to all opening types. The relationships used to compute all of the above adjustment factors are shown below.

Figures D-4 through D-7 are definition sketches of the four types of openings for which Matthai defined the coefficient of discharge. Figures D-8 through D-18 are the relationships defining the base coefficient of discharge and the factors used to adjust for nonstandard conditions. Except for type 1 openings, different curves are required for different embankment slopes. Most of these relationships are incorporated into HEC-RAS in the form of digitized values. The digitized values are shown in tabular form at the end of this appendix. Table D-1 cross-references the figures and tables pertaining to the base coefficient of discharge. Table D-2 cross-references those figures and tables pertaining to the various adjustment factors.

Generally each of the relationships are incorporated into HEC-RAS in the form of three arrays. Two one-dimensional arrays contain values of the two independent variables (the abscissa of the relationship and the family of curves), and a two-dimensional array contains the corresponding values of the dependent variable. Exceptions to this form of representation are discussed in the following paragraphs.

The type 1 opening Froude number adjustment (fig. D.8(b)) is adequately expressed in equation form as:

$$k_F = 0.9 + 0.2F \qquad (for\ 0.0 \le F \le 0.5) \tag{D-8}$$

and

$$k_F = 0.82 + 0.36F \qquad (for\ F > 0.5) \tag{D-9}$$

Where F is the Froude number with an arbitrary upper limit of F = 1.2 for the adjustment. The average depth adjustment for a type 3 opening with 2 to 1 embankment slope is determined by the following equations:

$$k_y = 1.00 + 0.3y \qquad (for\ 0.0 \le y \le 0.20) \tag{D-10}$$

and

$$k_y = 1.02 \pm 0.2\,\overline{y} \ \left(for\ \overline{y} > 0.2\right) \tag{D-11}$$

$$where \ \ \overline{y} = \frac{y_a + y_b}{2b} \ \ with \ \overline{y} = 0.30 \ as \ an \ upper \ Limit.$$

The type 4 opening wing wall adjustment factor, kθ, is computed using slopes of the family of curves (figs. D.15 and D.16). The equation for specified m-values is:

D-8

$$k_\theta = 1.0 + (WW - 30)\,Sk_\theta \qquad\qquad \text{(D-12)}$$

Where WW is the wing wall angle and Skθ is the appropriate slope from tables D.16 or D.18. kθ is obtained by interpolation for intermediate m-values.

Certain adjustments presented by Matthai were not incorporated into the WSPR0 bridge methodology. The skew adjustment was omitted because WSPR0 always computes the flow area normal to the flow for skewed bridge openings. An adjustment for submerged flow was also omitted because the FHWA methodology is used to compute pressure flow when girders are significantly submerged. The Froude number adjustment for type 4 openings with 2 to 1 embankment slope was intentionally omitted for reasons of consistency. There is no similar adjustment for type 4 openings with 1 to 1 embankment slopes, and the adjustment is rather minor. Matthai also applied an adjustment for eccentricity, which is a measure of unequal conveyances on left and right overbanks of the approach section. This factor was not included in WSPR0 on the bases that (1) it is a very minor adjustment, and (2) the effective flow length accounts for conveyance distribution.
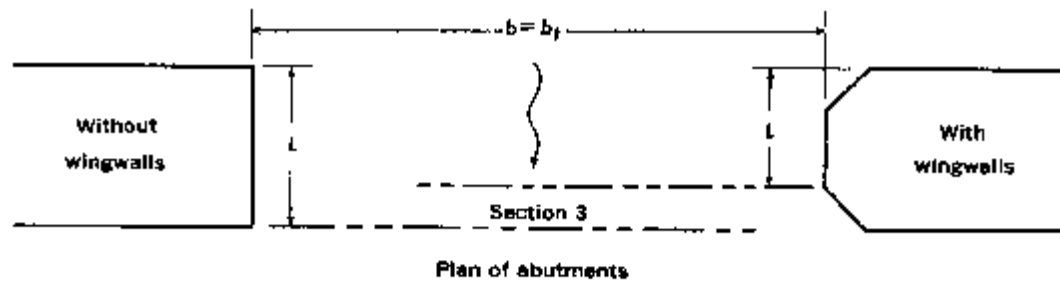
Figure D-4 Definition sketch of type 2 opening, sloping embankments without wing walls (after Matthai)
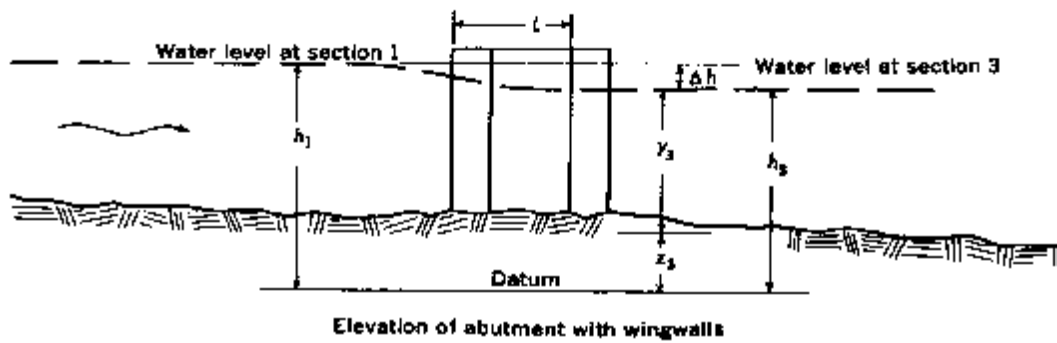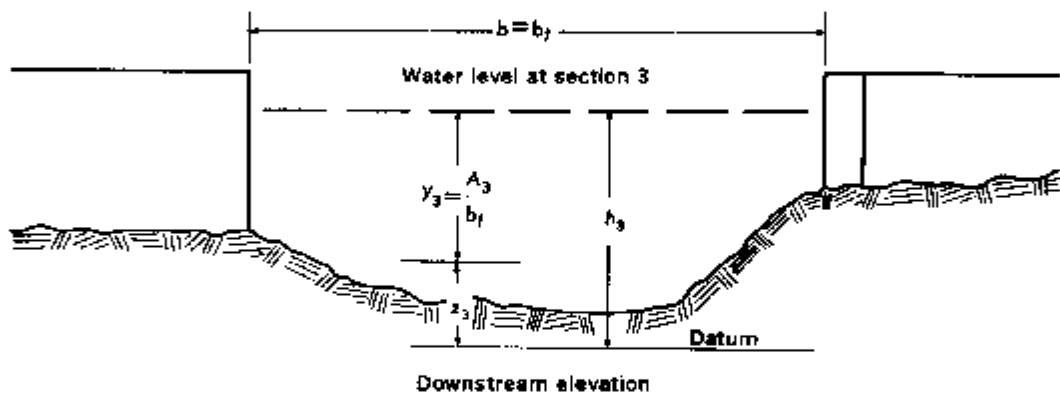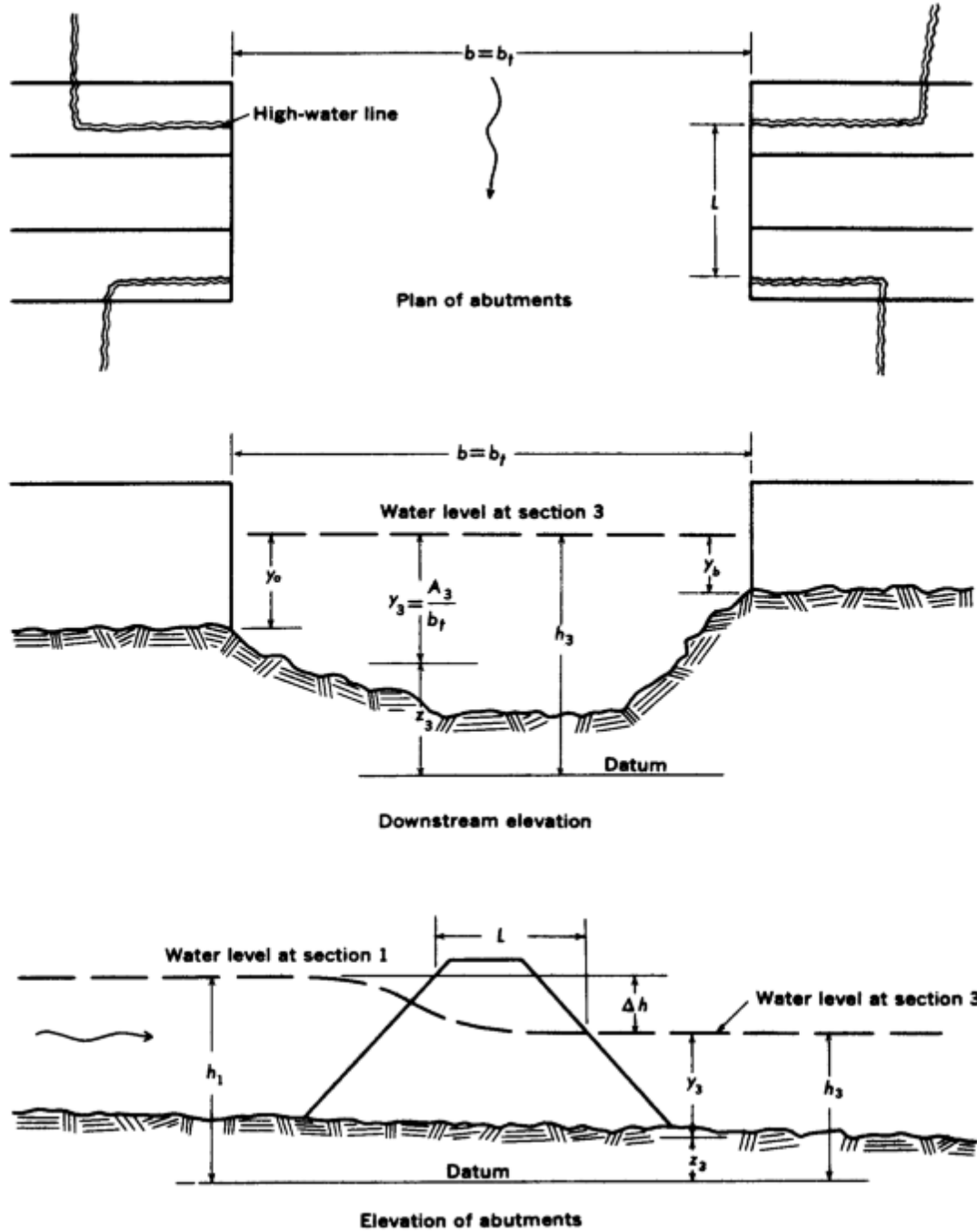
Figure D-5 Definition sketch of type 2 opening, sloping embankments without wing walls (after Matthai)
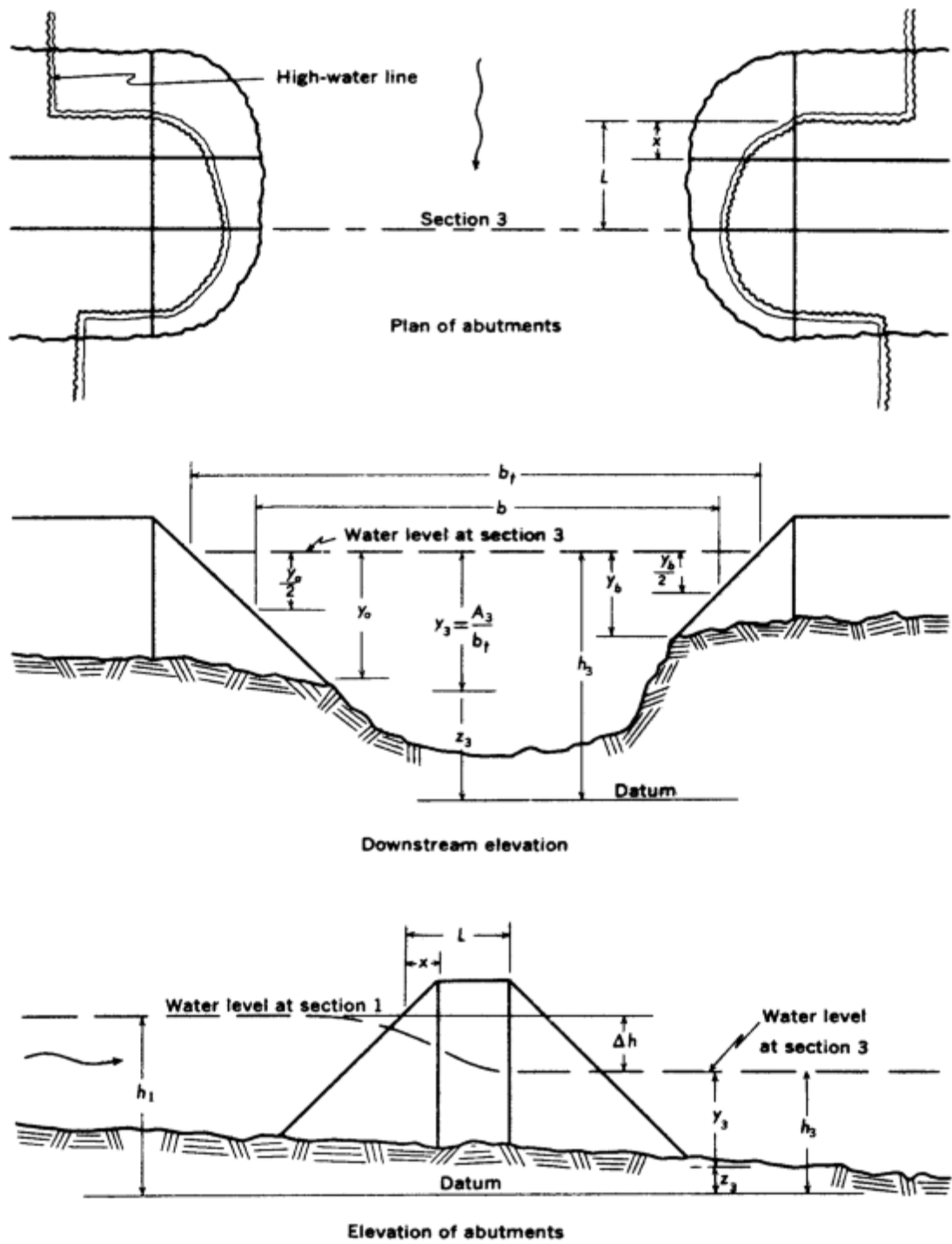
Figure D-6 Definition sketch of type 3 opening, sloping embankments and sloping abutments (spill through) (after Matthai)
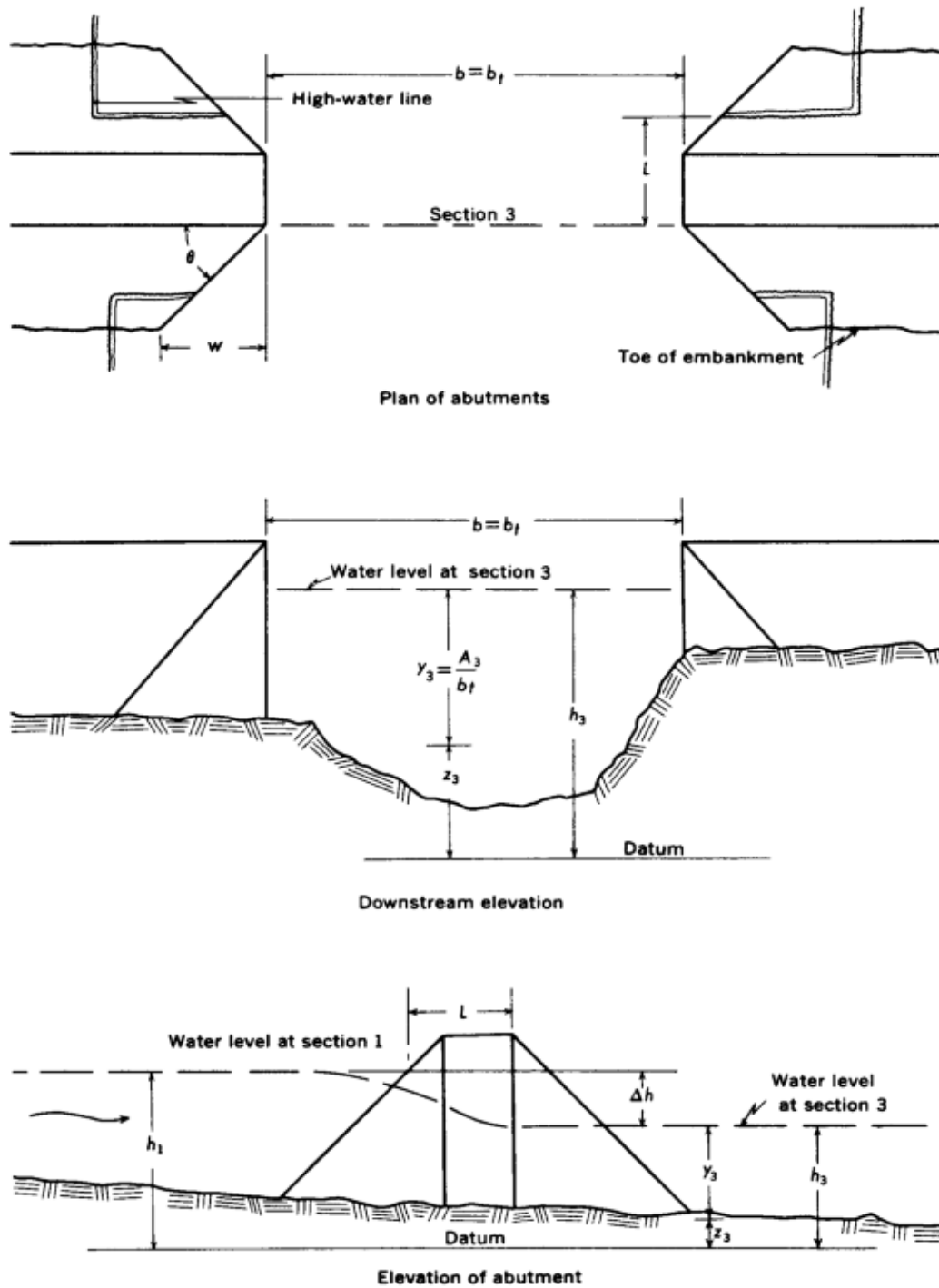
Figure D-7 Definition sketch of type 4 opening, sloping embankments and vertical abutments with wing walls (after Matthai)

Table D-1 Cross-reference of Figures and Tables pertaining to the base coefficient of discharge.

Type Opening	Embankment Slope	Figure No.	Table No.
1		D-8	D-3
2	1 to 1	D-10	D-6
	2 to 1	D-11	D-8
3	1 to 1	D-12	D-10
	1 2 to 1	D-13	D-12
	2 to 1	D-14	D-14
4	1 to 1	D-15	D-15
	2 to 1	D-16	D-17

Table D-2 Cross-reference of Figures and Tables pertaining to adjustment factors

Type Opening	Embankment Slope	Adjustment Factor For:	Figure No.	Table No.
1		Entrance Rounding	D-8	D-4
		Wingwalls	D-9	D-5
		Froude Number	Eqn.	Eqn.
2	1 to 1	Average Depth	D-10	D-7
	2 to 1	A	D-11	D-9
3	1 to 1	Entrance Geometry	D-12	D-11
	1 2 to 1	A	D-13	D-13
	2 to 1	A	Eqn.	Eqn.
4	1 to 1	Wingwalls	D-15	D-16
	2 to 1	A	D-16	D-18
All		Piers or Piles	D-17	D-19, D-20
		Spur Dikes	D-18	D-21
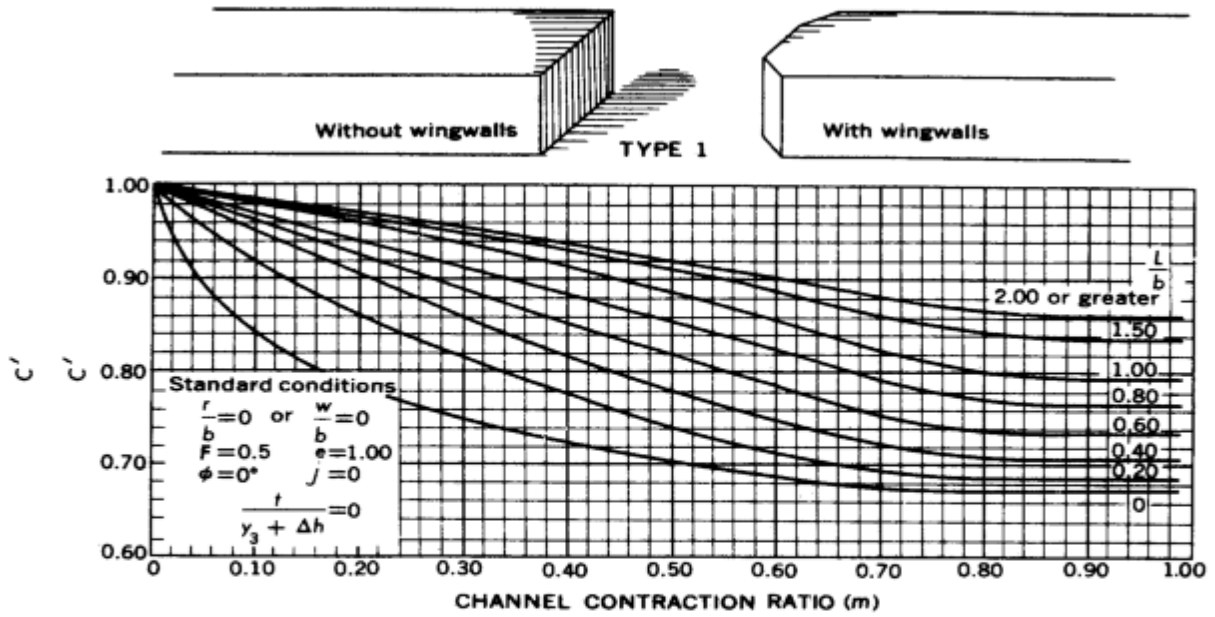
a) Base coefficient of discharge.
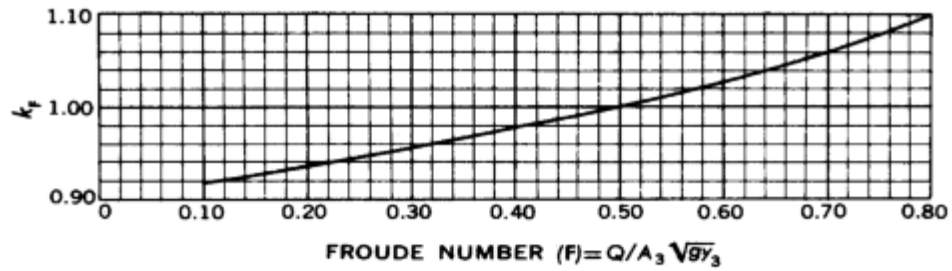
b) Froude number adjustment factor.
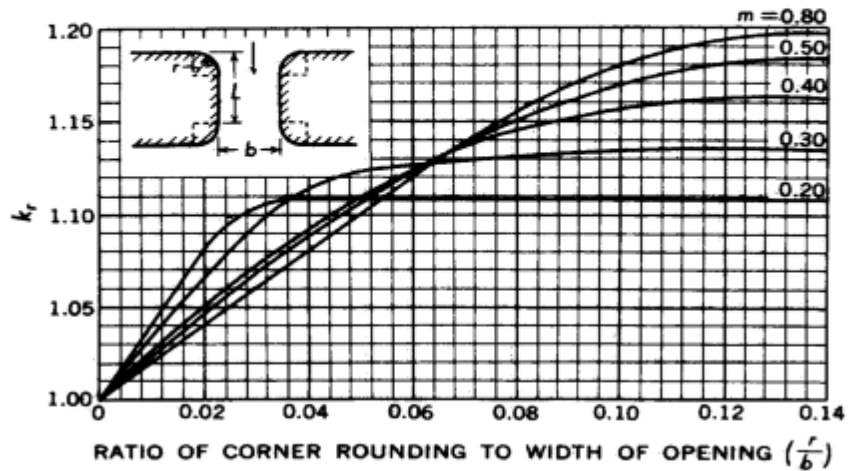
c) Corner rounding adjustment factor.

Figure D-8 Coefficients for type 1 openings (after Matthai)
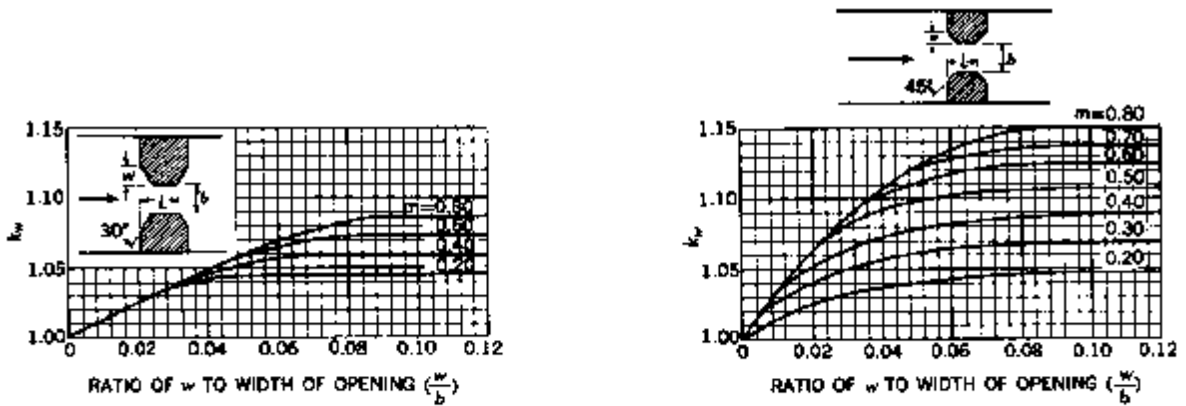
a) 30° wingwalls.

b) 45° wingwalls.
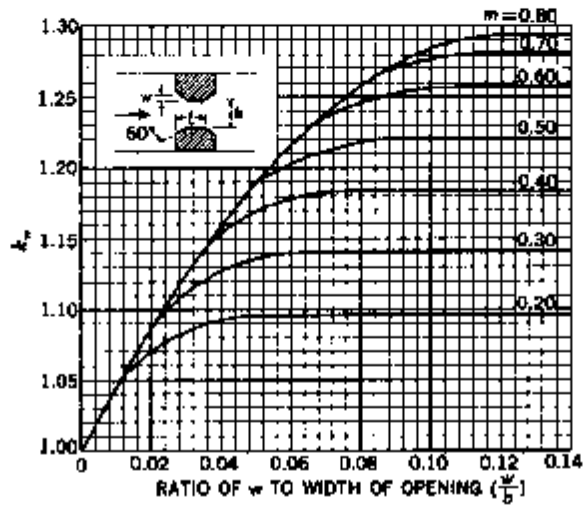
c) 60° wingwalls.

Figure D-9 Wingwall adjustment factors for type 1 openings (after Matthai).
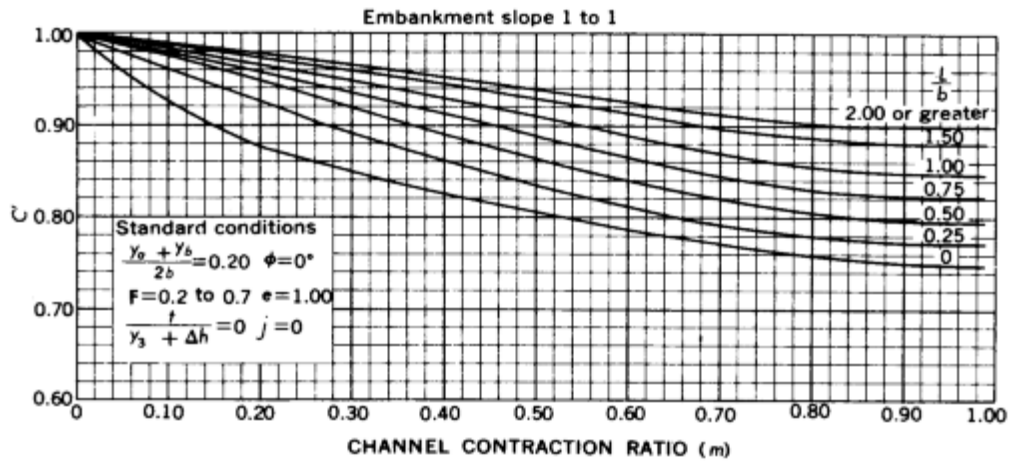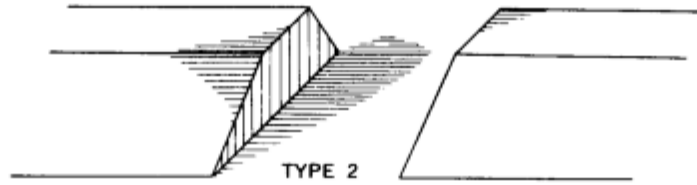
a) Base coefficient of discharge.
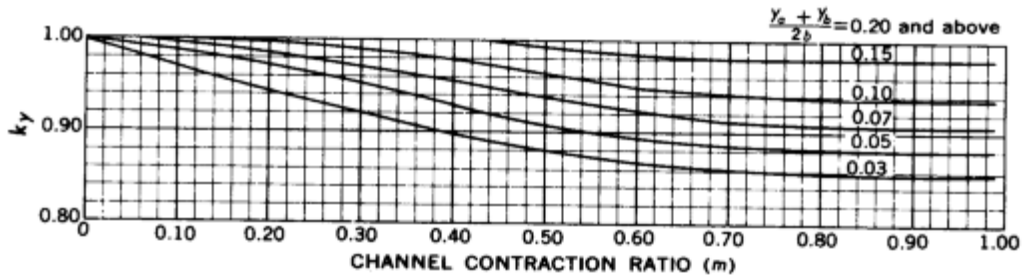
b) Average depth adjustment factor.

Figure D- 10 Coefficients for type 2 openings, embankment slope 1 to 1 (after Matthai)

TYPE 2

Embankment slope 2 to 1
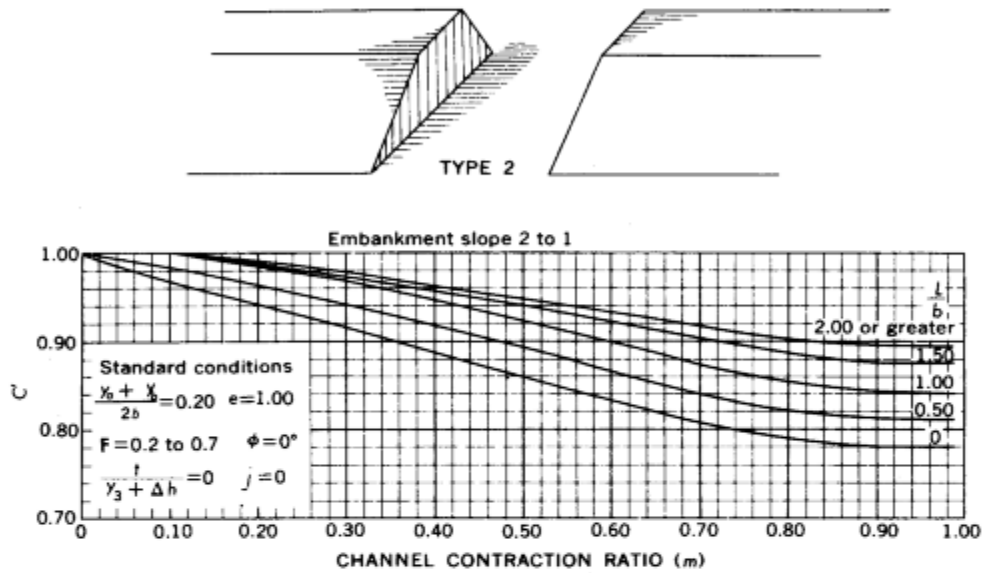
a) Base coefficient of discharge.
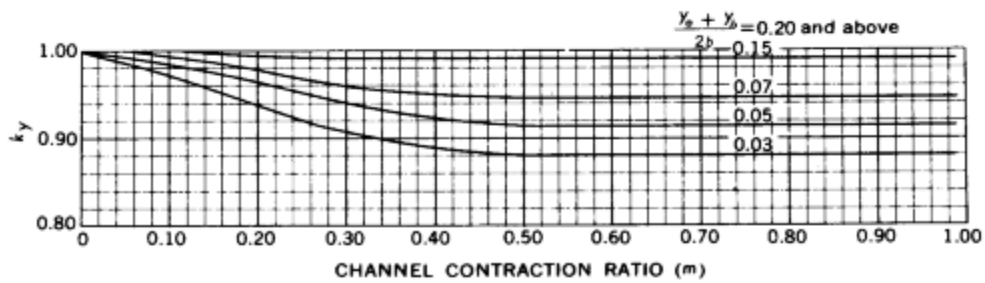
b) Average depth adjustment factor.

Figure D-11 Coefficients for type 2 openings, embankment slope 2 to 1 (after Matthai).
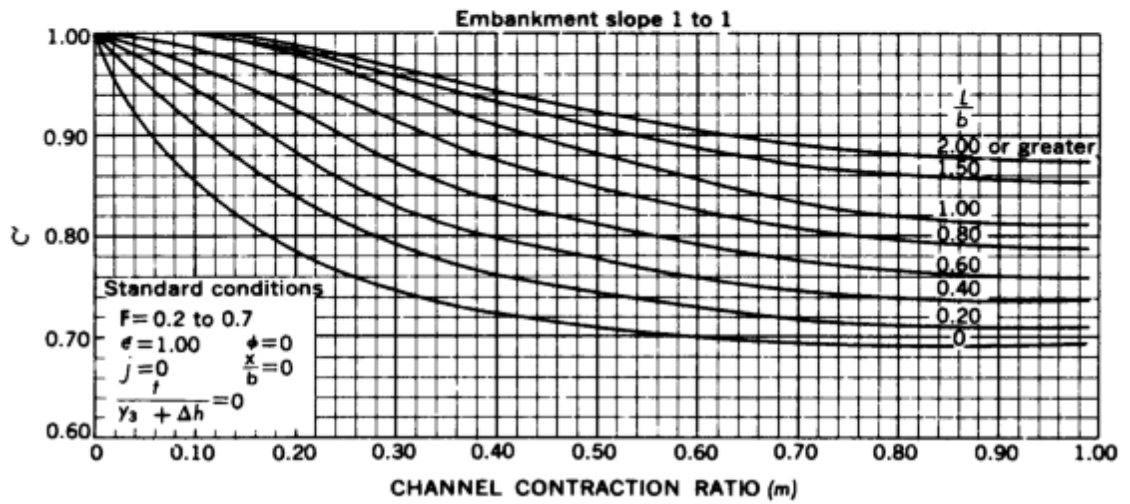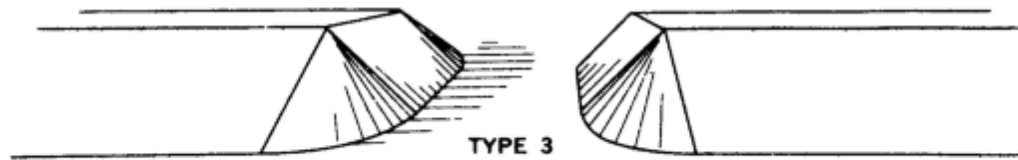
a) Base coefficient of discharge.
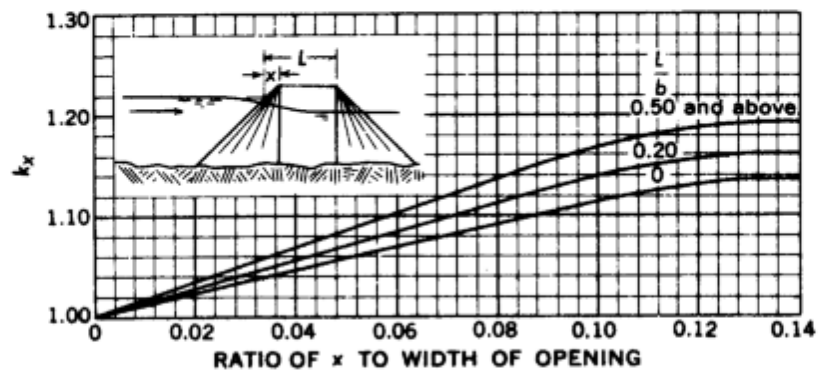
b) Unwetted abutment adjustment factor.

Figure D-12 Coefficients for type 3 openings, embankment slope 1 to 1 (after Matthai)
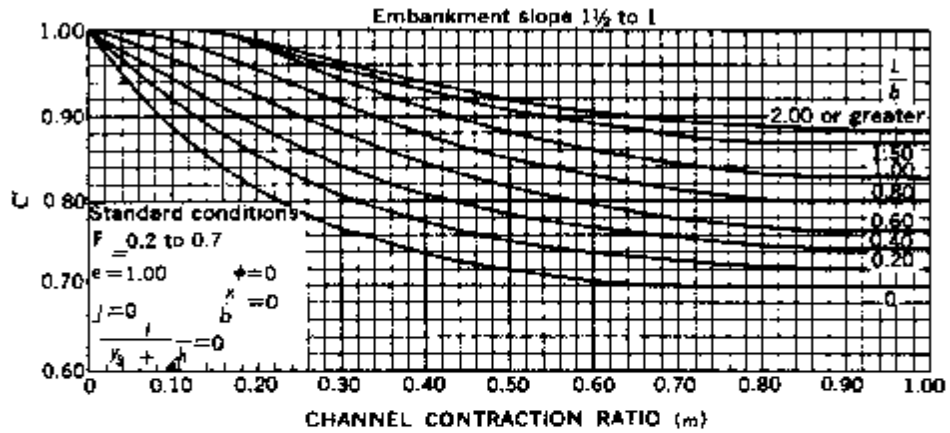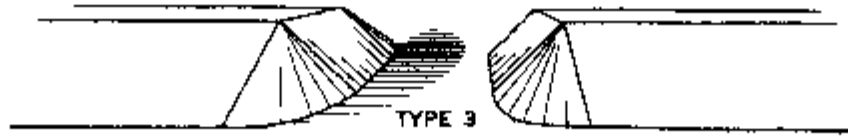
a) Base coefficient of discharge.
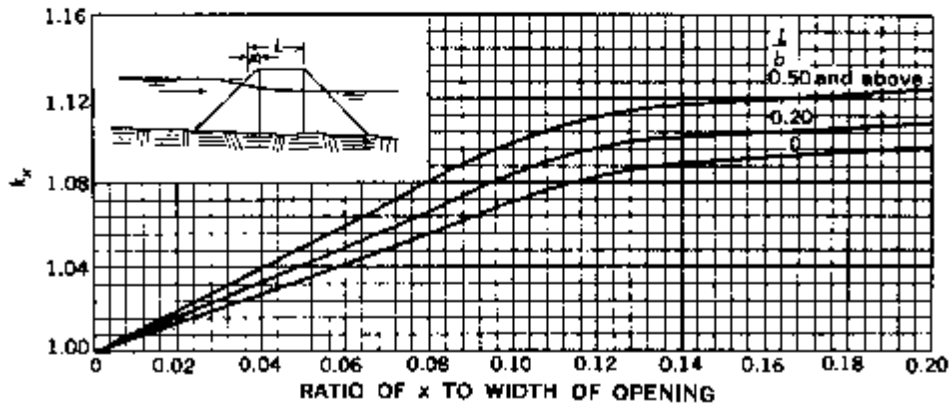
b) Unwetted abutment adjustment factor.

Figure D-13 Coefficients for type 3 openings, embankment slope 1-1/2 to 1 (after Matthai).
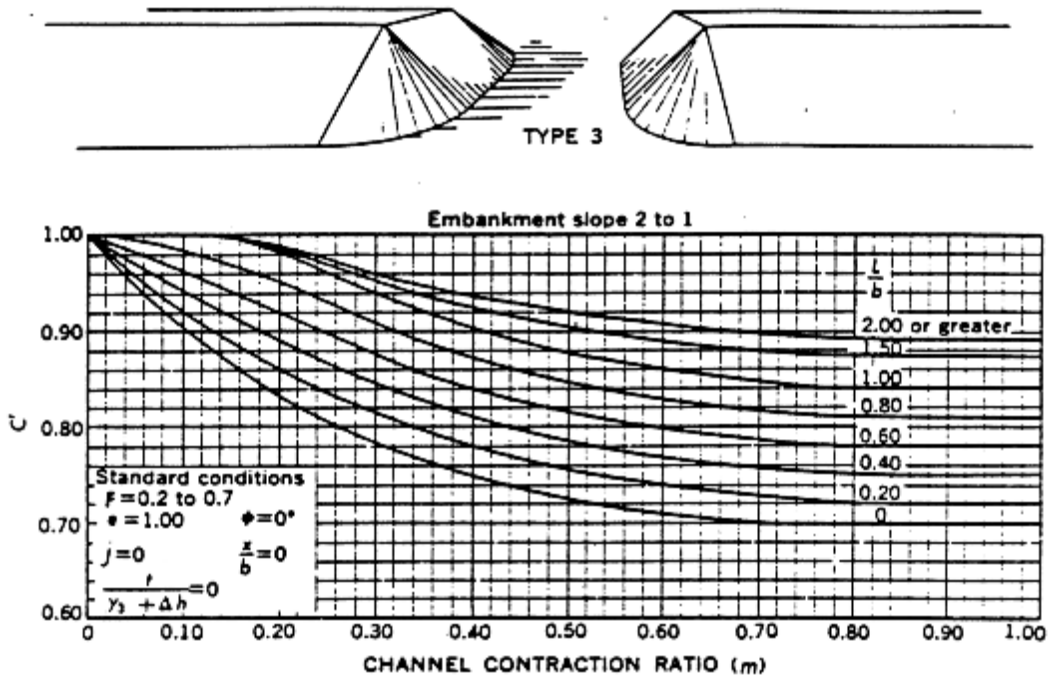
a) Base coefficient of discharge.
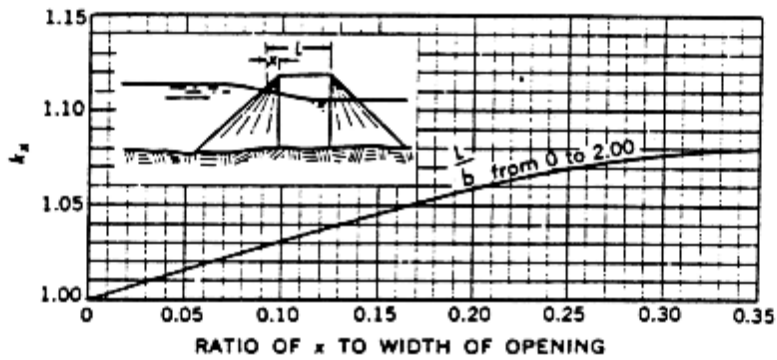
b) Unwetted abutment adjustment factor.

Figure D- 14 Coefficients for type 3 openings, embankment slope 2 to 1 (after Matthai)

TYPE 4

Embankment slope 1 to 1

$\frac{L}{b}$
2.00 or greater
1.50
1.00
0.60
0.40
0.20
0

Standard conditions
$\frac{w}{b} = 0.1$ $\phi = 0°$
$\frac{t}{y_3 + \Delta h} = 0$ $\theta = 30°$
F=0.2 to 0.7 $j = 0$
e = 1.00

CHANNEL CONTRACTION RATIO (m)

a) Base coefficient of discharge.

$m = 0.80$
0.60
0.50
0.40
0.30
0.20
0.10

ANGLE OF WINGWALL (m)
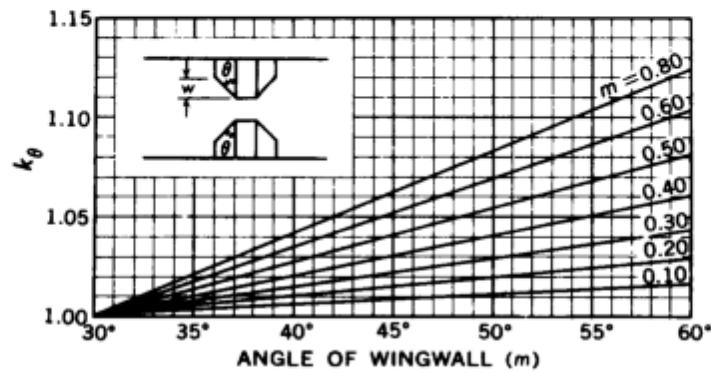
b) Wingwall adjustment factor.

Figure D- 15 Coefficients for type 4 openings, embankment slope 1 to 1 (after Matthai)

TYPE 4

Embankment slope 2 to 1
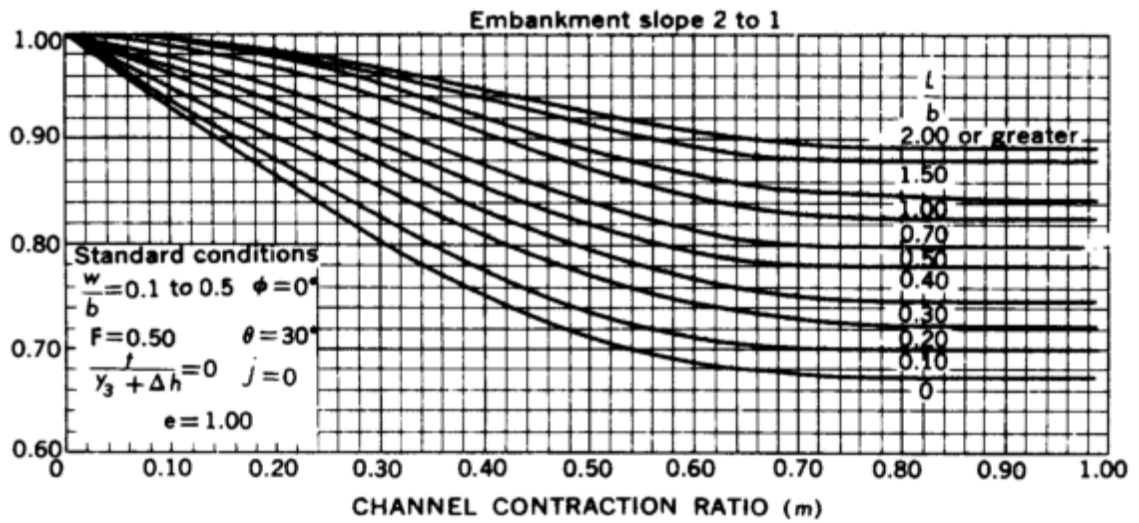
a) Base coefficient of discharge.
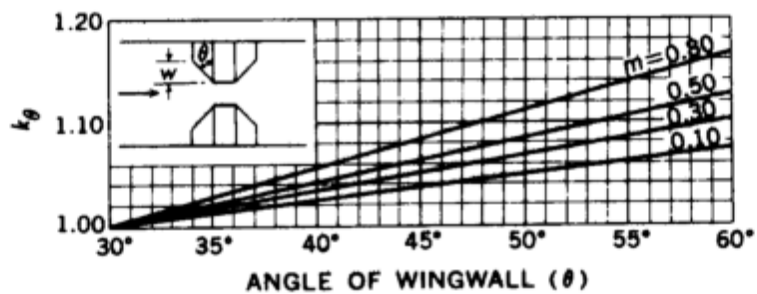
b) Wingwall adjustment factor.

Figure D-16 Coefficients for type 4 openings, embankment slope 2 to 1 (after Matthai)
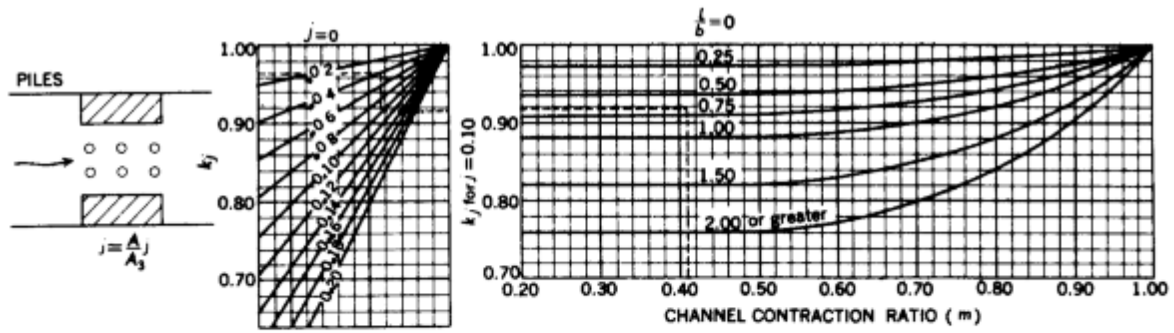
a) Adjustment factor for piles.
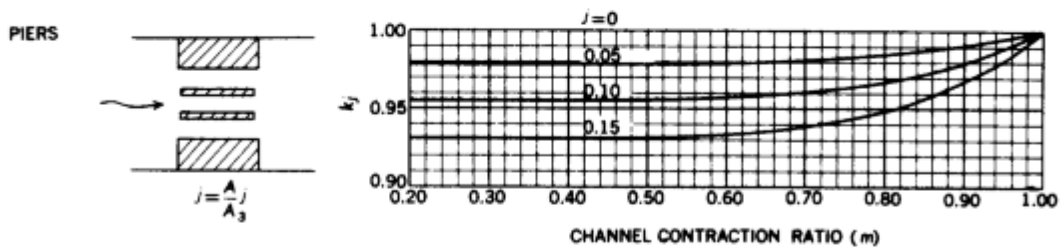
b) Adjustment factor for piers.

Figure D-17 Adjustment factors for piers or piles, all opening types (after Matthai)
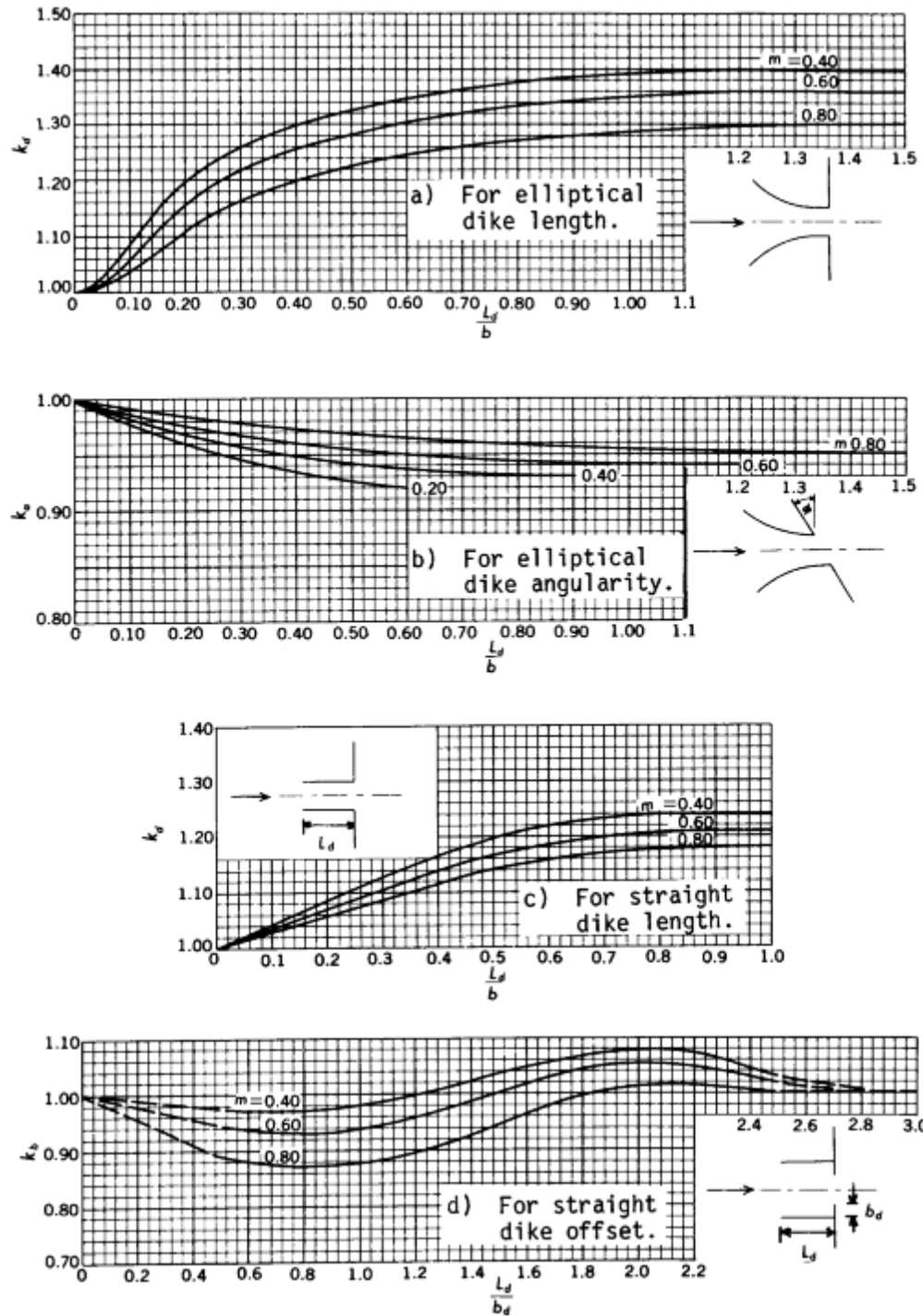
Figure D-18 Adjustment factors for spur dikes, all opening types (after Matthai)

Table D-3 Base coefficient of discharge, C', for type 1 opening, with or without wing walls

	m					
	0.0	0.1	0.3	0.5	0.8	1.0
0.0	1.00	0.83	0.745	0.70	0.67	0.67
0.2	1.00	0.92	0.81	0.74	0.685	0.685
0.4	1.00	0.95	0.86	0.755	0.71	0.71
L/b 0.6	1.00	0.965	0.89	0.82	0.735	0.735
0.8	1.00	0.97	0.91	0.855	0.77	0.765
1.0	1.00	0.98	0.935	0.885	0.80	0.795
1.5	1.00	0.985	0.95	0.91	0.845	0.835
2.0	1.00	0.99	0.955	0.92	0.87	0.86

m is the channel contraction ratio.

L/b is the ratio of flow length to bridge-opening width.

Table D-4 Variation of adjustment factor, k_r, for type 1 opening with entrance rounding

|		r/b						
		0.01	0.02	0.04	0.06	0.08	0.10	0.14
	0.1	1.06	1.07	1.07	1.07	1.07	1.07	1.07
	0.2	1.04	1.08	1.11	1.11	1.11	1.11	1.11
m	0.4	1.03	1.05	1.09	1.12	1.14	1.15	1.16
	0.6	1.02	1.04	1.08	1.12	1.15	1.17	1.18
	0.8	1.02	1.04	1.08	1.12	1.16	1.18	1.20
	1.0	1.02	1.04	1.08	1.12	1.16	1.18	1.22

r/b is the ratio of entrance rounding to bridge-opening width.

m is the channel contraction ratio.

Table D-5 Variation of adjustment factor, k0, for type 1 opening with wing walls (fig. D-9).

w/b

	0.01	0.02	0.04	0.06	0.08	0.10	0.14
0.1	1.01	1.02	1.02	1.02	1.02	1.02	1.02
0.2	1.01	1.025	1.04	1.04	1.04	1.04	1.04
m 0.4	1.01	1.025	1.04	1.06	1.06	1.06	1.06
0.6	1.01	1.025	1.05	1.06	1.07	1.07	1.07
0.8	1.01	1.025	1.05	1.07	1.08	1.09	1.09
1.0	1.01	1.025	1.05	1.07	1.08	1.09	1.10

(a) 30º wing walls

	0.01	0.02	0.04	0.06	0.08	0.10	0.14
0.1	1.00	1.01	1.01	1.02	1.02	1.02	1.02
0.2	1.01	1.02	1.04	1.04	1.05	1.05	1.05
m 0.4	1.03	1.05	1.07	1.08	1.09	1.09	1.09
0.6	1.03	1.06	1.10	1.11	1.12	1.12	1.12
0.8	1.03	1.06	1.11	1.13	1.15	1.15	1.15
1.0	1.03	1.06	1.11	1.13	1.15	1.16	1.17

(b) 45º wing walls

	0.01	0.02	0.04	0.06	0.08	0.10	0.14
0.1	1.02	1.04	1.05	1.05	1.05	1.05	1.05
0.2	1.04	1.07	1.09	1.10	1.10	1.10	1.10
m 0.4	1.04	1.09	1.15	1.18	1.18	1.18	1.18
0.6	1.04	1.09	1.15	1.21	1.24	1.25	1.26
0.8	1.04	1.09	1.15	1.22	1.26	1.28	1.29
1.0	1.04	1.09	1.15	1.22	1.26	1.28	1.32

(c) 60º wingwalls

w/b is the ratio of wing wall width to bridge-opening width.

Table D-6 Base coefficient of discharge, C', for type 2 opening, embankment slope 1 to 1

		m				
		0.0	0.1	0.3	0.5	0.8	1.0
	0.0	1.00	0.92	0.845	0.805	0.755	0.745
	0.2	1.00	0.955	0.88	0.83	0.775	0.765
	0.4	1.00	0.97	0.91	0.85	0.795	0.79
L/b	0.6	1.00	0.975	0.925	0.87	0.81	0.805
	0.8	1.00	0.98	0.94	0.895	0.835	0.825
	1.0	1.00	0.985	0.95	0.91	0.855	0.845
	1.5	1.00	0.988	0.96	0.93	0.885	0.88
	2.0	1.00	0.99	0.965	0.94	0.905	0.90

m is the channel contraction ratio.

L/b is the ratio of flow length to bridge-opening width.

Table D-7 Variation of adjustment factor, k_y, for type 2 opening, embankment slope 1 to 1

(see fig. D-10).

		m				
		0.0	0.2	0.4	0.7	1.0
$y_a + y_b$	0.03	1.00	0.94	0.895	0.86	0.86
-----	0.05	1.00	0.97	0.93	0.88	0.88
2b	0.07	1.00	0.985	0.955	0.91	0.91
	0.10	1.00	0.995	0.98	0.94	0.94
	0.15	1.00	1.00	1.00	0.98	0.98

m is the channel contraction ratio.

$(y_a + y_b)/2b$ is the ratio of average depth at the abutments to bridge-opening width.

Table D-8 Base coefficient of discharge, C', for type 2 opening, embankment slope 2 to 1

(see fig. D-10)

		m				
	0.0	0.1	0.3	0.5	0.8	1.0
0.0	1.00	0.965	0.915	0.86	0.79	0.78
0.2	1.00	0.97	0.925	0.87	0.80	0.79
0.4	1.00	0.98	0.935	0.89	0.81	0.80
L/b 0.6	1.00	0.99	0.95	0.90	0.83	0.82
0.8	1.00	0.995	0.96	0.91	0.845	0.83
1.0	1.00	1.00	0.97	0.925	0.855	0.84
1.5	1.00	1.00	0.975	0.94	0.89	0.875
2.0	1.00	1.00	0.98	0.95	0.905	0.895

m is the channel contraction ratio.

L/b is the ratio of flow length to bridge-opening width.

Table D-9 Variation of adjustment factor, k_y, for type 2 opening, embankment slope 2 to 1

(see fig. D-11)

		m				
		0.0	0.2	0.4	0.7	1.0
	0.03	1.00	0.935	0.89	0.88	0.88
	0.05	1.00	0.965	0.925	0.91	0.91
y_a+y_b	0.07	1.00	0.975	0.95	0.945	0.945
-----	0.10	1.00	0.985	0.97	0.97	0.97
2b	0.15	1.00	0.99	0.99	0.99	0.99

m is the channel contraction ratio

$(y_a + y_b)/2b$ is the ratio of average depth at the abutments to bridge-opening width.

Table D-10 Base coefficient of discharge, C', for type 3 opening, embankment slope1 to 1

(see fig. D-12)

	m					
	0.0	0.1	0.3	0.5	0.8	1.0
0.0	1.00	0.85	0.74	0.71	0.69	0.69
0.2	1.00	0.91	0.79	0.745	0.71	0.71
0.4	1.00	0.945	0.83	0.775	0.74	0.735
L/b 0.6	1.00	0.97	0.87	0.81	0.765	0.76
0.8	1.00	0.985	0.91	0.85	0.795	0.79
1.0	1.00	0.995	0.945	0.88	0.82	0.81
1.5	1.00	1.00	0.96	0.91	0.86	0.85
2.0	1.00	1.00	0.97	0.925	0.88	0.875

m is the channel contraction ratio.

L/b is the ratio of flow length to bridge-opening width.

Table D-11 Variation of adjustment factor, k_y, for type 3 opening, embankment slope 1 to 1. (see fig. D-12).

	x/b					
	0.00	0.08	0.12	0.16	0.20	0.25
0.0	1.00	1.09	1.13	1.14	1.14	1.14
L/b 0.2	1.00	1.11	1.155	1.16	1.16	1.16
0.5	1.00	1.135	1.19	1.20	1.20	1.20

x/b is the ratio of "unwetted" abutment length to bridge-opening width.

L/b is the ratio of flow length to bridge-opening width.

Table D-12 Base coefficient of discharge, C', for type 3 opening, embankment slope 1-1/2 to 1

(see fig. D-13).

	m					
	0.0	0.1	0.3	0.5	0.8	1.0
0.0	1.00	0.885	0.76	0.715	0.70	0.70
0.2	1.00	0.92	0.80	0.75	0.725	0.72
0.4	1.00	0.945	0.84	0.78	0.75	0.745
L/b 0.6	1.00	0.97	0.88	0.815	0.77	0.765
0.8	1.00	0.99	0.915	0.85	0.805	0.80
1.0	1.00	1.00	0.945	0.88	0.83	0.825
1.5	1.00	1.00	0.955	0.905	0.87	0.87
2.0	1.00	1.00	0.965	0.92	0.885	0.885

m is the channel contraction ratio.

L/b is the ratio of flow length to bridge-opening width.

Table D- 13 Variation of adjustment factor, kx, for type 3 opening, embankment slope 1-1/2 to 1

(see fig. D-13).

	x/b					
	0.00	0.08	0.12	0.16	0.20	0.25
0.0	1.00	1.055	1.085	1.09	1.095	1.10
L/b 0.2	1.00	1.065	1.10	1.105	1.11	1.115
0.5	1.00	1.08	1.11	1.12	1.125	1.13

x/b is the ratio of "unwetted" abutment length to bridge-opening width.

L/b is the ratio of flow length to bridge-opening width.

Table D-14 Base coefficient of discharge, C', for type 3 opening, embankment slope 2 to 1

(see fig. D-14).

			m			
	0.0	0.1	0.3	0.5	0.8	1.0
0.0	1.00	0.90	0.78	0.72	0.70	0.70
0.2	1.00	0.92	0.81	0.755	0.72	0.72
0.4	1.00	0.94	0.845	0.785	0.75	0.75
L/b 0.6	1.00	0.96	0.875	0.81	0.78	0.78
0.8	1.00	0.985	0.91	0.845	0.81	0.81
1.0	1.00	1.00	0.94	0.87	0.845	0.84
1.5	1.00	1.00	0.95	0.905	0.875	0.87
2.0	1.00	1.00	0.96	0.92	0.895	0.89

m is the channel contraction ratio.

L/b is the ratio of flow length to bridge-opening width.

Table D- 15 Base coefficient of discharge, C', for type 4 opening, embankment slope 1 to 1

(see fig. D-15)

			m			
	0.0	0.1	0.3	0.5	0.8	1.0
0.0	0.99	0.85	0.755	0.715	0.695	0.69
0.2	1.00	0.90	0.815	0.775	0.735	0.73
0.4	1.00	0.955	0.885	0.83	0.775	0.77
L/b 0.6	1.00	0.985	0.935	0.875	0.815	0.81
0.8	1.00	0.99	0.955	0.91	0.84	0.835
1.0	1.00	1.00	0.965	0.925	0.855	0.85
1.5	1.00	1.00	0.97	0.94	0.89	0.885
2.0	1.00	1.00	0.975	0.95	0.905	0.90

m is the channel contraction ratio.

L/b is the ratio of flow length to bridge-opening width.

m	Sk_θ
0.1	0.00057
0.2	0.001
0.4	0.002
0.6	0.00343
0.8	0.00413
1.0	0.00483

Table D- 16 Slopes of family of curves for determining adjustment factor, k_0, for wing wall

Angle for type 4 openings, embankment slope 1 to 1 (see fig. D-15).

Table D-17 Base coefficient of discharge, C', for type 4 opening, embankment slope 2 to 1

(see fig. D-16).

				m		
	0.0	0.1	0.3	0.5	0.8	1.0
0.0	1.00	0.93	0.80	0.705	0.67	0.67
0.2	1.00	0.95	0.855	0.765	0.725	0.725
0.4	1.00	0.97	0.895	0.815	0.78	0.78
L/b 0.6	1.00	0.985	0.925	0.845	0.805	0.805
0.8	1.00	0.99	0.94	0.87	0.825	0.825
1.0	1.00	0.995	0.95	0.89	0.85	0.85
1.5	1.00	0.995	0.965	0.91	0.88	0.88
2.0	1.00	1.00	0.97	0.925	0.89	0.89

m is the channel contraction ratio.

L/b is the ratio of flow length to bridge-opening width

Table D-18 Slopes of family of curves for determining adjustment factor, k_0, for wing wall

Angle for type 4 openings, embankment slope 2 to 1 (see fig. D-16).

m	Skθ
0.1	0.00243
0.2	0.00283
0.4	0.00373
0.6	0.00467
0.8	0.00557
1.0	0.00667

Table D-19 Adjustment factor, k_i for piers (see fig. D-17).

	m				
	0.40	0.60	0.80	0.90	1.00
0.00	1.00	1.00	1.00	1.00	1.00
0.05	0.978	0.979	0.985	0.991	1.00
j 0.10	0.955	0.957	0.967	0.98	1.00
0.15	0.93	0.933	0.948	0.968	1.00
0.20	0.903	0.907	0.928	0.956	1.00

Table D-20 Adjustment factor, kj, for piles (see fig. 17).

m

	0.40	0.60	0.80	0.90	1.00
0.00	1.00	1.00	1.00	1.00	1.00
0.25	0.973	0.976	0.984	0.99	1.00
L/b 0.50	0.933	0.94	0.96	0.976	1.00
1.00	0.88	0.888	0.92	0.953	1.00
2.00	0.76	0.772	0.84	0.905	1.00

(a) k_j for piles when j = 0.10

j

	0.00	0.04	0.08	0.12	0.16	0.20
.76	1.00	0.902	0.81	0.71	0.615	0.52
k_j for .80	1.00	0.92	0.841	0.761	0.684	0.605
j=.1 .90	1.00	0.961	0.921	0.88	0.842	0.802
1.0	1.00	1.00	1.00	1.00	1.00	1.00

(b) k_j for piles when j ⑤ 0.10

Ld/b						
	0.0	0.2	0.4	0.6	1.0	1.5
0.2	1.00	1.23	1.32	1.37	1.41	1.42
m 0.4	1.00	1.20	1.30	1.35	1.39	1.40
0.6	1.00	1.16	1.25	1.30	1.35	1.36
0.8	1.00	1.11	1.20	1.25	1.29	1.30

(a) Kd for elliptical dike length

Ld/b						
	0.0	0.2	0.4	0.6	1.0	1.5
0.2	1.00	0.96	0.935	0.92	0.91	0.905
m 0.4	1.00	0.968	0.95	0.935	0.93	0.925
0.6	1.00	0.976	0.96	0.95	0.94	0.935
0.8	1.00	0.984	0.973	0.965	0.955	0.95

(b) Ka for elliptical dike angularity

Ld/b						
	0.0	0.2	0.4	0.6	1.0	1.5
0.2	1.00	1.09	1.18	1.25	1.27	1.27
m 0.4	1.00	1.08	1.16	1.22	1.24	1.24
0.6	1.00	1.07	1.14	1.18	1.21	1.21
0.8	1.00	1.06	1.12	1.16	1.18	1.18

(c) Kd for straight dike length

Ld/b_d						
	0.0	0.5	1.0	1.5	2.0	2.8
0.2	1.00	0.99	1.00	1.06	1.10	1.00
m 0.4	1.00	0.97	0.98	1.04	1.08	1.00

| 0.6 | 1.00 | 0.94 | 0.94 | 1.00 | 1.05 | 1.00 |
| 0.8 | 1.00 | 0.89 | 0.88 | 0.945 | 1.01 | 1.00 |

(d) Kb for straight dike offset

Table D-21 Adjustment factors for spur dikes (see fig. D-18).

A P P E N D I X   E

Sediment Transport Functions – Sample Calculations

The following sample calculations were the basis for the algorithms used in the HEC-RAS sediment transport functions. They were computed for a single grain size, however they were adapted in the code to account for multiple grain sizes.

Ackers-White Sediment Transport Function

by Ackers-White (ASCE Jour. Of Hyd, Nov 1973)

Input Parameters

Temperature, F	T = 55	Average Velocity, ft/s	V = 2
Kinetic viscosity, ft^2/s	$\nu = 0.00001315$	Discharge, ft^3/s	Q = 5000
Depth, ft	D = 10	Unit Weight water, lb/ft^3	$\gamma_w = 62.385$
Slope	S = 0.001	Overall d50, ft	$d_{50} = 0.00232$
Median Particle Diamter, ft	$d_{si} = 0.00232$		
Specific Gravity of Sediment,		s = 2.65	

Constants

Acceleration of gravity, ft/s^2 g = 32.2

Solution

*note: Ackers-White required the use of d_{35} as the representative grain size for computations in their original paper. In the HEC-RAS approach, the median grain size will be used as per the 1993 update. The overall d_{50} is used for the hiding factor computations.

Hiding Factor from Profitt and Sutherland has been added for this procedure, but will be included as an option in HEC-RAS.

Computations are updated as per Acker's correction in Institution of Civil Engineers Water Maritime and Energy, Dec 1993.

Dimensionless grain diameter,

$$d_{gr} = d_{si} \left[\frac{g \cdot (s-1)}{v^2} \right]^{\frac{1}{3}}$$

$$d_{gr} = 15.655$$

Shear velocity u

$$u_{star} = \sqrt{g \cdot D \cdot S} \qquad\qquad u_{star} = 0.567$$

Sediment size-related transition exponent n,

$$n = \begin{vmatrix} 1 & \text{if } d_{gr} \leq 1 \\ (1 - .056 \cdot \log(d_{gr})) & \text{if } 1 < d_{gr} \leq 60 \\ 0 & \text{if } d_{gr} > 60 \end{vmatrix} \qquad\qquad n = 0.331$$

Initial motion parameter A,

$$A = \begin{vmatrix} \left(\dfrac{0.23}{\sqrt{d_{gr}}} + 0.14 \right) & \text{if } d_{gr} \leq 60 \\ 0.17 & \text{otherwise} \end{vmatrix} \qquad\qquad A = 0.198$$

Sediment mobility number F_{gr},

$$\alpha = 10 \quad \text{(assumed value used in HEC6 and SAM)} \qquad\qquad \alpha = 10$$

$$F_{gr} = \frac{u_{star}^{n}}{\sqrt{g \cdot d_{si} \cdot (s-1)}} \cdot \left(\frac{V}{\sqrt{32} \cdot \log\left(\alpha \cdot \frac{D}{d_{si}} \right)} \right)^{1-n} \qquad\qquad F_{gr} = 0.422$$

Hiding Factor HF,

Shield's Mobility Parameter $\square$

$$\theta = \frac{u_{star}^{2}}{g \cdot (s-1) d_{50}} \qquad\qquad \theta = 2.612$$

$$dRatio = \begin{vmatrix} 1.1 & \text{if } \theta \le 0.04 \\ (2.3 - 30 \cdot \theta) & \text{if } 0.04 < \theta \le 0.045 \\ (1.4 - 10 \cdot \theta) & \text{if } 0.045 < \theta \le 0.095 \\ 0.45 & \text{otherwise} \end{vmatrix}$$

dRatio = 0.45

$$dAdjust = d_{50} \cdot dRatio$$

dAdjust = 1.044 x 10^{-3}

$$HFRatio = \frac{d_{si}}{dAdjust}$$

HFRatio = 2.222

$$HF = \begin{vmatrix} 1.30 & \text{if } HFRatio \ge 3.7 \\ (0.53 \cdot \log(HFRatio) + 1) & \text{if } 0.075 \le HFRatio < 3.7 \\ 0.40 & \text{otherwise} \end{vmatrix}$$

HF = 1.184

Adjust Sediment Mobility Number for Hiding Factor

$$F_{gr} = HF \cdot F_{gr}$$

$F_{gr} = 0.5$

Check for too fine sediment based on F_{gr} and A,

$$Check = \frac{F_{gr}}{A}$$

Check = 2.522

Sediment transport function exponent m,

$$m = \begin{vmatrix} \left(\dfrac{6.83}{d_{gr}} + 1.67 \right) & \text{if } d_{gr} \le 60 \\ 1.78 & \text{otherwise} \end{vmatrix}$$

m = 2.106

Check for too fine sediment based on m,

$$Check = \begin{vmatrix} 0 & \text{if } m > 6 \\ Check & \text{otherwise} \end{vmatrix}$$

Check = 2.522

Sediment transport function coefficient C,

$$C = \begin{vmatrix} 10^{2.79 \cdot \log(d_{gr}) - 0.98(\log(d_{gr}))^2 - 3.46} & \text{if } d_{gr} \leq 60 \\ 0.025 & \text{otherwise} \end{vmatrix}$$

$C = 0.0298$

Transport parameter G_{gr},

$$G_{gr} = C \cdot \left(\frac{F_{gr}}{A} - 1 \right)^m$$

$G_{gr} = 0.072$

Sediment flux X, in parts per million by fluid weight,

$$X = \frac{G_{gr} s d_{si}}{D \left(\dfrac{u_{star}}{V} \right)^n}$$

$X = 6.741 \times 10^{-5}$

Sediment Discharge, lb/s

$$G = \gamma_w Q X$$

$G = 21.027$

Sediment Discharge, tons/day

$$G_s = \frac{86400}{2000} \cdot G$$

$G_s = 908$

Check to make sure particle diameter and mobility functions are not too low,

$$G_s = \begin{vmatrix} G_s & \text{if Check } > 1 \\ 0 & \text{otherwise} \end{vmatrix}$$

$G_s = 908$

Engelund Hansen Sediment Transport Function

by Vanoni (1975), and Raudkivi (1976)

Input Parameters

Temperature, F	$T = 55$	Average Velocity, ft/s	$V = 5.46$
Kinematic viscosity, ft²/s	$\nu = 0.00001315$		
Depth, ft	$D = 22.9$	Unit Weight water, lb/ft³	$\gamma_w = 62.385$
Slope	$S = 0.0001$		
Median Particle Diamter, ft	$d_{si} = 0.00232$	Channel Width, ft	$B = 40$
Specific Gravity of Sediment,		$s = 2.65$	

Constants

Acceleration of gravity, ft/s² $g = 32.2$

Solution

Bed level shear stress $\tau_\circ$

$$\tau_\circ = \gamma_w \cdot D \cdot S \qquad\qquad \tau_\circ = 0.143$$

Fall diameter d_f,

$$d_f = \begin{vmatrix} \left(-69.07 \cdot d_{si}^{\,2} + 1.0755 \cdot d_{si} + 0.000007\right) & \text{if } d_{si} \le 0.00591 \\ \left(0.1086 \cdot d_{si}^{\,0.6462}\right) & \text{otherwise} \end{vmatrix} \qquad d_f = 2.13 \times 10^{-3}$$

Sediment discharge lb/s,

$$g_s = 0.05 \cdot \gamma_w \cdot s \cdot V^2 \cdot \sqrt{\frac{d_f}{g \cdot (s-1)}} \cdot \left[\frac{\tau_\circ}{(\gamma_w \cdot s - \gamma_w) \cdot d_f}\right]^{\frac{3}{2}} \cdot B \qquad\qquad g_s = 32.82$$

Sediment discharge ton/day,

$$G_s = g_s \cdot \frac{86400}{2000} \qquad\qquad G_s = 1418$$

Laursen-Copeland Sediment Transport Function

by Copeland (from SAM code, 1996)

Input Parameters

Temperature, F	T = 55	Average Velocity, ft/s	V = 5.46
Kinematic viscosity, ft²/s	$\nu = 0.00001315$	Discharge, ft³/s	Q = 5000
Depth, ft	D = 22.90	Unit Weight water, lb/ft³	

$$\gamma_w = 62.385$$

Slope   S = 0.0001   84% Particle diameter, ft d_{84} = 0.00294

Median Particle Diamter, ft d_{si} = 0.00232

Specific Gravity of Sediment   s = 2.65

Constants

Acceleration of gravity, ft/s² $g = 32.2$

Solution

       *Note: the difference between the final result presented here and the result in SAM is due to

       the method for determining fall velocity. Rubey is used here, whereas SAM computes a

       value based on a drag coefficient determined from Reynolds number. Calculation routine   taken from SAM.

       Because the grain distribution is reduced to standard grade sizes representing each present

       grade class, the d_{84} will equal the standard grade size, d_{si}, in this procedure.

$$d_{84} = d_{si}$$

Grain-related hydraulic radius R

$$R' = \frac{0.0472 \cdot V^{\frac{3}{2}} \cdot \left(3.5 \cdot d_{84}\right)^{\frac{1}{4}}}{\left(g \cdot S\right)^{\frac{3}{4}}} \qquad\qquad R' = 14.189$$

R' = 15.248

$$u_*^{'} = \sqrt{g \cdot R' \cdot S} \qquad\qquad u_*^{'} = 0.222$$

$$FNRP = \left(\frac{V}{u_*^{'}}\right) - 3.28 - 5.75 \cdot \log\left(\frac{R'}{d_{84}}\right)$$

$$FNRP = 5.195 \times 10^{-4}$$

$$DFNRP = \frac{V + 5 \cdot u_*^{'}}{2.0 \cdot u_*^{'} \cdot R'} \qquad\qquad DFNRP = 0.972$$

$$RPRI2 = R' + \frac{FNRP}{DFNRP} \qquad\qquad RPRI2 = 15.249$$

$$\Delta R = |RPRI2 - R'| \qquad\qquad \Delta R = 5.345 \times 10^{-4}$$

$$R' = \begin{vmatrix} R' & \text{if } \Delta R \leq 0.001 \\ RPRI2 & \text{otherwise} \end{vmatrix}$$

$$R' = 15.248$$

Grain-related bed shear stress τ'_b,

$$\tau'_b = R' \cdot \gamma_w \cdot S \qquad\qquad \tau'_b = 0.095$$

$$\tau_b = D \cdot \gamma_w \cdot S \qquad\qquad \tau_b = 0.143$$

$$\tau'_b = \begin{vmatrix} \tau'_b & \text{if } \tau'_b < \tau_b \\ \tau_b & \text{otherwise} \end{vmatrix} \qquad\qquad \tau'_b = 0.095$$

$$u_*^{'} = \sqrt{\frac{\tau'_b \cdot g}{\gamma_w}} \qquad\qquad u_*^{'} = 0.222$$

$$RRP = \left(\frac{d_{si}}{R}\right)^{1.16667} \qquad\qquad RRP = 2.187 \times 10^{-5}$$

Dimensionless bed shear stress τ_b^*,

$$\tau_b^* = \frac{\tau'_b}{\gamma_w \cdot (s-1) \cdot d_{si}}$$

$$\tau_b^* = 0.398$$

Shield's parameter for course grains θ^*,

$$\theta^* = 0.647 \cdot \tau_b^* + 0.0064$$

$$\theta^* = \begin{vmatrix} 0.02 & \text{if } \theta^* < 0.02 \\ \theta^* & \text{otherwise} \end{vmatrix} \qquad\qquad \theta^* = 0.264$$

Critical shear stress, τ_{cr}

$$\tau_{cr} = \begin{vmatrix} \left[\theta^* \cdot \gamma_w \cdot (s-1) \cdot d_{si}\right] & \text{if } \tau_b^* \le 0.05 \\ \left[0.039 \cdot \gamma_w \cdot (s-1) \cdot d_{si}\right] & \text{otherwise} \end{vmatrix} \qquad \tau_{cr} = 9.315 \times 10^{-3}$$

Shear stress mobility parameter TFP,

$$\text{TFP} = \frac{\tau'_b}{\tau_{cr}} - 1 \qquad\qquad \text{TFP} = 9.214$$

Fall velocity ω,

Use Rubey's equation, Vanoni p. 169

$$F_1 = \sqrt{\frac{2}{3} + \frac{36 \cdot v^2}{g \cdot d_{si}^3 \cdot (s-1)}} - \sqrt{\frac{36 \cdot v^2}{g \cdot d_{si}^3 \cdot (s-1)}}$$

$F_1 = 0.725$

$$\omega = F_1 \cdot \sqrt{(s-1) \cdot g \cdot d_{si}}$$

$\omega = 0.255$

Particle velocity ratio SF,

$$SF = \frac{u_*^{'}}{\omega}$$

$SF = 0.870$

Particle velocity ratio parameter Ψ,

$$\Psi = \begin{vmatrix} \left[7.04 \cdot 10^{15} \cdot (SF)^{22.99} \right] & \text{if } SF \leq 0.225 \\ (40.0 \cdot SF) & \text{if } 0.225 < SF \leq 1.0 \\ (40 \cdot SF^{1.843}) & \text{if } SF > 1.0 \end{vmatrix}$$

$\Psi = 34.804$

Sediment transport G_s, tons/day

$$G_s = 0.432 \cdot \gamma_w \cdot Q \cdot RRP \cdot TFP \cdot \Psi$$

$G_s = 945$

Meyer-Peter Muller Sediment Transport Function

by Vanoni (1975), and Schlichting's Boundary Layer Theory, 1968

Input Parameters

Temperature, F	T = 55	Average Velocity, ft/s	V = 5.46
Kinematic viscosity, ft²/s	$\nu = 0.00001315$	Discharge, ft³/s	Q = 5000
Depth, ft	D = 22.9	Unit Weight water, lb/ft³	γ_w = 62.385
Slope	S = 0.0001	Overall d50, ft	d_{90} = 0.00306
Median Particle Diamter, ft	d_{si} = 0.00232	Channel Width, ft	B = 40
Specific Gravity of Sediment,		s = 2.65	

Constants

Acceleration of gravity, ft/s² $g = 32.2$

Solution

Shear velocity u,

$$u_* = \sqrt{g \cdot D \cdot S} \qquad\qquad u_* = 0.272$$

Shear Reynold's number, R_s,

$$R_s = \frac{u_* \cdot d_{90}}{\nu} \qquad\qquad R_s = 63.189$$

Schlichting's B coefficient, Bcoeff

$$BCoeff = \begin{vmatrix} (5.5 + 2.5 \cdot \ln(R_s)) & \text{if } R_s \leq 5 \\ \begin{bmatrix} 0.297918 + 24.8666 \cdot \log(R_s) - 22.9885 \cdot (\log(R_s))^2 \dots \\ + 8.5199 \cdot (\log(R_s))^3 - 1.10752 \cdot (\log(R_s))^4 \end{bmatrix} & \text{if } 5 < R_s \leq 70 \\ 8.5 & \text{otherwise} \end{vmatrix}$$

Friction factor due to sand grains f',

$$f' = \left(\frac{2.82843}{BCoeff - 3.75 + 2.5 \cdot \ln\left(2 \cdot \dfrac{D}{d_{90}}\right)} \right)^2$$

f' = 9.565 X 10⁻³

Nikaradse roughness ratio RKR,

$$RKR = \sqrt{\frac{f'}{8}} \cdot \frac{V}{\sqrt{g \cdot D \cdot S}}$$

RKR = 0.695

Sediment discharge lb/s,

$$g_s = \left[\frac{(RKR)^{\frac{3}{2}} \cdot \gamma_w \cdot D \cdot S - 0.047 \cdot (\gamma_w \cdot s - \gamma_w) \cdot d_{si}}{0.25 \cdot \left(\dfrac{\gamma_w}{g}\right)^{\frac{1}{3}} \cdot \left(\dfrac{\gamma_w \cdot s - \gamma_w}{\gamma_w \cdot s}\right)^{\frac{2}{3}}} \right]^{\frac{3}{2}} \cdot B$$

g_s = 7.073

Sediment discharge ton/day,

$$G_s = g_s \cdot \frac{86400}{2000}$$

G_s = 306

Toffaleti Sediment Transport Function

by Vanoni, for single grain size

Input Parameters

Slope,	S = 0.0001	Temperature, F	T = 55
Hydraulic Radius, ft	R = 10.68	viscosity, ft²/s	

$\nu = 0.00001315$

Width, ft	B = 40	Median Particle Size, ft	$d_{si} = 0.00232$
Velocity, ft/s		V = 5.46	65% finer Particle

Size, ft $d_{65} = 0.00257$

Fraction of Total Sediment $\quad p_i = 1$

Unit Weight of Water, lb/ft³ $\gamma_w = 62.385$

Constants

Acceleration of gravity, ft/s² $g = 32.2$

Solution

Nikaradse Roughness Value, using d_{65}, as per Einstein, 1950, p.

$$k_s = d_{65} \qquad k_s = 2.57 \times 10^{-3}$$

Grain-related shear velocity as per Einstein, 1950, p. 10

Guess $u'_{*try} = 0.199$

Assume hydraulically rough grain first.

$$r' = \frac{u'_{*try}{}^2}{g \cdot S}$$

r' = 12.298

$$u'_* = \frac{V}{\left(5.75 \cdot \log\left(12.27 \cdot \frac{r'}{k_s}\right)\right)}$$

Check $u'_* = 0.199$

Check for hydraulically rough or smooth grains…

Guess $u'_{*try} = 0.169$

$$r' = \frac{u'_{*try}{}^2}{g \cdot S} \qquad\qquad\qquad r' = 8.87$$

$$\delta' = \frac{11.6 \cdot v}{u'_{*try}} \qquad\qquad\qquad \delta' = 9.026 \times 10^{-4}$$

$$\text{Check} = \frac{k_s}{\delta'} \qquad\qquad \text{Check} = 2.847 \qquad\qquad \frac{k_s}{\delta'} = 2.847$$

$$u'_* = \left|\begin{array}{ll} \dfrac{V}{\left(5.75 \cdot \log\left(3.67 \cdot \dfrac{r' \cdot u'_{*try}}{v}\right)\right)} & \text{if Check} < 5 \quad \text{Smooth} \\[4ex] u'_* \quad \text{otherwise} & \text{Rough} \end{array}\right.$$

Check $u'_* = 0.169$

Check for Transitional regime

FIG. 2.97.—Factor *x* in Velocity Distribution Equation

$$\Phi = \frac{k_s}{\delta'} \qquad \Phi = 2.847 \qquad\qquad\qquad \Phi = 3.416$$

$$x = 1.14 \qquad\qquad\qquad \text{from figure 2.97, Vanoni, page 196}$$
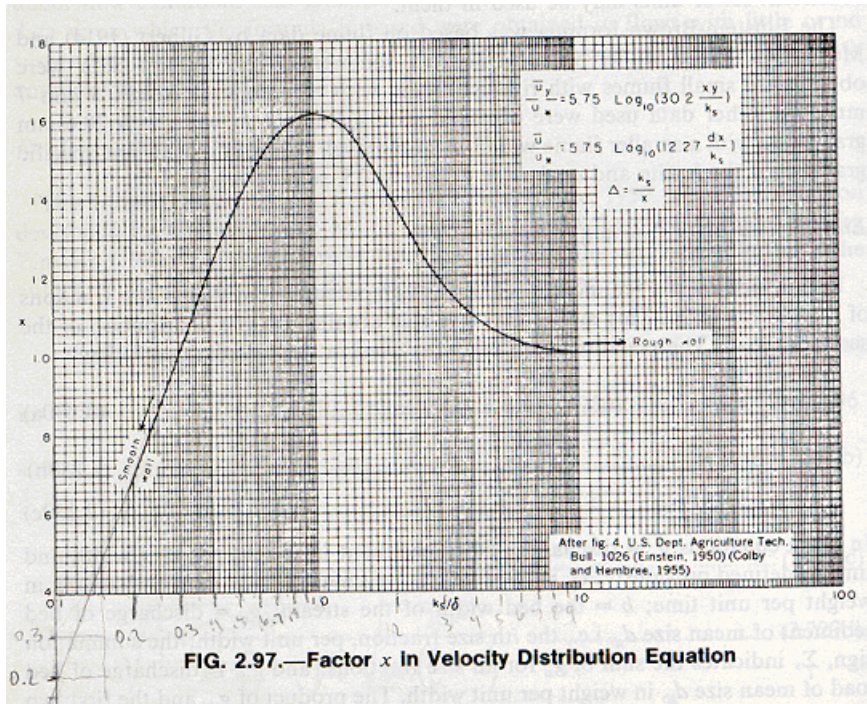
$$u'_* = \begin{vmatrix} \dfrac{V}{5.75 \cdot \log\left(12.27 \cdot \dfrac{r' \cdot x}{k_s}\right)} & \text{if } 0.1 < \Phi < 10 \\ u'_* & \text{otherwise} \end{vmatrix}$$

$$\delta' = \frac{11.6 \cdot v}{u'_*} \qquad\qquad \Phi = \frac{k_s}{\delta'} \qquad\qquad \Phi = 3.416$$

$$u'_* = 0.203$$

****Note: Einstein's method for determining u'* was compared with Toffaleti's graphical approach.

Results showed that the two methods are in acceptable agreement, with differences on the order

of less than 3%. Einstein's approach was selected for its established reputation and its relative

simplicity.

Toffaleti coefficients, A and k₄,

$$A_{factor} = \frac{\left(10^5 \cdot v\right)^{\frac{1}{3}}}{10 \cdot u'_*}$$

A$_{factor}$ = 0.54

$$A = \begin{vmatrix} \left(9.5987 \cdot A_{factor}^{-1.5445}\right) & \text{if } A_{factor} \leq 0.5 \\ \left(39.079 \cdot A_{factor}^{0.481}\right) & \text{if } 0.5 < A_{factor} \leq 0.66 \\ \left(221.85 \cdot A_{factor}^{4.660}\right) & \text{if } 0.66 < A_{factor} \leq 0.72 \\ 48 & \text{if } 0.72 < A_{factor} \leq 1.3 \\ \left(22.594 \cdot A_{factor}^{2.872}\right) & \text{if } A_{factor} > 1.3 \end{vmatrix}$$

A = 29.065

$$k_{4Factor} = \frac{\left(10^5 \cdot v\right)^{\frac{1}{3}}}{10 \cdot u'_*} \cdot 10^5 \cdot S \cdot d_{65}$$

K$_{4Factor}$ = 0.014

$$k_4 = \begin{vmatrix} (1.0) & \text{if } k_{4Facotr} \leq 0.25 \\ \left(5.315 \cdot k_{4Factor}^{1.205}\right) & \text{if } 0.25 \langle k_{4Factor} \leq 0.35 \\ \left(0.510 \cdot k_{4Factor}^{-1.028}\right) & \text{if } k_{4Factor} \rangle 0.35 \end{vmatrix}$$

k₄ = 1

$$Ak_4 = A \cdot k_4$$

Check for too low values for the product Ak₄,

$$Ak_4 = \begin{vmatrix} 16 & \text{if } Ak_4 \langle 16 \\ Ak_4 & \text{if } Ak_4 \geq 16 \end{vmatrix}$$

Ak$_4$ = 29.065

More Coefficients,

$$T_T = 1.10 \cdot (0.051 + 0.00009 \cdot T)$$

T$_T$ = 0.062

$$n_V = 0.1198 + 0.00048 \cdot T$$

n$_V$ = 0.146

$$c_z = 260.67 - 0.667 \cdot T$$

c$_Z$ = 223.985

Fall Velocity for Medium Sand from Toffaleti Tables at 55 degrees F,

$$w_i = 0.340$$

$$z_i = \frac{w_i \cdot V}{c_z \cdot R \cdot S}$$

$z_i = 7.76$

$$z_i = \begin{vmatrix} (1.5 \cdot n_V) & \text{if } z_i < n_V \\ z_i & \text{otherwise} \end{vmatrix}$$

$z_i = 7.76$

Empirical Relationship for g$_{ssLi}$,

$$g_{ssLi} = \frac{0.600 \cdot p_i}{\left(\dfrac{T_T \cdot Ak_4}{V^2}\right)^{\frac{5}{3}} \cdot \left(\dfrac{d_{si}}{0.00058}\right)^{\frac{5}{3}}}$$

$g_{ssLi} = 6.473$

$$M_i = \frac{g_{ssLi}}{\left[\dfrac{\left(\dfrac{R}{11.24}\right)^{1+n_V-0.756 \cdot z_i} - (2 \cdot d_{si})^{1+n_V-0.756 \cdot z_i}}{1 + n_V - 0.756 \cdot z_i}\right]}$$

M$_i$ = 2.948 X 10^{-10}

Concentration,

$$C_{Li} = \frac{M_i}{43.2 \cdot p_i \cdot (1 + n_V) \cdot V \cdot R^{0.756 \cdot z_i - n_V}}$$

C$_{Li}$ = 1.425 X 10^{-18}

Check for unrealistically high concentration and adjust M$_i$ if necessary,

$$C_{2d} = C_{Li} \cdot \left(\frac{2 \cdot d_{si}}{R} \right)^{-0.756 \cdot z_i} \qquad\qquad C_{2d} = 75.536$$

$$C_{Li} = \begin{vmatrix} C_{Li} & \text{if } C_{2d} < 100 \\ \dfrac{100}{\left(\dfrac{2 \cdot d_{si}}{R} \right)^{-0.756 \cdot z_i}} & \text{if } C_{2d} \geq 100 \end{vmatrix} \qquad C_{Li} = 1.425 \times 10^{-18}$$

$$M_i = C_{Li} \cdot \left[43.2 \cdot p_i \cdot (1 + n_V) \cdot V \cdot R^{0.756 \cdot z_i - n_V} \right] \qquad M_i = 2.948 \times 10^{-10}$$

Bed Load Transport,

$$g_{sbi} = M_i \cdot (2 \cdot d_{si})^{(1 + n_V - 0.756 z_i)} \qquad\qquad g_{sbi} = 30.555$$

Lower Layer Transport,

$$g_{ssLi} = M_i \cdot \left[\frac{\left(\dfrac{R}{11.24} \right)^{(1 + n_V - 0.756 \cdot z_i)} - (2 \cdot d_{si})^{(1 + n_V - 0.756 \cdot z_i)}}{1 + n_V - 0.756 \cdot z_i} \right] \qquad g_{ssLi} = 6.473$$

Middle Layer Transport,

$$g_{ssMi} = M_i \cdot \frac{\left(\dfrac{R}{11.24} \right)^{0.244 \cdot z_i} \cdot \left[\left(\dfrac{R}{2.5} \right)^{1 + n_V - z_i} - \left(\dfrac{R}{11.24} \right)^{1 + n_V - z_i} \right]}{1 + n_V - z_i} \qquad g_{ssMi} = 5.674 \times 10^{-1}$$

Upper Layer Transport,

$$g_{ssUi} = M_i \cdot \frac{\left(\dfrac{R}{11.24} \right)^{0.244 \cdot z_i} \cdot \left(\dfrac{R}{2.5} \right)^{0.5 \cdot z_i} \cdot \left[R^{(1 + n_V - 1.5 \cdot z_i)} - \left(\dfrac{R}{2.5} \right)^{1 + n_V - 1.5 \cdot z_i} \right]}{1 + n_V - 1.5 \cdot z_i} \qquad g_{ssUi} = 1.72 \times 10^{-15}$$

Total Transport per Unit Width,

$$g_{si} = g_{sbi} + g_{ssLi} + g_{ssMi} + g_{ssUi} \qquad\qquad g_{si} = 37.027$$

Total Transport,

$$G = g_{si} \cdot B \qquad\qquad \underline{G = 1481 \text{ tons/day}}$$

Yang Sediment Transport Function

by Yang, from ASCE Journal of Hydraulics, Oct 1973, Dec 1984

Input Parameters

Temperature, F	T = 55	Average Velocity, ft/s	V = 5.46
Kinematic viscosity, ft²/s	$v = 0.00001315$	Discharge, ft³/s	Q = 5000
Hydraulic Radius, ft	R = 10.68	Unit Weight water, lb/ft³	$\gamma_w = 62.385$
Slope,	S = 0.0001		
Meidan Particle Diamter, ft	$d_{si} = 0.00232$		
Specific Gravity of Sediment		s = 2.65	

Constants

Acceleration of gravity, ft/s² g = 32.2

Solution

Shear Velocity, ft/s,

$$u_* = \sqrt{g \cdot R \cdot S} \qquad\qquad u_* = 0.185$$

Particle Fall Velocity, ft/s,

Use Rubey's equation, Vanoni p. 169

$$F_1 = \sqrt{\frac{2}{3} + \frac{36 \cdot v^2}{g \cdot d_{si}^3 \cdot (s-1)}} - \sqrt{\frac{36 \cdot v^2}{g \cdot d_{si}^3 \cdot (s-1)}}$$

$F_1 = 0.725$

$$\omega = F_1 \cdot \sqrt{(s-1) \cdot g \cdot d_{si}} \qquad\qquad \omega = 0.255$$

Shear Reynold's Number,

$$R_s = \frac{u_* \cdot d_{si}}{v} \qquad\qquad R_s = 32.717$$

Critical Velocity, ft/s,

$$V_{cr} = \begin{vmatrix} \omega \cdot \left(\dfrac{2.5}{\log\left(\dfrac{u_* \cdot d_{si}}{v}\right) - 0.06} + 0.66 \right) & \text{if } 0 < R_s < 70 \\ (\omega \cdot 2.05) & \text{if } R_s \geq 70 \end{vmatrix}$$

$$V_{cr} = 0.606$$

Log of Concentration,

$$\log C_t = \begin{vmatrix} \left[5.435 - 0.286 \cdot \log\left(\dfrac{\omega \cdot d_{si}}{v}\right) - 0.457 \cdot \log\left(\dfrac{u_*}{\omega}\right) \ldots \\ + \left(1.799 - 0.409 \cdot \log\left(\dfrac{\omega \cdot d_{si}}{v}\right) - 0.314 \cdot \log\left(\dfrac{u_*}{\omega}\right) \right) \cdot \log\left(\dfrac{V \cdot S}{\omega} - \dfrac{V_{cr} \cdot S}{\omega}\right) \right] & \text{if } d_{si} < 0.00656 \quad \text{Sand} \\ \left[\left(6.681 - 0.633 \cdot \log\left(\dfrac{\omega \cdot d_{si}}{v}\right) - 4.816 \cdot \log\left(\dfrac{u_*}{\omega}\right) \right) \ldots \\ + \left(2.784 - 0.305 \cdot \log\left(\dfrac{\omega \cdot d_{si}}{v}\right) - 0.282 \cdot \log\left(\dfrac{u_*}{\omega}\right) \right) \cdot \log\left(\dfrac{V \cdot S}{\omega} - \dfrac{V_{cr} \cdot S}{\omega}\right) \right] & \text{if } d_{si} \geq 0.00656 \quad \text{Gravel} \end{vmatrix}$$

$$\log C_t = 1.853$$

Concentration, ppm

$$C_t = 10^{\log C_t}$$

$$C_t = 71.284$$

Sediment Discharge, lb/s

$$G = \frac{\gamma_w \cdot Q \cdot C_t}{1000000}$$

$G = 22.235$

Sediment Discharge, tons/day

$$G_s = \frac{86400}{2000} \cdot G$$

$G_s = 961$